NIST NCSTAR 1-3D

Federal Building and Fire Safety Investigation of the World Trade Center Disaster

Mechanical Properties of Structural Steels

William E. Luecke
J. David McColskey
Christopher N. McCowan
Stephen W. Banovic
Richard J. Fields
Timothy Foecke
Thomas A. Siewert
Frank W. Gayle

NIST National Institute of Standards and Technology • Technology Administration • U.S. Department of Commerce

NIST NCSTAR 1-3D

Federal Building and Fire Safety Investigation of the World Trade Center Disaster

Mechanical Properties of Structural Steels

William E. Luecke
J. David McColskey
Christopher N. McCowan
Stephen W. Banovic
Richard J. Fields*
Timothy Foecke
Thomas A. Siewert
Frank W. Gayle
Materials Science and Engineering Laboratory
National Institute of Standards and Technology

*Retired

September 2005

U.S. Department of Commerce
Carlos M. Gutierrez, Secretary

Technology Administration
Michelle O'Neill, Acting Under Secretary for Technology

National Institute of Standards and Technology
William Jeffrey, Director

Disclaimer No. 1

Certain commercial entities, equipment, products, or materials are identified in this document in order to describe a procedure or concept adequately or to trace the history of the procedures and practices used. Such identification is not intended to imply recommendation, endorsement, or implication that the entities, products, materials, or equipment are necessarily the best available for the purpose. Nor does such identification imply a finding of fault or negligence by the National Institute of Standards and Technology.

Disclaimer No. 2

The policy of NIST is to use the International System of Units (metric units) in all publications. In this document, however, units are presented in metric units or the inch-pound system, whichever is prevalent in the discipline.

Disclaimer No. 3

Pursuant to section 7 of the National Construction Safety Team Act, the NIST Director has determined that certain evidence received by NIST in the course of this Investigation is "voluntarily provided safety-related information" that is "not directly related to the building failure being investigated" and that "disclosure of that information would inhibit the voluntary provision of that type of information" (15 USC 7306c).

In addition, a substantial portion of the evidence collected by NIST in the course of the Investigation has been provided to NIST under nondisclosure agreements.

Disclaimer No. 4

NIST takes no position as to whether the design or construction of a WTC building was compliant with any code since, due to the destruction of the WTC buildings, NIST could not verify the actual (or as-built) construction, the properties and condition of the materials used, or changes to the original construction made over the life of the buildings. In addition, NIST could not verify the interpretations of codes used by applicable authorities in determining compliance when implementing building codes. Where an Investigation report states whether a system was designed or installed as required by a code *provision*, NIST has documentary or anecdotal evidence indicating whether the requirement was met, or NIST has independently conducted tests or analyses indicating whether the requirement was met.

Use in Legal Proceedings

No part of any report resulting from a NIST investigation into a structural failure or from an investigation under the National Construction Safety Team Act may be used in any suit or action for damages arising out of any matter mentioned in such report (15 USC 281a; as amended by P.L. 107-231).

National Institute of Standards and Technology National Construction Safety Team Act Report 1-3D
Natl. Inst. Stand. Technol. Natl. Constr. Sfty. Tm. Act Rpt. 1-3D, 322 pages (September 2005)
CODEN: NSPUE2

U.S. GOVERNMENT PRINTING OFFICE
WASHINGTON: 2005

For sale by the Superintendent of Documents, U.S. Government Printing Office
Internet: bookstore.gpo.gov — Phone: (202) 512-1800 — Fax: (202) 512-2250
Mail: Stop SSOP, Washington, DC 20402-0001

ABSTRACT

This report provides five types of mechanical properties for steels from the World Trade Center (WTC): elastic, room-temperature tensile, room-temperature high strain rate, impact, and elevated-temperature tensile. Specimens of 29 different steels representing the 12 identified strength levels in the building as built were characterized. Elastic properties include modulus, E, and Poisson's ratio, ν, for temperatures up to 900 °C. The expression for $E(T)$ for T < 723 °C is based on measurements of WTC perimeter column steels. Behavior for T > 723 °C is estimated from literature data. Room temperature tensile properties include yield and tensile strength and total elongation for samples of all grades of steel used in the towers. The report provides model stress-strain curves for each type of steel, estimated from the measured stress-strain curves, surviving mill test reports, and historically expected values. With a few exceptions, the recovered steels, bolts, and welds met the specifications they were supplied to. In a few cases, the measured yield strengths of recovered steels were slightly lower than specified, probably because of a combination of mechanical damage, natural variability, and differences in testing methodology. High-strain-rate properties for selected perimeter and core column steels include yield and tensile strength, total elongation and strain rate sensitivity for rates up to 400 s^{-1}. Measured properties were consistent with literature reports on other structural steels. Impact properties were evaluated with Charpy testing. Properties for perimeter and core column steels were consistent with other structural steels of the era. The impact toughness at room temperature of nearly all WTC steels tested exceeded 15 ft·lbf at room temperature. Elevated-temperature stress-strain curves were collected for selected perimeter and core column and truss steels. The report presents a methodology for estimating high-temperature stress-strain curves for the steels not characterized based on room-temperature behavior and behavior of other structural steels from the literature. The measured elevated-temperature stress-strain behavior of WTC steels is consistent with other structural steels from that era. For the truss steels, the report presents a complete constitutive law for creep deformation based on experimental measurements. For the steels not characterized, the report presents a methodology for estimating the creep deformation law.

Keywords: Creep, high strain rate, high temperature, impact, modulus, tensile strength, yield strength, World Trade Center.

This page intentionally left blank.

TABLE OF CONTENTS

List of Figures

This page intentionally left blank.

List of Tables

List of Acronyms and Abbreviations

Acronyms

AISC	American Institute of Steel Construction
AISI	American Iron and Steel Institute
ASTM	ASTM International
AWS	American Welding Society
BPS	Building Performance Study
CVN	Charpy V-notch
FATT	fracture appearance transition temperature
FEMA	Federal Emergency Management Agency
HAZ	heat-affected zone
HSR	high-rate style
HSLA	high-strength, low-alloy
JIS	Japan Industrial Standard
LERA	Leslie E. Robertson Associates
LRFD	load and resistance factor design
METT	mid-energy transition temperature
NIST	National Institute of Standards and Technology
PANYNJ	Port Authority of New York and New Jersey
PC&F	Pacific Car and Foundry
PONYA	Port of New York Authority
SEAoNY	Structural Engineers Association of New York
SHCR	Skilling, Helle, Christiansen, & Robertson
SMA	shielded metal arc
SRS	strain rate sensitivity
USC	United States Code
WF	wide-flange (a type of structural steel shape now usually called a W-shape)
WTC	World Trade Center
WTC 1	World Trade Center 1 (North Tower)
WTC 2	World Trade Center 2 (South Tower)

WTC 7	World Trade Center 7

Abbreviations

°C	degrees Celsius
°F	degrees Fahrenheit
μm	micrometer
ft	foot
F_y	yield strength
gal	gallon
GPa	gigapascal; 1×10^9 N/m^2
h	hour
in.	inch
L	liter
lb	pound
lbf	pound force
kip	a force equal to 1000 pounds
ksi	1,000 pounds per square inch
m	meter
min	minute
mm	millimeter
Mn	magnesium
min	minute
MPa	megapascal; 1×10^6 N/m^2
s	second

PREFACE

Genesis of This Investigation

Immediately following the terrorist attack on the World Trade Center (WTC) on September 11, 2001, the Federal Emergency Management Agency (FEMA) and the American Society of Civil Engineers began planning a building performance study of the disaster. The week of October 7, as soon as the rescue and search efforts ceased, the Building Performance Study Team went to the site and began its assessment. This was to be a brief effort, as the study team consisted of experts who largely volunteered their time away from their other professional commitments. The Building Performance Study Team issued its report in May 2002, fulfilling its goal "to determine probable failure mechanisms and to identify areas of future investigation that could lead to practical measures for improving the damage resistance of buildings against such unforeseen events."

On August 21, 2002, with funding from the U.S. Congress through FEMA, the National Institute of Standards and Technology (NIST) announced its building and fire safety investigation of the WTC disaster. On October 1, 2002, the National Construction Safety Team Act (Public Law 107-231), was signed into law. The NIST WTC Investigation was conducted under the authority of the National Construction Safety Team Act.

The goals of the investigation of the WTC disaster were:

- To investigate the building construction, the materials used, and the technical conditions that contributed to the outcome of the WTC disaster.
- To serve as the basis for:
  - Improvements in the way buildings are designed, constructed, maintained, and used;
  - Improved tools and guidance for industry and safety officials;
  - Recommended revisions to current codes, standards, and practices; and
  - Improved public safety.

The specific objectives were:

1. Determine why and how WTC 1 and WTC 2 collapsed following the initial impacts of the aircraft and why and how WTC 7 collapsed;
2. Determine why the injuries and fatalities were so high or low depending on location, including all technical aspects of fire protection, occupant behavior, evacuation, and emergency response;
3. Determine what procedures and practices were used in the design, construction, operation, and maintenance of WTC 1, 2, and 7; and
4. Identify, as specifically as possible, areas in current building and fire codes, standards, and practices that warrant revision.

NIST is a nonregulatory agency of the U.S. Department of Commerce's Technology Administration. The purpose of NIST investigations is to improve the safety and structural integrity of buildings in the United States, and the focus is on fact finding. NIST investigative teams are authorized to assess building performance and emergency response and evacuation procedures in the wake of any building failure that has resulted in substantial loss of life or that posed significant potential of substantial loss of life. NIST does not have the statutory authority to make findings of fault nor negligence by individuals or organizations. Further, no part of any report resulting from a NIST investigation into a building failure or from an investigation under the National Construction Safety Team Act may be used in any suit or action for damages arising out of any matter mentioned in such report (15 USC 281a, as amended by Public Law 107-231).

Organization of the Investigation

The National Construction Safety Team for this Investigation, appointed by the then NIST Director, Dr. Arden L. Bement, Jr., was led by Dr. S. Shyam Sunder. Dr. William L. Grosshandler served as Associate Lead Investigator, Mr. Stephen A. Cauffman served as Program Manager for Administration, and Mr. Harold E. Nelson served on the team as a private sector expert. The Investigation included eight interdependent projects whose leaders comprised the remainder of the team. A detailed description of each of these eight projects is available at http://wtc.nist.gov. The purpose of each project is summarized in Table P–1, and the key interdependencies among the projects are illustrated in Fig. P–1.

Table P–1. Federal building and fire safety investigation of the WTC disaster.

Technical Area and Project Leader	Project Purpose
Analysis of Building and Fire Codes and Practices; Project Leaders: Dr. H. S. Lew and Mr. Richard W. Bukowski	Document and analyze the code provisions, procedures, and practices used in the design, construction, operation, and maintenance of the structural, passive fire protection, and emergency access and evacuation systems of WTC 1, 2, and 7.
Baseline Structural Performance and Aircraft Impact Damage Analysis; Project Leader: Dr. Fahim H. Sadek	Analyze the baseline performance of WTC 1 and WTC 2 under design, service, and abnormal loads, and aircraft impact damage on the structural, fire protection, and egress systems.
Mechanical and Metallurgical Analysis of Structural Steel; Project Leader: Dr. Frank W. Gayle	Determine and analyze the mechanical and metallurgical properties and quality of steel, weldments, and connections from steel recovered from WTC 1, 2, and 7.
Investigation of Active Fire Protection Systems; Project Leader: Dr. David D. Evans; Dr. William Grosshandler	Investigate the performance of the active fire protection systems in WTC 1, 2, and 7 and their role in fire control, emergency response, and fate of occupants and responders.
Reconstruction of Thermal and Tenability Environment; Project Leader: Dr. Richard G. Gann	Reconstruct the time-evolving temperature, thermal environment, and smoke movement in WTC 1, 2, and 7 for use in evaluating the structural performance of the buildings and behavior and fate of occupants and responders.
Structural Fire Response and Collapse Analysis; Project Leaders: Dr. John L. Gross and Dr. Therese P. McAllister	Analyze the response of the WTC towers to fires with and without aircraft damage, the response of WTC 7 in fires, the performance of composite steel-trussed floor systems, and determine the most probable structural collapse sequence for WTC 1, 2, and 7.
Occupant Behavior, Egress, and Emergency Communications; Project Leader: Mr. Jason D. Averill	Analyze the behavior and fate of occupants and responders, both those who survived and those who did not, and the performance of the evacuation system.
Emergency Response Technologies and Guidelines; Project Leader: Mr. J. Randall Lawson	Document the activities of the emergency responders from the time of the terrorist attacks on WTC 1 and WTC 2 until the collapse of WTC 7, including practices followed and technologies used.

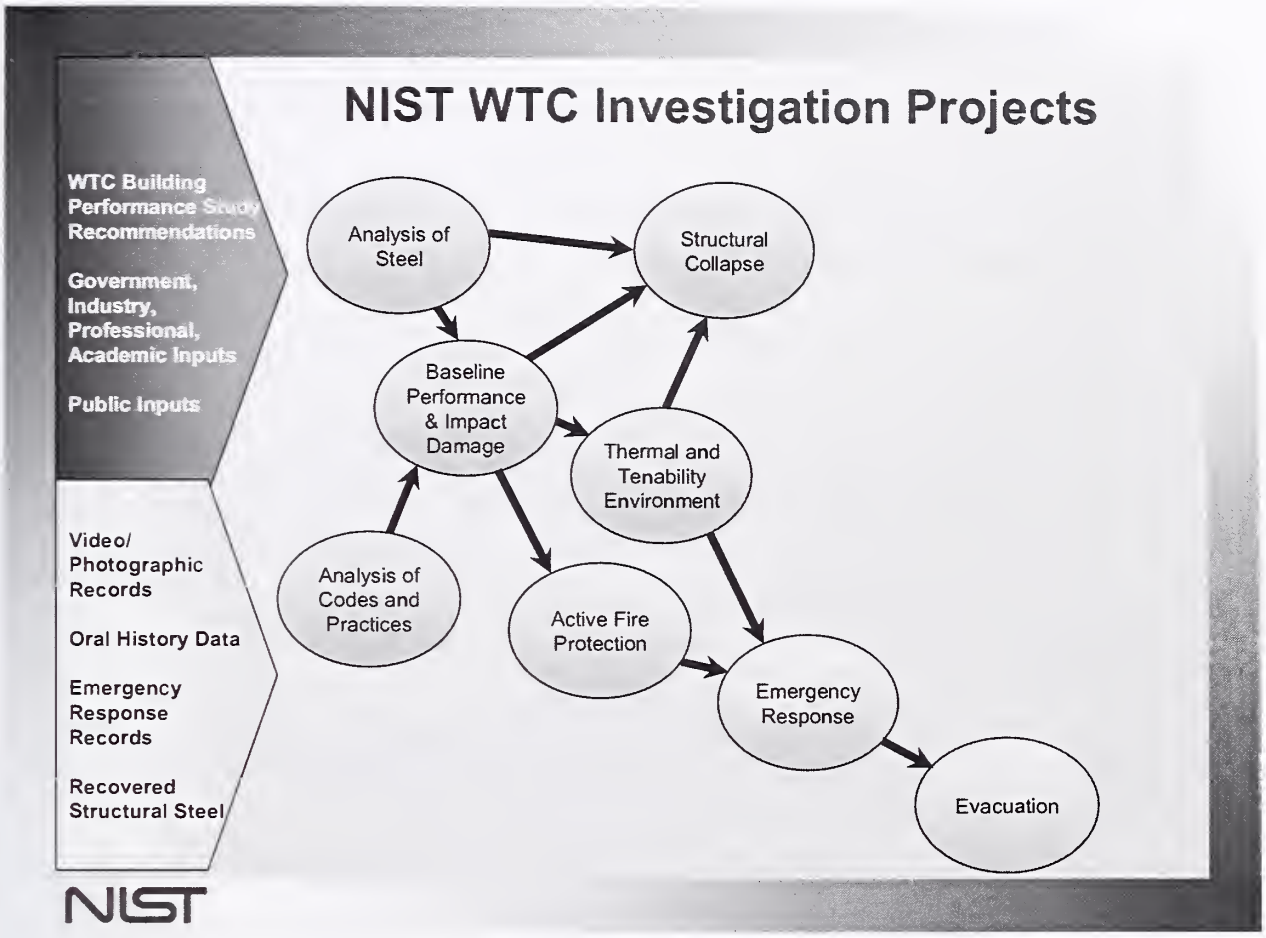

Figure P–1. The eight projects in the federal building and fire safety investigation of the WTC disaster.

National Construction Safety Team Advisory Committee

The NIST Director also established an advisory committee as mandated under the National Construction Safety Team Act. The initial members of the committee were appointed following a public solicitation. These were:

- Paul Fitzgerald, Executive Vice President (retired) FM Global, National Construction Safety Team Advisory Committee Chair
- John Barsom, President, Barsom Consulting, Ltd.
- John Bryan, Professor Emeritus, University of Maryland
- David Collins, President, The Preview Group, Inc.
- Glenn Corbett, Professor, John Jay College of Criminal Justice
- Philip DiNenno, President, Hughes Associates, Inc.

- Robert Hanson, Professor Emeritus, University of Michigan
- Charles Thornton, Co-Chairman and Managing Principal, The Thornton-Tomasetti Group, Inc.
- Kathleen Tierney, Director, Natural Hazards Research and Applications Information Center, University of Colorado at Boulder
- Forman Williams, Director, Center for Energy Research, University of California at San Diego

This National Construction Safety Team Advisory Committee provided technical advice during the Investigation and commentary on drafts of the Investigation reports prior to their public release. NIST has benefited from the work of many people in the preparation of these reports, including the National Construction Safety Team Advisory Committee. The content of the reports and recommendations, however, are solely the responsibility of NIST.

Public Outreach

During the course of this Investigation, NIST held public briefings and meetings (listed in Table P–2) to solicit input from the public, present preliminary findings, and obtain comments on the direction and progress of the Investigation from the public and the Advisory Committee.

NIST maintained a publicly accessible Web site during this Investigation at http://wtc.nist.gov. The site contained extensive information on the background and progress of the Investigation.

NIST's WTC Public-Private Response Plan

The collapse of the WTC buildings has led to broad reexamination of how tall buildings are designed, constructed, maintained, and used, especially with regard to major events such as fires, natural disasters, and terrorist attacks. Reflecting the enhanced interest in effecting necessary change, NIST, with support from Congress and the Administration, has put in place a program, the goal of which is to develop and implement the standards, technology, and practices needed for cost-effective improvements to the safety and security of buildings and building occupants, including evacuation, emergency response procedures, and threat mitigation.

The strategy to meet this goal is a three-part NIST-led public-private response program that includes:

- A federal building and fire safety investigation to study the most probable factors that contributed to post-aircraft impact collapse of the WTC towers and the 47-story WTC 7 building, and the associated evacuation and emergency response experience.
- A research and development (R&D) program to (a) facilitate the implementation of recommendations resulting from the WTC Investigation, and (b) provide the technical basis for cost-effective improvements to national building and fire codes, standards, and practices that enhance the safety of buildings, their occupants, and emergency responders.

Table P–2. Public meetings and briefings of the WTC Investigation.

Date	Location	Principal Agenda
June 24, 2002	New York City, NY	Public meeting: Public comments on the *Draft Plan* for the pending WTC Investigation.
August 21, 2002	Gaithersburg, MD	Media briefing announcing the formal start of the Investigation.
December 9, 2002	Washington, DC	Media briefing on release of the *Public Update* and NIST request for photographs and videos.
April 8, 2003	New York City, NY	Joint public forum with Columbia University on first-person interviews.
April 29–30, 2003	Gaithersburg, MD	NCST Advisory Committee meeting on plan for and progress on WTC Investigation with a public comment session.
May 7, 2003	New York City, NY	Media briefing on release of *May 2003 Progress Report.*
August 26–27, 2003	Gaithersburg, MD	NCST Advisory Committee meeting on status of the WTC investigation with a public comment session.
September 17, 2003	New York City, NY	Media and public briefing on initiation of first-person data collection projects.
December 2–3, 2003	Gaithersburg, MD	NCST Advisory Committee meeting on status and initial results and release of the *Public Update* with a public comment session.
February 12, 2004	New York City, NY	Public meeting on progress and preliminary findings with public comments on issues to be considered in formulating final recommendations.
June 18, 2004	New York City, NY	Media/public briefing on release of *June 2004 Progress Report.*
June 22–23, 2004	Gaithersburg, MD	NCST Advisory Committee meeting on the status of and preliminary findings from the WTC Investigation with a public comment session.
August 24, 2004	Northbrook, IL	Public viewing of standard fire resistance test of WTC floor system at Underwriters Laboratories, Inc.
October 19–20, 2004	Gaithersburg, MD	NCST Advisory Committee meeting on status and near complete set of preliminary findings with a public comment session.
November 22, 2004	Gaithersburg, MD	NCST Advisory Committee discussion on draft annual report to Congress, a public comment session, and a closed session to discuss pre-draft recommendations for WTC Investigation.
April 5, 2005	New York City, NY	Media and public briefing on release of the probable collapse sequence for the WTC towers and draft reports for the projects on codes and practices, evacuation, and emergency response.
June 23, 2005	New York City, NY	Media and public briefing on release of all draft reports for the WTC towers and draft recommendations for public comment.
September 12–13, 2005	Gaithersburg, MD	NCST Advisory Committee meeting on disposition of public comments and update to draft reports for the WTC towers.
September 13–15, 2005	Gaithersburg, MD	WTC Technical Conference for stakeholders and technical community for dissemination of findings and recommendations and opportunity for public to make technical comments.

- A dissemination and technical assistance program (DTAP) to (a) engage leaders of the construction and building community in ensuring timely adoption and widespread use of proposed changes to practices, standards, and codes resulting from the WTC Investigation and the R&D program, and (b) provide practical guidance and tools to better prepare facility owners, contractors, architects, engineers, emergency responders, and regulatory authorities to respond to future disasters.

The desired outcomes are to make buildings, occupants, and first responders safer in future disaster events.

National Construction Safety Team Reports on the WTC Investigation

A final report on the collapse of the WTC towers is being issued as NIST NCSTAR 1. A companion report on the collapse of WTC 7 is being issued as NIST NCSTAR 1A. The present report is one of a set that provides more detailed documentation of the Investigation findings and the means by which these technical results were achieved. As such, it is part of the archival record of this Investigation. The titles of the full set of Investigation publications are:

NIST (National Institute of Standards and Technology). 2005. *Federal Building and Fire Safety Investigation of the World Trade Center Disaster: Final Report on the Collapse of the World Trade Center Towers.* NIST NCSTAR 1. Gaithersburg, MD, September.

NIST (National Institute of Standards and Technology). 2006. *Federal Building and Fire Safety Investigation of the World Trade Center Disaster: Final Report on the Collapse of World Trade Center 7.* NIST NCSTAR 1A. Gaithersburg, MD.

Lew, H. S., R. W. Bukowski, and N. J. Carino. 2005. *Federal Building and Fire Safety Investigation of the World Trade Center Disaster: Design, Construction, and Maintenance of Structural and Life Safety Systems.* NIST NCSTAR 1-1. National Institute of Standards and Technology. Gaithersburg, MD, September.

Fanella, D. A., A. T. Derecho, and S. K. Ghosh. 2005. *Federal Building and Fire Safety Investigation of the World Trade Center Disaster: Design and Construction of Structural Systems.* NIST NCSTAR 1-1A. National Institute of Standards and Technology. Gaithersburg, MD, September.

Ghosh, S. K., and X. Liang. 2005. *Federal Building and Fire Safety Investigation of the World Trade Center Disaster: Comparison of Building Code Structural Requirements.* NIST NCSTAR 1-1B. National Institute of Standards and Technology. Gaithersburg, MD, September.

Fanella, D. A., A. T. Derecho, and S. K. Ghosh. 2005. *Federal Building and Fire Safety Investigation of the World Trade Center Disaster: Maintenance and Modifications to Structural Systems.* NIST NCSTAR 1-1C. National Institute of Standards and Technology. Gaithersburg, MD, September.

Grill, R. A., and D. A. Johnson. 2005. *Federal Building and Fire Safety Investigation of the World Trade Center Disaster: Fire Protection and Life Safety Provisions Applied to the Design and Construction of World Trade Center 1, 2, and 7 and Post-Construction Provisions Applied after Occupancy.* NIST NCSTAR 1-1D. National Institute of Standards and Technology. Gaithersburg, MD, September.

Razza, J. C., and R. A. Grill. 2005. *Federal Building and Fire Safety Investigation of the World Trade Center Disaster: Comparison of Codes, Standards, and Practices in Use at the Time of the Design and Construction of World Trade Center 1, 2, and 7.* NIST NCSTAR 1-1E. National Institute of Standards and Technology. Gaithersburg, MD, September.

Grill, R. A., D. A. Johnson, and D. A. Fanella. 2005. *Federal Building and Fire Safety Investigation of the World Trade Center Disaster: Comparison of the 1968 and Current (2003) New*

York City Building Code Provisions. NIST NCSTAR 1-1F. National Institute of Standards and Technology. Gaithersburg, MD, September.

Grill, R. A., and D. A. Johnson. 2005. *Federal Building and Fire Safety Investigation of the World Trade Center Disaster: Amendments to the Fire Protection and Life Safety Provisions of the New York City Building Code by Local Laws Adopted While World Trade Center 1, 2, and 7 Were in Use*. NIST NCSTAR 1-1G. National Institute of Standards and Technology. Gaithersburg, MD, September.

Grill, R. A., and D. A. Johnson. 2005. *Federal Building and Fire Safety Investigation of the World Trade Center Disaster: Post-Construction Modifications to Fire Protection and Life Safety Systems of World Trade Center 1 and 2*. NIST NCSTAR 1-1H. National Institute of Standards and Technology. Gaithersburg, MD, September.

Grill, R. A., D. A. Johnson, and D. A. Fanella. 2005. *Federal Building and Fire Safety Investigation of the World Trade Center Disaster: Post-Construction Modifications to Fire Protection, Life Safety, and Structural Systems of World Trade Center 7*. NIST NCSTAR 1-1I. National Institute of Standards and Technology. Gaithersburg, MD, September.

Grill, R. A., and D. A. Johnson. 2005. *Federal Building and Fire Safety Investigation of the World Trade Center Disaster: Design, Installation, and Operation of Fuel System for Emergency Power in World Trade Center 7*. NIST NCSTAR 1-1J. National Institute of Standards and Technology. Gaithersburg, MD, September.

Sadek, F. 2005. *Federal Building and Fire Safety Investigation of the World Trade Center Disaster: Baseline Structural Performance and Aircraft Impact Damage Analysis of the World Trade Center Towers*. NIST NCSTAR 1-2. National Institute of Standards and Technology. Gaithersburg, MD, September.

Faschan, W. J., and R. B. Garlock. 2005. *Federal Building and Fire Safety Investigation of the World Trade Center Disaster: Reference Structural Models and Baseline Performance Analysis of the World Trade Center Towers*. NIST NCSTAR 1-2A. National Institute of Standards and Technology. Gaithersburg, MD, September.

Kirkpatrick, S. W., R. T. Bocchieri, F. Sadek, R. A. MacNeill, S. Holmes, B. D. Peterson, R. W. Cilke, C. Navarro. 2005. *Federal Building and Fire Safety Investigation of the World Trade Center Disaster: Analysis of Aircraft Impacts into the World Trade Center Towers,* NIST NCSTAR 1-2B. National Institute of Standards and Technology. Gaithersburg, MD, September.

Gayle, F. W., R. J. Fields, W. E. Luecke, S. W. Banovic, T. Foecke, C. N. McCowan, T. A. Siewert, and J. D. McColskey. 2005. *Federal Building and Fire Safety Investigation of the World Trade Center Disaster: Mechanical and Metallurgical Analysis of Structural Steel*. NIST NCSTAR 1-3. National Institute of Standards and Technology. Gaithersburg, MD, September.

Luecke, W. E., T. A. Siewert, and F. W. Gayle. 2005. *Federal Building and Fire Safety Investigation of the World Trade Center Disaster: Contemporaneous Structural Steel Specifications*. NIST Special Publication 1-3A. National Institute of Standards and Technology. Gaithersburg, MD, September.

Banovic, S. W. 2005. *Federal Building and Fire Safety Investigation of the World Trade Center Disaster: Steel Inventory and Identification.* NIST NCSTAR 1-3B. National Institute of Standards and Technology. Gaithersburg, MD, September.

Banovic, S. W., and T. Foecke. 2005. *Federal Building and Fire Safety Investigation of the World Trade Center Disaster: Damage and Failure Modes of Structural Steel Components.* NIST NCSTAR 1-3C. National Institute of Standards and Technology. Gaithersburg, MD, September.

Luecke, W. E., J. D. McColskey, C. N. McCowan, S. W. Banovic, R. J. Fields, T. Foecke, T. A. Siewert, and F. W. Gayle. 2005. *Federal Building and Fire Safety Investigation of the World Trade Center Disaster: Mechanical Properties of Structural Steels.* NIST NCSTAR 1-3D. National Institute of Standards and Technology. Gaithersburg, MD, September.

Banovic, S. W., C. N. McCowan, and W. E. Luecke. 2005. *Federal Building and Fire Safety Investigation of the World Trade Center Disaster: Physical Properties of Structural Steels.* NIST NCSTAR 1-3E. National Institute of Standards and Technology. Gaithersburg, MD, September.

Evans, D. D., R. D. Peacock, E. D. Kuligowski, W. S. Dols, and W. L. Grosshandler. 2005. *Federal Building and Fire Safety Investigation of the World Trade Center Disaster: Active Fire Protection Systems.* NIST NCSTAR 1-4. National Institute of Standards and Technology. Gaithersburg, MD, September.

Kuligowski, E. D., D. D. Evans, and R. D. Peacock. 2005. *Federal Building and Fire Safety Investigation of the World Trade Center Disaster: Post-Construction Fires Prior to September 11, 2001.* NIST NCSTAR 1-4A. National Institute of Standards and Technology. Gaithersburg, MD, September.

Hopkins, M., J. Schoenrock, and E. Budnick. 2005. *Federal Building and Fire Safety Investigation of the World Trade Center Disaster: Fire Suppression Systems.* NIST NCSTAR 1-4B. National Institute of Standards and Technology. Gaithersburg, MD, September.

Keough, R. J., and R. A. Grill. 2005. *Federal Building and Fire Safety Investigation of the World Trade Center Disaster: Fire Alarm Systems.* NIST NCSTAR 1-4C. National Institute of Standards and Technology. Gaithersburg, MD, September.

Ferreira, M. J., and S. M. Strege. 2005. *Federal Building and Fire Safety Investigation of the World Trade Center Disaster: Smoke Management Systems.* NIST NCSTAR 1-4D. National Institute of Standards and Technology. Gaithersburg, MD, September.

Gann, R. G., A. Hamins, K. B. McGrattan, G. W. Mulholland, H. E. Nelson, T. J. Ohlemiller, W. M. Pitts, and K. R. Prasad. 2005. *Federal Building and Fire Safety Investigation of the World Trade Center Disaster: Reconstruction of the Fires in the World Trade Center Towers.* NIST NCSTAR 1-5. National Institute of Standards and Technology. Gaithersburg, MD, September.

Pitts, W. M., K. M. Butler, and V. Junker. 2005. *Federal Building and Fire Safety Investigation of the World Trade Center Disaster: Visual Evidence, Damage Estimates, and Timeline Analysis.* NIST NCSTAR 1-5A. National Institute of Standards and Technology. Gaithersburg, MD, September.

Hamins, A., A. Maranghides, K. B. McGrattan, E. Johnsson, T. J. Ohlemiller, M. Donnelly, J. Yang, G. Mulholland, K. R. Prasad, S. Kukuck, R. Anleitner and T. McAllister. 2005. *Federal Building and Fire Safety Investigation of the World Trade Center Disaster: Experiments and Modeling of Structural Steel Elements Exposed to Fire.* NIST NCSTAR 1-5B. National Institute of Standards and Technology. Gaithersburg, MD, September.

Ohlemiller, T. J., G. W. Mulholland, A. Maranghides, J. J. Filliben, and R. G. Gann. 2005. *Federal Building and Fire Safety Investigation of the World Trade Center Disaster: Fire Tests of Single Office Workstations.* NIST NCSTAR 1-5C. National Institute of Standards and Technology. Gaithersburg, MD, September.

Gann, R. G., M. A. Riley, J. M. Repp, A. S. Whittaker, A. M. Reinhorn, and P. A. Hough. 2005. *Federal Building and Fire Safety Investigation of the World Trade Center Disaster: Reaction of Ceiling Tile Systems to Shocks.* NIST NCSTAR 1-5D. National Institute of Standards and Technology. Gaithersburg, MD, September.

Hamins, A., A. Maranghides, K. B. McGrattan, T. J. Ohlemiller, and R. Anleitner. 2005. *Federal Building and Fire Safety Investigation of the World Trade Center Disaster: Experiments and Modeling of Multiple Workstations Burning in a Compartment.* NIST NCSTAR 1-5E. National Institute of Standards and Technology. Gaithersburg, MD, September.

McGrattan, K. B., C. Bouldin, and G. Forney. 2005. *Federal Building and Fire Safety Investigation of the World Trade Center Disaster: Computer Simulation of the Fires in the World Trade Center Towers.* NIST NCSTAR 1-5F. National Institute of Standards and Technology. Gaithersburg, MD, September.

Prasad, K. R., and H. R. Baum. 2005. *Federal Building and Fire Safety Investigation of the World Trade Center Disaster: Fire Structure Interface and Thermal Response of the World Trade Center Towers.* NIST NCSTAR 1-5G. National Institute of Standards and Technology. Gaithersburg, MD, September.

Gross, J. L., and T. McAllister. 2005. *Federal Building and Fire Safety Investigation of the World Trade Center Disaster: Structural Fire Response and Probable Collapse Sequence of the World Trade Center Towers.* NIST NCSTAR 1-6. National Institute of Standards and Technology. Gaithersburg, MD, September.

Carino, N. J., M. A. Starnes, J. L. Gross, J. C. Yang, S. Kukuck, K. R. Prasad, and R. W. Bukowski. 2005. *Federal Building and Fire Safety Investigation of the World Trade Center Disaster: Passive Fire Protection.* NIST NCSTAR 1-6A. National Institute of Standards and Technology. Gaithersburg, MD, September.

Gross, J., F. Hervey, M. Izydorek, J. Mammoser, and J. Treadway. 2005. *Federal Building and Fire Safety Investigation of the World Trade Center Disaster: Fire Resistance Tests of Floor Truss Systems.* NIST NCSTAR 1-6B. National Institute of Standards and Technology. Gaithersburg, MD, September.

Zarghamee, M. S., S. Bolourchi, D. W. Eggers, Ö. O. Erbay, F. W. Kan, Y. Kitane, A. A. Liepins, M. Mudlock, W. I. Naguib, R. P. Ojdrovic, A. T. Sarawit, P. R Barrett, J. L. Gross, and

T. P. McAllister. 2005. *Federal Building and Fire Safety Investigation of the World Trade Center Disaster: Component, Connection, and Subsystem Structural Analysis.* NIST NCSTAR 1-6C. National Institute of Standards and Technology. Gaithersburg, MD, September.

Zarghamee, M. S., Y. Kitane, Ö. O. Erbay, T. P. McAllister, and J. L. Gross. 2005. *Federal Building and Fire Safety Investigation of the World Trade Center Disaster: Global Structural Analysis of the Response of the World Trade Center Towers to Impact Damage and Fire.* NIST NCSTAR 1-6D. National Institute of Standards and Technology. Gaithersburg, MD, September.

McAllister, T., R. W. Bukowski, R. G. Gann, J. L. Gross, K. B. McGrattan, H. E. Nelson, L. Phan, W. M. Pitts, K. R. Prasad, F. Sadek. 2006. *Federal Building and Fire Safety Investigation of the World Trade Center Disaster: Structural Fire Response and Probable Collapse Sequence of World Trade Center 7.* (Provisional). NIST NCSTAR 1-6E. National Institute of Standards and Technology. Gaithersburg, MD.

Gilsanz, R., V. Arbitrio, C. Anders, D. Chlebus, K. Ezzeldin, W. Guo, P. Moloney, A. Montalva, J. Oh, K. Rubenacker. 2006. *Federal Building and Fire Safety Investigation of the World Trade Center Disaster: Structural Analysis of the Response of World Trade Center 7 to Debris Damage and Fire.* (Provisional). NIST NCSTAR 1-6F. National Institute of Standards and Technology. Gaithersburg, MD.

Kim, W. 2006. *Federal Building and Fire Safety Investigation of the World Trade Center Disaster: Analysis of September 11, 2001, Seismogram Data.* (Provisional). NIST NCSTAR 1-6G. National Institute of Standards and Technology. Gaithersburg, MD.

Nelson, K. 2006. *Federal Building and Fire Safety Investigation of the World Trade Center Disaster: The Con Ed Substation in World Trade Center 7.* (Provisional). NIST NCSTAR 1-6H. National Institute of Standards and Technology. Gaithersburg, MD.

Averill, J. D., D. S. Mileti, R. D. Peacock, E. D. Kuligowski, N. Groner, G. Proulx, P. A. Reneke, and H. E. Nelson. 2005. *Federal Building and Fire Safety Investigation of the World Trade Center Disaster: Occupant Behavior, Egress, and Emergency Communication.* NIST NCSTAR 1-7. National Institute of Standards and Technology. Gaithersburg, MD, September.

Fahy, R., and G. Proulx. 2005. *Federal Building and Fire Safety Investigation of the World Trade Center Disaster: Analysis of Published Accounts of the World Trade Center Evacuation.* NIST NCSTAR 1-7A. National Institute of Standards and Technology. Gaithersburg, MD, September.

Zmud, J. 2005. *Federal Building and Fire Safety Investigation of the World Trade Center Disaster: Technical Documentation for Survey Administration.* NIST NCSTAR 1-7B. National Institute of Standards and Technology. Gaithersburg, MD, September.

Lawson, J. R., and R. L. Vettori. 2005. *Federal Building and Fire Safety Investigation of the World Trade Center Disaster: The Emergency Response Operations.* NIST NCSTAR 1-8. National Institute of Standards and Technology. Gaithersburg, MD, September.

ACKNOWLEDGMENTS

Many people contributed valuable skills, facilities and information that made this report possible. We thank:

Professor George Krauss (University Emeritus Professor, Colorado School of Mines) and Dr. Elliot Brown (EB Consulting, Golden, CO) for technical discussions regarding the metallurgy of the steels in the World Trade Center.

Dr Hugh MacGillivray (Professor, Imperial College, London, UK) for technical discussions regarding high strain rate testing,

Professor David Matlock (Colorado School of Mines) for use of the high-rate tensile testing machine,

Tessa Dvorak and Brian Goudy (National Institute of Standards and Technology [NIST]) for data reduction,

Lonn Rodine (NIST) for specimen and drawing preparation,

Ray Santoyo (NIST) and Mark Iadicola (NIST) for conducting many of the room temperature tensile tests,

Donald Harne (NIST) for conducting some of the creep tests,

Richard Rhorer and Michael Kennedy (NIST) and Debasis Basek (University of Tennessee) for conducting the high-rate Kolsky bar tests,

Dr. T. Weerasooriya and Mr. P. Moy (Impact Physics and High Rate Laboratory, Weapons and Materials Directorate, Army Research Laboratory, Aberdeen, MD) for performing initial Kolsky bar tests and assisting in calibrating the NIST Kolsky bar facility,

Richard Ricker and David Dayan (NIST) for conducting the tests to determine the elastic modulus as a function of temperature,

Kazushige Tokuno (Nippon Steel USA) for supplying historical information on Yawata steel properties,

Former employees of Laclede Steel (St. Louis, MO) including David McGee and Larry Hutchison for locating Laclede records for NIST investigators during a visit to the Laclede Steel Mill.

This page intentionally left blank.

EXECUTIVE SUMMARY

National Institute of Standards and Technology (NIST) had several objectives in characterizing the recovered World Trade Center (WTC) steels. One was to characterize the mechanical properties of steels recovered from the impact and fire zone as a function of temperature to provide data for fire modeling, and deformation rate to provide data for impact modeling. The second was to determine whether the mechanical properties of the steels, bolts and welds were consistent with both the specifications that they were delivered to, and the expected properties of structural steels from the construction era.

The experimentally determined mechanical property data can be divided into five groups:

- Elastic properties as a function of temperature were determined from recovered perimeter column steels.
- Room temperature yield and tensile strength, and total elongation were determined from specimens of recovered steel of all grades from the fire and impact zones. Complete stress-strain curves are reported for 29 different steels with 12 yield strength levels. Load-displacement curves were measured from recovered A 325 bolts. Stress-strain curves and strengths of several different perimeter column and truss weld geometries are reported.
- Yield and tensile strengths and total elongations of selected perimeter and core column steels were determined as a function strain rate at rates up to 400 s^{-1}. Strain-rate sensitivities and complete stress-strain curves for these steels are reported. Several steels were characterized at higher rates using Kolsky bar tests.
- Impact properties as a function of temperature were determined using Charpy tests for selected perimeter column, core column, truss, and truss-seat steels.
- Elevated-temperature yield and tensile strength, and total elongation were determined on selected specimens of recovered perimeter and core column, truss, and truss seat steels. Complete stress-strain curves for temperatures up to 650 °C are reported for all steels characterized. Creep deformation as a function of temperature and stress was determined for the truss chord steel.

By combining these measured properties with historical averages from the literature, and in some cases recovered mill test reports, NIST developed values for properties of the important grades of steel including

- Elastic modulus and Poisson's ratio as a function of temperature,
- Model room-temperature stress-strain curves for all WTC steel grades from the fire and impact zones corrected for dynamic effects,
- Room-temperature load-displacement curves for A 325 bolts,

- Yield and tensile strength for weld metals,
- Strain rate sensitivity of steel for high strain rate properties,
- Elevated-temperature yield and tensile strength and complete stress-strain behavior for all WTC steel grades from the fire and impact zones,
- Elevated-temperature load-displacement curves for A 325 bolts,
- Creep response for all WTC steel grades from the fire and impact zones.

This report makes several findings concerning the steel used in the WTC:

- Steels, bolts, and welds generally have properties that are consistent with the specifications to which they were supplied.
- Infrequently, the measured yield strengths are lower than called for by the appropriate specifications. The measured yield strengths of 2 of 24 perimeter column samples are lower than the specified minimum. This probably occurred from a combination of the natural variability of steel properties, and small differences between the mill and NIST testing protocols. The measured yield strengths of 2 of 8 core column samples are lower than the specified minimum. In this case, mechanical damage that occurred in the collapse and subsequent recovery removed the expected yield point behavior and lead to the low values.
- The average measured yield strength of the steels from the perimeter columns exceeds the specified minimum values by about 10 percent, which is consistent with historically expected values for steel plates.
- The measured yield strengths of the $F_y = 36$ ksi wide-flange core columns are lower than expected from historical measurements of other structural steels.
- The strain rate sensitivities of the yield and tensile strengths of perimeter and core columns are similar to other structural steels from the WTC construction era.
- The impact properties of the steels, evaluated by Charpy testing, are similar to structural steels from the WTC era. The ductile-to-brittle transition temperatures of the perimeter and core column steels are at or below room temperature.
- The behavior of the yield and tensile strengths of WTC steels with temperature is similar to that of other structural steels from the WTC construction era.

Chapter 1
INTRODUCTION

1.1 OVERVIEW OF REPORT

National Institute of Standards and Technology (NIST) had three objectives in characterizing the mechanical properties of the structural steels, bolts and welds recovered from the World Trade Center (WTC) site. The first was to compare the measured properties of the steels with the requirements of the specifications that they were purchased under. The second was to determine whether their properties were consistent with the properties and quality of other structural steel from the WTC construction era. The third was to determine the constitutive behavior of the steels for input into finite element models of the response of the building components to the airplane impact and to the high temperatures produced by the subsequent fires. In support of these three goals, the Investigation characterized the elastic properties at elevated temperatures, the room-temperature tensile behavior, the high-strain-rate behavior, the impact behavior using Charpy tests, and the elevated-temperature tensile and creep behavior.

This report comprises five chapters that summarize the results of investigations into the mechanical properties of the WTC steels. Chapter 2 covers the temperature dependence of the elastic properties. Chapter 3 covers the room-temperature, quasi-static stress-strain behavior. Chapter 4 details investigations into the properties of the steel at high strain-rate, which are relevant for modeling the airplane impact. Chapter 5 summarizes the results of Charpy tests to characterize the impact properties of the steels. Chapter 6 addresses the elevated-temperature deformation behavior of the steel, which is relevant for modeling the response of the steel to the fires. Within each chapter, where appropriate, individual sections address the relation of the measured properties to the standards and specifications used in the WTC construction. Each chapter also compares the measured properties to literature data from the WTC construction era as a means to establish whether the properties of the steel were anomalous or ordinary. Finally, separate sections explain the methods by which experimental results, literature and construction data, and theoretical models were combined to produce constitutive laws for input to the finite element models.

1.1.1 Elastic Properties (Chapter 2)

After examining reported literature values of the change in elastic properties with temperature, the Investigation characterized specimens of perimeter column steels. The scatter in the literature data is large and probably results from differences in test technique. Analysis of the experimental data generated in the Investigation produced expressions for Young's modulus, shear modulus, and Poisson's ratio for temperatures up to 700 °C. For higher temperatures, the Investigation produced a methodology for estimating the modulus.

1.1.2 Room Temperature Tensile Properties (Chapter 3)

Metallurgically and mechanically, only the room-temperature stress-strain behavior detailed in Chapter 3 is relevant to the standards and specifications that the steel was to meet. In support of the first objective,

NIST characterized the room-temperature tensile stress-strain behavior of several hundred tensile specimens from the perimeter columns, core columns, trusses, and truss seats. The specimens represent samples of all major strength levels of steel from all the fabricators who supplied steel for the floors in the impact and fire zones of the towers. In addition, NIST characterized the load-displacement behavior of recovered bolts and the strength of selected welds and weld assemblies.

In comparing the properties of the recovered steels to their intended specifications, NIST used chemical analyses, room-temperature tensile tests, and archival information. A number of experimental difficulties complicated the positive identification of the exact specifications used for a given steel. Despite these limitations, the Investigation made several findings regarding the properties of the recovered steel in relation to the original specifications.

The yield and tensile strengths of the perimeter columns, with only a few exceptions, are consistent with the strength requirements of the original specifications. The number of slightly under-strength plates and the amount by which they fall short is consistent with expected values for the average strength and coefficient of variation of yield strengths of plate steels from the WTC construction era. The ratio of measured yield strength to specified yield strength is also consistent with literature estimates from the WTC construction era.

Unlike the perimeter columns, the NIST-measured yield strengths of several of the wide-flange core columns recovered from the core were less than specified. It is likely that these low values arose from damage that removed the yield point behavior, which could easily lead to NIST-measured strengths up to 3 ksi below the value in the mill test report. The average measured yield strengths and yield points for the wide-flange specimens whose yield points were larger than the specified minimum are still several ksi less than the expected value predicted from the literature of the WTC construction era, however.

Many of the components in the floor trusses were fabricated from high-strength, low-alloy (HSLA) steels, even when they were only required to meet the A 36 minimum requirements. The strengths of recovered bolts are consistent with the ASTM A 325 specification, but are much higher than expected based on reports from the contemporaneous literature. The limited number of tests on welds indicates that their strengths are consistent with the expected values from the welding procedures used.

To provide constitutive data for finite element models of the Investigation, the third objective for the room-temperature tensile testing program, NIST produced representative stress-strain curves for each of the many grades of steel in the towers. For the perimeter column and truss steels, the yield strengths were corrected for testing-rate effects and, where possible, experimental data were combined with surviving WTC mill test reports to produce better estimates of the characteristic strength. NIST-measured stress-strain curves from specimens taken from recovered components, modeled using the Voce work-hardening law, were used to describe the plastic deformation of each steel grade. For the core columns, either plates or wide-flange shapes, the yield strength was assumed to be the historical average from the literature of the WTC construction era, corrected for dynamic effects. NIST-measured stress-strain curves from specimens recovered from core columns, also modeled using Voce work hardening, supplied the plastic behavior. For the truss steels, based on chemistry and mechanical characterization, the angles were assumed to be a high-strength low-alloy steel regardless of specification. Experimental stress-strain data were used to estimate the yield and work-hardening behavior. For the A 325 bolts, NIST supplied load-displacement curves measured on recovered bolts. For the perimeter and core column welds, NIST

estimated mechanical properties by combining data from archival materials and tests on welds in recovered components.

1.1.3 High-Strain-Rate Properties (Chapter 4)

Because the strength of steel depends on the rate at which it is deformed, it is necessary to quantify this relation for the steels in the impact zone. Failing to properly account for the increased strength with deformation rate could lead to an incorrect estimates of the damage caused by the airplane impact. In support of this goal, the Investigation employed two types of high-strain-rate tests. For rates, $50\,s^{-1} < \dot{\varepsilon} < 500\,s^{-1}$, tests used a servohydraulic tensile test machine and special tensile specimens. For higher rates, tests employed a Kolsky bar test apparatus in which the test specimen is a right circular cylinder loaded in compression.

Like other structural steels, the strength of the WTC steels increase with increasing strain rate. The strain rate sensitivity of the WTC steels was evaluated for eight perimeter column plates, four wide-flange core columns, and one plate from a core box column. The measured strain rate sensitivities are of the same magnitude as other structural steels reported in the literature and decrease with increasing yield strength.

1.1.4 Impact Properties (Chapter 5)

Charpy impact tests are a type of dynamic fracture test that probes the ability of steels to absorb energy before fracturing. As such, they are particularly relevant to the airplane impact. In the Charpy test, the energy used to break a notched specimen is measured as a function of temperature.

None of the ASTM International (ASTM) specifications for steels used in the WTC, then or current, put limits on the impact properties, but the measured impact properties are similar to those of other structural steels of the WTC construction era. All the perimeter column steels have large upper shelf energies and transition temperatures well below 0 °F. The transition temperatures of the wide-flange specimen and the truss rods and angles are near room temperature. The transition temperatures of the truss-seat steels are above room temperature, and the absorbed energy of these steels is low even at room temperature, indicating a propensity for brittle failure.

1.1.5 Elevated-Temperature Properties (Chapter 6)

The high-temperature testing program had two thrusts. One was to characterize the elevated-temperature stress-strain behavior of the steels most likely to have been affected by the post-impact fires. The second was to characterize the creep, or time-dependent deformation, behavior of the steels from the floor trusses. In each of these two areas, in addition to the experimental characterization, NIST developed methodologies to predict the behavior of untested steels.

For the elevated-temperature stress-strain behavior, the methodology recognized that the yield and tensile strengths of structural steels, normalized to their room-temperature values, follow a master curve with temperature. A modified form of this master strength curve, developed using literature data on bolt steels, describes the more rapid strength degradation of the bolts with temperature.

To produce elevated-temperature stress-strain curves of WTC steel, NIST developed a methodology to account for the change in the work-hardening behavior using literature data for structural steels scaled by the ratio of room-temperature tensile strengths.

NIST also characterized the creep deformation behavior of the floor truss steels. To estimate the creep properties of untested steels, NIST developed a methodology that used either existing literature data or the Investigation-generated floor truss creep data after scaling by the ratios of room-temperature tensile strength.

1.2 DESCRIPTION OF THE MAJOR BUILDING COMPONENTS

This section summarizes the major structural elements of the WTC buildings in the impact and fire areas. (NIST NCSTAR 1-3A[1]) contains a more detailed description of the structure of the building.

The WTC towers had a frame-tube construction consisting of closely spaced perimeter columns with a rectangular core. The buildings had a square footprint, 207 ft 2 in. on a side with chamfered corners. From the 9th to the 107th floors, the perimeter columns were closely spaced, built-up box columns. The core of the building was approximately 87 ft by 137 ft and connected to the perimeter columns by a floor panel system that provided column-free office space.

1.2.1 Perimeter Columns

Each building face consisted of 59 columns spaced at 40 in. The columns were fabricated by welding four plates to form an approximately 14 in. square section, Fig. 1–1. The perimeter columns were joined by horizontal spandrel plates to form panels, which were typically three stories (36 ft) tall and three columns wide, Fig. 1–2. Heavy end, or "butt" plates 1.375 in. to 3 in. thick were welded to the top and bottom of each column. The columns were also bolted to the adjacent columns using ASTM A 325 bolts except for the heaviest butt plates, which used ASTM A 490 bolts. Other than at the mechanical floors, the panels were staggered vertically so that only one third of them were spliced in any one story. Adjacent spandrels were bolted together using splice plates.

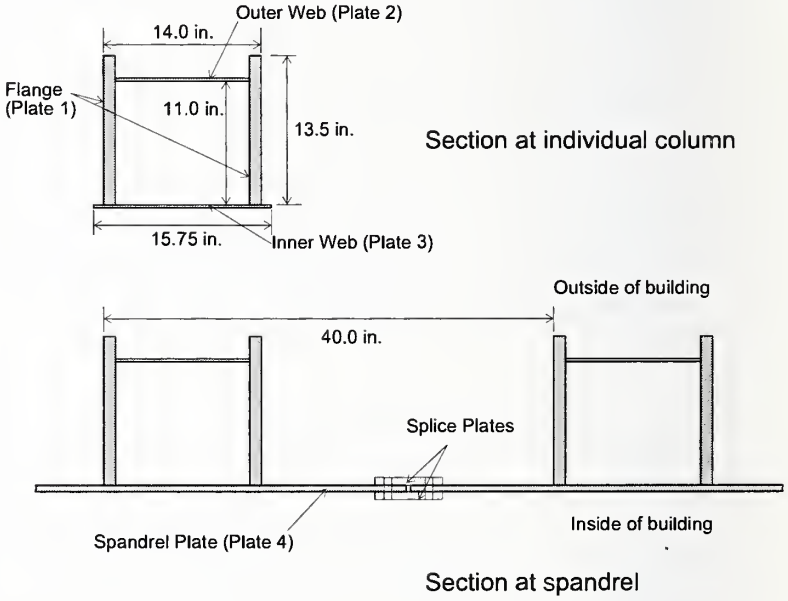

Figure 1–1. Cross section of a perimeter column; sections with and without spandrels.

[1] This reference is to one of the companion documents from this Investigation. A list of these documents appears in the Preface to this report.

The structural steel documents specified 14 grades of steel for the plates of the perimeter columns, with minimum yield strengths of (36, 42, 45, 46, 50, 55, 60, 65, 70, 75, 80, 85, 90, and 100) ksi.

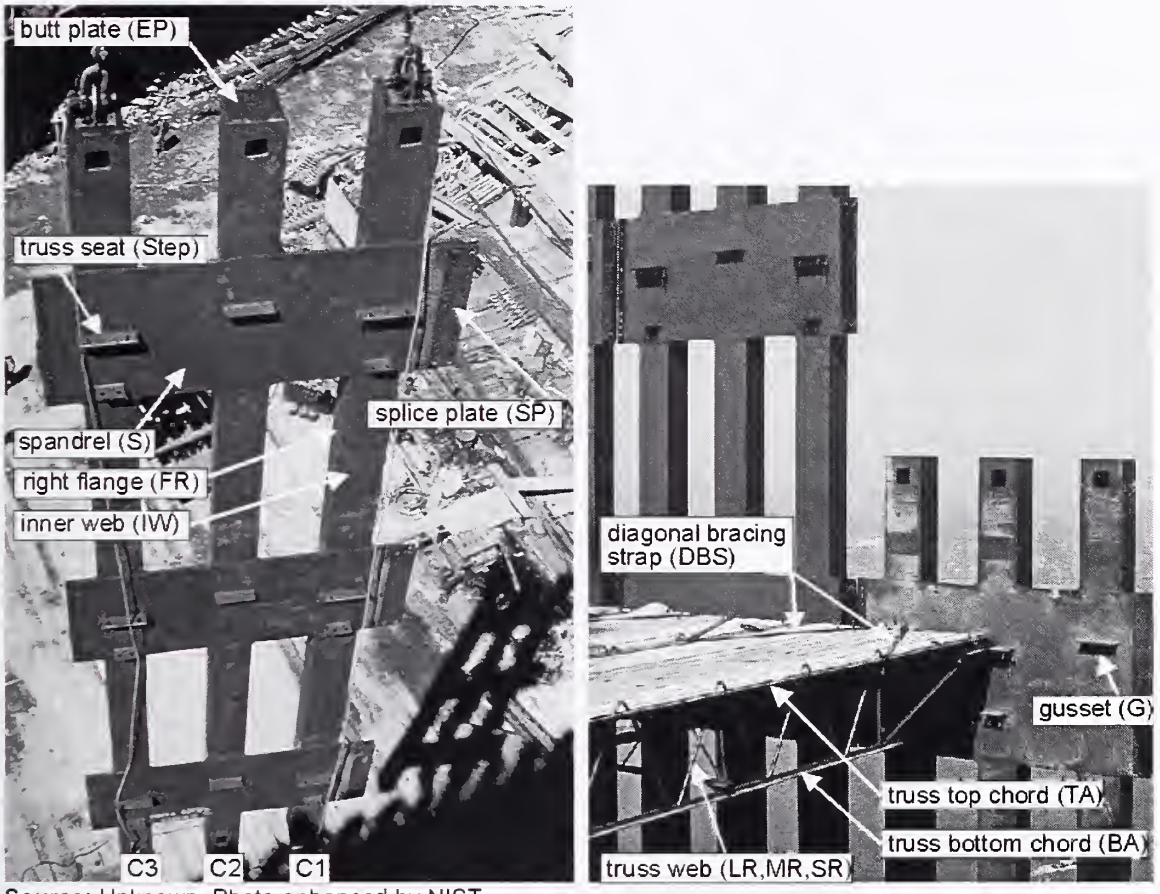

Source: Unknown. Photo enhanced by NIST.

Figure 1–2. Characteristic perimeter column panel illustrating the various components. Designations in parentheses refer to the specimen nomenclature of Table 1–1.

The side plates of a column are termed the flanges, Fig. 1–1, and the inner and outer plates are termed the webs. In an individual column, the flanges were always at least as thick as the webs. Although the yield strengths of the webs and flanges of an individual column were identical, the yield strengths of the columns within a three-story, three-column panel could differ.

As the elevation in the building increased, the thickness of the plates in the columns decreased, but the plates were always at least 0.25 in. thick. About one half of the recovered perimeter columns in the NIST inventory are type 120, in which the flange and web plates are both 0.25 in. thick. In the WTC 1 fire and impact zone, floors 92–100, columns of this type make up about 2/3 of the total columns

Twelve grades of steel were specified for the spandrels, with the same strength levels as the columns but with a maximum F_y = 85 ksi. In a panel, the yield strength of the spandrel plate was generally lower than that of the webs and flanges, and its thickness was greater than the adjacent inner web plate. Where the spandrels crossed the columns there was no inner web plate.

1.2.2 Core Columns

Core columns were of two types: welded box columns and rolled wide flange (WF) shapes. Fig. 1–3 shows some examples of the shapes of core columns. In the lower floors, the core columns were primarily very large box columns, as large as 12 in.×52 in. with plates up to 7 in. thick. In the upper floors, the columns were primarily rolled wide-flange shapes. Like the perimeter columns, the core columns were typically spliced at three-story intervals. Core box columns were specified with F_y = 36 ksi or F_y = 42 ksi. Core wide-flange columns were specified to be one of four grades, but were primarily F_y = 36 ksi and F_y = 42 ksi steel.

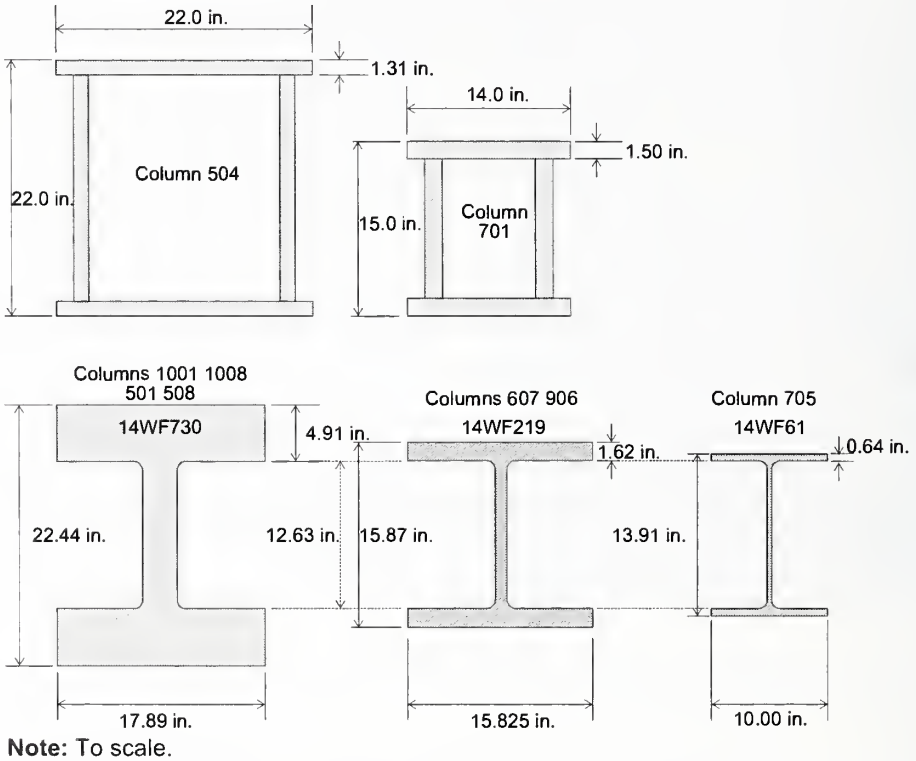

Note: To scale.

Figure 1–3. Typical welded box columns and rolled wide-flange shapes used for core columns between the 83rd and 86th floors.

1.2.3 Flooring System

Other than in a few special mechanical floors, the floor outside the core was supported by a two-dimensional network of 29 in. deep floor trusses. Figure 1–4 illustrates the major components of an individual floor truss. The most common floor trusses were nominally 60 ft or 36 ft long. Although there were dozens of variants, the top chord was usually fabricated from two sections of 2 in.×1.5 in.×0.25 in. thick angle specified to conform to ASTM A 242 with F_y = 50 ksi. In the 60 ft trusses, the lower chord was usually fabricated from two slightly larger angles, 3 in.×2 in.×0.37 in. thick specified to conform to A 36. The 36 ft trusses generally used a 2 in.×1.5 in.×0.25 in. thick angle for the lower chord as well. The truss web was a continuous round bar, which was usually D = 1.09 in. for the 60 ft trusses and D = 0.92 in. or D = 0.98 in. for the 36 ft trusses.

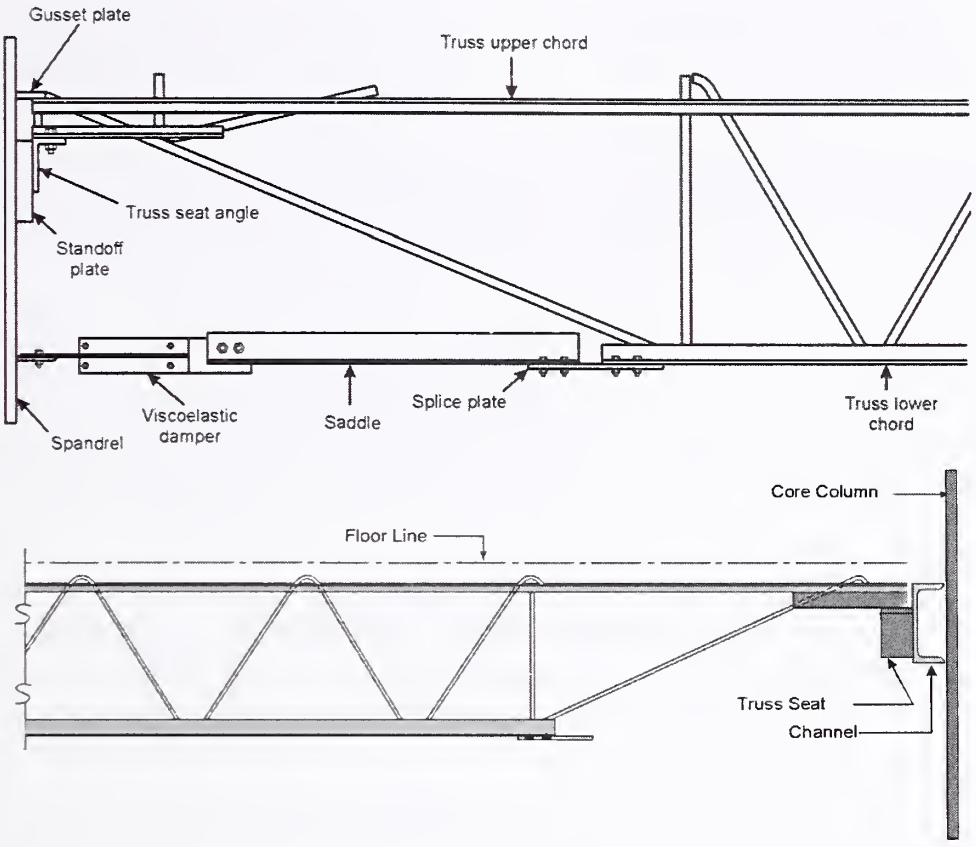

Figure 1–4. Schematic diagram of a floor truss.

Before erection, the individual trusses were assembled into modules typically 20 ft wide. Each module contained two sets of doubled trusses in the interior and a single truss along each edge. Smaller bridging trusses ran perpendicular to the main trusses at 13 ft 4 in. spacing. The bridging trusses were usually fabricated from 1.5 in. × 1.25 in. × 0.23 in. angles and $D = 0.75$ in. round webs.

At the core, the floor trusses were bolted to seats on channels that ran continuously along the core columns. At the perimeter columns, the floor trusses were bolted and welded to seats mounted on the spandrels at every other column, Fig. 1–2. Diagonal bracing straps welded to gusset plates secured the installed floor truss modules to the perimeter columns, Fig. 1–2.

1.3 SPECIMEN NOMENCLATURE

The specimen nomenclature of the Investigation captures the vital information about the location of the individual specimens within the larger component. Because the recovered sections arrived at NIST unidentified, and it often required weeks or months to establish the original location in the building, the nomenclature does not capture details about the original location. The NIST report "Steel Inventory and Identification within Buildings" (NIST NCSTAR 1-3B) contains tables that map the specimen designation to its location in the building and specified dimensions and strength. Furthermore, because of the significant damage, it was not possible to identify all the recovered sections.

Table 1–1 describes the naming convention for the perimeter column samples with an example. Figure 1–2 illustrates the naming convention for the perimeter column and truss components graphically. The example specimen name, N8-C1T2-IW-L2, describes the second specimen in a series of longitudinal tension specimens from the inner web of a perimeter column panel from WTC 1 column line 143 near top of the panel at floor 100. This panel is from the north face of the tower, just above and to the east of the impact zone. In this nomenclature, the column numbering within a given panel is reversed from the scheme used in the structural engineering drawings.

Table 1–2 describes the naming convention for all other specimens using an example from a core column. The example specimen name, C65-F1, describes the first sample taken from the flange of the core wide-flange column from WTC 1 on column line 904 somewhere between floors 86-89. This column is below and on the opposite side of the building from the impact zone. The sample that the example describes supplied the tension specimens used for characterizing the tensile behavior of the core columns.

1.4 SYMBOLS AND ABBREVIATIONS

The preface to this report contains tables of acronyms and units used in this report. Table 1–3 defines several symbols and terms relating to mechanical testing.

Table 1–1. Specimen nomenclature for perimeter column specimens.

Example N8-C1T2-IW-L2

Sub Element	Possible Values	Description
N8		Recovered item tag (letter denotes the recycling yard where specimen originated)[a]
C1		Describes column # in panel[b]
	C1	Column 1: column on the left, looking into the building
	C2	Column 2: center column
	C3	Column 3: column on the right looking into the building
T		Describes specimen location in column
	T	Near top
	M	Near middle
	B	Near bottom
2		1, 2, 3 etc., chronological by specimen cut from this larger section
IW		Describes plate location within column or other component within assembly
	IW	Inner web[c]
	LF	Left flange (looking into building); sometimes abbreviated as FL
	RF	Right flange (looking into building); sometimes abbreviated as FR
	OW	Outer web
	S	Can refer to either spandrels or truss seats
	SP	Can refer to either spandrels or splice plates
	Step	Truss seat
	EP	End or butt plate of column
	DBS	Diagonal bracing strap that ties floor truss to column
	G	Gusset plate that attaches diagonal bracing strap to perimeter column panel
	Tab	Plate welded to perimeter column panel and truss
L		Describes orientation with respect to rolling direction[d]
	L	Longitudinal
	T	Transverse
2	1, 2, 3…	Specimen number within series of orientations

a. The structural engineering drawings identify the perimeter column panels by the column number of the center column and the floors at the splices. For example, WTC 1 142 97-100 is tower 1, column line 142 floors 97–100. In the Investigation notation, this is recovered panel N8. The structural engineering drawings number the columns looking from outside the building.

b. C1 corresponds to column line 143; C2 corresponds to column line 142; C3 corresponds to column line 141 in the example above.

c. The structural engineering plans also number the four plates in each perimeter column: RF and LF correspond to plate 1, OW corresponds to plate 2, IW corresponds to plate 3, and S or SP corresponds to plate 4.

d. For spandrel plates, the orientation designation refers to the orientation with respect to the vertical axis of the building. Metallographic analysis later revealed that the rolling direction of the spandrel plates is along their long direction. Therefore all spandrel specimens designated with an "L" are oriented transverse to the rolling direction.

Table 1–2. Specimen nomenclature for core box and wide-flange shapes, trusses, and all other specimens.

Example C65-F1

Sub Element	Possible Values	Description
C65		Recovered item tag (denotes the recycling yard where the specimen was recovered)
F		Describes location within recovered item
	F	Flange (for WF shapes or wider plate for box columns)
	FL	Flange (for WF shapes or wider plate for box columns)
	W	Web (for WF shapes or narrower plate for box columns)
	WEB	Web (for WF shapes or narrower plate for box columns)
	BA	Bottom chord bulb angle (for trusses)
	TA	Top chord bulb angle (for trusses)
	TR	Round bar (for truss webs)
	LR	Large diameter round bar (for truss webs)
	MR	Medium diameter round bar (for truss webs)
	SR	Small diameter round bar (for truss webs)
	TS	Core truss seat
	Weld	Taken from a weld in the component
–		Describes orientation with respect to rolling direction (used for tensile specimens)
	L	Longitudinal
	T	Transverse
1	1, 2, 3…	Specimen number within series of orientations

Table 1–3. Mechanical testing definitions used in this report.

F_y	Yield strength Generally used as the specified minimum yield strength or yield point depending on the steel standard in use. (AISC usage)
ROA	reduction of area (ASTM usage Standard E 6)
TS	Tensile Strength The maximum engineering stress in a tensile test (ASTM E 6 usage) Often referred to in other literature as ultimate tensile strength, *UTS*, or by the symbol S_u.
YP	Yield point The first maximum in the engineering stress-engineering strain curve, associated with discontinuous yielding. Also called upper yield strength (ASTM E 6 usage). This report uses the symbol *YP* to denote a measured value of the yield point as opposed to its specified minimum value.
YS	Yield strength The engineering stress at which it is considered that plastic elongation has commenced. This document uses the 0.2 % offset stress. (ASTM E 6 usage) This report uses the symbol *YS* to denote a measured value of the yield strength as opposed to its specified minimum value.
El_t	Total Elongation The elongation (of a tensile specimen) determined after fracture by realigning and fitting together of the broken ends of the specimen. (ASTM E 6 usage)

Chapter 2
ELASTIC PROPERTIES

2.1 INTRODUCTION

This section reports the expressions for the temperature dependence of the elastic properties of steel supplied to other NIST Investigation Team members. Expressions include Young's modulus E, Poisson's ratio ν, and shear modulus G. World Trade Center (WTC) structural steels can be assumed to be elastically isotropic, so the shear modulus is related to E and ν:

$$G = \frac{E}{2(1+\nu)} \qquad 2\text{–}1$$

Because structural steels contain relatively low fractions of alloying elements, there is no significant difference in modulus between structural steel variants.

From room temperature up to about 720 °C the primary metal phase in iron-carbon alloys such as structural steel is ferrite, usually denoted as α-phase. Above this temperature steel undergoes a phase transformation to a mixture of α-phase and γ-gamma phase, or austenite. At still higher temperatures, 910 °C in pure iron, but lower in most structural steels, the phase transformation to all austenite is complete. In the two-phase region, the fraction of α-phase and γ-gamma phase, and therefore modulus, depends strongly on carbon content and temperature. This phase change introduces some difficulty in representing the change in modulus with temperature.

2.2 EXPERIMENTAL PROCEDURE

Three specimens of WTC steels, summarized in Table 2–1, were characterized in a thermomechanical analyzer (Model DMA 2980, TA Instruments) over the temperature range –140 °C < T<600 °C. Rectangular specimens nominally 50 mm×10 mm×1 mm were loaded in three-point bending. The thermomechanical analyzer oscillated the specimens at 1.0 hz at a constant amplitude of 15 μm. Measurements were conducted in two stages. The first was at temperatures, –140 °C < T < 50 °C. The second was in the range 50 °C < T < 600 °C. In both cases, modulus determinations were made at 5 °C intervals while the furnace temperature increased at 5 °C/min. During the high-temperature characterization the specimen chamber was filled with an inert gas to suppress oxidation.

2.3 ELASTIC PROPERTIES (E, ν, G) FOR 0°C < T < 723 °C

The literature is rich with determinations of the change of Young's modulus, E, with temperature for T<723 °C. Figure 2–1 shows some examples. The wide variation in the values is an artifact of the different measurement techniques. The data sets with the highest values were obtained using ultrasonic techniques. These data represent adiabatic determinations, and are not appropriate for estimating elevated-temperature modulus in structures. The data sets with the lowest values were probably determined from

the loading portion of high-temperature tensile tests, and therefore include inelastic specimen deformation. These determinations are also inappropriate.

Figure 2–1 also plots Young's modulus, E, determined for the three specimens of perimeter columns, summarized in Tab. 2–1, determined using the thermomechanical analyzer.

A third-order polynomial was sufficient to represent the data for 0 °C < T<600 °C for the three steels summarized in Table 2–1 and plotted in Fig. 2–2.

$$E(T) = e_0 + e_1 T + e_2 T^2 + e_3 T^3$$

where

e_0= 206.0 GPa
e_1= –0.04326 GPa/°C
e_2= -3.502×10^{-5} GPa/(°C)^2
e_3= -6.592×10^{-8} GPa/(°C)^3

2–2

The constant term, e_0, was fixed as the average of the three steels at 0 °C and was not part of the polynomial fit. The room-temperature value for E for the fit lies within the range of the highly regarded data that Galambos (1978) recommends.

Figure 2–3 summarizes the relatively scarce literature data for Poisson's ratio, ν, as a function of temperature. The data for iron (Dever 1972) and mild steel (Clark 1953 cited in Cooke 1988) do not differ significantly. The solid line is the fit of a fourth-order polynomial to all the data for 0 °C < T < 725 °C:

$$\nu(T) = n_0 + n_1 T + n_2 T^2 + n_3 T^3 + n_4 T^4$$

where

n_0= 0.28737362
n_1= 2.5302417×10^{-5} (°C)$^{-1}$
n_2= 2.6333384×10^{-8} (°C)$^{-2}$
n_3= -9.9419588×10^{-11} (°C)$^{-3}$
n_4= 1.2617779×10^{-13} (°C)$^{-4}$

2–3

for T in the range 0 °C < T < 725 °C. The room-temperature value, (ν = 0.288), is 4 percent smaller than the commonly used value ν = 0.3, which has been rounded to one significant digit.

The shear modulus, G, was determined from E and ν, using Eq. 2–1. To generate the curve shown in Fig. 2–2, values for the shear modulus as a function of temperature, G (T), were calculated at discrete points from Eq. 2–1 using the expressions for E (T) and ν (T), Eqs. 2–2 and 2–3. The resulting data were fit using a fifth-order polynomial.

$$G(T) = g_0 + g_1 T + g_2 T^2 + g_3 T^3 + g_4 T^4 + g_5 T^5$$

where

g_0= 80.005922 GPa
g_1= –0.018303811 GPa/°C
g_2= -1.5650288×10^{-5} GPa/(°C)^2
g_3= -1.5160921×10^{-8} GPa/(°C)^3
g_4= -1.6242911×10^{-11} GPa/(°C)^4
g_5= 7.7277543×10^{-15} GPa/(°C)^5

2–4

for T in the range $0 < T < 725$ °C. The room-temperature value of the shear modulus, G, calculated this way differs by 3.5 percent from the actual measurements cited in Galambos (1978) and the Metals Handbook (ASM 1978), but it is consistent with the values for E and ν from Equations 2–2 and 2–3.

In using the expressions for modulus at elevated temperature, it is important to recognize that the flow stress of structural steel above the α-γ phase transformation may be only 10 percent or less of the room-temperature value. Calculations that use the high-temperature value of the modulus and do not account for the very reduced strength may be inaccurate.

2.4 ELASTIC PROPERTIES (E, ν, G) FOR $T > 910$ °C

The literature data for elastic modulus of γ-Fe, the high-temperature phase, is sparse. Köster (1948) provided data for a function for calculating the modulus, $E_\gamma(T)$, of austenite (γ-phase) in the range 910 °C < T < 1000 °C, which is also plotted in Fig. 2–1.

$$E_\gamma(T) = \gamma_1\left(1-(T-\gamma_2)\gamma_3\right) \qquad 2\text{–}5$$

$\gamma_1 =$ 216.0 GPa
$\gamma_2 =$ 26.85 °C
$\gamma_3 =$ 4.7×10^{-4} °C^{-1}

Data for the Poisson's ratio for austenite are not available. The shear modulus, G, can be calculated from Eq. 2–1 after a suitable estimate of Poisson's ratio is made.

2.5 ELASTIC PROPERTIES (E, ν, G) FOR 723 °C < T < 910 °C

In principle, it is possible to do a rule-of-mixtures calculation to evaluate the modulus as a function of temperature in the two-phase field. Many assumptions are necessary to make the problem tractable, and even then, each steel, because of its composition, would have a different value for the composite modulus. Some of these assumptions include

- The extrapolation of Eq. 2–5 correctly describes the modulus of austenite in the two-phase field.
- The extrapolation of Eq. 2–2 correctly describes the modulus of ferrite in the two-phase field.
- All alloying elements other than carbon have no effect on the positions of the phase boundaries.
- The phase change is infinitely fast so that the time-dependence can be ignored. This may be a good approximation on heating, but it is much less appropriate for cooling.

The uncertainties that these assumptions introduce probably exceed the added fidelity that a rule-of-mixtures calculation might provide. Instead of the complicated rule-of-mixtures calculation, a much simpler method for approximating the elastic modulus in the two-phase region, $E_{\alpha\text{-}\gamma}$ is to interpolate between the two endpoints:

$$E_{\alpha-\gamma}(T) = E_{\alpha}(A_1) + \frac{E_{\gamma}(A_3) - E_{\alpha}(A_1)}{A_3 - A_1}(T - A_1) \qquad 2\text{–}6$$

where A_1 = 723 °C and A_3 = 910 °C.

2.6 UNCERTAINTIES

The expression for Young's modulus, Eq. 2–2, represents the experimental data obtained at NIST (Table 2–1) to within 2 percent for all cases, Fig. 2–4

2.7 REFERENCES

AISC. 1973. *Manual of Steel Construction.* American Institute of Steel Construction. New York p. 6-11.

ASME. 2004. Boiler and Pressure Vessel Code. Section II Materials, Part D Properties (Customary), Subpart 2 Physical Properties Tables, Table TM-1. ASME International. New York. p. 696

Clark, C.L. 1953. *High-temperature Alloys*. Pitman, New York.

Cooke, G.M.E. 1988. An Introduction to the Mechanical Properties of Structural Steel at Elevated Temperatures. *Fire Safety Journal*. 13 45-54.

Dever, D.J. 1972. Temperature Dependence of the Elastic Constants in a-Iron Single Crystals: Relationship to Spin Order and Diffusion Anomalies. *J. Appl. Phys.* 43 (8). 3293-3301.

Fields, R.J. T. Weerasooriya, and M. F. Ashby. 1980. Fracture-Mechanisms in Pure Iron, Two Austenitic Stainless Steels, and One Ferritic Steel. *Met. Trans. A.* 11A 333-347.

Galambos T.V. and M. K. Ravindra. 1978. Properties of Steel for Use in LRFD, *J. Struct. Div. ASCE.* 104 (9). 1459-1468.

Köster, W. 1948. Die Temperaturabhängigkeit des Elastizitätsmoduls reiner Metalle, *Z. Metallkd.* **39**(1). 1-9.

Uddin T. and C. G. Culver. 1975. Effects of Elevated Temperature on Structural Members. *J. Struct. Div. ASCE*. 101 (7). 1531-1549.

Table 2–1. Specimen data for Young's modulus (*E*) determination.

Specimen	Tower Column Line and Floor Range	Specified Yield Point F_y (ksi)	Location in Column
N9-C2B-FR-1	WTC 1 Column 154 Floors 101–104	55	Right flange
C68-C3T1-EP-2	Unknown butt plate from perimeter column	50	Unknown
S9-C3T-FL-1	WTC 1 Column 133 Floors 97–100	55	Left flange

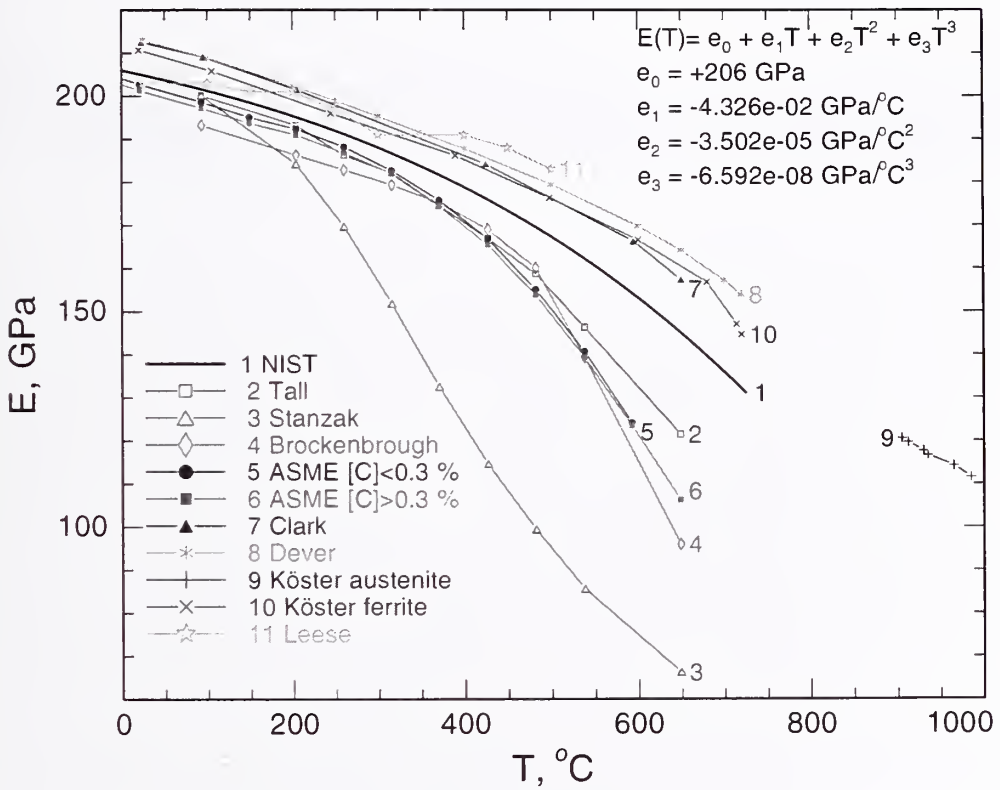

Sources: Clark 1953; Cooke 1988; Köster 1948; Dever 1972; Uddin 1975; ASME 2004.

Figure 2–1. Young's modulus as a function of temperature.

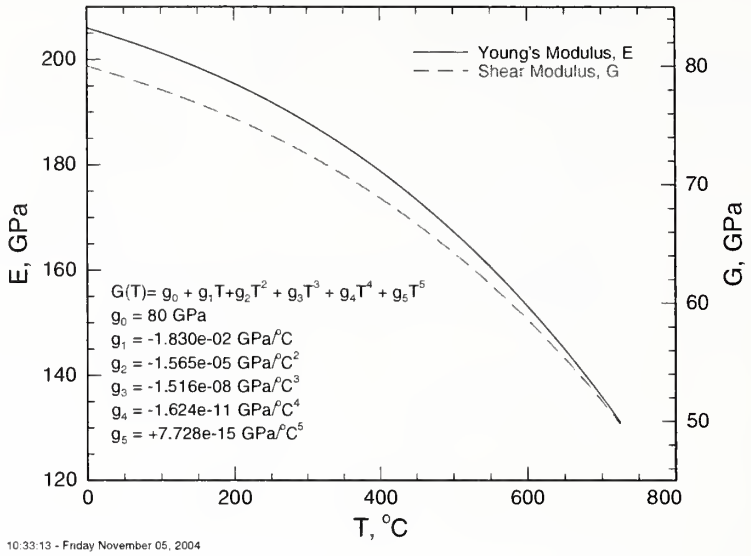

Figure 2–2. Young's modulus, *E*(*T*), and shear modulus, *G(T)* for 0°C < *T*< 725°C. Young's modulus was measured on the WTC steels summarized in Table 2–1. Solid line is Eq. 2–2. Shear modulus, *G*, calculated from *E* and ν via Eq. 2–4.

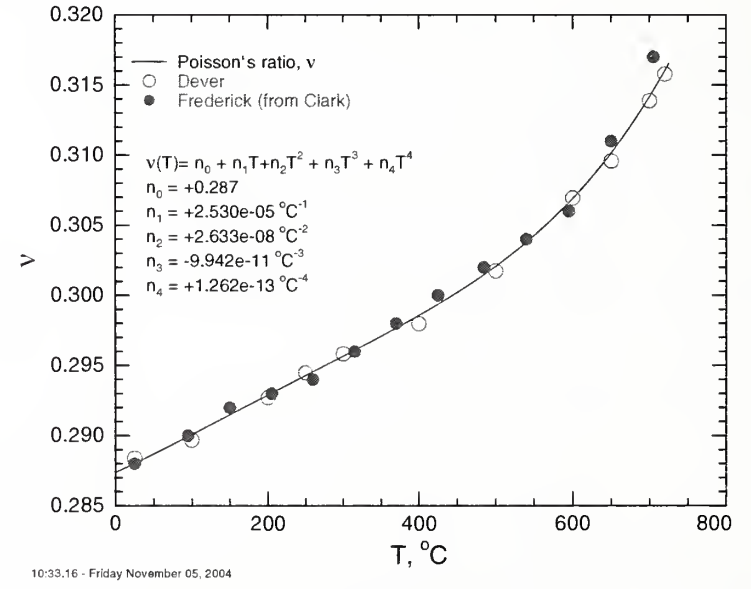

Source: Dever 1972; Clark 1953; Cooke 1988.

Figure 2–3. Poisson's ratio (ν) as a function of temperature. The solid line is the fit of a 4th order polynomial (Eq. 2–3) for 0 °C < *T* < 725 °C.

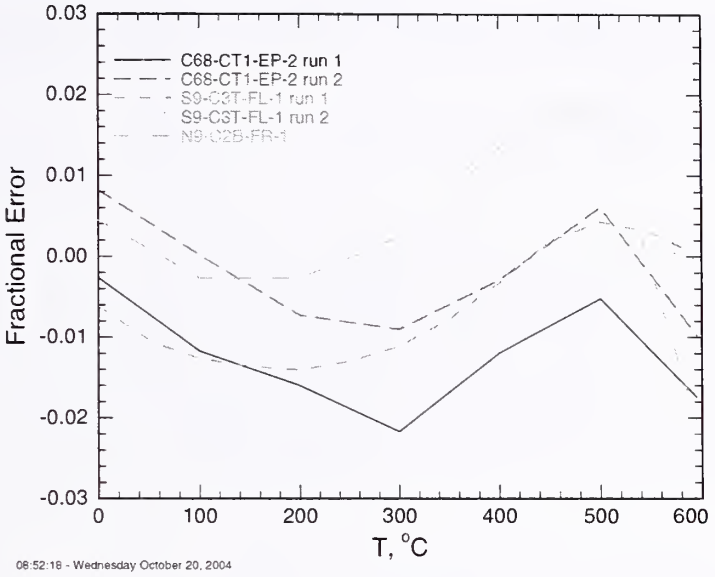

Figure 2–4. Fractional error in representing the Young's modulus data for the three specimens of perimeter column steel (Table 2–1) using Eq. 2–2.

This page intentionally left blank.

Chapter 3
ROOM-TEMPERATURE TENSILE PROPERTIES

3.1 INTRODUCTION

The National Institute of Standards and Technology (NIST) had three goals in characterizing the tensile properties of the steels, bolts and welds. The first was to compare the measured properties of the steels with the specifications they were purchased under. The second was to determine whether their properties were consistent with the properties and quality of other structural steel from the World Trade Center (WTC) construction era. The third was to determine the constitutive behavior for input into the finite element models of the Investigation, which modeled the response of the building components to the airplane impact and to the high temperatures produced by the subsequent fires.

To satisfy the first and objectives, NIST tested several hundred specimens taken from columns, trusses, and truss seats that represent all the major strength levels and most of the grades of steel in the fire and impact zones of the two towers.

To satisfy the third objective, NIST produced values yield strengths and representative stress-strain curves for each of the many grades of steel in the towers and supplied these to other Investigation Team members. The representative tensile stress-strain curves were corrected for dynamic effects. The curves drew on experimental data as well as surviving WTC mill test reports and literature data. The Voce work-hardening law (Voce 1948) described behavior of the representative curves. The parameters for the Voce law originated from the tensile behavior of recovered WTC steels.

3.2 TEST PROCEDURES

3.2.1 Steel

Standard tensile tests were generally conducted according to ASTM International (ASTM) E 8-01, "Standard Test Methods for Tension Testing of Metallic Materials" using a closed-loop, servo-hydraulic or a screw-driven, electro-mechanical test machine. In most cases, yield strength determination was made at a running crosshead rate that produced post-yield strain rates between 0.001 min^{-1} and 0.005 min^{-1}. In some tests the extension rate was increased to produce a plastic strain rate of 0.05 min^{-1} for tensile strength determination. In other cases, the entire test was conducted at a constant extension rate. Several tests were conducted at a slightly higher extension rate 0.0325 mm/s, which produced plastic strain rates that conform to ASTM A 370-67, the test method used by steel mills to qualify steel.

Much of the recovered steel was damaged in the collapse of the towers or subsequent handling during clearing of the WTC site. Specimens were selected from the least deformed regions. Even so, some of the resulting stress-strain curves of the low-strength steels do not exhibit a yield point. In such cases, yield strength was determined by the 0.2 percent offset method as specified in ASTM E 8-01.

The geometrical and thickness differences in the various components did not allow for a single, standard specimen geometry for the tensile testing. Whenever possible, specimens were made using the full

thickness of the material, according to ASTM E 8. For plates less than 0.75 in. thick, the specimens were a mixture of the standard flat and round geometries. For plates greater than 0.75 in. thick, the specimens were generally the ASTM standard 0.500 in. diameter round geometry. Truss rods were machined into round tensile specimens while truss angles were machined into subsize flat tensile specimens. Truss seats and core columns were machined into rounds. Figures 3–1 to 3–11 show the various tensile specimen configurations.

Specimen strain was measured using class B2 extensometers that conformed to ASTM E 83, "Standard Practice for Verification and Classification of Extensometer System." In most cases, the operator removed the extensometer prior to specimen failure. Total elongation was calculated by measuring gauge marks on the specimen prior to testing and again following fracture. Reductions of area for the round specimens were measured by comparing the original cross-sectional area to the area of the minimum cross section at the fracture location. Reductions of area for the rectangular and square cross section specimens were calculated based on the parabolic shape of the fracture surface, according to note 42 of ASTM E 8-01.

The notch sensitivity of two types of core column steels was evaluated using notched round tensile specimens, Fig. 3–11, taken from the quarter depth of plates. All three specimens have identical minor diameters of 0.25 in., but each has a different notch radius. Specimens were instrumented using an axial extensometer mounted on the major diameter and a diametral extensometer mounted on the notch root. Specimens were loaded at 0.00033 in./s, which produced an initial, elastic stressing rate of approximately 0.6 ksi/s.

3.2.2 Bolts

Tensile tests for determining the room-temperature load-displacement relation on the A 325 bolts generally followed ASTM Recommended Practice F 606, "Test Methods for Determining the Mechanical Properties of Externally and Internally Threaded Fasteners, Washers, and Rivets." Although many columns were recovered, very few contained undamaged fasteners suitable for mechanical testing. In all, only one A 490 and seven A 325 bolts were suitable for testing. Of all the perimeter columns recovered, only one, the unidentified C-68, had any associated A 325 bolts from the endplates. These seven bolts were the only A 325 bolts characterized. The single A 490 bolt tested came from a "bow-tie" section from floor 7. A commercial metallurgical testing firm tested three A 325 bolts and the A 490 bolt. To provide load-displacement data and assess the magnitude of strain rate effects, NIST tested four A 325 bolts: two bolts at each of two displacement rates. The rates chosen were very slow (0.0007 in/s crosshead displacement) and as fast as the machine would go (2.0 in/s). For these tests, two threads were exposed rather than the four required by ASTM F 606. Forensic observations of recovered perimeter column sections showed that failed bolts had from zero to four threads exposed. In addition, to obtain unambiguous load-displacement data, the NIST tests did not employ the wedge required by A 325.

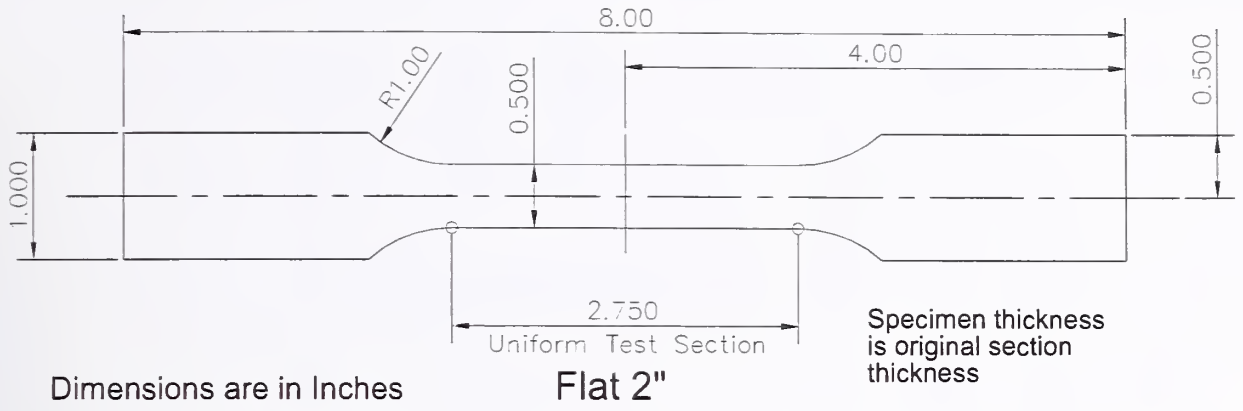

Figure 3–1. Flat tensile specimen typically used for standard room-temperature quasi-static tensile tests.

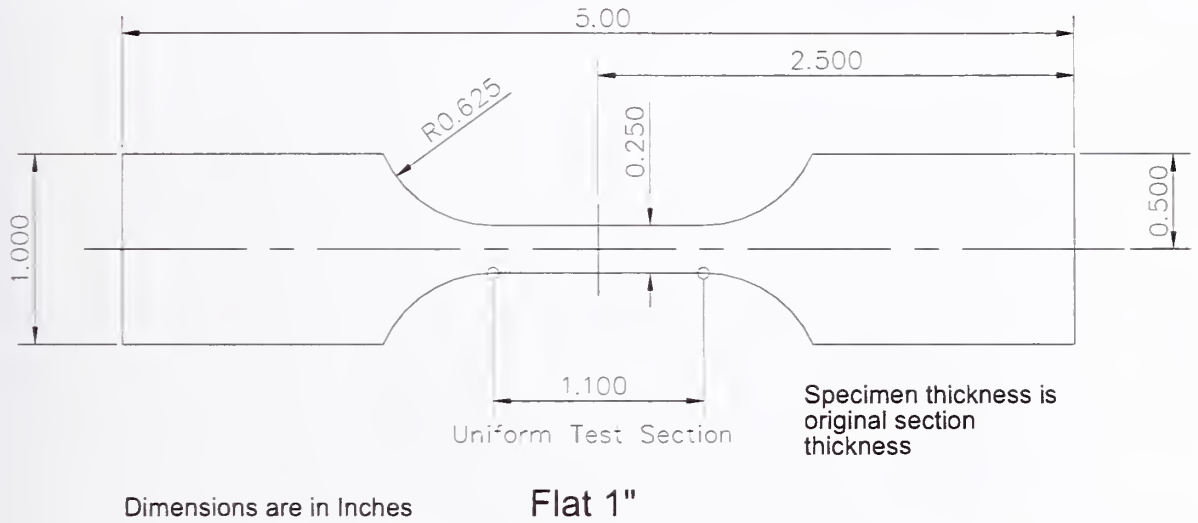

Figure 3–2. Flat tensile specimen typically used for elevated-temperature tensile tests.

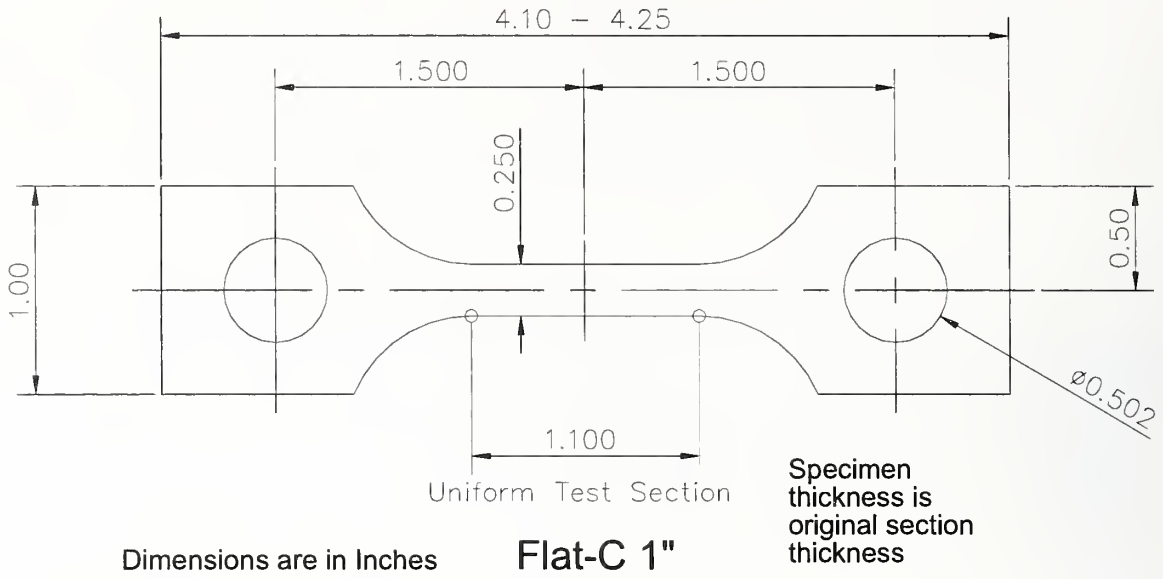

Figure 3–3. Flat tensile specimen used for room and elevated-temperature tensile tests.

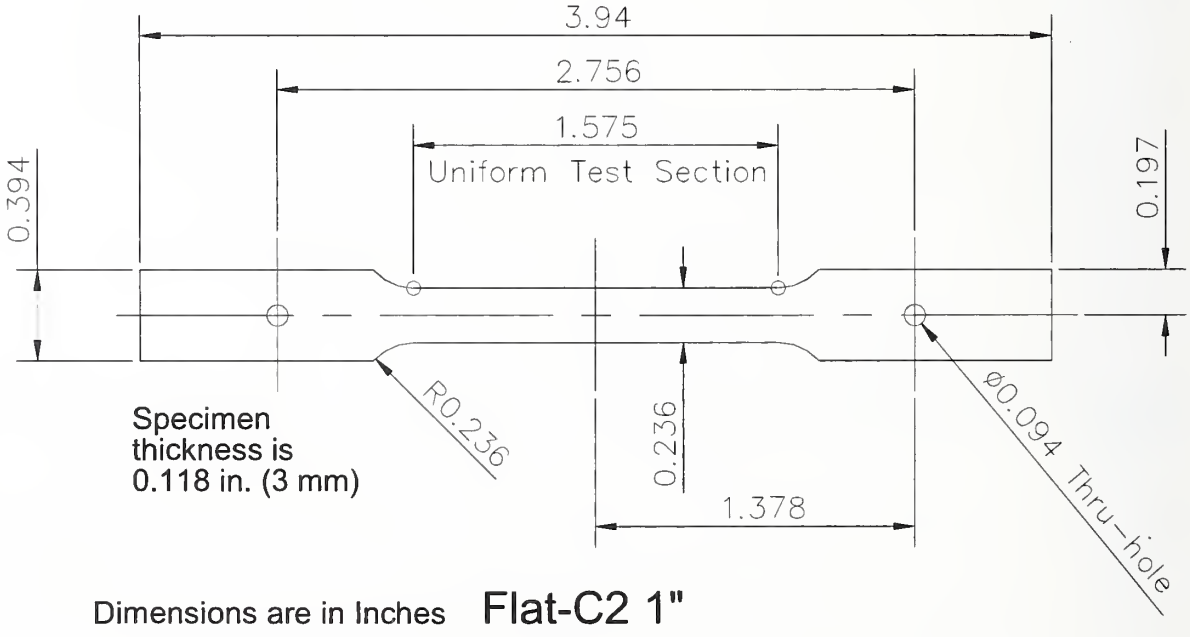

Figure 3–4. Flat tensile test specimen used for some creep tests.

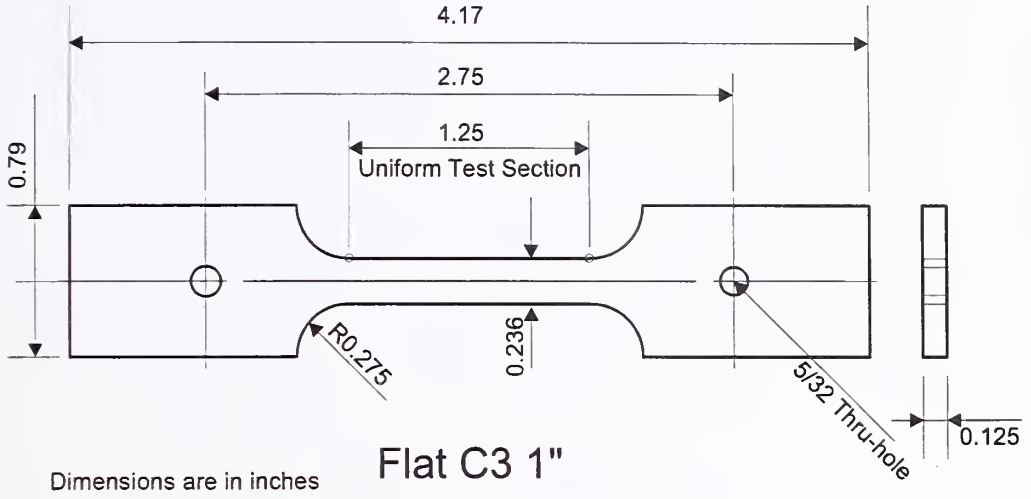

Figure 3–5. Flat tensile test specimen used for some creep and elevated-temperature tests.

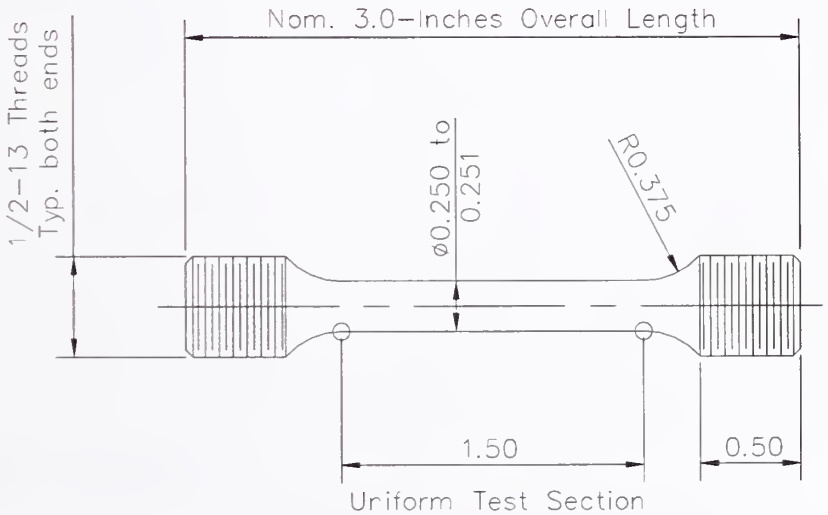

Figure 3–6. Round tensile specimen used for room-temperature and elevated-temperature tensile tests.

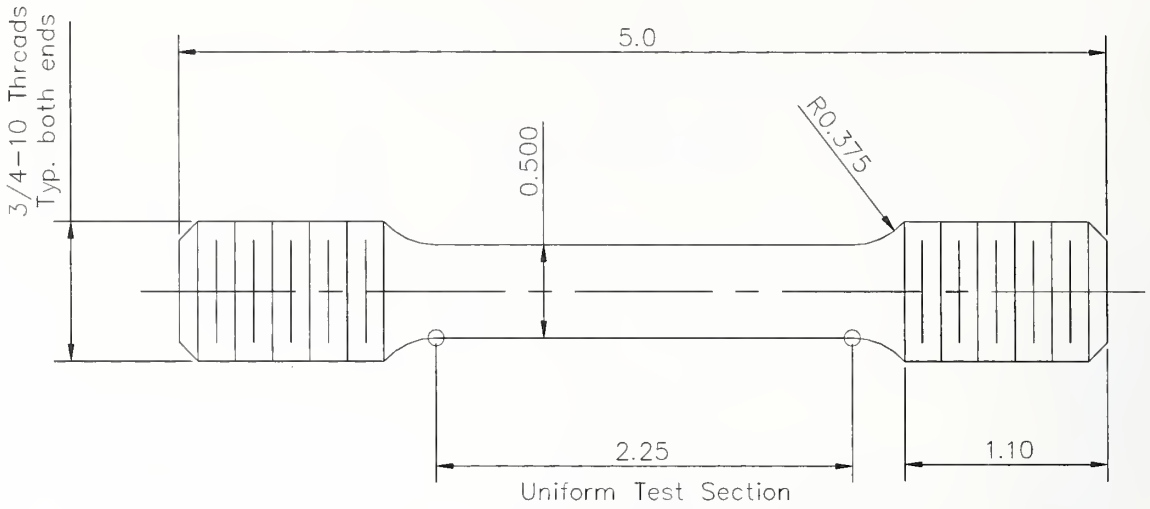

Figure 3–7. Round tensile specimen used for room-temperature tensile testing.

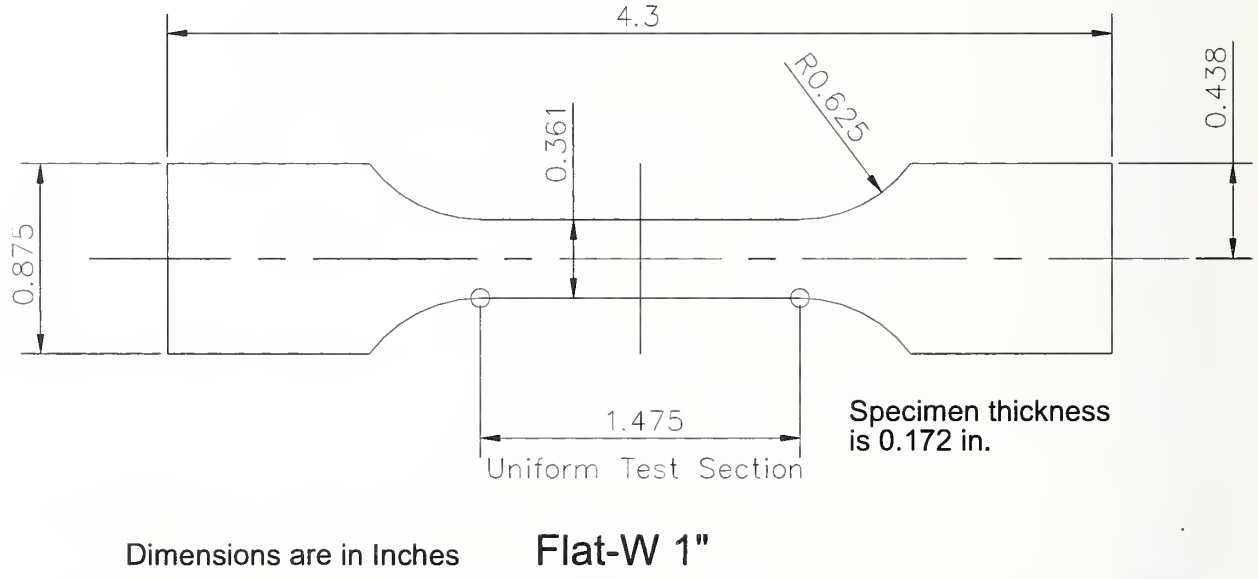

Figure 3–8. Flat tensile specimen typically used for tensile testing of all-weld metal specimens.

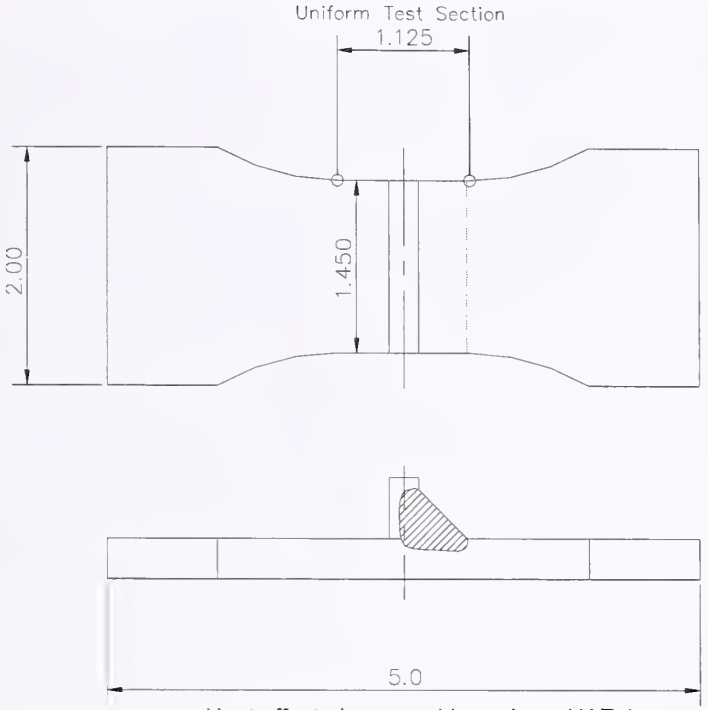

Figure 3–9. Heat affected zone tensile test specimen with flange/web weld intact. The flange is the specimen portion that is in tension.

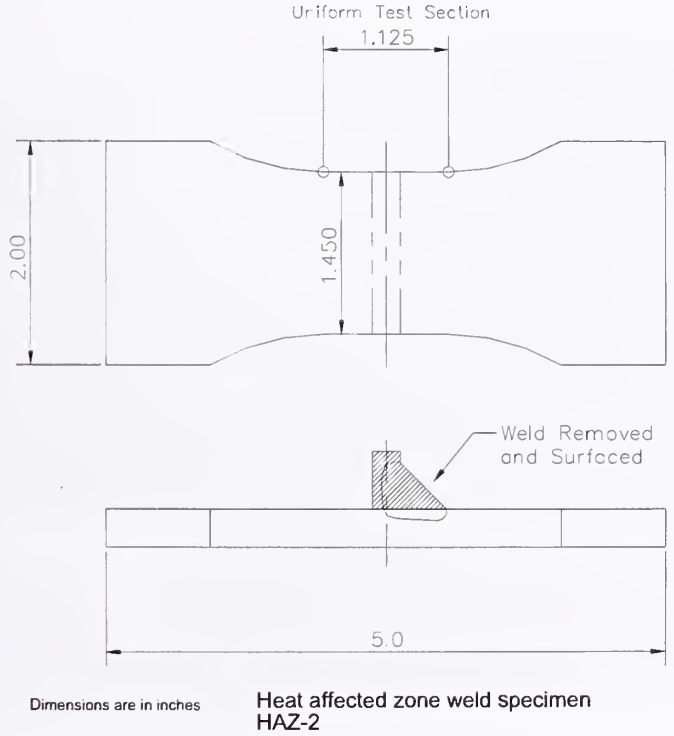

Figure 3–10. Heat affected zone tensile specimen with weld and web machined flush to the flange surface. The flange is the specimen portion that is in tension.

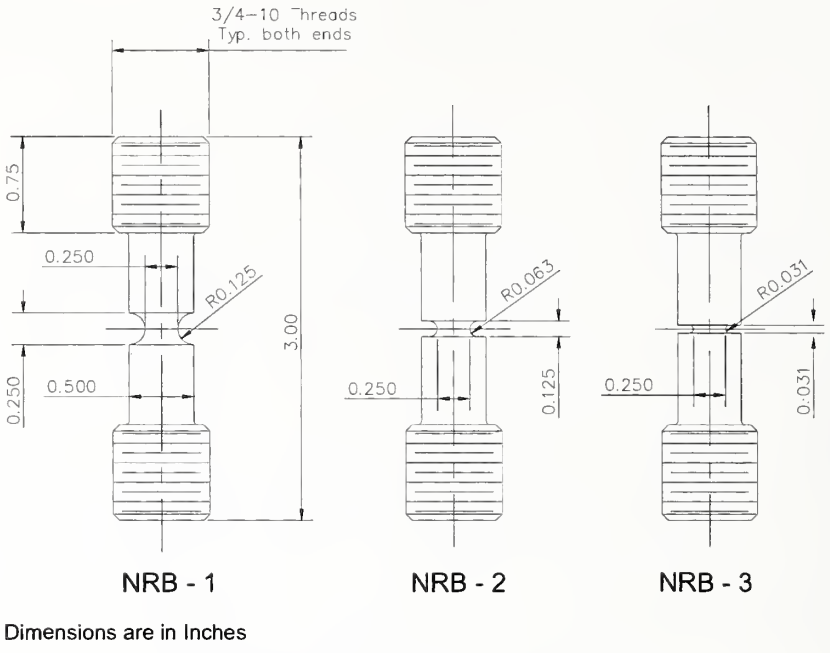

Figure 3–11. Notched tensile specimens.

3.2.3 Welds

Tests on specimens of all-weld metal from perimeter columns followed ASTM E 8 and used flat specimen type Flat-W1", Fig. 3–8.

Transverse tensile tests on perimeter column welds also followed ASTM E 8 and used specimen types K-1 and K-2, Figs. 3–9 and 3–10. In these flange specimens, the weld and the two heat affected zones (HAZ) are oriented transverse to the pull direction. The reduced section region extends from within the base metal (plate), through the weld and surrounding HAZ, and well into the base metal on the other side of the web. The type K-1 specimen retains a stub of the perimeter column outside web about 0.5 in. long, which extends at a right angle from the center of the specimen. In the type K-2 specimen, the stub of the web is removed entirely.

The shear strength of the resistance welds in the floor trusses was evaluated on a segment of the lower chord of a truss. A push rod gripped in the upper hydraulic grip of a 220,000 lbf closed-loop, servo-hydraulic test machine loaded the truss rod at 0.001 in./s while the angles of the lower chord rested on a clevis, Fig. 3–12.

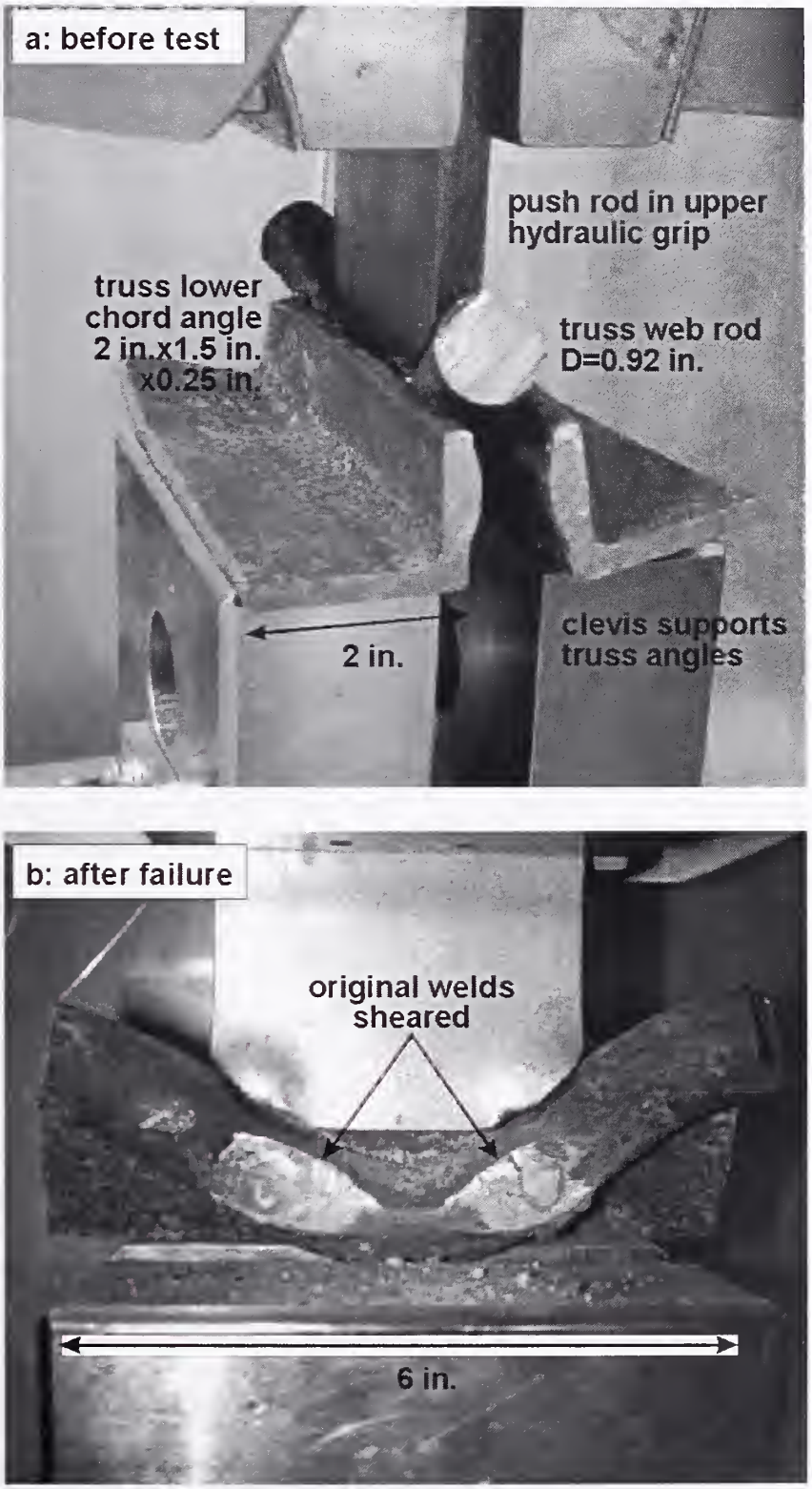

Source: NIST.

Figure 3–12. The resistance weld shear strength test (a) before loading, (b) after failure.

3.3 RESULTS

3.3.1 Steel

Figure 3–13 displays some example stress-strain curves for perimeter column, core column, and truss steels. Appendix A of this report summarizes the measured yield and tensile strengths, total elongations, and reductions of area for all the specimens tested. It also contains stress-strain curves for most specimens. Sections 3.4.1 and 3.5.1 analyze these results in terms of engineering specifications.

Figure 3–14 shows stress-strain curves for two sets notched bar tension tests on core column steels. Specimen C71-1-F2 is from the flange of a F_y = 36 ksi 12WF190 shape from WTC 1 column line 904 between floors 77-80, oriented longitudinally. The un-notched specimen, labeled $R = \infty$, has an unexpectedly high yield strength and lacks the expected yield point behavior, probably from damage incurred in the collapse and subsequent recovery. The flange was 1.736 in. thick. Specimen B6152-1-F1 is from a flange plate of a F_y = 36 ksi type 380 box column from WTC 1 column line 803 between floors 15–18. The original plate was 2.06 in. thick.

Stresses were calculated on the 0.25 in. diameter reduced cross section. The axial strain was calculated using the notch height, $2R$, as the gauge length, see Fig. 3–11. The diametral strain was calculated using the 0.25 in. reduced cross section diameter, which is the same for the three specimen geometries. Figure 3–14 plots the diametral strains in the negative direction and includes the results of tests on unnotched specimens for comparison. Because the operator sometimes removed the extensometers before failure, the strains may not represent failure strain. All fractures occurred by ductile hole growth; there was no evidence of a transition to cleavage fracture. The increasing tensile strength with decreasing notch radius shows that neither steel is notch-sensitive under the test conditions.

3.3.2 Bolts

Table 3–1 summarizes the results of tests on bolts. Figure 3–15 plots the load-displacement data for the four WTC A 325 bolts tested. All seven A 325 bolts failed in the threads, as expected.

3.3.3 Welds

Perimeter Columns

The yield strengths of two specimens of all weld metal produced by submerged arc welding from specimen N-9 (WTC 1, column 154, floors 101–104 specified F_y = 55 ksi) are F_y = 85.1 ksi and F_y = 84.8 ksi, Table 3–2. Their tensile strengths are TS = 103 ksi and TS = 103.3 ksi.

Transverse tests on weld specimens were conducted on fillet welds from specimen N-8 (WTC 1, column 142, floors 97-100, specified F_y = 60 ksi). The yield and tensile strengths are independent of the specimen type, Tables 3–3 and 3–4, so the presence of the stub of the web did not create a stress concentration. Because none of these transverse specimens broke in the weld, the strengths do not represent the weld strength, but rather represent the strength of the weakest region across the entire joint, which encompasses base metal to weld to base metal.

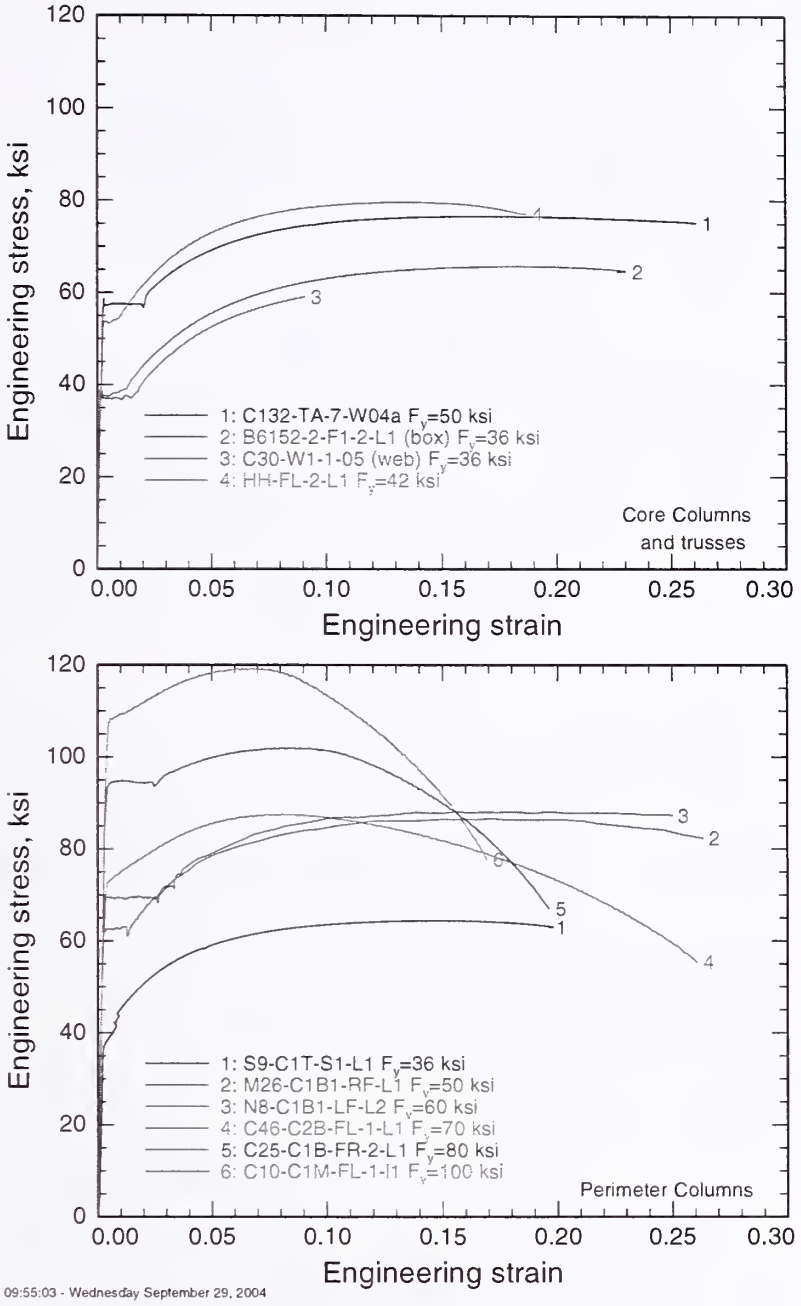

Figure 3–13. Examples of stress-strain curves for perimeter column, core column, and truss steels. In most cases, the strains do not represent failure.

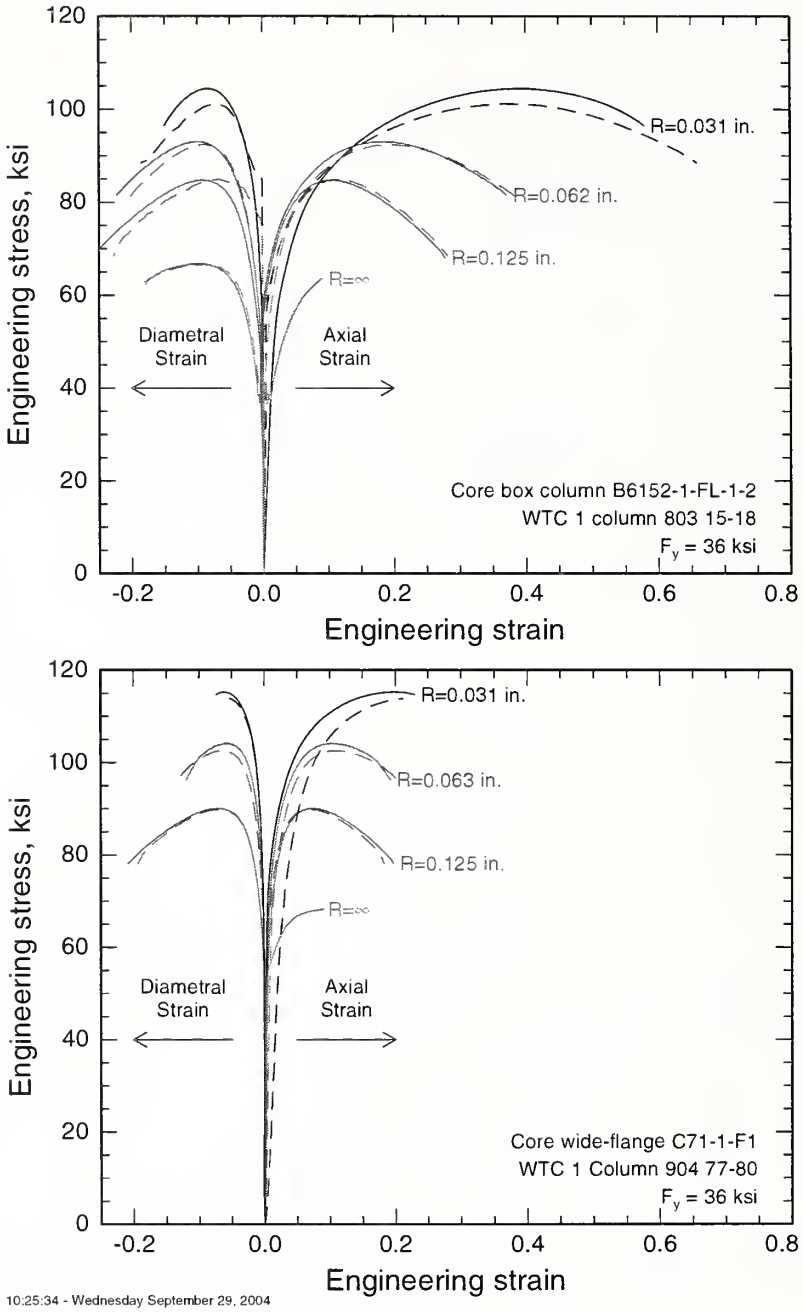

Figure 3–14. Stress-strain curves for notched round bar tests using the specimens in Fig. 3–11.

Table 3–1. Results of tensile tests on bolts.

Tests on A 325 Bolts				
Test Type	**Bolt Size**		**Tensile Strength (lbf)[a]**	**Notes**
ASTM F 606-02	7/8 in.×4.25 in.		69,000	failed in threads
ASTM F 606-02	7/8 in.×4.25 in.		68,000	failed in threads
ASTM F 606-02	7/8 in.×4.25 in.		63,900	failed in threads
		Test Rate (in./s)	**Tensile Strength (lbf)**	
load-elongation	7/8 in.×4.5 in.	0.00065	67,900	failed in threads
load-elongation	7/8 in.×4.0 in.	0.00065	68,300	failed in threads
load-elongation	7/8 in.×4.0 in.	2.0	68,800	failed in threads
load-elongation	7/8 in.×4.0 in.	2.0	68,200	failed in threads
Test on an A 490 Bolt				
Test	**Bolt Size**	**F_y (psi)**	***TS*** **(psi)[b]**	**Notes**
A 370 tensile[c]	1 in.×5 in.	153,500	163,400	EL_t = 16 % (2 in. gage length) ROA = 59.5 %

a. For A 325 bolts TS_{min} = 120,000 psi. For 7/8 in. bolts minimum tensile strength = 55,450 lbf based on A = 0.462 in.^{2} for 7/8 in. diameter bolts.

b. For A 490 bolts TS_{min} = 150,000 psi; minimum F_y = 130,000 psi; minimum EL_t = 14 percent (based on 2 in. gage length); minimum reduction in area ROA = 40 percent.

c. A 490 bolt was tested as a round tension specimen machined from the bolt.

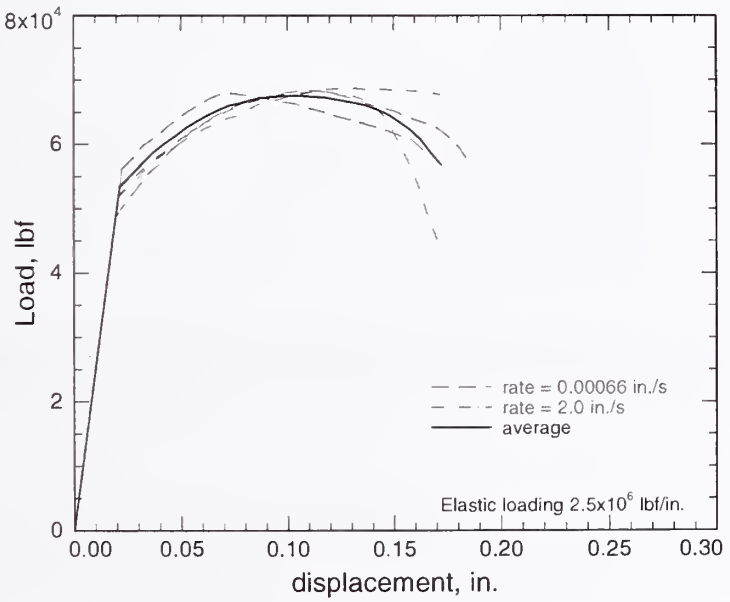

Figure 3–15. Load-displacement curves from four tensile tests of A 325 bolts, and the average curve.

Table 3–2. Room-temperature weld properties as measured.

Weld Location and Type	F_y (ksi)	*TS* (ksi)	Comments
Perimeter column fillet weld from N9 WTC 1 column 154 101-104 base metal F_y = 55 ksi test 1	85.1	103.0	All weld metal NIST test
Perimeter column fillet weld from N9 WTC 1 column 154 101-104 base metal F_y = 55 ksi test 2	84.8	103.3	All weld metal NIST test
Perimeter column lower strength steels	81.0	92.3	From PC&F Procedures
Perimeter column higher strength steels	105.0	118.0	From PC&F Procedures
Truss resistance welds (in shear)		46.4	NIST test Total Load 104,000 lbf
5/8 in. Core column weld in shear Test 1		82.9	From Stanray Pacific Procedures
5/8 in. Core column weld in shear Test 2		84.9	From Stanray Pacific Procedures
0.5 in. submerged arc weld for core column in shear		129.6	From Stanray Pacific Procedures

Table 3–3. Results of transverse tensile tests on welds from specimen N-8 (WTC 1, column 142, floors 97-100, specified F_y = 60 ksi).

Specimen	Specimen Type	F_y (ksi)	*TS* (ksi)	Total Elongation (%)	Comments
N8-C3B1-RF-HAZ-2	HAZ-1 (with stub Fig. 3–9)	70.0	95.8	12	Broke at weld root
N8-C3B1-RF-HAZ-4	HAZ-1 (with stub Fig. 3–9)	n/a	92.6	n/d	
N8-C3B1-RF-HAZ-1R	HAZ-2 (without stub Fig. 3–10)	65.3	92.2	15	Broke 0.5 in. from weld
N8-C3B1-RF-HAZ-3R	HAZ-2 (without stub Fig. 3–10)	67.8	92.9	17	

Key: n/d, not determined.

Table 3–4. Fillet weld sizes for various plate thicknesses in the core box columns.

Plate Thickness Range (in.)	Fillet Weld Size (in.)
0.75 to 1.5	3/8
1 5/8 to 1 7/8	7/16
2 1/8 to 2 5/8	1/2

Trusses

Although much of truss T1 was seriously deformed, it was possible to select several 5 in. to 6 in. long, relatively undamaged lower chord sections with resistance welds. The load for shear failure was 104,000 lbf, using the geometry of Fig. 3–12. On the fracture surface, the two weld areas that make up the resistance weld measure 0.45 in.^{2} and 0.67 in.^{2}. Assuming the two angles shared the load equally, and that the two welds on the side that did not fail have the same area as those on the side that did fail, the weld shear strength is 46.4 ksi.

3.4 COMPARISON WITH ENGINEERING SPECIFICATIONS

3.4.1 Steel

There are a number of issues in testing recovered steel that complicate answering the question, "Are the NIST-measured properties of the steel consistent with the appropriate specification?" They fall into three main groups: differences between the NIST test procedures and those in the mill test, natural variability of steel properties, and confounding effects from the post-fabrication handling of the steel. This section first discusses these complicating factors, and then summarizes the mechanical property data for each representative steel specimen in relation to the requirements of the original specifications.

Test Method Differences

One issue that complicates comparing the NIST-measured properties of the steel to the requirements of the original specification arises from differences between the test methodology used in establishing the mill test report and the test methodology that the NIST Investigation team used.

For structural steel, ASTM A 6 specifies that mill tests are conducted in accord with ASTM A 370. Most of the NIST tests on recovered steel were conducted in accord with ASTM E 8, which is a more generic standard for tensile testing. The major differences between the two are in the testing rate. E 8 prescribes that the testing rate, r, lie in the range 1.15 MPa/s < r < 11.5 MPa/s. A 370 prescribes only that the maximum strain rate in the uniform cross section to be 0.00104 s^{-1}. In general, the operator calculates this strain rate by assuming that all the actuator motion produces elastic strain in the specimen, which is frequently a poor assumption, because the test machine is not infinitely stiff. It is a reasonable assumption, however, that the A 370 rate used for the mill test report is between 5 and 10 times the rate used in the E 8 tests at NIST. A rule of thumb is that the measured yield strength increases between 2 ksi to 5 ksi per decade of strain rate. (Rao 1966, Johnson 1967, Barsom, 1987) On the average, then, the yield point measured in the NIST Investigation could be up to 3 ksi less than the one measured in the mill test report from rate effects alone. Unfortunately, the "rule of thumb value" is approximate: some steels exhibit almost no rate sensitivity, so it is impossible to predict the magnitude of the effect.

Another problem is that A 370 specifies three alternative methods for determining yield point and does not require the mill to report which method it used. In any case, very few mill test reports have survived, and none exist for the particular plates or shapes that are in the NIST inventory. The three methods are

- Drop of the beam method (for quasi-load controlled systems)
- Position of the knee or first maximum load in the curve

- Total extension under load

In any given test, these three methods all yield slightly different values for the yield point. If a definite yield point exists, it will generally be the highest of the possible values. NIST is unaware of any studies that document whether one of the other methods consistently yields higher values, however.

A 370 requires that plates and shapes with $t \leq 1.5$ in. must be tested full thickness with an 18 in. long, 1.5 in. wide specimen. Because of test machine limitations and lack of suitable, undamaged material, NIST frequently tested smaller specimens than ASTM A 370 calls for. NIST generally used 8 in. long, 0.5 in. wide full thickness flat specimens for plates with $t \leq 0.5$ in. For most other plates, NIST employed 0.5 in. diameter round specimens. Most ASTM standards prescribe that total elongation is to be measured on the 18 in. long specimen using an 8 in. gauge length, instead of the 2 in. gauge length used for the 8 in. specimen. For tests on samples taken from the same plate, the total elongations measured using 8 in. long flat specimens will be larger than those measured using 18 in. long specimens, because the necked region in the shorter specimen will occupy a greater fraction of the total gauge length. There is no absolute scaling law between the two gauge lengths, however.

During the WTC era ASTM A 6 prescribed that specimens for mill tests of wide-flange shapes originate from a section of the web. In some cases due to material quality problems, NIST harvested specimens from the flanges of wide-flange shapes. In general, because they are thicker than the webs, and therefore cool more slowly, the flanges will exhibit a yield point that can be several ksi lower than tests from the webs. In the 1974 AISI report on property variability, the average for the difference between product flange tests and official mill test reports is nearly zero for low strength ($F_y < 40$ ksi) steels, but is about 4 ksi for higher strength steels.

Natural Variability

ASTM steel standards require very little tension testing for mill acceptance. For example A 36-66 required only two tension tests from each heat, unless the heat was less than 50 tons, where only one test was necessary. The standard does not clarify how the yield point shall be reported when the two tests yield different values. In the early 1970s the American Iron and Steel Institute (AISI) conducted an extensive study on the variability of mechanical properties and chemistry of structural steel. That report has a great deal of information on product tension tests as they relate to the mill test report. The critical aspect is that the mill test report is a single tension test, conducted on one piece of a large lot of steel. It is a check that the quality of the steel is acceptable. The contemporary version of A 6 specifically calls out the AISI report (1974) and points out that a mill test report of $YP > 36$ ksi is **not** a guarantee that all the product supplied has $YP > 36$ ksi:

> "These testing procedures are not intended to define the upper or lower limits of tensile properties at all possible test locations within a heat of steel. It is well known and documented that tensile properties will vary with a heat or individual piece of steel. It is, therefore, incumbent on designers and engineers to use sound engineering judgement when using tension test results shown on mill reports. The testing procedures of Specification A6/A6M have been found to provide material adequate for normal structural design criteria."

The AISI property variability study (1974) has a substantial amount of data on product tests on both wide-flange and plate steels, where the product tests are taken from the same plate or shape as the mill test specimen. The variability within the entire heat, which encompasses many plates or shapes, will certainly be larger than this. The chapter on wide-flange sections indicates that the standard deviation of the difference between the mill test report and a product test from the same shape is about 2.3 ksi for shapes with $YP < 40$ ksi. In other words, it is not uncommon for product tests to be significantly lower than the mill test report. Barsom and Reisdorf (1988) reached similar conclusions from tension tests on heavyweight rolled A 36 wide-flange shapes.

Effects Arising From Prior Deformation

All steels relevant to the WTC Investigation except the $F_y = 100$ ksi steels were qualified at the mill based on yield point, *YP*, rather than on yield strength F_y or *YS*. Figure 3–16 defines yield point, yield strength, and yield point elongation graphically. Alpsten (1972, Fig. 5) reported a typical difference between the yield point (the maximum stress reached before yielding) and the yield strength (for instance defined by the 0.2 percent offset method) as about 3 ksi. Individual values were as large as 10 ksi. Testing at NIST has borne out this observation. Plain carbon steels, such as A 36, will almost always exhibit a yield point. Microalloyed steels (A 572, A 441) may or may not exhibit a yield point, but there is no a priori method to predict the existence or magnitude.

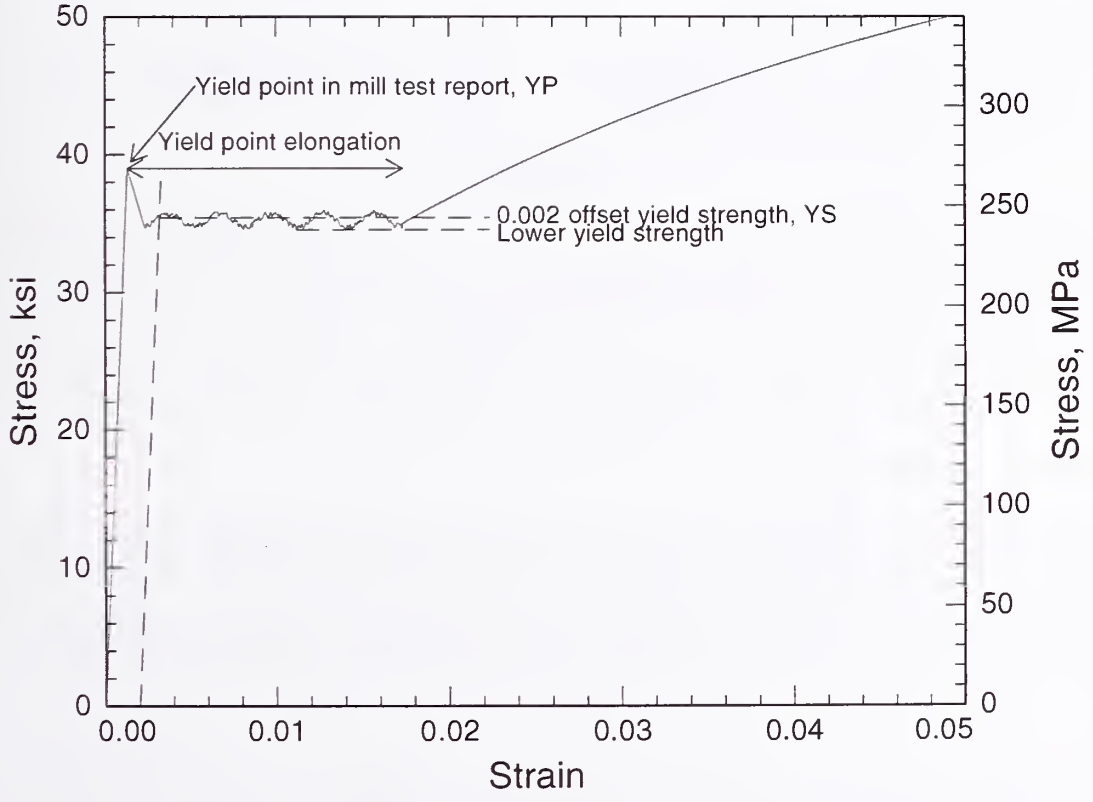

Figure 3–16. Schematic diagram of the various definitions of yield behavior in mechanical testing of steel.

The yield point elongation, or Lüders' strain, in Fig. 3–16 arises because of inhomogeneous deformation in the gauge length. Mobile interstitial impurities, mostly carbon and nitrogen, can diffuse to the cores of dislocations and pin them in place. An overstress is necessary to break the dislocation free of its atmosphere of interstitials. Rather than homogeneous deformation throughout the gauge length, the early stages of deformation of such steels proceeds as deformation bands sweep through the gauge section. A pre-strained specimen, where dislocations have already been freed from their interstitial atmospheres, will not exhibit yield point elongation.

Any prior deformation of the material for the test specimens typically removes the yield point. Two scenarios exist. The prior deformation may be sufficient to remove the yield point, but only partially remove the yield point elongation. In this case the NIST-reported value will almost certainly be less than what the mill test report would have stated. Larger prior deformation will eliminate the yield point elongation entirely and result in a work-hardened steel. In this case, the NIST-measured yield strength may be more or less than what the mill test would have reported, and it may still be less than the specified value.

The A 36 steels should exhibit a yield point and yield point elongation if undeformed. If a low-strength steel does not exhibit yield point behavior, and the resulting yield strength is expressed as 0.2 percent offset yield strength, there is a significant probability that the NIST-reported yield strength will be less than the specification called for. This does not imply, however, that the NIST-measured mechanical properties of the steel are inconsistent with original specification. In general, a fraction of a percent strain will remove the yield point, and a further (1–3) percent will remove the yield point elongation. The strains induced by the collapse and subsequent handling are probably sufficient to remove the yield point elongation. Any test of a F_y = 36 ksi steel that does not result in the appearance of a yield point and yield point elongation should be regarded with caution.

The pre-strain that removed the yield point elongation can further reduce the measured yield strength through the Bauschinger effect (Uko 1980). The measured yield strength of a specimen that has been strained in the positive direction and subsequently tested in the negative direction will be less than originally measured in the positive direction. The yield strength of a deformed flange may be lower if the direction of the tensile test is opposite to the direction of its pre-strain. The literature is not clear on the possible magnitudes of the reduction for pre-strains less than the typical yield point elongation, however.

Identification Methodology

The results of the NIST-conducted chemical and mechanical characterizations can be compared to the requirements of the various ASTM steel specifications allowed in the steel contracts. In some cases, it is possible to determine with reasonable confidence that the properties of the steel are consistent with the requirements of individual ASTM or proprietary specifications. In other cases, especially for the perimeter columns where the historical record indicates that many proprietary steels were used, this chapter attempts to identify the specific mill that rolled the steel. Identification of the specific mill cannot be made with the same level of certainty as correspondence with intended specifications, because it requires combining information from several disparate sources and making reasonable assumptions based on historical data and steelmaking practice. No documents exist that identify whether a given column was to be fabricated from steel meeting a given ASTM standard or proprietary specification. Instead, the structural engineering plans specify only the minimum yield strengths of the steel. The fabricator was free

to choose from a large list of acceptable steels. One exception to this rule is for columns with specified F_y = 36 ksi. ASTM A 36 is the only structural steel specification in the list of approved steels that supplies steel with this yield point.

Figure 3–17 illustrates the method for identifying possible steel grades graphically. The Port of New York Authority (PONYA) contract with the steel fabricators allowed them to use steels that met enumerated ASTM standards, as well as specific proprietary steels, without further approval. In addition, fabricators could request permission from PONYA to use certain unlisted steels after providing property data. The Port Authority of New York and New Jersey (PANYNJ) documents reviewed during the Investigation contain many examples of these requests. These documents do not provide sufficient information to identify an unknown steel, however, because the standards generally only specify the allowable ranges of a few chemical elements. Steel mills have much more specific recipes for individual steels. Occasionally, NIST has identified literature examples of named steels that can help identify unknown steels. The boundaries of the diagram should be considered porous, since NIST has incomplete information on construction era approvals of steels, as well as chemical and mechanical characterization of proprietary steels. Furthermore, as discussed above, each steel exhibits a natural variability in properties. From the chemical and mechanical analyses and the historical record, it is never possible to state with certainty that a specific mill rolled a specific plate. Where the historical record indicates that one mill supplied a proprietary steel, the analysis discusses whether the specimen in the NIST inventory was likely to have met that specification.

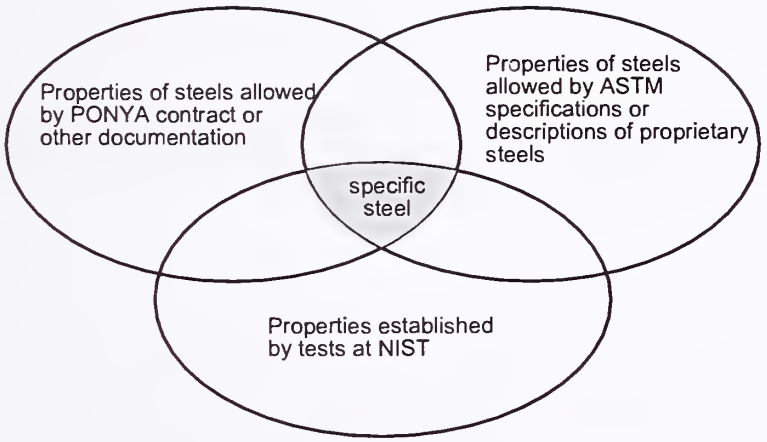

Figure 3–17. Methodology for identifying recovered steels.

The rest of this section summarizes the representative specimens and attempts to discern whether it was likely that the steel met the original specifications, subject to the constraints that the complicating factors detailed above induce. A separate document (NIST NCSTAR 1-3B) summarizes the chemistries of all steels characterized as part of the Investigation. Another document (NIST NCSTAR 1-3A) summarizes the standard specifications for the steels used in the construction.

Perimeter Columns

Contemporaneous construction documents (White 1967; Symes 1968) indicate that Pacific Car and Foundry (PC&F) fabricated the perimeter columns primarily with steel it purchased from Yawata Iron and Steel, and possibly Kawasaki Steel. One contemporaneous document (White 1967) indicates that

Yawata was to supply the steels with F_y > 36 ksi and Kawasaki was to supply steels with F_y = 36 ksi. At least one surviving shipping manifest (Mitsui 1968) shows PC&F received 190 t of A 36 spandrel plates that originated in Chiba, Japan, the location of a Kawasaki Steel mill. One contemporaneous construction document clearly indicates that Yawata also supplied A 36 for spandrels (Symes 1969b).

Another contemporaneous document (Symes 1969) also indicates that PC&F used domestic steel for plate 3, the inner web, of the perimeter columns. By weight, the plate 3 steel represents less than 10 percent of the mass of the perimeter columns, because the spandrel plates make up much of the inside wall of the perimeter column.

Except for the F_y = 36 ksi steel, which it supplied to meet A 36, Yawata supplied all other grades of steel to its own specifications, which the PONYA chief engineer approved. NIST was unable to locate the complete specification for these steels. The only document that NIST located (White 1967b) details required changes to the complete specifications for Yawata steels during the negotiations over acceptance. Unfortunately, NIST could not locate the original specification document that describes the tensile strength and total elongation requirements of any of the Yawata steels with F_y > 36 ksi. It is therefore impossible to compare the measured tensile strengths and total elongations of perimeter column steels to specification documents. Generally, the measured total elongations of the intermediate-strength steels are greater than the 24 percent minimum that A 441-66 specified.

In general, the measured yield strengths perimeter column steels exceed the minimum requirements. Figure 3–18 plots the ratio of the measured yield strength to the specified minimum yield strength for all tests using specimens oriented parallel to the original rolling direction of the plate, which was the specified test orientation for plates in the WTC construction era. The points that lie below the line of unity ratio at specified F_y = 60 ksi originated in two inner web plates from the same perimeter column panel, and thus probably came from the same plate.

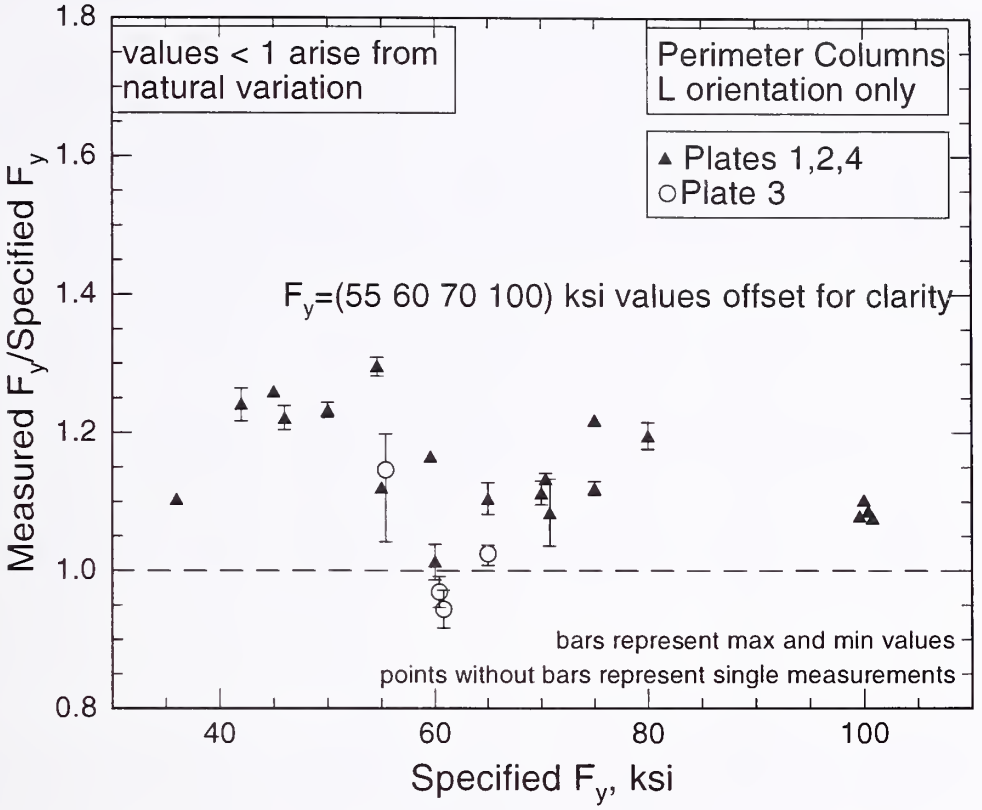

Figure 3–18. Ratio of measured yield strength to specified minimum yield strength for all longitudinal tests of perimeter column steels.

F_y = 36 ksi S-9 Spandrel

The representative F_y = 36 ksi specimen, S9-C1T-S1, came from the 100th floor spandrel of rccovcred perimeter column S-9 (WTC 1 Column line 133 floors 97–100), which is just above thc airplane impact hole. The rolling, or longitudinal, direction of the spandrel plates lies in their long direction, or perpendicular the axis of the building. The measured yield strengths in longitudinal tests exceed the requirements of A 36; the average F_y = 38.2 ksi. The tensile strength and total elongations are also consistent with the requirements of A 36.

The chemistry of specimen S9-C1T-S1, Table 3-5 column 1, is also consistent with the requirements of A 36, Table 3–5. The Mn and Si contents are higher, and the C content is lower, than most of the other F_y = 36 ksi spandrels, but A 36 has no requirements for Mn or Si for plates that are 0.75 in. thick or less. Two of the thirteen characterized spandrels specified as F_y = 36 ksi have this chemistry; the chemistry of the other eleven is different, but also consistent with the requirements of A 36.

Table 3–5. Summary of mechanical properties and chemical compositions for steels from low-strength perimeter columns.

	S9-C3T-S-1 (note a)	ASCE3-C1B-FL-2	S14-C2B-S-1	M26-C1T-FR-1	N9-C1M-FR-1	N8-C1B-F-1	N8-C3T-OW-1	
C	0.10	0.19	0.16	0.16	0.17	0.16	0.18	C
Mn	1.41	1.21	1.18	1.36	1.27	1.50	1.39	Mn
P	0.011	0.020	<0.005	0.024	0.016	0.023	0.018	P
S	0.016	0.016	0.024	0.022	0.011	0.016	0.012	S
Si	0.55	0.25	0.36	0.29	0.40	0.44	0.40	Si
Ni	0.02	0.01	0.06	0.01	0.01	0.01	0.02	Ni
Cr	0.04	0.03	0.05	0.02	0.02	0.02	0.04	Cr
Mo	<0.01	<0.01	<0.01	<0.01	<0.01	<0.01	<0.01	Mo
Cu	0.08	0.05	0.14	0.04	0.05	0.05	0.05	Cu
V	0.018	<0.005	0.024	<0.005	<0.005	0.005	0.011	V
Nb	<0.005	0.040	<0.005	0.047	0.042	0.064	<0.005	Nb
Ti	0.026	<0.005	0.018	<0.005	<0.005	0.007	<0.005	Ti
Zr	<0.005	<0.005	<0.005	<0.005	<0.005	<0.005	<0.005	Zr
Al	<0.005	<0.005	<0.005	0.018	0.024	0.042	0.029	Al
B	<0.0005	<0.0005	<0.0005	<0.0005	<0.0005	<0.0005	<0.0005	B
N	0.0032	0.0070	0.0060	0.0186	0.0065	0.0033	0.0050	N
F_y (ksi) specified	36	45	46	50	55	60	60	F_y (ksi) specified
F_y avg (long)	38.2	56.7	55.8	61.7	61.8	69.2 (note b)	60.8	F_y avg (long)
t (in.)	3/8	1 7/8	3/8	9/16	1/4	5/16	1/4	t (in.)

a. S9-C3T-S-1 and S9-C1T-S-1 originate from different locations on the same plate

b. The average of 4 longitudinal tests of N8-C1B-F-1 is F_y = 68.7 ksi. Value reported is the average of 4 tests on N8-C1B-F-1 and 3 tests on N8-C3B-RF

Key: long, longitudinal.

Note: Highlighted entries are particularly relevant for steel identification.

F_y = 45 ksi ASCE3

The representative F_y = 45 ksi specimen ASCE3-C1B-FL came from an unidentified location. A stamping at one end identified the yield strength of the plates, however. The yield strength measured in the single longitudinal test, F_y = 56.7 ksi, far exceeds the specified F_y = 45 ksi. The yield and tensile strengths and total elongation are consistent with values from a group of recovered Yawata mill test reports for F_y = 45 ksi steels of similar thickness. In that group of mill test reports, the averages of 25 individual plates are F_y = 51.6 ksi, TS = 72.8 ksi; the total elongation in 8 in. is El_t = 28.0 percent.

The chemistry of ASCE3-C1B-FL is consistent with the Yawata "A441-modified" chemistry specification, Table 3–7 under the heading "Yawata 50." The important features of that specification are the high allowable Si content and the use of Nb as a micro-alloying agent. That specification also expresses the Cu content as a maximum rather than the usual minimum.

F_y = 46 ksi S-14 Spandrel

The representative F_y = 46 ksi specimen S14-C3B-S1 came from the 91st floor spandrel of a panel from the north face of WTC 2 on column line 217. The structural engineering plans specify this spandrel as F_y = 46 ksi. For unknown reasons, the plans include spandrel plates specified as F_y = 45 ksi and F_y = 46 ksi, sometimes even in the same perimeter column panel. However, none of the surviving contemporaneous construction communication between PC&F and SHCR and PONYA ever mention F_y = 46 ksi steel. All surviving Yawata specifications describe F_y = 45 ksi and F_y = 50 ksi steels only. Furthermore, none of the contemporaneous ASTM structural steel specifications describe a steel supplied with F_y = 46 ksi for the thickness of this spandrel: t = 3/8 in. For example, plates meeting A 242, A 440, or A 441 would be supplied with F_y = 50 ksi for this thickness. A 572 does not have a F_y = 46 ksi entry.

In any case, the measured yield strength far exceeds the specified minimum; the average value of three tests is F_y = 55.8 ksi, which is also consistent with any of the F_y = 50 ksi specifications.

The chemistry of the specimen is consistent with the requirements for the specification for the Yawata F_y = 50 ksi steel, Table 3–5. It does differ from the chemistry of the other two F_y = 50 ksi plates recovered, however.

F_y = 50 ksi M-26

The representative F_y = 50 ksi specimen M26-C1T-FR came from the north face of WTC 1 on column line 131 near the 93rd floor, which is just below the impact zone. The test specimen originated in a section of flange (plate 1) 9/16 in. thick. The average measured longitudinal yield strength is more than 10 ksi higher than the specified minimum: F_y = 61.7 ksi.

The chemistry of the specimen is consistent with the Yawata specification for F_y = 50 ksi. Like many of the other perimeter column steels, it is strengthened by addition of Nb. The Yawata hot-rolled steels in the range 50 ksi ≤ F_y ≤ 60 ksi share a common chemistry specification, which the contemporaneous construction correspondence denotes as "A441-modified." That specification only puts an upper limit of 0.15 percent on Nb+V, so many different chemistries could satisfy this specification.

F_y = 55 ksi N-9

The representative F_y = 55 ksi specimen N9-C1M-FR came from the north face of WTC 1 column line 155 near the 102nd floor. The test specimen originated from a section of flange (plate 1) 0.25 in. thick. The measured average yield strength is consistent with the specification: F_y = 61.8 ksi.

The chemistry is consistent with the Yawata F_y = 55 ksi specification, and is very similar to those of perimeter column steels specified as F_y = 50 ksi and F_y = 60 ksi.

F_y = 60 ksi N-8

The representative F_y = 60 ksi specimens came from several of the flange and outer web plates in specimen N-8, which is from the north face of WTC 1, centered on column line 142 between floors 97–100. This panel was just above the impact zone. The average yield strength of seven tests of longitudinal specimens taken from two different 5/16 in. thick flanges (plate 1) is F_y = 69.2 ksi, which is much greater than the specified minimum. The average yield strength of three longitudinal specimen taken from the

outer web (plate 2) of N8-C3-B1 (column line 141, near the bottom) is F_y = 60.8 ksi. One of these tests was slightly lower than the specified minimum (F_y = 59.2 ksi vs. F_y = 60 ksi).

The chemistries of the flange (plate 1) and outer web (plate 2) are consistent with the Yawata specification for F_y = 60 ksi steel, Table 3–7, but they are not identical. In particular, the outer web (plate 2) does not contain Nb, and the V content is rather low (0.011 percent). But because the Yawata specification only limits the sum of Nb+V, both chemistries are consistent with this specification.

F_y = 65 ksi N-99

The representative F_y = 65 ksi specimen came from the flange (plate 1) of specimen N99-C3T1-RF, which originated in WTC 1, column line 147 near the 102nd floor. This location is several floors above the impact zone. The average measured yield strength of two longitudinal specimens is F_y = 71.8 ksi, which exceeds the minimum F_y = 65 ksi in the Yawata specification.

The chemistry of N99-C3M-FR-1, which is from a different location in the same plate, is also consistent with the Yawata F_y = 65 ksi specification, Table 3–6, which contemporaneous construction documents denote as WEL-TEN 60R. According to these documents, this was the highest strength hot-rolled grade, and it was only used at thicknesses up to 0.5 in. Thicker plates required the quenched and tempered WEL-TEN 60. The hot-rolled WEL-TEN 60R is alloyed with V instead of Nb, and has added Cr.

F_y = 70 ksi C-46, S-1, and S-14

NIST tested three different examples of F_y = 70 ksi perimeter-column steels. They are S1-C2M-FL, a 7/16 in. thick flange (plate 1) from the west face of WTC 1 column line 433 near floor 89, C46-C2M-FL, a 3/4 in. thick flange from west face of WTC 2 column line 157 near floor 69, and S14-C3M-FR, a 1/4 in. thick flange (plate 1) from the north face of WTC 2 column line 218 near floor 92. The global average longitudinal yield strength is F_y = 77.7 ksi, which exceeds the minimum requirements of the Yawata specification for F_y = 70 ksi WEL-TEN 62.

The chemistries of all three specimens are similar, Table 3–6. All are consistent with the F_y = 70 ksi WEL-TEN 62 specification, Table 3-7, which has V and Cr additions.

F_y = 75 ksi C-22

The representative F_y = 75 ksi specimen C22-C2M-FL came from a 1/4 in. thick flange (plate 1) from the north face of WTC 1 column line 157 near floor 94. This location is just above the impact opening. The average longitudinal yield strength, F_y = 83.7 ksi exceeds the requirements of the F_y = 75 ksi WEL-TEN 62 specification.

The chemistry is consistent with the F_y = 75 ksi WEL-TEN 62 specification, Table 3–6, and is similar to the chemistry of the F_y = 70 ksi steels.

Table 3–6. Summary of mechanical properties and chemical compositions for steels from high-strength perimeter columns.

	N99-C3M-FR-1 (note a)	S1-C2M-FL-1	C46-C2M-FL-1	S14-C3M-FR-1	C22-C2M-FL-1	C25-C1B-FR-1	M10b-C3M-FR-1	
C	0.16	0.13	0.12	0.13	0.15	0.13	0.14	C
Mn	1.25	1.08	1.10	1.07	1.13	0.97	0.84	Mn
P	0.018	0.008	0.014	0.010	0.016	0.014	0.009	P
S	0.018	0.013	0.015	0.013	0.013	0.015	0.016	S
Si	0.38	0.41	0.40	0.39	0.39	0.33	0.23	Si
Ni	0.01	0.01	0.04	0.01	0.01	0.01	0.01	Ni
Cr	0.19	0.22	0.21	0.21	0.23	0.32	0.88	Cr
Mo	<0.01	< 0.01	< 0.01	< 0.01	<0.01	0.20	0.40	Mo
Cu	0.05	0.04	0.05	0.05	0.04	0.28	0.23	Cu
V	0.053	0.020	0.024	0.020	0.041	< 0.005	<0.005	V
Nb	<0.005	< 0.005	< 0.005	< 0.005	<0.005	0.024	<0.005	Nb
Ti	<0.005	< 0.005	< 0.005	< 0.005	<0.005	< 0.005	<0.005	Ti
Zr	<0.005	< 0.005	< 0.005	< 0.005	<0.005	< 0.005	<0.005	Zr
Al	0.031	0.110	0.097	0.110	0.110	0.100	0.075	Al
B	<0.0005	< 0.0005	< 0.0005	< 0.0005	<0.0005	0.0016	<0.0005	B
N	0.0120	0.0060	0.0070	0.0070	0.0020	0.0070	0.0051	N
F_y (ksi)	65	70	70	70	75	80	100	F_y (ksi)
F_y avg (long)	71.8	77.9	75.9	79.4	83.7	95.7	107.7	F_y avg (long)
t (in)	1/4	7/16	3/4	1/4	1/4	1/4	1/4	I (in)

a. N99-C3M-FR-1 and N99-C3T1-RF are from different locations in the same plate. In the specimen designation system, occasionally "FR" and "RF" are used interchangeably to indicate specimens from the right flange.

Key: long, longitudinal.

Note: Highlighted entries are particularly relevant for steel identification.

F_y = 80 ksi C-25

The representative F_y = 80 ksi specimen C25-C1B-FR-2 came from a 1/4 in. thick flange (plate 1) from the east face of WTC 1 column line 207 near floor 89. The average longitudinal yield strength for two specimens, F_y = 95.7 ksi, is significantly higher than the minimum requirement of the Yawata WEL-TEN 70 specification.

The chemistry, which identifies it as a chrome-molybdenum steel, is also consistent with the WEL-TEN 70 specification, Table 3–7 The chemistries of three other F_y = 80 ksi plates from different columns are similar. A thicker F_y = 80 ksi section, C46-C1B with t = 5/8 in. contains 0.43 percent Ni and small amounts of V instead of the small amounts of Nb of the other F_y = 80 ksi steels. The specification for WEL-TEN 70 has no limits on Ni, Nb, or V, however, so the chemistry of C46-C1B is also consistent with the WEL-TEN 70 specification.

F_y = 85 ksi to F_y = 100 ksi M-10b, C-10, B-1043, and C-14

Contemporaneous construction documents (White 1968) indicate that PC&F requested and received permission to use F_y = 100 ksi steel wherever the plans called for steels with yield strengths greater than 85 ksi. Forensic investigation of the recovered steel confirmed this finding. Ten of the fourteen columns of recovered steel that were specified to have $F_y \geq 85$ ksi or $F_y \geq 90$ ksi had legible yield strength stampings. In each case the columns were stamped as F_y = 100 ksi.

NIST tested four different specimens of nominally F_y = 100 ksi perimeter column steel.

Specimen M-10b-C3B1-RF came from 1/4 in. thick flange (plate 1) from the north face of WTC 2 column line 205 near floor 83. Although the structural engineering drawings specify it as F_y = 85 ksi, markings on the plate indicate that it is F_y = 100 ksi. Specimen C10-C1M-FL came from a 1/4 in. thick flange from the west face of WTC 1 column line 452 near floor 86. Although specified as F_y = 90 ksi, markings on the plate indicate that it is F_y = 100 ksi. Specimen C14-C1-RF came from a 1/4 in. thick flange from the northeast corner of WTC 2 column line 301. Specimen B1043-C2T-FL is an example of a thicker section, t = 1.125 in., specified as F_y = 100 ksi from the south face of WTC 2 column line 406 near floor 43.

As a group, the average yield strength is F_y = 109.2 ksi; the minimum of the group is F_y = 107.5 ksi. All the yield strengths exceed the minimum requirement of F_y = 100 ksi for Yawata WEL-TEN 80C, Table 3–6 and Table 3–7. The total elongations to failure for specimen C14-C1-RF are less than those of the other specimens: 16 percent and 17 percent compared to an average of 22 percent for the others. Some contemporaneous construction correspondence (White 1967b) indicates that the F_y = 100 ksi WEL-TEN 80C was to meet the strength and total elongation requirements of A 514-66, which mandates a minimum total elongation of 18 percent in a 2 in. gauge length. A 1966 Yawata steel advertisement (WEL-TEN 1966) states a 16 percent minimum. The total elongation of each specimen from F_y = 100 ksi plate is larger than this value.

Inner Web (Plate 3)

Contemporaneous construction documents (Symes 1969) indicate that PC&F generally fabricated the flanges, outer webs and spandrels (plates 1, 2 and 4) from Japanese steel (primarily Yawata) and the inner web (plate 3) from domestic steel. For this reason, this section reviews the properties of steel specimens from the inner webs separately. Chemical analyses of specimens from the inner web confirm that the steel is frequently different from the steel used in plates 1 and 2. In some cases, however, the composition of the inner web plate is identical to the other plates in the column, indicating that it was fabricated from a Yawata steel. All inner web plates with $F_y > 75$ ksi have chemistries consistent with the Yawata grades. In terms of mass, the inner web represents less than 10 percent of the total steel used in the perimeter columns, because the spandrel plates cover part of the inside of the perimeter column, and because the inner web is often thinner than the flange plates.

Other contemporaneous construction documents provide evidence that Bethlehem steel supplied most of the domestically produced steel for the PC&F perimeter column contract. The actual fraction is unknown, and those same construction documents also show that PC&F purchased or requested approval to purchase plate from nearly every domestic steel company. None of the recovered plate 3 steels with $F_y < 100$ ksi contain Nb, which means that they do not correspond to USS Ex-Ten, which specifies a

minimum Nb content. Because of the lack of information in the construction record, it is impossible to unambiguously identify the source of the steel used for plate 3.

Table 3–7. Summary of mechanical properties, chemical compositions, and relevant ASTM and Yawata specifications for steels from high-strength perimeter columns.

	C10-C1M-FL-1	B1043-C2T-FL-1	A 441	Yawata50	WEL-TEN 62	WEL-TEN 70	WEL-TEN 80C	
C	0.17	0.15	0.22	0.22	0.18	0.18	0.18	C
Mn	0.89	0.80	0.85–1.25	1.1–1.6	1.40	1.20	0.6–1.2	Mn
P	0.015	0.005	0.040	0.040	0.035	0.030	0.030	P
S	0.012	0.012	0.050	0.050	0.035	0.030	0.030	S
Si	0.24	0.23	0.30	0.55	0.55	0.55	0.15–0.35	Si
Ni	0.01	0.01						Ni
Cr	0.90	0.88		0.30	0.30	1.3 max	0.7–1.3	Cr
Mo	0.43	0.33				0.6 max	0.6 max	Mo
Cu	0.28	0.31	0.20	0.20		0.15–0.5	0.15–0.5	Cu
V	0.007	<0.005	0.02 min		0.12 max			V
Nb	<0.005	<0.005		0.15 Nb+V max				Nb
Ti	<0.005	<0.005						Ti
Zr	<0.01	<0.005						Zr
Al	0.081	0.053						Al
B	<0.0005	<0.0005					0.006 max	B
N	0.0040	0.0080						N
F_y (ksi)	100	100	50	50-60	70	75–80	100	F_y (ksi)
F_y avg (long)	108.7	110.3						F_y avg (long)
t (in.)	1/4	1 1/8						t (in.)

Key: long, longitudinal.

N9-C1T1-IW is a specimen of plate 3 with specified F_y = 55 ksi from the north face of WTC 1 column line 155 near the 102nd floor. The original plate is 0.25 in. thick. The average yield strength of three longitudinal specimens is F_y = 61.3 ksi, which is larger than the specified F_y = 55 ksi Chemically, the steel has slightly too much Mn to meet the Bethlehem V-series specification (1.31 percent vs. a maximum 1.25 percent) even after accounting for the relaxed requirements of product testing, assuming the increased compositional ranges allowed by A 572-70 for Mn. This difference would have an insignificant effect on mechanical properties.

NIST tested three examples of F_y = 60 ksi plate 3 steel. N8-C1B1-A-IW is a specimen of inner web from the north face of WTC 1, column line 143 near floor 98. The average yield strength of two longitudinal specimens of N8-C2M-IW is F_y = 56.7 ksi, which is below the specified minimum: F_y = 60 ksi. The average of three transverse specimens, an orientation which would not have been used for mill testing is similarly low: F_y = 56.8 ksi. N8-C2M-E-IW came from the adjacent column 142. The average yield strengths of longitudinal and transverse specimens are similarly low: F_y = 56.7 ksi and F_y = 57.2 ksi

respectively. Given that the columns are adjacent and the inner web plate thickness is the same, it is likely that these two inner web plates came from the same original plate. Specimen C40-C2M-IW originated from the north face of WTC 1, column line 136 at floor 100. The average yield strength of two longitudinal specimens of C40-C2M-IW, F_y = 64.6 ksi, exceeds the specified minimum.

The chemistries of the two plates are very similar to each other, as well as to the compositions of many of the other plate 3 specimens. All are high in V, and contain Cr and Ni. The magnitudes of the alloy contents are consistent with the Bethlehem V-series specification.

Specimen N99-C3M1-IW is an example of an inner web plate with specified F_y = 65 ksi from WTC 1 column line 147 between floors 99 and 102. The average yield strength of three longitudinal specimens is F_y = 66.6 ksi, which exceeds the specified minimum. The chemistry of the plate is very similar to all of the other plate 3 specimens. It has vanadium added for strength, as well as trace amounts of Ni and Cr.

Specimen S14-C3T-IW-1 is an example of an inner web plate with specified F_y = 70 ksi from WTC 2 column line 217 between floors 91-94. The average yield strength of two longitudinal specimens is F_y = 76.0 ksi, which exceeds the specified minimum: F_y = 70 ksi. The chemistry is similar to the rest of the plate 3 specimens and consistent with the construction correspondence on the chemistry specifications for the Bethlehem V-series steels.

The measured yield strengths of two of the inner web plates are less than the specified minimum. The relevant question is, "If the measured yield strength of a plate measured in the course of the investigation is lower than the specified minimum, is this an anomalous or an expected event?" That question is the convolution of at least two other questions:

1. What is the distribution of yield strengths from mill test reports for a given specified minimum yield strength?

2. What is the distribution of product test values of yield strength for a given strength in a mill test report?

The literature data on variation in structural steel properties (Alpsten 1972, Galambos 1978, AISI 1974), while reasonably large, is not structured in a manner that makes it easy to use. Alpsten (1972) and Galambos (1978) provide partial answers to question 1, and the AISI report (1974) on "Variation of Product Analysis and Tensile Properties..." helps answer question 2. One might also attempt to estimate how frequently in construction that steels with inappropriate specified minimum yield strengths are used, but this question is fundamentally different from the objective answers to questions 1 and 2. Ideally, we would like to answer the question by calculating the probability that a plate specified as F_y = 60 ksi would actually have a measured (product) F_y = 56.7 ksi, the average yield strength of test specimens from the inner web of perimeter column N-8.

Several 1960's era studies (Alpsten 1972, Galambos 1978) summarize the distribution of mill-test-report yield strengths for given steel grades. One shortfall of these studies in applying them to the questions at hand is that they usually report just a mean value and a standard deviation or coefficient of variation (C_v). Because each grade of steel is supplied to a specified minimum value, the distributions of mill test report values are non-normal. Instead, they are truncated at the specified minimum and therefore skewed to the positive values. Estimating the fraction of plates with strength near the specified minimum is not accurate.

A second problem is that no studies exist that examine the variability in these distributions between steel mills. It is likely that individual steel mills have different production practices that result in different shapes to the distributions. The reported values for the distributions usually represent the output of a single mill.

The AISI report on product variability (1974) appears at first glance to be the answer to these questions, but it codes its data in a manner that removes some of the utility. The probabilities that it expresses for product tests are given as the expected difference between the measured value and the mill test report value. In other words, knowledge of the original mill test report value is necessary, which is impossible for the WTC steels. In that sense, it answers question 2, but a good answer to question 1 is still absent.

Given the uncertainties in the AISI report (1974), it is not prudent to attempt a detailed statistical calculation. Instead, the calculation should simply establish whether it is reasonable to have found a product tension test result that is less than the specified minimum in the suite of tests that characterize the WTC steels.

To proceed with the estimation, define the following variables:

Variable	Value	Definition
F_y	60 ksi	the specified minimum yield strength for the plate in question, N-8
F_y^p	56.7 ksi	the NIST-measured (product) yield strength
k_p	$\frac{F_y^{mtr}}{F_y} = 1.092$	the historical average of the ratio of yield strength in mill test reports, F_y^{mtr}, to the specified minimum yield strength, F_y, for high-strength steel plates
C_v	0.054	the coefficient of variation of the historical average of mill test reports of a given specified minimum yield strength

Galambos (1978) estimated k_p and C_v from Alpsten's (1973) data on Swedish $F_y = 58$ ksi plates.

The AISI report on variability (1974) expresses its statistics for results of product tests in terms of deviation from the official value (i.e. the value stated on the mill test report). To estimate this value, calculate the deviation, $\Delta\sigma$, from the mill test report as

$$\Delta\sigma = k_p F_y - F_y^p = 1.092 \times 60 \text{ ksi} - 56.7 \text{ ksi} = -8.82 \text{ ksi}$$

From Table 11 of study SU/18 in the AISI report (1974), the minimum fraction, f, of tests higher than this difference from the official test is $f = 0.87$ for steels with $F_y \geq 50$ ksi. Therefore 13 percent of the time, product tests of plates would have produced values such as those for plates N8-C2M-IW and N8-C1B1-IW. Given that they were physically located next to each other, and are the same thickness and specified minimum yield strength, it is likely that these inner web plates originated from a common plate.

In comparison, NIST tested more than 20 distinct perimeter column plates. Of these, only the inner web plates from N8-C2M-1W and N8-C1B1-1W, or about 5 percent of the total, had a product tension test that was less than the specified minimum. Therefore, it is not unreasonable or anomalous that the measured yield strengths of inner web plates from perimeter column N-8 are less than the specified minimum.

The previous calculation is approximate and should be regarded only as an order-of-magnitude calculation. It shows that it is possible that a product tension test of WTC steel could be less than the specified minimum without being considered anomalous. Comprehensive data on the range of possible values of k_p and C_v do not exist. The data from study SU/18 of the AISI report (1974) is based on only 168 mill test reports. That report does not contain sufficient information to decide if those 168 mill test reports came from steels made to high-strength specifications, or if they were simply very high mill test reports for steels made to low strength specifications.

Core Columns

NIST tested representative samples of the four most common core columns: box and wide-flange in F_y = 36 ksi and F_y = 42 ksi. Table 3–8 summarizes these results. Appendix A of this report tabulates the complete test data and plots the stress-strain curves for the individual tension tests. Mechanically, the yield stress of some of the specimens is less than the specified minimum, but these differences probably arise from damage to the column that removed the yield point or test differences between the mill test report and the NIST protocol. Figure 3–19 plots the ratio of measured yield strength or yield point to the specified minimum for longitudinal tests.

Table 3–8 and Table 3–9 also summarize the chemistry data on specimens of identified core column steel. With one exception, the steels are unremarkable. The chemistry of specimens from all the columns (shapes and plates) specified as F_y = 36 ksi are consistent with ASTM A 36. The chemistries of the high-strength shapes are consistent with A 441 or A 572. Although A 572 is not listed in the PONYA steel contract, both HH-F1-1 and C-26 (a beam from the 107th floor) could have been supplied to the Bethlehem V-series requirements. That steel is listed in the PONYA steel contract and could be sold to meet A 572. The combination of chemistry and measured yield strength of specimen C-88c is inconsistent with every ASTM specification listed in the PONYA contract, but that contract lists proprietary steels for which NIST does not have typical compositions for comparison.

Most of the core columns recovered were significantly deformed, which made it difficult to select undeformed regions to harvest test specimens from. Even the relatively straight sections were often slightly bent. Appendix B summarizes the extent of the deformation in the regions from which specimens were taken for columns C-30, C-65, C-70, and C-155. From the geometry of the deformed column, it was possible to estimate the magnitude of the changes to the stress-strain curves for the web and flange specimen. Generally, the disappearance of the yield point and the elevated strengths of the flange specimens are consistent with the magnitude of the deformation measured from the shape of the core columns.

This section describes each column and the individual specimens harvested from it.

F_y = 36 ksi Wide-Flange C-30

Specimen C-30 is a F_y = 36 ksi 14WF237 shape from WTC 2 column line 1008, between floors 104–106. This location is on the opposite side of the building and well above the impact zone. All six tensile specimens, three from the web and three from the flange, exhibit both yield point and yield point elongation behavior. All six tests produced $YP > 36$ ksi. The segment of the column from which the test specimens originated had no measurable deformation, see Appendix B, which is consistent with the appearance of the yield point and the similarity of the stress-strain curves from the webs and flanges.

Figure 3–20 plots the stress-strain curves for the longitudinal tests of C-30, along with the corresponding curves for the three other wide-flange core columns specified as F_y = 36 ksi for which web tests were conducted. The chemistry, tensile strength, and total elongation of C-30 meet ASTM A 36.

Table 3–8. Summary of mechanical properties and chemical compositions for steels from core column wide-flange shapes.

Shapes	C30-F1-1 WTC 2 1008 104-106	C65-F1-1 WTC 1 904 86-89	C71-FL-2 WTC 1 904 77-80	C80-F1-1 WTC 1 603 92-95	C155-F1-1 WTC 1 904 83-86	HH-F1-1 WTC 1 605 98-101	C26-F1-1 WTC 1 beam 107	
C	0.17	0.23	0.23	0.23	0.23	0.17	0.19	C
Mn	1.06	0.74	0.73	0.90	0.87	1.08	1.19	Mn
P	<0.005	0.006	0.027	0.008	<0.005	<0.005	<0.005	P
S	0.014	0.015	0.016	0.008	0.017	0.014	0.015	S
Si	0.10	0.02	0.03	0.03	0.03	0.03	0.03	Si
Ni	0.05	0.02	0.02	0.01	0.02	0.02	0.04	Ni
Cr	0.04	0.02	0.02	0.02	0.03	0.02	0.03	Cr
Mo	<0.01	0.01	0.04	0.01	<0.01	<0.01	<0.01	Mo
Cu	0.24	0.05	0.08	0.05	0.06	0.24	0.02	Cu
V	0.036	<0.005	< 0.005	<0.005	<0.005	0.065	0.059	V
Nb	<0.005	<0.005	< 0.005	<0.005	<0.005	<0.005	<0.005	Nb
Ti	<0.005	<0.005	< 0.005	<0.005	<0.005	<0.005	<0.005	Ti
Zr	<0.005	<0.005	< 0.005	<0.005	<0.005	<0.005	<0.005	Zr
Al	<0.005	<0.005	< 0.005	<0.005	<0.005	<0.005	0.018	Al
B	<0.0005	<0.0005	< 0.0005	<0.0005	<0.0005	<0.0005	<0.0005	B
N	0.0067	0.0041	0.003	0.004	0.0049	0.0099	0.0065	N
V/N ratio	5.4					6.6	9.1	
specified F_y (ksi)	36	36	36	36	36	42	50	
F_y avg (web) (ksi)	41.9	31.1	33.2	n/d	42.2	n/d	50.3	
Yield behavior[a]	YP	NYP	YP	NYP	YP	YP	NYP	
F_y avg (flange) (ksi)	39.6	32.4	53.4	34.4	50.9	54.1	n/d	

Shapes	C30-F1-1 WTC 2 1008 104-106	C65-F1-1 WTC 1 904 86-89	C71-FL-2 WTC 1 904 77-80	C80-F1-1 WTC 1 603 92-95	C155-F1-1 WTC 1 904 83-86	HH-F1-1 WTC 1 605 98-101	C26-F1-1 WTC 1 beam 107	
Type	14WF237	12WF161	12WF190	14WF184	12WF161	12WF92	27WF94	
t_w (in.) (b)	1.090	0.905	1.060	0.840	0.905	0.545	0.576	
t_f (in.) (b)	1.748	1.486	1.736	1.378	1.486	0.865	0.872	

a. Yield behavior
YP = yield point behavior exists in stress-strain curve
NYP = no yield point behavior exists in stress-strain curve
b. t_f = flange thickness; t_w = web thickness.

Key: n/d, not determined.

Note: Highlighted items are particularly relevant for steel identification.

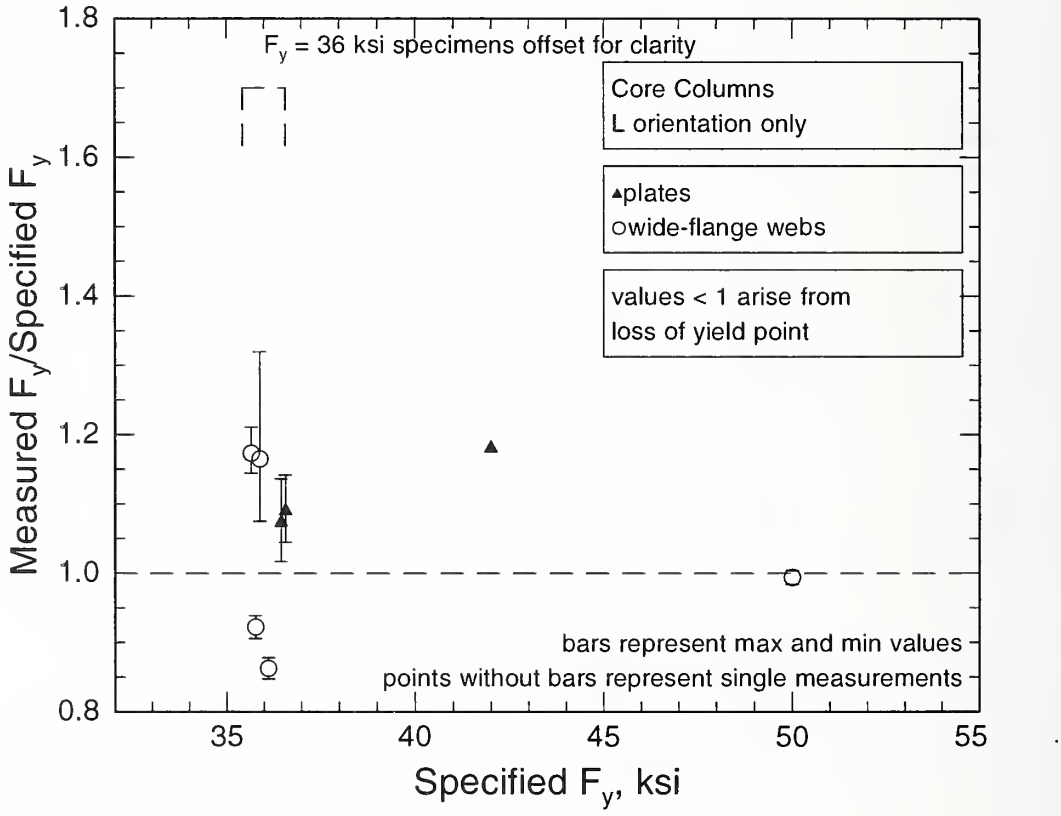

Figure 3–19. Ratio of measured yield strength to specified minimum yield strength for all longitudinal tests of core column steels.

Table 3–9. Summary of mechanical properties and chemical compositions for steels from core box columns.

Specimen	B6152-2-FL-3	B6152-1-FL-1	Fuji mill test report[a]	C88C-F2-1	C88A-F1-1	C88B-F1-1	C88B-F2-1	C88B-F3-1
Location	WTC 1 504 33-36	WTC 2 803 15-18		WTC 2 801 80-83	WTC 2 801 80-83	WTC 2 801 77-80	WTC 2 801 77-80	WTC 2 801 77-80
C	0.17	0.16	0.20	0.18	0.19	0.15	0.18	0.18
Mn	0.81	0.98	0.96	0.98	1.15	1.11	0.86	0.87
P	<0.005	0.024	0.013	0.029	0.013	<0.005	<0.005	<0.005
S	0.011	0.013	0.008	0.020	0.021	0.011	0.014	0.016
Si	0.20	0.24	0.20	0.04	0.05	0.09	0.03	0.03
Ni	0.02	0.01		0.02	0.02	0.02	0.02	0.02
Cr	0.03	0.02		0.02	0.03	0.01	0.01	0.02
Mo	<0.01	< 0.01		0.06	0.02	<0.01	<0.01	<0.01
Cu	0.05	0.05		0.05	0.05	0.02	0.02	0.03
V	<0.005	< 0.005		< 0.005	<0.005	<0.005	<0.005	<0.005
Nb	<0.005	< 0.005		< 0.005	<0.005	0.030	0.011	0.013
Ti	<0.005	< 0.005		< 0.005	<0.005	<0.005	<0.005	<0.005
Zr	<0.005	< 0.005		< 0.005	<0.005	<0.005	<0.005	<0.005
Al	0.013	0.031		< 0.005	<0.005	<0.005	<0.005	<0.005
B	<0.0005	< 0.0005		< 0.0005	0.0024	<0.0005	<0.0005	<0.0005
N	0.0100	0.0070		0.005	0.004	0.006	0.004	0.006
specified F_y (ksi)	36	36	36	42	42	42	42	42
F_y avg (ksi)	40.4	38.8	38.4	49.7	n/d	n/d	n/d	n/d
Yield behavior[b]	YP	YP	n/d	NYP	n/d	n/d	n/d	n/d
Column Type	Type 354	Type 380	n/a	Type 378	n/a	n/a	n/a	n/a
t (in.)[c]	1.88	2.06	3.0	1.5	1.5	1.44	1.44	

a. Data for 25,263 lb plate 65.5 in. by 453.75 in. tested Aug 5 1969, rolled at Fuji Hirohata Works.
TS = 64.9 ksi; total elongation measured on gage length of 8 in: = El_t = 32 percent.

b. Yield behavior:
YP = yield point behavior exists in stress-strain curve.
NYP = no yield point behavior exists in stress-strain curve.

c. t = plate thickness.

Key: n/a, not applicable; n/d, not determined.

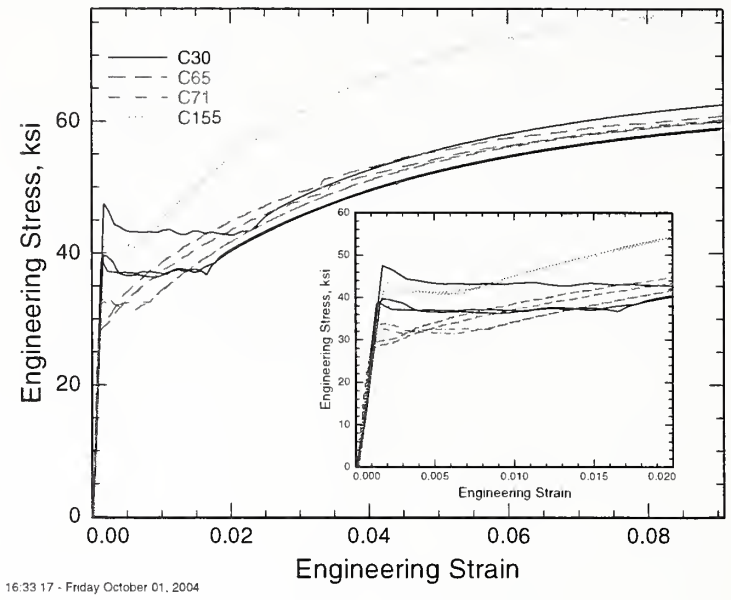

Figure 3–20. Yield behavior in tests of webs of four wide-flange core columns specified as F_y = 36 ksi.

F_y = 36 ksi Wide-Flange C-65

Specimen C-65 is a F_y = 36 ksi 12WF161 shape from WTC 1 column line 904 between floors 86–89. This location is on the opposite side of and well-below the impact zone. None of the eight specimens tested, six from a flange and two from the web, exhibit either yield point or significant yield point elongation. There is a small yield point elongation in the two specimens from the web (Fig. 3–20), but it is only one tenth as long as the usual (1–3) percent. Only one of the eight tests produced a yield strength above 36 ksi. The section that is the source of the web specimens is deformed into an "S" shape, see Appendix B, although the specimens were harvested away from the large tear in the web. The section that is the source of specimens from the flange, see Appendix B, shows no evidence of significant deformation, but the lack of yield point and yield point elongation indicate that the material has more than several percent prior strain.

There are several possible explanations for the low yield strength, given the absence of yield point behavior. Galambos (1978) reported the mean value of yield strength in mill test reports for English A 36 shapes as 1.22×36 ksi = 44 ksi, which is consistent with data in Barsom (1988) on U.S. heavy A 36 wide-flange shapes from slightly after the WTC construction era. For such a mean large excess strength, the AISI variability study (1974) predicts virtually no possibility of finding under-strength product tests, unlike the estimate for high-strength perimeter column plates in the previous section. The measured yield strengths of the other WTC wide-flange specimens tested that exhibit yield point phenomena are all less than this mean value. One limitation of the AISI variability study is that 97 percent of the members of its data set for wide-flange shapes are ASTM Group 1 and 2 shapes, while the WTC core columns tested are all much heavier Group 3 and 4 shapes. Because these heavier shapes undergo much less reduction during rolling, and cool more slowly from the rolling temperature, their average strengths may be much closer to the specified minimum than the heavily rolled, fast-cooling lighter shapes in the AISI study. It is also

possible that this difference represents different steelmaking practice for the wide-flange columns, which probably came from Yawata Iron and Steel.

There are several other possible origins for the low value of the measured yield strength. The typical difference between yield point *YP* and yield strength *YS* or F_y (3 ksi or more) could account for part of the shortfall, although the mean of the two tests is only 30.5 ksi. The slower testing rate in the NIST tests could account for an additional 2 ksi. Finally, were the prior strain in the opposite direction from the tensile tests, the Bauschinger effect (Uko 1980, Tipper 1952, Elliot 2004) could further reduce the measured yield strength (10-20) percent from the expected value. In particular, the flow stress in the first 3 percent strain after pre-straining in the opposite direction is much less than in the forward direction, but the difference decreases with increasing strain. The sum of these three effects could raise the yield strength above $F_y = 36$ ksi.

Although the yield strength of column C-65 is less than the specified minimum, the stress-strain behavior is very similar to the other $F_y = 36$ ksi columns, Fig. 3–20. By approximately 3 percent strain, the flow stress is similar to column C-30. Furthermore, the tensile strength and total elongation measured in specimens from C-65 are consistent with the requirements of A 36.

The chemistry of C-65 meets ASTM A 36.

$F_y = 36$ ksi Wide-Flange C-71

Specimen C-71 is a 12WF190 shape from WTC 1 column line 904 between floors 77–80 specified to have $F_y = 36$ ksi. Both web specimens exhibit yield point and yield point elongation behavior, but the measured yield point is less than 36 ksi; the mean value is $YP = 33.2$ ksi. In contrast the flange specimens exhibit significant evidence of substantial prior deformation: $F_y = 53.3$ ksi and absence of yield point elongation. The measured chemistry, total elongation, and tensile strength are all consistent with the requirements of A 36.

Arguments made for explaining the low measured yield strengths of specimen C-65 apply to specimen C-71 as well.

It is likely that the high strength and lack of yield point behavior of the specimens from the flanges arose from bending of the column about the web axis. Appendix B summarizes an analysis of the shape of the deformed columns and estimates the strain in the flanges from the bending of the column. The measured deformation of the column is consistent with the elevated strength of the flange specimens, which came from the portion of the flange with tensile strain.

$F_y = 36$ ksi Wide-Flange C-80

Specimen C-80 is a 14WF184 shape from WTC 1 column line 603 between floors 92–95 specified to have $F_y = 36$ ksi. The yield strength of the single flange specimen tested is slightly lower than the specified minimum: $F_y = 34.4$ ksi. The stress-strain curve does not exhibit yield point or yield point elongation. Reintroducing the expected yield point behavior to the measured yield strength would probably increase the yield strength enough to be consistent with the requirements of A 36. The chemistry, tensile strength, and total elongation of C-80 are consistent with the requirements of ASTM A 36.

F_y = 36 ksi Wide-Flange C-155

Specimen C-155 is a 14WF184 shape from WTC 1 column line 603 between floors 92–95 specified to have F_y = 36 ksi. All three web specimens exhibit yield point and yield point elongation behavior, and the yield points of all three are well above 36 ksi; the average yield point is YP = 42.2 ksi. The chemistry, tensile strength, and total elongation all meet A 36.

Like specimens from C-71, the flange specimens show evidence of prior deformation: elevated yield strength, and lack of yield point and yield point elongation. Like column C-71, the magnitude of the elevated strength and lack of yield point in the flanges is consistent with the measured deformation in the column. The tensile specimens came from the portion of the flange that had been strained in tension. Appendix B details the calculation.

F_y = 42 ksi Wide-Flange HH

Specimen HH is a 12WF92 shape from WTC 1 column line 605 between floors 98–101 specified to have F_y = 42 ksi. The two longitudinally oriented specimens from the flange exhibit yield point and yield point elongation behavior with YP = 54.1 ksi. Although the mill test report requires data from a web specimen, given that the flanges usually have lower strength than the webs, it is likely that a web test from specimen HH would have produced a yield point YP > 42 ksi. The chemistry of specimen HH is consistent with the requirements of both ASTM A 441 and A 440 with its Cu content and A 572 types 2 and 4 because of its high vanadium content. The chemistry of HH-FL-1 is inconsistent with USS Ex-Ten, because it lacks Nb.

Both ASTM A 441 or A 440 require a group 2 shape like HH to have YP = 50 ksi, which is less than the measured yield point of HH-FL-1. The measured yield point is also consistent with the requirements of A 572 Grades 42, 45, 50, and 55, but A 572 does not appear in the list of approved steels in the PONYA contract. However, A 572 Type 4 is written to be satisfied by the Bethlehem V-series of steels, which were permitted under the PONYA contract and presumably could be supplied in 42 ksi and 45 ksi grades. Historical documents (Betts 1967) indicate that Yawata supplied about half of the mass of the steel for the rolled shapes in the core. Other documents (Monti 1967) indicate that Yawata requested and was granted an exception to supply its own "A 441 modified" composition, which HH-FL-1 does not meet. The historical documents do not indicate whether Yawata intended to supply all rolled shapes with F_y > 36 ksi to this specification or not. It is most likely that HH-FL-1 represents a Yawata A 441 shape, which would have been supplied to F_y = 50 ksi.

F_y = 50 ksi Wide-Flange C-26

Specimen C-26 is a 27WF94 shape from a beam in the WTC 1 107th floor specified to have F_y = 50 ksi. The measured yield strengths of two of the three web specimens are less than 50 ksi, but both by less than 1 ksi. None of the stress-strain curves exhibit yield point or yield point elongation. The web that is the source of the specimens is quite deformed. Indeed, the flat, full-thickness, 8 in. tensile specimens bowed about 1/8 in, so the absence of a yield point and significant yield point elongation is not surprising.

The chemistry of C-26 is consistent with the requirements of A 572 Type 2 and Type 4 as well, based on the vanadium and nitrogen content. Because it lacks of sufficient Cu, the chemistry is inconsistent with the requirements of A 441.

Given the yield strength and chemistry C-26 could be a Bethlehem V-series shape, which the PONYA steel contract did allow.

F_y = 36 ksi Box B6152-1

Specimen B6152-1 is a 2.06 in. thick flange plate from a type 380 box column from WTC 1 column line 803 between floors 15–18 specified to have F_y = 36 ksi. The two stress-strain curves are very similar, but only one exhibits a definite yield point. The measured yield strengths are both F_y > 36 ksi, however.

The chemistry is consistent with the requirements of ASTM A 36 and is rather similar to the chemistry of a Fuji steel A 36 plate (Morris 1969) shipped to Stanray Pacific, Table 3–8. That similarity and its thickness (2.06 in) are consistent with the historical documents (Warner 1967) that Fuji Steel supplied most of the plates with t < 3 in. in the Stanray Pacific contract for the welded core columns.

F_y = 36 ksi Box B6152-2

Specimen B6152-2 is a 1.88 in. thick flange plate from a type 354 box column from WTC 1 column line 504 between floors 33-36 specified to have F_y = 36 ksi. Both longitudinal specimens exhibit a yield point and yield point elongation. The yield points exceed the requirements of A 36: YP = 40.4 ksi. The chemistry of B6152-2-F1-2 is similar to B6152-1-F1 and consistent with A 36.

F_y = 42 ksi Box C-88c

Specimen C-88c is a 1.5 in. thick flange plate from a type 378 box column from WTC 2 column line 801 between floors 80–83 specified to have F_y = 42 ksi. Originally, it was part of C-88a, Fig. 3–21. Note that the junction between C-88a and C-88b is the intact welded splice at the 80th floor. The yield strength of the single longitudinal test, YS = 49.7 ksi, (0.2 percent offset) is much larger than the F_y = 42 ksi yield strength requirement.

The chemistry of C-88c is anomalous, Table 3–9. It is inconsistent with all ASTM specifications listed in the PONYA steel contract. Its lack of vanadium makes it inconsistent with the requirements of A 441. Because it does not contain Nb either, it inconsistent with the chemistry requirements of all the variants of the A 572 specification. Although the PONYA steel contracts do not mention A 572, there is archival evidence (Marubeni-Iida 1967) of shipments of A 572 steels to Stanray Pacific. Its low Cu content is inconsistent with the requirements of A 440. There are several steels listed in the PONYA contract, most notably proprietary Lukens grades, for which NIST cannot locate typical or specified compositions, so possibly it could have been shipped to one of those specifications. Summaries such as Woldman's (1990) indicate only specified minimum compositions, and are thus of limited utility in identifying specific alloys. Contemporaneous documents (Warner 1967) indicate that Fuji steel supplied all plates with t < 1.75 in. The thickness of the C-88 plates (1.5 in.) identifies Fuji as a possible source. However, plates with $F_y \geq 42$ ksi for the box columns were rather uncommon; only 69 of the 1202 columns per building are specified as F_y = 42 ksi. Because of their rarity, Stanray Pacific could have purchased these outside their general contract. The PANYNJ documents reviewed by NIST yielded no correspondence on substitutions or approvals of such a plate, but it is certainly possible that the PANYNJ documents do not contain a complete record of the construction correspondence. NIST was not been able to identify which mills might have supplied this plate.

The other F_y = 42 ksi steels from the adjacent plate and column respectively, C-88a, are chemically similar, but not identical, Table 3–9. The chemistry of the flange opposite C-88c (C-88a-F1) is different and contains B, but much less Mo. The plates of C-88b, which are slightly thinner and originate from the floors below, contain Nb; their chemistries are consistent with the requirements of A 572, grade 42.

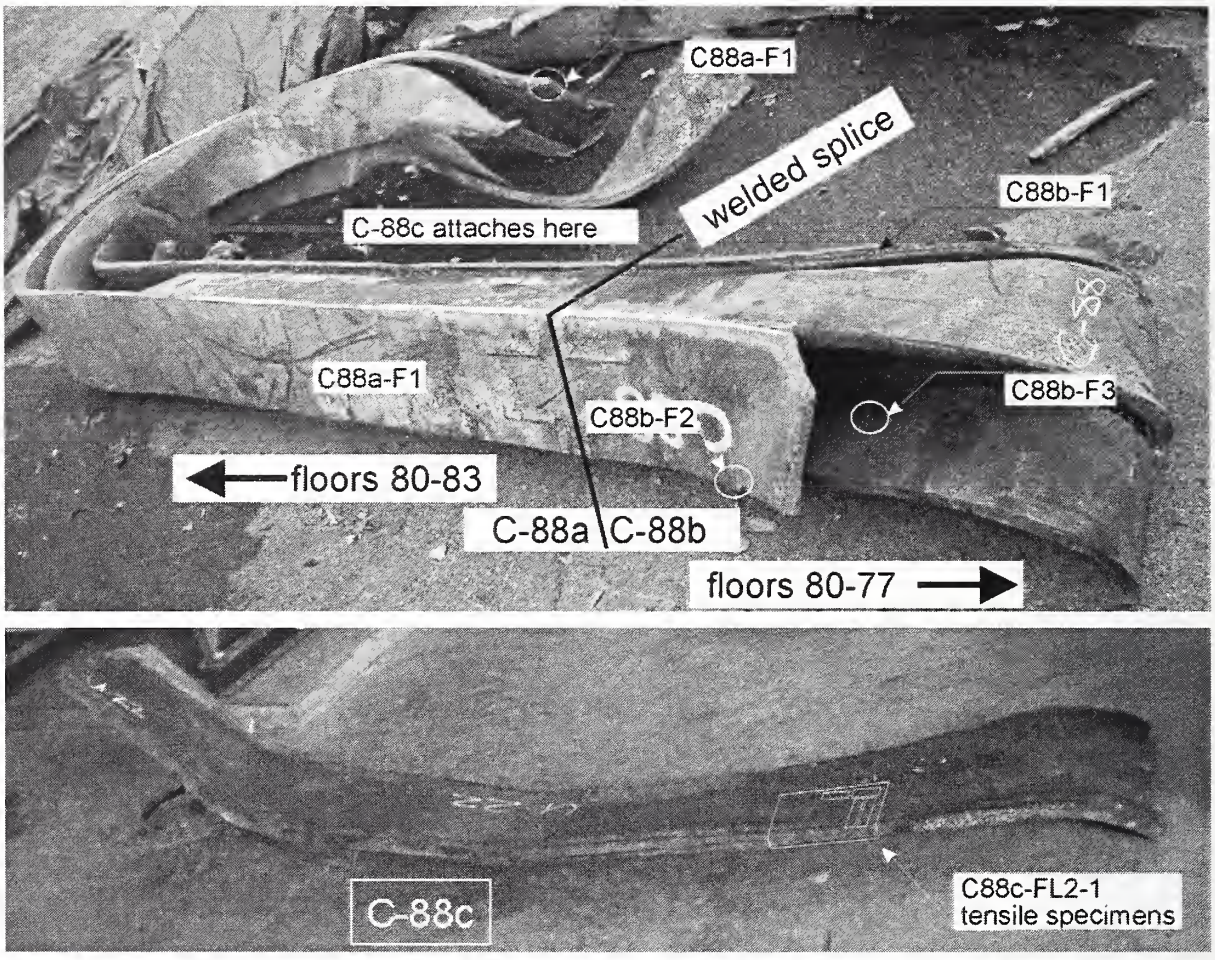

Circled locations denote approximate specimen locations for chemical analysis

Source: NIST.

Figure 3–21. Section of C-88c that is the source of the specimens.

Trusses

Contemporaneous construction documents indicate that Laclede (1968b, 1968c) supplied the steel in the floor trusses to two specifications: A 36 and A 242. Although modern versions of A 242 specify requirements for corrosion resistance, A 242-66 left the buyer and seller to set these requirements. A 36 specifies a minimum yield point, F_y = 36 ksi, while A 242 specifies a higher yield point, F_y = 50 ksi. Table 3–10 summarizes the dimensions of the main truss components, the specifications they were supplied to, and where they were commonly used. Figure 3–22 plots the ratio of the NIST-measured yield strength or yield point to the specified minimum value for all truss steels tested.

The chemistries of all of the truss components tested are consistent with the requirements of both A 36 and A 242. Their strengths all exceed the specified minima. Table 3–11 summarizes the chemistry and mechanical property data for the truss steels.

Table 3–10. Common truss component dimensions and standards.

Specification	Shape	Used For
A 36	3 in. × 2 in. bulb angle	Lower chord of many common 60 ft trusses
A 36	1.09 in. round bars	Main web of many 60 ft trusses
A 36	1 13/16 in. round bars	Unknown
A 242	2 in. × 1.5 in. bulb angle	Upper chord of many common 60 ft trusses Upper and lower chord of many common 36 ft trusses
A 242	0.75 in round bars	Main web of bridging trusses
A 242	0.92 in. 0.98 in. 1.14 in. round bars	Main web of many common 36 ft trusses

Truss Angles

Four of the seven 2 in. × 1.5 in. bulb angles have added vanadium, which makes them similar to a modern A 572 steel. The measured yield strengths of all of the truss angles tested are all $F_y > 50$ ksi, even if they were supplied to A 36, which is consistent with the requirements of both A 36 and A 242. The tensile strength of one of the three bulb angles specified as A 36 exceeds the required maximum by 1 ksi.

Truss Round Bars

The yield strength of an A 36 web round bar with $D = 1.09$ in. is $F_y = 47.4$ ksi. The chemistries of both the $D = 1.09$ in. diameter bars are consistent with the requirements of A 36. The chemistries and mechanical properties of all round bars originally specified as A 242 are consistent with the requirements of that standard.

Table 3–11. Summary of mechanical properties and chemical compositions, and specifications for truss steels tested.

Truss Bulb Angles									
	T1-BA-Plate[a, b]	**C53-TA-1**	**C53-TA-2**	**C132-TA-3**	**C137f-TA-5**	**T-1-TA-Plate[a]**	**C137a-TA-3**	**N8[c]**	**C53-BA3**
C	0.20	0.22	0.18	0.19	0.18	0.18	0.19		0.17
Mn	0.77	0.46	0.84	0.82	0.84	0.86	0.90		0.60
P	0.009		0.024	0.010	0.020	0.016	0.021		0.013
S	0.032	0.028	0.024	0.029	0.020	0.028	0.029		0.040
Si	0.06	0.15	0.04	0.07	0.07	0.04	0.06		0.02
Ni	0.09	0.10	0.08	0.08	0.06	0.08	0.08		0.09
Cr	0.12	0.09	0.10	0.10	0.05	0.12	0.08		0.08
Mo	<0.01	< 0.01	< 0.01	< 0.01	0.01	0.02	0.05		0.01
Cu	0.26	0.48	0.28	0.32	0.22	0.29	0.30		0.32
V	0.036	< 0.005	< 0.005	0.038	< 0.005	0.044	0.043		0.039
Nb	<0.005	< 0.005	0.018	< 0.005	< 0.005	0.009	< 0.005		< 0.005
Ti	<0.005	< 0.005	< 0.005	< 0.005	< 0.005	<0.005	< 0.005		< 0.005
Zr	<0.005	< 0.005	0.011	< 0.005	< 0.005	<0.005	< 0.005		< 0.005
Al	0.045	< 0.005	0.028	0.032	0.038	0.015	0.029		n/d
B	<0.0005	<0.0005	<0.0005	<0.0005	<0.0005	<0.0005	< 0.0005		< 0.0005
N	0.0080	0.0080	0.0010	0.0080	0.0100	0.0066	0.0160		0.0090
dimensions	1.5 in. x 1.25 in.	2 in. x 1.5 in. x 0.25 in.	2 in. x 1.5 in. x 0.25 in.	2 in. x 1.5 in. x 0.25 in.	2 in. x 1.5 in. x 0.25 in.	2 in.x 1.5 in.x 0.25 in.	2 in. x 1.5 in. x 0.37 in.	2 in. x 1.5 in. x 0.25 in	3 in. x 2 in. x 0.37 in.
Spec	A 242	A 242	A 242	A 242	A 242	A 242	A 242	A 242	A 36
Fy (ksi)	n/d	n/d	n/d	58.8	n/d	52.2	n/d	55.5	57.2

Truss Round Bars									
	T1-SR-1	**C53-MR-1**	**C137a-SR-3**	**T1-LR-1[d]**	**C53-LR-1[e]**	**M32-LR-1**	**C106-SR-1**	**A 36-66**	**A 242-66 Type 1[e]**
C	0.20	0.22	0.24	0.21	0.18	0.20	0.21	0.26	0.22
Mn	0.84	0.92	0.99	0.79	0.79	0.86	0.64		1.25
P	0.008	0.018	0.007	0.008	0.018	0.020	0.011	0.04	
S	0.027	0.031	0.025	0.019	0.030	0.032	0.023	0.05	0.05
Si	0.07	0.08	0.08	0.05	0.06	0.07	0.05		
Ni	0.05	0.07	0.08	0.04	0.03	0.08	0.06		
Cr	0.07	0.05	0.11	0.04	0.10	0.06	0.09		
Mo	<0.01	0.03	< 0.01	<0.01	0.01	0.03	0.01		
Cu	0.12	0.22	0.27	0.08	0.27	0.04	0.26		
V	0.035	0.041	0.038	0.038	<0.005	<0.005	0.031		
Nb	<0.005	<0.005	< 0.005	<0.005	<0.005	<0.005	<0.005		
Ti	<0.005	<0.005	< 0.005	<0.005	<0.005	<0.005	<0.005		
Zr	<0.005	<0.005	< 0.005	<0.005	<0.005	<0.005	<0.005		
Al	0.044	0.032	0.033	0.033	<0.005	0.033	0.017		
B	<0.0005	<0.0005	< 0.0005	<0.0005	<0.0005	<0.0005	<0.0005		
N	0.0083	0.0100	0.0110	0.0080	0.0110	0.0100	0.0110		
diameter	0.75 in.	0.92 in.	0.92 in.	0.92 in.	1.09 in.	1.09 in.			
Spec.	A 242	A 242	A 242	A 242	A 36	A 36		A 36	A 242
Fy (ksi)	n/d	n/d	n/d	60.0	47.4	n/d	n/d	36	50

a. From a bridging truss.
b. Thickness approximately 0.23 in.
c. Originally attached to perimeter column N8. Chemistry not determined.
d. Originally assigned as $D = 1.0$ in.
e. Yield point reported. Other alloying elements must be reported.
Key: n/d not determined

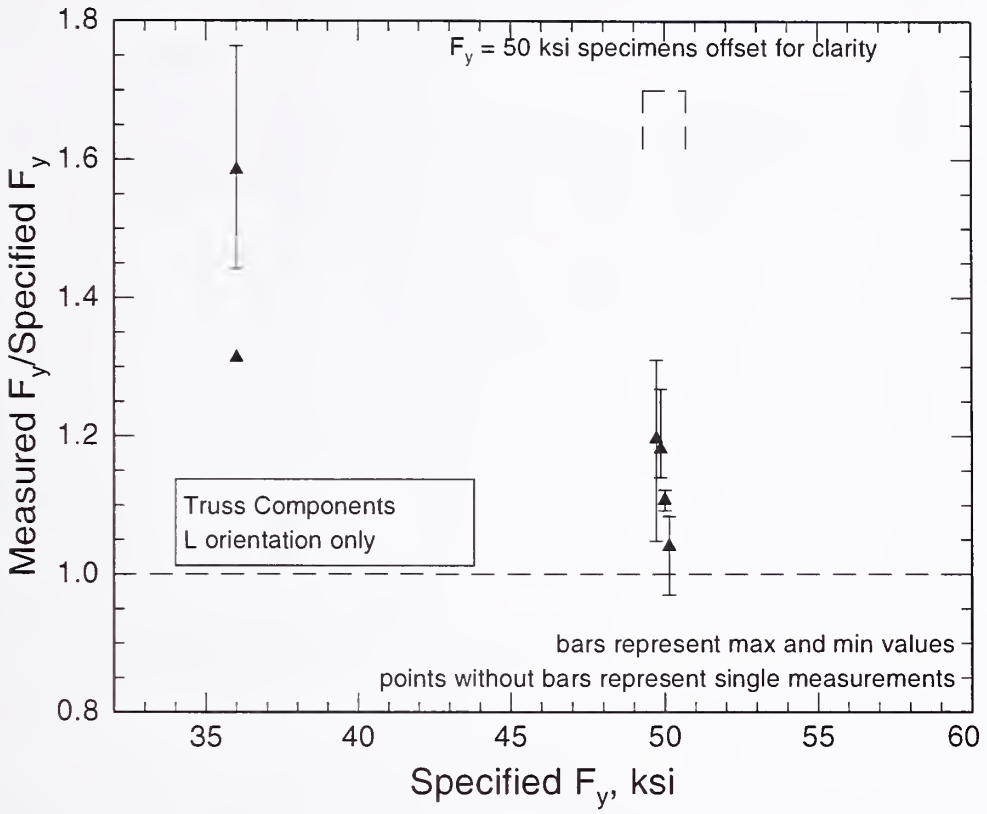

Figure 3–22. Ratio of measured yield strength to specified minimum yield strength for all longitudinal tests of truss steels.

Truss Seats

The structural engineering plans specify that all truss seats were to have a minimum yield strength F_y = 36 ksi. Presumably, the fabricators would have used A 36 steel. The plans do not require that the steel conform to a specific ASTM standard, however. Figure 3–23 plots the ratio of the NIST-measured yield strength or yield point to the specified minimum for all longitudinal tests of truss seat steels. Table 3–12 summarizes the chemistry and yield data for all truss seats characterized. The chemistry data are summarized in terms of averages and ranges because the mechanical data come from one set of specimens and the chemistry data come from another. The chemistries of all the perimeter truss seats characterized are consistent with the requirements of A 36. All the perimeter column truss seats meet A 36 for yield and tensile strength and total elongation. The yield point of the core truss seats (C128-T1) is slightly less than A 36 allows: F_y = 34 ksi. Because of the natural variability in product tests, this slightly low value is not remarkable. One of the other core column truss seats tested is substantially stronger than required: F_y = 58.6 ksi and TS = 82.2 ksi. The tensile strength slightly exceeds the TS = 80 ksi maximum that A 36 allows. This truss seat is strengthened with vanadium, see Table 3–12; the high strength is consistent with the chemistry.

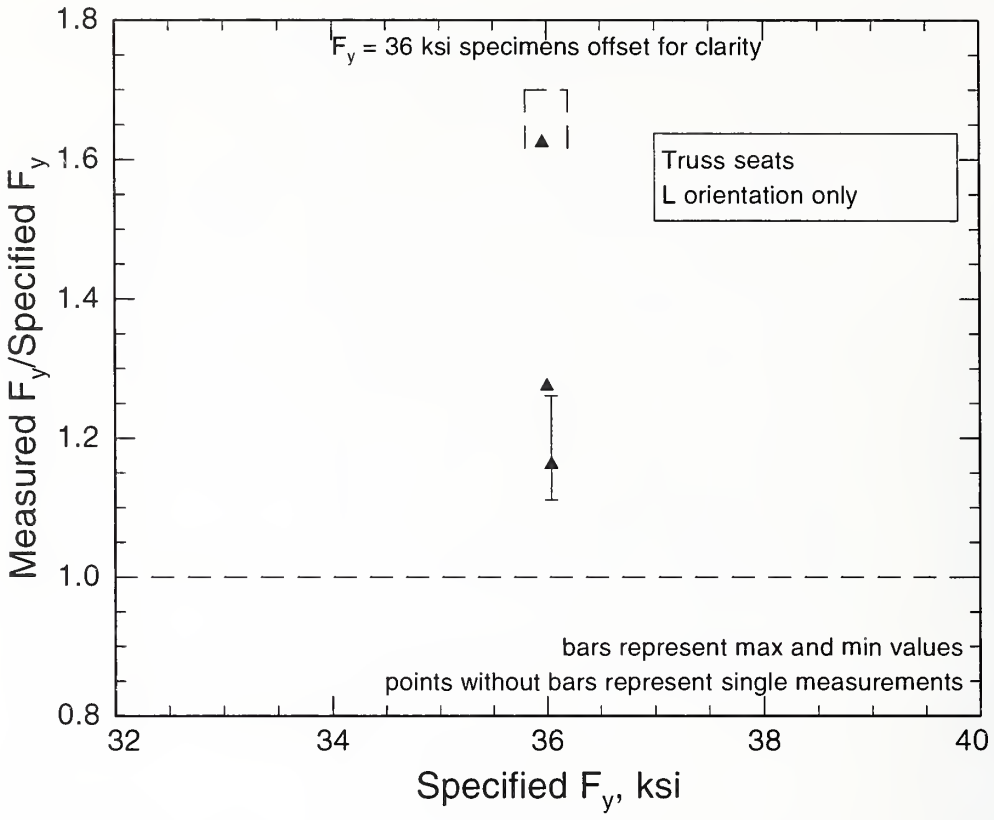

Figure 3–23. Ratio of measured yield strength to specified minimum yield strength for all longitudinal tests of truss seat steels.

3.4.2 Bolts

Table 3–1 summarizes the results of tests of the A 325 and A 490 bolts. The measured strengths exceed the requirements of their respective standards. The chemistry of an A 325 bolt recovered from perimeter panel M-2 is consistent with the requirements of the specification for A 325 Type 1.

3.4.3 Welds

One problem in comparing weld properties to those reported in fabrication documents is that the fabrication documents usually reference welding procedure data. These data are taken from test welds with very large gaps between the base plates. The advantage of this large gap is that it makes it easy to remove mechanical test specimens (tensile, impact and bend) that are purely weld metal, and so accurately reflect the performance of the weld metal itself. The disadvantage is that this large gap does not simulate the conditions of the production weld in the component, where dilution of the weld with some of the base metal will change its properties. The change is usually to higher strength since the carbon content in the base metal, which is higher than that of the filler metal, increases the hardenability of the weld composition.

Table 3–12. Summary of mechanical properties, chemical compositions for truss seat steels tested.

	Perimeter Seat Chemistry							
	Average %	Max %	Min %	N8-C1B1	N9-C1T1	N99-C1B	M34-TS-A-L5 %	C128-T1 %
C	0.19	0.24	0.16				0.24	0.19
Mn	0.44	0.47	0.41				1.16	0.83
P	0.006	0.008	<0.005				0.013	0.01
S	0.022	0.030	0.015				0.006	0.005
Si	0.06	0.07	0.06				0.05	0.038
Ni	0.09	0.16	0.06				0.022	0.014
Cr	0.07	0.10	0.05				0.053	0.018
Mo	<0.01	<0.01					0.035	0.02
Cu	0.24	0.32	0.20				0.27	0.027
V	<0.005	<0.005					0.048	0.002
Nb	(a)	0.046	<0.005				0.002	n/d
Ti	<0.005	<0.005					0.002	n/d
Zr	<0.005	<0.005					n/d	n/d
Al	(b)	0.034	<0.005				n/d	n/d
B	<0.0005	<0.0005					n/d	n/d
N	0.0090	0.0280	0.0040				n/d	n/d
Description	Perimeter seat	Perimeter seat	Perimeter seat	Perimeter seat[c, e]	Perimeter seat[c]	Perimeter seat[d]	Core seat	Core seat
Specification				A 36	A 36	A 36	A 36	A 36
F_y (ksi)				40.7	40.9	41.1	58.6	34.0
Yield behavior				YP	YP	YP	YP	YP

a. One specimen with [Nb] =0.046 percent, all others <0.005.
b. One specimen with [Al]=0.034 percent, all others < 0.005.
c. Longitudinal orientation.
d. Transverse orientation.
e. Two of three specimens have YP.
Key: n/d. not determined; NYP: no yield point behavior; YP. yield point behavior in stress-strain curve.
Notes: Chemistry averages based on 7 specimens of perimeter truss seats not characterized for strength. Chemistry expressed in mass fraction.

Welds in the Perimeter Columns

The perimeter column panels were large and complicated, so a variety of welding processes were used during the various steps in their fabrication. Although welding procedures were sometimes changed during the construction (SHCR 1968), the floors that the aircraft struck appear to have been constructed using gas-shielded flux-core electrodes to make the butt welds that joined the spandrels to the inner web of the panels, shielded-metal-arc electrodes for tacking the diaphragm plates inside the columns, tandem submerged arc to make the long longitudinal fillet welds that formed the box shape, and a combination of flux-core and shielded-metal-arc electrodes to finish the ends (PCF 1967).

Pacific Car and Foundry requested permission (SHCR 1968) to change to a different flux-cored electrode that produced F_y = 84.5 ksi, TS = 94.5 ksi, total elongation El_t = 24 percent, and impact toughness of 52 ft·lbf at 0 °F, when welded with 14 passes on 0.75 in. thick plate. Apparently, they wished to use this electrode for the butt welds that connected the spandrels to the inner web. It is likely that they used this procedure for the columns at the level of impact. Pacific Car and Foundry's welding procedure (PCF 1967) specifies a series of weld strength ranges that correspond to the base metal strength ranges, and typical properties of the flux-cored electrodes to be used.

Similarly, the submerged-arc fillet welds used two types of flux, one with higher alloying levels, to produce two strength levels: F_y = 81 ksi, TS = 92.3 ksi, and F_y = 105 ksi, TS = 118 ksi (PCF 1967). The lower-strength flux would have been specified for the F_y = 55 ksi (nominal) strength of perimeter column N-9 (WTC 1, column 154). These procedure data compare well with the measured strengths for a fillet weld in N-9 of F_y = 85.1 ksi, TS = 103 ksi, and F_y = 84.8 ksi, TS = 103.3 ksi. The strengths are slightly higher than those listed in the procedure document (F_y = 81 ksi, TS = 92.3 ksi), probably because of dilution of the weld by the higher-carbon base metal.

Tests of the transverse strength of the perimeter columns at the region of the fillet welds in column N-8, Table 3–3, show that the weld region was stronger than the adjacent plate material. With the weld metal milled from the surface of the flange, the failure occurred outside the weld region. Without the weld removed, the failure occurred at the weld root, indicating that residual stress or geometrical effects explain the rips that occurred adjacent to the longitudinal welds in many of the recovered columns.

Together, these transverse data provide a measure of the strength and ductility of the longitudinal fillet welds in the columns. Since none of these transverse specimens actually broke in the weld, the results are not a true measure of the weld strength, but rather of the weakest region across the entire joint (base metal to weld to base metal). The failure location, which is adjacent to the weld, matches the general observations on the recovered sections, where rips progressed through the regions adjacent to the welds, but seldom through the welds.

Welds in the Core Columns

The longitudinal fillet welds used to fabricate the core box columns from plates tended to be much smaller than the plates. An example (Stanray Pacific 1967) is a nominal 5/8 in. fillet used to join a 1 in. thick A 36 plate to a 1.25 in. thick A 36 plate using a tandem submerged arc weld. The average shear load at failure for two transversely loaded fillet weld tests was 42,400 lbf per linear inch. The equivalent shear strengths, calculated using the actual cross-sectional areas, are 82.9 ksi and 84.9 ksi. Stanray Pacific also measured longitudinal shear loads for these fillet welds of 25,600 lb per linear inch and 26,200 lbf per linear inch in two tests. Another document, (Stanray Pacific, undated) provides transverse fillet weld property data on a 0.5 in. triple-wire submerged-arc weld used to join a 1.5 in. A 36 plate to a 1.25 in. plate to fabricate a column. Just over 5 linear inches of this weld failed at 236,000 lbf, for a shear load of 45,900 lbf per linear inch.

Because submerged arc welding was not suitable for the ends of the columns or for the tack welds used to align plates during construction. Stanray Pacific (1967b) used a self-shielded FCAW electrode for these locations, with E7018 used as a root pass when full penetration welds were required. The weld procedure was developed on a 1.25 in-thick plate with a 20 degree bevel on a butt weld, and a root gap of 0.5 in.

Two transverse tensile tests gave tensile strengths $TS = 84.4$ ksi (failure in the HAZ) and $TS = 84.25$ ksi (failure in the weld). The wide gap also permitted determination of the all-weld-metal tensile strength $TS = 81$ ksi.

Welds in the Trusses

Truss T1 is built from 2 in. × 1.5 in. × 0.25 in. thick bulb angle with a 0.92 in. diameter rod. The manufacturer, Laclede (1968) designated this resistance weld assembly as type R-21. Unfortunately there are no strength data for this assembly type, but it is very similar to several others for which data do exist. Extrapolating from the data for R-12 (56,900 lbf) and R-17 (56,800 lbf) suggests an average load at failure of 56,700 lbf for the R-21 assembly (per the manufacturers shear test procedure). This procedure was based on loading of an entire and intact truss.

The shear load of 104,000 lbf in the test of the section from truss T1 is significantly higher than the 56,700 lbf suggested by the manufacturer's data. Some strengthening may have occurred by aging during the lifetime of the truss. The different test methods between the manufacturer, who tested an entire truss with a slightly different loading geometry, and NIST is another possible source of the difference, but the measured load at failure is still higher than expected.

There were a few non-resistance welds in the trusses, primarily fillet welds near the ends, but the weld geometry of these welds was not suitable for test. However, documents (Laclede 1969) provide weld strength data from procedure and welder qualification tests for both shielded-metal-arc and flux-cored-arc electrodes. They indicate shear strengths of 6.8 ksi/in to 7.5 ksi/in for about 9 in. of a 1/8 in. fillet weld (total shear load of 60,500 lbf to 67,000 lbf) produced with an E7018 shielded metal arc electrode, and about 9 ksi/in for about 9 in. of a 1/8 in. fillet weld (total shear load near 80,000 lbf) produced with a fluxed cored electrode.

3.5 MECHANICAL PROPERTY VALUES

3.5.1 Steel

Early in the Investigation, other NIST Investigation Team members requested estimates for the stress-strain behavior of the many WTC steels. Responding to these requests in a timely manner necessitated estimating some properties based solely on historical averages, rather than on experimentally determined properties. Experimental measurements on recovered steels formed the basis for estimating the stress-strain behavior for perimeter column and truss steels. The stress-strain curves for core column steels, however, are based mostly on literature estimates of the properties of WTC-construction era plates and shapes.

Estimating the constitutive behavior of the WTC steels required two steps. The first step was to make the best estimate of the yield strength for each grade of steel by combining measured values, literature estimates of expected properties, and historical mill test reports. The second step was to estimate the work-hardening behavior for each grade using stress-strain relations measured from WTC steels, because work-hardening behavior is not available in the literature for any WTC steel.

For step 1, two types of correction are necessary to estimate the yield strength for input into a constitutive model. The first is to correct the experimentally derived or mill test report data for artifacts of testing.

These corrections are expressed as factors to be added to the measured yield strengths. If only the specified minimum yield strength is available, a second type of correction is necessary. This was the case for the core column steels at the time that the modeling groups needed the constitutive behavior. In this case, correction must be made for the fact that the yield strength of the as-supplied steel exceeds the specified minimum. This correction is expressed as a multiplicative correction factor to the specified minimum yield.

An important additive correction to the estimated yield strength is necessary because the experimental and mill test report values are enhanced because the tests are not conducted at zero strain rate (Beedle 1960). Properly, the yield strength in a mill test report or experimental determination is a dynamic yield strength, σ_{yd}. For modeling building performance, the appropriate strength is the static, or zero strain rate, yield strength σ_{ys}. Starting from the static yield strength, all the strength enhancements due to strain rate effects, such as produced in the aircraft impact, can be calculated. From tests on several different structural steels, Rao et al. (1963) estimated that for strain rates, $16\times10^{-4}\,\mathrm{s}^{-1} > \dot{\varepsilon} > 2\times10^{-4}\,\mathrm{s}^{-1}$, the difference between and static, σ_{ys}, and dynamic σ_{yd}, yield strength can be represented by

$$\sigma_{ys} - \sigma_{yd} = -\left(3.2 + 1000\dot{\varepsilon}\right) = k_{\text{dynamic}}, \qquad 3\text{–}1$$

where the strain rate, $\dot{\varepsilon}$, is measured in inverse seconds, and the strengths are measured in ksi. Rao (1963) measured the static yield strength by straining the specimen past yield, and then locking the actuator. With the actuator locked, the load drops slightly at nominally constant strain. This constant value is the static yield strength, σ_{ys}. The difference between the static and dynamic yield strengths, termed k_{dynamic}, is an additive correction factor, which is less than zero. Galambos (1978) used this relation to estimate the properties of structural steel for use in Load and Resistance Factor Design (LRFD). In computing the static yield strength for this Investigation, the strain rate in mill test reports is assumed to be $6\times10^{-4}\ \mathrm{s}^{-1}$, and the strain rate in NIST-conducted tests is assumed to be $3.3\times10^{-4}\ \mathrm{s}^{-1}$.

For estimating the yield strength of steel in rolled wide-flange shapes, it is necessary to make an another additive correction for the variation in yield strength with location from which the test specimen is taken. During the WTC era, but not currently, ASTM standards specified that the test specimen for the mill test report be taken from the web section (in the "cross bar" of an "H" shaped specimen) of the rolled shape, rather than the flange. In typical rolled shapes, however, the flange is thicker than the web, and accounts for most of the load-carrying capacity of the column. Because it is thicker, it cools more slowly from the rolling temperature, and its yield strength is generally lower than the web. Many studies, summarized by Alpsten (1972), have characterized this strength difference between web and flange as 2 ksi to 4 ksi for nominally 36 ksi shapes. It was not uncommon for the measured yield strength of a flange to be 1 ksi to 2 ksi below the specified nominal value reported in the mill test report for samples from the web. The correction for variation with location, k_{flange}, is also an additive correction factor:

$$\sigma_y^{\text{flange}} - \sigma_y^{\text{web}} = k_{\text{flange}}. \qquad 3\text{–}2$$

When insufficient experimental or mill test report data are available for a steel grade, it is necessary to use a second, multiplicative correction factor to estimate the yield strength from the historical averages of that grade. During the 1960s and 70s, several studies (AISI 1973; Galambos 1976; Alpsten 1972) characterized the variability in properties of steels supplied to various standards. These studies answered questions like, "What is the mean value of the yield strength of the plates or shapes that meet A 36?"

They answered this question by examining thousands of mill reports, but not by doing independent product testing. Because the tension test to certify the mechanical properties is conducted near the end of the production process, scrapping a heat of steel because it did not meet the intended specification is undesirable. Thus, steel mills generally strive to make steels in which the strength exceeds the intended specification. Typically, the yield strengths in the mill reports from the WTC-construction era exceed the specified minimum values by 5 percent to 10 percent. The exact value depended on the specified minimum yield strength, and whether the steel was supplied as plates or shapes. Of course, the yield strength in the mill report will never be less than the standard calls for, because the steel could not have been sold as meeting the standard. The results of these studies are necessary in estimating the properties of WTC steels when no other corroborating evidence is available.

The correction, k_p, from specified minimum to historical average yield strength is a multiplicative factor. For example, for rolled plates, the mean yield strength from the mill test reports, *YS*, is

$$YS = k_p F_y , \qquad 3\text{–}3$$

where F_y is the specified minimum yield strength.

Estimating the yield strength of a given WTC steel requires some or all of these three correction factors. The static yield strength, σ_{ys}, for perimeter columns and truss steels was calculated from the average value of the NIST-measured yield strengths, *YS*, corrected for dynamic effects.

$$\sigma_{ys} = YS + k_{\text{dynamic}} , \qquad 3\text{–}4$$

where k_{dynamic} is calculated from Eq. 3–1. Where mill test report data exist for a grade of perimeter column steel, these data were combined with the NIST-measured data. No correction for location effects or historical averages was necessary.

The static yield strength for rolled shapes was calculated using the expected historical value from literature data (Alpsten 1972) rather than the measured values, with correction for dynamic and location effects:

$$\sigma_{ys} = k_s F_y + k_{\text{dynamic}} + k_{\text{flange}} , \qquad 3\text{–}5$$

where F_y is the specified minimum yield strength, The factor $k_s = 1.2$ corrects for the fact that, historically, the mill test report value of the yield strength of rolled shapes exceeds the specified minimum value by 20 percent. (Alpsten, 1972). The factor $k_{\text{flange}} = -2.6$ ksi corrects for the fact that, until recently, the specimen for the mill test report came from the higher-strength web, but the flange represents the majority of the load-carrying area. The factor k_{dynamic} is calculated from Eq. 3–1.

For core rolled plates no correction for location effects was necessary:

$$\sigma_{\text{ys}} = k_p F_{\text{y}} + k_{\text{dynamic}} , \qquad 3\text{–}6$$

where $k_p = 1.092$ (Alpsten 1972). Table 3–13 summarizes the estimated static yield strengths for all the steels in the fire and impact zones.

The second step in estimating constitutive behavior was to estimate the work hardening of the steel after yield. There is no historical or literature information on work hardening behavior of WTC steels, so the work hardening behavior for all WTC steels was modeled using stress-strain data generated in the Investigation. Early in the Investigation, based on requests from other Investigation Team members, NIST selected the Voce hardening law to represent the increase in stress, σ, with plastic strain, ε_p, in the plastic regime. In this hardening rule the flow stress, σ, reaches a limiting stress, R_∞, with an exponential decay:

$$\sigma = R_0 \varepsilon_p + R_\infty \left(1 - \exp\left(-b\varepsilon_p\right)\right) \qquad 3\text{–}7$$

This relation is available in most finite element packages.

Table 3–13. Estimated static yield strengths and work-hardening parameters, Eq. 3–5, for perimeter column steels.

Description	F_y ksi	σ_{ys} ksi	TS ksi	ε_{max}[a]	b	R_∞ ksi	R_0 ksi
All F_y =36 ksi perimeter column steels in plates 1 2 4 (i.e.. not inner plate – plate 3)	36	35.6	61.2	0.190	30.337	24.467	67.973
All F_y =45 ksi perimeter column steels in plates 1 2 4 (i.e.. not inner plate – plate 3)	45	53.1	74.9	0.153	24.965	27.198	62.245
All F_y =50 ksi perimeter column steels in plates 1 2 4 (i.e.. not inner plate – plate 3)	50	54.0	75.6	0.220	28.659	27.870	74.790
All F_y =55 ksi perimeter column steels in plates 1 2 4 (i.e.. not inner plate – plate 3) with thickness $\leq$ 1.5 in.	55	60.8	82.6	0.259	18.479	24.698	76.770
All F_y =60 ksi perimeter column steels in plates 1 2 4 (i.e.. not inner plate – plate 3) with t $\leq$ 1.25 in.	60	62.0	87.3	0.176	27.535	24.543	74.925
All F_y =65 ksi perimeter column steels in plates 1 2 4 (i.e.. not inner plate – plate 3) with t $\leq$ 0.5 in.	65	69.6	90.4	0.138	38.284	23.847	89.520
All F_y =70 ksi perimeter column steels in plates 1 2 4 (i.e.. not inner plate – plate 3)	70	76.7	92.0	0.103	19.499	26.777	10.714
All F_y =75 ksi perimeter column steels in plates 1 2 4 (i.e.. not inner plate – plate 3)	75	82.5	96.8	0.070	29.008	17.463	17.826
All F_y =80 ksi perimeter column steels all plates	80	91.5	99.4	0.079	32.567	14.203	29.522
All F_y =85 F_y =90 F_y =100 ksi perimeter column steels, regardless of plate	85	104.8	116.0	0.081	13.857	32.500	1.793
Perimeter Plate 3 (inner web)	42	42.6	67.2	0.153	24.974	26.843	62.110
Perimeter Plate 3 (inner web)	45	45.9	69.8	0.153	24.977	26.785	62.147
Perimeter Plate 3 (inner web)	50	51.4	74.2	0.220	28.777	24.729	73.369
Perimeter Plate 3 (inner web)	55	56.9	78.5	0.259	18.455	25.244	76.857

Description	F_y ksi	σ_{ys} ksi	TS ksi	ε_{max}[a]	b	R_∞ ksi	R_θ ksi
Perimeter Plate 3 (inner web)	60	62.4	82.9	0.176	27.547	24.298	74.922
Perimeter Plate 3 (inner web)	65	67.9	87.3	0.138	38.407	21.774	88.546
Perimeter Plate 3 (inner web)	70	78.9	96.0	0.070	31.698	29.734	0.000
Perimeter Plate 3 (inner web)	75	78.9	96.0	0.070	31.698	29.734	0.000

a. ε_{max} is the true strain at the tensile strength, *TS*.

The procedure for determining the parameters of Eq. 3–7 was multi-step:

1. For each experimental stress-strain curve for a given steel, remove yield point and yield point elongation or truncate curve at the 0.2 percent offset yield strength for stress-strain curves without this yield point behavior.

2. Truncate the curve at the tensile strength, *TS*, which is the beginning of necking.

3. Shift the stress-strain curve to zero stress and strain.

4. Fit the parameters of Eq. 3–7 to the resulting curve segment.

5. For the set of replicated tests, determine the smallest of the strains at tensile strength, ε_{max}, which is the point at which necking begins.

6. Create a fitted plasticity curve for each experimental curve that terminates at ε_{max}.

7. Numerically average each family of fitted curves at each strain point to produce an average behavior.

8. Refit the parameters of Eq. 3–7 to the average curve produce the average work-hardening properties.

Tables 3–13 and 3–14 and Figs. 3–24 to 3–27 summarize the representative tensile stress-strain curves for the 33 WTC steels characterized in the Investigation. The elastic portion of those curves use the value of elastic modulus (205 GPa = 29.7 Msi) extended to the value of the static yield strength. The strain at which this occurs will be close to, but not equal to the 0.2 percent offset yield strength, *YS*.

3.5.2 Bolts

The vertical column connections between exterior wall panels were fastened using either four or six high-strength bolts, depending on the vertical location on the building. The bolts were specified to conform to either the ASTM A 325 or A 490 standards. The joints lower on the building were generally composed of six A 490 bolts, and those higher up of four A 325 bolts. These bolt types are designed for use in general structural assembly in buildings and other structures, and are not designed for either high-temperature or severe environmental exposure.

Bolts are characterized by a smooth section, the shank, and a threaded section. Because the two sections have different diameters, the load bearing section is not uniform along the length of the bolt. As a

consequence, the tensile stresses that each section of the bolt feels are not uniform, and are higher in the threaded area. In addition, the threads complicate the characterization of the mechanical behavior in three ways. First, the roots of the threads concentrate stresses in those areas and cause preferential locations for both plastic flow and fracture initiation. Second, the interaction of the bolt threads and the nut threads in making the mechanical joint is complex. The first three or four threads toward the bolt shaft take up most of the load of the joint. Finally, the threads deform under shear, rather than under tension, Fig. 3–28. These peculiarities both require the mechanical properties of bolts to be specified differently from ordinary structural steel and introduce additional variations in bolt performance in service.

The use of stress-strain constitutive behavior to describe the mechanical behavior of bolts does not fully capture their behavior. The aforementioned effects of the threads in localizing plastic response require that the mechanical behavior be described in terms of load-elongation curves from a tensile test of an actual bolt and nut sample. Nevertheless, for each bolt diameter ASTM A 325 specifies a minimum tensile strength in pounds derived from a minimum tensile strength, TS = 120,000 ksi, calculated on the load-bearing area in the threads for bolts less than 1.125 in. diameter. For ASTM A 490 bolts, the standard specifies minimum values for yield strength, F_y, tensile strength, TS, total elongation to failure and reduction of area, ROA. Tests on A 490 bolts are conducted on specimens machined from the bolts rather than on the bolts themselves.

Table 3–14. Estimated static yield strengths and work-hardening parameters, Eq. 3–5, for core column and truss steels.

Description	F_y ksi	σ_{ys} ksi	TS ksi	ε_{max}[a]	b	R_∞ ksi	R_0 ksi
Truss rounds specified as A 36	36	38.1	59.6	0.126	20.523	31.539	0.000
Truss angles (regardless of ASTM specification) and all rounds specified as A 242	36	55.3	74.1	0.190	31.113	20.583	64.369
F_y =36 ksi core WF shapes	36	37.0	n/d	0.190	30.337	24.467	67.973
Core Group 1&2 shapes	42	53.8	n/d	0.202	23.023	32.116	30.495
Core Group 3 shapes	42	49.0	n/d	0.202	23.023	32.116	30.495
Core Group 4&5 shapes	42	44.2	n/d	0.202	23.023	32.116	30.495
Core Group 1&2 shapes	45	53.8	n/d	0.202	23.023	32.116	30.495
Core Group 3 shapes	45	49.0	n/d	0.202	23.023	32.116	30.495
Core Group 4&5 shapes	45	47.8	n/d	0.202	23.023	32.116	30.495
Core Group 1&2 shapes	50	53.8	n/d	0.202	23.023	32.116	30.495
Core Group 3 shapes	50	53.8	n/d	0.202	23.023	32.116	30.495
All 36 ksi core box column steels	36	36.7	64.5	0.204	21.723	30.729	58.392
Core Plates with $t \leq 0.75$ in.	42	51.4	n/d	0.202	23.023	32.116	30.495
Core Plates with 0.75 in. $< t \leq 1.5$ in.	42	47.0	n/d	0.202	23.023	32.116	30.495
Core Plates with 1.5 in. $< t \leq 4.0$ in.	42	42.6	n/d	0.202	23.023	32.116	30.495

Key: n/d, not determined.

a. ε_{max} is the true strain at the tensile strength, TS.

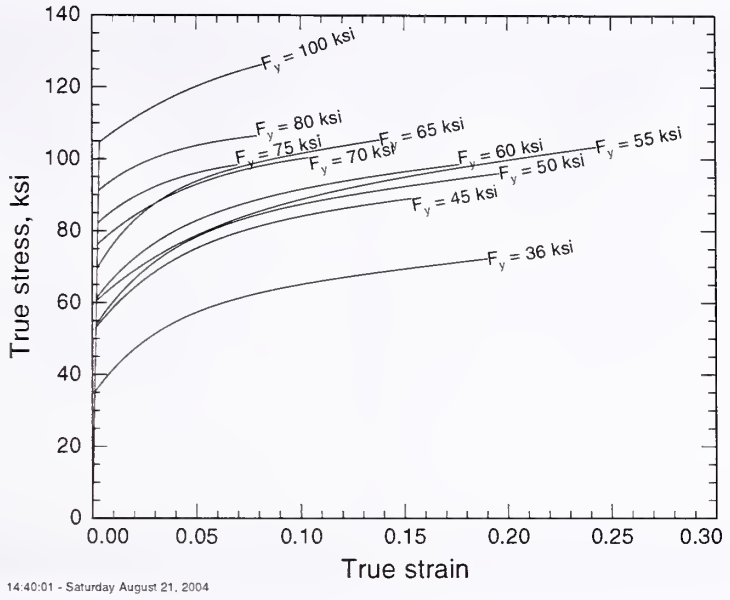

Figure 3–24. Representative tensile stress-strain behavior for perimeter column steels from flanges, outer webs, and spandrels (plates 1, 2, and 4).

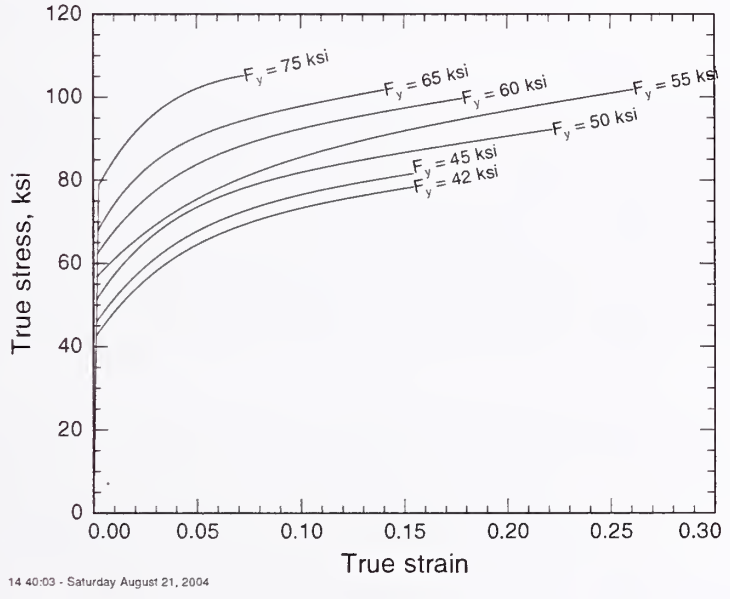

Figure 3–25. Representative tensile stress-strain behavior for perimeter column steels from inner webs (plate 3).

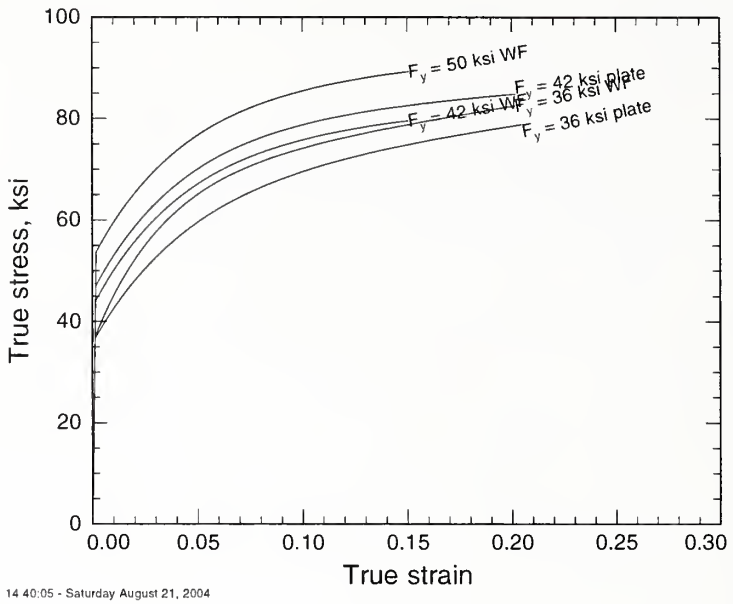

Figure 3–26. Representative tensile stress-strain behavior for selected core column steels.

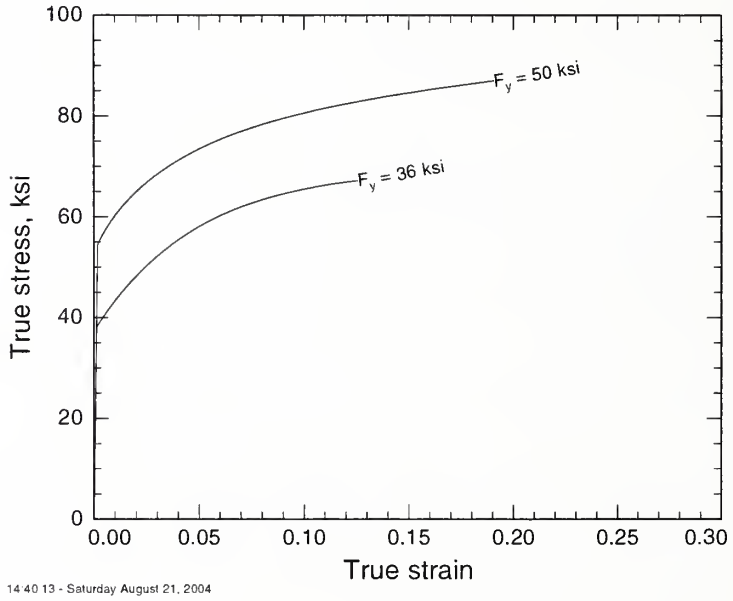

Figure 3–27. Representative tensile stress-strain behavior for truss steels.

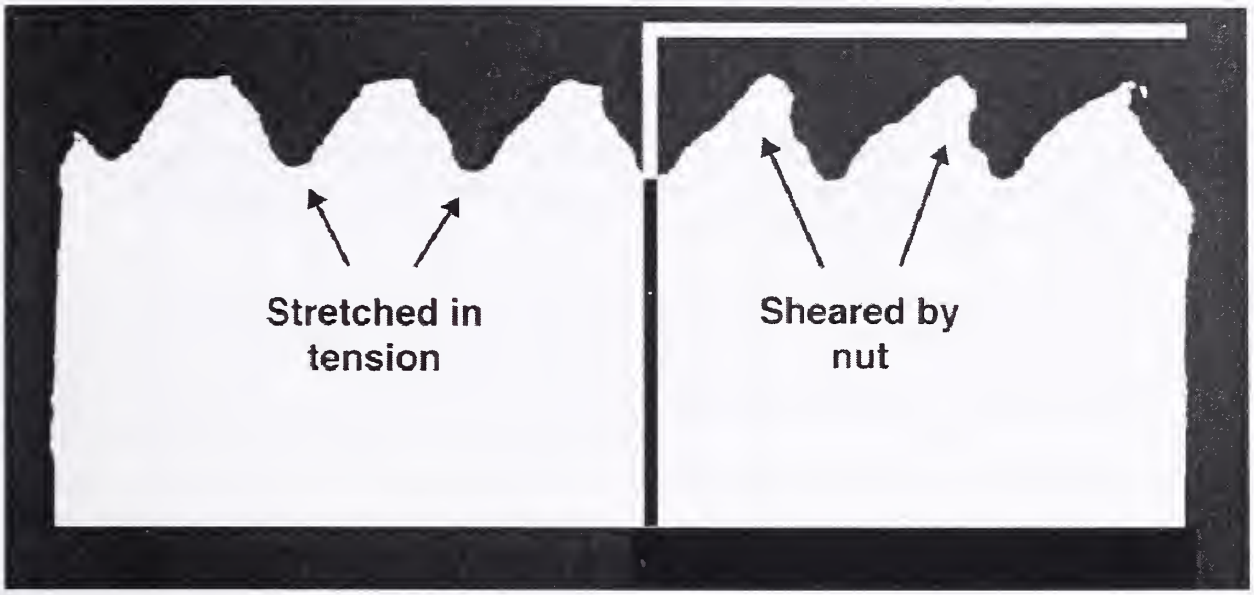

Figure 3–28. Representation of deformation that occurs in exposed bolt threads (left) and in bolt threads coupled with nut threads (right).

In simulating the response of the bolts as a feature of the finite element model, one would take stress-strain behavior measured for the base metal of the bolt, mesh the bolt with all of its non-uniformities, and then generate the load-displacement behavior up to failure. However, it is easier and more accurate to simply test bolts in tension and supply the actual load-displacement curves.

Figure 3–15, a plot of the four load-displacement curves for the A 325 bolts, shows that the bolt strength is independent of the strain rate. The high-rate Kolsky bar tests and quasi-static compression tests on specimens taken from the same bolt, described in Chapter 4, produced similar results. In consequence, an average load-displacement curve was calculated from all four tests and is plotted in bold. This average curve was produced by calculating the average failure displacement for the four tests, then modifying each curve by truncating at or extending to this displacement (in the case of extension, using a spline fit). The load values of the four tests were then averaged to produce the bold curve, which should be used in calculating the mechanical response of the bolted joints at room temperature.

Relatively few experimental studies of A 325-type bolts have been published. Rumpf and Fisher (1963) presented load-elongation data for A 325 bolts and measured the actual change in length of the bolt during the test. Other studies (Kirby 1995, Li 2003, Sakumoto 1993, Salih 1992) reported proof loads or failure loads while investigating temperature or other effects on strength.

The tensile strengths of A 325 bolts from the WTC towers, Table 3–1, are higher than measured in previous studies and much larger than the A 325 specification. The average tensile strength of the WTC A 325 bolts is (67,700±300) lbf, or 22 percent greater than the specified minimum. The failure loads taken from ten batches of 7/8 in. bolts in the 1960s (Rumpf 1963) range from 53,000 lbf to 67,500 lbf with an average of 58,500 lbf or 10 percent greater than the specified minimum. When Rumpf et al. conducted these tests, the A 325 standard was based on TS = 115,000 lbf, so the specified minimum tensile load was 53,200 lbf. The strength of the WTC bolts is comparable to the 1990s era 7/8 in. A 325

bolts characterized by Salih et al. (1992), whose mean tensile strength was (65,000± 400) lbf, or 17 percent greater than the specified minimum.

Bolt strengths that exceeded the requirements of A 325 were apparently quite common, but the high values for the WTC bolts are unexpected. Use of the literature values for the bolt strengths in the models would under predict the strength of the vertical perimeter column connections, and might tend to incorrectly predict a global collapse mode.

Studies in the literature have established the effect of the number of exposed threads above the nut on both ultimate load and elongation of the bolt. Figures 3–29 and 3–30 show the results from the literature studies graphically. Because bolts have a non-uniform cross section, deformation tends to concentrate within the exposed threads above the nut. Increasing the number of exposed threads increases the length over which this deformation occurs and increases the total elongation to failure. Exposing fewer threads has the opposite effect. In terms of critical load at failure, the threads act as stress concentrators, and failure will occur at the location within the threads that has the greatest stress concentration. Increasing the number of exposed threads increases the number of stress concentrators, and increases the chance of loading a more severe stress concentrator, which produces failure at lower loads. The data of Rumpf et al. (1963) indicate that the linear strength decrease stops above nine exposed threads, however.

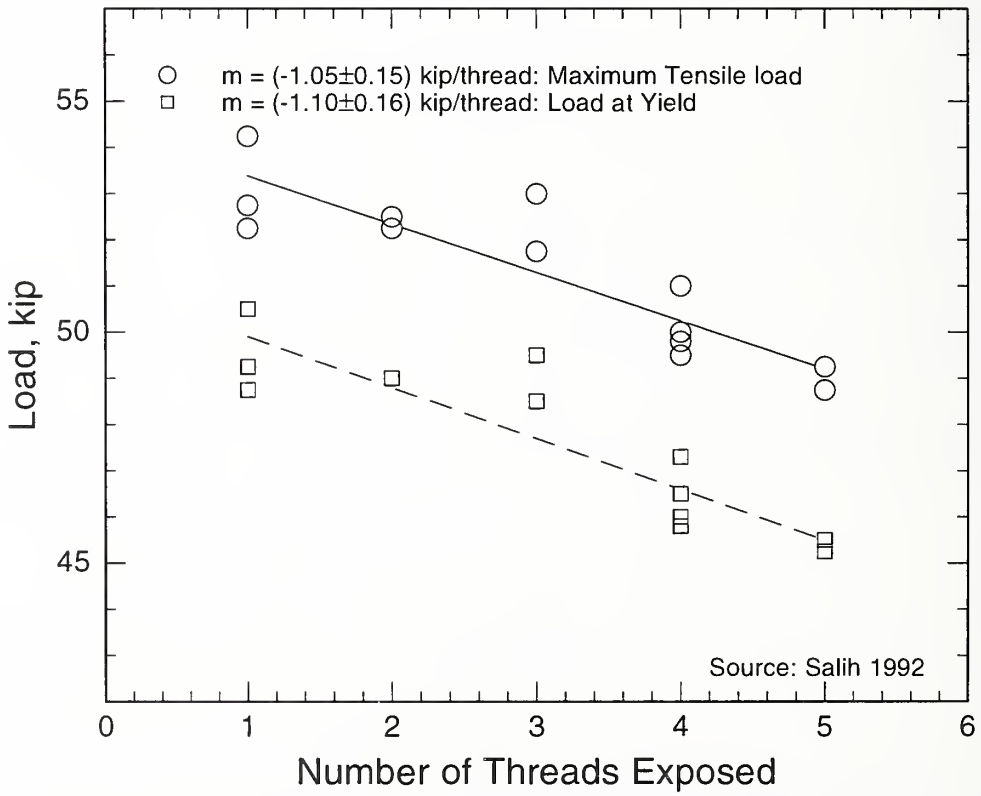

Figure 3–29. Tensile strength change of A 325 bolts with exposed thread length.

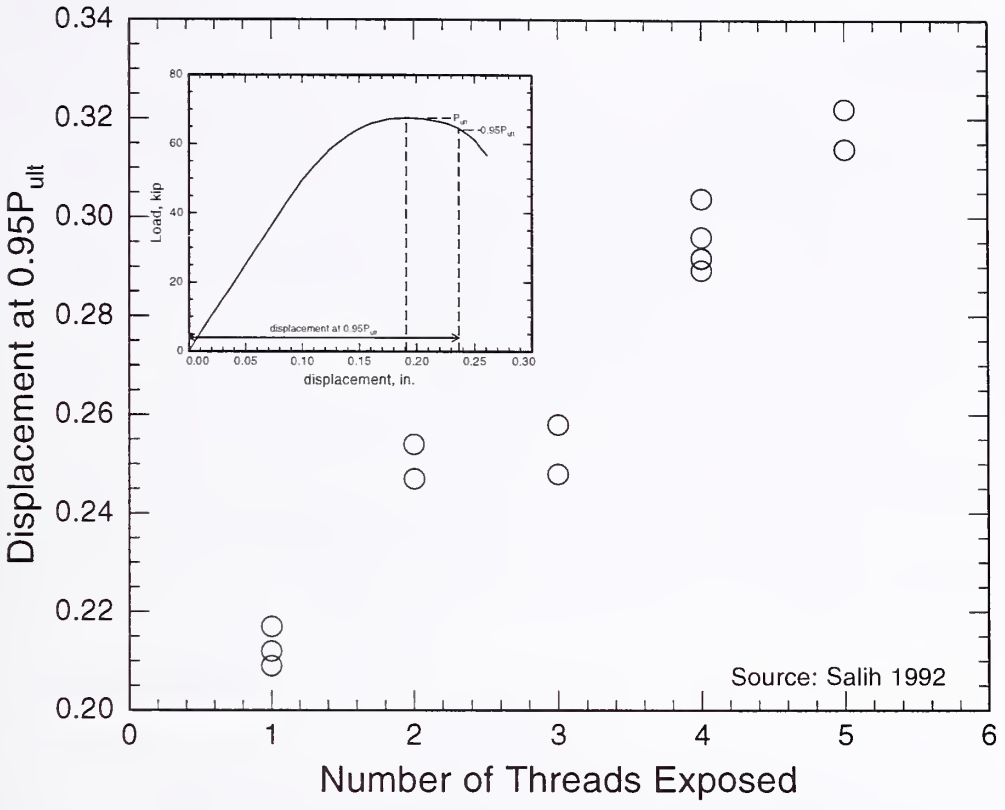

Figure 3–30. Displacement near failure of A 325 bolts as a function of number of threads exposed.

The Investigation generally followed the procedures in ASTM F 606 for testing threaded fasteners which mandates leaving four threads exposed during the load-displacement test of heavy head bolts. The study deviated from F 606 in that only two threads were exposed, which is an average value of the number of exposed threads on failed bolts seen in the WTC recovered components. During the WTC construction era, A 370 governed the test requirements for A 325 bolts, and mandated six exposed threads. In the absence of other data, it is reasonable to assume that the statistical variation of the percent change in strength with thread exposure is the same as literature values from contemporary materials.

The slopes of the linear portions of the experimentally measured load-displacement curves are significantly lower than those published in the literature. Both Rumpf (1963) and Salih (1992) used an extensometer on the bolt. The data of Fig. 3–15 represent the displacement of the crosshead of the testing machine, which includes the elastic compliances of the load frame, grips, etc. To reproduce the load-displacement curve of the bolt itself, the load-displacement curve from the test, Fig. 3–15 has been modified in Fig. 3–31 to increase the slope of the linear portion to match that reported in the literature, 2,500,000 lbf/in. (Rumpf 1963).

Using Bolt Data

Use the average curve of the actual tests, Fig. 3–31, for the A 325 bolts from the World Trade Center. Using literature values, which are lower, may result in inaccurate failure mode predictions.

Use literature values for the linear portion of the load-displacement curve for A 325 bolts. Figure 3–31 shows this corrected data.

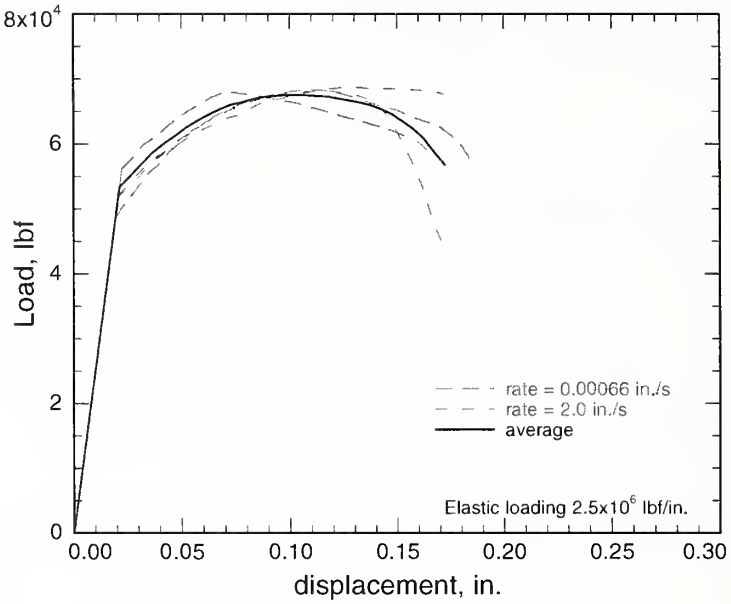

Figure 3–31. Data for load-displacement of A 325 bolts from Fig. 3–15 corrected for initial elastic slope from literature.

Assume no strain rate effects on strength, because the Kolsky data in Chapter 4, and the tensile data, Fig. 3–15, do not show a strong effect.

Use the data of Figures 3–29 and 3–30 to estimate the effect of different exposed thread lengths on tensile strength and elongation at failure. Assume no further strength reduction for more than nine exposed threads.

3.5.3 Welds

To assist in modeling the structural performance, Tables 3–2 and 3–15 summarize the as-measured and as-designed weld data. Table 3–2 contains data generated as part of this study. Table 3–15 contains data for the strength ranges listed in the construction documents.

Table 3–15. Room-temperature weld metal properties as designed.

For Applications With	Weld Metal Properties[a]
F_y < 60 ksi	F_y = 65 ksi, TS = 80 ksi
60 ksiF_y75 ksi	F_y = 77.5 ksi, TS = 85 ksi
F_y > 75 ksi	F_y = 107.5 ksi, TS = 115 ksi

a. Theoretical weld properties (not including the strengthening due to dilution by base metal).

3.6 SUMMARY

The Investigation made several findings regarding the properties of the recovered steel and the original specifications and expectations. The yield and tensile strengths of the perimeter columns in 22 of 24 cases are larger than the minimum requirements. The number of slightly under-strength plates and the amount by which they fall short are consistent with expected values for the average strength and coefficient of variation of yield strengths of plate steels from the WTC-construction era. The ratio of measured yield strength to specified yield strength, approximately 1.1, is also consistent with literature estimates from the WTC-construction era. Unlike the perimeter columns, the measured yield strengths of 2 of 8 samples of wide-flange shapes recovered from the core are less than minimum F_y = 36 ksi specified in A 36. It is possible that these low values arose from damage that removed the yield point behavior. The average measured yield strength and yield point for the wide-flange specimens is about 10 percent lower than expected value predicted from the literature of the WTC-construction era, however. Many of the steels in the floor trusses were high-strength, low-alloy (HSLA) steels, even when they were specified to conform to A 36, and so were much stronger than specified. Recovered bolts were stronger than the minimum specified in A 325, and were much stronger than expected based on reports from the contemporaneous literature. The welds tested had strengths consistent with the requirements of the design documents.

3.7 REFERENCES

3.7.1 References Available from Publicly Available Sources

AISI. 1974. The Variation of Product Analysis and Tensile Properties Carbon Steel Plates and Wide Flange Shapes. in *Contributions to the Metallurgy of Steel.* American Iron and Steel Institute. Washington, DC.

Alpsten G. A. 1972. Variations in Mechanical and Cross-Sectional Properties of Steel. in *Planning and Design of Tall Buildings volume 1b.* American Society of Civil Engineers. New York. 755–805.

Banovic S. W., C. McCowan and W. E. Luecke. 2005. *Federal Building and Fire Safety Investigation of the World Trade Center Disaster: Physical Properties of Steels.* NIST NCSTAR 1-3E. National Institute of Standards and Technology. Gaithersburg, Md. April.

Banovic S. W., Foecke T. 2005b. *Federal Building and Fire Safety Investigation of the World Trade Center Disaster: Damage and Failure Modes of Structural Steel Components.* NIST NCSTAR 1-3C. National Institute of Standards and Technology. Gaithersburg, Md. April.

Barsom, J. M. 1988. Characteristics of Heavyweight Wide-Flange Structural Shapes. *Welding Research Council Bulletin.* 332. 1–19 April.

Barsom, J. M. 1987. Material Considerations in Structural Steel Design. *AISC Engineering Journal.* 24[3] 127–139.

Beedle, L. S. and L. Tall. 1960. Basic Column Strength. *ASCE J. Struct. Div.* ST 7. 139-173.

Elliot, R. A., E. Orowan, T. Udoguchi, and A. S. Argon. 2004. Absence of yield points on strain reversal after aging, and the Bauschinger overshoot. *Mechanics of Materials.* 36. 1143-1153.

Johnson, R. F. 1967. The Measurement of Yield Stress. In *Strong tough structural steels: proceedings of the joint conference organized by the British Iron and Steel Research Association and the Iron and Steel Institute at the Royal Hotel Scarborough, 4-6 April 1967.* ISI Publication 104. Iron & Steel Institute. London. 51-60.

Kirby, B. R. 1995. "The Behaviour of High-strength Grade 8.8 Bolts in Fire." *J. Construct. Steel. Research.* **33.** 3–38.

Li, G.-Q., S.-C. Jian, Y.-Z. Yin, K. Chen and M.-F. Li. 2003 "Experimental Studies on the Properties of Constructional Steel at Elevated Temperatures." *J. Struct. Eng.* 129[12]. 1717–1721.

Luecke, W. E, T. A. Siewert, and F. W Gayle. 2005. *Federal Building and Fire Safety Investigation of the World Trade Center Disaster: Contemporaneous Structural Steel Specifications.* NIST NCSTAR 1-3A. National Institute of Standards and Technology. Gaithersburg, Md. April.

Rao, N. R. N, M. Lohrmann, and L. Tall. 1966. Effect of Strain Rate on the Yield Stress of Structural Steels. *Journal of Materials.* 1[2] 241–261.

Rumpf, J. L. and J. W. Fisher. 1963. "Calibration of A325 Bolts." *J. Struct. Div. ASCE.* 89[ST6]. 215–234.

Sakumoto, Y., K. Keira, F. Furuyama and T. Ave. 1993. "Tests of Fire-Resistant Bolts and Joints." *J. Struct. Eng.* 119[11]. 3131–3150.

Salih, N., J. Smith, H. M. Aktan and M. Usmen. (1992) "An Experimental Appraisal of the Load-Deformation Properties of A325 High-Strength Bolts." *J. Test. Eval.* 20[6]. 440–448.

Tipper, C. F. 1952. Effect of Direction of Rolling, Direction of Straining, and Ageing on the Mechanical Properties of Mild-Steel Plate. *J. Iron Steel Inst.* 172[10]. 143-148.

Uko, D. R. Sowerby, and J. D. Embury. 1980. "Bauschinger Effect in Structural Steels and Role in Fabrication of Line Pipe: Part 1 Analysis of Bauschinger Effect in Structural Steels." *Metals Technology.* 7. 359-367.

Voce, E. 1948. "The Relationship between Stress and Strain for Homegeneous Deformation. *J. Inst. Metals.* **74** 537-562.

WEL-TEN. 1966. *Iron Age* **198** p 18 Advertisement showing representative properties of Yawata WEL-TEN steels. "Nickel may be added to WEL-TEN 60 and 62 if necessary." October 6.

Woldman's Engineering Alloys. 1990. Frick J.P. editor. ASM International. Materials Park, OH.

3.7.2 References Available from Nonpublic Sources

Betts, Jr, W. E. 1967. Letter to R.M. Monti (PONYA) that details Montague-Betts steel purchase. August 25. "We have had five representatives of Yawata Iron & Steel, Ltd. of Japan in our office for several days discussing the Contract which we are placing with them for a minimum of 12,000 tons of wide flange beams and columns."

Laclede. 1968. Document QC-101 "Quality Control Data Resistance Weld Designation and Strength." March 23.

Laclede. 1968b Memorandum No. 4. Interoffice memorandum from R.D. Bay that contains specifications and drawings for bulb angles used to construct floor trusses. January 16.

Laclede. 1968c Memorandum No. 11. Interoffice memorandum from R.D. Bay that contains specifications and drawings round bars used to construct floor trusses. February 28.

Laclede. 1969. Memorandum from E.M. Elgan, General Welding Foreman, to Fred Deppe, St Louis Testing Laboratories, that contains qualification data on fillet welds for welder and procedure certification. December 18. NIST Document WTCI-509-LERA

Marubeni-Iida. 1967. Memorandum from H. Yamada (Marubeni-Iida (America)) to I. Soffer (PONYA) that contains copies of shipping orders for first three shipments of steel plate to Stanray Pacific. The shipping order lists three plates marked as A 572 Grade 42. 5 pages, July 18.

Mitsui. 1968. Shipping invoice from Mitsui & Co. to Pacific Car and Foundry for 382,892 lb of steel plate conforming to A 36-66 for spandrels. Originating port was Chiba, Japan, site of a Kawasaki steel mill. June 10.

Monti, R.M. 1967. Memorandum from R.M. Monti (PONYA) to William Clarkson (Montague-Betts) that contains approval to use the Yawata "A 441 modified" steel composition. Includes supporting correspondence from Yawata Steel to Montague Betts (dated November 2, 1967) with chemical and mechanical requirements. 5 pages. November 21.

Morris, R. E. 1969. Letter to James White (SHCR) that contains a mill test report H9-5386 for an A 36 plate from Fuji Steel Hirohata works. Aug. 5.

PCF. 1967. Pacific Car and Foundry. Documents WS-11A through WS-11C "Weld Procedure." June 1. NIST document number WTCI-158-LERA

Skilling-Helle-Christiansen-Robertson. 1968. Inter-office memo, October 25.

Stanray Pacific. 1967. Memorandum from H. Kjerulf, VP of Engineering (Stanray Pacific), to L. Feld (PONYA) that describes the use of tandem submerged arc welding to join core column plates. May 23.

Stanray Pacific. 1967b. Memorandum from F. Allen (Controller, Stanray Pacific) to L. Feld (PONYA) that describes the use of a self-shielded FCAW electrode for welding the ends of columns. June 2.

Stanray Pacific. 1968. Memorandum from R.E. Morris (Contract Administrator, Stanray Pacific) to J. White (SHCR) that describes modifications to the welding procedure SA-4 during the contract. April 8.

Stanray Pacific. undated. "Stanray Pacific Welding Procedure Qualification SA-2 (revised)," Report includes transverse fillet weld strength data. Filed with documents dated October 1967.

Symes. R.C. 1968. PCF Memo #666-90 Control Procedure for Material Substitution. Memorandum from R.C. Symes (PCF) to R.M. Monti (PONYA) that details the procedure for substituting steel with yield strength larger than specified. May 29.

Symes R.C. 1969 Memorandum PCF D-666 # T-40. Letter to M. Gerstman, Tishman Realty and Construction, February 5. "Our original buying plan for this contract was that plates #1, 2 and 4 would be imported and stripped in our plant, while plate #3 would be domestic. In fact, we have occasionally bought minor quantities of domestic material instead of planned imported, to maintain fabrication schedules and so on, but in general we have adhered to our original concept."

Symes. R.C. 1969b. PCF Memorandum D-666 -#T-178. Memorandum from Symes (PCF) to R.M. Monti (PONYA) that contains the results of a Yawata Iron and Steel investigation (dated Dec. 18, 1968) into "minor laminar discontinuities" in A 36 spandrel plates. "all FY 36 spandrels incorporated into panels up to the present time meet the contract specifications for this material and that discontinuities found do not represent injurious defects."

Warner, H. L. 1967. Letter to Malcolm Levy (PONYA) that details Stanray Pacific steel purchasing plan. July 7. The memo shows 10,240 tons of "British" steel 1.75 in. and thicker and 21,760 tons of "Japanese" steel of all gauges. Other documents identify Fuji as the Japanese supplier and Colvilles as the British supplier.

White, J. 1967. Memorandum from James White (SHCR) to R.M. Monti (PONYA) on sources of steel for Pacific Car and Foundry. September 6. "Information now in our hands indicates that only Kawasaki and Yawata are producing steel for PCF."

White, J. 1967b. Memorandum from James White (SHCR) to R.M. Monti (PONYA) that details required changes to original specification for proprietary Yawata steel grades, "A441-modified,", WEL-TEN 60R, WEL-TEN 60, WEL-TEN 62, WEL-TEN 70, WEL-TEN 80C (described as "A 514-modified.")

White, J. 1968. Letter on SHCR letterhead to R.M. Monti (PONYA) that approves the substitution of F_y = 100 ksi steel for F_y = 90 ksi in all instances. Feb. 15.

Chapter 4
HIGH-STRAIN-RATE PROPERTIES

4.1 INTRODUCTION

It is well known that the yield and ultimate strengths of steels increase with increasing strain rate (Harding 1979, Hutchinson 1977, Wiesner 1999). In terms of the mechanical response of the steels in the towers, the high-speed impact of the aircraft is a high-strain-rate event, which is well above the conventional strain rates normally associated with mechanical properties measurements. It is estimated that the strain rates on the World Trade Center (WTC) steels, due to the aircraft impacts, were up to 1000 s^{-1}. Accurate models of the aircraft impact and the resulting damage to the towers require knowledge of the mechanical properties of the steels at high strain rates.

The goal of the high-strain-rate testing plan was to develop a database of high-strain-rate properties on WTC steels for use in modeling the extent of structural damage to the perimeter and core columns as a result of the aircraft impacts. For strain rates up to 500 s^{-1}, the test plan employed high-rate tension tests on eight perimeter- and five core-column steels. These data were used to develop models for strain rate sensitivity for the Investigation. For higher rates up to 2500 s^{-1} the plan employed high-rate compression tests, using a split Hopkinson pressure bar or Kolsky test, on one bolt and two perimeter-column steels.

4.2 TEST PROCEDURES

4.2.1 High Strain-Rate Tension Tests

High-strain-rate tension tests were conducted on eight perimeter-column steels and five core-column steels at rates between 50 s^{-1} and 500 s^{-1}. High-strain-rate tension specimens, Fig. 4–1, had a gauge length of 1.0 in., a width of 0.25 in., and a thickness of either 0.125 in. or 0.063 in. Strain was measured using open-grid, high-elongation strain gauges attached to the specimen test section with high-elongation strain gauge adhesive. An additional strain gauge attached to the fixed-grip end of the specimen was used to measure the load and to validate that the specimen grip-end did not deform plastically.

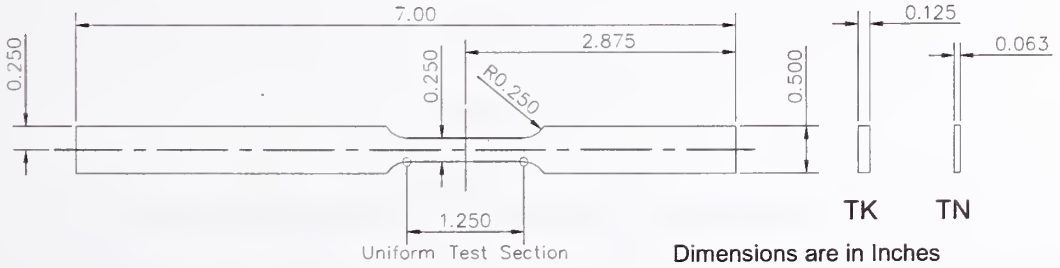

Flat-HSR-1" TK Flat-HSR-1" TN

Figure 4–1. Specimen used for high-strain-rate tension tests.

The high-strain-rate test machine is a closed-loop, servo-hydraulic machine with an 11,240 lb capacity actuator mounted in a 110,000 lb load frame (Bruce 2003). A 400 gal per min. servo-valve, supplied by a 5 gal capacity accumulator, controls the high rates for this machine. A digital controller and associated computer system provide system control. The specified peak velocity for the system is 13.5 m/s at zero load and 10 m/s at 50 percent of the maximum load. Data are acquired using commercially available software and a data acquisition board capable of acquiring 500,000 data points per second. The typical acquisition rate is 10 ms per point, which allows 5,000 data points per test. The system employs two load measurement devices: a piezoelectric load washer attached to the fixed end of the load train and a strain gauge bonded to the grip end of the specimen.

A slack-adaptor in the load train, Fig. 4–2, allows the actuator to achieve the desired displacement rate before loading the specimen. The tension specimen is gripped using bolt-tightened wedge grips. Triggering the system starts the data acquisition and accelerates the actuator to the desired testing speed. At the end of its travel, the slack adapter engages the lower grip rod and loads the specimen at the desired extension rate. The targeted strain rates were not always achieved, but the resulting rates could be calculated and are used in this report.

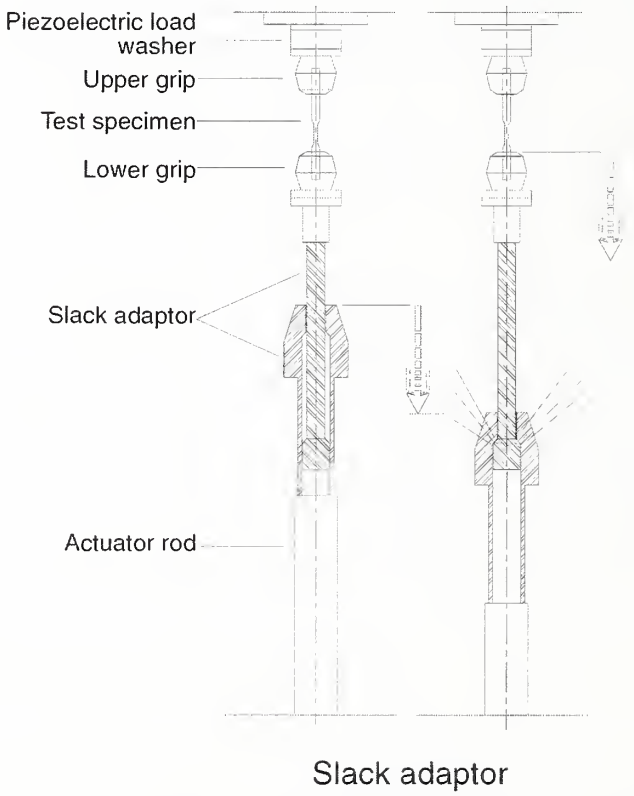

Figure 4–2. Schematic diagram of the slack adaptor apparatus.

Data collected during high-strain-rate tension tests include the load from the piezoelectric load washer, the actuator displacement, the strains in the test section and the grip-end of the specimen from the strain gauges, and the time. The reported strain rate realized by the specimen is obtained from the slope of the strain vs. time curve recorded for each test.

4.2.2 Analysis of High-Strain-Rate Tension Test Data

The data were analyzed using a multi-step technique (Bruce 2003):

1. Correct the specimen gauge section and grip section strain data for Wheatstone bridge non-linearity.

2. Plot the engineering strain, e, versus time, t, using the gauge-section strain gauge data. Determine the engineering strain rate, $\dot{e}_p$, in the plastic region by fitting a line through the linear part of the data over a time range $t_1 < t < t_2$. Calculate the engineering strain at each time increment, Δt, for $t > t_2$ as

$$e(t + \Delta t) = e(t) + \Delta t \cdot \dot{e}_p \qquad 4\text{–}1$$

3. Convert the grip-section strain data to load, using the calculated modulus and cross-sectional area of the grip-end of the specimen. Overlay the grip section load curve on the data from the piezoelectric load washer curve, and, if necessary, adjust the modulus in the grip load signal to align it with the mean of the load washer signal to produce the corrected load signal.

4. Calculate the engineering stress based on the corrected load signal and the cross-sectional area of the test section of the specimen.

5. Calculate the true strain and true stress values from the engineering strain and engineering stress values.

6. Choose the uniform strain limit as the strain value at the tensile strength.

7. Compute the total elongation, El_t, or engineering strain at fracture, e_f, from the distance, L_0, between gauge marks made on the specimen prior to testing to that following testing, L_f:

$$El_t = \frac{L_f - L_o}{L_o} \qquad 4\text{–}2$$

8. Compute the reduction of area, ROA, from the original cross-sectional area, A_0, of the specimen test section prior to testing, and that measured after testing, A_f:

$$ROA = \frac{A_0 - A_f}{A_0} \qquad 4\text{–}3$$

9. Plot the engineering- and true-stress-strain curves up to the point of instability (uniform strain limit).

10. Determine the yield strength by visually estimating the mean value of stress just prior to the onset of strain hardening. In cases where the ringing of the load signal precludes reliable visual estimation, fit a third order polynomial to the yielding and strain hardening regions (1 percent $\leq e \leq$ 5 percent) of the curve. Draw a line parallel to the linear-elastic part of the

stress-strain curve at an offset of 1 percent. The intersection of these two constructed lines is the estimated yield strength, see Fig. 4–3. The value of 1 percent was chosen because the downside of the peak maximum load curve often fell slightly less than this offset point and significantly skewed the data. The ESIS Procedure for Dynamic Tensile Tests (2000) describes the procedure in greater detail.

11. Determine the tensile strength, *TS*, by dividing the maximum load by the original cross-sectional area of the test section.

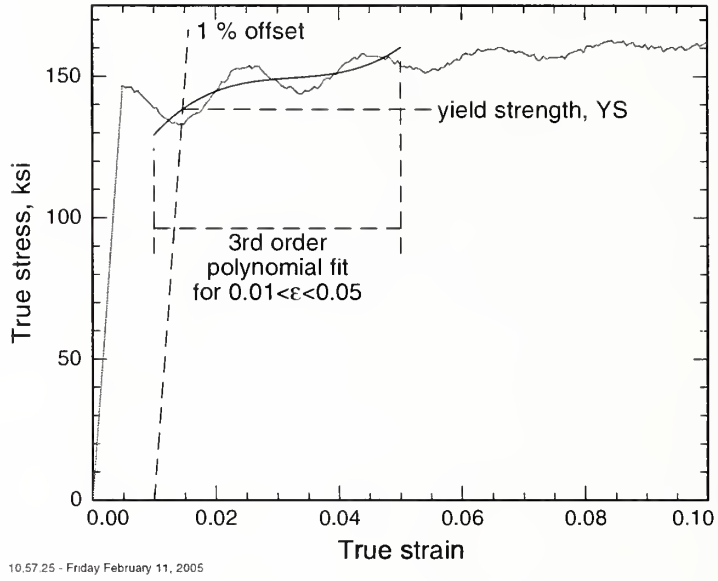

Figure 4–3. Schematic of the procedure for estimating the tensile yield strength when ringing in the load signal precludes reliable visual estimation.

4.2.3 Kolsky Bar Tests

Tests at very high strain rates employed the split Hopkinson pressure bar, or Kolsky, test. This test method is well known, and the literature of high-rate testing describes it in detail, for example Follansbee (1985). The device consists of two hardened steel bars lightly supported in a frame as shown schematically in Fig. 4–4. The test specimen, which is lubricated to reduce friction, is placed between two hardened (58 HRC) maraging steel bars, 15 mm in diameter and 1.5 m long. A gas gun fires a 0.5 m long striker bar at the end of the input bar. The impact generates an elastic compressive pulse in the input bar as shown in Fig. 4–5. This pulse, which travels down the input bar at nearly 5000 m/s, compresses the test

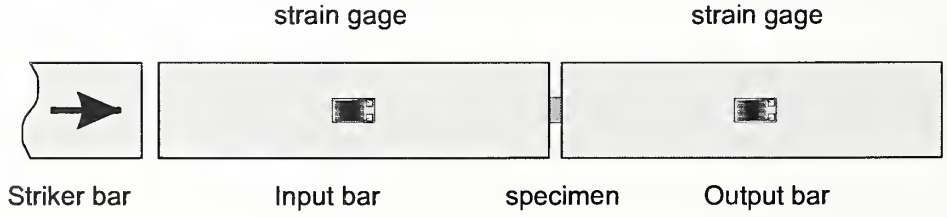

Figure 4–4. Schematic diagram of Kolsky bar apparatus.

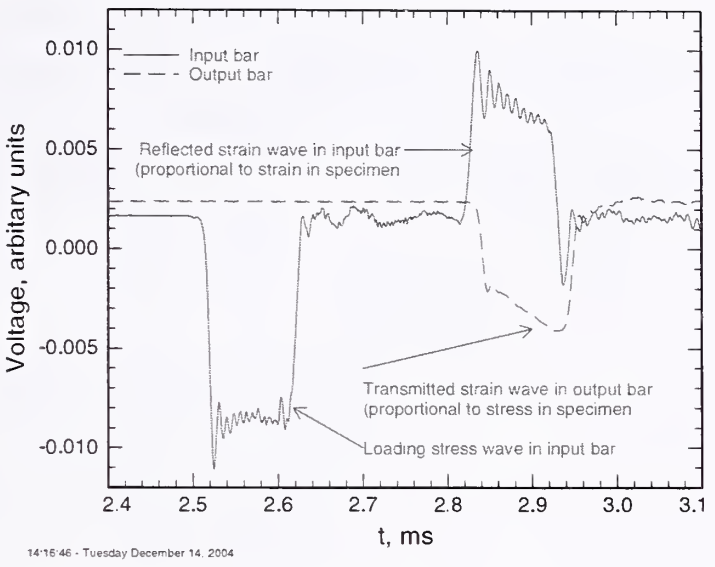

Figure 4–5. Oscillograph record of an incident pulse that is partially transmitted to the output bar and partially reflected in the input or incident bar.

specimen between the input and output bars at strain rates between 200 $s^{-1}$and 10,000 s^{-1}. Thin copper disks placed between the striker bar and the input bar shape the loading pulse and reduce oscillations during dynamic loading of the specimen. The exact strain rate depends on parameters such as the length and velocity of the striker bar, and the test specimen dimensions. Some of the loading pulse on the test specimen enters the output bar as a transmitted strain wave, and some is reflected back into the input bar, see Fig. 4–5. The reflected and transmitted strain waves are recorded using strain gauges mounted on the bars, dynamic Wheatstone resistance bridges, and dual trace oscilloscopes. The stress, σ, in the test specimen at time t is related to the transmitted strain, ε_T, in the output bar by

$$\sigma(t) = E\frac{A_0}{A}\varepsilon_T(t) \qquad 4\text{–}4$$

where E is Young's modulus of the bar, A_0 is the cross-sectional area of the bar, and A is the cross-sectional area of the test specimen. The strain rate in the test specimen at any instant is related to the reflected strain, ε_R, in the incident bar by

$$\frac{d\varepsilon}{dt} = -2\frac{C}{L}\varepsilon_R(t) \qquad 4\text{–}5$$

where C is the longitudinal sound speed in the bar and L is the length of the test specimen. The strain rate is integrated to obtain the strain at any time during the test. Combining the strain rate data with the stress record provides the high rate constitutive behavior, or stress-strain curve. In the Kolsky test, strains in the range $0.01 < \varepsilon < 0.20$ are usually considered reliable. At strains below this range, which includes the elastic and early yielding regions, the test specimen stress has not reached equilibrium. At strains greater than this range, the test specimen may deform nonuniformly.

The Kolsky bar test specimens were cylinders, 4 mm or 6 mm in diameter and 2 mm high, whose longitudinal axis was parallel to the rolling direction of the plate. Specimens originated from two perimeter columns and an A 325 bolt. Specimen C22-C2M-FL3 is a F_y = 75 ksi plate from WTC 1 column line 157 between floors 93–96. Specimen N8-C3M-FR2 is a F_y = 60 ksi plate from WTC 1 column line 141 between floors 97–100. The original location of the A 325 bolt is unknown. Chapter 3 summarizes the results of the bolt tests.

4.2.4 Quasi-Static Compression Tests

Because the lowest strain rate that the Kolsky test can achieve is about 200 s^{-1}, quasi-static compression tests using Kolsky specimens were conducted to extend the strain rate data to low rates. These tests employed an ordinary servo-hydraulic test machine in extension control at constant extension rate. In most cases, the specimen strain was estimated from the crosshead displacement, after correcting for machine compliance. Tests on the A 325 bolt steel employed an extensometer clipped to the ends of the loading rams as well.

4.3 RESULTS

4.3.1 High Strain-Rate Tension Tests

Figure 4–6 is an example of a set of high-strain-rate stress-strain curves for F_y = 50 ksi perimeter column M26-C1-RF, from WTC 1 column 131 floors 90-93, north face, just above impact zone. Although the stress measurement was taken from the strain gauge on the grip-end of the test specimen, the ringing in the stress signal is not completely eliminated.

Tables 4–1 and 4–2 summarize the results of the high strain-rate tension tests of the eight perimeter-column steels and five core-column steels. Appendix A tabulates the individual test data and presents the stress-strain curves for each test.

Table 4–1. Summary of specimens and results for high strain-rate tests of perimeter columns.

F_y (ksi)	Specimen	Location[a] in Building and Shape	Specimen Orientation	m Eq. 4–9
50	M26-C1-RF	WTC 1 131 90-93 9/16 in. flange plate	longitudinal	F_y: m=0.0121±0.0033 *TS:* m=0.0118±0.0023
			transverse	F_y: m=0.0178±0.0044 *TS:* m=0.0158±0.0026
60	N8-C1-RF	WTC 1 143 97-100 5/16 in. flange plate	longitudinal	F_y: m=0.0160±00033 *TS:* m=0.0133±0.0032
			transverse	F_y: m=0.0115±0.0032 *TS:* m=0.0127±0.0012
65	N99-C3-RF	WTC 1 147 99-102 1/4 in. flange plate	longitudinal	F_y: m=0.0125±0.0023 *TS:* m=0.0131±0.0028
			transverse	F_y: m=0.0094±0.0036 *TS:* m=0.0112±0.0022
75	C22-FL	WTC 1 157 93-96 1/4 in. flange plate	longitudinal	F_y: m=0.0067±0.0021 *TS:* m=0.0138±0.0003
			transverse	F_y: m=0.0061±0.0016 *TS:* m=0.0145±0.0038
75	C14-SP	WTC 2 300 86 3/8 in. spandrel plate	longitudinal	F_y: m=n/d *TS:* m=0.0108±0.0015
			transverse	F_y: m=0.0083±0.0021 *TS:* m=0.0098±0.0016
100	M10B-RF	WTC 2 206 83-86 1/4 in. flange plate	longitudinal	F_y: m=0.0053±0.0014 *TS:* m=0.0085±0.0013
			transverse	F_y: m=0.0039±0.0038 *TS:* m=0.0083±0.0010
100	C10-IW	WTC 1 451 85-88 1/4 in. inner web plate	longitudinal	F_y: m=0.0077±0.0033 *TS:* m=0.0113±0.0006
			transverse	n/d
100	C10-FL	WTC 1 451 85-88 1/4 in/ flange plate	longitudinal	F_y: m=0.0044±0.0014 *TS:* m=0.0080±0.0026
			transverse	F_y: m=0.0051±0.0014 *TS:* m=0.0091±0.0021

a. WTC # XXX YY-ZZ: #=tower 1 or 2; XXX=column line; YY-ZZ=floor range

Key: n/d, not determined, generally because of a lack of low strain rate data

Note: Reported uncertainties are defined as the estimated standard uncertainty of m, s_m

$$s_m = \frac{s}{\sqrt{SS_{xx}}} = \frac{1}{n-2}\frac{\sum(y_i - \hat{y}_i)^2}{\sqrt{\sum(x_i - \bar{x})^2}}$$

Table 4–2. Summary of specimens and results for high strain-rate tests of core columns.

F_y ksi	Specimen	Location[a] in Building and Shape	Specimen Orientation	m (Eq. 4–9)
36	C65-WEB	WTC 1 904 86-89 web of 12WF161	longitudinal	F_y: m=0.0336±0.0030 *TS:* m=0.0207±0.0010
			transverse	n/d
36	C65-FL	WTC 1 904 86-89 flange of 12WF161	longitudinal	F_y: m=0.0290±0.0042 *TS:* m=0.0130±0.0014
			transverse	n/d
36	B6152-2-FL	WTC 1 504 33-36 flange of box column	longitudinal	F_y: m=0.0239±0.0038 *TS:* m=0.0165±0.0012
			transverse	F_y: m=0.0396±0.0009 *TS:* m=0.0196±0.0017
36	C80	WTC 1 603 92-95 flange of 14WF184	longitudinal	F_y: m=0.0317±0.0027 *TS:* m=0.0175±0.0039
			transverse	n/d
42	HH1-WEB	WTC 1 605 89-101 web of 12WF92	longitudinal	F_y: m=0.0265±0.0014 *TS:* m=0.0200±0.0058
			transverse	n/d

a. WTC # XXX YY-ZZ: #=tower 1 or 2; XXX=column line; YY-ZZ=floor range.
Key: n/d, not determined, generally because of a lack of low strain rate data
Note: Reported uncertainties are defined as the estimated standard uncertainty of m, s_m

$$s_m = \frac{s}{\sqrt{SS_{xx}}} = \frac{1}{n-2}\frac{\sum(y_i - \hat{y}_i)^2}{\sqrt{\sum(x_i - \bar{x})^2}}$$

4.3.2 High Strain-Rate Kolsky Bar Tests

Figure 4–7 is an example of the results of a Kolsky test. The plot shows both the stress-strain behavior and the corresponding strain-rate-strain behavior for a perimeter column steel. Note that the strain rate is not constant during the test. Table 4–3 summarizes the Kolsky bar tests for the two perimeter column steels and the A 325 bolt steel. Appendix A presents the results of the other tests.

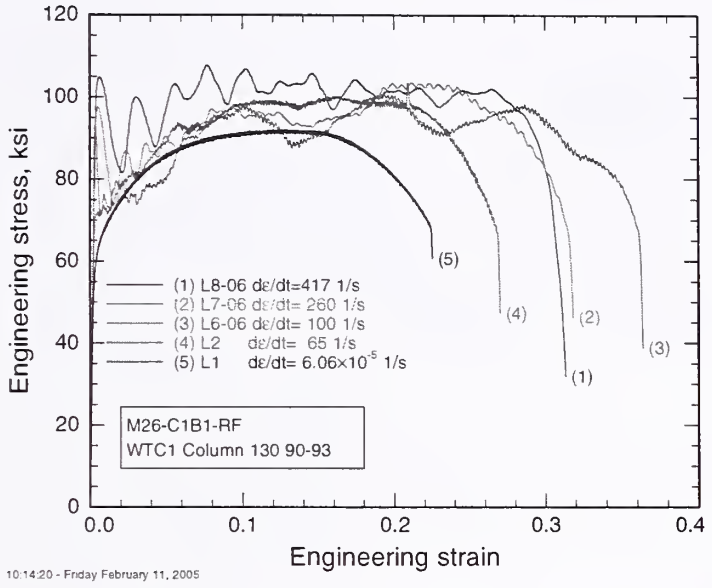

Figure 4–6. Examples of tensile high-rate stress-strain curves for F_y = 50 ksi perimeter column steel M26-C1B1-RF.

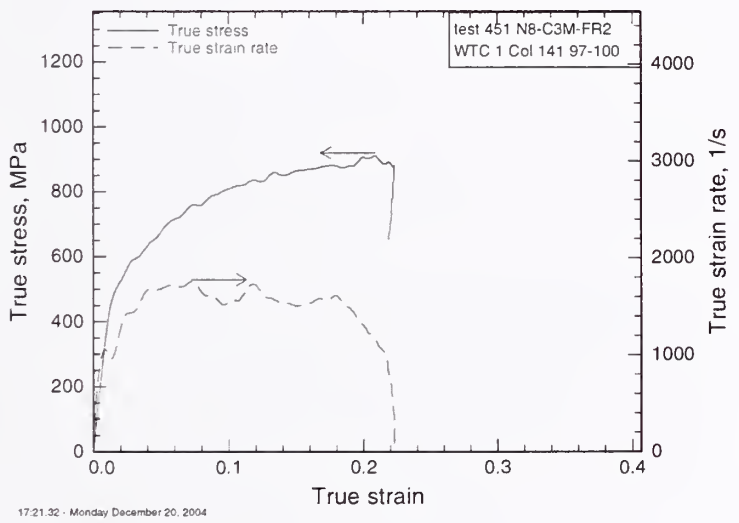

Figure 4–7. Example stress-strain and strain rate-strain curves for Kolsky tests.

Table 4–3. Summary of Kolsky bar tests.

Test Specimen and Location	Nominal F_y (ksi)	Test #	Average Flow Stress[a] (MPa)	Average Strain Rate[b] (1/s)
C22-C2M-FL3 WTC 1 Column 157 93–96	100	434	943±43	1562±408
		435	895±55	1134±123
		436	804±46	579±42
		437	675±65	389±95
		438	1015±43	2102±283
		439	1029±31	2571±423
		440	829±42	529±76
		441	835±53	1141±125
N8-C3M-FR2 WTC 1 Column 141 97–100	60	450	831±64	1533±159
		451	808±64	1609±80
		452	776±71	1016±81
		453	621±82	759±119
		454	453±95	443±87
		455	860±52	2169±204
		456	906±55	2354±246
		457	921±55	2799±344
		458	898±56	2689±206
A 325 bolt unknown location	92	324	691±36	917±335
		325	795±179	711±434
		326	836±227	688±445
		327	992±70	1145±338
		328	957±86	1060±382
		329	1077±44	2395±566

a. Average flow stress represents the average in the range $0.2\varepsilon_{max} < \varepsilon < 0.8\ \varepsilon_{max}$.

b. Average strain rate represents the average in the range $0.2\varepsilon_{max} < \varepsilon < 0.8\ \varepsilon_{max}$.

Note: Uncertainties represent the standard deviation of the value: $s = \sqrt{\frac{1}{N-1}(x_i - \bar{x})^2}$.

4.3.3 Quasi-Static Compression Tests

Table 4–4 and Fig. 4–8 summarize the quasi-static compression test conditions and results that are used for analyzing the strain rate sensitivity from the Kolsky bar tests. The plots are graphically truncated at 10 percent strain.

Table 4–4. Summary of quasi-static compression tests

F_y (ksi)	Specimen	Location in Building	Initial Strain Rate (1/s)
60	N8-C3M-FR2-1	WTC 1 142 97-100 5/16 in. flange plate	0.001
			0.01
75	C22-C2M-FL3	WTC 1 157 93-96 1/4 in. flange plate	0.01
			0.001
100	C10-C1M-FL2	WTC 1 451 85-88 1/4 in. flange plate	0.01
n/a	A 325 bolt	unknown	0.002

Key: WTC # XXX YY-ZZ: #=tower 1 or 2; XXX, column line; YY-ZZ, floor range; n/a = not applicable.

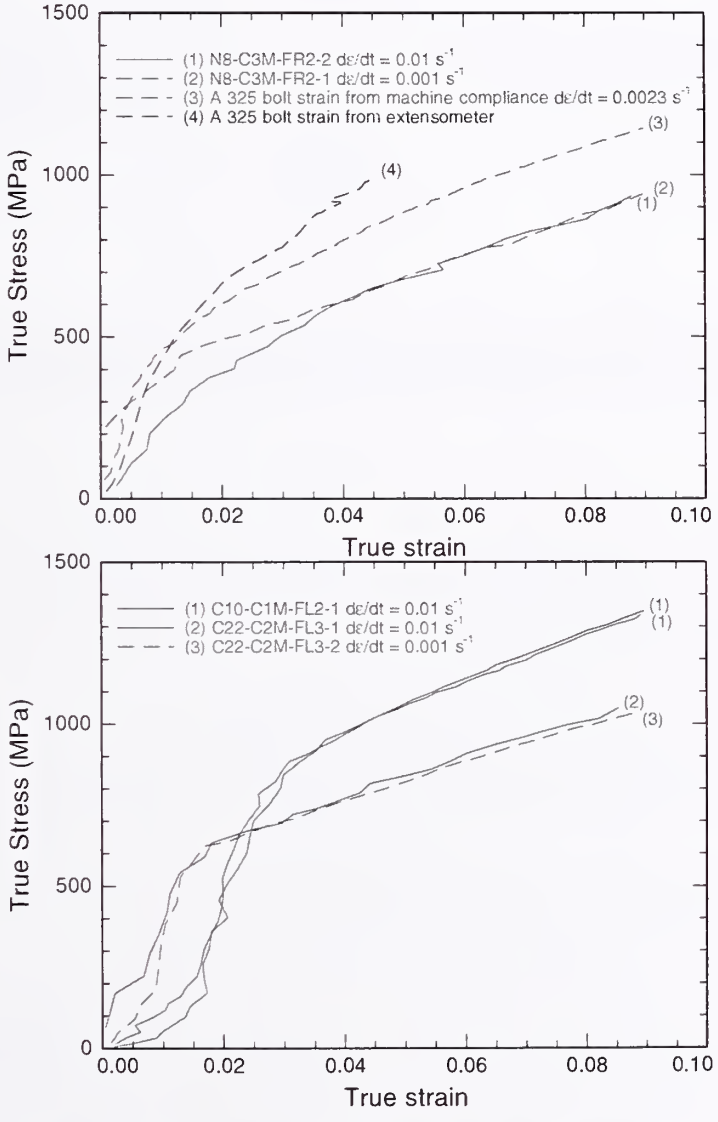

Figure 4–8. Quasi-static compression stress-strain curves for the tests summarized in Table 4–4.

4.4 DISCUSSION

There are several important limitations in understanding the data from the high-rate tensile tests. At testing rates greater than about 200 s^{-1} (Follansbee 1985b) the propagation of the stress wave that loads the specimen through the loading train begins to influence the measurement of the test load. At these rates, the time necessary for the test specimen to achieve an equilibrium stress state throughout the gauge section can be a significant portion of the total time of the test. In this case, the experimentally derived

low strain behavior does not represent the deformation behavior of the steel. An upper limit for the rate at which the stress wave propagates through the specimen (Follansbee 1985b) is the elastic wave velocity v_e:

$$v_e = \sqrt{\frac{E}{\rho}} \qquad 4\text{–}6$$

where E is the elastic modulus and ρ is the density. A lower limit is the velocity of the plastic stress wave:

$$v_p = \sqrt{\frac{\left(\frac{d\sigma}{d\varepsilon}\right)}{\rho}} \qquad 4\text{–}7$$

where $d\sigma/d\varepsilon$ is the instantaneous slope of the true-stress true-strain curve. Follansbee (1985b) asserts that the stress wave velocity is closer to the elastic wave velocity even after yielding. The minimum valid strain can be estimated (Follansbee 1985b) from the time necessary for three passages of the stress wave:

$$\varepsilon_{\min} = \frac{3\dot{\varepsilon}L_0}{v_e} \qquad 4\text{–}8$$

through the specimen of gauge length L_0 deforming at a strain rate $\dot{\varepsilon}$. For the high rate tension tests, the 1 percent offset strain used for the yield strength is more than sufficient strain to ensure an equilibrium stress state in the gauge section.

A second issue in high-rate tests is the heating of the test specimen by the work of plastic deformation (Follansbee 1985b). Quasistatic tests are often assumed to be isothermal, where the heat generated by the work of deformation can escape from the specimen via the grips. In contrast, high-rate tests are generally assumed to be adiabatic. In the short time of the test, the heat generated in deforming the specimen cannot escape the specimen. An upper limit estimate, following Follansbee (1985b), for the temperature rise under adiabatic deformation is about 80 °C. The Investigation made no attempt to correct for changes in yield and tensile strength or elongation resulting from adiabatic heating.

Ringing of the load signal. (Gillis 1985) introduces a third problem in interpreting the stress-strain curves. The ringing generally occurs at about the natural frequency of the load cell. The problem can be particularly severe for high-rate tests that employ conventional load cells (Bruce 2004). Even with test specimens instrumented with strain gauges in the grip section away from the load application, like those used in the Investigation, it is not always possible to eliminate the ringing (Bleck 2000; ESIS 2000; Wiesner 1999; Yan 2002). Many tests reported in the literature have been heavily filtered to remove the

load ringing (Gillis 1985). In reporting the data, the Investigation did not attempt to mathematically remove the ringing.

4.4.1 Calculation of Strain-Rate Sensitivity for Tension Tests

Strain-rate sensitivity (SRS) is an indication of the effects of strain rate on material properties such as yield and tensile strength. This report defines the SRS as the slope of the log(stress)-log(strain rate) curve. Although there are other representations of the stress-strain rate behavior, this analysis expresses the effect of strain rate on yield, F_y, and tensile strength, TS, via a simple relation:

$$\frac{\sigma}{\sigma_0} = \left(\frac{\dot{\varepsilon}}{\dot{\varepsilon}_0} \right)^m \qquad 4\text{–}9$$

where σ is the yield, F_y, or tensile, TS, strength, $\sigma_0 = 1$ ksi is a normalizing parameter, $\dot{\varepsilon}_0$ is a fitted reference strain rate, and m is the strain rate sensitivity. From the parameters of Eq. 4–9, it is straightforward to calculate the parameters of the other possible representations.

To calculate the strain rate sensitivity, the natural logarithm of Eq. 4–9 is fit to the data:

$$\log_e\left(\frac{\sigma}{\sigma_0} \right) = m \log_e(\dot{\varepsilon}) - m \log_e(\dot{\varepsilon}_0) \qquad 4\text{–}10$$

where $\sigma_o = 1$ ksi. The slope of the fit is the strain rate sensitivity, m, and the intercept is the second term in Eq. 4–10.

Tables 4–1 and 4–2 summarize the fitted value of the strain rate sensitivity, m. In all cases the yield and tensile strength increase with increasing strain rate. Appendix A contains strain rate sensitivity plots of both F_y and TS for each steel. Some of the calculations utilize data developed using the standard Flat 2" and round specimens for the quasi-static rates. The tables in Appendix A identify which specimen was used for each test. Appendix E provides justification for combining the data from the different specimens to evaluate the strain rate sensitivity. Figure 4–9 plots the measured strain rate sensitivity, m, for the yield and tensile strengths as a function of specified minimum yield strength. The uncertainties in Fig. 4–9 and Tables 4–1 and 4–2 are the estimated standard uncertainties of the calculated strain rate sensitivities, m, as described in the footnote of Table 4–1. There is no significant difference in the strain rate sensitivity, m, measured in the longitudinal and transverse directions.

Because the total elongation, El_t, depends on the specimen geometry, it is not possible to use all the quasi-static test data to evaluate the strain rate sensitivity. For many of the core column steels, however, there is quasi-static test data obtained using the high-rate style specimens of Fig. 4–1. Many of the quasi-static tests on perimeter column steels employed the $t = 0.25$ in. Flat 2" specimen, which is geometrically identical to the $t = 0.125$ in. Flat-HSR 1"specimen. Appendix E provides theoretical and experimental justification for combining data generated using these two specimens for evaluating the total elongation behavior.

4.4.2 Calculation of Strain-Rate Sensitivity for Kolsky Tests

Figure 4–10 shows the strain rate dependence of the flow stress for the three steels evaluated in the Kolsky bar tests. For the two perimeter columns, the flow stress is evaluated at a 1 percent offset strain. For the A 325 bolt steel the flow stress is evaluated at a 5 percent offset strain. Table 4–5 summarizes the data plotted in Fig. 4–10. Table 4–6 compares the strain rate sensitivities evaluated in tension with those evaluated in the compression Kolsky bar tests. The absolute values of the strain rate sensitivities evaluated by the two techniques are similar. The larger scatter of the Kolsky data, Fig. 4–10, results in uncertainties in the calculated strain rate sensitivities, *m,* that are roughly two times larger than those from the tensile data.

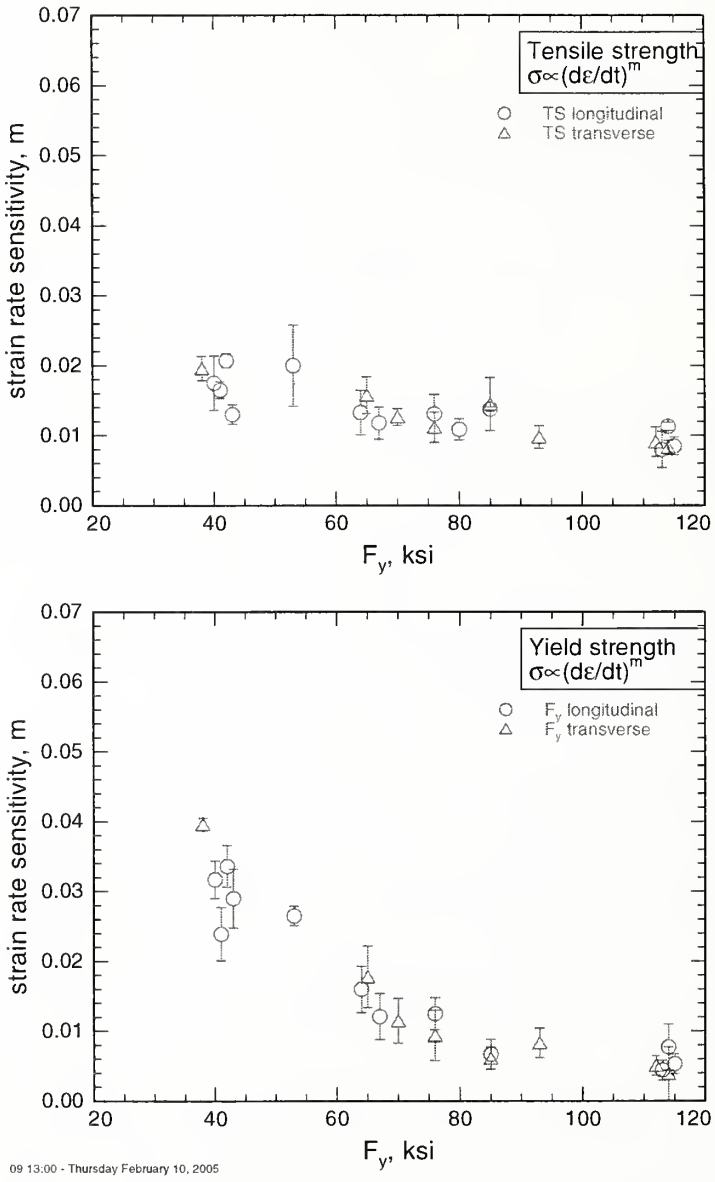

Figure 4–9. Strain rate sensitivity of yield and tensile strength as a function of specified minimum yield strength.

Figure 4–11 plots the strain rate dependence of the flow stress at different strain levels for the A 325 bolt. Note that by 5 percent strain the flow stress is independent of the strain rate. This behavior, summarized in Table 4–6, agrees with the strain rate independent strength found in the full bolt tests described in Section 3.5.2.

Table 4–5. Summary of stress-strain rate data plotted in Fig. 4–10.

N8-C3M-FR2 *Fy* = 60 ksi WTC 1 142 97-100		C22-C2M-FL3 *Fy* = 75 ksi WTC 1 157 93-96		A 325 Bolt Location Unknown	
Stress (MPa)	Strain Rate (1/s)	Stress (MPa)	Strain Rate (1/s)	Stress (MPa)	Strain Rate (1/s)
500	0.001	650	0.001	990	0.0023
460	0.01	650	0.01	988	24
470	500	700	500	1020	384
550	750	800	600	968	1150
550	750	700	600	992	915
650	2400	700	1200	991	2970
575	1500	720	1200		
650	2200	740	1250		
620	2400	840	1750		
620	2200	800	2400		
550	3000				

Notes: N8-C3M-FR2 and C22-C2M-FL3 evaluated at 1 percent offset strain.
A 325 bolt evaluated at 5 percent offset strain.
Slow rate tests evaluated using method of Section 4.2.4.

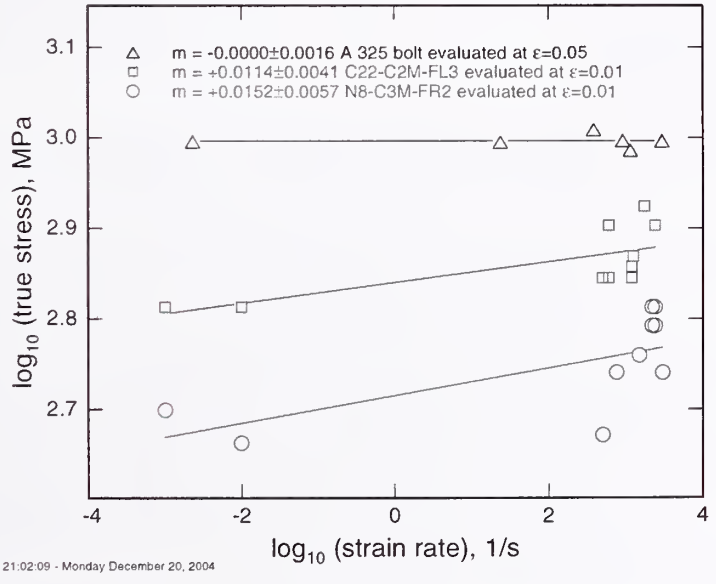

Figure 4–10. Flow stress as a function of strain rate for Kolsky tests.

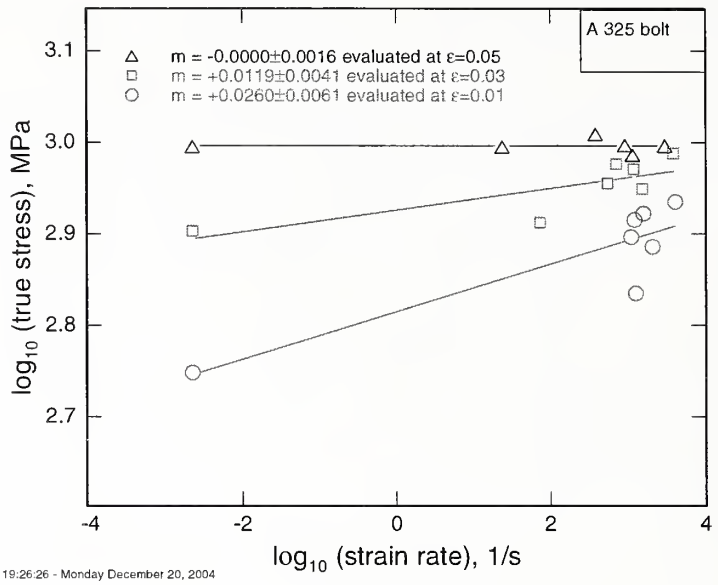

Figure 4–11. Flow stress as a function of strain rate evaluated at different strains for Kolsky tests on the A 325 bolt.

Table 4–6. Comparison of strain rate sensitivity measured in tension and compression.

Specimen	F_y, ksi	Strain Rate Sensitivity from Tension Tests[a]	Strain Rate Sensitivity from Kolsky Bar and Compression Tests[a]
C22-C2M-FL3	75	F_y: m=0.0067±0.0021	m=0.0114±0.0041
N8-C3M-FR2	60	F_y: m=0.0160±00033	m=0.0152±0.0057
A 325 Bolt	TS_{min} 120 ksi	TS: m=0.001±0.001	m=0.0000±0.0016 Stress evaluated at 5 % plastic strain

a. Strengths evaluated at 1 percent offset strain for both tension and compression.

4.5 HIGH-STRAIN-RATE DATA PROVIDED TO THE INVESTIGATION

Early in the Investigation, before the tensile testing was complete or fully analyzed, it was necessary to provide estimates of the high-strain rate behavior of the WTC steels to other Investigation team members. These estimates were based on a provisional set that contained only six perimeter-column and no core-column steels. The provisional model predicted the increase in flow stress as a function of the strain rate and the quasi-static yield strength, using the Cowper-Symonds equation. After the full set of high strain-rate data from the thirteen steels was complete, the strain rate sensitivities for the full set were analyzed using the same methodology. The prediction of the high-strain-rate behavior of the perimeter column steels was generally similar for the provisional and complete models. The provisional model based on the six perimeter-column steels over-predicts the increase in flow stress in the low-strength core-column steels. Appendix C summarizes the analysis of both data sets.

4.6 COMPARISON WITH LITERATURE DATA

Table 4–7 summarizes the strain rate sensitivities of several structural steels for comparison with those of the WTC steels in Table 4–2. It is not a comprehensive list, but it does include several plain-carbon (Couque 1988, Krafft 1962, Manjoine 1944) and HSLA (Chatfield 1974, Davies 1975, Langseth 1991) structural steels. The data from Chatfield (1974) and Davies (1975) are for automotive rather than structural steels, but the chemistries are similar to the WTC steels. Most of the references, except Krafft (1962) and Couque (1988) provide little information on the microstructure of the steels characterized.

Table 4–7. Literature data for strain rate sensitivities of structural steels.

Steel	Reference	F_y (ksi)	m Determined for F_y (Eq. 4–9)	m Determined for TS (Eq. 4–9)	Notes	Chemistry % mass
1020 T1[a]	Couque 1988	28	0.043	n/r	(a) to	Not reported
1020 T7[a]	Couque 1988	30	0.059	n/r	(a) to	Not reported
Commercial low-carbon open hearth[a]	Manjoine 1944	31	0.054±0.007	0.019±0.005	(a) te	Not reported
HSLA-40	Chatfield 1974	40	0.045±0.004	0.031±0.007	te	C 0.06 Mn 0.34 Si 0.02 Cu 0.04 Cr 0.03 Ni 0.03 Al 0.055
EM-3[b]	Krafft 1962	44.6	0.064	0.053	(b) c	C 0.20 Mn 1.12 Si 0.31
HSLA-45-1	Chatfield 1974	45	0.035±0.003	0.034±0.0009	te	C 0.18 Mn 0.78 Si 0.06 Cu 0.04 Cr 0.03 Ni 0.03 Mo 0.016 Al 0.001
HSLA-45-2	Chatfield 1974	45	0.024±0.002	0.023±0.005	te	C 0.18 Mn 0.69 Si 0.63 Cu 0.07 Cr 0.03 Ni 0.12 Mo 0.012 Al 0.007
HSLA-50	Chatfield 1974	50	0.026±0.003	0.019±0.0001	te	C 0.13 Mn 0.55 Si 0.94 Cu 0.04 Cr 0.42 Ni 0.12 Mo 0.020 Al 0.012
YST-50	Davies 1975	50	0.014±0.002	0.010±0.0018	te	C 0.10 Mn 0.54 Ti 0.12
ST52-3N	Langseth 1991	51	0.021±0.002	0.0098±0.0005	te	C 0.12 Mn 1.30 Si 0.40 Cu 0.20 Cr 0;08 Ni 0.20 Mo 0.03 Al 0.03
Hot-rolled	Davies 1975	60	n/r	0.022±0.003	te	C 0.19 Mn 0.75
HSLA-80-1	Chatfield 1974	80	0.020±0.002	0.016±0.003	te	C 0.14 Mn 0.76 Si 0.60 Cu 0.03 Cr 0.49 Ni 0.03 Mo 0.005 Al 0.02
HSLA-80-2	Chatfield 1974	80	0.018±0.007	0.018±0.005	te	C 0.05 Mn 1.55 Si 0.16 Cu 0.01 Cr 0.02 Ni 0.01 Mo 0.29 Al 0.068
YST-80	Davies 1975	80	0.012±0.0007	0.0087±0.001	te	C 0.11 Mn 0.54 Ti 0.30 V 0.018

a. Actual value for F_y.
b. Reported value.
Key: te, tension test; to, torsion test; c, compression test; n/r = not reported.
Note: See Table 4–1 for definition of uncertainties of parameters.

Figure 4–12 plots the strain rate sensitivities, m, from Table 4–7, as a function of yield strength, F_y, along with the data from the WTC steels. The behavior and magnitude of the strain rate sensitivities of the WTC steels is entirely consistent with those from the literature of similar steels.

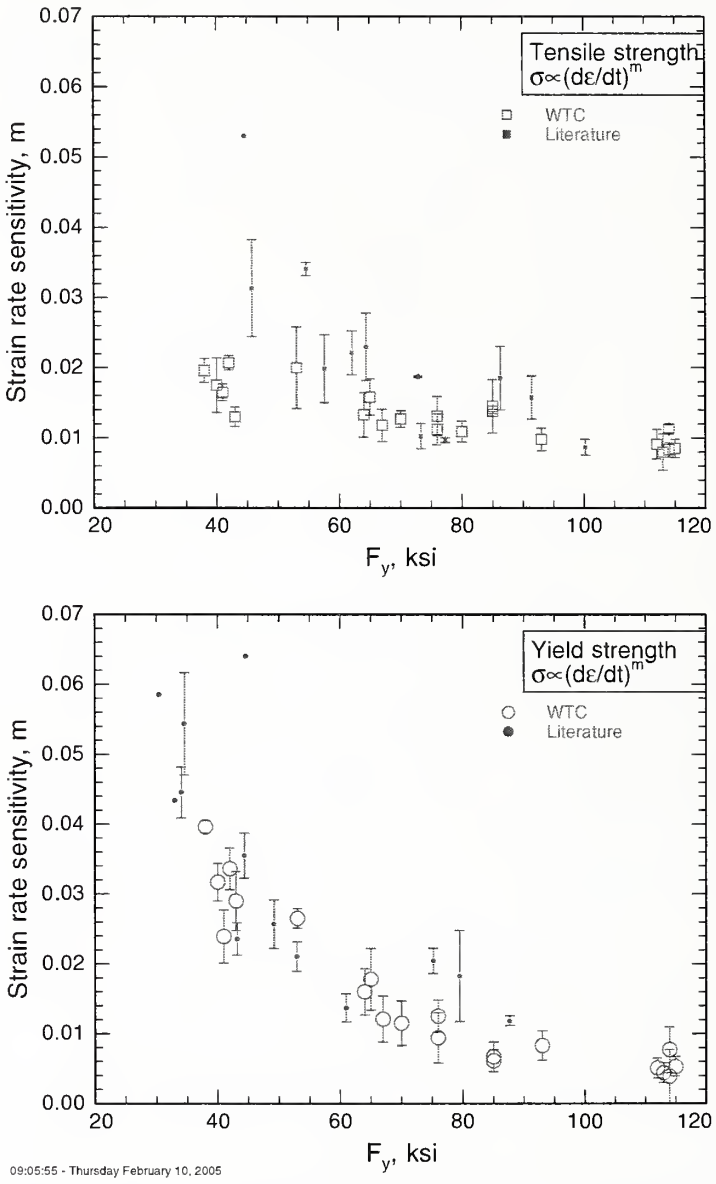

Figure 4–12. Comparison of strain rate sensitivities of NIST WTC steels to values for structural steels from the literature.

One limitation of the data from the WTC steels is that the strain rate sensitivity is determined using data only at the extremes of the strain rates. Gilat et al. (1997) found that the strain rate sensitivity of AISI 1020 steel at strain rates near 1 s^{-1} was negative. They argued that it arose from dynamic strain aging. Other investigations of plain-carbon and HSLA steels either did not probe this strain rate range (Couque 1988) or did and found that the strength increases monotonically with strain rate (Chatfield 1974, Davies 1975, Krafft 1962). Even steels likely to be susceptible to dynamic strain aging (Chatfield

1974, Krafft 1962, Manjoine 1944) exhibit this monotonic increase in strength with strain rate. In contrast to Gilat (1997), Harding (1972) found three regimes of constant, but positive, strain rate sensitivity of the yield strength of BS 968, a ferrite-pearlite structural steel. At strain rates less than 0.1 s^{-1}, the strain rate sensitivity is nearly zero. At rates up to 10^3 s^{-1} the strain rate sensitivity is $m \approx 0.07$. At rates above 10^3 s^{-1} the strain rate sensitivity is even higher.

There is no consistent relation between total elongation and strain rate in structural steels in the strain-rate range used in this investigation. Although Bleck et al. (2000) found that total elongation, El_t, in mild steel (C = 0.05 percent) decreases with increasing strain rate, they also found that values for other steels do not depend equally on strain rate. Manjoine (1944), Kendall (1965), Chatfield (1974), Davies (1975), Langseth (1991), and Harding (1972) also found no strong correlation between strain rate and total elongation. Bruce (2003) reported that ductility increases with increasing strain rate in HSLA steels.

Figures 4–13 and 4–14 compare the strain rate sensitivities of the total elongation of various structural steels from the literature to those obtained in the Investigation. The data for the WTC steels were all obtained using specimens of constant, identical geometry, but possibly different size, or using identical Flat-HSR 1" specimens at all rates. The data tables in Appendix A identify the specific specimen types employed. The elongation behavior of the steels from the perimeter and core columns is similar to the behavior of other structural steels. Uncertainties in the strain rate sensitivities of the total elongation are large for both literature and WTC steels. In many cases, the measured strain rate sensitivities are statistically indistinguishable from zero.

4.7 SUMMARY

The strain rate sensitivity of the yield and tensile strength of the perimeter and core column steels tested is similar to that of other structural steels reported. The total elongation of perimeter and core column steels generally increases slightly with increasing strain rate. The magnitude of the increase is several absolute percent and is similar to behavior reported for other structural steels.

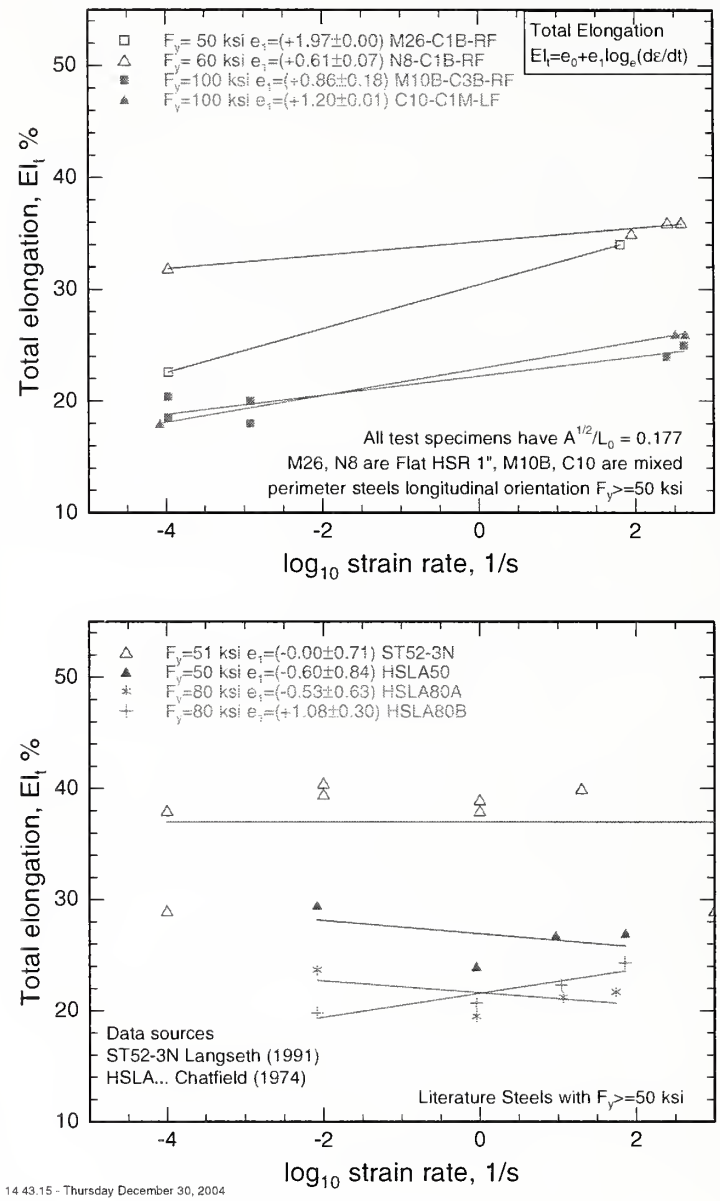

Figure 4–13. Total elongation, *El$_t$*, as a function of strain rate for high-strength, perimeter column steels and high-strength steels in the literature.

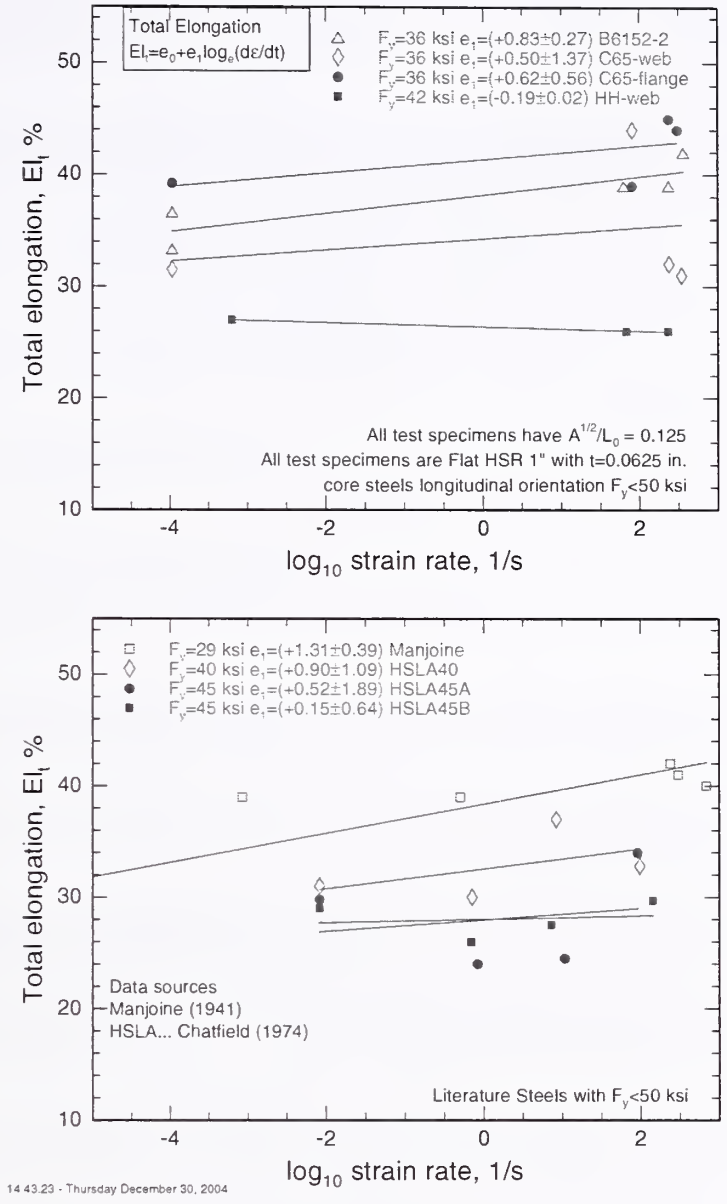

Figure 4–14. Total elongation, El_t, as a function of strain rate for low-strength, core column steels and low-strength steels in the literature.

4.8 REFERENCES

Bleck, W and I. Schael. 2000. Determination of crash-relevant material parameters by dynamic tensile tests. *Archiv für das Eisenhuttenwesen.* 71 173-178.

Bruce, D. M. 2003. *Dynamic Tensile Testing of Sheet Steels and Influence of Strain Rate on Strengthening Mechanisms in Sheet Steels.* Ph.D. Thesis. Colorado School of Mines.

Bruce, D. M. D. K. Matlock, J. G. Speer, and A. K. De. 2004. Assessment of the Strain-Rate Dependent Tensile Properties of Automotive Sheet Steels. SAE Technical paper 2004-01-0507. Presented at the SAE 2004 World Congress. March 8-11.

Chatfield, D. and R. Rote. 1974. Strain Rate Effects on Properties of High Strength, Low Alloy Steels. Society of Automotive Engineers. publication no. 740177.

Couque, H., R. J. Asaro, J. Duffy, and S. H. Lee. 1988. Correlations of Microstructure with Dynamic and Quasi-Static Fracture in a Plain Carbon Steel. *Met. Trans. A.* 19A .2179–2206.

Davies, R. and C. Magee. 1975. The Effect of Strain-Rate Upon the Tensile Deformation of Materials. *J Eng. Mater. Tech.* 97[2]. 151-155.

ESIS Designation P7-00. 2000. "Procedure for Dynamic Tensile Tests," European Structural Integrity Society. KH. Schwalbe, Editor. Approved August 2000.

Follansbee, P. S. 1985. High Strain Rate Compression Testing, The Hopkinson Bar. p.p 198-203. in *Metals Handbook 9th ed. Volume 8 Mechanical Testing.* American Society for Metals, Metals Park, Ohio.

Follansbee, P. S. 1985b. High Strain Rate Compression Testing, Introduction. in *Metals Handbook 9th ed. Volume 8 Mechanical Testing.* American Society for Metals, Metals Park, Ohio. 190-192.

Gilat, A. and X. Wu. 1997. Plastic Deformation of 1020 steel over a wide range of strain rates and temperatures. *Int. J. Plasticity.* 13[6-7]. 611-632.

Gillis. P. P and T. S. Gross. 1985. Effect of Strain Rate on Flow Properties. *Metals Handbook Ninth Edition, Volume 8 Mechanical Testing.* American Society for Metals. Metals Park, OH. p.p. 38-46.

Harding, J. 1972. Effect of High Strain Rate on the Room-Temperature Strength and Ductility of Five Alloy Steels. *J. Iron Steel Inst.* 210. 425-432.

Harding J. 1987. The Effect of High Strain Rate on Material Properties. Chapter 4 of *Materials at High Strain Rates.* T.Z. Blazynski, ed. Elsevier. London.

Hutchinson, J. W. and K. W. Neale. 1977. Influence of Strain-Rate Scnsitivity on Necking Under Uniaxial Tension. *Acta Metallurgica.* 25. 839–846.

Krafft, J. M. and A. M. Sullivan. 1962. On Effects of Carbon and Manganese Content and of Grain Size on Dynamic Strength Properties of Mild Steel. *Trans. A.S.M.* 55. 101–118.

Langseth, M. U. S. Lindholm, P. K. Larsen, and B. Lian. 1991. Strain Rate Sensitivity of mild steel grade ST-52-3N. *J. Eng. Mech.* 117[4]. 719–731.

Manjoine M. J. 1944. Influence of Rate of Strain and Temperature on Yield Stresses of Mild Steel. *Trans. A.S.M.* 66. A-211-A-218.

Wiesner, C. S. and H. MacGillivray. 1999. Loading Rate Effects on Tensile Properties and Fracture, *Proceedings of the Seventh Symposium Toughness of Steel, Fracture, Plastic Flow and Structural Integrity*. April 29, Abingdon, UK. 149–173.

Yan, B. and K. Xu. 2002. High-strain-rate behavior of advanced high strength steels for automotive applications. *44th Mechanical Working and Steel Processing Conference Proceedings.* Volume 40. Association for Iron and Steel Technology. Warrendale, PA.

This page intentionally left blank.

Chapter 5
IMPACT PROPERTIES

5.1 INTRODUCTION

Charpy impact tests were performed on steels from the World Trade Center (WTC) to provide data for comparison with the WTC-construction era literature data, and to provide additional information on how strain-rate affects the fracture mode of the steels. Estimates of the energy absorbed during an impact and the characteristic fracture mode of the steel are both of interest. As strain rates increase, the strength of steel tends to increase, and the fracture behavior tends to be less ductile and more notch-sensitive. Charpy impact testing is one of the methods used to evaluate these effects. This chapter discusses the data from the impact tests with respect to the transition temperature from ductile to brittle behavior, the absorbed energy levels associated with a given test temperature, and the influence of specimen orientation on the absorbed energy. The impact data generated in the Investigation were not used quantitatively used in the modeling efforts, however.

Figure 5–1 is a schematic example of the definition of the transition temperature expressed in terms of the energy absorbed. At high temperature there is an upper shelf of relatively constant absorbed energy where fracture is ductile. At low temperature the absorbed energy is also relatively constant, but low, and fracture is brittle. An S-shaped curve connects the two shelves. The transition temperature from ductile to brittle behavior can be defined in many different ways. Common definitions based on absorbed energy include the midpoint of the S-curve, a specific fraction of the upper shelf energy, or some fixed energy level, such as 20 ft lbf (27 J) or 30 ft lbf (41 J). The transition temperature can also be characterized by examining the change in appearance of the fracture surface with temperature. The fracture appearance transition temperature (or FATT) represents the temperature at which fibrous features occupy a specific fraction of the fracture surface. In this chapter, transition temperatures based on energy are defined as the midpoint between the upper and lower shelf energies. Transition temperatures based on fracture appearance are defined as the temperature at which ductile fracture features occupy 50 percent of the fracture surface. For any steel, the transition temperatures measured by these two definitions will rarely be identical, but frequently they will be similar.

5.2 PROCEDURES

To obtain the most useful data, representative samples of the steels found near the impact zone were evaluated. These samples do not represent the thicker sections and the types of steels found in the lower stories of the towers. Impact test specimens were oriented according to the requirements of ASTM International (ASTM) Standard Test Method A 370-97a. Tests were conducted according to the requirements of ASTM Standard Test Method E 23-02. Some components were thick enough to permit full-size (10 mm × 10 mm) specimen cross sections to be taken, but for many components the plates were too thin, and sub-size specimens were used. The ASTM Type A specimen, with $B = 5$ mm thickness (5 mm × 10 mm cross section), was used for the sub-size specimens. Figure 5–2 shows the geometries of the two specimens.

The specimens were oriented according to Section 4 of A 370. Figure 5–2 illustrates the sample orientations with respect to the rolling direction of the steel using a composite micrograph of the microstructure of a plate from perimeter column N9-C1T1-LF (F_y = 55 ksi). In the figure, the dark features are the bands of pearlite. The grains are the slightly elongated shapes with varied contrast. The inclusions are also elongated in the direction of rolling, but are not visible on this scale. The longitudinal orientation is such that the long dimension of the specimen is parallel to the rolling direction, and the fracture direction is perpendicular to the rolling direction. The long dimension of the transverse specimen is across the plate or structural shape, perpendicular to the rolling direction, and the fracture direction is parallel to the rolling direction. These longitudinal (L) and transverse (T) specimens are often referred to as L-T and T-L specimens respectively in other specimen orientation designation systems. For the samples taken at or near welds that join flanges and webs on perimeter columns, the welding direction coincides with the rolling direction of the steels. A transverse specimen can be located with the notch tip adjacent to the fusion line of the weld and promote crack growth in a direction parallel to the weld (parallel) in the heat affected zone (HAZ).

All specimens were tested on a 300 ft·lbf capacity impact machine that was verified to the requirements of E 23-02. The striker velocity at impact was approximately 17.7 ft/s. Strain rates at the notch are estimated (Poussard 2003) to approach 5000 s^{-1}. The average strain rate across the ligament of the sample is estimated to be about 100 s^{-1}, which is near that of the high-rate tensile tests. When testing sub-size specimens, the standard anvil supports for 10 mm thick specimens were replaced with higher ones, so the center of the striker met the center of the specimen.

Specimens were tested over a range of temperatures to characterize the transition behavior of the steels. Because of the scatter that is common in impact testing, multiple specimens were tested at most temperatures. All impact energy data were collected digitally using a precision encoder. The fracture surface appearance was assessed to estimate the fracture appearance transition temperature (FATT), which was defined as the temperature at which the fracture surface exhibited 50 percent ductile fracture features. Evaluations were made using the chart comparison technique of ASTM E 23 Annex A6. These estimates of percent shear provide qualitative information, complementary to the absorbed energy data.

This investigation employed only one sub-size specimen geometry, so these results can be compared to each other, but they cannot be directly compared to handbook data, which are usually developed on standard, full-thickness specimens. There is a large literature on methods for predicting the results of full-size specimen Charpy tests using sub-size specimens. Lucon (2001) presents a concise summary of the various methods for predicting the upper shelf energy, E_{us} as well as the ductile-to-brittle transition temperature. When unlimited material is available and plate thickness is greater than the Charpy specimen thickness, many methods simply develop an empirical correction factor by analyzing both full- and sub-size specimens. Because many of the plates of interest for the Investigation were less than 10 mm thick, this type of analysis was not possible.

For the scaling of energies, methods generally define a correction factor, K, that scales the upper shelf energy obtained from sub-size specimen, E_{ss}, to the expected energy from full-size specimens, E_{fs}:

$$E_{fs} = KE_{ss} \qquad 5\text{–}1$$

The correction factors, K, take many different forms. Table 5–1 summarizes some common ones. All include some permutation of the specimen width, B, and ligament depth, b, Fig. 5–2. More recent correction factors incorporate details of the notch, including the notch radius, R, and notch angle, θ.

The individual studies on specimen size effect (Corwin 1986, Kayano 1991, Lucas 1986, Lucon 2001, Louden 1988, Manahan 1990, Schubert 1995, Schwartzbart 1954, Uehira 2004) reach different, incompatible conclusions about the suitability of the different correction factors. These discrepancies probably arise because each investigator characterized different steels, using test specimens with different notch and loading geometries. Several of the correction factors (Corwin 1986, Lucas 1986) do not incorporate information about the notch geometry.

This investigation uses a correction factor, K, first proposed by Lucas (1986)

$$K = \frac{B_{fs} b_{fs}^2}{B_{ss} b_{ss}^2} = \frac{10\ \text{mm} \times (8\ \text{mm})^2}{5\ \text{mm} \times (8\ \text{mm})^2} = 2 \qquad 5\text{–}2$$

Note that nearly all the proposed correction factors in Table 5–1 predict $K = 2$ because the full-size and sub-size specimens have identical notch geometries. These scaling factors do not explicitly consider the effect of increased constraint for larger specimens, as ASTM E 23-04 (2004) Appendix X1 discusses.

Different scaling methods must be used for estimating the full-size specimen transition temperature from sub-size specimens (Lucon, 2001). The transition temperatures in this report, which were estimated from fracture appearance, have not been scaled.

5.3 RESULTS

Appendix A of this report tabulates the data from individual impact tests. Table 5–2 summarizes some of the important experimental results. The rest of this section summarizes the results for the steels arranged by location in the building.

5.3.1 Perimeter Columns

The upper shelf energy of longitudinal specimens from flange material from perimeter column N8-C1M1 (F_y = 60 ksi specified strength, F_y = 68.8 ksi measured), located between the 97th and 100th floors of WTC 1, is 38.3 ft·lbf, Fig. 5–3. At about -5 °F the absorbed energy begins to decrease as the fracture mode enters the transition region. For the transverse specimens, the absorbed energy drops from an upper shelf of 10.4 ft lbf beginning at about -40 °F. For both orientations, fracture surface evaluations indicate that the transition temperature (FATT) is about -95 °F. After correcting for sub-size specimen effects using Eq. 1–2, the estimated upper shelf absorbed energy is 76.6 ft·lbf and 20.8 ft·lbf for full-thickness longitudinal and transverse orientations respectively. The ratio of the upper shelf energies for the longitudinal to transverse orientations is approximately 3.7.

The impact data for the flange of the C10-C1M1 perimeter column from WTC 1 west face, column 452, floors 85-88 in Fig. 5–3 show that the upper shelf for both the longitudinal and transverse orientations extends throughout the temperature range evaluated. Fracture surface evaluations confirm this result and indicate that the transition temperature (FATT) is below -100 °F for this quenched and tempered steel

(specified F_y = 90 ksi, supplied F_y = 100 ksi, measured F_y = 109.4 ksi). As is the case for the N8-C1M1 flange, there are two upper shelves: 47.1 ft·lbf for longitudinal specimens and 11.4 ft·lbf for the transverse specimens. After correcting for sub-size specimen effects, the upper shelf absorbed energies for full-size longitudinal and transverse specimens are 94.2 ft·lbf and 22.8 ft·lbf respectively.

The transition curve of steel from the perimeter column spandrel N8-C1B1 (specified F_y = 42 ksi, measured F_y = 54.4 ksi), Fig. 5–4, is similar to that for the flange material from the same column. The absorbed energy drops from the upper shelf at temperatures below about -40 °F. The upper shelves for the longitudinal and transverse specimen orientations are 40.9 ft·lbf and 13.3 ft·lbf respectively. Fracture surface evaluations indicate the transition to 100 percent brittle fracture is nearly complete at -112 °F. After correcting for the effects of the sub-size specimen using Eq. 1–2, the estimated upper shelf energy for full-size longitudinal specimens is 81.8 ft·lbf, and the upper shelf energy for the transverse specimens is 26.6 ft·lbf.

5.3.2 HAZ Materials from Perimeter Columns

The upper-shelf absorbed energy values of HAZ (heat affected zone) specimens, notched near the toe of a fillet weld on the flange of perimeter column N8-C1M1, are similar to those of the unaffected flange materials, Fig. 5–3. The upper shelf is 44.3 ft·lbf for the longitudinal specimens, and 9.4 ft·lbf for the transverse specimens. The data and fracture surface evaluations indicate that the specimens with longitudinal orientations have entered the transition region at 0 °F, but the transverse specimens have not. Again, after correcting to full-size using Eq. 1–2, the upper shelf absorbed energies for the longitudinal and transverse specimens are 88.6 ft·lbf and 18.8 ft·lbf respectively. The transition temperature of the HAZ region appears to be higher than the unaffected flange material, but this has little practical significance considering the transition temperature is still quite low and likely below 0 °F.

The upper shelf absorbed energies from the HAZ material from the C10-C1M1 flange, tested using transversely oriented specimens are similar to those of the unaffected C10-C1M1 transverse flange material, Fig. 5–3. The average absorbed energy is 11.0 ft·lbf down to temperatures below-100 °F. After correcting for sub-size specimen effects, the upper shelf absorbed energy for the transverse specimens is 22.0 ft·lbf.

5.3.3 Core Columns

Impact properties of specimens from the web of core column C-80, a 14WF184 shape from WTC 1 column 603 floors 92–95, (specified F_y = 36 ksi, measured F_y = 34.4 ksi) also vary as a function of sample orientation, Fig. 5–4. The average absorbed energy of the room temperature tests is (53.8±6.3) ft·lbf for the longitudinal specimens, and (26.1±1.2) ft·lbf for the transverse specimens. The absorbed energy decreases with temperature throughout the range tested, indicating transition behavior over the range of 0 °F < T < 172 °F. Fracture surface evaluations show approximately 95 percent ductile features at 172 °F for both longitudinal and transverse specimen orientations, and less than 50 percent ductile features at room temperature. The transition temperatures (FATT) for both orientations are greater than room temperature and less than 140 °F.

5.3.4 Trusses

The data for the $D = 0.92$ in. diameter truss rod longitudinal samples (specified $F_y = 50$ ksi, measured $F_y = 60.0$ ksi) show a gradual transition in impact behavior throughout most of the temperature range tested (Fig. 5–5). The absorbed energy drops from 107 ft·lbf at 172 °F to 4.9 ft·lbf at -4 °F. At room temperature the absorbed energy is (32.4±4.8) ft·lbf. Fracture surface evaluations show about 90 percent ductile fracture at 172 °F and about 30 percent ductile fracture at room temperature. The transition temperature (FATT) is higher than room temperature, likely about 100 °F.

The steel from the floor-truss angles (2 in.×1.5 in.×0.25 in.) (specified $F_y = 50$ ksi, measured $F_y = 52.2$ ksi-58.8 ksi) also shows transition behavior throughout the temperature range tested (Fig. 5–5). The absorbed energy drops from (31.1±1.1) ft·lbf at room temperature to 1.6 ft·lbf at -76 °F. Fracture surface evaluations indicate that the transition temperature (FATT) is likely below room temperature (50 percent to 70 percent ductile at room temperature). After correcting for sub-size specimen effects using Eq. 1–2, the absorbed energy is (62.2±2.2) ft·lbf at room temperature, (17.8±1.1) ft·lbf at -4 °F, and 3.2 ft·lbf on the lower shelf at -76 °F.

5.3.5 Truss Seats

The $F_y = 36$ ksi truss seats from perimeter columns, like the floor-truss angle and rod, show transition behavior throughout the temperature range tested, Fig. 5–5. The absorbed energies for transverse specimens range from 27.5 ft·lbf to 36.8 ft·lbf at 172 F, and drop to about 2.3 ft·lbf at –40 °F. At room temperature the absorbed energies of truss seats N13-C3B1, M4-C3T, and N8-C3T are (7.7±1.1) ft·lbf, (11.9±0.5) ft·lbf, and (21.2±0.5) ft·lbf respectively. Fracture surface evaluations indicate that the N13 and M4 samples were about 10 percent ductile at 77 °F, 50 percent ductile at 140 °F, and about 80 percent ductile at 172 °F. The N8 samples were 20 percent ductile at 77 °F, 50 percent ductile at a temperature between room temperature and 104 °F, and nearly 100 percent ductile at 172 °F.

5.3.6 Bolts

At 68 °F, the averaged absorbed energy for the A 325 bolt material in Fig. 5–6 is (41.1±12.4) ft·lbf, and the fractures were 100 percent ductile. The scatter and scarcity of data prevent a more accurate estimate of the average. Again, correcting for sub-size specimen effects, the room temperature absorbed energy is (82.2±24.8) ft·lbf. As the temperature drops to 32 °F, fracture surface evaluations indicate the transition temperature region is entered. At -40 °F the fracture mode is approximately 75 percent brittle, so the lower shelf energy starts somewhere below this temperature.

5.4 DISCUSSION

5.4.1 Perimeter Columns

Figures 5–7 and 5–8 summarize the impact toughness data for the various building components tested. Data for sub-size specimens are normalized for comparison with data for full-size specimens using Eq. 1–2. The summary plots use the same scales to facilitate comparison.

The transition temperatures of the N8 perimeter column steels, Fig. 5–7 and Table 5–2 are in the expected range based on the relationships shown in Fig. 5–9 for the strength and toughness of HSLA steels in 1967 (Irvine 1967b). These data show that a fine-grain ferrite-pearlite steel (or a controlled rolled steel) with a strength 50 ksi $\leq F_y \leq$ 65 ksi would be expected to have a transition temperature in the range -50 °F $\leq T \leq$ -100 °F.

The impact data for the higher strength quenched and tempered C10-C1M1 flange steel (F_y = 109.6 ksi), Fig. 5–7, show no indication of transition behavior down to –120 °F. The transition temperature of this material, as well as the HAZ samples tested from it, is well below –100 °F, which is far below the temperatures predicted by the historic data in Fig. 5–9.

The transition temperatures of the perimeter column steels are similar and are lower than those predicted by historical data. These steels are very tough at 70 °F, the temperature at the time of the aircraft impact. There is no reason to expect that they would fail in a brittle manner at high strain rate.

The upper shelf energies of the perimeter column longitudinal specimens, which have a notch orientation that is transverse to the rolling direction, are approximately three times larger than those of the transverse specimens. By the mid 1970's this effect was understood (Irvine 1967, Wells 1975, Kozasu 1975, DeArdo 1975, Farrar 1975, Tamura 1988). The toughness of steel in the upper shelf region is influenced by the morphology of inclusions, pearlite, grains and other constituents in the steel. Banded pearlite and increasing inclusion lengths, for example, were known to reduce the through-thickness (short transverse) impact toughness of structural steels (Fig. 5–2).

One of the key issues in understanding the effect of microstructure on the toughness of these plate steels is that sulfide inclusions become more plastic relative to the steel with decreasing rolling temperatures and approach the deformability of the ferrite matrix at 1650 °F (900 °C) (Baker 1972). In the 1960's, the development of controlled rolled steel technologies resulted in the use of lower rolling temperatures than had been common in the past. This approach to plate production, for which a lower rolling temperature was key, produced high strength, fine grain, ferrite-pearlite steels, with the adverse effect of elongating the sulfide inclusions along the rolling direction. Since inclusions and other microstructural features that can reduce toughness are oriented with their longest lengths and largest areas on planes parallel to the plane of rolling, toughness can depend strongly on sample orientation in heavily rolled or controlled rolled steels.

Figures 5–10 and 5–11 show that the fracture surfaces of longitudinal and transverse specimens are characteristically different, which reflects the influence of the microstructure on the fracture process. When the plane of crack growth is perpendicular to the rolling direction, the fracture surface is convoluted and has circular ductile dimple features where voids initiated at manganese sulfide inclusions grew and coalesced just prior to failure. When the direction of crack growth is parallel to the rolling direction, the fracture surface has ductile linear features, which form a corduroy texture with long parallel peak-valley features, Fig. 5–12. For this orientation, the void growth is tubular rather than spherical, because the lengths of the elongated inclusions are parallel to the crack growth direction. Fracture features on the surfaces of these elongated ductile dimples, Figs. 5–11c and 5–11d, have morphologies that might be expected for disrupted pearlite colonies and remnants of manganese sulfide inclusions. Figure 5–13 shows the locations and morphologies of manganese sulfides on the fracture surface of a transverse impact specimen using an elemental x-ray map. These results indicate that many of the film or plate-like

features on the fracture surface are manganese sulfides. As the number and length of the manganese sulfide inclusions in the steels increase, the resistance to crack growth in this orientation decreases.

The impact energies of these perimeter column flange and spandrel steels are in the range expected, compared with data from the literature, see Table 5–3. The corrected upper shelf impact energies for the longitudinal specimens, for example, are about 75 ft·lbf, which is similar to the 84 ft·lbf reported for a 0.012 S low carbon structural steel (Hulka 1993).

Although the upper shelf energies for the flange and spandrel steels are within the range expected for steels of the late 1960's, the ratio of longitudinal to transverse energy is near the maximum reported in literature. Ratios of longitudinal to transverse properties of about 3 have been reported in WTC-era HSLA ferrite-pearlite steel (Korchynsky 1970) and also for heavily rolled niobium X60 steels (Kozasu 1973). These differences in the impact toughness of longitudinal and transverse orientations were of concern at the time, but were not improved significantly for HSLA structural steels until the 1970's, when sulfur control in steelmaking became common practice (Gladman 1997). As late as 1970 the reduction in sulfur content to a level below 0.01 mass percent, where transverse toughness begins to increase significantly, was cited as uneconomical in large scale steel production (Korchynsky 1970).

One of the common concerns for low through-thickness toughness was cracking under welds on structural members, which was being discussed in relation to controlled rolled steels in the 1960's. The problem was primarily viewed as a concern for thick sections, in which the high post-weld stresses could produce large cracks under the welds due to delamination. In the case of the WTC perimeter columns and spandrels, delaminations due to welding have not been observed to be a problem, but the lower transverse toughness relates to the ductile tearing that occurred along the direction of rolling and the "pull-out" failure modes at welded components on the faces of the columns.

5.4.2 HAZ Materials from Perimeter Columns

The impact energies of the perimeter column HAZ samples indicate that the welding operation had little practical effect on the toughness, Fig. 5–7. The lower impact toughness for the transverse HAZ specimen orientation is relevant to the fractures seen along the edges and at the joints of some of the columns, presumably due to overload during the collapse.

5.4.3 Core Columns

The absorbed energy at 77 °F of transverse web specimens from core column C-80, (26.1±1.2) ft·lbf, are similar to those that Barsom (1988) reported for slightly heavier wide-flange shapes, Table 5–3. In those tests, the average room-temperature absorbed energy was 37 ft·lbf, but the data ranged over $12 < CVN < 80$ ft·lbf. The estimate that the FATT is between room temperature and 140 °F is consistent with the average value of 113 °F that Barsom (1988) reported.

5.4.4 Trusses

The impact energies for the truss angle and rod, Fig. 5–8, increase with increasing temperature, which indicates transition behavior in the temperature range tested. The upper shelf is not apparent in these data, but fracture surface evaluations indicate that the FATT is near room temperature. Literature data (Wilson

1978) indicate that a range in transition temperature (FATT) from about 70 °F to 145 °F might be expected for steel plate grades such as A 36 and A 537, having thickness of 0.75 in. to 1.5 in. The transition temperatures of other late 1960's, 0.17 C – 0.8 Mn steels are also at or above room temperature (Duckworth 1967). Considering the nominal composition of the WTC truss angle and rod (0.04 Al, 0.20 C, 0.8 Mn, 0.004 N, 0.05 Si, and 0.01 to 0.03 S) and the other factors known to influence the transition temperature, such as pearlite content, precipitation strengthening, and free nitrogen content, only pearlite content would be expected to raise the transition temperature higher than that predicted for the 0.17 C – 0.8 Mn steels. This is because the higher carbon content would increase the pearlite content, if all other factors remained unchanged. The nitrogen and silicon contents of the truss steels are low, and the sulfur content affects only the absorbed energy and not the transition temperature. So, the near-room-temperature transition temperatures of the angle and rod shapes from the trusses are consistent the properties expected for this steel. Clearly, these materials were ductile enough for fabrication, which was the primary consideration.

5.4.5 Truss Seats

Figure 5–8 summarizes the impact data for the F_y = 36 ksi seat materials from perimeter columns N8, N13, and M4. The transition temperatures for the truss seats are all above room temperature, and fracture surface evaluations indicate very low ductility at room temperature. In Fig. 5–14, for example, the fracture surfaces of the N-13 and M-4 samples show that fracture occurred in a predominantly brittle manner at room temperatures. This finding may be relevant to possible scenarios for floor collapse.

5.4.6 Expected Values of Impact Toughness

The measured impact properties of the recovered steels must be kept in proper context to be useful. One context is their similarity to the properties of other structural steels of the era. For this context, it is important to remember that there were no specified requirements for impact properties on the steels used to build the WTC. No ASTM specifications for structural steel intended for use in buildings, then or now, require Charpy impact tests. The current AISC LRFD manual (2001) only requires impact testing in one very limited case: steels for heavy Group 4 and 5 rolled shapes used in tension and spliced by welding must have a minimum CVN impact toughness of 20 ft·lbf at 70 °F. Furthermore, the literature discussions of the era indicate that not even the simplest of minimum toughness requirements for structural steels had been agreed upon in the late 1960's (Irvine 1967). One criterion, that the steel possess a CVN impact toughness of 15 ft·lbf at the operating temperature, originated with the WWII experience of the catastrophic failure of the Liberty ships. (Barsom 1987b)

Table 5–3 summarizes the historical data on Charpy impact toughness of structural steel supplied to ASTM specifications. The impact toughness of WTC steel evaluated at room temperature is quite similar to the historical values. The data for core wide-flange column C80 can be compared to the heavyweight A 36 wide-flange data in Table 5–3. The perimeter column plate steels N8-C1M1 and N8-C1-B1 can be compared to the A 572 plate steels. Finally the F_y = 100 ksi perimeter column plate C10-C1M has properties similar to the A 514 Type E steel. The impact toughness of all the of the historical and WTC column steels exceeds 15 ft·lbf at 70 °F. Only the impact toughnesses of some of the truss seats steels are less than this value.

5.5 SUMMARY

Table 5–2 summarizes the results of the Charpy tests. The upper shelf energies of the perimeter column steels, including material from the heat-affected zones of welds, average 76 ft·lbf longitudinal and 19 ft·lbf transverse. Their transition temperatures are all well below room temperature, and room temperature is on the upper shelf. The room temperature absorbed energies of the truss and core-column wide-flange steels are about 40 ft·lbf longitudinal, and their transition temperatures are at room temperature or above. The room-temperature transverse absorbed energies of the truss seat steels are as low as 7 ft·lbf, and their transition temperatures are all above room temperature. Fracture-surface evaluations demonstrated that the failure of the truss seat steels at room temperature was predominantly brittle.

The impact properties of the steels, except some of the truss seat steels, are consistent with contemporaneous structural steels intended for use in buildings.

5.6 REFERENCES

AISC (American Institute of Steel Construction). 2001. *Load and Resistance Factor Design Specification for Structural Steel Buildings*. Chicago, Il. Section A.3.1c, page 3 and commentary on p.p. 168-169. Sept. 4.

ASTM (American Society for Testing and Materials). 2004. E 23-04 Standard Test Methods for Notched Bar Impact Testing of Metallic Materials. Book of Standards volume 03.01. American Society for Testing and Materials. West Conshohocken, Pa.

Baker, T. J. 1975. Use of Scanning Electron Microscopy in Studying Sulfide Morphology on Fracture Surfaces. In *Sulfide inclusions in steel: proceedings of an international symposium, 7-8 November 1974, Port Chester, New York.* J. J. DeBarbadillo and E. Snape, eds. American Society for Metals. Metals Park, Ohio. 135-158.

Baker T. J. and J. A. Charles. 1972. Deformation of MnS Inclusions in Steel. *Journal of the Iron and Steel Institute.* **210**. 680-690.

Barsom J. M. and S. R. Novak. 1977. *Subcritical Crack Growth and Fracture of Bridge Steels.* National Cooperative Highway Research Program Report 181. Transportation Research Board, National Research Council.

Barsom J. M. 1987. Material Considerations in Structural Steel Design. *AISC Engineering Journal.* **24**[3] 127-139.

Barsom, J. M. and S. T. Rolfe. 1987b. *Fracture and Fatigue Control in Structures. Applications of Fracture Mechanics*. 2nd edition. Prentice-Hall, Inc. New Jersey. Section 15.4.

Barsom J. M. and B. G. Reisdorf. 1988. Characteristics of Heavyweight Wide-Flange Structural Shapes. *Welding Research Council Bulletin.* Number 332. 1-19. April.

Corwin, W.R. and A.M. Hoagland 1986. Effect of Specimen Size and Material Condition on the Charpy Impact Properties of 9Cr-1Mo-V-Nb Steel. *p.p.* 32-388in *The Use of Small-Scale Specimens for Testing Irradiated Material*, ASTM STP 888. W.R. Corwin and G.E. Lucas, eds. American Society for Testing and Materials. Philadelphia, Pa.

DeArdo Jr. A. J. and E. G. Hamburg. 1975. Influence of Elongated Inclusions on the Mechanical Properties of High Strength Steel Plate. In *Sulfide inclusions in steel: proceedings of an international symposium, 7-8 November 1974, Port Chester, New York.* J. J. DcBarbadillo and E. Snape, eds. American Society for Metals. Metals Park, Ohio.309-337.

Duckworth, W. E. 1967. Metallurgy of Structural Steels: Present and Future Possibilities. 1967. In *Strong tough structural steels: proceedings of the joint conference organized by the British Iron and Steel Research Association and the Iron and Steel Institute at the Royal Hotel Scarborough, 4-6 April 1967.* ISI Publication 104. Iron & Steel Institute. London. 61-73.

Farrar J. C. M. and R. E. Dolby. 1975. Lamellar Tearing in Welded Steel Fabrication. The Role of Sulfide Inclusions. In *Sulfide inclusions in steel: proceedings of an international symposium, 7-8 November 1974, Port Chester, New York.* J. J. DeBarbadillo and E. Snape, eds. American Society for Metals. Metals Park, Ohio. 253-285.

Frank, K. H., J. M. Barsom, and R. O. Hamburger. 2000. *State of the Art Report, Base Metals and Fracture.* SAC-2000-5a. Federal Emergency Management Agency.

Gladman, T. 1997. *The Physical Metallurgy of Microalloyed Steels.* Thc Institute of Materials. London

Hulka, K. and F. Heisterkamp. Low Carbon Structural Steels, The Key to Economic Constructions. 1993. *Low Carbon Steels for the 1990's.* R. Asfahani and G. Tither, eds. TMS. 211-218.

Irvine, K. J. 1967. The Development of High-Strength Structural Steels. In Strong tough structural steels: proceedings of the joint conference organized by the British Iron and Steel Research Association and the Iron and Steel Institute at the Royal Hotel Scarborough, 4-6 April 1967. ISI Publication 104. Iron & Steel Institute. London. 1-10.

Kayano, H., H. Kurishita, A. Kimura, M.Narui, M. Yamazaki, and Y. Suzuki. 1991. Charpy Impact Testing using Miniature Specimens and its Application to the Study of Irradiation Behavior of Low-Activation Ferritic Steels. *J. Nucl. Mater.* **179-181** 425-428.

Korchynsky, M. and H. Stuart. 1970. The role of strong carbide and sulfide forming elements in the manufacture of formable high strength low alloy steels. Symposium low alloy high alloy steels. Symposium jointly organized by the Metallurg Companies held at Nuremberg, BRD, on May 21-23, 1970. 17-27

Kozasu, I. and T. Osuka. 1973. Processing Conditions and Properties of Control-Rolled Steel Plates. In Processing and Properties of Low Carbon Steel, J. M. Gray, ed. The Metallurgical Society of AIME. New York. 47-68.

Kozasu, I. and J. Tanaka. 1975. Effects of Sulfide Inclusions on Notch Toughness and Ductility of Structural Steels. In Sulfide inclusions in steel: proceedings of an international symposium, 7-8 November 1974, Port Chester, New York. J. J. DeBarbadillo and E. Snape, eds. American Society for Metals. Metals Park, Ohio. 287-308.

Kumar, A.S., B.S. Louden, F.A. Garner, and M.L. Hamilton. 1993. Recent Improvements in Size Effects Correlations for DBTT and Upper Shelf Energy of Ferritic Steels. *p.p.* 47-61 in *Small- Specimen Test Techniques Applied to Nuclear Reactor Vessel Thermal Annealing and Plant Life Extension.* ASTM STP 1204. W.R. Corwin et al., eds. American Society for Testing and Materials. Philadelphia, Pa.

Louden, B.S., A.S. Kumar, F.A. Garner, M.L. Hamilton, and W.L. Hu. 1988. The Influence of Specimen Size on Charpy Impact Testing of Unirradiated HT-9. *J. Nucl. Mater.* **155-157**. 662-667.

Lucas, G.E., G.R. Odette, J.W. Sheckherd, P. McConnell, and J. Perrin. 1986. Subsized Bend and Charpy V-Notch Specimens for Irradiated Testing. *p.p.* 305-324in *The Use of Small-Scale Specimens for Testing Irradiated Material*, ASTM STP 888. W.R. Corwin and G.E. Lucas, eds. American Society for Testing and Materials. Philadelphia, Pa.

Lucon, E. 2001. Material Damage Evaluation of Primary Power Plant Components Using Sub-size Specimens. Advanced Engineering Materials. 3[5]. 291-302.

Manahan, M.P. and C. Charles. 1990. A Generalized Methodology for Obtaining Quantitative Charpy Data from Test Specimens on Nonstandard Dimensions. *Nucl. Tech.* **90**. 245-259.

Poussard, C., C. Sainte Catherine, P. Forget, and B. Marini, 2003. On the Identification of Critical Damage Mechanisms Parameters to Predict the Behavior of Charpy Specimens on the Upper Shelf. in Predictive Material Modeling: Combining Fundamental Physics Understanding, Computational Methods and Empirically Observed Behavior. M. T. Kirk and M. Erickson Natishan, eds. ASTM STP 1429. American Society for Testing and Materials, West Conshohocken, Pa.

Schubert, L.E. A.S. Kumar, S.T. Rosinski, and M.L Hamilton. 1995. Effect of Specimen Size on the Impact Properties of Neutron Irradiated A533B Steel. *J. Nucl. Mater.* **225**. 231-237.

Schwartzbart, H and J.P. Sheehan. 1954. Effect of Specimen Size on Notched Bar Impact Properties of Quenched-and-Tempered Steels. *ASTM Proc.* **54** 939-963.

Tamura, I., C. Ouchi, T. Tanaka, and H. Sekine. 1988. Thermomechanical Processing of High Strength Low Alloy Steels. Butterworth & Co. Ltd. London.

Uehira A. and S. Ukai. 2004. Empirical Correlation of Specimen Size Effects in Charpy Impact Properties of 11Cr-0.5Mo-2W, V, Nb Ferritic-Martensitic Stainless Steel. *J. Nucl. Sci. Tech.* **41**[10] 973-980.

Wells, R. G. 1975. Metallographic Techniques in the Identification of Sulfide Inclusions in Steel. In Sulfide inclusions in steel: proceedings of an international symposium, 7-8 November 1974, Port Chester, New York. J. J. DeBarbadillo and E. Snape, eds. American Society for Metals. Metals Park, Ohio. 123-134.

Wilson A. D. 1978. Comparisons of Dynamic Tear and Charpy V-notch Impact Properties of Plate Steels. Trans. ASME. **100**. 204-211.

Table 5–1. Common sub-size to full-size upper shelf energy correction factors.

Reference	Correction Factor, K	K Note a	Definitions
Corwin 1986	$\frac{B_{fs}b_{fs}}{B_{ss}b_{ss}}$	2	B = specimen width b = ligament depth (see Figure 5–2)
Corwin 1986	$\frac{\left(B_{fs}b_{fs}\right)^{1.5}}{\left(B_{ss}b_{ss}\right)^{1.5}}$	2.8	
Lucas 1986	$\frac{B_{fs}b_{fs}^2}{B_{ss}b_{ss}^2}$	2	
Louden 1988	$\frac{B_{fs}b_{fs}^2}{L_{fs}K_t} \Big/ \frac{B_{ss}b_{ss}^2}{L_{ss}K_t}$	2	L = span = 40 mm per Fig. A1.2 of ASTM E 23 K_t = notch stress concentration factor[b]
Schubert 1995	$\frac{B_{fs}b_{fs}^2}{L_{fs}K_t'} \Big/ \frac{B_{ss}b_{ss}^2}{L_{ss}K_t'}$	2	K_t' = alternate notch stress concentration factor

a. K is evaluated for the NIST Charpy specimen geometries.

b. K_t and K_t' depend only on the notch angle, θ, root radius, R, and ligament depth, b. These three parameters are identical in the full-size and sub-size specimens of the Investigation. Formulas for K_t can be found in Kumar (1993).

Note: Subscripts *ss* and *fs* refer to sub-size and full-size specimens, respectively.

Table 5–2. Summary of Charpy data.

Specimen	Description	F_y ksi	Location[a]	E_{us} longitudinal ft·lbf (Note c)	E_{us} transverse ft·lbf	Transition T (FATT) °F (Note b)	E_{77} longitudinal[c] ft·lbf (Note d)	E_{77} transverse[d] ft·lbf
N8-C1M1	flange t=0.3125 in. plate sub-size specimen	60	WTC 1 142 97-100	76.6	20.8	-95	76.7±2.9	21.6±0.3
C10-C1M1	flange t=0.25 in. plate sub-size specimen	100	WTC 1 452 85-88	94.2	22.8	<-100	92.0±2.4	23.3±0.7
N8-C1B1	spandrel t=0.375 in. plate sub-size specimen	42	WTC 1 142 99	81.8	26.6	n/d	83.6±2.2	26.4±0.8
N8-C1M1	Heat-affected zone sub-size specimen	n/a	WTC 1 142 97-100	88.6	18.8	<0	87.6±6.2	19.2±0.4
C10-C1M1	Heat-affected zone sub-size specimen	n/a	WTC 1 452 85-88	n/d	22.0	<-100	n/d	23.1±1.2
C80	core WF web 14WF184 full-size specimen	36	WTC 1 603 92-95	n/d	n/d	77 < T < 140	53.8±6.3	26.1±1.2
truss rod	D=0.92 in. full-size specimen	50	unknown	n/d	n/d	~100	32.4±4.8	n/d
truss angle	2 in.×1.5 in. ×0.25 in. sub-size specimen	50	unknown	n/d	n/d	<77	62.2±2.2	n/d
N13	truss seat full-size specimen	36	WTC 1 130 99-102	n/d	n/d	140	n/d	7.7±1.1
N8	truss seat full-size specimen	36	WTC 1 142 97-100	n/d	n/d	77 < T < 104	n/d	21.2±0.5
M4	truss seat full-size specimen	36	unknown	n/d	n/d	140	n/d	11.9±0.5
A 325 bolt	D=7/8 in. bolt sub-size specimen	n/a	unknown	82.2	n/d	-40 < T<32	n/d	n/d

a. Location code example: WTC 1 142 97-100: Tower 1, column line 142, between floors 97 and 100.
b. Transition temperature evaluated from fracture surface appearance (FATT).
c. E_{us} = upper shelf absorbed energy, corrected using Eq. 1–2 where appropriate.
d. E_{77} =room temperature absorbed energy, average and standard uncertainty, corrected using Eq. 1–2 where appropriate.
Key: HAZ, heat affected zone; long, longitudinal orientation; trans, transverse orientation.
n/a = not applicable; n/d, not determined.
Note: The reported uncertainty, u, is the estimated uncertainty of the mean of n values:

$$u(E_{77}) = \left[\frac{1}{n(n-1)} \sum E_i - \overline{E})^2 \right]^{1/2}$$

Table 5–3. Historical data on Charpy impact toughness of structural steel.

Reference	Year	Steel	Type	CVN ft·lbf	T °F	Orient	Notes
Barsom and Novak 1977	1977	A36	plate	28	72	L&T	single plate t=1 in, Figure C-1 and Table 3
Barsom and Reisdorf 1988	1988	A36	wide-flange W14 shapes >342 lb/ft	37	70		28 individual shapes. Range: 12 ft·lbf<CVN<80 ft·lbf
Frank 2000	1994	A36	wide-flange shapes	95	70		91% of the specimens had CVN>30ftlb @70 °F, Table 6-4
Barsom 1987	1972	A572 Gr 50	plate	55	70	L	also appears in (Frank 2000) 52 plates from 6 mills
Barsom 1987	1972	A572 Gr 50	plate	37	40	L	"
Barsom 1987	1972	A572 Gr 50	plate	21	0	L	"
Barsom 1987	1972	A572 Gr 50	plate	25	70	T	"
Barsom 1987	1972	A572 Gr 50	plate	18	40	T	"
Barsom 1987	1972	A572 Gr 50	plate	12	0	T	"
Barsom and Reisdorf 1988	1988	A572	wide-flange W14 shapes >342 lb/ft	38	70	T	22 individual shapes Range: 11 ft·lbf<CVN<81 ft·lbf
Frank 2000	1994	A572	wide-flange	61	70		77% of specimens had CVN>30ftlb @70 °F, Table 6-4
Barsom and Novak 1977	1977	A514 Type E	plate	65	70	L	single plate, t = 1 in. Figure C-10 and Table 3
Barsom and Novak 1977	1977	A514 Type E	plate	40	70	T	"

a. Year refers to first year of publication for references that cite other sources.
b. CVN: absorbed energy in Charpy test.
c. Orient: specimen orientation with respect to rolling direction
Key: L, longitudinal; T, transverse.

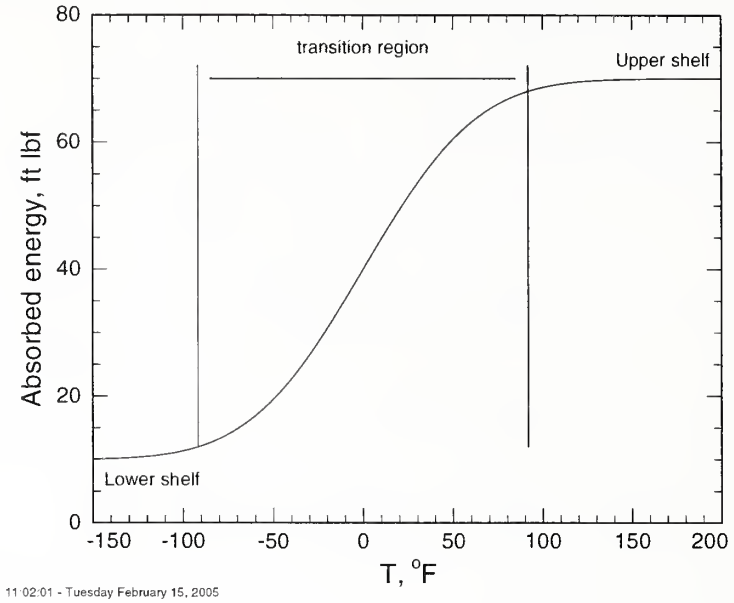

Figure 5–1. An example transition curve.

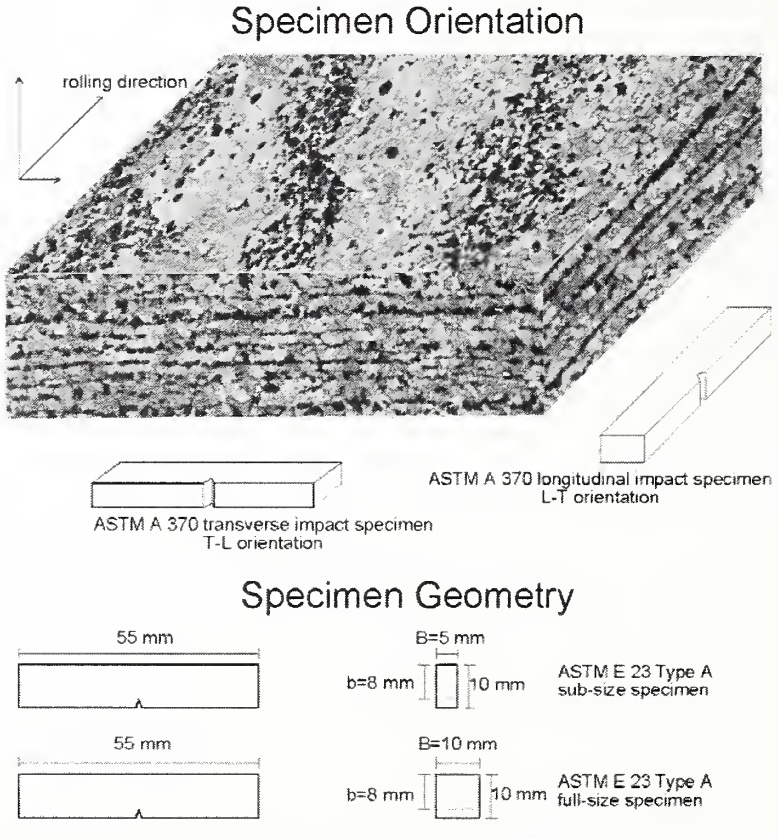

Figure 5–2. Charpy impact specimen geometries and orientations with respect to the plate rolling direction.

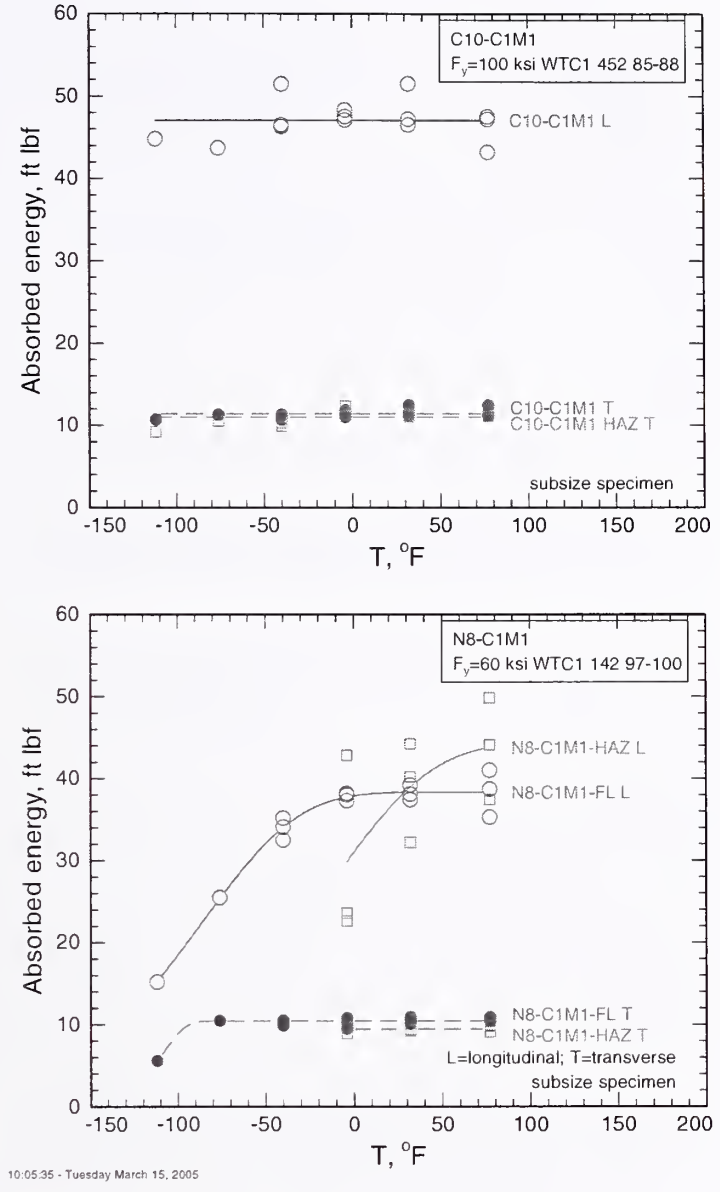

Figure 5–3. Longitudinal and transverse Charpy impact data of samples from the flange and adjacent HAZ of perimeter column N8-C1M1, the flange and adjacent HAZ of perimeter column C10-C1M1.

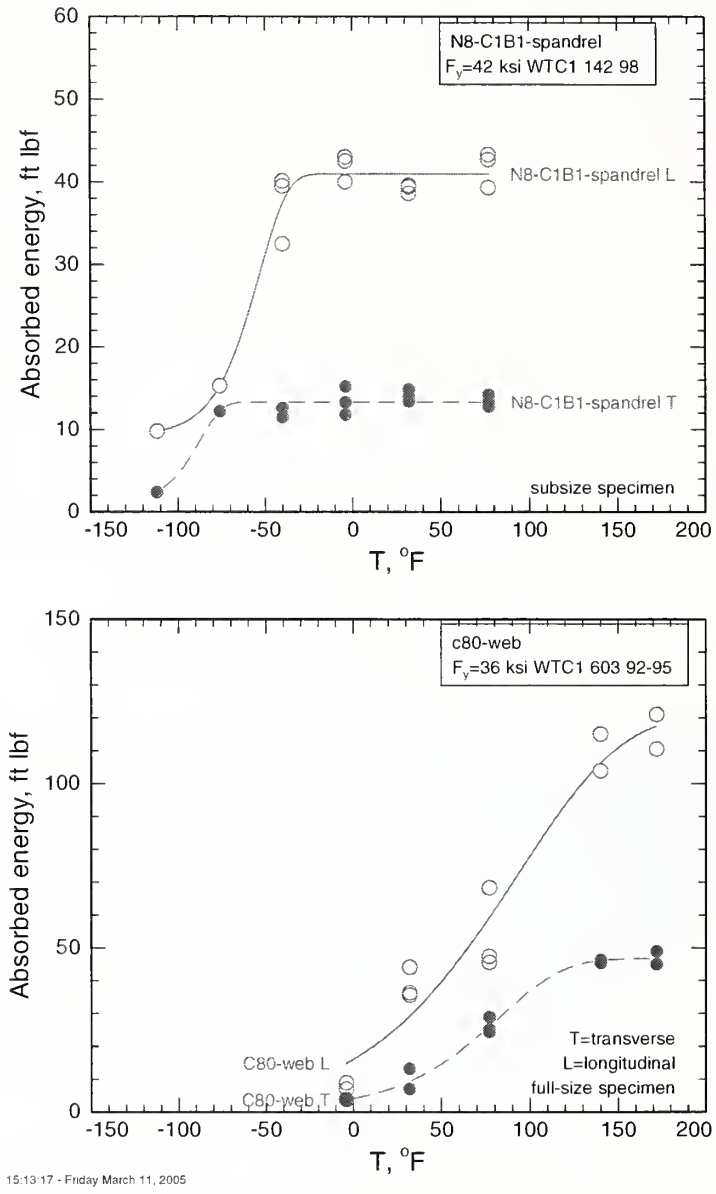

Figure 5–4. Longitudinal and transverse Charpy impact data for the spandrel associated with perimeter column N8 and the web of wide-flange core column C-80.

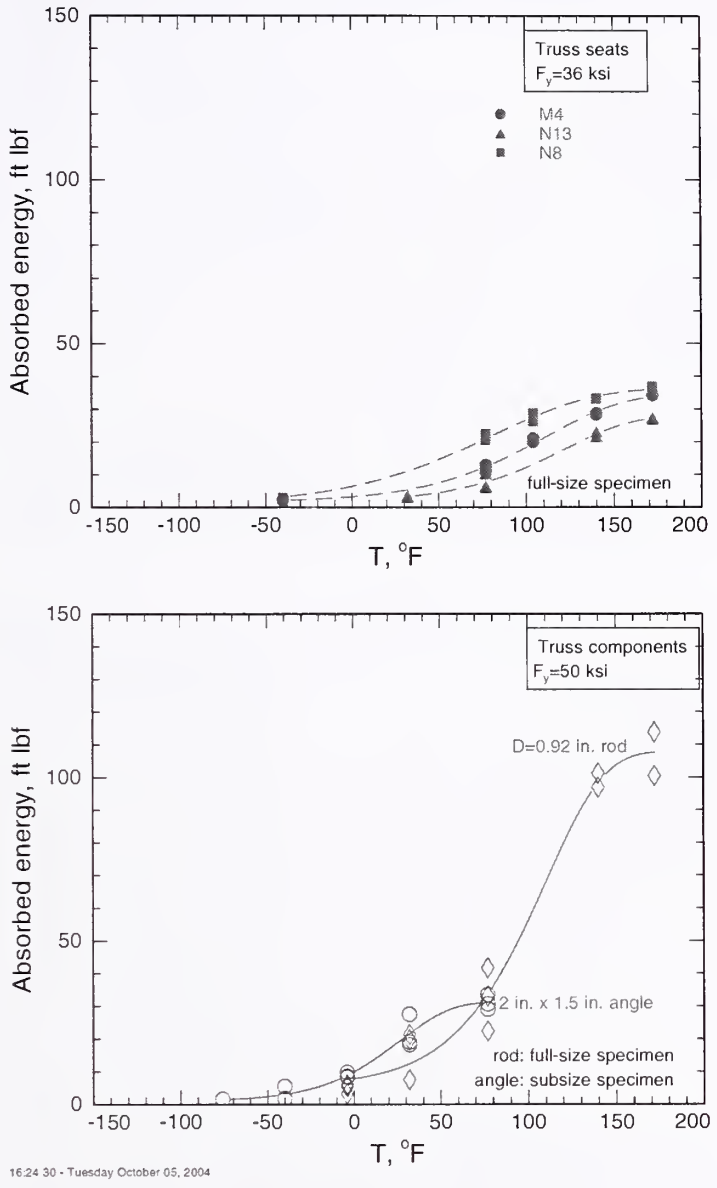

Figure 5–5. Transverse Charpy impact data from samples from perimeter column truss seats M4, N13, and N8, and from floor truss components.

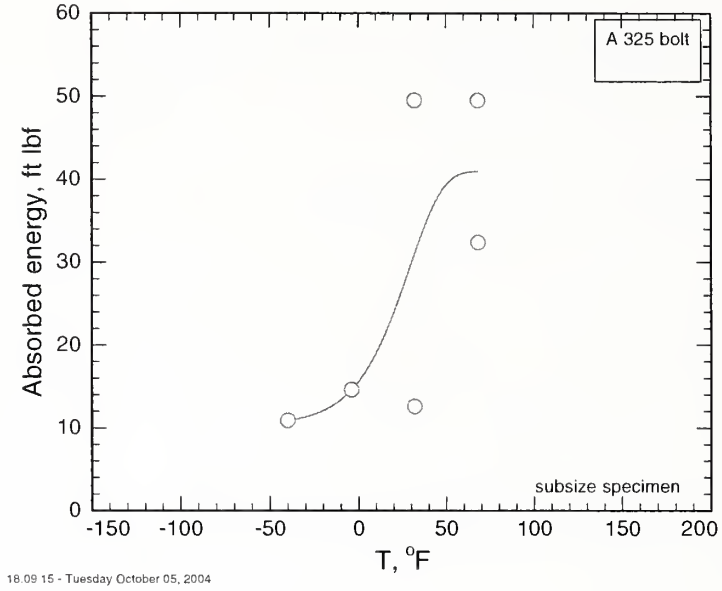

Figure 5–6. Longitudinal Charpy impact data for A 325 bolts.

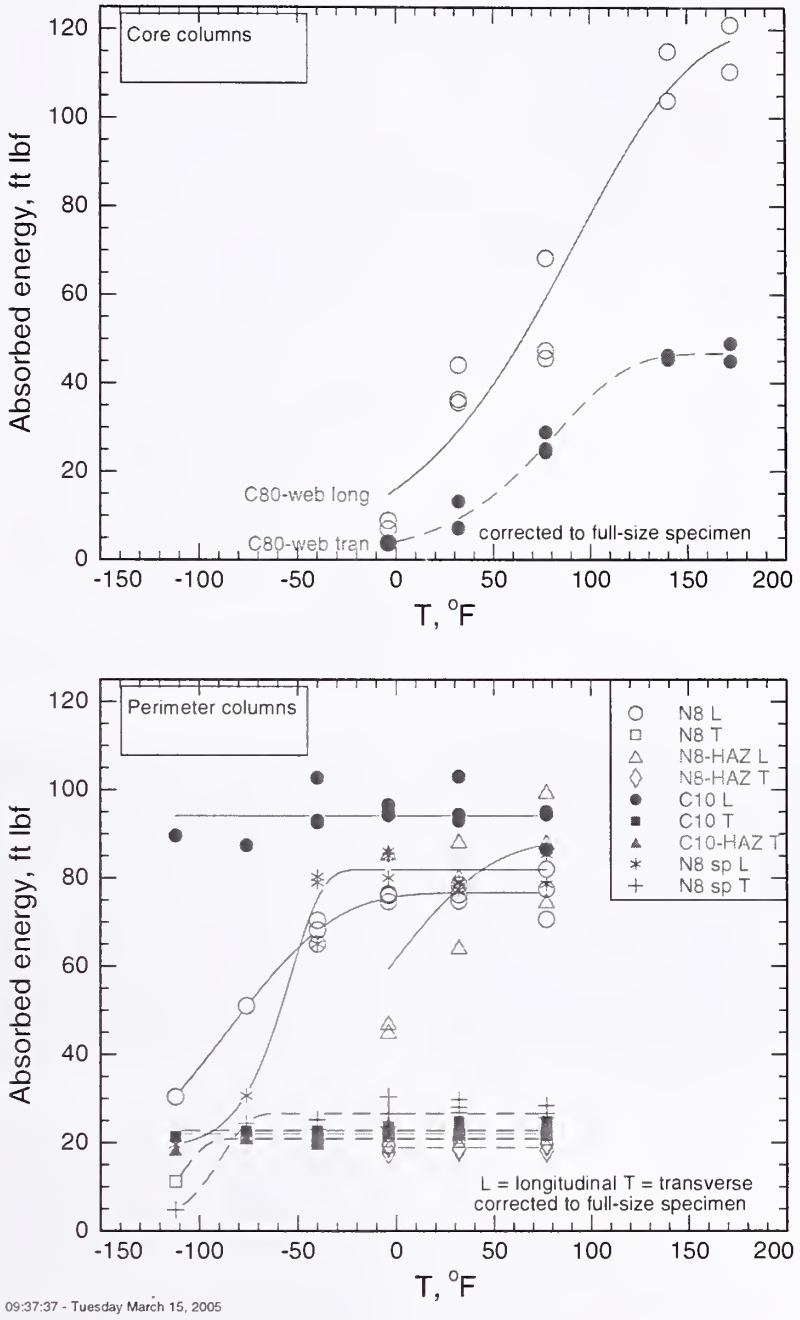

Figure 5–7. Summary plot of the dependence of absorbed energy on test temperature for all perimeter and core column steels. The absorbed energy values of the sub-size specimens have been corrected using Eq. 5–2 to compare them to data from full-size (10 mm by 10 mm) specimens.

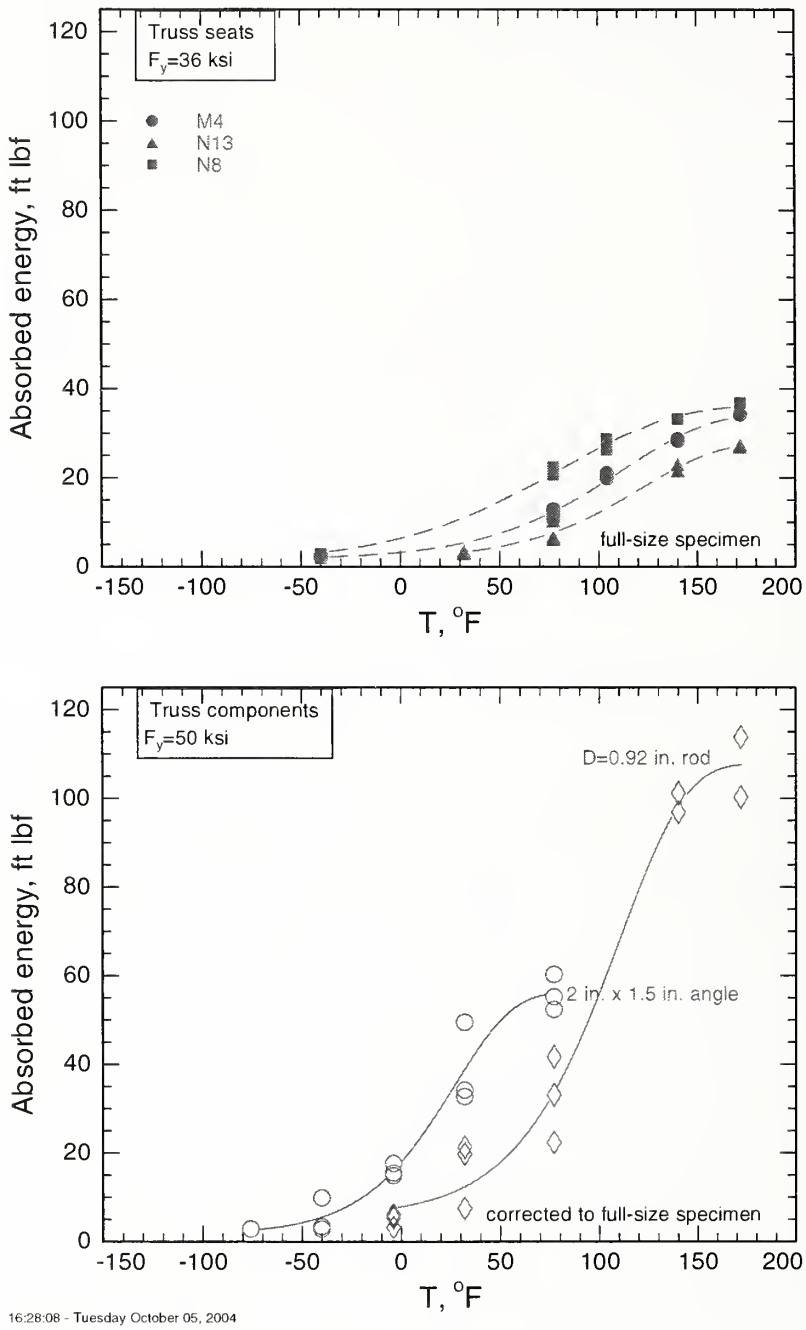

Figure 5–8. Summary plot of the dependence of absorbed energy on test temperature for all truss component and truss seat steels. The absorbed energy values of the sub-size specimens have been corrected using Eq. 5–2 to compare them to data from full-size (10 mm by 10 mm) specimens.

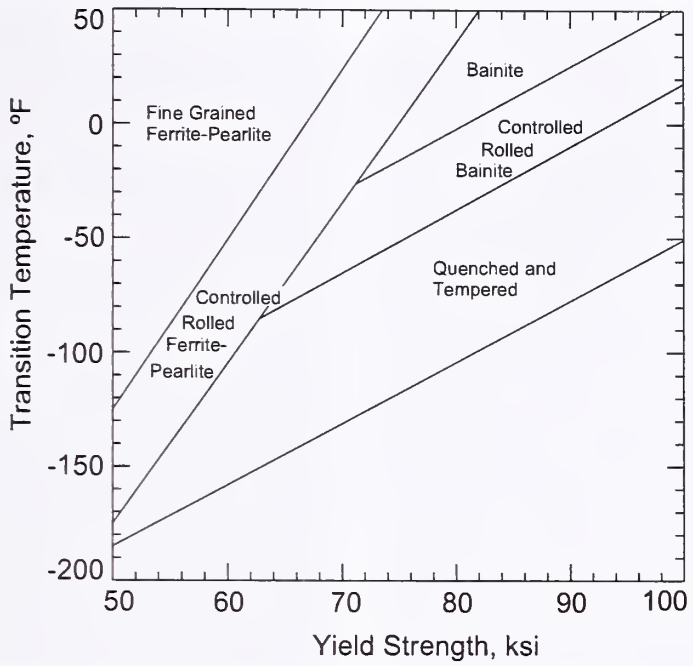

Figure 5–9. Strength-toughness relationships for several types of structural steels from the WTC construction era, after Irvine (1969).

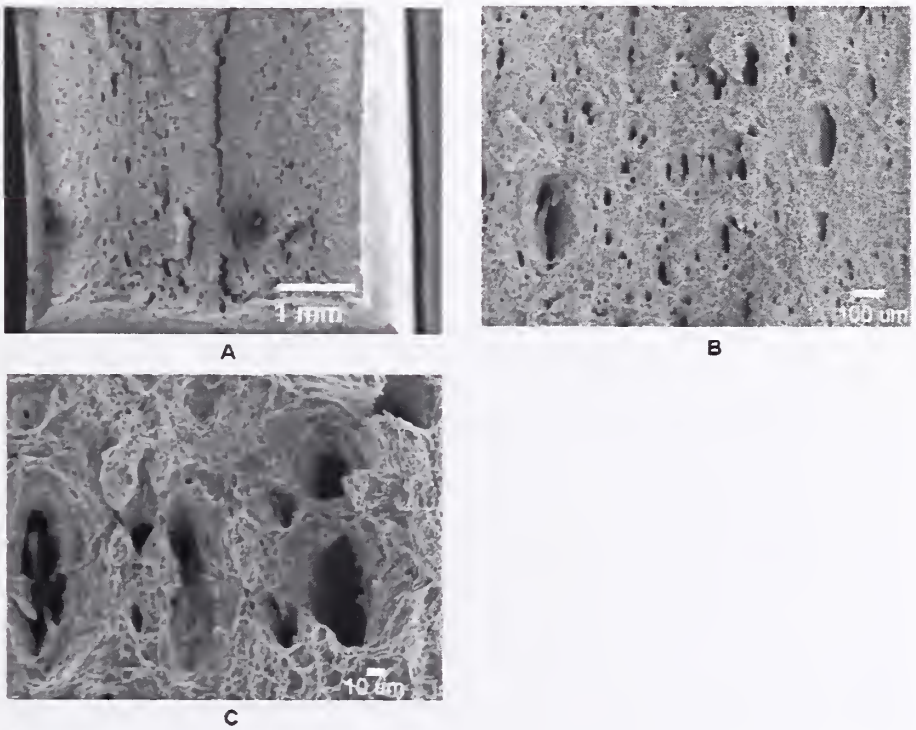

Source: NIST.

Figure 5–10. Scanning electron micrographs of the fracture surface of a Charpy V-notch longitudinal specimen orientation from an N8-C1M1 perimeter column (WTC 1-142-97-100). (a) ductile dimples (oval features) and general surface morphology, (b) low magnification view of large and small ductile dimples on the fracture surface, (c) higher magnification view.

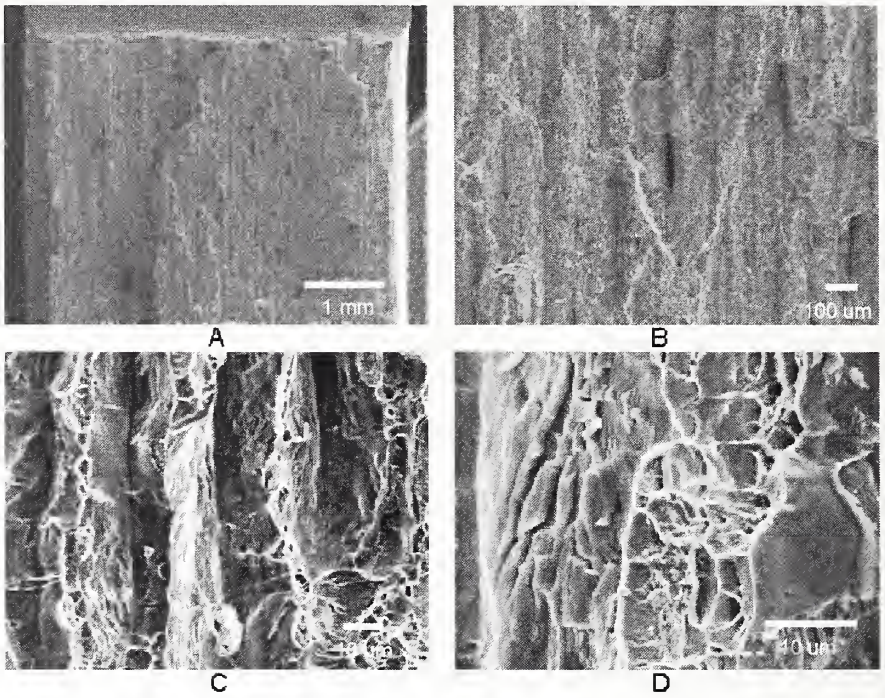

Source: NIST.

Figure 5–11. Scanning electron micrographs of the fracture surface of an N8-C1M1 perimeter column sample showing ductile tearing features that form due to fracture initiation and growth at elongated inclusions and pearlite on planes parallel to the rolling plane. The "ductile dimples" in this case are linear features with a peak-valley morphology

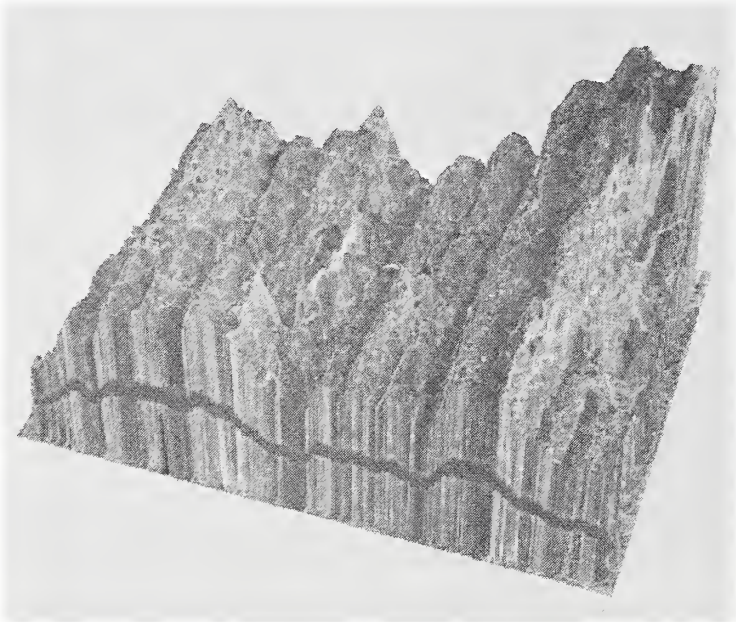

Figure 5–12. Perspective view of the fracture surface of sample N8-C1M1 showing the long peak-valley features characteristic of the fracture surface for transversely oriented impact specimens. The green line indicates the topography of the fracture surface.

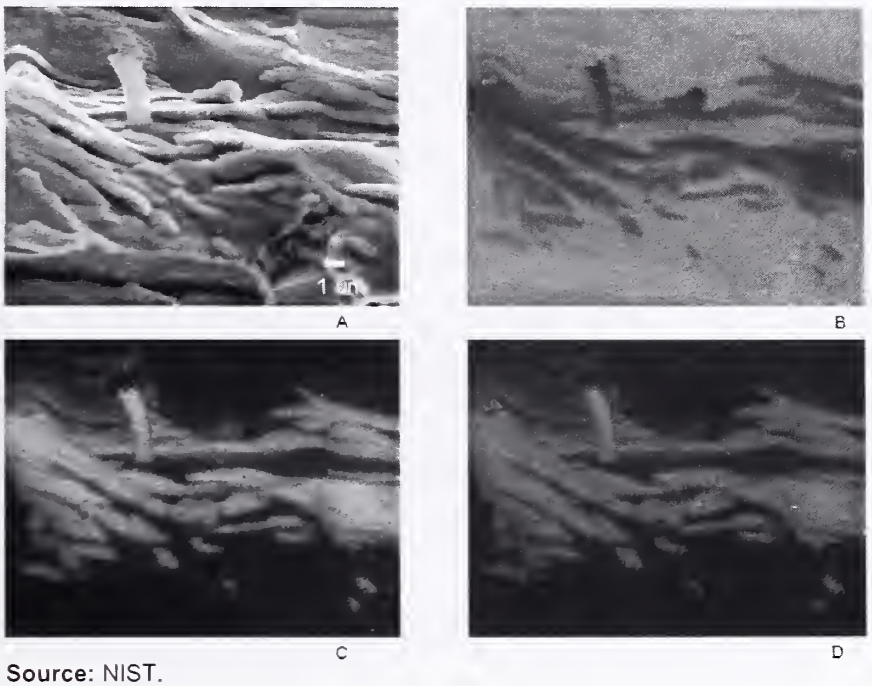

Source: NIST.

Figure 5–13. A gray-scale image (a) and compositional maps from fracture surface of an N8-C1M1 perimeter column Charpy V-notch specimen. The relative concentrations of (b) iron, (c) manganese, and (d) sulfur. The surface of the "ductile dimple" is littered with the remnants of manganese sulfide inclusions.

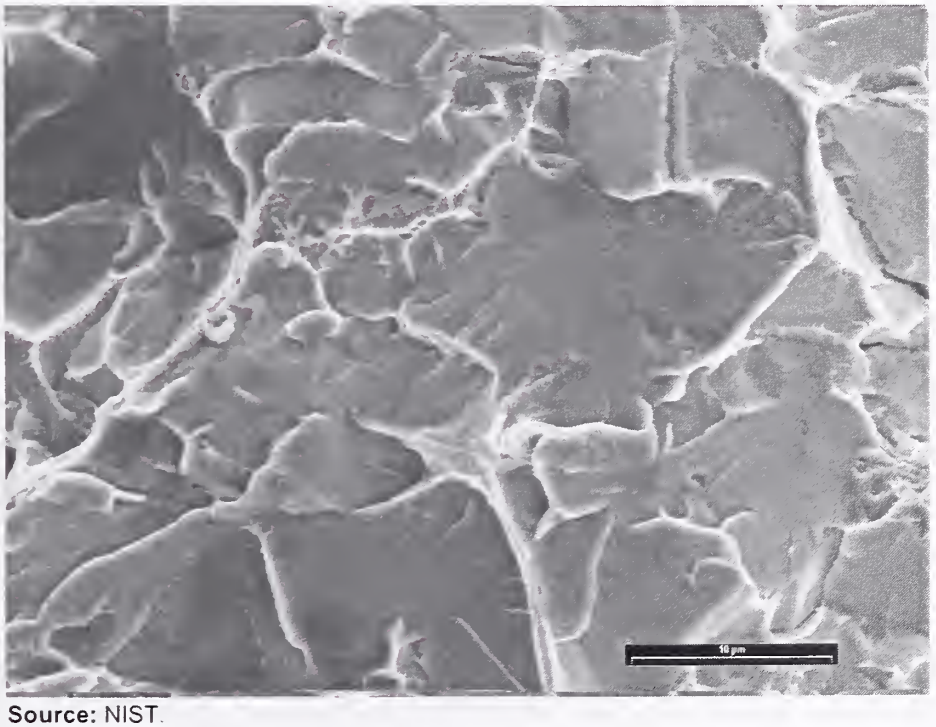

Source: NIST.

Figure 5–14. The fracture surface of a perimeter truss seat, N13-C3B1 that was tested at room temperature shows cleavage facets, which indicate a brittle fracture mode.

This page intentionally left blank.

Chapter 6
ELEVATED TEMPERATURE PROPERTIES

6.1 INTRODUCTION

The high temperature tensile deformation and creep behavior of structural steels are important inputs to finite element models of the response of the World Trade Center (WTC) structures to the fires. This segment of the Investigation used two approaches to provide that information. The first was to experimentally characterize the high-temperature mechanical properties of the steels that were most likely to have been exposed to the fires. The second was to develop methodologies to estimate the tensile and creep properties of those steels that were not experimentally characterized.

The experimental characterization of the high-temperature tensile properties focused on the steels that were most likely to have been exposed to high temperature from the fires: the floor trusses and truss seats, the core columns, and the inner web plates of the perimeter columns. The experimental characterization of creep properties focused on the steel from the floor trusses

The methodology to estimate high-temperature tensile properties of untested steels recognizes that the yield and tensile strength of structural steels, normalized to their room temperature values, degrade with temperature along a master curve. To estimate the dependence of the shape of the stress-strain curves with temperature, the methodology uses both literature and experimental data.

For estimating creep properties of all WTC structural steels, except those in the floor trusses, the methodology uses 1970s literature data for creep of structural steel scaled by the ratios of their tensile strengths. For the properties of the truss steels, the methodology uses data generated from tests on recovered truss steels themselves.

6.2 TEST PROCEDURES

6.2.1 Tensile Tests

High-temperature tensile tests employed two different machines. The tests on the floor truss steels employed an electromechanical testing machine (Instron 8562) with a contact extensometer that had a 12.5 mm gauge length. The furnace is a split, $MoSi_2$-element design. The specimens, designated type Flat C2, conform to Fig. 1 of ASTM International (ASTM) E 21. The uniform cross section is 32 mm long and 3 mm × 6 mm wide. They were loaded using pin-aligned, superalloy, wedge grips. The specimen temperature was monitored using a K-type thermocouple mounted within 1 mm of the specimen surface. The specimens were loaded as soon as possible after the furnace temperature stabilized at the test temperature, which was generally within 20 min. During the temperature stabilization step, the specimen temperature was always within 5 °C of the desired temperature. The crosshead speed in these tests was 0.0325 mm/s, which produced a strain rate after yielding of approximately 0.001 s^{-1}, measured using the extensometer. Prior to yield, the crosshead displacement rate produced a specimen stressing rate of 4±2 MPa/s. These rates meet the requirements of ASTM E 8 and E 21.

Most other tests used a second electromechanical machine with a high-temperature extensometer with a 1.0 in. gauge length. The furnace is a split design in which quartz lamps heat the specimen. The specimens, Type Flat C1, have a 1.1 in. uniform long cross section 0.25 in. wide. The specimen thickness was usually the original thickness of the plate. These tests followed the loading protocol of ASTM E 21. The initial crosshead displacement rate was 0.00167 mm/s. After several percent strain, the crosshead rate was increased to 0.0167 mm/s, as required by E 21,which produces a discernible step in the flow stress for elevated temperature tests.

6.2.2 Creep Tests

Creep testing employed two types of machines. Some employed the same electromechanical test machine with $MoSi_2$ furnace used in the high-temperature tensile tests. Most tests employed two identical, traditional dead-load, lever-arm creep frames (Applied Test Systems) with split, wire-wound, three-zone NiCr furnaces. Extensometers in these furnaces are averaging, clamp-on types with a nominal gauge length of 25.4 mm. The specimens were loaded by hand by adding masses to the weight pan. Generally, it took less than three minutes to reach full load. During the test, the operator removed mass to maintain constant stress from the weight pan at approximately 3 percent strain increments. These corrections manifest themselves as kinks in the strain-time curves. Specimen C132-2w-2 shows such a correction at approximately 6,000 s (as shown later in Fig. 6–3). The test specimens were the type Flat C2. Creep tests were conducted at temperatures 400 °C, 500 °C, 600 °C, and 650 °C. One stress-temperature condition was used per specimen. Individual specimen stresses lay in the range 100 MPa < σ < 445.8 MPa. Tests were generally discontinued after 2 h if the specimen had not failed, though some tests were allowed to run longer.

6.3 RESULTS

6.3.1 Tensile Tests

Table 6–1 describes the specimens from the three perimeter column, two core column and two floor truss steels tested at high temperature and their original locations in the buildings. The curves of Fig. 6–1, which illustrate data from specimen N8-C1B1A-FL, are typical of the high-temperature stress-strain curves for all the specimens tested. Appendix A contains the stress-strain curves for the other specimens. In most cases, the experimenter removed the extensometer prior to failure, so the end points of the curves do not necessarily represent failure. Because some of these tests followed the loading protocol of ASTM E 21, there is a jump in the flow stress at about $\varepsilon = 0.02$ that corresponds to the mandatory extension rate change. At low temperatures, where the strain rate sensitivity is low, the jump is small, but at elevated temperatures, it can be as large as 5 ksi.

6.3.2 Creep Tests

Truss steel from a 2 in. × 1.5 in. × 0.25 in. truss top chord angle from specimen C-132 was characterized for creep. This steel was specified to conform to A 242 with $F_y = 50$ ksi. Chemical and mechanical analyses of the larger lower chord angles, which were specified to conform to A 36, indicate that they were made from the same steel, however.

Table 6–1. Specimens and locations for high-temperature tensile tests with full stress-strain data.

Specimen	Description	Source	F_y (ksi)
C40-C2M-IW-2	Perimeter column inner web	WTC 1 Column 136 floors 98-101	60
N8-C1B1A-FL	Perimeter column flange	WTC 1 Column 142 floors 97-100	60
C10-C1M-FL-1	Perimeter column flange	WTC 1 Column 451 floors 85-88	100
C65	12WF161 core column	WTC 1 Column 904 floors 86–89	36
HH-FL-1	12WF92 core column	WTC 1 Column 605 floors 98-101	42
C-132	2 in.×1.5 in×0.25in. truss bulb angle	Unknown	50
C-53	3 in. ×2 in×0.37 in. truss bulb angle	Unknown	36

Note: F_y is the specified value, rather than the NIST-measured value.

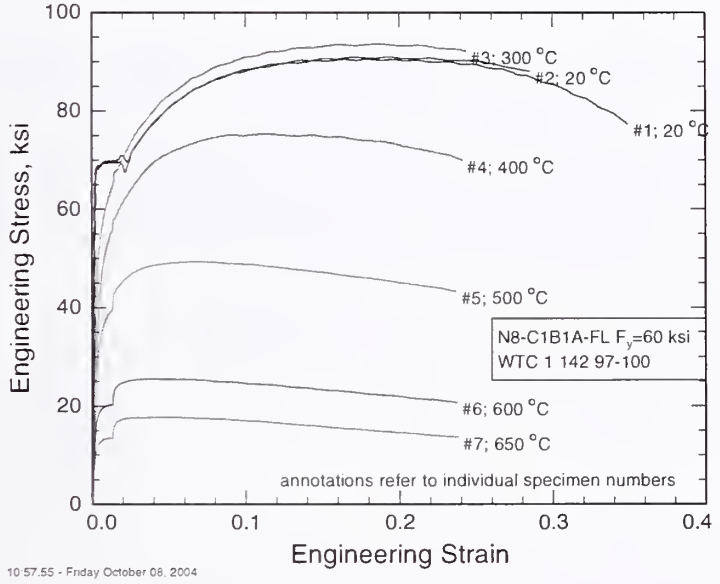

Figure 6–1. Elevated-temperature stress-strain curves. Specimen N8-C1B1A-FL is from a F_y = 60 ksi perimeter column flange plate from WTC 1 column 142 between floors 97–100. Annotations refer to individual test specimen numbers.

The creep test matrix consisted of 20 creep tests taken to failure or discontinued after several hours. Figures 6–2, 6–3, 6–4, and 6–5 display the creep curves for specimens from the truss upper chord.

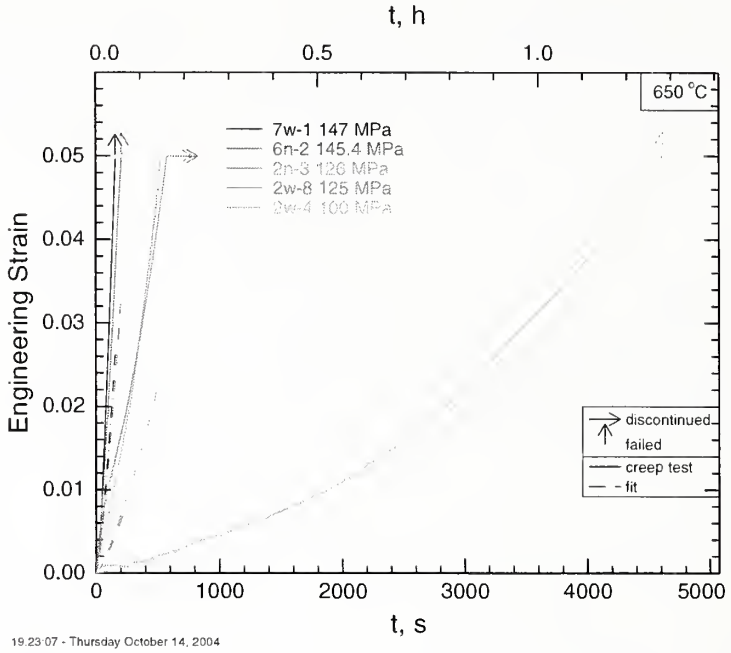

Figure 6–2. Creep curves of A 242 truss steel from specimen C-132 at 650 °C. Dashed lines represent the fit from Eq. 6–14 using the parameters in Eqs. 6–16, 6–17, and 6–18. Experimental curves are graphically truncated at ε = 0.05.

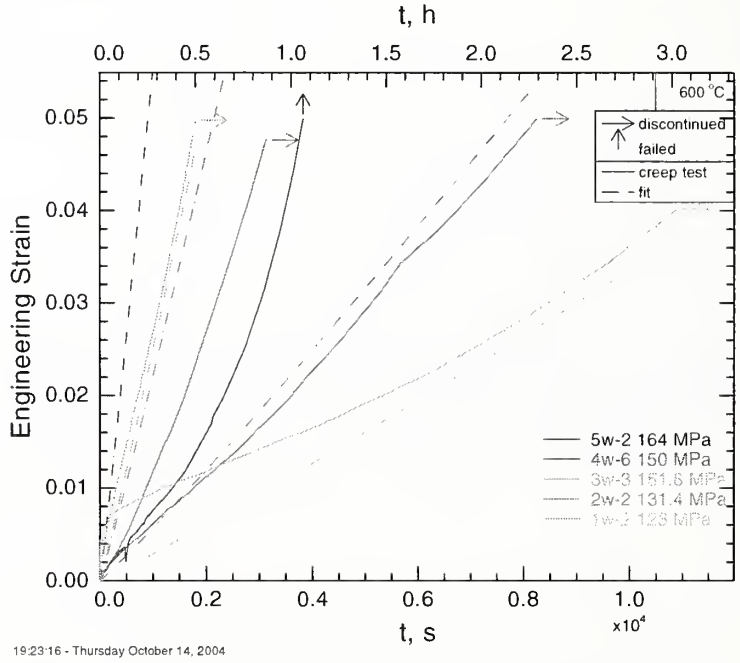

Figure 6–3. Creep curves of A 242 truss steel from specimen C-132 at 600 °C. Dashed lines represent the fit from Eq. 6–14 using the parameters in Eqs. 6–16, 6–17, and 6–18. Experimental curves are graphically truncated at ε = 0.05.

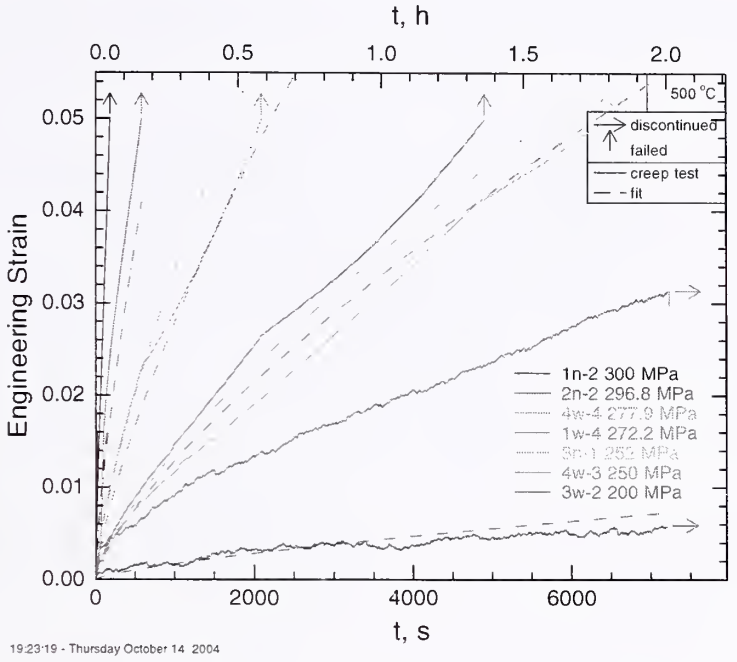

Figure 6–4. Creep curves of A 242 truss steel from specimen C-132 at 500 °C. Dashed lines represent the fit from Eq. 6–14 using the parameters in Eqs. 6–16, 6–17, and 6–18. Experimental curves are graphically truncated at ε = 0.05.

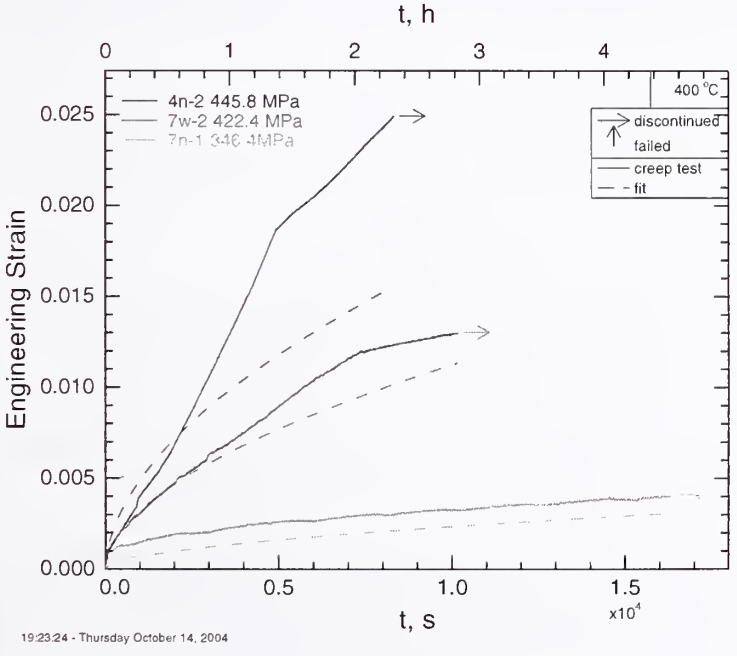

Figure 6–5. Creep curves of A 242 truss steel from specimen C-132 at 400 °C. Solid lines represent measured creep strain. Dashed lines represent the fit from Eq. 6–14 using the parameters in Eqs. 6–16, 6–17, and 6–18. Experimental curves are graphically truncated at ε = 0.05.

6.4 MECHANICAL PROPERTY VALUES FOR STEELS

6.4.1 A Universal Curve for Elevated-Temperature Tensile Properties

Early in the Investigation, before any significant tensile testing was completed, it was necessary to provide other NIST Investigation Team members with a relation to describe the yield and tensile strength of structural steel as a function of temperature. This relation forms the basis for estimating the elevated-temperature stress-strain behavior of the recovered steels. Because it was not experimentally feasible to characterize all of the different grades, the relation is necessary to estimate the properties of the steels that were not characterized. The WTC steels tested for elevated temperature behavior were those that were particularly relevant for modeling the fire-affected floors. These were primarily the steels in the core columns and the floor trusses, though several perimeter column steels were also characterized.

The literature contains very few summaries of the properties of structural steels at elevated temperature. The small data set that is available is particularly appropriate to the Investigation, however, because it comprises structural steels from the WTC construction era. A strong disadvantage of the sources is that they do not typically report the strain rate used in the tests.

A useful and often recognized relation is that the strength of structural steel as a function of temperature, normalized to the room-temperature value, follows a universal curve, independent of strength level. Both the normalized yield, F_y, and tensile, TS, strength curves are roughly sigmoidal. The normalized curve for yield strength drops away from unity more quickly than does the curve for tensile strength, which has a plateau out to about 300 °C. A function that represents this behavior with a smooth curve and a minimum of parameters is

$$f = \frac{F_y(T)}{F_y(23°C)} = (1 - A_2)\exp\left(-\frac{1}{2}\left[\left(\frac{T}{s_1}\right)^{m_1} + \left(\frac{T}{s_2}\right)^{m_2}\right]\right) + A_2 \qquad 6\text{–}1$$

and

$$f = \frac{TS(T)}{TS(23°C)} = (1 - A_2)\exp\left(-\frac{1}{2}\left[\left(\frac{T}{t_1}\right)^{n_1} + \left(\frac{T}{t_2}\right)^{n_2}\right]\right) + A_2 \qquad 6\text{–}2$$

where T is measured in °C. The parameters in Eqs. 6–1 and 6–2 are completely empirical and have no physical significance.

Figures 6–6 and 6–7 plot the master curves for yield and tensile strength overlaid on the literature data, which are the small solid symbols (Chijiiwa 1993, Goda 1964, Harmathy 1973, Holt 1964, Melloy 1963, USS 1972). The model curves, Eq. 6–1 and 6–2, are not fits to the literature data. Instead, the parameters of Eqs. 6–1 and 6–2 were adjusted to provide a visually accurate representation of the bulk of the data, particularly in the region of steep slope in the range 500 °C < T < 700 °C. Furthermore, the values of the parameters, summarized in Table 6–2, have no physical significance. The scatter in the literature data arises from several sources. At intermediate temperatures, the sensitivities of the different steels to dynamic strain aging differ. Dynamic strain aging can actually raise the flow stress above the room temperature value. Furthermore, the literature sources do not report the testing rates employed, which

may differ between the sources. Rate effects can make a significant contribution to the measured flow stress at temperatures above about 500 °C.

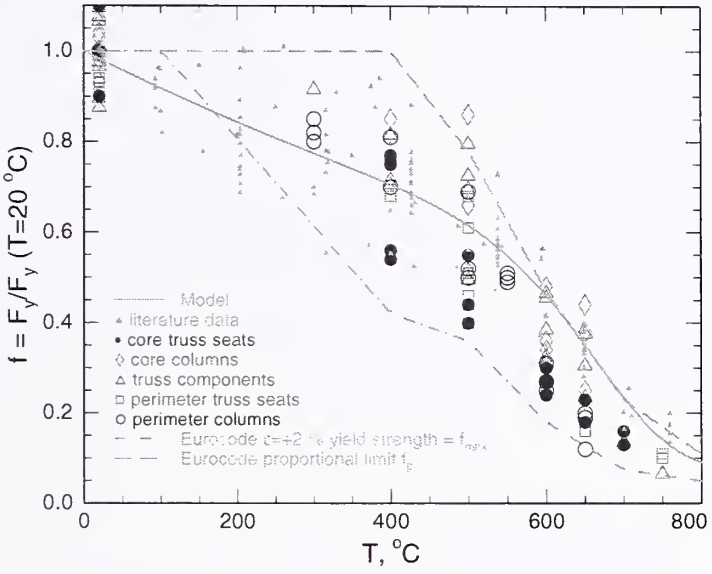

Figure 6–6. Ratio, *f*, of room- to high-temperature yield strength (F_y) for all steels characterized. The data spread at room temperature exists because the individual test results are normalized to their mean. The solid line is the expression, Eq. 6–1, developed using literature data on structural steels, which are denoted by the smaller symbols.

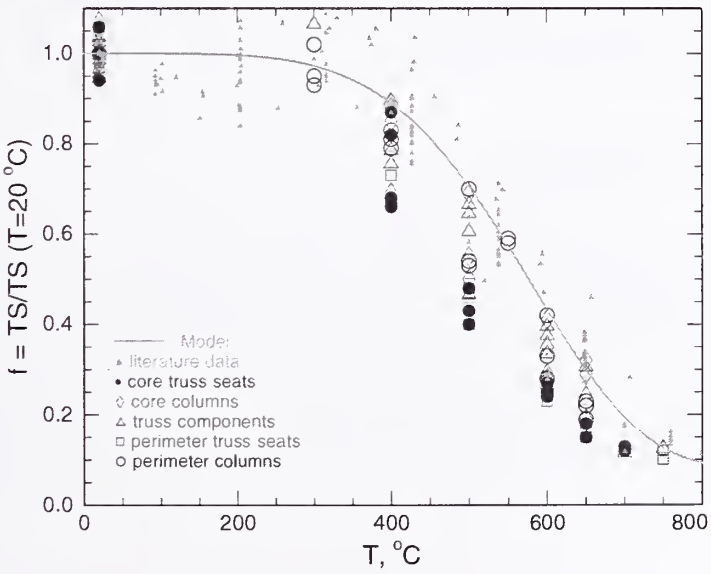

Figure 6–7. Ratio of room- to high-temperature tensile strength (*TS*) for the steels in Table 6–1. The data spread at room temperature exists because the individual tests are normalized to their mean. The solid line is the expression developed for literature data on structural steels, Eq. 6–2, denoted by the smaller symbols.

Table 6–2. Values for the parameters in the strength reduction equations (Eqs. 6–1 and 6–2).

Yield Strength Reduction Parameters (Eq. 6–1)	Tensile Strength Reduction Parameters (Eq. 6–2)
$A_2 = 0.074692$	$A_2 = 0.086327$
$m_1 = 8.325929$	$n_1 = 5.0004$
$m_2 = 1.000000$	$n_2 = 4.992176$
$s_1 = 638.384277$ °C	$t_1 = 531.403687$ °C
$s_2 = 523.523132$ °C	$t_2 = 1032.864014$ °C

The recent Eurocodes (EN 1993-1-2 Fire) recommend expressions for the proportional limit, f_p, and flow stress, f_{max}, of structural steel as functions of temperature. These two parameters define specific points on the recommended stress-strain behavior for steel at elevated temperature in the Eurocode. That curve has four regions:

1. a small region of linear-elastic behavior up to the proportional limit, f_p,
2. a work-hardening region that extends to $e = 0.02$,
3. a plastic regime that extends at constant, maximum flow stress, f_{max}, and
4. a failure range where the strength decreases to zero.

An important feature of this stress-strain curve is that it reaches the maximum stress, f_{max}, at $e = 0.02$. Figure 6-6 compares both of these to the Investigation data. Neither the Eurocode proportional limit, f_p, nor the $e = 0.02$ yield strength, f_{max}, corresponds to the $e = 0.002$ offset yield strength reported in Figure 6-6, but they do represent lower and upper bounds. There is no analogous definition for the tensile strength, *TS*.

6.4.2 Analysis of Tensile Data

Figures 6–6 and 6–7 also summarize the normalized yield (F_y) and tensile (*TS*) strength for all the steels tested, segregated by component. At temperatures up to 400 °C the data from the WTC steels generally lie in the same range as the literature data. At 500 °C and above, the WTC data average only 75 percent of the curve that represents the literature data. This deviation probably arises from the differences in the testing rates. The strain rates used for the WTC data were as low as $\dot{\varepsilon} = 8.3 \times 10^{-4} s^{-1}$ while the literature data were probably generated using rates appropriate to ASTM A 370, which are ten times higher: $\dot{\varepsilon} = 8.3 \times 10^{-3} s^{-1}$. The expected difference between the two testing rates can be evaluated by recognizing that the high-temperature flow stress, σ, depends on the strain rate $\dot{\varepsilon}$ in a power-law relation:

$$\sigma = \dot{\varepsilon}_0 \dot{\varepsilon}^m \qquad 6\text{–}3$$

where $\dot{\varepsilon}_0$ is a constant and m is designated as the strain rate sensitivity.

The necessary strain rate sensitivity, m, to raise the average of the WTC data to the prediction of the model curve is $m = 0.13$. Reported elevated-temperature strain rate sensitivities for low-carbon structural

steel are near this value: $m = 0.105$ at 600 °C (Manjoine 1944), $m = 0.08$ at 649 °C (Gowda 1978). An analysis of the strain rate sensitivities of six WTC steels, from the stress jump that occurs when the extension rate is changed at about 2 percent strain yielded similar values. The strain rate sensitivity, m, evaluated from the individual strain rate jumps, increases with temperature: $m = 0.055 \pm 0.029$ at 500 °C, $m = 0.119 \pm 0.020$ at 600 °C, and $m = 0.146 \pm 0.029$ at 650 °C.

6.4.3 Estimating Elevated-Temperature Stress-Strain Curves

A complete stress-strain curve as a function of temperature is necessary as input for finite element modeling. Because it was not feasible to characterize all twenty different WTC steels for their high-temperature stress-strain behavior, a methodology was necessary to estimate the stress-strain curves for each steel. The stress-strain (σ-ε) curves of the more than twenty different WTC structural steels can be grouped into two classes based on their shape and specified minimum yield strength. The shapes of the σ-ε curves of low yield strength (A 36, $F_y = 36$ ksi) steels differ from those of higher yield strength ($F_y > 36$ ksi) steels. The low strength steels work harden over a larger strain range, even when they develop the same tensile strength (TS) as the higher strength steels.

At elevated temperatures, of course, the yield and tensile strengths decrease, see Figs. 6–6 and 6–7. Some steels initially increase in strength with increasing temperature, through the process of dynamic strain-aging, (Baird 1970) but this behavior is not *a priori* predictable. The analysis does not attempt to predict the effects of dynamic strain aging. The limited quantity of literature stress-strain curves, as well as those generated in the Investigation, indicates that the shape of the work-hardening portion of the stress-strain curve changes with increasing temperature. The model to describe the stress-strain curves must capture this shape change.

The methodology for creating stress-strain curves for WTC steels has three steps.

1. Choose a representative low-strength (A 36 $F_y = 36$ ksi) and a high-strength ($F_y > 36$ ksi) steel for which literature or experimental stress-strain curves at different elevated temperatures are available.

2. Develop a model that can predict the stress-strain behavior of these steels as a function of temperature.

3. Apply this model stress-strain behavior to all other WTC steels by appropriately scaling the resulting stress-strain behavior of the steel in question to that of the steel used to develop the model.

The stress-strain curves for 0 °C < T < 650 °C for all steels are represented using a power-law work-hardening model:

$$\sigma = R_{TS} R_C K(T) \varepsilon^{n(T)} \qquad 6\text{–}4$$

where σ has units of ksi, T has units of °C and

$$K(T) = (k_4 - k_0)\exp\left(-\frac{1}{2}\left[\left(\frac{T}{t_{k1}}\right)^{k_1} + \left(\frac{T}{t_{k2}}\right)^{k_2}\right]\right) + k_0 \qquad 6\text{–}5$$

and

$$n(T) = (n_4 - n_0)\exp\left(-\frac{1}{2}\left[\left(\frac{T}{t_{n1}}\right)^{n_1} + \left(\frac{T}{t_{n2}}\right)^{n_2}\right]\right) + n_0 \qquad 6\text{–}6$$

The parameter R_{TS} is the ratio of the room temperature tensile strength of the steel of interest, TS_i, to the room temperature tensile strength, TS_{ref}, of the steel used to develop the model expressed by Eqs. 6–5 and 6–6.

$$R_{TS} = \frac{TS_i}{TS_{\text{ref}}} \qquad 6\text{–}7$$

Because the work hardening decreases with increasing temperature, scaling by the room-temperature tensile strength, *TS*, is more appropriate than scaling by the room-temperature yield strength, F_y. The parameter R_C corrects for two additional phenomena. The temperature-dependent functions (Eqs. 6–5 and 6–6) were originally developed using data that were not corrected to zero strain rate, whereas the stress-strain curves supplied to the Investigation teams for room temperature behavior are corrected to the zero strain rate. Secondly, because the temperature dependence of all the possible steels is represented using the behavior of only two different steels, it is possible that the stress-strain behavior predicted by Eq. 6–4 at room temperature could differ from that predicted by the already generated and supplied room-temperature stress-strain curve. The parameter R_C corrects the elevated-temperature stress-strain curve so that the value of stress predicted by Eq. 6–4 for $T = 25$ °C at $\varepsilon = 0.05$ equals that of the room temperature model curve. In general, the correction is small: $0.9 < R_C < 1.04$.

The functions *K(T)* and *n(T)* have the same form as the functions that describe the reduction in yield and tensile strength with temperature in Figs. 6–6 and 6–7. Although they are not based on a physical model, they represent the behavior of *n(T)* and *K(T)*, and are relatively easy to evaluate. Their functional form produces a monotonic decrease in the strength of the work hardening with temperature, which agrees with the trend of the literature data. The maxima of the functional forms of *n(T)* and *K(T)* occur at $T = 0$ °C.

To calculate the six parameters in each expression for *K(T)* and *n(T)*, the plastic portion of each tensile test stress-strain curve, i.e. the strain at stress greater than the yield strength, was modeled with a power-law work hardening expression,

$$\sigma = K\varepsilon^n \qquad 6\text{–}8$$

using a non-linear least-squares fitting method, to estimate an individual K_i and n_i. The individual K_i and n_i were then fitted with Eqs. 6–5 and 6–6 respectively. The fits for *n(T)* were subject to constraints on the maximum values for n_1 and n_2, which were necessary to avoid introducing anomalous behavior in Eq. 6–4 at intermediate temperature. Note also that the functional form of Eqs. 6–5 and 6–6 does not capture the small strength increase caused by dynamic strain aging at temperatures less than 300 °C. In

addition to depending sensitively on testing rate, the magnitude of this increase varies from steel to steel. It may be absent in many steels, particularly the higher strength, microalloyed steels. Computationally, one of the modeling groups required stress-strain behavior in which the strength decreased monotonically with temperature, which this functional form supplies.

The model for the low-strength steel stress-strain curves is based on the A 36 data of Harmathy (1970). Table 6–3 summarizes some of the properties of this steel. Table 6–4 and Figs. 6–8 and 6–9 show the individual K_i and n_i to which Eqs. 6–5 and 6–6 were fit. Table 6–5 summarizes the values of those parameters in Eqs. 6–5 and 6–6 for steels with F_y = 36 ksi. Figure 6–10 shows the prediction of the model plotted over the original data used to generate the parameters for Eqs. 6–5 and 6–6. Note that although some of the K_i and n_i in Figs. 6–8 and 6–9 deviate strongly from the fitted curves, the prediction of the model for the stress-strain behavior, Fig. 6–10, agrees with the data quite well.

Table 6–3. Property data for the A 36 steel reported in Harmathy (1970).

Grade	A 36
Composition	C 0.19 % P 0.007 % S 0.03 % Mn 0.71 % Si 0.09 % semi-killed, from 1/2 in. plate compositions expressed in mass percent
F_y (20 °C)	44 ksi (reported, not corrected to zero strain rate)
TS (20 °C)	64 ksi (reported, not corrected to zero strain rate)
Range of data	20 °C – 649 °C
Number of tests	10

Table 6–4. Individual K_i and n_i used for steels with F_y = 36 ksi.

T °C	K_i ksi	n_i
24	92.95	0.1404
99	82.2	0.1335
149	108.8	0.1947
204	140.0	0.2458
260	155.9	0.2766
315	152.6	0.2928
427	105.3	0.2352
535	54.98	0.1402
593	38.41	0.1316
649	24.81	0.1167

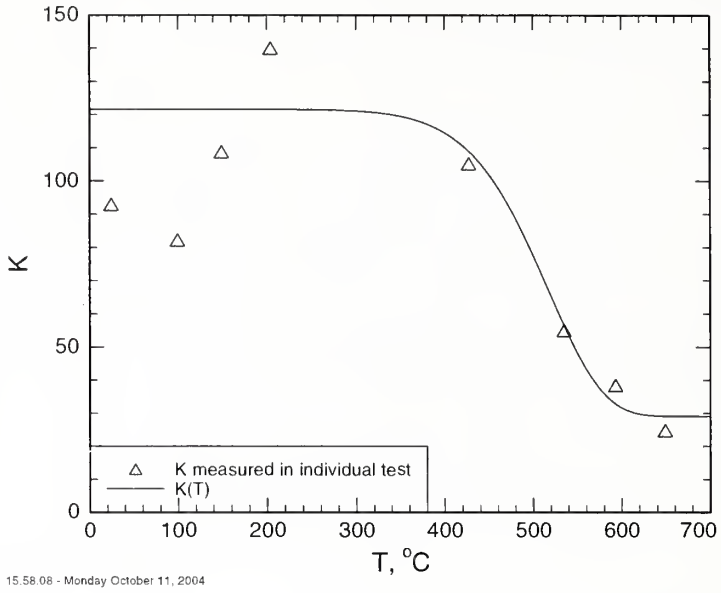

Figure 6–8. *K(T)*, Eq. 6–5, for the A 36 steel of Harmathy (1970), used to model the behavior of steel with F_y = 36 ksi.

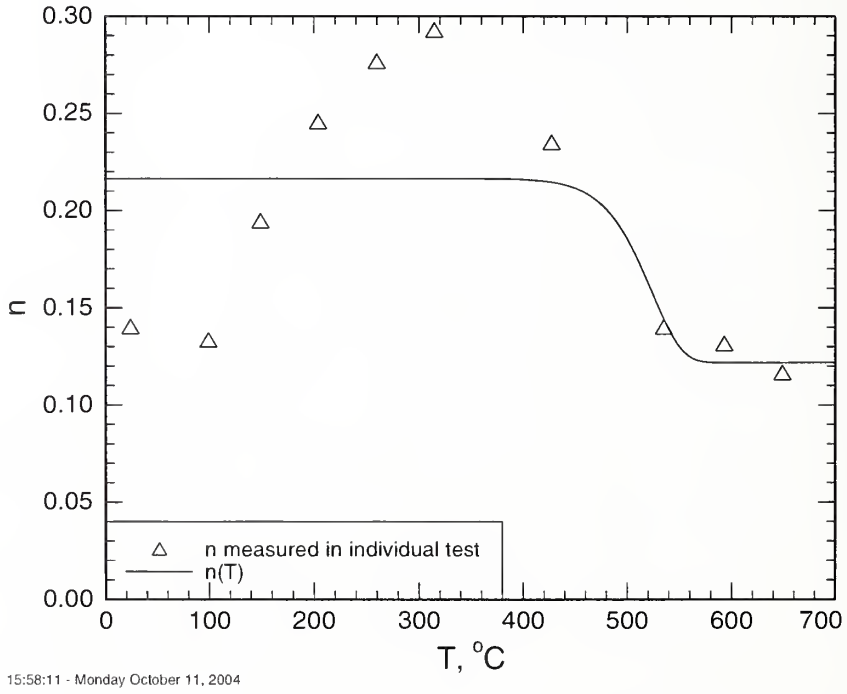

Figure 6–9. *n(T)*, 6–6, for the A 36 steel of Harmathy (1970) used to model the behavior of steel with F_y = 36 ksi.

Table 6–5. Values of the parameters of Eqs. 6–5 and 6–6 for steels with F_y = 36 ksi.

k_0	29.0492 ksi
t_{k1}	524.1812 °C
t_{k2}	523.6799 °C
k_1	9.4346
k_2	9.3532
k_4	121.6056 ksi
n_0	0.1235
t_{n1}	524.4304 °C
t_{n2}	521.2410 °C
n_1 [a]	19.0000
n_2	19.0000
n_4	0.2168

a. Fits on n_1 and n_2 were constrained to have $n \leq 19$.

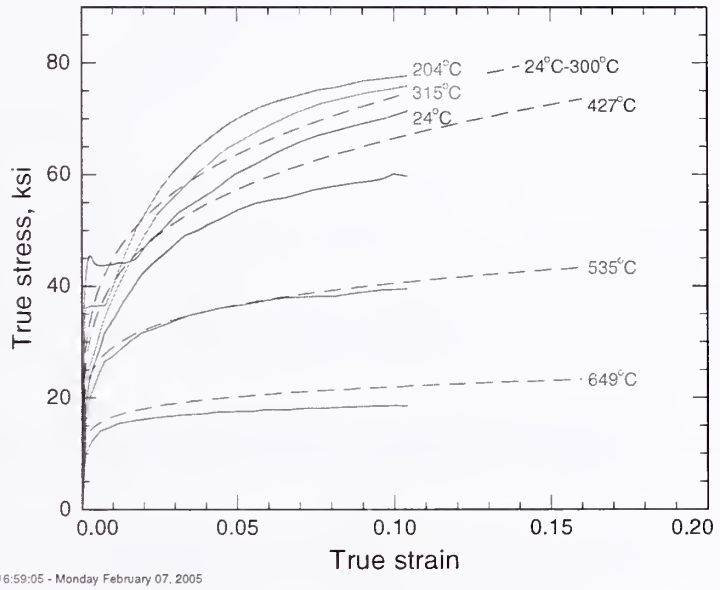

Figure 6–10. Predictions for the model (dashed lines) for A 36 steel (F_y = 36 ksi nominal) overlaid on the original data used to generate the model (solid lines). The model (Eqs. 6–4, 6–5, and 6–6 and Table 6–4) makes essentially identical predictions for 0°C < T < 300 °C, so only one line is plotted. Note that the model should not be used for strains in the elastic region (ε~ < 0.003), but the curves are shown in this region. Instead, elastic lines of the appropriate modulus should be used.

The model for the high-strength steel stress-strain curves is based on measurements made in the NIST laboratory of steel taken from the truss angles C-132 and C-53, used in WTC 1 and WTC 2 (location in building unknown). The Laclede truss steel, summarized in Table 6–6 is a good model for most of the high strength steels. Its composition and mechanical behavior are similar to an ASTM A 572 Grade 50 steel. Chemical and mechanical characterization indicates that although the truss angles of C-132 were

supplied to A 242 and the truss angles of C-53 were supplied to A 36, the steels are identical, high-strength, low-alloy (HSLA) steels similar to current ASTM A 572. Most of the perimeter steels in the towers are also micro-alloyed steels, especially those up to about F_y = 60 ksi.

Table 6–6. Property data for the A 242 Laclede truss steel tested as part of the Investigation.

Grade	A 242 (F_y = 50 ksi)
Composition	C 0.19 % Mn 0.82 % P 0.010 % S 0.029 % Si 0.07 % Ni 0.08 % Cr 0.10 % Cu 0.32 % V 0.038 % from 2.5 in. x 1.5 in. x 0.25 in. open web floor truss angle compositions expressed in mass percent
F_y(20 °C)	59 ksi (static F_y-corrected to zero strain rate)
TS (20 °C)	77.8 ksi (static *TS*-corrected to zero strain rate)
Range of data	20 °C – 650 °C
Number of tests	14

Table 6–7 and Figs. 6–11 and 6–12 show the individual K_i and n_i to which Eqs. 6–5 and 6–6 were fit. Table 6–8 summarizes the values of those parameters in Eqs. 6–5 and 6–6 for steels with F_y > 36 ksi. Figure 6–13 shows the prediction of the model plotted over the original data used to generate the parameters for Eqs. 6–5 and 6–6. The model captures the shapes of the stress-strain curves. The actual data show the reduced ductility characteristic of the Laclede truss steel.

Table 6–7. Individual K_i and n_i used for steels with F_y > 36 ksi.

T (°C)	*K* (ksi)	*n*
25	117.52	0.1276
25	122.9	0.1699
25	113.6	0.1141
300	137.4	0.1763
400	95.48	0.1460
400	111.3	0.1614
500	64.72	0.0815
500	68.12	0.0833
600	35.32	0.0415
600	30.16	0.0267
600	31.0	0.0250
600	37.03	0.0451
650	23.0	0.0327
650	27.46	0.0353

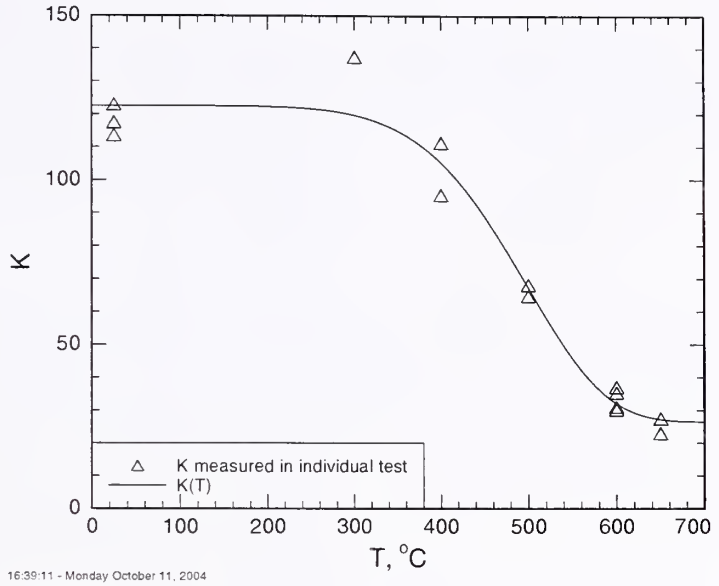

Figure 6–11. ***K(T),*** **Eq. 6–5,for the A 242 Laclede steel used to model the behavior of steel with F_y > 36 ksi.**

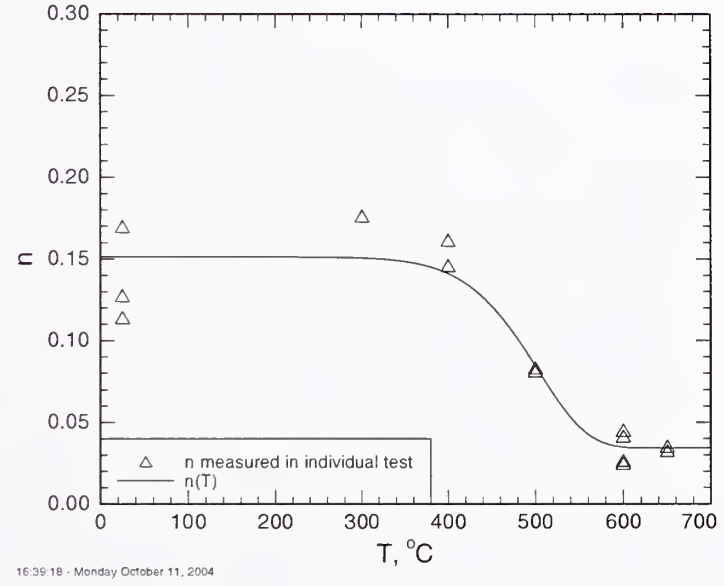

Figure 6–12. ***n(T),*** **Eq. 6–6,for the A 242 Laclede steel, used to model the behavior of steel with F_y > 36 ksi.**

Table 6–8. Values of the parameters of Eqs. 6–5 and 6–6 for steels with F_y > 36 ksi.

k_0	26.4721 ksi
t_{k1}	511.8266 °C
t_{k2}	511.8938 °C
k_1	6.5764
k_2	6.5971
k_4	122.5167 ksi
n_0	0.0342
t_{n1}	519.6340 °C
t_{n2}	499.6031 °C
n_1 [a]	10.0000
n_2	10.0000
n_4	0.1511

a. fits on n_1 and n_2 were constrained to have $n \leq 10$.

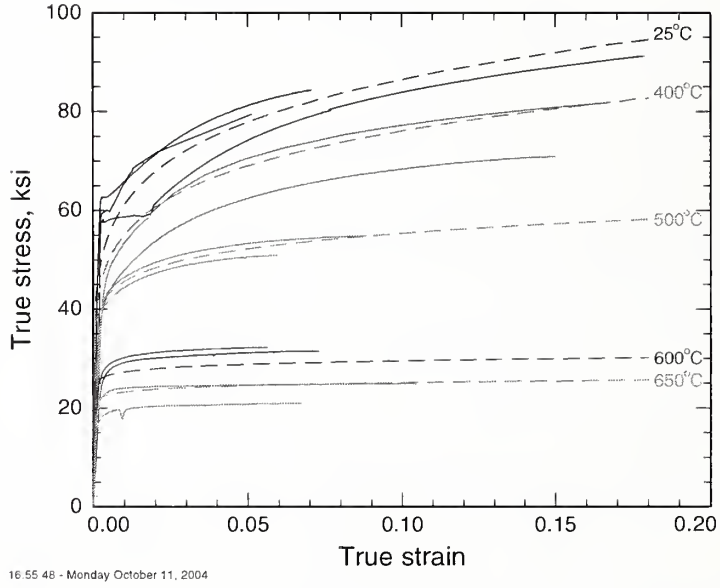

Figure 6–13. Predictions for the model (dashed lines) for steel with F_y > 36 ksi overlaid on the original data used to generate the model (solid lines). Note that the model should not be used for strains in the elastic region (ε~ < 0.003), but the curves are shown in this region. Instead, elastic lines of the appropriate modulus should be used.

A small disadvantage of this method is that the very low strain ($\varepsilon < 0.001$) behavior is neither linear nor does it have a slope equal to the Young's modulus appropriate to that temperature. In terms of the stress-strain behavior, this is a very small error, however. One way of introducing linear stress-strain behavior for small strains is to solve Eq. 6–4 for the intersection point, ε_y, with the correct Young's modulus, $E(T)$, which can be evaluated using Eq. 1–2 of the Chapter 1

$$R_{TS} R_C K(T) \varepsilon_y^{n(T)} = E(T) \varepsilon_y \qquad 6\text{–}9$$

For $\varepsilon < \varepsilon_y$ use the linear Young's modulus relation; for $\varepsilon > \varepsilon_y$ use Eq. 6–4. Figure 6–14 shows stress-strain curves calculated using the method of Eq. 6–9. Figure 6–15 compares the yield points calculated by that method with the expression for the yield point as a function of temperature for many structural steels, Fig. 6–6. The agreement is within the band of the scatter of the data, confirming the suitability of this method. Further accuracy is not warranted, because as temperature increases the yield strength depends increasingly strongly on the testing rate. In these cases, the proportional limit may be much less than the 0.02 percent offset yield strength.

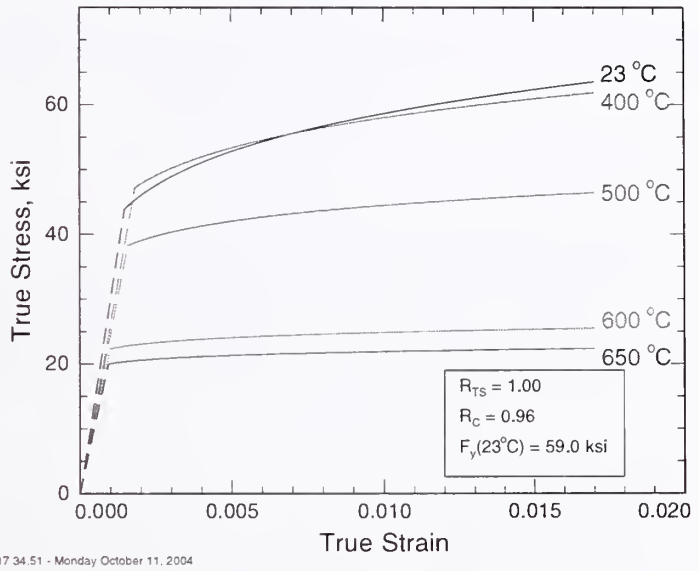

Figure 6–14. Simulated elevated temperature stress-strain curves for the Laclede A 242 truss steel. The small-strain behavior is modeled using the appropriate Young's modulus, while the large-strain behavior comes from Eq. 6–4.

Generally, the correspondence between the original room temperature stress-strain curves and those predicted by Eq. 6–4 is quite good. For the steels with $F_y > 75$ ksi, the agreement is less satisfactory because these steels do not strongly work harden. During the development of this methodology NIST could not locate any elevated temperature stress-strain curves for such high-strength steels, and had not yet conducted the tests reported in Appendix A.

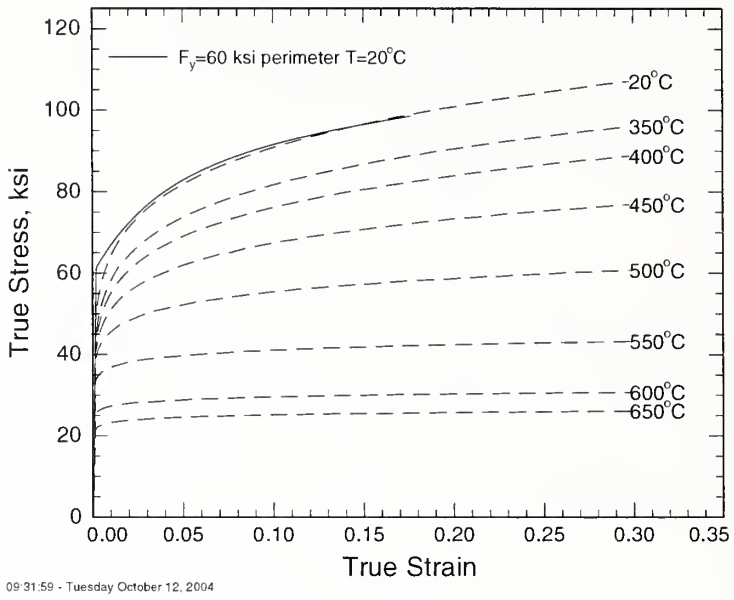

Figure 6–15. Example of predicted stress-strain curves for F_y = 60 ksi perimeter columns calculated using Eq. 6–4.

Limitations of Elevated-Temperature Stress-Strain Curves

There are important limitations to the high-temperature stress-strain curves. At room temperature the stress-strain curves are time-invariant, and, to a good approximation rate-invariant as well. At elevated temperature, beginning at about 400 °C, where thermally activated dislocation motion is easier, these assumptions are no longer valid. In particular the yield strength, defined as the stress below which no permanent deformation occurs, is very poorly defined.

Summary of Data for All WTC Steels

Table 6–9 shows the values of R_{TS} and R_C for all the different steels in WTC 1 and WTC 2.

Example Calculations

To estimate the stress-strain behavior of a F_y = 60 ksi perimeter column steel use the supporting data from Table 6–8 and Table 6–9 with R_{TS} = 1.1800 and R_C = 0.8900. Figure 6–16 shows the stress-strain curves generated using Eqs. 6–4, 6–5, and 6–6 and these parameters. Note, of course, that there is no distinct yield point in the curves generated by Eq. 6–4.

Table 6–9. Scaling parameters (Eq. 6–4) for all WTC steels.

Static F_y (ksi)	Static TS (ksi)	R_{TS}	R_c	Summary Description
36.7	64.5	1.09	0.86	All 36 ksi core box column steels
37.0	63.5	1.07	0.95	All 36 ksi core WF
51.4	79.2	1.07	0.88	All 42 ksi box column steels t ≤ 0.75in
47.0	74.8	1.01	0.88	All 42 ksi box column steels 0.75in < t ≤ 1.5 in
42.6	70.4	0.95	0.88	All 42 ksi box column steels t > 1.5 in
53.8	74.4	1.00	0.98	42 ksi Group 1&2 shapes WF Core Columns
49.0	71.1	0.96	0.95	42 ksi Group 3 shapes WF Core Columns
44.2	66.6	0.90	0.95	42 ksi Group 4&5 shapes WF Core Columns
53.8	74.4	1.00	0.98	45 ksi Group 1&2 shapes WF Core Columns
49.0	71.1	0.96	0.95	45 ksi Group 3 shapes WF Core Columns
47.8	71.1	0.96	0.94	45 ksi Group 4&5 shapes WF Core Columns
53.8	74.4	1.00	0.98	50 ksi Group 1&2 shapes WF Core Columns
53.8	74.4	1.00	0.98	50 ksi Group 4&5 shapes WF Core Columns
35.6	61.2	1.03	0.88	All 36 ksi perimeter column steels plates 1 2 4 (not inner web = plate 3)
53.1	74.9	1.01	0.95	All 45 ksi perimeter column steels plates 1 2 4 (not inner web = plate 3)
54.0	75.6	1.02	0.98	All 50 ksi perimeter column steels plates 1 2 4 (not inner web = plate 3)
60.8	82.6	1.11	0.90	All 55 ksi perimeter column steels plates 1 2 4 (i.e. not -plate 3) with thickness ≤ 1.5 in
62.0	87.3	1.18	0.89	All 60 ksi perimeter column steels plates 1 2 4 (i.e. not inner plate –plate 3) with t ≤ 1.25 in
69.6	90.4	1.22	0.98	All 65 ksi perimeter column steels plates 1 2 4 (i.e. not inner plate –plate 3) with t ≤ 0.5 in
76.7	92.0	1.24	0.96	All 70 ksi perimeter column steels plates 1 2 4 (not inner web = plate 3)
82.5	96.8	1.31	0.94	All 75 ksi perimeter column steels plates 1 2 4 (not inner web = plate 3)
91.5	99.4	1.34	0.99	All 80 ksi perimeter column steels all plates
104.8	116.0	1.57	0.98	All 85, 90, 100 ksi perimeter column steels, regardless of plate
38.1	59.6	1.00	0.94	Truss rounds specified as A 36
55.3	74.1	1.00	0.96	Truss angles (A 36 or A 242) and all rounds specified as A242
42.6	n/d	0.90	0.91	All F_y = 42 ksi perimeter column plate 3 steels
45.9	n/d	0.94	0.92	All F_y = 45 ksi perimeter column plate 3 steels
51.4	n/d	1.00	0.93	All F_y = 50 ksi perimeter column plate 3 steels
56.9	n/d	1.07	0.91	All F_y = 55 ksi perimeter column plate 3 steels
62.4	n/d	1.13	0.95	All F_y = 60 ksi perimeter column plate 3 steels
67.9	n/d	1.19	0.98	All F_y = 65 ksi perimeter column plate 3 steels
78.9	n/d	1.31	1.00	All F_y = 70 ksi and F_y = 75 ksi perimeter column plate 3 steels

Key: n/d, not determined.

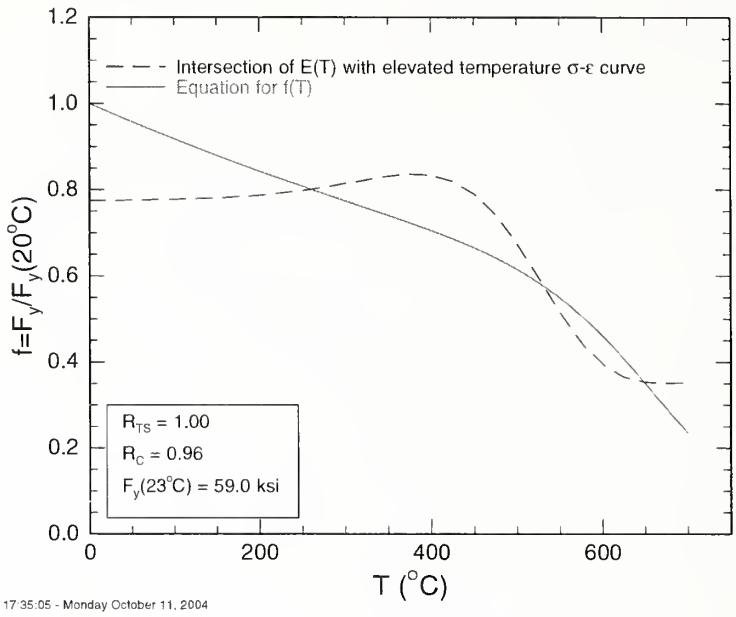

Figure 6–16. Yield point calculated from intersection of appropriate Young's modulus and Eq. 6–4 compared with the expression for the decrease in yield strength for structural steels in general Eq. 6–1. The correspondence is within the uncertainty of either expression.

To estimate the stress-strain behavior of a F_y = 36 ksi core column WF steel use the supporting data from Table 6–5 and Table 6–9 with R_{TS} = 1.0700 and R_C = 0.9500. Figure 6–17 shows the stress-strain curves generated using Eqs. 6–4, 6–5, and 6–6 and the parameters above. Note that Eq. 6–4 slightly overpredicts the already supplied room temperature curve (the solid line), but this difference is within the range of behavior NIST has observed for other A 36 grades of steel.

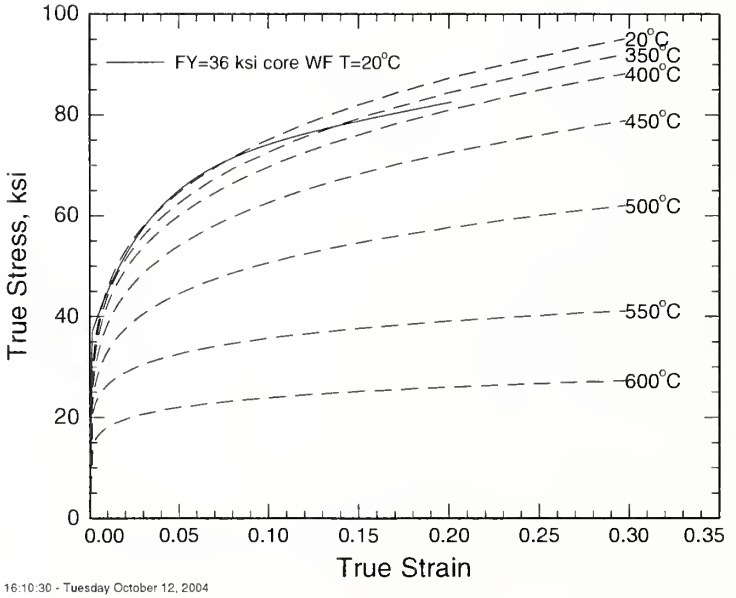

Figure 6–17. Example stress-strain curves for F_y = 36 ksi WF core columns calculated using Eq. 6–4.

6.4.4 Analysis of Creep Data

Background

The literature contains very few strain-time curves for short-term creep of structural steel. One source is Knight (1971) who characterized four Australian steels: AS A135, AS A149, X-60, and Aus-Ten 50. The first two are similar to US ASTM A 36 steels. X-60 is a pipeline steel conforming to API 5LX. Aus-Ten 50 is a weathering steel with Cr and Ni additions. A second source is Fujimoto (1979), who characterized the creep of three Japanese structural steels: SS41, SM50, and SM58. SS41 is similar to A 36. SM50 is a higher strength grade (F_y = 350 MPa (51 ksi) , TS = 530 MPa). SM58 is a Cr-Mo-V steel (F_y = 540 MPa (78 ksi), TS = 660 MPa). Williams-Leir (1983) reanalyzed the data in both these studies and developed a very useful analytical model for predicting creep strain as a function of time, stress, and temperature for all seven steels.

Fields and Fields (1988) reanalyzed Knight's creep data of AS A149 steel. The data set for the AS A149 steel consists of 44 tests in the range 350 °C < T < 650 °C. They also used their model to predict the strain-time creep behavior of SS41 in Fujimoto (1979). The analysis of this section preserves the notation of Fields and Fields, and refers to the predicted strain using these parameters as the "AS A149 model."

Fields and Fields (1988) represented the creep strain, ε_c, using a function that separates the time and stress dependence into independent functions:

$$\varepsilon_c = A t^B \sigma^C \qquad 6\text{–}10$$

The functions A, B, and C are all functions of temperature.

$$B(T) = B_0 + B_1 T$$

where
$B_0 = -1.1$
$B_1 = 0.0035$ 6–11

where T is in °C and t is in minutes.

$$C(T) = C_0 + C_1 T$$

where
$C_0 = 2.1$
$C_1 = 0.0064$ 6–12

where T is in °C and σ is in ksi. The parameter C is the temperature dependent creep stress exponent, often denoted by the symbol n.

$$A(T) = 10^{-(A_0 + A_1 T)}$$

where

for $T < 500$ °C

$A_0 = 6.10$

$A_1 = 0.00573$

for $T > 500$ °C

$A_0 = 13.25$

$A_1 = -0.00851$

6–13

where T is in °C and strain is in percent.

The analysis of the remainder of this section has two goals. One is to characterize the actual creep behavior of the important truss angle steel that made up the chords of the floor trusses. The second is to develop a methodology for estimating from literature data the creep behavior of the other steels in the trusses, truss seats, perimeter columns, and core columns.

Results for A 242 F_y = 50 ksi Truss-Angle Steel

The A 242 steel tested came from the upper and lower chords of truss specimen C-132, of unknown location in the buildings. The steel was specified to conform to ASTM A 242. Chemical analysis showed that, although its chemistry is consistent with the A 242 specification, it contains reduced levels of the usual Cr and Ni alloying elements added to A 242 steels for corrosion resistance. Chemically it is similar to a contemporary A 572 steel.

The solid lines in Figs. 6–2 through 6–5 plot the creep curves for A 242. The curves have been graphically truncated at 5 percent strain. Horizontal arrows denote tests that were suspended. Vertical arrows denote tests that ended with specimen failure.

Analysis of A 242 F_y = 50 ksi Truss-Angle Creep Data

The analysis retains the formalism of the 1988 analysis of Fields and Fields, which describes the creep (not total) strain as

$$\varepsilon_c = A t^B \sigma^C \qquad 6\text{–}14$$

where A, B, and C are all functions of temperature.

In practice it was not possible to evaluate both A and C independently in a single creep test. While Fields and Fields evaluated C from plots of creep strain as a function of stress at different times, we evaluated C as the stress exponent for creep rate, $d\varepsilon/dt$:

$$\frac{d\varepsilon}{dt} = A' \sigma^{C(T)} \qquad 6\text{–}15$$

Calculating C this way enabled the use of extra strain rate data from the high-temperature tensile tests. A non-linear least squares fit to the ($d\varepsilon/dt$, σ, T) data shown in Table 6–10, using the natural logarithm of Eq. 6–15 resulted in

$$C(T) = C_0 + C_1 T \qquad 6\text{–}16$$

where
$C_0 = 3.233$
$C_1 = 0.0117$

where T is in °C and σ is in MPa. Using the entire data set simultaneously results in a fit that weights the temperatures with more data points more strongly. Figure 6–18 shows the strain rate data and the fits to Eq. 6–16. The range of $C(T)$ is $7.9 < C(T) < 10.8$ for $400\ °C < T < 650\ °C$.

Table 6–10. Stress-temperature-strain rate data used to evaluate the parameters of Eq. 6–16.

Specimen	Flow Stress MPa	T °C	Strain Rate 1/s
C132TA6W-1	165	650	9.02E-04
C132TA7W-1	147.2	650	2.69E-04
C132TA6N-2	145.4	650	2.13E-04
C132TA2N-3	126	650	1.39E-04
C132TA2W-8	125	650	3.20E-04
C132TA2W-4	100	650	2.95E-05
C132TA4N-3	212	600	7.62E-04
C132TA1W-8	202	600	2.50E-04
C132TA3W-4	190	600	2.62E-04
C132TA5W-2	164	600	2.79E-05
C132TA3W-3	152	600	2.85E-05
C132TA4W-6	150	600	1.90E-05
C132TA2W-2	131	600	9.91E-06
C132TA1W-2	123	600	2.44E-06
C132TA1N-3	349	500	8.60E-04
C132TA1N-2	300	500	2.50E-04
C132TA2N-2	297	500	4.11E-05
C132TA4W-4	278	500	1.53E-05
C132TA1W-4	272	500	7.75E-06
C132TA3N-1	252	500	6.77E-06
C132TA4W-3	250	500	3.48E-06
C132TA3W-2	200	500	5.17E-07
C132TA4N-2	445.8	400	2.67E-06
C132TA7W-2	422.4	400	8.81E-07
C132TA7N-1	346.4	400	8.40E-08

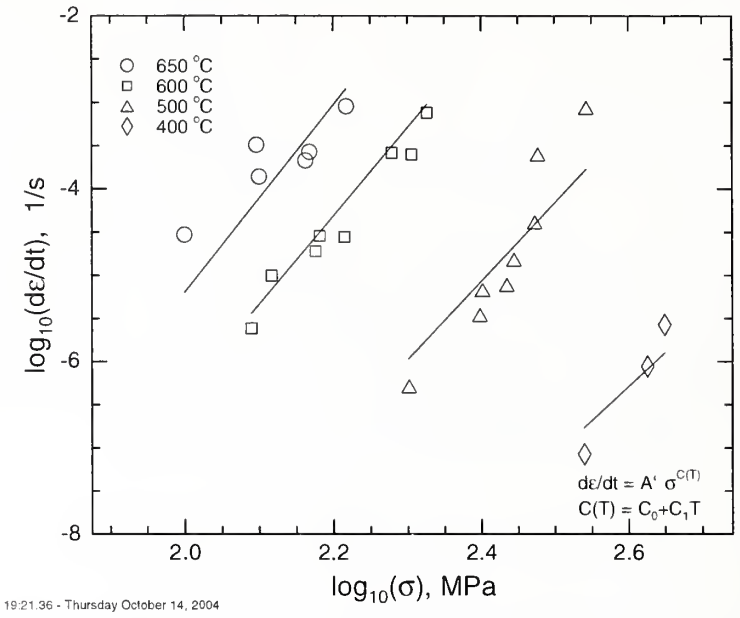

Figure 6–18. Prediction of the function *C(T)*, Eq. 6–16, from strain rate data for A 242 truss steels.

Unlike the data for the AS A149 steel, the time-hardening exponent, B, does not increase linearly with temperature, so the representation of Eq. 6–11 is inappropriate. To ensure accurate representation of the creep behavior near and outside the boundaries of the experimental conditions requires choosing a function for B that does not diverge or produce negative values of B at low temperature. Of course, creep at temperatures less than about 400 °C is insignificant, so the specifics of the behavior at low temperatures will not affect the measurable strain. The chosen function for $B(T)$ has a minimum value for low temperature:

$$B(T) = B_0 + B_1 T^{B_2} \qquad 6\text{–}17$$

where

$B_0 = 0.3982$

$B_1 = 3.5531 \times 10^{-11}$

$B_2 = 3.6975$

where T is in °C and t is in seconds. The parameters have no physical significance. Figure 6–19 shows the behavior of $B(T)$ over the temperature range where creep is important.

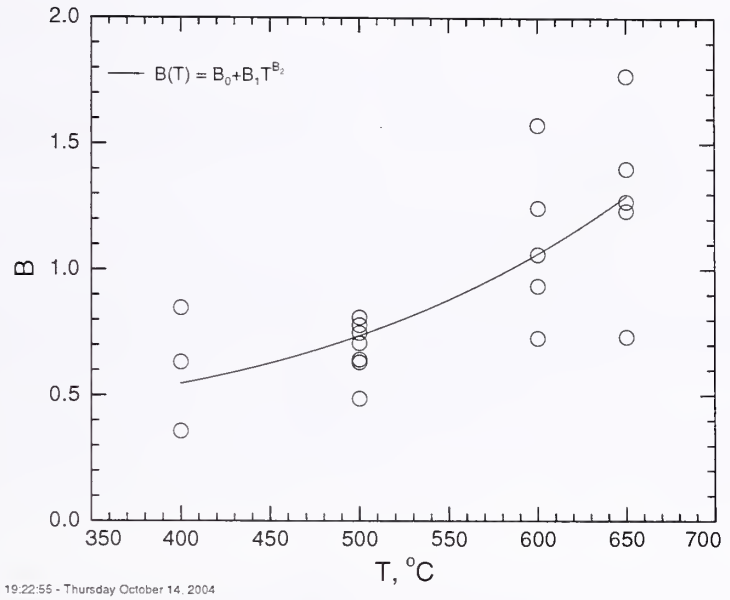

Figure 6–19. Variation of the parameter *B* with temperature. Solid line is Eq. 6–17.

The prefactor, A, in Eq. 6–14 could be represented by a quadratic polynomial.

$$A(T) = \exp(A_0 + A_1 T + A_2 T^2) \text{ where}$$
$$A_0 = -55.4504 \qquad 6\text{–}18$$
$$A_1 = 9.47600\times10^{-3}$$
$$A_2 = -3.52064\times10^{-5}$$

where T is in °C and strain is in natural units.

Evaluating the parameters of Eqs. 6–16, 6–17, and 6–18 required several steps. The first step was to evaluate C_0 and C_1 of Eq. 6–16 using the data of Table 6–10. After that, Eq. 6–14 was fit to each individual creep curve, using the appropriate values of $C(T)$ and σ. This resulted in a set of 20 individual (A_i, T_i) and (B_i, T_i) pairs, from which the values of the parameters in Eqs. 6–17 and 6–18 were evaluated by linear regression in the case of Eq. 6–18 and non-linear, least-squares fitting in Eq. 6–17.

Comparison of the A 242 Model with Actual Creep Curves.

Figures 6–2 through 6–5 also plot the model creep curves developed using the methodology of the previous sections. In general the agreement is acceptable and is of the same magnitude as the model fits of Williams-Leir (1983) to Knight's (1971) and Fujimoto's (1979) data, as well as Fujimoto's (1979) fits to his own data. It is important to realize that the model curves in the figures are not fits to the individual creep curves, but are rather the prediction of the model from the global fit, using the methodology of the previous section.

Estimating Creep Properties of WTC Steels.

The general goal of the second part of this analysis is to develop a methodology to estimate the creep properties of the other WTC steels using either literature-generated models or models generated from creep data from the NIST laboratory.

Previous analysis has indicated that both the yield (F_y) and tensile (TS) strengths follow a universal curve with temperature, when normalized to their room temperature values. This behavior suggests that it is possible to use the creep data developed for one steel to predict the creep behavior of another steel by appropriate scaling by one of these parameters. A second advantage of this approach is that F_y, TS, and total elongation to failure are frequently the only steel parameters reported in the literature. To use the AS A149 model to predict creep behavior of an untested steel, Eq. 6–14 uses a corrected stress, σ_c, equal to the applied stress, σ_a, times the ratio, R_σ, of the yield or tensile strength of the AS A149 to that of the untested steel. For example,

$$\sigma_c = R_\sigma \sigma_a = \frac{TS_{\text{A149}}}{TS_{\text{unt}}} \sigma_a \qquad 6\text{–}19$$

So, for an untested steel that is stronger than the reference AS A149 steel, the corrected stress used to predict the creep behavior will be less than the actual applied stress ($R_\sigma < 1$). An alternative approach, which is even simpler, is to set $R_\sigma = 1$, which is equivalent to assuming that all steels have identical creep properties.

The best of the three possible scaling ratios, R_σ, (F_y, TS, and no scaling) was evaluated subjectively. Williams-Leir's (1983) analytical expressions for creep strain as a function of time for the four Australian steels of Knight (1971) and three Japanese steels of Fujimoto (1979) facilitated this intercomparison. Although Williams-Leir used an expression for creep strain as a function of time, stress, and temperature that differs from Eq. 6–14, his fits produced creep curves of similar fidelity. Using his analytical expression removed the need to re-fit all seven data sets. At four temperatures (500 °C, 550 °C, 600 °C, and 650 °C) the ratio, R, of the creep strain at 3600 s predicted by the scaling ratio approach of Eq. 6–19 to that predicted from the Williams-Leir analytical expression was plotted as a function of stress for each steel. The range of stresses plotted was constrained to produce strains in the range $5\times10^{-4} < \varepsilon < 0.25$. Strains outside this range are irrelevant for creep modeling. This procedure produced 28 plots (seven steels at four temperatures) where each plot has seven plotted ratio lines. Perfect prediction by one steel of another's creep strain would produce a horizontal ratio line with $R = 1$. For each steel at each scaling ratio, R_σ, the quality of the prediction was ranked by visually judging the distance from the distance of the predicted line from unity.

The results of the ranking established the tensile strength ratio scaling as the best approach. In about 1/2 of the cases, tensile-strength ratio scaling and no scaling produced similar results. In about 1/3 of the cases, tensile-strength ratio scaling produced the best results, and in the remaining 1/6 of the cases, no scaling produced the best results. Thus, in about 5/6 of the cases, scaling the creep behavior by the room temperature tensile strength ratio produced creep curves that most closely approximated the measured curves. Scaling by the yield strength ratio almost always produced the worst predicted strains. Frequently it produced estimates that differed from the actual data by more than a factor of ten. The only times that

scaling by the yield strength ratio produced acceptable results was when the scaling ratio was fortuitously identical to the scaling ratio produced by the tensile strengths.

Values for Creep Parameters

To estimate the creep strain as a function of time for all truss bulb angles use Eq. 6–14 with the parameters in Eqs. 6–16, 6–17 and 6–18.

To estimate the creep strain as a function of time for all other steels use Eq. 6–14 with the parameters of Eqs. 6–11, 6–12 and 6–13. Scale the applied stress by the ratio of the tensile strength of the AS A149 steel (TS_{A149} = 70.6 ksi) to that of the steel in question using Eq. 6–19.

6.4.5 Values for Bolts

Background

NIST did not test any bolts at elevated temperatures. Given the lack of experimental data, it is necessary to predict the bolt properties using the methodology of Section 6.4.1.

Because A 325 and A 490 bolts are not intended to be used above room temperature, very little elevated temperature property data exist in the literature. The limited strength data for bolts plotted in Fig. 6–20 come from tensile specimens of bolt steels rather than the bolts themselves, made to British, Japanese and Chinese bolt standards. In general, these bolt standards are similar to the corresponding ASTM standards, however. Table 6–11, and the rest of this section, summarize the literature data used to construct Fig. 6–20.

Table 6–11. Sources of bolt data.

Reference	Steel	*TS* (spec) MPa	F_y (Spec) MPa	Steel Chemistry
Kirby	Grade 8.8	785-981	628	C-Mn-Cr-Mo-B-Ti
Li	20MnTiB	1040-1240	940	C-Mn-Ti-B
Sakumoto	Bol-Ten	981-1177	883	unknown
	A 325	827	634	C-Mn-B

Kirby (1995) studied British Grade 8.8 bolts supplied to BS 3692 from two manufacturers. These bolts are very similar to A 325 bolts in both strength and chemistry. He conducted tensile strength tests at temperatures up to 800 °C on actual bolts, as well as on the steels used to fabricate the bolts. In the bolt tests, the mode of tensile failure depended on choice of nut. Even though the nuts were made to identical specifications, in one set the bolt failed by ductile necking in the thread, while in the other set, the bolt threads stripped out.

Li et al. (2003) tested bolt steel identified as "20MnTiB," which apparently corresponds to a Chinese bolt specification. In terms of strength, these bolts are similar to A 490 bolts, rather than to A 325 bolts. They tested tensile specimens fabricated from bolt steel at temperatures up to 700 °C.

Sakumoto (1993) reported the properties of ordinary and "fire-resistant" (FR) bolts made to JSS II-09-1981. Both were identified as "BOL-TEN110N" steel. This bolt steel is stronger than the A 325 bolt steels.

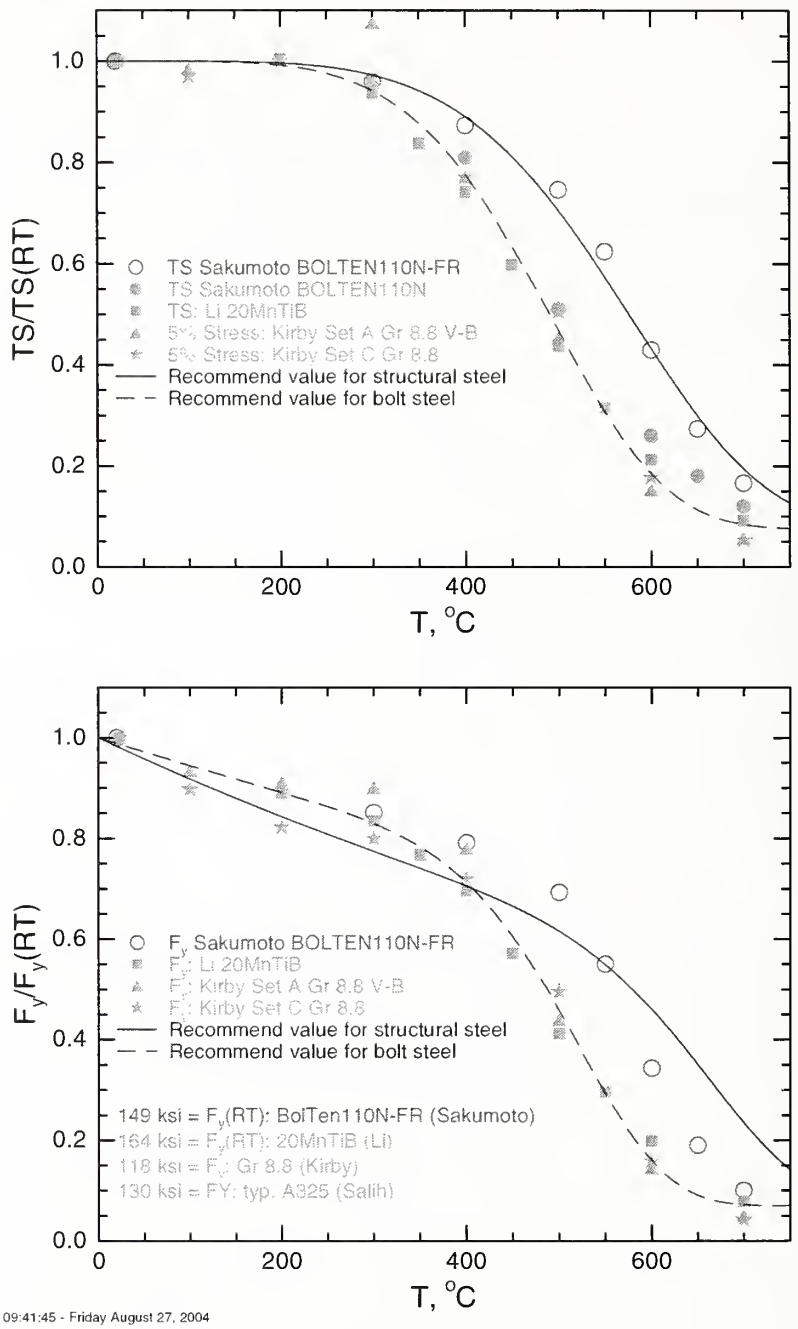

Figure 6–20. Comparison of high-temperature yield, F_y, and tensile, *TS*, strength for bolt steels and the expression for structural steels in general, Eqs. 6–1 and 6–2. Solid symbols are bolt steels. Open symbols are "fire-resistant" bolt steels. Expression for bolt steels is the dashed line.

Figure 6–20 shows the ratio of yield (F_y) and tensile (TS) strengths to their room-temperature values for the various bolt steels. The solid line is the expression for structural steels in general. The bolt steels,

however, with the exception of the FR BOL-TEN steel, lose strength more rapidly than do the structural steels.

Results

Because the bolt steels lose strength more rapidly with increasing temperature than do structural steels, it is necessary to use a different set of parameters for Eqs. 6–1 and 6–2 to describe the strength loss. Table 6–12 shows the values for the parameters for yield (Eq. 6–1) and tensile (Eq. 6–2) strength reduction. The dashed curve in Fig. 6–20 corresponds to the expression for the strength reduction of bolt steels.

Table 6–12. Values for the parameters in the strength reduction equations (Eqs. 6–1 and 6–2) for use with bolts.

Yield Strength Reduction Parameters (Eq. 6–1)	Tensile Strength Reduction Parameters (Eq. 6–2)
$A_2 =$ 0.07	$A_2 =$ 0.09
$m_1 =$ 6.8221	$n_1 =$ 5.0237
$m_2 =$ 1.0000	$n_2 =$ 5.0245
$s_1 =$ 491.0	$t_1 =$ 478.0
$s_2 =$ 810.0	$t_2 =$ 585.0

Values for Bolt Strength Parameters

The yield and tensile strength of bolt steels degrade more rapidly with temperature than do ordinary structural steels. The reductions can be represented by Eqs. 6–1 and 6–2, using the parameters in Table 6–12.

Limitations

Most of the data in Fig. 6–20 come from tests on bolt steels, rather than on bolts themselves. Only Kirby (1995) provides data from actual bolt tests. No information exists on changes in failure mechanisms with increasing temperature for structural steel bolts. The ductility measured in tensile tests of bolt steels cannot be directly applied to predict bolt failure, because bolts generally fail in the threads. There is relatively little data on the expected (versus specified) strength of bolts. Fisher (1963) and Salih (1993) found very different values for the average strength of A 325 bolts, though as expected, the average strength was much higher than the specified strength.

In the absence of data to the contrary, the reduction in bolt strength with temperature can be modeled with Eq. 6–2 using the parameters of Table 6–12.

6.5 SUMMARY

The yield and tensile strength of structural steel follow a master curve when normalized to their room temperature values, Eqs. 6–1 and 6–2.

The shapes of stress-strain curves at elevated temperature can be modeled based on the room-temperature shape of a model curve scaled by the ratio of their tensile strengths. The model accounts for the decrease in work-hardening with increasing temperature, Eqs. 6–4, 6–5 and 6–6. The behavior of steels with F_y = 36 ksi is based on the behavior of A 36 steel from the literature. The behavior of steels with F_y > 36 ksi is based on the behavior of F_y = 50 ksi steel recovered from the WTC floor trusses.

Creep behavior can be modeled using a function that breaks the time and stress dependence of the creep strain into separate functions, Eq. 6–14. The behavior of steels with F_y = 36 ksi is based on a literature analysis of Australian AS A149 steel. To apply this model to other F_y = 36 ksi steels, it is necessary to scale the applied stress by the ratios of their room-temperature tensile strengths, Eq. 6–19. The creep behavior of steels with F_y > 36 ksi is based on results of tests on F_y = 50 ksi steel recovered from the WTC floor trusses.

Bolt properties are estimated from literature data.

6.6 REFERENCES

Baird, J.D. 1971. The effects of strain-ageing due to interstitial solutes on the mechanical properties of metals, Review 149. *Metall. Rev.* 16 1–18.

Chijiiwa, R. *et al.* 1993. Development and Practical Application of Fire-Resistant Steel for Buildings. Nippon Steel Technical Report 58. 47–55.

Fields. B.A. and R.J. Fields. 1989. Elevated Temperature Deformation of Structural Steel. NISTIR 88-3899.

Fujimoto, M. *et al.* 1979. Primary Creep of Structural Steel at High Temperatures. Report of the Research Laboratory of Engineering Materials, Tokyo Institute of Technology. Number 4. p.p. 1–27.

Goda, S. *et al.* 1964. Present Status of Weldable High Strength Steel. Yawata Technical Report (Yawata Seitetsu Kenkyu) 248 5086–5163 (in Japanese).

Gowda, B.C. 1978. Tensile Properties of SA 516, Grade 55 Steel in the Temperature Range of 25°–927°C and Strain Rate Range of 10^{-4} to 10^{-1} sec^{-1}. In, *Characterization of Materials for Service at Elevated Temperatures.* Smith, G.V. ed. American Society of Mechanical Engineers. New York. "presented at the 1978 ASME/CSME Montreal Pressure Vessel & Piping Conference, Montreal, Quebec, Canada, June 25–29 1978." 145–158

Harmathy T.Z. and W.W. Stanzak. 1970. Elevated-Temperature Tensile and Creep Properties of Some Structural and Prestressing Steels. in *Fire Test Performance, ASTM STP 464*, American Society for Testing and Materials. 186–208.

Holt, J.M. 1963. Short-time Elevated-Temperature Tensile Properties of USS "T-1" and USS "T-1" Type A Constructional Alloy Steels. United States Steel Report (57.019-901)(3)(a-AS-EA-2). Also reported in (USS 1972).

Holt, J.M. 1964. Short-Time Elevated-Temperature Tensile Properties of USS Cor-Ten and USS Tri-Ten High-strength Low-alloy steels, USS Man-Ten (A 440) High-strength Steel, and ASTM A 36 Steel. United States Steel Corp. Report 57.19–901(1). Monroeville, Pa, Applied Research Laboratory. Oct. 16 (much of this data appear in (USS 1972)

Jerath, V., K.J. Cole and C.I. Smith. 1980. Elevated Temperature Tensile Properties of Structural Steels Manufactured by the British Steel Corporation. Unpublished Report # T/RS/1189/11/80/C. British Steel Corporation, Teeside Laboratories. July 24.

Kirby, B. R. 1995. The Behaviour of High-strength Grade 8.8 Bolts in Fire. *J. Construct. Steel. Research.* 33 3–38.

Knight, D., D.H. Skinner and M.G. Lay. 1971. Short Term Creep Data on Four Structural Steels. Report MRL 6/3 Melbourne Research Laboratories. The Broken Hill Proprietary Company. Clayton, Victoria, Australia. January.

Li, Guo-Qiang, Shou-Chao Jian, Ying-Zhi Yin, Kai Chen and Ming-Fei Li. 2003. Experimental Studies on the Properties of Constructional Steel at Elevated Temperatures. *J. Struct. Eng.* 129[12] 1717–1721.

Manjoine, M.J. 1944. Influence of Rate of Strain and Temperature on Yield Stresses of Mild Steel. *Trans. ASME.* 66. A-211–A-218.

Melloy, G.F. and J.D.Dennison. 1963. Short-time Elevated-Temperature Properties of A7, A440, A441, V50, and V65 Grades. Internal memorandum to J.W. Frame. Report 1900-4g. Bethlehem Steel. April 17.

Rumpf, John L. and John W. Fisher. 1963. Calibration of A325 Bolts. *J. Struct. Div. ASCE.* 89[ST6]. 215–234.

Sakumoto, Y., K. Keira, F. Furuyama and T. Ave. 1993. Tests of Fire-Resistant Bolts and Joints. *J. Struct. Eng.* 119[11] 3131–3150.

Salih, Nazir, John Smith, *et al.* 1992 An Experimental Appraisal of the Load-Deformation Properties of A325 High-Strength Bolts. *J. Test. Eval.* 20[6] 440–448.

(USS) 1972. *Steels for Elevated Temperature Service.* United States Steel Corporation. Pittsburgh, Pa.

Williams-Leir, G. 1983. Creep of Structural Steel in Fire: Analytical Expressions. *Fire and Materials.* 7[2] 73-78.

This page intentionally left blank.

Chapter 7
SUMMARY AND FINDINGS

7.1 SUMMARY

The experimentally determined mechanical property data of World Trade Center (WTC) steels can be divided into five groups:

- Elastic properties as a function of temperature were determined from recovered perimeter column steels.
- Room temperature yield and tensile strength, and total elongation were determined from specimens of recovered steel of all grades from the fire and impact zones. Complete stress-strain curves are reported for 29 different steels with 12 yield strength levels. Load-displacement curves were measured from recovered A 325 bolts. Stress-strain curves and strengths of several different perimeter column and truss weld geometries are reported.
- Yield and tensile strengths and total elongations of selected perimeter and core column steels were determined as a function strain rate at rates up to 400 s^{-1}. Strain-rate sensitivities and complete stress-strain curves for these steels are reported. Several steels were characterized at higher rates using Kolsky bar testing.
- Impact properties as a function of temperature were determined using Charpy tests for selected perimeter column, core column, truss, and truss-seat steels.
- Elevated-temperature yield and tensile strength, and total elongation were determined on selected specimens of recovered perimeter and core column, truss, and truss seat steels. Complete stress-strain curves for temperatures up to 650 °C are reported for all steels characterized. Creep deformation as a function of temperature and stress was determined for the truss chord steel.

By combining these measured properties with historical averages from the literature, and in some cases recovered mill test reports, National Institute of Standards and Technology (NIST) developed expressions and values for properties of the important grades of steel:

- Elastic modulus and Poisson's ratio as a function of temperature,
- Model room-temperature stress-strain curves for all WTC steel grades from the fire and impact zones corrected for dynamic effects,
- Room-temperature load-displacement curves for A 325 bolts,
- Yield and tensile strength for weld metals,
- Strain rate sensitivity of steel for high strain rate properties,

- Elevated-temperature yield and tensile strength and complete stress-strain behavior for all WTC steel grades from the fire and impact zones,
- Elevated-temperature load-displacement curves for A 325 bolts,
- Creep response for all WTC steel grades from the fire and impact zones.

7.2 FINDINGS

This report makes a number of findings concerning the steel used in the WTC:

- Steels, bolts, and welds generally have properties that indicate that they met the specifications to which they were supplied.
- Infrequently, the measured yield strengths are lower than called for by the appropriate specifications. The measured yield strengths of 2 of 24 perimeter column samples were lower than the specified minimum. This probably occurred from a combination of the natural variability of steel properties, and small differences between the mill and NIST testing protocols. The measured yield strengths of 2 of 8 core column samples were lower than the specified minimum. In this case, mechanical damage that occurred in the collapse and subsequent recovery removed the expected yield point behavior leading to the low values.
- The average measured yield strength of the steels from the perimeter columns exceeds the specified minimum values by about 10 percent, which is consistent with historically expected values for steel plates.
- The measured yield strengths of the F_y = 36 ksi wide-flange core columns are lower than expected from historical measurements of other structural steels.
- The strain rate sensitivities of the yield and tensile strengths of perimeter and core columns are similar to other structural steels from the WTC construction era.
- The impact properties of the steels, evaluated by Charpy testing, are similar to structural steels from the WTC era. The ductile-to-brittle transition temperatures of the perimeter and core column steels are at or below room temperature.
- The behavior of the yield and tensile strengths of WTC steels with temperature is similar to that of other structural steels from the WTC construction era.

Appendix A
DATA TABLES AND SUPPLEMENTAL FIGURES

A.1 DATA TABLES FOR ROOM-TEMPERATURE MECHANICAL PROPERTIES

The following tables summarize the room-temperature mechanical properties.

Table A–4. Room-temperature tensile test results for perimeter column steels.

Specified yield (F_y)	Location in Bldg (Bldg.-Center column number, floor level)	Test axis with respect to RD	Temp	Specimen type and nominal GL	Area	Yield point, *YP*	0.2 % Yield Strength, *YS*	0.2 % Yield Strength, *YS*	Tensile Strength, *TS*	Tensile Strength, TS	El_t	*ROA*	Measured yield/F_y	Sample #
ksi			°C		in.²	ksi	ksi	MPa	ksi	MPa	%	%		
45	unknown	L	RT	Flat 2"	0.1963	56.7	56.20	387	75.4	520	33 (2in.)	69	1.26	ASCE3-C1B-FL-1-
45	unknown	T	RT	Flat 2"	0.1963	56.7	51.80	357	75.2	519	29 (2in.)	58	1.26	ASCE3-C1B-FL-1-
45	unknown	T	RT	Flat 2"	0.1963	53.6	51.90	358	75.0	517	33 (2in.)	57	1.19	ASCE3-C1B-FL-1-
50	1-124-70/73	T	20	Flat-C 1"	0.0745	NYP	53.5	369	80.4	554	40 (1in.)	66	1.07	CC-C3T-IW-2-1
50	1-124-70/73	T	20	Flat-C 1"	0.0747	NYP	53.3	368	80.9	558	39 (1in.)	66	1.07	CC-C3T-IW-2-2
50	1-130-90/93	L	20	Flat 2"	0.2954	NYP	62.2	429	85.5	590	36 (2in.)	61	1.24	M26-C1B1-RF-L1
50	1-130-90/93	L	20	Flat 2"	0.2948	NYP	61.1	421	86.1	594	35 (2in.)	61	1.22	M26-C1B1-RF-L2
50	1-130-90/93	T	20	Flat 2"	0.2964	NYP	61.6	425	84.8	585	30 (2in.)	41	1.23	M26-C1B1-RF-T1
50	1-130-90/93	T	20	Flat 2"	0.2952	NYP	61.7	425	84.7	584	30 (2in.)	37	1.23	M26-C1B1-RF-T2
55	2-154-101/104	L	20	Flat 2"	0.1313	NYP	57.3	395	84.5	583	27 (2in.)	60	1.04	N9-C1T1-IW-L-1
55	2-154-101/104	L	20	Flat 2"	0.1320	65.9	60.6	418	87.1	601	26 (2in.)	60	1.10	N9-C1T1-IW-L-2
55	2-154-101/104	L	20	Flat 2"	0.1290	65.9	64.3	454	89.2	615	27 (2in.)	61	1.20	N9-C1T1-IW-L-3
55	2-154-101/104	T	20	Flat 2"	0.1303	NYP	65.2	450	88.3	609	24 (2in.)	49	1.19	N9-C1T1-IW-T-1
55	2-154-101/104	T	20	Flat 2"	0.1310	66.4	66.4	458	88.6	611	24 (2in.)	50	1.21	N9-C1T1-IW-T-2
55	2-154-101/104	L	20	Flat 2"	0.1358	NYP	61.0	421	82.3	567	32 (2in.)	66	1.11	N9-C1T1-LF-L-2
55	2-154-101/104	L	20	Flat 2"	0.1330	NYP	62.0	427	82.7	570	34 (2in.)	65	1.13	N9-C1T1-LF-L-3
55	2-154-101/104	T	20	Flat 2"	0.1355	NYP	61.5	424	83.9	578	27(2in.)	43	1.12	N9-C1T1-LF-T-1
55	2-154-101/104	T	20	Flat 2"	0.1330	NYP	63.9	441	82.7	570	27 (2in.)	44	1.16	N9-C1T1-LF-T-3
55	2-154-101/104	T	20	Flat 2"	0.1338	NYP	63.4	437	82.1	566	26 (2in.)	34	1.15	N9-C1T1-LF-T-4
55	2-154-101/104	L	20	Flat 2"	0.1375	NYP	61.6	425	83.3	574	34 (2in.)	65	1.12	N9-C1T1-RF-L-2
55	2-154-101/104	L	20	Flat 2"	0.1370	NYP	62.0	427	83.9	578	31 (2in.)	64	1.13	N9-C1T1-RF-L-3
55	2-154-101/104	L	20	Flat 2"	0.1378	NYP	61.6	425	81.5	562	30 (2in.)	47	1.12	N9-C1T1-RF-T-1
55	2-154-101/104	T	20	Flat 2"	0.1396	NYP	61.2	422	80.9	558	29 (2in.)	52	1.11	N9-C1T1-RF-T-2
55	2-154-101/104	T	20	Flat 2"	0.1385	NYP	61.2	422	82.7	570	29 (2in.)	48	1.11	N9-C1T1-RF-T-3
55	2-154-101/104	L	20	Flat 2"	0.1350	NYP	70.5	486	97.7	674	25 (1in.)	54	1.28	N9-C1T1-OW-L-1
55	2-154-101/104	L	20	Flat 2"	0.1345	NYP	72.0	496	96.9	668	35 (1in.)	58	1.31	N9-C1T1-OW-L-2
55	2-154-101/104	L	20	Flat 2"	0.1363	NYP	71.5	493	95.2	656	33 (1in.)	56	1.30	N9-C1T1-OW-L-3
55	2-154-101/104	T	20	Flat 2"	0.1347	NYP	72.0	496	94.6	652	18 (2in.)	24	1.31	N9-C1T1-OW-T-1
55	2-154-101/104	T	20	Flat 2"	0.1362	NYP	71.5	493	93.9	647	17 (2in.)	24	1.30	N9-C1T1-OW-T-2
55	2-154-101/104	T	20	Flat 2"	0.1375	NYP	70.0	483	93.2	643	19 (2in.)	27	1.27	N9-C1T1-OW-T-3
60	1-142-97/100	T	20	Flat 2"	0.1300	60.4	61.9	427	81.1	559	27 (2in.)	50	1.03	N8-C2M-IW-1-T1
60	1-142-97/100	T	20	Flat 2"	0.1300	58.5	59.6	411	80.4	554	29 (2in.)	48	0.99	N8-C2M-IW-1-T2
60	1-142-97/100	L	20	Flat 2"	0.1348	NYP	56.8	392	77.5	534	33 (2in.)	64	0.95	N8-C2M-IW-1-L2
60	1-142-97/100	L	20	Flat 2"	0.1336	59.5	59.9	413	78.6	542	30 (2in.)	61	1.00	N8-C2M-IW-1-L1

Table A–1. Room-temperature tensile test results for perimeter column steels (continued).

Specified yield (F_y) ksi	Location in Bldg (Bldg.-Center column number, floor level)	Test axis with respect to RD	Temp °C	Specimen type and nominal GL	Area in.²	Yield point, *YP* ksi	0.2 % Yield Strength, *YS* ksi	0.2 % Yield Strength, *YS* MPa	Tensile Strength, *TS* ksi	Tensile Strength, TS MPa	El_t %	*ROA* %	Measured yield/F_y	Sample #
60	1-142-97/100	L	20	Flat 2"	0.1300	NYP	62.3	430	93.5	645	28 (2in.)	55	1.04	N8-C3B1-OW-L1
60	1-142-97/100	L	20	Flat 2"	0.1310	NYP	59.2	408	91.6	632	27 (2in.)	57	0.99	N8-C3B1-OW-L2
60	1-142-97/100	L	20	Flat 2"	0.1320	NYP	61.0	421	92.4	637	28 (2in.)	58	1.02	N8-C3B1-OW-L3
60	1-142-97/100	T	20	Flat 2"	0.1342	NYP	64.8	447	92.9	641	21 (2in.)	33	1.08	N8-C3B1-OW-T1
60	1-142-97/100	T	20	Flat 2"	0.1362	NYP	64.4	444	91.4	630	23 (2in.)	37	1.07	N8-C3B1-OW-T2
60	1-142-97/100	T	20	Flat 2"	0.1342	NYP	65.2	450	92.8	640	20 (2in.)	24	1.09	N8-C3B1-OW-T3
60	1-142-97/100	L	20	Flat 2"	0.1650	NYP	69.0	476	89.9	620	32 (2in.)	60	1.15	N8-C3B1-RF-L1
60	1-142-97/100	L	20	Flat 2"	0.1660	NYP	70.2	484	90.1	621	30 (2in.)	63	1.17	N8-C3B1-RF-L2
60	1-142-97/100	L	20	Flat 2"	0.1660	70.1	70.1	483	90.4	623	31 (2in.)	58	1.17	N8-C3B1-RF-L3
60	1-142-97/100	T	20	Flat 2"	0.1636	68.3	68.3	471	89.3	616	24 (2in.)	30	1.14	N8-C1B1-D3-RF-
60	1-142-97/100	T	20	Flat 2"	0.1675	67.1	67.1	463	87.9	606	24 (2in.)	32	1.12	N8-C1B1-D3-RF-
60	1-142-97/100	L	20	Flat 2"	0.1651	70.3	68.8	474	88.8	612	35 (2in.)	47	1.15	N8-C1B1-D3-LF-
60	1-142-97/100	L	20	Flat 2"	0.1651	70.3	69.2	477	88.1	607	34 (2in.)	43	1.15	N8-C1B1-D3-LF-
60	1-142-97/100	T	20	Flat 2"	0.1657	70.0	68.5	472	89.3	616	25 (2in.)	32	1.14	N8-C1B1-D3-LF-
60	1-142-97/100	T	20	Flat 2"	0.1667	NYP	67.8	467	89.1	614	24 (2in.)	35	1.13	N8-C1B1-D3-LF-
60	1-142-97/100	L	20	Flat 2"	0.1316	NYP	55.0	379	76.3	526	34 (2in.)	44	0.92	N8-C1B1-A-IW-L1
60	1-142-97/100	L	20	Flat 2"	0.1305	NYP	58.3	402	77.0	531	37 (2in.)	45	0.97	N8-C1B1-A-IW-L2
60	1-142-97/100	T	20	Flat 2"	0.1307	NYP	58.2	401	79.3	547	27 (2in.)	38	0.97	N8-C1M1-E-IW-T1
60	1-142-97/100	T	20	Flat 2"	0.1313	NYP	57.8	399	79.7	550	28 (2in.)	35	0.96	N8-C1M1-E-IW-T2
60	1-142-97/100	T	20	Flat 2"	0.1300	NYP	56.5	390	80.1	552	29 (2in.)	49	0.94	N8-C1M1-E-IW-T3
60	1-142-97/100	T	20	Flat 2"	0.1280	NYP	56.2	387	81.0	558	29 (2in.)	44	0.94	N8-C1M1-E-IW-T4
60	1-142-97/100	T	20	Flat-C 1"	0.0745	NYP	68.4	472	91.0	627	39 (1in.)	65	1.14	N8-C1B1A-FL-1
60	1-142-97/100	T	20	Flat-C 1"	0.0743	NYP	68.4	472	91.9	634	39 (1in.)	68	1.14	N8-C1B1A-FL-2
60	1-136-98/101	T	20	Flat-C 1"	0.0611	NYP	64.7	446	83.0	572	33 (1in.)	63	1.08	C40-C2M-IW-2-1
60	1-136-98/101	T	20	Flat-C 1"	0.0614	NYP	64.4	444	83.2	574	36 (1in.)	65	1.07	C40-C2M-IW-2-2
65	1-148-99/102	L	20	Flat 2"	0.1380	NYP	70.3	485	93.1	642	29 (2in.)	60	1.08	N99-C3T1-RF-L1
65	1-148-99/102	L	20	Flat 2"	0.1351	NYP	73.3	505	94.0	648	30 (2in.)	60	1.13	N99-C3T1-RF-L2
65	1-148-99/102	T	20	Flat 2"	0.1364	74.0	73.7	508	93.8	647	23 (2in.)	40	1.13	N99-C3T1-RF-T1
65	1-148-99/102	T	20	Flat 2"	0.1351	NYP	74.4	513	94.0	648	23 (2in.)	40	1.14	N99-C3T1-RF-T2
65	1-148-99/102	T	20	Flat 2"	0.1330	NYP	63.2	436	92.1	635	21 (2in.)	43	0.97	N99-C3M1-IW-T1
65	1-148-99/102	T	20	Flat 2"	0.1313	NYP	65.1	449	92.5	638	23 (2in.)	44	1.00	N99-C3M1-IW-T2
65	1-148-99/102	L	20	Flat 2"	0.1320	NYP	65.5	452	92.4	637	25 (2in.)	61	1.01	N99C3M1-IW-L3
65	1-148-99/102	L	20	Flat 2"	0.1315	NYP	66.9	461	93.5	645	26 (2in.)	59	1.03	N99-C3M1-IW-L2
65	1-148-99/102	L	20	Flat 2"	0.1305	NYP	67.4	465	93.9	647	28 (2in.)	60	1.04	N99-C3M1-IW-L1

Table A–1. Room-temperature tensile test results for perimeter column steels (continued).

Specified yield (F_y) ksi	Location in Bldg (Bldg.-Center column number, floor level)	Test axis with respect to RD	Temp °C	Specimen type and nominal GL	Area in.²	Yield point, *YP* ksi	0.2 % Yield Strength, *YS* ksi	0.2 % Yield Strength, *YS* MPa	Tensile Strength, *TS* ksi	Tensile Strength, TS MPa	El_t %	*ROA* %	Measured yield/F_y	Sample #
70	2-157-68/71	L	20	Flat 2"	0.3850	NYP	72.5	500	87.8	605	30 (2in.)	70	1.04	C46-C2B-FL-1-L1
70	2-157-68/71	L	20	Flat 2"	0.3840	NYP	79.3	547	92.1	635	31 (2in.)	70	1.13	C46-C2B-FL-1-L2
70	2-157-68/71	T	20	Flat 2"	0.3844	NYP	75.7	522	90.8	626	20 (2in.)	50	1.08	C46-C2B-FL-1-T1
70	2-157-68/71	T	20	Flat 2"	0.3837	NYP	72.1	497	88.8	612	22 (2in.)	51	1.03	C46-C2B-FL-1-T2
70	2-218-91/94	T	20	Flat-C 1"	0.0630	NYP	72.6	501	102.2	705	30 (1in.)	61	1.04	S14-C3B-IW-1-1
70	2-218-91/94	T	20	Flat-C 1"	0.0627	NYP	79.3	547	103.6	714	28 (1in.)	54	1.13	S14-C3B-IW-1-2
70	2-218-91/94	L	20	Flat 2"	0.1407	NYP	79.9	551	92.8	640	21 (2in.)	66	1.14	S14-C3M-FR-1-L1
70	2-218-91/94	L	20	Flat 2"	0.1418	NYP	78.8	543	91.7	632	22 (2in.)	67	1.13	S14-C3M-FR-1-L2
70	2-218-91/94	T	20	Flat 2"	0.1419	NYP	80.3	554	92.1	635	17 (2in.)	43	1.15	S14-C3M-FR-1-T1
70	2-218-91/94	T	20	Flat 2"	0.1397	NYP	78.7	543	93.3	643	21 (2in.)	47	1.12	S14-C3M-FR-1-T2
70	1-433-79/82	L	20	Flat 2"	0.2292	NYP	79.1	545	93.5	645	26 (2in.)	69	1.13	S1-C2M-FL-2-L1
70	1-433-79/82	L	20	Flat 2"	0.2304	NYP	76.7	529	93.1	642	30 (2in.)	69	1.10	S1-C2M-FL-2-L2
70	1-433-79/82	T	20	Flat 2"	0.2299	NYP	77.6	535	93.3	643	21 (2in.)	45	1.11	S1-C2M-FL-2-T1
70	1-433-79/82	T	20	Flat 2"	0.2314	NYP	77.6	535	92.8	640	17 (2in.)	41	1.11	S1-C2M-FL-2-T2
75	1-157-93/96	L	20	Flat 2"	0.1367	NYP	83.2	574	93.7	646	24 (2in.)	70	1.11	C22-C2M-FL-2-L1
75	1-157-93/96	L	20	Flat 2"	0.1363	84.7	83.8	578	94.1	649	24 (2in.)	68	1.12	C22-C2M-FL-2-L2
75	1-157-93/96	T	20	Flat 2"	0.1365	NYP	82.7	570	93.8	647	18 (2in.)	52	1.10	C22-C2M-FL-2-T1
75	1-157-93/96	T	20	Flat 2"	0.1331	NYP	82.6	570	93.3	643	17 (2in.)	52	1.10	C22-C2M-FL-2-T2
80	1-206-89/92	L	20	Flat 2"	0.1418	NYP	94.1	649	102.2	705	21 (2in.)	64	1.18	C25-C1B-FR-2-L1
80	1-206-89/92	L	20	Flat 2"	0.1419	97.2	95.9	661	102.8	709	24 (2in.)	64	1.20	C25-C1B-FR-2-L2
80	1-206-89/92	T	20	Flat 2"	0.1411	NYP	93.6	645	102.7	708	17 (2in.)	46	1.17	C25-C1B-FR-2-T1
80	1-206-89/92	T	20	Flat 2"	0.1414	97.1	95.6	659	103.2	712	19 (2in.)	47	1.20	C25-C1B-FR-2-T2
85*	2-206-83/86	L	20	Flat 2"	0.1316	NYP	107.5	741	120.4	830	20 (2in.)	55	1.26	M10B-C3B1-RF-
85*	2-206-83/86	L	20	Flat 2"	0.1320	NYP	107.9	744	120.5	831	18 (2in.)	62	1.27	M10B-C3B1-RF-
85*	2-206-83/86	T	20	Flat 2"	0.1315	NYP	109.5	755	120.5	831	12 (2in.)	40	1.29	M10B-C3B1-RF-
85*	2-206-83/86	T	20	Flat 2"	0.1326	NYP	108.6	749	119.9	827	14 (2in.)	36	1.28	M10B-C3B1-RF-

Table A–1. Room-temperature tensile test results for perimeter column steels (continued).

Specified yield (F_y) ksi	Location in Bldg (Bldg.-Center column number, floor level)	Test axis with respect to RD	Temp °C	Specimen type and nominal GL	Area in.²	Yield point, *YP* ksi	0.2 % Yield Strength, *YS* ksi	0.2 % Yield Strength, *YS* MPa	Tensile Strength, *TS* ksi	Tensile Strength, TS MPa	El_t %	*ROA* %	Measured yield/F_y	Sample #
90*	1-451-85/88	L	20	Flat-C 1"	0.0686	NYP	na	na	124.0	855	24 (1in.)	65	n/a	C10-C1M-IW-1-1
90*	1-451-85/88	L	20	Flat-C 1"	0.0691	NYP	110.0	758	122.7	846	23 (1in.)	64	1.29	C10-C1M-IW-1-2
90*	1-451-85/88	L	20	Flat 2"	0.1400	NYP	108.3	747	119.5	824	18 (2in.)	61	1.20	C10-C1B-FL-1-L1
90*	1-451-85/88	L	20	Flat 2"	0.1397	NYP	109.1	752	119.9	827	18 (2in.)	60	1.21	C10-C1B-FL-1-L2
90*	1-451-85/88	T	20	Flat 2"	0.1400	NYP	109.5	755	120.2	829	16 (2in.)	43	1.22	C10-C1B-FL-1-T1
90*	1-451-85/88	T	20	Flat 2"	0.1396	NYP	110.1	759	120.9	834	16 (2in.)	41	1.22	C10-C1B-FL-1-T2
90*	1-451-85/88	L	20	Flat-C 1"	0.0709	NYP	110.0	758	124.7	860	27 (1in.)	67	1.10	C10-C1M-FL-1-1
90*	1-451-85/88	L	20	Flat-C 1"	0.0705	NYP	110.6	763	124.4	858	23 (1in.)	66	1.11	C10-C1M-FL-1-2
90*	2-406-40/43	L	20	Rd 2"	0.1936	NYP	110.6	763	121.2	836	22 (2in.)	45	1.23	B1043-C2T-FL-2-
90*	2-406-40/43	L	20	Rd 2"	0.1940	NYP	109.7	756	119.9	827	23 (2in.)	45	1.22	B1043-C2T-FL-2-
90*	2-406-40/43	L	20	Rd 2"	0.1936	NYP	110.6	763	121.4	837	22 (2in.)	45	1.23	B1043-C2T-FL-2-
100*	2-300-85/87	L	20	Flat 2"	0.1323	NYP	107.9	744	117.9	813	16 (2in.)	54	1.08	C14-C1-RF-L1
100*	2-300-85/87	L	20	Flat 2"	0.1324	NYP	108.0	745	118.6	818	17 (2in.)	60	1.08	C14-C1-RF-L2
100*	2-300-85/87	T	20	Flat 2"	0.1328	NYP	106.6	735	117.5	810	15 (2in.)	35	1.07	C14-C1-RF-T1
100*	2-300-85/87	T	20	Flat 2"	0.1319	NYP	106.9	737	117.9	813	17 (2in.)	33	1.07	C14-C1-RF-T2

* Denotes that this specification was replaced with 100 ksi material
El_t = total elongation to failure

Table A–5. Room-temperature tensile test results for perimeter column spandrel steels.

Specified yield (F_y) ksi	Location in Bldg (Bldg.-Center column number, floor level)	Test axis with respect to RD	Temp °C	Specimen type and nominal GL	Area in.²	Yield point, *YP* ksi	0.2 % Yield Strength, *YS* ksi	0.2 % Yield Strength, *YS* MPa	Tensile Strength, *TS* ksi	Tensile Strength, TS MPa	El_t %	*ROA* %	Measured yield/F_y	Sample #
36	1-133-97/100	T	20	Flat 2"	0.1916	NYP	38.3	264	64.4	444	30 (2in.)	63	1.06	S9-C1T-S1-L1
36	1-133-97/100	T	20	Flat 2"	0.1932	NYP	38.6	266	63.6	439	33 (2in.)	61	1.07	S9-C1T-S1-L2
36	1-133-97/100	T	20	Flat 2"	0.1928	NYP	37.6	259	63.2	436	32 (2in.)	62	1.04	S9-C1T-S1-L3
36	1-133-97/100	L	20	Flat 2"	0.1925	NYP	39.9	275	65.4	451	30 (2in.)	57	1.11	S9-C1T-S1-T2
36	1-133-97/100	L	20	Flat 2"	0.1928	39.9	39.6	273	63.3	436	33 (2in.)	57	1.10	S9-C1T-S1-T1
42	1-142-97/100	T	20	Flat 2"	0.2000	NYP	55.8	385	74.8	516	31 (2in.)	42	1.33	N8-C1B1-S-L-1
42	1-142-97/100	T	20	Flat 2"	0.1990	NYP	59.8	412	75.3	519	28 (2in.)	44	1.42	N8-C1B1-S-L-2
42	1-142-97/100	L	20	Flat 1"	0.0980	NYP	51.1	352	75.7	522	42 (1in.)	63	1.22	N8-C1B1-S-T-1
42	1-142-97/100	L	20	Flat 1"	0.0990	NYP	52.3	361	74.9	516	42 (1in.)	63	1.25	N8-C1B1-S-T-2
42	1-142-97/100	L	20	Flat 1"	0.0980	NYP	53.1	366	74.8	516	42 (1in.)	61	1.26	N8-C1B1-S-T-3
46	2-218-91/94	T	20	Flat 2"	0.2058	57.4	55.2	381	78.6	542	32 (2in.)	69	1.20	S14-C3B-S1-L1
46	2-218-91/94	T	20	Flat 2"	0.2063	57.0	55.9	385	78.4	541	33 (2in.)	n/d	1.22	S14-C3B-S1-L2
46	2-218-91/94	T	20	Flat 2"	0.2071	57.0	56.3	388	77.7	536	32 (2in.)	70	1.22	S14-C3B-S1-L3
46	2-218-91/94	L	20	Flat 2"	0.2063	57.0	57.1	394	78.5	541	23 (2in.)	37	1.24	S14-C3B-S1-T1
46	2-218-91/94	L	20	Flat 2"	0.2049	n/d	55.4	382	79.6	549	27 (2in.)	48	1.20	S14-C3B-S1-T2
75	2-300-85/87	L	20	Flat HSR 1"	0.0156	NYP	91.4	630	105.4	727	18 (1in.)	56	1.22	C14-SP-5T
75	2-300-85/87	T	20	Flat HSR 1"	0.0314	NYP	92.4	637	105.7	729	17 (1in.)	46	1.23	C14-SP-4L

Note:
In the spandrel specimen names, the orientation designation is reversed from the usual practice, and originally referred to the orientation with respect to the building long axis

Table A–6. Room-temperature tensile test results for core column steels.

Specified yield (F_y) ksi	Location in Bldg (Bldg.-Center column number, floor level)	Test axis with respect to RD	Temp °C	Specimen type and nominal GL	Area in.²	Yield point, *YP* ksi	0.2 % Yield Strength, *YS* ksi	0.2 % Yield Strength, *YS* MPa	Tensile Strength, *TS* ksi	Tensile Strength, *TS* MPa	El_t %	*ROA* %	Measured yield/F_y	Sample #	Structural Type
36	1-904-86/89	L	20	Rd 1"	0.0490	NYP	32.0	221	66.9	461	43 (1")	63	0.89	C65-H.25-L1	12WF161 flange
36	1-904-86/89	L	20	Rd 1"	0.0489	NYP	30.3	209	65.0	448	42 (1")	61	0.84	C65-H.25-L2	12WF161 flange
36	1-904-86/89	L	20	Rd 1"	0.0489	NYP	33.4	230	70.0	483	43 (1")	62	0.93	C65-H.25-L3	12WF161 flange
36	1-904-86/89	L	20	Rd 1"	0.0489	NYP	36.5	252	68.0	469	38 (1")	63	1.01	C65-H.5-L1	12WF161 flange
36	1-904-86/89	L	20	Rd 1"	0.0488	NYP	33.7	232	66.0	455	42 (1")	62	0.94	C65-H.5-L2	12WF161 flange
36	1-904-86/89	L	20	Rd 1"	0.0488	NYP	29.1	201	64.0	441	43 (1")	62	0.81	C65-H.5-L3	12WF161 flange
36	1-904-86/89	L	20	Rd 1"	0.0488	NYP	32.6	221	65.6	452	42 (1")	62	0.91	C65-H.5-L4	12WF161 flange
36	1-904-86/89	L	20	Rd 1"	0.0487	NYP	30.5	210	63.5	438	41 (1")	66	0.85	C65-2-WEB-L1	12WF161 web
36	1-904-86/89	L	20	Rd 1"	0.0487	NYP	31.6	218	64.0	441	42 (1")	63	0.88	C65-2-WEB-L2	12WF161 web
36	1-603-92/95	L	20	Rd 1"	0.0495	NYP	34.4	237	67.3	464	38 (1")	69	0.96	C80-L18	14WF184 flange
36	1-504-33/36	L	20	Rd 2"	0.1963	NYP	37.6	259	65.7	453	35 (2")	69	1.04	B6152-2-FL-2-L	Type 354 Box
36	1-504-33/36	L	20	Rd 2"	0.1963	41.1	38.2	263	65.4	451	36 (2")	67	1.06	B6152-2-FL-2-L	Type 354 Box
36	1-504-33/36	T	20	Rd 2"	0.1963	40.3	38.6	266	65.8	454	32 (2")	58	1.07	B6152-2-FL-2-T	Type 354 Box
36	1-504-33/36	T	20	Rd 2"	0.1963	38.1	38.6	266	65.1	449	32 (2")	55	1.07	B6152-2-FL-2-T	Type 354 Box
36	1- 803-15/18	L	20	Rd 2"	0.1963	40.9	38.6	266	66.8	461	n/d	n/d	1.14	B6152-1-F1-15	Type 380 Box
36	1- 803-15/18	L	20	Rd 2"	0.1963	36.6	36.3	250	66.7	460	n/d	n/d	1.02	B6152-1-F1-16	Type 380 Box
36	2-1008-104/106	L	20	Rd 2"	0.1963	37.4	34.4	237	62.2	429	40 (2in)	62	1.04	C30-1-F1-2-17	14WF237 flange
36	2-1008-104/106	L	20	Rd 2"	0.1963	36.7	33.9	234	60.9	420	39 (2in)	67	1.02	C30-1-F1-1-18	14WF237 flange
36	2-1008-104/106	L	20	Rd 2"	0.1963	44.7	42.4	292	61.7	426	38 (2in)	69	1.24	C30-1-F1-1-19	14WF237 flange
36	2-1008-104/106	L	20	Rd 2"	0.1963	39.6	37.8	261	62.6	432	38 (2in)	65	1.10	C30-2-W1-04	14WF237 web
36	2-1008-104/106	L	20	Rd 2"	0.1963	38.7	37.1	256	62.8	433	38 (2in)	63	1.08	C30-1-W1-05	14WF237 web
36	2-1008-104/106	L	20	Rd 2"	0.1963	47.5	44.3	305	66.4	458	38 (2in)	70	1.32	C30-1-W1-06	14WF237 web

Table A–3. Room-temperature tensile test results for core column steels (continued).

Specified yield (F_y) ksi	Location in Bldg (Bldg.-Center column number, floor level)	Test axis with respect to RD	Temp °C	Specimen type and nominal GL	Area in.²	Yield point, *YP* ksi	0.2 % Yield Strength, *YS* ksi	0.2 % Yield Strength, *YS* MPa	Tensile Strength, *TS* ksi	Tensile Strength, *TS* MPa	*El*, %	*ROA* %	Measured yield/F_y	Sample #	Structural Type
36	1-904-77/80	L	20	Rd 2"	0.1963	n/a	53.4	368	68.3	471	28 (2in)	59	1.48	C71-1-F2-20	12WF190 flange
36	1-904-77/80	L	20	Rd 2"	0.1963	n/a	53.3	368	68.4	472	28 (2in)	58	1.48	C71-1-F2-21	12WF190 flange
36	1-904-77/80	L	20	Rd 2"	0.1963	33.8	32.1	222	63.2	436	36 (2in)	59	0.94	C71-1-W1-13	12WF190 web
36	1-904-77/80	L	20	Rd 2"	0.1963	32.6	31.5	217	63.6	438	37 (2in)	60	0.91	C71-1-W1-14	12WF190 web
36	1-904-83/86	L	20	Rd 2"	0.1963	n/a	49.1	339	70.7	487	30 (2in)	62	1.36	C155-1-F1-10	12WF161 flange
36	1-904-83/86	L	20	Rd 2"	0.1963	n/a	52.6	363	71.8	495	29 (2in)	52	1.46	C155-1-F1-11	12WF161 flange
36	1-904-83/86	L	20	Rd 2"	0.1963	n/a	51.0	352	70.4	485	28 (2in)	59	1.42	C155-1-F1-12	12WF161 flange
36	1-904-83/86	L	20	Rd 2"	0.1963	43.6	41.7	288	79.2	546	30 (2in)	54	1.21	C155-1-W1-07	12WF161 web
36	1-904-83/86	L	20	Rd 2"	0.1963	41.2	40.8	282	79.4	547	31 (2in)	49	1.14	C155-1-W1-08	12WF161 web
36	1-904-83/86	L	20	Rd 2"	0.1963	41.9	41.2	284	79.4	547	29 (2in)	53	1.16	C155-1-W1-09	12WF161 web
42	2-801-80/83	L	20	Rd 2"	0.1963	NYP	49.7	343	72.2	498	27 (2")	59	1.18	C88C-FL-2-L2	Type 378 Box
42	2-801-80/83	T	20	Rd 2"	0.1963	NYP	52.7	363	72.7	501	27 (2")	56	1.25	C88C-FL-2-T2	Type 378 Box
42	2-801-80/83	T	20	Rd 2"	0.1963	NYP	53.5	369	72.5	500	n/d	n/d	1.27	C88C-FL-2-T1	Type 378 Box
42	1-605-98/101	L	20	Rd 2"	0.1963	56.3	53.6	370	79.8	550	26 (2")	68	1.28	HH-FL-1-2-L1	12WF92 from flange
42	1-605-98/101	L	20	Rd 2"	0.1963	56.3	54.5	376	79.9	551	29 (2")	67	1.30	HH-FL-1-2-L2	12WF92 from flange
42	1-605-98/101	T	20	Rd 2"	0.1963	52.2	50.0	345	75.6	521	28 (2")	58	1.19	HH-FL-1-2-T1	12WF92 from flange
42	1-605-98/101	T	20	Rd 2"	0.1963	52.7	50.7	350	75.4	520	27 (2")	60	1.21	HH-FL-1-2-T2	12WF92 from flange
42	1-605-98-101	L	20	Flat-C2 1"	0.0297	NYP	52.1	359	74.2	512	38 (1")	70	1.24	HH-FL-1-16	12WF92 from flange
50	WTC1 beam on 10	L	20	Flat 2"	0.2485	NYP	49.7	343	n/d	n/d	42 (2")	66	0.99	C26-F2-1-1	27WF94 web
50	WTC1 beam on 10	L	20	Flat 2"	0.2463	NYP	50.2	346	74.0	510	41 (2")	66	1.00	C26-F2-1-2	27WF94 web
50	WTC1 beam on 10	L	20	Flat 2"	0.2412	NYP	49.2	339	74.9	516	37 (2")	66	0.98	C26-F2-1-3	27WF94 web

Table A–7. Room-temperature tensile test results for truss component steels.

Specified yield (F_y) ksi	Location in Bldg (Bldg.-Center column number, floor level)	axis with respect to RD	Temp °C	Specimen type and nominal GL	Area in.²	Yield point, *YP* ksi	0.2 % Yield Strength, *YS* ksi	0.2 % Yield Strength, *YS* MPa	Tensile Strength, *TS* ksi	Tensile Strength, *TS* MPa	El_t %	*ROA* %	Measured yield/F_y	Sample #
Truss Rods (from T1) Initial Dia of 0.92"														
50	n/a	L	20	Rd 2"	0.1928	NYP	58.4	403	77.8	536	27 (2")	65	1.17	TR1
50	n/a	L	20	Rd 2"	0.1928	NYP	65.5	452	83.0	572	24 (2")	65	1.31	TR2
50	n/a	L	20	Rd 2"	0.1928	NYP	52.4	361	76.5	527	15 (2")	67	1.05	TR3
50	n/a	L	20	Rd 1"	0.0485	NYP	63.4	437	86.7	598	26 (1")	62	1.27	TR4
50	n/a	L	20	Rd 1"	0.0491	NYP	57.5	396	75.7	522	35 (1")	67	1.15	TR5
50	n/a	L	20	Rd 1"	0.0485	NYP	62.6	432	83.1	573	26 (1")	63	1.25	TR6
Truss Rods Initial Dia of 1.09" (0.250" specimen dia)														
36	n/a	L	20	Rd 1"	0.0489	47.4	41.4	285	63.3	436	38 (1")	60	1.15	C53-1L
Truss Angles (from T1)														
50	n/a	L	20	Flat-C 1"	0.0636	NYP	53.7	370	74.9	516	33 (1")	59	1.07	T1A-1
50	n/a	L	20	Flat-C 1"	0.0643	NYP	48.5	334	73.3	505	31 (1")	60	0.97	T1A-2
50	n/a	L	20	Flat-C 1"	0.0640	NYP	54.2	374	74.1	511	35 (1")	61	1.08	T1A-4
50	n/a	L	20	Flat-C 1"	0.0635	NYP	50.7	350	74.7	515	32 (1")	56	1.01	T1A-8
50	n/a	L	20	Flat-C 1"	0.0626	NYP	53.8	371	75.3	519	30 (1")	60	1.08	T1A-7
Truss Angles (from N8) 2 in. x 1.5 in. x 0.25 in. bulb angle														
50	1-142-97/100	L	20	Flat-C 1"	0.0643	NYP	55.9	385	79.2	546	32 (1")	64	1.12	N8A-1
50	1-142-97/100	L	20	Flat-C 1"	0.0631	NYP	56.1	387	79.5	548	33 (1")	62	1.12	N8A-2
50	1-142-97/100	L	20	Flat-C 1"	0.0631	NYP	54.6	376	79.9	551	32 (1")	60	1.09	N8A-3
Truss Angles (Room Temperature A242 specimens tested according to A370) 2" X 1.5" bulb angle"														
50	n/a	L	20	Flat-C2 1"	0.0283	NYP	57.3	395	76.6	528	38 (1")	n/d	1.15	C132TA7W
50	n/a	L	20	Flat-C2 1"	0.0281	NYP	63.4	437	n/d	n/d	n/f	n/d	1.27	C132TA6N
50	n/a	L	20	Flat-C2 1"	0.0284	NYP	57.0	393	79.6	549	33 (1")	65	1.14	C132TA2N3a
50	n/a	L	20	Flat-C2 1"	0.0283	59.2	57.4	396	76.5	527	n/f	n/f	1.15	C132TA7W-4a
Truss Angles 3 in. x 2 in. x 0.37 in. bulb angle														
36	n/a	L	20	Flat-C2 1"	0.0300	NYP	63.5	438	81.3	561	26 (1")	58	1.76	C53BA2-12N
36	n/a	L	20	Flat-C2 1"	0.0294	NYP	51.9	358	75.3	519	24 (1")	56	1.44	C53BA1-6N
36	n/a	L	20	Flat-C2 1"	0.0290	NYP	56.1	387	n/a	n/a	n/a	n/a	1.56	C53BA3-2

Table A–8. Room-temperature tensile test results for truss seat steels.

Specified yield (F_y)	Location in Bldg (Bldg.-Center column number, floor level)	Test axis with respect to RD	Temp	Specimen type and nominal GL	Area	Yield point, *YP*	0.2 % Yield Strength, *YS*	0.2 % Yield Strength, *YS*	Tensile Strength, *TS*	Tensile Strength, *TS*	El_t	*ROA*	Measured yield/F_y	Sample #	Type
ksi			°C		in.²	ksi	ksi	MPa	ksi	MPa	%	%			
36	1-142-97/100	L	20	Rd 1"	0.0495	NYP	45.4	313	67.0	462	29 (1")	36	1.26	N8-C1B1-S-C-1-L	perimeter truss seat
36	1-142-97/100	L	20	Rd 1"	0.0485	41.5	38.5	265	64.6	445	33 (1")	38	1.07	N8-C1B1-S-C-2-L	perimeter truss seat
36	1-142-97/100	L	20	Rd 1"	0.0479	40.0	38.1	263	65.2	450	34 (1")	38	1.06	N8-C1B1-S-C-3-L	perimeter truss seat
36	1-142-97/100	T	20	Rd 1"	0.0489	38.4	38.3	264	67.8	467	30 (1")	31	1.06	N8-C1B1-S-C-13-	perimeter truss seat
36	1-142-97/100	T	20	Rd 1"	0.0491	NYP	47.0	324	67.0	462	21 (1")	33	1.31	N8-C1B1-S-C-14-	perimeter truss seat
36	1-142-97/100	T	20	Rd 1"	0.0489	NYP	37.3	257	67.4	465	32 (1")	31	1.04	N8-C1B1-S-C-15-	perimeter truss seat
36	2-154-101/104	L	20	Rd 1"	0.0475	40.9	40.9	282	69.6	480	31 (1")	52	1.14	N9-C1T1-S-C-9-L	perimeter truss seat
36	1-148-99/102	T	20	Rd 1"	0.0483	41.9	39.0	269	63.8	440	34 (1")	55	1.08	N99-C1B-T-51	perimeter truss seat
36	1-148-99/102	T	20	Rd 1"	0.0487	42.5	42.0	290	66.0	455	31 (1")	53	1.17	N99-C1B-T-56	perimeter truss seat
36	1-148-99/102	T	20	Rd 1"	0.0487	45.6	44.0	303	67.0	462	33 (1")	53	1.22	N99-C1B-T-53	perimeter truss seat
36	Unknown	L	20	Rd 1"	0.0489	46.0	44.9	310	68.8	474	36 (1")	62	1.25	M4-C3T-L1	perimeter truss seat
36	na	L	20	Rd 1"	0.0489	58.6	57.5	396	82.2	567	30 (1")	69	1.60	M34-TS-A-L5	core truss seat
36	na	T	20	Rd 1"	0.0489	NYP	70.1	483	92.8	640	22 (1")	45	1.95	M34-TS-A-T1	core truss seat
36	na	T	20	Rd 1"	0.0483	34.0	33.3	230	66.6	459	40 (1")	68	0.93	C128-T1	core truss seat

Table A–9. Room-temperature tensile test results for notched round bars.

Specified yield (F_y) ksi	Location in Bldg (Bldg.-Center column number, floor level)	Test axis with respect to RD	Temp °C	Specimen type and nominal GL	Area in.²	Yield point, *YP* ksi	0.2 % Yield Strength, *YS* ksi	0.2 % Yield Strength, *YS* MPa	Tensile Strength, *TS* ksi	Tensile Strength, *TS* MPa	El_t %	*ROA* %	Measured yield/F_y	Sample #	Structural Type
36	1- 803-15/18	L	20	NRB-3	0.0491	n/a	n/a	n/a	104.5	720	n/d	n/d	0.031	B6152-1-F1-1-01	Type 380 Box
36	1- 803-15/18	L	20	NRB-3	0.0491	n/a	n/a	n/a	101.2	698	n/d	n/d	0.031	B6152-1-F1-1-02	Type 380 Box
36	1- 803-15/18	L	20	NRB-2	0.0491	n/a	n/a	n/a	93.0	641	n/d	n/d	0.063	B6152-1-F1-1-03	Type 380 Box
36	1- 803-15/18	L	20	NRB-2	0.0491	n/a	n/a	n/a	92.4	637	n/d	n/d	0.063	B6152-1-F1-1-04	Type 380 Box
36	1- 803-15/18	L	20	NRB-1	0.0491	n/a	n/a	n/a	84.8	585	n/d	n/d	0.125	B6152-1-F1-1-05	Type 380 Box
36	1- 803-15/18	L	20	NRB-1	0.0491	n/a	n/a	n/a	84.9	585	n/d	n/d	0.125	B6152-1-F1-1-06	Type 380 Box
36	1- 803-15/18	L	20	Rd 2"	0.1963	40.9	38.6	266	66.8	461	34.8 (2in.)	62.0	n/a	B6152-1-F1-15	Type 380 Box
36	1- 803-15/18	L	20	Rd 2"	0.1963	36.6	36.3	250	66.7	460	37.0 (2in.)	67.6	n/a	B6152-1-F1-16	Type 380 Box
36	1-904-77/80	L	20	NRB-1	0.0491	n/a	n/a	n/a	90.1	621	n/d	n/d	0.125	C71-1-F1-07	12WF190 flange
36	1-904-77/80	L	20	NRB-1	0.0491	n/a	n/a	n/a	89.9	620	n/d	n/d	0.125	C71-1-F1-08	12WF190 flange
36	1-904-77/80	L	20	NRB-2	0.0491	n/a	n/a	n/a	104.1	718	n/d	n/d	0.063	C71-1-F1-09	12WF190 flange
36	1-904-77/80	L	20	NRB-2	0.0491	n/a	n/a	n/a	102.6	707	n/d	n/d	0.063	C71-1-F1-10	12WF190 flange
36	1-904-77/80	L	20	NRB-3	0.0491	n/a	n/a	n/a	115.3	795	n/d	n/d	0.031	C71-1-F1-11	12WF190 flange
36	1-904-77/80	L	20	NRB-3	0.0491	n/a	n/a	n/a	113.8	785	n/d	n/d	0.031	C71-1-F1-12	12WF190 flange
36	1-904-77/80	L	20	Rd 2"	0.1963	n/a	53.4	368	68.3	471	28 (2in.)	59	n/a	C71-1-F2-20	12WF190 flange
36	1-904-77/80	L	20	Rd 2"	0.1963	n/a	53.3	368	68.4	472	28 (2in.)	58	n/a	C71-1-F2-21	12WF190 flange

Table A–10. Room-temperature test results for welded components.

Specified yield (F_y) ksi	Location in Bldg (Bldg.-Center column number, floor level)	Test axis with respect to RD	Temp °C	Specimen type and nominal GL	Area in.²	Yield point, *YP* ksi	0.2 % Yield Strength, *YS* ksi	0.2 % Yield Strength, *YS* MPa	Tensile Strength, *TS* ksi	Tensile Strength, *TS* MPa	El_t %	Sample #
Heat-Affected Zone Specimens												
n/a	1-142-97/100	T	20	HAZ-2	0.443	NYP	65.3	450	92.2	636	15 (1")	N8-C3B1-RF-HAZ-1R
n/a	1-142-97/100	T	20	HAZ-1	0.443	NYP	70.0	483	95.8	661	12 (1")	N8-C3B1-RF-HAZ-2
n/a	1-142-97/100	T	20	HAZ-2	0.443	NYP	67.8	467	92.9	641	17 (1")	N8 C3B1 RF-HAZ-3R
n/a	1-142-97/100	T	20	HAZ-1	0.443	NYP	n/a	n/a	92.6	638	n/a	N8-C3B1-RF-HAZ-4
Truss-Section Specimens												
n/a	n/a	20	20	2.0 (est)	NYP	n/a	n/a	n/a	52.3	361	n/a	Truss-Section-Shear

Table A–11. Room-temperature tensile test results for all-weld metal specimens.

Specified yield (F_y)	Location in Bldg (Bldg.-Center column number, floor level)	Test axis with respect to RD	Temp	Specimen type and nominal GL	Area	Yield point, *YP*	0.2 % Yield Strength, *YS*	0.2 % Yield Strength, *YS*	Tensile Strength, *TS*	Tensile Strength, *TS*	El_t	*ROA*	Measured yield/F_y	Sample #
ksi			°C		in.²	ksi	ksi	MPa	ksi	MPa	%	%		
n/a	55	L	20	Flat-W 1"	0.0628	NYP	85.1	587	103.0	710	27	49.7	n/a	W1 (N9)
n/a	55	L	20	Flat-W 1"	0.0621	NYP	84.8	585	103.3	712	na	43.2	n/a	W2 (N9)
Commercially supplied weld metals														
n/a	n/a	n/a	20	Rd-W 2"	0.0995	80.9	77.3	533	87.4	603	22 (2")	69	n/a	1254-1
n/a	n/a	n/a	400	Rd-W 2"	0.0995	NYP	59.6	411	77.6	535	19 (2")	62	n/a	1254-2
n/a	n/a	n/a	650	Rd-W 2"	0.0990	NYP	14.9	103	16.6	114	30 (2")	81	n/a	1254-3
n/a	n/a	n/a	20	Rd-W 2"	0.0995	65.7	63.7	439	74.0	510	24 (2")	76	n/a	1255-Y-1
n/a	n/a	n/a	400	Rd-W 2"	0.0984	NYP	46.7	322	65.8	454	23 (2")	75	n/a	1255-Y-2
n/a	n/a	n/a	650	Rd-W 2"	0.0995	NYP	15.4	106	17.0	117	36 (2")	95	n/a	1255-Y-3

A.2 DATA TABLES FOR HIGH STRAIN RATE PROPERTIES

The following table summarizes the high-strain-rate properties.

Table A–12. Room-temperature, high-rate tensile test results for perimeter column steels.

Specified yield (F_y)	Location in Bldg (Bldg.-Center column number, floor level)	Test axis with respect to rolling direction	Strain Rate for F_y	Yield Strength 1 % offset F_y	Yield Strength 1 % offset F_y	Strain Rate for TS	Tensile Strength, TS	Tensile Strength, TS	total elongation El_t	Gage length L_g	ROA	Specimen type and nominal gage length	Sample #	thickness, t	$A^{0.5}/L_g$
ksi			1/s	ksi	MPa	1/s	ksi	MPa	%	in.	%			in.	
50	1-130-90/93	L	6.061E-05	63.2	436	1.21E-03	85.5	590	36	2	61	Flat 2"	M26-C1B1-RF-L1	0.5625	0.265
50	1-130-90/93	L	6.061E-05	61.7	425	1.21E-03	86.1	594	35	2	61	Flat 2"	M26-C1B1-RF-L2	0.5625	0.265
50	1-130-90/93	L	1.07E-04	70.6	487	1.07E-04	91.8	633	23	1	58	Flat HSR 1" TK	M26-C1B1-L1	0.125	0.177
50	1-130-90/93	L	65	72.2	498	65	99.9	689	34	1	55	Flat HSR 1" TK	M26-C1B1-RF-L2	0.125	0.177
50	1-130-90/93	L	100	75.9	523	100	100.4	692	28	1	58	Flat HSR 1" TN	M26-C1B1-RF-L6-06	0.0625	0.125
50	1-130-90/93	L	260	75.9	523	260	102.8	709	32	1	54	Flat HSR 1" TN	M26-C1B1-RF-L7-06	0.0625	0.125
50	1-130-90/93	L	417	85.0	586	417	106.7	736	30	1	57	Flat HSR 1" TN	M26-C1B1-RF-L8-06	0.0625	0.125
50	1-130-90/93	T	6.061E-05	62.6	432	1.21E-03	84.8	585	30	2	41	Flat 2"	M26-C1B1-RF-T1	0.5625	0.265
50	1-130-90/93	T	6.061E-05	62.5	431	1.21E-03	84.7	584	30	2	37	Flat 2"	M26-C1B1-RF-T2	0.5625	0.265
50	1-130-90/93	T	99	73.4	506	99	96.2	663	30	1	41	Flat HSR 1" TK	M26-C1B1-RF-T1	0.125	0.177
50	1-130-90/93	T	255	77.9	537	255	101.2	698	32	1	42	Flat HSR 1" TK	M26-C1B1-RF-T2	0.125	0.177
50	1-130-90/93	T	316	83.7	577	316	103.3	712	27	1	44	Flat HSR 1" TN	M26-C1B1-RF-T5	0.0625	0.125
50	1-130-90/93	T	360	92.0	634	360	108.8	750	28	1	43	Flat HSR 1" TN	M26-C1B1-RF-T4	0.0625	0.125
60	1-142-97/100	L	1.07E-04	62.0	427	1.07E-04	84.3	581	32	1	63	Flat HSR 1" TK	N8-C1B1-RF3-L2	0.125	0.177
60	1-142-97/100	L	90	73.2	505	90	102.7	708	35	1	57	Flat HSR 1" TK	N8-C1B1-RF-L3	0.125	0.177
60	1-142-97/100	L	257	79.0	545	257	107.8	743	36	1	56	Flat HSR 1" TK	N8-C1B1-RF-L4	0.125	0.177
60	1-142-97/100	L	277	81.5	562	277	106.2	732	30	1	54	Flat HSR 1" TN	N8-C1B1-C-RF-L7-06	0.0625	0.125
60	1-142-97/100	L	387	81.8	564	387	99.9	689	35	1	56	Flat HSR 1" TN	N8-C1B1-C-RF-L8-06	0.0625	0.125
60	1-142-97/100	L	386	75.0	517	386	98.2	677	36	1	56	Flat HSR 1" TK	N8-C1B1-RF-L5	0.125	0.177
60	1-142-97/100	T	6.061E-05	68.3	471	1.21E-03	89.3	616	24	2	30	Flat 2"	N8-C1B1-D3-RF-T1	0.25	0.177
60	1-142-97/100	T	6.061E-05	67.1	463	1.21E-03	87.9	606	24	2	32	Flat 2"	N8-C1B1-D3-RF-T2	0.25	0.177
60	1-142-97/100	T	54	75.3	519	54	102.8	709	26	1	39	Flat HSR 1" TK	N8-C1B1-C-RF-T1	0.125	0.177
60	1-142-97/100	T	297	84.1	580	297	102.7	708	28	1	40	Flat HSR 1" TK	N8-C1B1-C-RF-T2	0.125	0.177
65	1-148-99/102	L	1.07E-04	76.2	525	1.07E-04	98.0	676	24	1	51	Flat HSR 1" TN	N99-C3M1-RF-L6	0.0625	0.125
65	1-148-99/102	L	6.061E-05	70.8	488	1.21E-03	93.1	642	29	2	60	Flat 2"	N99-C3T1-RF-L1	0.25	0.177
65	1-148-99/102	L	6.061E-05	73.9	510	1.21E-03	94.0	648	30	2	60	Flat 2"	N99-C3T1-RF-L2	0.25	0.177
65	1-148-99/102	L	60	87.3	602	60	104.9	723	28	1	42	Flat HSR 1" TN	N99-C3M1-RF-L6-06	0.0625	0.125
65	1-148-99/102	L	95	87.6	604	95	111.4	768	27	1	47	Flat HSR 1" TN	N99-C3M1-RF-L9	0.0625	0.125
65	1-148-99/102	L	236	83.1	573	236	112.1	773	33	1	51	Flat HSR 1" TN	N99-C3M1-RF-L10	0.0625	0.125
65	1-148-99/102	L	367	94.6	652	367	120.5	831	32	1	50	Flat HSR 1" TN	N99-C3M1-RF-L8-06	0.0625	0.125
65	1-148-99/102	T	6.061E-05	74.7	515	1.21E-03	93.8	647	23	2	40	Flat 2"	N99-C3T1-RF-T1	0.25	0.177
65	1-148-99/102	T	6.061E-05	74.8	516	1.21E-03	94.0	648	23	2	40	Flat 2"	N99-C3T1-RF-T2	0.25	0.177
65	1-148-99/102	T	79	77.9	537	79	101.5	700	32	1	43	Flat HSR 1" TK	N99-C3M1-RF-T1	0.125	0.177
65	1-148-99/102	T	270	88.0	607	270	109.1	752	30	1	45	Flat HSR 1" TK	N99-C3M1-RF-T2	0.125	0.177
65	1-148-99/102	T	515	91.1	628	515	110.7	763	31	1	44	Flat HSR 1" TK	N99-C3M1-RF-T3	0.125	0.177

Table A–9. Room-temperature, high-rate tensile test results for perimeter column steels (continued).

Specified yield (F_y) ksi	Location in Bldg (Bldg.-Center column number, floor level)	Test axis with respect to rolling direction	Strain Rate for F_y 1/s	Yield Strength 1 % offset F_y ksi	Yield Strength 1 % offset F_y MPa	Strain Rate for TS 1/s	Tensile Strength, TS ksi	Tensile Strength, TS MPa	total elongation El_t %	Gage length L_g in.	ROA %	Specimen type and nominal gage length	Sample #	thickness, t in.	$A^{0.5}/L_g$
75	1-157-93/96	L	8.333E-05	83.7	577	8.33E-05	93.7	646	24	2	70	Flat 2"	C22-C2M-FL-2-L1	0.25	0.177
75	1-157-93/96	L	8.333E-05	83.8	578	8.33E-05	94.1	649	24	2	68	Flat 2"	C22-C2M-FL-2-L2	0.25	0.177
75	1-157-93/96	L	77	94.9	654	77	114.0	786	27	1	54	Flat HSR 1" TN	C22-C2B-FL-L4	0.0625	0.125
75	1-157-93/96	L	225	89.9	620	225	114.9	792	29	1	60	Flat HSR 1" TN	C22-C2B-FL-L5	0.0625	0.125
75	1-157-93/96	T	8.333E-05	83.9	578	8.33E-05	93.8	647	18	2	52	Flat 2"	C22-C2M-FL-2-T1	0.25	0.177
75	1-157-93/96	T	8.333E-05	83.9	578	8.33E-05	93.3	643	17	2	52	Flat 2"	C22-C2M-FL-2-T2	0.25	0.177
75	1-157-93/96	T	121	92.2	636	121	106.5	734	24	1	55	Flat HSR 1" TN	C22-C2B-FL-T4	0.0625	0.125
75	1-157-93/96	T	276	88.9	613	276	114.6	790	30	1	54	Flat HSR 1" TK	C22-C2B-FL-T-2	0.125	0.177
75	1-157-93/96	T	358	94.7	653	358	125.9	868	26	1	52	Flat HSR 1" TN	C22-C2B-FL-T5	0.0625	0.125
85	2-206-83/86	L	1.07E-04	113.5	783	1.07E-04	122.6	845	18.45	1	54.1	Flat HSR 1" TK	M10B-C3B1-RF-L4	0.125	0.177
85	2-206-83/86	L	1.07E-04	114.5	789	1.07E-04	123.4	851	20.37	1	54.45	Flat HSR 1" TK	M10B-C3B1-RF-L5	0.125	0.177
85	2-206-83/86	L	6.061E-05	111.6	769	1.21E-03	120.4	830	20	2	55	Flat 2"	M10B-C3B1-RF-L1	0.25	0.177
85	2-206-83/86	L	6.061E-05	113.3	781	1.21E-03	120.5	831	18	2	62	Flat 2"	M10B-C3B1-RF-L2	0.25	0.177
85	2-206-83/86	L	83	119.2	822	83	130.8	902	17	1	45	Flat HSR 1" TN	M10B C3B1-RF-L6-06	0.0625	0.125
85	2-206-83/86	L	250	117.3	809	250	138.9	958	24	1	63	Flat HSR 1" TK	M10B C3B1-RF-L2	0.125	0.177
85	2-206-83/86	L	283	123.1	849	283	136.9	944	18	1	48	Flat HSR 1" TN	M10B C3B1-RF-L7-06	0.0625	0.125
85	2-206-83/86	L	416	129.5	893	416	140.0	965	25	1	65	Flat HSR 1" TK	M10B C3B1-RF-L3	0.125	0.177
85	2-206-83/86	T	6.061E-05	113.3	781	1.21E-03	120.5	831	12	2	40	Flat 2"	M10B-C3B1-RF-T1	0.25	0.177
85	2-206-83/86	T	6.061E-05	112.2	774	1.21E-03	119.9	827	14	2	36	Flat 2"	M10B-C3B1-RF-T2	0.25	0.177
85	2-206-83/86	T	63	112.0	772	63	129.8	895	23	1	37	Flat HSR 1" TK	M10B C3B1-RF-T1	0.125	0.177
85	2-206-83/86	T	252	125.7	867	252	134.4	927	23	1	39	Flat HSR 1" TK	M10B C3B1-RF-T2	0.125	0.177

Table A–9. Room-temperature, high-rate tensile test results for perimeter column steels (continued).

Specified yield (F_y)	Location in Bldg (Bldg.-Center column number, floor level)	Test axis with respect to rolling direction	Strain Rate for F_y	Yield Strength 1 % offset F_y	Yield Strength 1 % offset F_y	Strain Rate for TS	Tensile Strength, TS	Tensile Strength, TS	total elongation El_t	Gage length L_g	ROA	Specimen type and nominal gage length	Sample #	thickness, t	$A^{0.5}/L_g$
ksi			1/s	ksi	MPa	1/s	ksi	MPa	%	in.	%			in.	
90	1-451-85/88	L	1.10E-04	113.6	783	7.88E-04	124.7	860	27	1	67	Flat-C 1"	C10-C1M-FL-1-1	0.25	0.250
90	1-451-85/88	L	1.19E-04	112.9	778	8.10E-04	124.4	858	23	1	66	Flat-C 1"	C10-C1M-FL-1-2	0.25	0.250
90	1-451-85/88	L	8.333E-05	109.9	758	8.33E-05	119.5	824	18	2	61	Flat 2"	C10-C1B-FL-1-L1	0.25	0.177
90	1-451-85/88	L	8.333E-05	110.5	762	8.33E-05	119.9	827	18	2	60	Flat 2"	C10-C1B-FL-1-L2	0.25	0.177
90	1-451-85/88	L	70	123.4	851	70	137.3	947	19	1	40	Flat HSR 1" TN	C10-C1M1-FL-L4	0.0625	0.125
90	1-451-85/88	L	241	116.0	800	241	127.9	882	18	1	45	Flat HSR 1" TN	C10-C1M1-FL-L5	0.0625	0.125
90	1-451-85/88	L	325	115.0	793	325	129.8	895	26	1	53	Flat HSR 1" TK	C10-C1M-1-L-2	0.125	0.177
90	1-451-85/88	L	433	123.3	850	433	149.4	1030	26	1	62	Flat HSR 1" TK	C10-C1M-1-L-3	0.125	0.177
90	1-451-85/88	T	8.333E-05	110.7	763	8.33E-05	120.2	829	16	2	43	Flat 2"	C10-C1B-FL-1-T1	0.25	0.177
90	1-451-85/88	T	8.333E-05	111.4	768	8.33E-05	120.9	834	16	2	41	Flat 2"	C10-C1B-FL-1-T2	0.25	0.177
90	1-451-85/88	T	99	115.0	793	99	132.7	915	23	1	43	Flat HSR 1" TK	C10-C1M-1-T-1	0.125	0.177
90	1-451-85/88	T	235	123.7	853	235	143.7	991	20	1	40	Flat HSR 1" TN	C10-C1M1-FL-T5	0.0625	0.125
90	1-451-85/88	T	307	120.7	832	307	132.4	913	24	1	40	Flat HSR 1" TK	C10-C1M-1-T-2	0.125	0.177
90	1-451-85/88	T	479	119.2	822	479	143.1	987	25	1	41	Flat HSR 1" TK	C10-C1M-1-T-3	0.125	0.177
90	1-451-85/88	L	1.19E-04	na	na	8.08E-04	124.0	855	24	1	65	Flat-C 1"	C10-C1M-IW-1-1	0.25	0.250
90	1-451-85/88	L	1.19E-04	112.5	776	8.17E-04	122.7	846	23	1	64	Flat-C 1"	C10-C1M-IW-1-2	0.25	0.250
90	1-451-85/88	L	81	119.8	826	81	139.2	960	17	1	53	Flat HSR 1" TN	C10-C1M1-IW-L1	0.0625	0.125
90	1-451-85/88	L	233	126.3	871	233	141.7	977	22	1	54	Flat HSR 1" TN	C10-C1M1-IW-L2	0.0625	0.125
90	1-451-85/88	L	350	132.0	910	350	144.0	993	23	1	42	Flat HSR 1" TN	C10-C1M1-IW-L3	0.0625	0.125
90	1-451-85/88	T	83	119.8	826	83	140.2	967	19	1	39	Flat HSR 1" TN	C10-C1M1-IW-T1	0.0625	0.125
90	1-451-85/88	T	297	128.5	886	297.3	145.3	1002	19	1	40	Flat HSR 1" TN	C10-C1M1-IW-T3	0.0625	0.125
90	1-451-85/88	T	371	124.7	860	371	148.5	1024	20	1	40	Flat HSR 1" TN	C10-C1M1-IW-T2	0.0625	0.125

Table A–13. Room-temperature, high-rate tensile test results for perimeter-column spandrel steels.

Specified yield (F_y) ksi	Location in Bldg (Bldg.-Center column number, floor level)	Test axis with respect to rolling direction	Strain Rate for F_y 1/s	Yield Strength 1% offset F_y ksi	Yield Strength 1% offset F_y MPa	Strain Rate for TS 1/s	Tensile Strength, TS ksi	Tensile Strength, TS MPa	total elongation El_t %	Gage length L_g in.	ROA %	Specimen Type	Sample #	thickness, t in.	$A^{0.5}/L_g$
75	2-300-85/87	T	1.07E-04	91.3	629	1.07E-04	104	717	18	1	37	Flat HSR 1" TK	C14-SP-5L	0.125	0.177
75	2-300-85/87	T	1.07E-04	91.7	632	1.07E-04	104	717	18	1	41	Flat HSR 1" TK	C14-SP-6L	0.125	0.177
75	2-300-85/87	T	6.20E-04	93.3	643	6.20E-04	105.7	729	17	1	46	Flat HSR 1" TK	C14 Spandrel 4L	0.125	0.177
75	2-300-85/87	T	73	95.4	658	73	114.6	790	24	1	40	Flat HSR 1" TK	C14 Spandrel L1	0.125	0.177
75	2-300-85/87	T	93	96.2	663	93	114.9	792	25	1	44	Flat HSR 1" TK	C14 Spandrel HAZ L	0.125	0.177
75	2-300-85/87	T	270	106.9	737	270	124.4	858	25	1	41	Flat HSR 1" TK	C14 Spandrel L2	0.125	0.177
75	2-300-85/87	T	388	108.9	751	388	117.9	813	27	1	44	Flat HSR 1" TK	C14 Spandrel HAZ L	0.125	0.177
75	2-300-85/87	T	456	105.9	730	456	125.3	864	26	1	46	Flat HSR 1" TK	C14 Spandrel L3	0.125	0.177
75	2-300-85/87	L	5.62E-04	92.2	636	5.62E-04	105.4	727	18	1	56	Flat HSR 1" TK	C14 Spandrel-5T	0.0625	0.125
75	2-300-85/87	L	86	100.5	693	86	119.4	823	28	1	50	Flat HSR 1" TK	C14 Spandrel T1	0.125	0.177
75	2-300-85/87	L	241	107.0	738	241	124.3	857	26	1	42	Flat HSR 1" TN	C14-SP-3T	0.0625	0.125
75	2-300-85/87	L	264	105.9	730	264	119.2	822	27	1	57	Flat HSR 1" TK	C14 Spandrel T2	0.125	0.177
75	2-300-85/87	L	402	102.1	704	402	121.8	840	26	1	51	Flat HSR 1" TN	C14-SP-4T	0.0625	0.125

Table A–14. Room-temperature, high-rate tensile test results for core-column steels.

Specified yield (F_y) ksi	Location in Bldg (Bldg.-Center column number, floor level)	Test axis with respect to rolling direction	Strain Rate for F_y 1/s	Yield Strength 1% offset F_y ksi	Yield Strength 1% offset F_y MPa	Strain Rate for TS 1/s	Tensile Strength, TS ksi	Tensile Strength, TS MPa	total elongation El_t %	Gage length L_g in.	ROA %	Specimen Type	Sample #	thickness, t in.	$A^{0.5}/L_g$
36	1-603-92/95	L	8.75E-05	37.1	256	5.52E-04	67.3	464	38	1	69	Rd 1"	C80-L18	0.25	0.222
36	1-603-92/95	L	84	57.3	395	84	85.0	586	40	1	56	Flat HSR 1" TN	C80-A-3-1	0.0625	0.125
36	1-603-92/95	L	100	55.5	383	100	82.5	569	44	1	62	Flat HSR 1" TK	C80-A-2-1	0.125	0.177
36	1-603-92/95	L	299	62.5	431	299	80.1	552	n/a	1	57	Flat HSR 1" TK	C80-A-2-2	0.125	0.177
36	1-603-92/95	L	401	59.5	410	401	89.1	614	45	1	60	Flat HSR 1" TK	C80-A-2-3	0.125	0.177
36	1-504-33/36	L	1.07E-04	39.6	273	1.07E-04	64.5	445	33	1	53	Flat HSR 1" TN	B6152-2-FL-2-L4	0.0625	0.125
36	1-504-33/36	L	1.07E-04	40.8	281	1.07E-04	66.1	456	37	1	51	Flat HSR 1" TN	B6152-2-FL-2-L5	0.0625	0.125
36	1-504-33/36	L	1.17E-03	39.8	274	1.17E-03	65.7	453	35	2	69	Rd 2"	B6152-2-FL-2-L1	0.5	0.222
36	1-504-33/36	L	1.20E-03	37.6	259	1.20E-03	65.4	451	36	2	67	Rd 2"	B6152-2-FL-2-L2	0.5	0.222
36	1-504-33/36	L	63	58.0	400	63	78.6	542	39	1	52	Flat HSR 1" TN	B6152-2-FL2-L1	0.0625	0.125
36	1-504-33/36	L	235	52.5	362	235	81.8	564	39	1	52	Flat HSR 1" TN	B6152-2-FL2-L2	0.0625	0.125
36	1-504-33/36	L	361	54.1	373	361	83.8	578	42	1	55	Flat HSR 1" TN	B6152-2-FL2-L3	0.0625	0.125
36	1-504-33/36	T	1.20E-03	38.2	263	1.20E-03	65.8	454	32	2	58	Rd 2"	B6152-2-FL-2-T1	0.5	0.222
36	1-504-33/36	T	1.20E-03	39.0	269	1.20E-03	65.1	449	32	2	55	Rd 2"	B6152-2-FL-2-T2	0.5	0.222
36	1-504-33/36	T	82	59.2	408	82	79.8	550	37	1	49	Flat HSR 1" TN	B6152-2-FL1-2-T1	0.0625	0.125
36	1-504-33/36	T	253	62.7	432	253	82.1	566	37	1	50	Flat HSR 1" TN	B6152-2-FL1-2-T2	0.0625	0.125
36	1-504-33/36	T	377	64.3	443	377	86.3	595	36	1	49	Flat HSR 1" TN	B6152-2-FL1-2-T3	0.0625	0.125
36	1-904-86/89	L	8.75E-05	37.9	261	4.37E-04	63.5	438	41	1	66	Rd 1"	C65-2-WEB-L1	0.25	0.222
36	1-904-86/89	L	8.75E-05	39.5	272	4.37E-04	64.0	441	42	1	63	Rd 1"	C65-2-WEB-L2	0.25	0.222
36	1-904-86/89	L	1.07E-04	38.8	268	1.07E-04	60.9	441	32	1	55	Flat HSR 1" TN	C65-WEB-L4	0.0625	0.125
36	1-904-86/89	L	81	57.1	394	81	82.5	569	44	1	49	Flat HSR 1" TN	C65-WEB-L1	0.0625	0.125
36	1-904-86/89	L	238	62.4	430	238	84.4	582	32	1	49	Flat HSR 1" TN	C65-WEB-L2	0.0625	0.125
36	1-904-86/89	L	346	69.3	478	346	81.9	565	31	1	49	Flat HSR 1" TN	C65-WEB-L3	0.0625	0.125
36	1-904-86/89	T	90	63.1	435	90	90.8	626	27	1	50	Flat HSR 1" TN	C65-WEB-T1	0.0625	0.125
36	1-904-86/89	T	226	70.2	484	226	88.8	612	25	1	47	Flat HSR 1" TN	C65-WEB-T2	0.0625	0.125
36	1-904-86/89	T	318	71.5	493	318	88.0	607	32	1	45	Flat HSR 1" TN	C65-WEB-T3	0.0625	0.125

Table A–11. Room-temperature, high-rate tensile test results for core-column steels (continued).

Specified yield (F_y) ksi	Location in Bldg (Bldg.-Center column number, floor level)	Test axis with respect to rolling direction	Strain Rate for F_y 1/s	Yield Strength 1% offset F_y ksi	Yield Strength 1% offset F_y MPa	Strain Rate for TS 1/s	Tensile Strength, TS ksi	Tensile Strength, TS MPa	total elongation El_t %	Gage length L_g in.	ROA %	Specimen Type	Sample #	thickness, t in.	$A^{0.5}/L_g$
36	1-904-86/89	L	8.75E-05	39.7	274	4.37E-04	66.6	459	43	1	63	Rd 1"	C65-H.25-L1	0.25	0.222
36	1-904-86/89	L	8.75E-05	37.8	261	4.37E-04	65.0	448	42	1	61	Rd 1"	C65-H.25-L2	0.25	0.222
36	1-904-86/89	L	8.75E-05	38.3	264	4.37E-04	70.0	483	43	1	62	Rd 1"	C65-H.25-L3	0.25	0.222
36	1-904-86/89	L	8.75E-05	47.0	324	4.37E-04	68.0	469	38	1	63	Rd 1"	C65-H.5-L1	0.25	0.222
36	1-904-86/89	L	8.75E-05	42.5	293	4.37E-04	66.0	455	42	1	62	Rd 1"	C65-H.5-L2	0.25	0.222
36	1-904-86/89	L	8.75E-05	37.1	256	4.37E-04	64.0	441	43	1	62	Rd 1"	C65-H.5-L3	0.25	0.222
36	1-904-86/89	L	2.19E-03	38.7	267	2.19E-03	65.6	452	42	1	62	Rd 1"	C65-H.5-L4	0.25	0.222
36	1-904-86/89	L	1.07E-04	40.1	276	1.07E-04	65.3	450	39	1	54	Flat HSR 1" TN	C65-FL2-L4	0.0625	0.125
36	1-904-86/89	L	81	57.6	397	81	76.4	527	39	1	51	Flat HSR 1" TN	C65-FL2-L1	0.0625	0.125
36	1-904-86/89	L	238	57.6	397	238	78.6	542	45	1	53	Flat HSR 1" TN	C65-FL2-L2	0.0625	0.125
36	1-904-86/89	L	307	68.2	470	307	80.5	555	44	1	53	Flat HSR 1" TN	C65-FL2-L3	0.0625	0.125
36	1-904-86/89	T	75	55.4	382	75	76.3	526	38	1	45	Flat HSR 1" TN	C65-FL2-T1	0.0625	0.125
36	1-904-86/89	T	234	58.6	404	234	78.9	544	38	1	49	Flat HSR 1" TN	C65-FL2-T2	0.0625	0.125
36	1-904-86/89	T	318	70.6	487	318	84.0	579	42	1	45	Flat HSR 1" TN	C65-FL2-T3	0.0625	0.125
42	1-605-86/89	L	6.30E-04	52.0	359	6.30E-04	73.1	504	27	1	66	Flat HSR 1" TN	HH1-WEB-L4	0.0625	0.125
42	1-605-98/101	L	68	69.9	482	68	96.6	666	26	1	50	Flat HSR 1" TN	HH1-WEB-L1	0.0625	0.125
42	1-605-98/101	L	233	73.7	508	233	91.2	629	26	1	50	Flat HSR 1" TN	HH1-WEB-L2	0.0625	0.125
42	1-605-98/101	T	62	70.9	489	62	92.0	634	26	1	49	Flat HSR 1" TN	HH1-WEB-T1	0.0625	0.125
42	1-605-98/101	T	245	78.8	543	245	95.6	659	32	1	50	Flat HSR 1" TN	HH1-WEB-T2	0.0625	0.125
42	1-605-98/101	T	346	86.3	595	346	101.7	701	30	1	50	Flat HSR 1" TN	HH1-WEB-T3	0.0625	0.125

A.3 DATA TABLES FOR IMPACT PROPERTIES

The following table summarizes the Charpy test results.

Table A–15. Charpy V-notch impact data for samples tested.[a]

Building Location	Specimen Thickness in.	Specimen Orientation	Test Temp °F	Energy ft-lbf	Energy Corrected ft-lbf	Specimen ID	Specimen Type
1-42-97/100	0.2	T	77	14.2	25.6	SL-1	N8-C1B1Spandrel_T
1-142-97/100	0.2	T	77	12.8	23.0	SL-2	N8-C1B1Spandrel_T
1-142-97/100	0.2	T	77	13.3	24.0	SL-3	N8-C1B1Spandrel_T
1-142-97/100	0.2	T	32	14.0	25.2	SL-7	N8-C1B1Spandrel_T
1-142-97/100	0.2	T	32	14.9	26.9	SL-8	N8-C1B1Spandrel_T
1-142-97/100	0.2	T	32	13.4	24.1	SL-9	N8-C1B1Spandrel_T
1-142-97/100	0.2	T	-4	11.8	21.2	SL-10	N8-C1B1Spandrel_T
1-142-97/100	0.2	T	-4	13.3	23.9	SL-11	N8-C1B1Spandrel_T
1-142-97/100	0.2	T	-4	15.2	27.4	SL-12	N8-C1B1Spandrel_T
1-142-97/100	0.2	T	-40	12.6	22.8	SL-13	N8-C1B1Spandrel_T
1-142-97/100	0.2	T	-40	12.6	22.8	SL-14	N8-C1B1Spandrel_T
1-142-97/100	0.2	T	-40	11.5	20.7	SL-15	N8-C1B1Spandrel_T
1-142-97/100	0.2	T	-76	12.2	21.9	SL-4	N8-C1B1Spandrel_T
1-142-97/100	0.2	T	-112	2.4	4.4	SL-5	N8-C1B1Spandrel_T
1-142-97/100	0.2	L	77	43.3	78.0	ST-1	N8-C1B1-Spandrel_L
1-142-97/100	0.2	L	77	42.7	76.9	ST-2	N8-C1B1-Spandrel_L
1-142-97/100	0.2	L	77	39.3	70.7	ST-3	N8-C1B1-Spandrel_L
1-142-97/100	0.2	L	32	39.4	70.8	ST-7	N8-C1B1-Spandrel_L
1-142-97/100	0.2	L	32	38.6	69.4	ST-8	N8-C1B1-Spandrel_L
1-142-97/100	0.2	L	32	39.6	71.3	ST-9	N8-C1B1-Spandrel_L
1-142-97/100	0.2	L	-4	43.0	77.5	ST-10	N8-C1B1-Spandrel_L
1-142-97/100	0.2	L	-4	42.5	76.6	ST-11	N8-C1B1-Spandrel_L
1-142-97/100	0.2	L	-4	40.0	72.0	ST-12	N8-C1B1-Spandrel_L
1-142-97/100	0.2	L	-40	32.5	58.5	ST-13	N8-C1B1-Spandrel_L
1-142-97/100	0.2	L	-40	39.5	71.2	ST-14	N8-C1B1-Spandrel_L
1-142-97/100	0.2	L	-40	40.1	72.2	ST-15	N8-C1B1-Spandrel_L
1-142-97/100	0.2	L	-76	15.3	27.5	ST-4	N8-C1B1-Spandrel_L
1-142-97/100	0.2	L	-112	9.8	17.6	ST-5	N8-C1B1-Spandrel_L
1-142-97/100	0.2	L	77	35.3	63.6	NL-1	N8-C1M1-Flange_L
1-142-97/100	0.2	L	77	41.0	73.9	NL-2	N8-C1M1-Flange_L
1-142-97/100	0.2	L	77	38.7	69.6	NL-3	N8-C1M1-Flange_L
1-142-97/100	0.2	L	32	37.4	67.4	NL-7	N8-C1M1-Flange_L
1-142-97/100	0.2	L	32	38.1	68.6	NL-8	N8-C1M1-Flange_L
1-142-97/100	0.2	L	32	39.2	70.5	NL-9	N8-C1M1-Flange_L
1-142-97/100	0.2	L	-4	38.2	68.8	NL-10	N8-C1M1-Flange_L
1-142-97/100	0.2	L	-4	38.0	68.5	NL-11	N8-C1M1-Flange_L
1-142-97/100	0.2	L	-4	37.3	67.2	NL-12	N8-C1M1-Flange_L
1-142-97/100	0.2	L	-40	35.2	63.4	NL-13	N8-C1M1-Flange_L
1-142-97/100	0.2	L	-40	32.5	58.5	NL-14	N8-C1M1-Flange_L

Building Location	Specimen Thickness in.	Specimen Orientation	Test Temp °F	Energy ft-lbf	Energy Corrected ft-lbf	Specimen ID	Specimen Type
1-142-97/100	0.2	L	-40	34.1	61.3	NL-15	N8-C1M1-Flange_L
1-142-97/100	0.2	L	-76	25.5	46.0	NL-4	N8-C1M1-Flange_L
1-142-97/100	0.2	L	-112	15.2	27.3	NL-5	N8-C1M1-Flange_L
1-142-97/100	0.2	T	77	10.4	18.7	NT-1	N8-C1M1-Flange_T
1-142-97/100	0.2	T	77	10.9	19.7	NT-2	N8-C1M1-Flange_T
1-142-97/100	0.2	T	77	10.9	19.7	NT-3	N8-C1M1-Flange_T
1-142-97/100	0.2	T	32	10.6	19.0	NT-7	N8-C1M1-Flange_T
1-142-97/100	0.2	T	32	10.9	19.6	NT-8	N8-C1M1-Flange_T
1-142-97/100	0.2	T	32	10.1	18.2	NT-9	N8-C1M1-Flange_T
1-142-97/100	0.2	T	-4	10.2	18.3	NT-10	N8-C1M1-Flange_T
1-142-97/100	0.2	T	-4	9.5	17.1	NT-11	N8-C1M1-Flange_T
1-142-97/100	0.2	T	-4	10.8	19.4	NT-12	N8-C1M1-Flange_T
1-142-97/100	0.2	T	-40	9.9	17.8	NT-13	N8-C1M1-Flange_T
1-142-97/100	0.2	T	-40	10.5	18.9	NT-14	N8-C1M1-Flange_T
1-142-97/100	0.2	T	-40	10.5	18.9	NT-15	N8-C1M1-Flange_T
1-142-97/100	0.2	T	-76	10.5	18.9	NT-4	N8-C1M1-Flange_T
1-142-97/100	0.2	T	-112	5.6	10.1	NT-5	N8-C1M1-Flange_T
1-142-97/100	0.2	L	77	44.1	79.4	HL	N8-C1M1-HAZ_L
1-142-97/100	0.2	L	77	37.4	67.3	HL	N8-C1M1-HAZ_L
1-142-97/100	0.2	L	77	49.8	89.7	HL	N8-C1M1-HAZ_L
1-142-97/100	0.2	L	32	32.2	57.9	HL	N8-C1M1-HAZ_L
1-142-97/100	0.2	L	32	40.2	72.4	HL	N8-C1M1-HAZ_L
1-142-97/100	0.2	L	32	44.2	79.5	HL	N8-C1M1-HAZ_L
1-142-97/100	0.2	L	-4	22.6	40.7	HL	N8-C1M1-HAZ_L
1-142-97/100	0.2	L	-4	42.8	77.0	HL	N8-C1M1-HAZ_L
1-142-97/100	0.2	L	-4	23.6	42.6	HL	N8-C1M1-HAZ_L
1-142-97/100	0.2	T	77	9.8	17.7	HT	N8-C1M1-Weld_T
1-142-97/100	0.2	T	77	9.9	17.8	HT	N8-C1M1-Weld_T
1-142-97/100	0.2	T	77	9.1	16.3	HT	N8-C1M1-Weld_T
1-142-97/100	0.2	T	32	9.2	16.6	HT	N8-C1M1-Weld_T
1-142-97/100	0.2	T	32	9.4	16.9	HT	N8-C1M1-Weld_T
1-142-97/100	0.2	T	32	9.2	16.6	HT	N8-C1M1-Weld_T
1-142-97/100	0.2	T	-4	9.8	17.6	HT	N8-C1M1-Weld_T
1-142-97/100	0.2	T	-4	9.6	17.3	HT	N8-C1M1-Weld_T
1-142-97/100	0.2	T	-4	8.9	15.9	HT	N8-C1M1-Weld_T
1-451-85/88	0.2	L	77	43.2	77.8	C10_L	C10-C1M1- Flange_L
1-451-85/88	0.2	L	77	47.5	85.5	C10_L	C10-C1M1- Flange_L
1-451-85/88	0.2	L	77	47.2	85.0	C10_L	C10-C1M1- Flange_L
1-451-85/88	0.2	L	32	47.2	85.0	C10_L	C10-C1M1- Flange_L
1-451-85/88	0.2	L	32	46.5	83.7	C10_L	C10-C1M1- Flange_L
1-451-85/88	0.2	L	32	51.5	92.7	C10_L	C10-C1M1- Flange_L
1-451-85/88	0.2	L	-4	47.1	84.8	C10_L	C10-C1M1- Flange_L
1-451-85/88	0.2	L	-4	48.3	86.9	C10_L	C10-C1M1- Flange_L
1-451-85/88	0.2	L	-4	47.5	85.5	C10_L	C10-C1M1- Flange_L

Building Location	Specimen Thickness in.	Specimen Orientation	Test Temp °F	Energy ft-lbf	Energy Corrected ft-lbf	Specimen ID	Specimen Type
1-451-85/88	0.2	L	-40	46.3	83.3	C10_L	C10-C1M1- Flange_L
1-451-85/88	0.2	L	-40	51.4	92.5	C10_L	C10-C1M1- Flange_L
1-451-85/88	0.2	L	-40	46.5	83.7	C10_L	C10-C1M1- Flange_L
1-451-85/88	0.2	L	-76	43.7	78.7	C10_L	C10-C1M1- Flange_L
1-451-85/88	0.2	L	-112	44.8	80.6	C10_L	C10-C1M1- Flange_L
1-451-85/88	0.2	T	77	11.2	20.2	C10_T	C10-C1M1- Flange_T
1-451-85/88	0.2	T	77	12.4	22.3	C10_T	C10-C1M1- Flange_T
1-451-85/88	0.2	T	77	11.4	20.5	C10_T	C10-C1M1- Flange_T
1-451-85/88	0.2	T	32	12.4	22.3	C10_T	C10-C1M1- Flange_T
1-451-85/88	0.2	T	32	11.2	20.2	C10_T	C10-C1M1- Flange_T
1-451-85/88	0.2	T	32	11.6	20.9	C10_T	C10-C1M1- Flange_T
1-451-85/88	0.2	T	-4	11.8	21.2	C10_T	C10-C1M1- Flange_T
1-451-85/88	0.2	T	-4	11.4	20.5	C10_T	C10-C1M1- Flange_T
1-451-85/88	0.2	T	-4	11.0	19.8	C10_T	C10-C1M1- Flange_T
1-451-85/88	0.2	T	-40	10.7	19.3	C10_T	C10-C1M1- Flange_T
1-451-85/88	0.2	T	-40	10.9	19.6	C10_T	C10-C1M1- Flange_T
1-451-85/88	0.2	T	-40	11.3	20.3	C10_T	C10-C1M1- Flange_T
1-451-85/88	0.2	T	-76	11.3	20.3	C10_T	C10-C1M1- Flange_T
1-451-85/88	0.2	T	-112	10.7	19.3	C10_T	C10-C1M1- Flange_T
1-451-85/88	0.2	T	77	11.1	20.0	C10_HAZ	C10-C1M1-HAZ_T
1-451-85/88	0.2	T	77	12.0	21.6	C10_HAZ	C10-C1M1-HAZ_T
1-451-85/88	0.2	T	32	11.4	20.5	C10_HAZ	C10-C1M1-HAZ_T
1-451-85/88	0.2	T	32	11.2	20.2	C10_HAZ	C10-C1M1-HAZ_T
1-451-85/88	0.2	T	32	11.0	19.8	C10_HAZ	C10-C1M1-HAZ_T
1-451-85/88	0.2	T	-4	12.3	22.1	C10_HAZ	C10-C1M1-HAZ_T
1-451-85/88	0.2	T	-4	11.7	21.1	C10_HAZ	C10-C1M1-HAZ_T
1-451-85/88	0.2	T	-4	11.3	20.3	C10_HAZ	C10-C1M1-HAZ_T
1-451-85/88	0.2	T	-40	10.3	18.5	C10_HAZ	C10-C1M1-HAZ_T
1-451-85/88	0.2	T	-40	11.0	19.8	C10_HAZ	C10-C1M1-HAZ_T
1-451-85/88	0.2	T	-40	9.9	17.8	C10_HAZ	C10-C1M1-HAZ_T
1-451-85/88	0.2	T	-76	10.5	18.9	C10_HAZ	C10-C1M1-HAZ_T
1-451-85/88	0.2	T	-112	9.2	16.6	C10_HAZ	C10-C1M1-HAZ_T
1-603-92/95	0.4	T	172	48.9	48.9	C80_T	C80-web-column 603_T
1-603-92/95	0.4	T	172	45.0	45.0	C80_T	C80-web-column 603_T
1-603-92/95	0.4	T	140	45.4	45.4	C80_T	C80-web-column 603_T
1-603-92/95	0.4	T	140	46.3	46.3	C80_T	C80-web-column 603_T
1-603-92/95	0.4	T	77	28.9	28.9	C80_T	C80-web-column 603_T
1-603-92/95	0.4	T	77	24.4	24.4	C80_T	C80-web-column 603_T
1-603-92/95	0.4	T	77	25.1	25.1	C80_T	C80-web-column 603_T
1-603-92/95	0.4	T	32	7.1	7.1	C80_T	C80-web-column 603_T
1-603-92/95	0.4	T	32	7.3	7.3	C80_T	C80-web-column 603_T
1-603-92/95	0.4	T	32	13.2	13.2	C80_T	C80-web-column 603_T
1-603-92/95	0.4	T	-4	3.8	3.8	C80_T	C80-web-column 603_T
1-603-92/95	0.4	T	-4	4.0	4.0	C80_T	C80-web-column 603_T

Building Location	Specimen Thickness in.	Specimen Orientation	Test Temp °F	Energy ft-lbf	Energy Corrected ft-lbf	Specimen ID	Specimen Type
1-603-92/95	0.4	T	-4	3.6	3.6	C80_T	C80-web-column 603_T
1-603-92/95	0.4	L	172	110.5	110.5	C80_L	C80-web-column 603_L
1-603-92/95	0.4	L	172	121.1	121.1	C80_L	C80-web-column 603_L
1-603-92/95	0.4	L	140	115.1	115.1	C80_L	C80-web-column 603_L
1-603-92/95	0.4	L	140	103.9	103.9	C80_L	C80-web-column 603_L
1-603-92/95	0.4	L	77	45.6	45.6	C80_L	C80-web-column 603_L
1-603-92/95	0.4	L	77	47.4	47.4	C80_L	C80-web-column 603_L
1-603-92/95	0.4	L	77	68.3	68.3	C80_L	C80-web-column 603_L
1-603-92/95	0.4	L	32	36.3	36.3	C80_L	C80-web-column 603_L
1-603-92/95	0.4	L	32	44.1	44.1	C80_L	C80-web-column 603_L
1-603-92/95	0.4	L	32	35.6	35.6	C80_L	C80-web-column 603_L
1-603-92/95	0.4	L	-4	8.9	8.9	C80_L	C80-web-column 603_L
1-603-92/95	0.4	L	-4	7.0	7.0	C80_L	C80-web-column 603_L
1-603-92/95	0.4	L	-4	3.8	3.8	C80_L	C80-web-column 603_L
unknown	0.2	L	77	29.1	52.3	T1-1	Angle (2X1.5X0.25 inch)
unknown	0.2	L	77	33.5	60.4	T1-2	Angle (2X1.5X0.25 inch)
unknown	0.2	L	77	30.7	55.3	T1-3	Angle (2X1.5X0.25 inch)
unknown	0.2	L	32	18.2	32.7	T1-7	Angle (2X1.5X0.25 inch)
unknown	0.2	L	32	27.5	49.4	T1-8	Angle (2X1.5X0.25 inch)
unknown	0.2	L	32	19.0	34.2	T1-9	Angle (2X1.5X0.25 inch)
unknown	0.2	L	-4	8.3	14.9	T1-10	Angle (2X1.5X0.25 inch)
unknown	0.2	L	-4	9.8	17.7	T1-11	Angle (2X1.5X0.25 inch)
unknown	0.2	L	-4	8.6	15.5	T1-12	Angle (2X1.5X0.25 inch)
unknown	0.2	L	-40	5.5	9.9	T1-13	Angle (2X1.5X0.25 inch)
unknown	0.2	L	-40	1.9	3.4	T1-14	Angle (2X1.5X0.25 inch)
unknown	0.2	L	-40	1.6	2.9	T1-15	Angle (2X1.5X0.25 inch)
unknown	0.2	L	-76	1.6	3.0	T1-4	Angle (2X1.5X0.25 inch)
unknown	0.4	L	172	100.3	100.3	TR	Rod (0.92 inch)
unknown	0.4	L	172	113.8	113.8	TR	Rod (0.92 inch)
unknown	0.4	L	140	101.2	101.2	TR	Rod (0.92 inch)
unknown	0.4	L	140	96.9	96.9	TR	Rod (0.92 inch)
unknown	0.4	L	77	22.4	22.4	TR	Rod (0.92 inch)
unknown	0.4	L	77	41.7	41.7	TR	Rod (0.92 inch)
unknown	0.4	L	77	33.1	33.1	TR	Rod (0.92 inch)
unknown	0.4	L	32	21.3	21.3	TR	Rod (0.92 inch)
unknown	0.4	L	32	19.8	19.8	TR	Rod (0.92 inch)
unknown	0.4	L	32	7.5	7.5	TR	Rod (0.92 inch)
unknown	0.4	L	-4	5.4	5.4	TR	Rod (0.92 inch)
unknown	0.4	L	-4	3.2	3.2	TR	Rod (0.92 inch)
unknown	0.4	L	-4	6.1	6.1	TR	Rod (0.92 inch)
	0.4	T	172	27.4	27.4	N13	Scat
	0.4	T	172	26.9	26.9	N13	Scat
	0.4	T	140	21.6	21.6	N13	Scat
	0.4	T	140	23.0	23.0	N13	Scat

Building Location	Specimen Thickness in.	Specimen Orientation	Test Temp °F	Energy ft-lbf	Energy Corrected ft-lbf	Specimen ID	Specimen Type
	0.4	T	77	6.1	6.1	N13	Seat
	0.4	T	77	10.3	10.3	N13	Seat
	0.4	T	77	6.7	6.7	N13	Seat
	0.4	T	32	3.6	3.6	N13	Seat
	0.4	T	32	3.0	3.0	N13	Seat
	0.4	T	32	3.3	3.3	N13	Seat
1-142-97/100	0.4	T	172	36.8	36.8	N8	Seat
1-142-97/100	0.4	T	140	33.2	33.2	N8	Seat
1-142-97/100	0.4	T	140	33.2	33.2	N8	Seat
1-142-97/100	0.4	T	104	26.3	26.3	N8	Seat
1-142-97/100	0.4	T	104	28.7	28.7	N8	Seat
1-142-97/100	0.4	T	77	20.7	20.7	N8	Seat
1-142-97/100	0.4	T	77	22.4	22.4	N8	Seat
1-142-97/100	0.4	T	77	20.6	20.6	N8	Seat
1-142-97/100	0.4	T	-40	1.9	1.9	N8	Seat
1-142-97/100	0.4	T	-40	2.9	2.9	N8	Seat
unknown	0.4	T	172	34.2	34.2	M4	Seat
unknown	0.4	T	140	28.7	28.7	M4	Seat
unknown	0.4	T	140	28.3	28.3	M4	Seat
unknown	0.4	T	104	19.9	19.9	M4	Seat
unknown	0.4	T	104	21.1	21.1	M4	Seat
unknown	0.4	T	77	10.8	10.8	M4	Seat
unknown	0.4	T	77	12.9	12.9	M4	Seat
unknown	0.4	T	77	11.9	11.9	M4	Seat
unknown	0.4	T	-40	2.1	2.1	M4	Seat
unknown	0.4	T	-40	2.5	2.5	M4	Seat

a. The orientation of spandrel specimens appears to be reversed because the specimen identifications (L and T) were in reference to the building, rather than the rolling direction of the steel.

A.4 DATA TABLES FOR ELEVATED-TEMPERATURE PROPERTIES

The following tables summarize the data from the elevated temperature tensile tests.

Table A–16. High-temperature, tensile test results for perimeter column steels.

Specified yield (F_y) ksi	Location in Bldg (Bldg.-Center column number, floor level)	Test axis with respect to RD	Temp °C	Specimen type and nominal GL	Area in.²	Yield point, *YP* ksi	0.2 % Yield Strength, *YS* ksi	0.2 % Yield Strength, *YS* MPa	Tensile Strength, *TS* ksi	Tensile Strength, *TS* MPa	El_t %	*ROA* %	Measured yield/F_y	Sample #	Type
60	1-136-98/101	L	20	Flat-C 1"	0.0611	NYP	64.7	446	83.0	572	33 (1")	63	1.08	C40-C2M-IW-2-1	
60	1-136-98/101	L	20	Flat-C 1"	0.0614	NYP	64.4	444	83.2	574	36 (1")	65	1.07	C40-C2M-IW-2-2	
60	1-136-98/101	L	300	Flat-C 1"	0.0594	n/a	54.7	377	78.9	544	27 (1")	53	n/a	C40-C2M-IW-2-3	
60	1-136-98/101	L	400	Flat-C 1"	0.0609	n/a	52.0	359	67.6	466	32 (1")	60	n/a	C40-C2M-IW-2-4	
60	1-136-98/101	L	500	Flat-C 1"	0.0615	n/a	33.4	230	44.2	305	28 (1")	41	n/a	C40-C2M-IW-2-5	
60	1-136-98/101	L	600	Flat-C 1"	0.0611	n/a	20.1	139	27.1	187	44 (1")	78	n/a	C40-C2M-IW-2-6	
60	1-136-98/101	L	650	Flat-C 1"	0.0596	n/a	12.8	88	18.1	125	55 (1")	86	n/a	C40-C2M-IW-2-7	
60	1-142-97/100	L	20	Flat-C 1"	0.0745	68.6	68.4	472	91.0	627	39 (1")	65	1.14	N8-C1B1A-FL-1	
60	1-142-97/100	L	20	Flat-C 1"	0.0743	68.4	68.4	472	91.9	634	39 (1")	68	1.14	N8-C1B1A-FL-2	
60	1-142-97/100	L	300	Flat-C 1"	0.0745	n/a	54.4	375	93.6	645	36 (1")	60	n/a	N8-C1B1A-FL-3	
60	1-142-97/100	L	400	Flat-C 1"	0.0738	n/a	47.6	328	72.0	496	37 (1")	73	n/a	N8-C1B1A-FL-4	
60	1-142-97/100	L	500	Flat-C 1"	0.0743	n/a	34.2	236	49.3	340	45 (1")	80	n/a	N8-C1B1A-FL-5	
60	1-142-97/100	L	600	Flat-C 1"	0.0740	n/a	18.5	128	25.3	174	48 (1")	80	n/a	N8-C1B1A-FL-6	
60	1-142-97/100	L	650	Flat-C 1"	0.0743	n/a	12.7	88	17.8	123	54 (1")	84	n/a	N8-C1B1A-FL-7	
100	1-451-85/88	L	20	Flat-C 1"	0.0709	NYP	110.0	758	124.7	860	27 (1")	67	1.10	C10-C1M-FL-1-1	
100	1-451-85/88	L	20	Flat-C 1"	0.0705	NYP	110.6	763	124.4	858	23 (1")	66	1.11	C10-C1M-FL-1-2	
100	1-451-85/88	L	300	Flat-C 1"	0.0713	n/a	90.7	625	116.1	801	24 (1")	60	n/a	C10-C1M-FL-1-3	
100	1-451-85/88	L	400	Flat-C 1"	0.0706	n/a	88.8	612	103.2	712	23 (1")	64	n/a	C10-C1M-FL-1-4	
100	1-451-85/88	L	500	Flat-C 1"	0.0706	n/a	76.0	524	86.7	598	25 (1")	72	n/a	C10-C1M-FL-1-5	
100	1-451-85/88	L	550	Flat-C 1"	0.0708	n/a	54.3	374	72.2	498	30 (1")	79	n/a	C10-C1M-FL-1-8	
100	1-451-85/88	L	550	Flat-C 1"	0.0704	n/a	55.0	379	72.2	498	29 (1")	79	n/a	C10-C1M-FL-1-9	
100	1-451-85/88	L	550	Flat-C 1"	0.0707	n/a	56.2	387	73.4	506	27 (1")	80	n/a	C10-C1M-FL-1-10	
100	1-451-85/88	L	600	Flat-C 1"	0.0705	n/a	27.2	188	51.7	356	37 (1")	76	n/a	C10-C1M-FL-1-6	
100	1-451-85/88	L	650	Flat-C 1"	0.0709	n/a	13.6	94	28.8	199	44 (1")	75	n/a	C10-C1M-FL-1-7	

Table A–17. High-temperature, tensile test results for core column steels.

Specified yield (F_y) ksi	Location in Bldg (Bldg.-Center column number, floor level)	Test axis with respect to RD	Temp °C	Specimen type and nominal GL	Area in.²	Yield point, *YP* ksi	0.2 % Yield Strength, *YS* ksi	0.2 % Yield Strength, *YS* MPa	Tensile Strength, *TS* ksi	Tensile Strength, *TS* MPa	El_t %	*ROA* %	Measured yield/F_y	Sample #	Structural Type
36	1-504-33/36	L	20	Rd 2"	0.1963	39.6	37.6	259	65.7	453	35 (2")	69	1.04	B6152-2-FL-2-L1	Type 354 Box
36	1-504-33/36	L	650	Flat-C3 1"	0.0296	n/a	16.7	115	19.0	131	n/d	n/d	n/a	B6152-2-FL-2-20	Type 354 Box
36	1-904-86/89	L	20	Rd 1"	0.0490	NYP	32.0	221	66.9	461	43 (1")	63	0.89	C65-H.25-L1	12WF161 flange
36	1-904-86/89	L	20	Rd 1"	0.0489	NYP	30.3	209	65.0	448	42 (1")	61	0.84	C65-H.25-L2	12WF161 flange
36	1-904-86/89	L	20	Rd 1"	0.0489	NYP	33.4	230	70.0	483	43 (1")	62	0.93	C65-H.25-L3	12WF161 flange
36	1-904-86/89	L	20	Rd 1"	0.0489	NYP	36.5	252	68.0	469	38 (1")	63	1.01	C65H-.5-L1	12WF161 flange
36	1-904-86/89	L	20	Rd 1"	0.0488	NYP	33.7	232	66.0	455	42 (1")	62	0.94	C65-H-.5-L2	12WF161 flange
36	1-904-86/89	L	20	Rd 1"	0.0488	NYP	29.1	201	64.0	441	43 (1")	62	0.81	C65-H.5-L3	12WF161 flange
36	1-904-86/89	L	20	Rd 1"	0.0488	NYP	32.0	221	65.6	452	42 (1")	62	0.89	C65-H.5-L4	12WF161 flange
36	1-904-86/89	L	400	Rd 1"	0.0494	n/a	27.5	190	56.9	392	42 (1")	72	n/a	C65-FL-L-1	12WF161 flange
36	1-904-86/89	L	500	Rd 1"	0.0495	n/a	21.6	149	33.5	231	43 (1")	74	n/a	C65-FL-L-2	12WF161 flange
36	1-904-86/89	L	600	Rd 1"	0.0495	n/a	11.7	81	18.5	128	91 (1")	97	n/a	C65-FL-L-3	12WF161 flange
36	1-904-86/89	L	650	Rd 1"	0.0495	n/a	7.4	51	11.0	76	na	97	n/a	C65-FL-L-4	12WF161 flange
36	1-904-86/89	L	20	Rd 1"	0.0487	29.1	30.5	210	63.5	438	41 (1")	66	0.85	C65-2-WEB-L1	12WF161 flange
36	1-904-86/89	L	20	Rd 1"	0.0487	30.5	31.6	218	64.0	441	42 (1")	63	0.88	C65-2-WEB-L2	12WF161 flange
36	1-603-92/95	L	20	Rd 1"	0.0495	34.5	34.4	237	67.3	464	38 (1")	69	0.96	C80-L18	14WF184 flange
36	1-603-92/95	L	400	Rd 1"	0.0494	n/a	26.0	179	59.0	407	37 (1")	73	n/a	C80-FL-L-13	14WF184 flange
36	1-603-92/95	L	500	Rd 1"	0.0494	n/a	29.5	203	37.0	255	42 (1")	72	n/a	C80-FL-L-14	14WF184 flange
36	1-603-92/95	L	600	Rd 1"	0.0494	n/a	11.6	80	19.6	135	61 (1")	98	n/a	C80-FL-L-15	14WF184 flange
36	1-603-92/95	L	650	Rd 1"	0.0494	n/a	8.5	59	12.8	88	83 (1")	98	n/a	C80-FL-L-17	14WF184 flange
42	1-605-98/101	L	23	Flat-C3 1"	0.0297	n/a	52.1	359	74.2	512	38 (1")	70	1.24	HH-FL-1-16	12WF92 from flange
42	1-605-98/101	L	400	Flat-C3 1"	0.0299	n/a	39.8	275	65.1	449	n/d	75	n/a	HH-FL-1-19	12WF92 from flange
42	1-605-98/101	L	500	Flat-C3 1"	0.0295	n/a	34.5	238	51.0	352	n/d	64	n/a	HH-FL-1-18	12WF92 from flange
42	1-605-98/101	L	600	Flat-C3 1"	0.0294	n/a	24.8	171	30.2	208	n/d	n/d	n/a	HH-FL-1-20	12WF92 from flange
42	1-605-98/101	L	650	Flat-C3 1"	0.0298	n/a	19.6	135	24.0	166	n/d	84	n/a	HH-FL-1-17	12WF92 from flange

Table A–18. High-temperature, tensile test results for truss steels.

Specified yield (F_y) ksi	Location in Bldg (Bldg.-Center column number, floor level)	Test axis with respect to RD	Temp °C	Specimen type and nominal GL	Area in.²	Yield point, *YP* ksi	0.2 % Yield Strength, *YS* ksi	0.2 % Yield Strength, *YS* MPa	Tensile Strength, *TS* ksi	Tensile Strength, *TS* MPa	El_f %	*ROA* %	Measured yield/F_y	Sample #	Type
50	n/a	L	20	Rd 2"	0.1928	NYP	58.4	403	77.8	536	27 (2")	65	1.17	TR1	Truss Rods (from T1) D=0.92 in.
50	n/a	L	20	Rd 2"	0.1928	NYP	65.5	452	83.0	572	24 (2")	65	1.31	TR2	Truss Rods (from T1) D=0.92 in.
50	n/a	L	20	Rd 2"	0.1928	NYP	52.4	361	76.5	527	15 (2")	67	1.05	TR3	Truss Rods (from T1) D=0.92 in.
50	n/a	L	20	Rd 1"	0.0485	NYP	63.4	437	86.7	598	26 (1")	62	1.27	TR4	Truss Rods (from T1) D=0.92 in.
50	n/a	L	20	Rd 1"	0.0491	NYP	57.5	396	75.7	522	35 (1")	67	1.15	TR5	Truss Rods (from T1) D=0.92 in.
50	n/a	L	400	Rd 1"	0.0487	n/a	42.5	293	56.1	387	26 (1")	42	n/a	T1-TR-G1-	Truss Rods (from T1) D=0.92 in.
50	n/a	L	500	Rd 1"	0.0489	n/a	31.2	215	37.6	259	9 (1")	22	n/a	T1-TR-G1-	Truss Rods (from T1) D=0.92 in.
50	n/a	L	600	Rd 1"	0.0487	n/a	19.1	132	23.8	164	26 (1")	28	n/a	T1-TR-G1-	Truss Rods (from T1) D=0.92 in.
50	n/a	L	700	Rd 1"	0.0487	n/a	8.2	56.5	9.6	66	30 (1")	42	n/a	T1-TR-G1-1	Truss Rods (from T1) D=0.92 in.
36	n/a	L	20	Rd 1"	0.0489	47.4	41.4	285	63.3	436	38 (1")	60	1.15	C53-1L	Truss Rods D=1.09 in.
36	n/a	L	400	Rd 1"	0.0489	n/a	33.8	233	47.9	330	31 (1")	46	n/a	C53-3L	Truss Rods D=1.09 in.
36	n/a	L	500	Rd 1"	0.0487	n/a	20.8	143	30.0	207	31 (1")	39	n/a	C53-4L	Truss Rods D=1.09 in.
36	n/a	L	600	Rd 1"	0.0483	n/a	13.7	94	16.9	117	37 (1")	39	n/a	C53-6L	Truss Rods D=1.09 in.
36	n/a	L	650	Rd 1"	0.0489	n/a	10.1	70	n/a	n/a	n/a	n/a	n/a	C53-9L	Truss Rods D=1.09 in.
36	n/a	L	650	Rd 1"	0.0487	n/a	9.8	68	12.7	88	42 (1")	45	n/a	C53-10L	Truss Rods D=1.09 in.
50	n/a	L	20	Flat-C 1"	0.0636	NYP	53.7	370	74.9	516	33 (1")	59	1.07	T1A-1	Truss Angles 2 in. x 1.5 in. x 0.25 in.
50	n/a	L	20	Flat-C 1"	0.0643	NYP	48.5	334	73.3	505	31 (1")	60	0.97	T1A-2	Truss Angles 2 in. x 1.5 in. x 0.25 in.
50	n/a	L	20	Flat-C 1"	0.0640	NYP	54.2	374	74.1	511	35 (1")	61	1.08	T1A-4	Truss Angles 2 in. x 1.5 in. x 0.25 in.
50	n/a	L	20	Flat-C 1"	0.0635	NYP	50.7	350	74.7	515	32 (1")	56	1.01	T1A-8	Truss Angles 2 in. x 1.5 in. x 0.25 in.
50	n/a	L	500	Flat-C 1"	0.0628	n/a	33.1	228	42.6	294	18 (1")	18	n/a	T1A-3	Truss Angles 2 in. x 1.5 in. x 0.25 in.
50	n/a	L	750	Flat-C 1"	0.0636	n/a	3.1	21	8.5	59	39 (1")	29	n/a	T1A-9	Truss Angles 2 in. x 1.5 in. x 0.25 in.
50	1-142-97/100	L	20	Flat-C 1"	0.0643	NYP	55.9	385	79.2	546	32 (1")	64	1.12	N8A-1	Truss Angles 2 in. x 1.5 in. x 0.25 in.
50	1-142-97/100	L	20	Flat-C 1"	0.0631	NYP	56.1	387	79.5	548	33 (1")	62	1.12	N8A-2	Truss Angles 2 in. x 1.5 in. x 0.25 in.
50	1-142-97/100	L	20	Flat-C 1"	0.0631	NYP	54.6	376	79.9	551	32 (1")	60	1.09	N8A-3	Truss Angles 2 in. x 1.5 in. x 0.25 in.
50	n/a	L	20	Flat-C2	0.0283	NYP	57.3	395	76.6	528	38 (1")	n/d	1.15	C132TA7	Truss Angles 2 in. x 1.5 in. x 0.25 in.
50	n/a	L	20	Flat-C2	0.0281	NYP	63.3	436	n/d	n/d	n/a	n/d	1.27	C132TA6N-	Truss Angles 2 in. x 1.5 in. x 0.25 in.
50	n/a	L	20	Flat-C2	0.0284	NYP	57.0	393	79.6	549	33 (1")	65.0	1.14	C132TA2N	Truss Angles 2 in. x 1.5 in. x 0.25 in.
50	n/a	L	20	Flat-C2	0.0283	59.2	57.4	396	76.5	528	n/f	n/f	1.15	C132TA7W	Truss Angles 2 in. x 1.5 in. x 0.25 in.
50	n/a	L	500	Flat-C2	0.0280	n/a	42.8	295	50.6	349	16 (1")	n/d	n/a	C132TA1N-	Truss Angles 2 in. x 1.5 in. x 0.25 in.
50	n/a	L	600	Flat-C2	0.0283	n/a	27.1	187	30.8	212	n/f	n/a	n/a	C132TA4N-	Truss Angles 2 in. x 1.5 in. x 0.25 in.
50	n/a	L	650	Flat-C2	0.0280	n/a	22.6	156	23.9	165	n/d	n/d	n/a	C132TA6W	Truss Angles 2 in. x 1.5 in. x 0.25 in.
50	n/a	L	400	Flat-C2	0.0285	n/a	48.3	333	70.0	483	32 (1")	n/d	n/a	C132TA2W	Truss Angles 2 in. x 1.5 in. x 0.25 in.
50	n/a	L	600	Flat-C2	0.0283	n/a	19.2	133	27.6	190	n/d	n/d	n/a	C132TA3W	Truss Angles 2 in. x 1.5 in. x 0.25 in.
50	n/a	L	600	Flat-C2	0.0279	n/a	22.7	156	29.3	202	n/f	n/a	n/a	C132TA1W	Truss Angles 2 in. x 1.5 in. x 0.25 in.
36	n/a	L	20	Flat-C3	0.0300	NYP	63.5	438	81.3	560	26 (1")	58	1.76	C53BA2-12	Truss Angles 3 in. x 2 in. x 0.37 in.
36	n/a	L	20	Flat-C3	0.0294	NYP	51.9	358	75.3	519	24 (1")	59	1.44	C53BA1-6N	Truss Angles 3 in. x 2 in. x 0.37 in.
36	n/a	L	300	Flat-C3	0.0299	n/a	53.2	367	83.9	579	n/d	n/d	n/a	C53BA2-5W	Truss Angles 3 in. x 2 in. x 0.37 in.
36	n/a	L	400	Flat-C3	0.0283	n/a	40.9	282	61.9	427	n/d	54	n/a	C53BA3-6	Truss Angles 3 in. x 2 in. x 0.37 in.
36	n/a	L	500	Flat-C3	0.0291	n/a	40.6	280	48.1	332	11 (1")	n/d	n/a	C53BA2-2W	Truss Angles 3 in. x 2 in. x 0.37 in.
36	n/a	L	600	Flat-C3	0.0291	n/a	27.0	186	29.7	205	8 (1")	30	n/a	C53BA3-8	Truss Angles 3 in. x 2 in. x 0.37 in.
36	n/a	L	600	Flat-C3	0.0295	n/a	26.3	182	26.6	183	16 (1")	28	n/a	C53BA1-3W	Truss Angles 3 in. x 2 in. x 0.37 in.
36	n/a	L	650	Flat-C3	0.0294	n/a	18.1	125	19.9	138	20 (1")	n/d	n/a	C53BA2-4W	Truss Angles 3 in. x 2 in. x 0.37 in.

Table A–19. Elevated-temperature, tensile test results for truss seat steels.

Specified yield (F_y) ksi	Location in Bldg (Bldg.-Center column number, floor level)	Test axis with respect to RD	Temp °C	Specimen type and nominal GL	Area in.²	Yield point, *YP* ksi	0.2 % Yield Strength, *YS* ksi	0.2 % Yield Strength, *YS* MPa	Tensile Strength, *TS* ksi	Tensile Strength, *TS* MPa	El_t %	*ROA* %	Measured yield/F_y	Sample #	Type
36	1-142-97/100	L	20	Rd 1"	0.0495	45.0	45.4	313	67.0	462	29 (1")	36	1.26	N8-C1B1-S-C-1-L	Perimeter truss seat
36	1-142-97/100	L	20	Rd 1"	0.0485	41.5	38.5	265	64.6	445	33 (1")	38	1.07	N8-C1B1-S-C-2-L	Perimeter truss seat
36	1-142-97/100	L	20	Rd 1"	0.0479	38.6	37.7	260	65.2	450	34 (1")	38	1.06	N8-C1B1-S-C-3-L	Perimeter truss seat
36	1-142-97/100	T	20	Rd 1"	0.0489	38.4	38.3	264	67.8	467	30 (1")	31	1.06	N8-C1B1-S-C-13-	Perimeter truss seat
36	1-142-97/100	T	20	Rd 1"	0.0491	NYP	47.0	324	67.0	462	21 (1")	33	1.31	N8-C1B1-S-C-14-	Perimeter truss seat
36	1-142-97/100	T	20	Rd 1"	0.0489	NYP	37.3	257	67.4	465	32 (1")	31	1.04	N8-C1B1-S-C-15-	Perimeter truss seat
36	1-142-97/100	T	500	Rd 1"	0.0489	n/a	27.8	192	32.9	227	30 (1")	45	n/a	N8-C1B1-S-C-16T	Perimeter truss seat
36	1-142-97/100	L	750	Rd 1"	0.0479	n/a	4.3	30	8.0	55	39 (1")	51	n/a	N8-C1B1-S-C-6L	Perimeter truss seat
36	2-154-101/104	L	20	Rd 1"	0.0475	40.9	40.9	282	69.6	480	31 (1")	52	1.14	N9-C1T1-S-C-9-L	Perimeter truss seat
36	2-154-101/104	T	500	Rd 1"	0.0487	n/a	20.9	144	32.6	225	30 (1")	40	n/a	N9-C1T1-S-C-35T	Perimeter truss seat
36	2-154-101/104	L	500	Rd 1"	0.0470	n/a	24.9	172	32.0	221	36 (1")	42	n/a	N9-C1T1-S-C-17L	Perimeter truss seat
36	2-154-101/104	L	500	Rd 1"	0.0491	n/a	20.7	143	31.8	219	33 (1")	42	n/a	N9-C1T1-S-C-18L	Perimeter truss seat
36	2-154-101/104	T	750	Rd 1"	0.0485	n/a	4.2	29	7.0	48	34 (1")	54	n/a	N9-C1T1-S-C-34T	Perimeter truss seat
36	unknown	L	20	Rd 1"	0.0489	46.0	44.9	310	68.8	474	36 (1")	62	1.25	M4-C3T-L1	Perimeter truss seat
36	unknown	L	400	Rd 1"	0.0489	n/a	30.6	211	50.3	347	32 (1")	50	n/a	M4-C3T-L2	Perimeter truss seat
36	unknown	L	500	Rd 1"	0.0487	n/a	20.7	143	27.6	190	36 (1")	54	n/a	M4-C3T-L3	Perimeter truss seat
36	unknown	L	600	Rd 1"	0.0487	n/a	11.4	79	15.6	108	61 (1")	93	n/a	M4-C3T-L4	Perimeter truss seat
36	unknown	L	650	Rd 1"	0.0489	n/a	7.0	48	10.1	70	75 (1")	91	n/a	M4-C3T-L5	Perimeter truss seat
36	n/a	L	20	Rd 1"	0.0489	58.6	57.5	396	82.2	567	30 (1")	69	1.60	M34-TS-A-L5	Core truss seat
36	n/a	T	20	Rd 1"	0.0489	NYP	70.1	483	92.8	640	22 (1")	45	1.95	M34-TS-A-T1	Core truss seat
na	n/a	T	400	Rd 1"	0.0492	n/a	48.0	331	72.0	496	24 (1")	47	n/a	M34-TS-A-T2	Core truss seat
na	n/a	T	400	Rd 1"	0.0487	n/a	34.7	239	57.5	397	32 (1")	55	n/a	M34-TS-B-T7	Core truss seat
na	n/a	T	500	Rd 1"	0.0490	n/a	27.9	192	38.0	262	36 (1")	51	n/a	M34-TS-C-T16	Core truss seat
na	n/a	T	500	Rd 1"	0.0490	n/a	25.3	174	35.2	243	37 (1")	80	n/a	M34-TS-B-T8	Core truss seat
na	n/a	T	700	Rd 1"	0.0488	n/a	8.0	55	11.0	76	52 (1")	78	n/a	M34-TS-B-T9	Core truss seat
na	n/a	T	600	Rd 1"	0.0490	n/a	15.5	107	22.0	152	62 (1")	79	n/a	M34-TS-C-T17	Core truss seat
na	n/a	T	650	Rd 1"	0.0490	n/a	14.4	99	15.8	109	39 (1")	88	n/a	M34-TS-A-T3	Core truss seat
na	n/a	T	700	Rd 1"	0.0490	n/a	10.1	70	11.0	76	67 (1")	82	n/a	M34-TS-C-T18	Core truss seat
na	n/a	L	400	Rd 1"	0.0485	n/a	36.0	248	59.5	410	58 (1")	47	n/a	M34-TS-B-L10	Core truss seat
na	n/a	L	600	Rd 1"	0.0485	n/a	17.4	120	23.4	161	n/a	90	n/a	M34-TS-B-L11	Core truss seat
na	n/a	L	700	Rd 1"	0.0487	n/a	8.0	55	10.3	71	n/a	85	n/a	M34-TS-B-L12	Core truss seat
36	n/a	T	20	Rd 1"	0.0483	34.0	33.3	230	66.6	459	40 (1")	68	0.93	C128-T1	Core truss seat
na	n/a	T	400	Rd 1"	0.0487	n/a	25.7	177	58.2	401	37 (1")	71	n/a	C128-T2	Core truss seat
na	n/a	T	500	Rd 1"	0.0485	n/a	18.2	125	32.0	221	46 (1")	79	n/a	C128-T3	Core truss seat
na	n/a	T	600	Rd 1"	0.0485	n/a	9.9	68	15.7	108	68 (1")	97	n/a	C128-T4	Core truss seat
na	n/a	T	650	Rd 1"	0.0487	n/a	6.0	41	9.9	68	79 (1")	92	n/a	C128-T5	Core truss seat

Table A–20. High-temperature, tensile creep test results for truss steels.

Specified Yield (F_y) ksi	Bldg (Bldg.-Center column number, floor level)	Test axis with respect to RD	Temp °C	Spec. type and nominal GL	Area in.²	Stress ksi	*A*	*b*	t_{max} s	e_{max}	Failure	Sample #
50	n/a	L	400	Flat-C2-1"	0.0278	50.2	1.203E-04	0.3595	16442	0.0087	discontinue	C132TA7N-1
50	n/a	L	400	Flat-C2-1"	0.0284	61.3	4.001E-05	0.6340	10504	0.0529	discontinue	C132TA7W-2
50	n/a	L	400	Flat-C2-1"	0.0284	64.7	1.230E-05	0.8493	8540	0.0883	discontinue	C132TA4N-2
50	n/a	L	500	Flat-C2-1"	0.0276	36.3	1.019E-04	0.6420	7200	0.0296	discontinue	C132TA4W-3
50	n/a	L	500	Flat-C2-1"	0.0284	36.5	1.579E-05	0.9244	10549	0.0920	failure	C132TA3N-1
50	n/a	L	500	Flat-C2-1"	0.0278	39.5	2.800E-05	0.8856	6824	0.0838	failure	C132TA1W-4
50	n/a	L	500	Flat-C2-1"	0.0283	40.3	1.420E-04	0.7711	3358	0.0889	failure	C132TA4W-4
50	n/a	L	500	Flat-C2-1"	0.0283	43.0	2.959E-04	0.7686	665	0.0516	failure	C132TA2N-2
50	n/a	L	500	Flat-C2-1"	0.0279	43.5	8.260E-04	0.7790	377	0.1810	failure	C132TA1N-2
50	n/a	L	600	Flat-C2-1"	0.0280	17.9	2.324E-06	1.2095	10901	0.0401	discontinue	C132TA1W-2
50	n/a	L	600	Flat-C2-1"	0.0283	19.1	2.984E-07	1.3406	13740	0.1181	failure	C132TA2W-2
50	n/a	L	600	Flat-C2-1"	0.0286	21.8	2.089E-06	1.2458	3131	0.0476	discontinue	C132TA4W-6
50	n/a	L	600	Flat-C2-1"	0.0281	22.0	2.210E-05	1.0312	2367	0.0685	failure	C132TA3W-3
50	n/a	L	600	Flat-C2-1"	0.0277	23.8	9.129E-09	1.8830	4659	0.0786	failure	C132TA5W-2
50	n/a	L	650	Flat-C2-1"	0.0283	14.5	1.595E-08	1.7701	5701	0.0931	failure	C132TA2W-4
50	n/a	L	650	Flat-C2-1"	0.0284	18.1	9.285E-05	0.9800	856	0.1010	failure	C132TA2W-8
50	n/a	L	650	Flat-C2-1"	0.0282	18.3	1.720E-05	1.2630	541	0.0514	discontinue	C132TA2N-3
50	n/a	L	650	Flat-C2-1"	0.0284	21.1	6.796E-04	0.8598	1256	0.2842	failure	C132TA6N-2
50	n/a	L	650	Flat-C2-1"	0.0281	21.4	4.000E-04	0.9496	911	0.1829	failure	C132TA7W-1
50	n/a	L	700	Flat-C2-1"	0.0283	8.5	7.687E-14	2.7995	23117	0.1388	failure	C132TA5W-4

Notes

t_{max} time at which specimen failed or test was discontinued

e_{max} engineering strain at which specimen failed or test was discontinued

A,b strain = At**b, where t has units of s, strain in engineering units (not percent)

A.5 SUPPLEMENTAL FIGURES FOR ROOM-TEMPERATURE PROPERTIES

Figures A–1 through A–17 summarize the room-temperature stress-strain behavior of specimens taken from the perimeter columns. Figures A–18 through A–26 summarize the room-temperature stress-strain behavior of specimens taken from the core wide-flange and box columns. Figure A–27 summarizes the behavior of the truss steels.

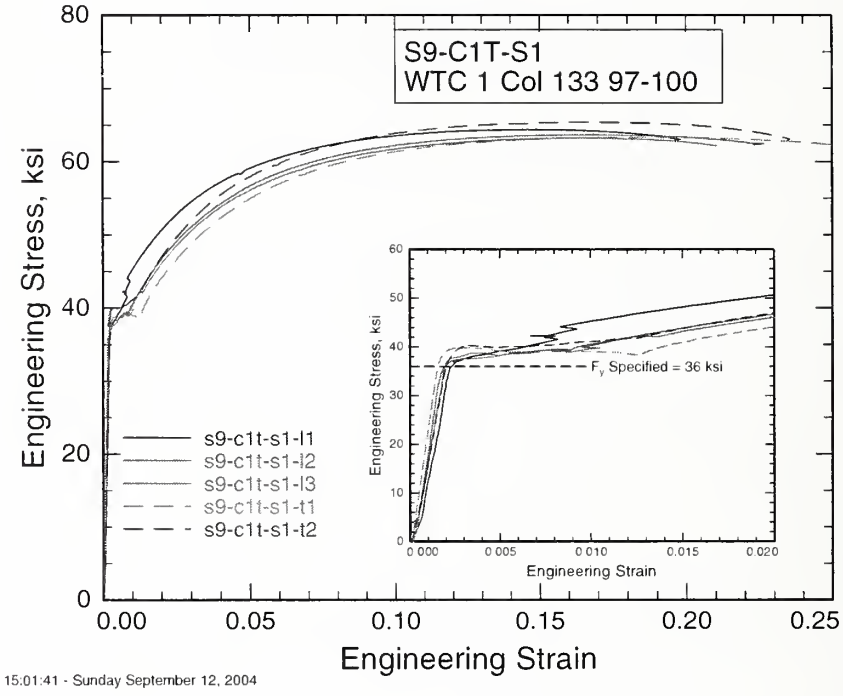

Figure A–1. Stress-strain curves for F_y = 36 ksi S-9 spandrel.

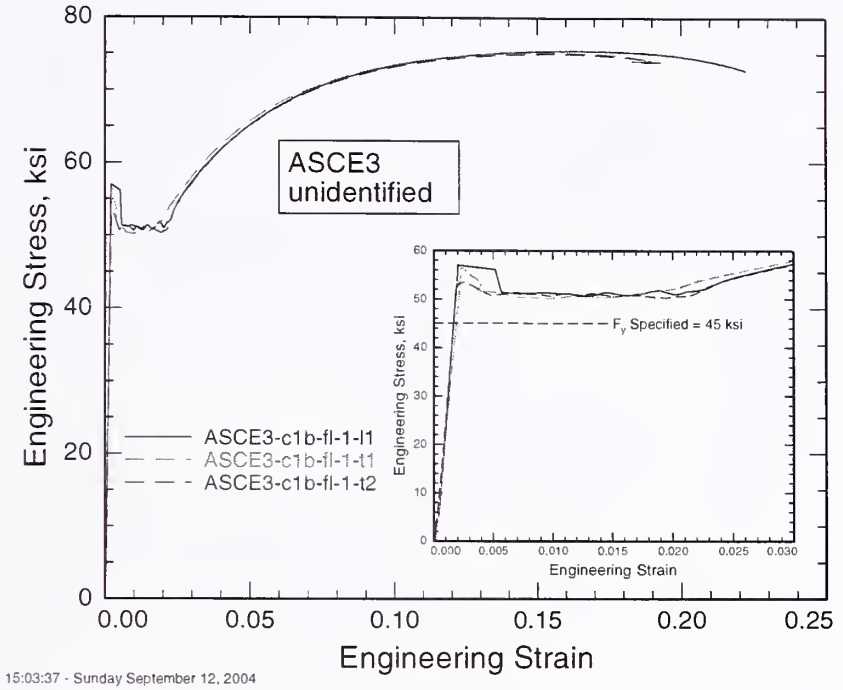

Figure A–2. Stress-strain curves for F_y = 45 ksi ASCE3.

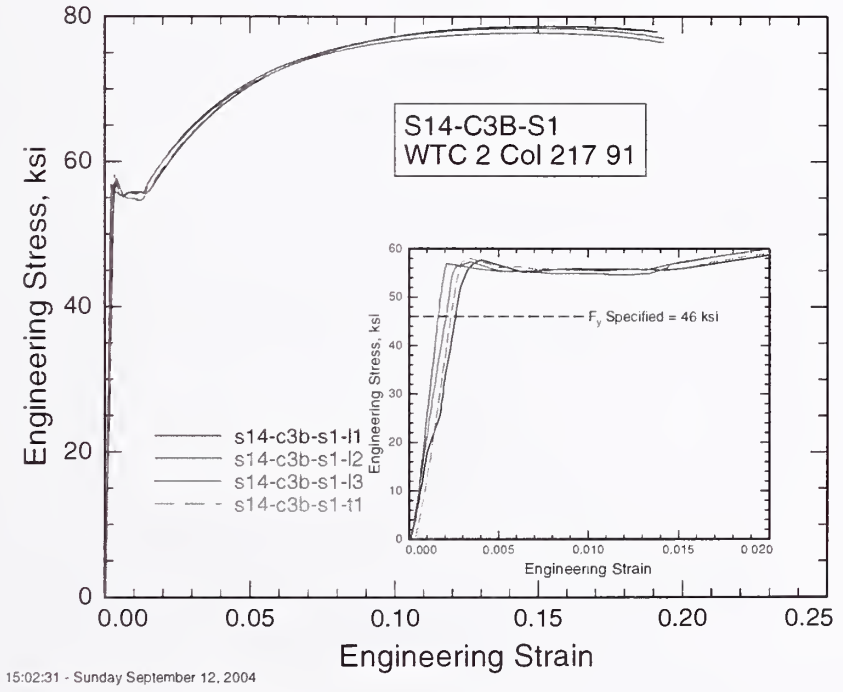

Figure A–3. Stress-strain curves for F_y = 46 ksi S-14 spandrel.

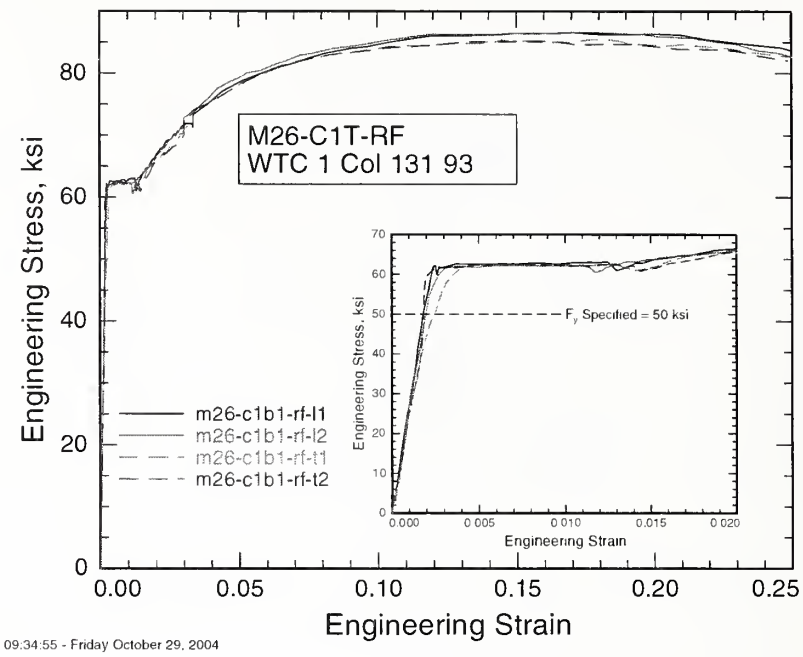

Figure A–4. Stress-strain curves for F_y = 50 ksi M-26.

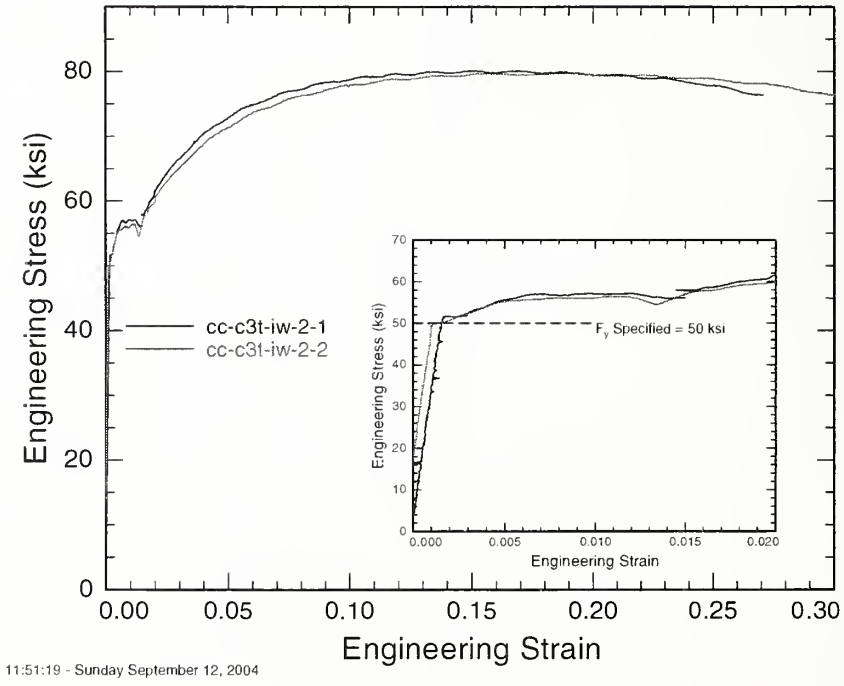

Figure A–5. Stress-strain curves F_y = 50 ksi CC-C3T-IW.

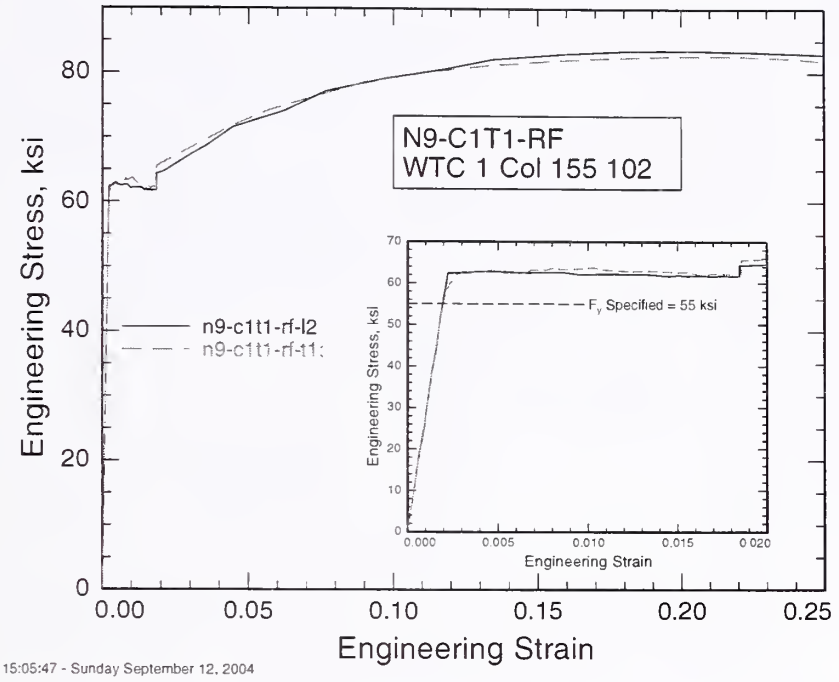

Figure A–6. Stress-strain curves for F_y = 55 ksi N-9.

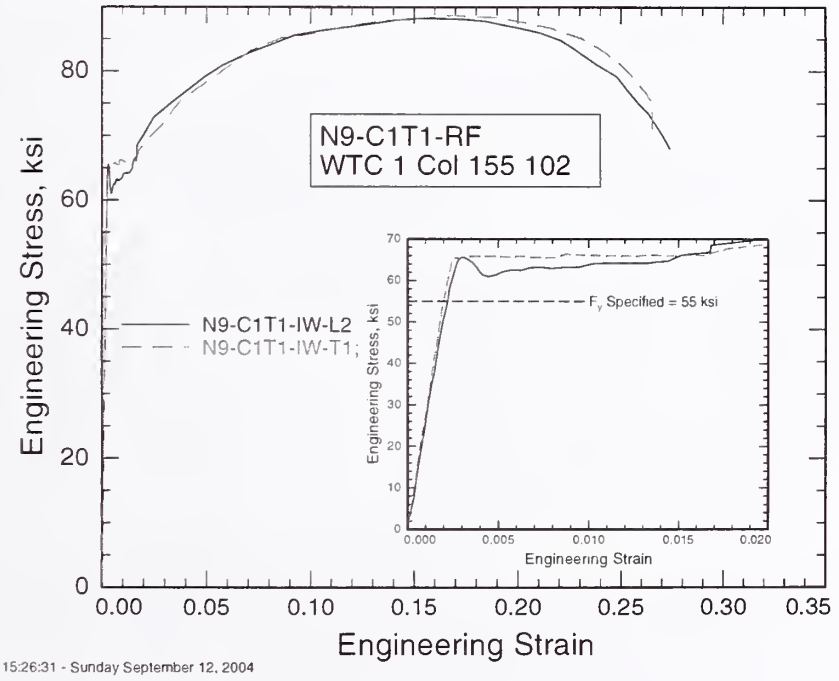

Figure A–7. Stress-strain curves for F_y = 55 ksi N-9 inner web.

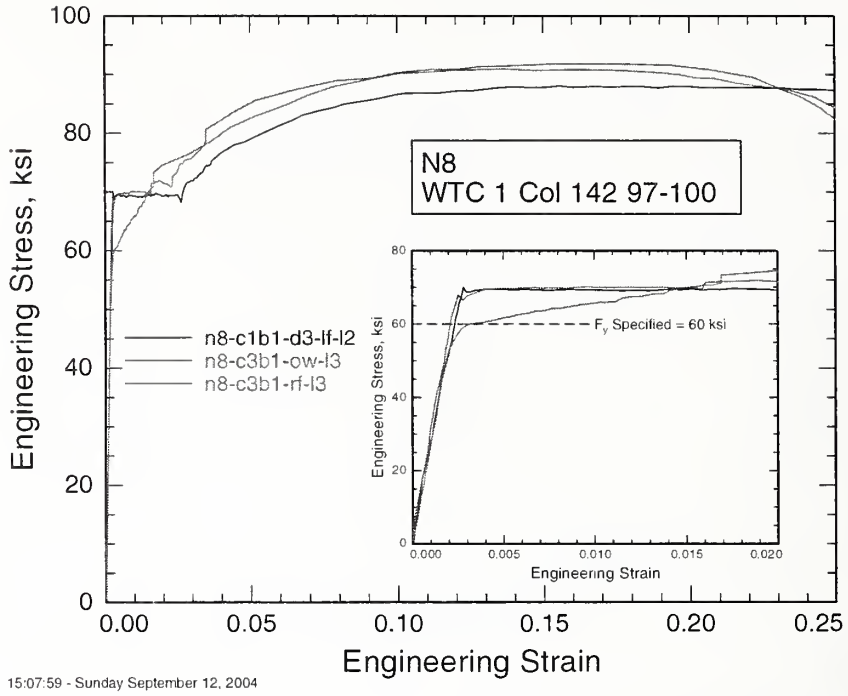

Figure A–8. Stress-strain curves for F_y = 60 ksi N-8.

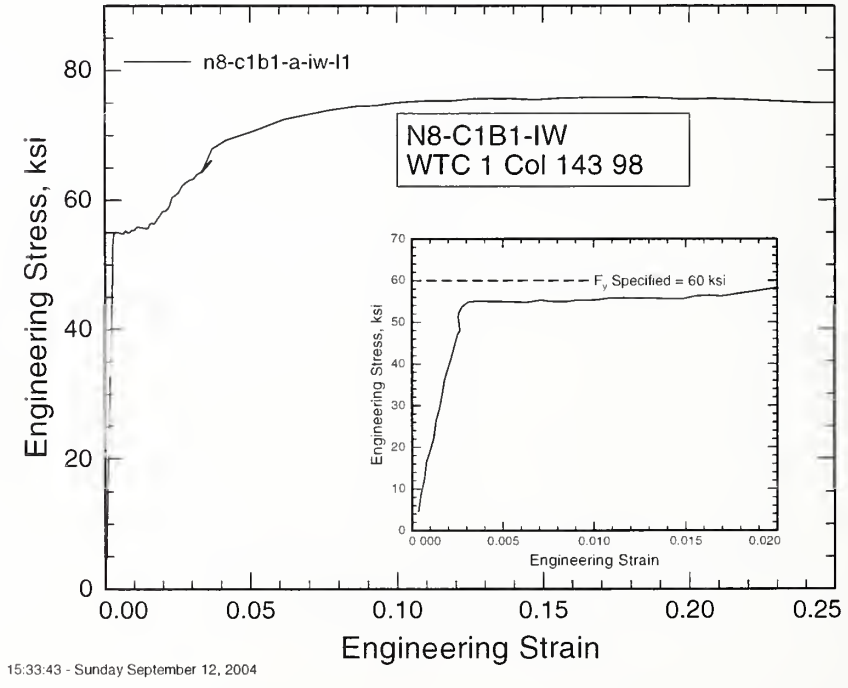

Figure A–9. Stress-strain curves for F_y = 60 ksi N-8 inner web.

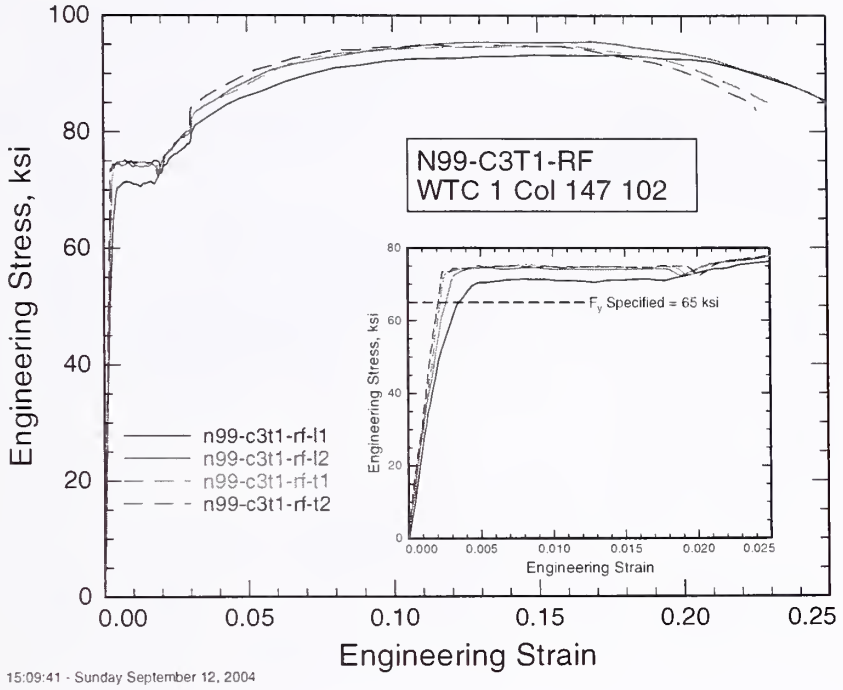

Figure A–10. Stress-strain curves for F_y = 65 ksi N-99.

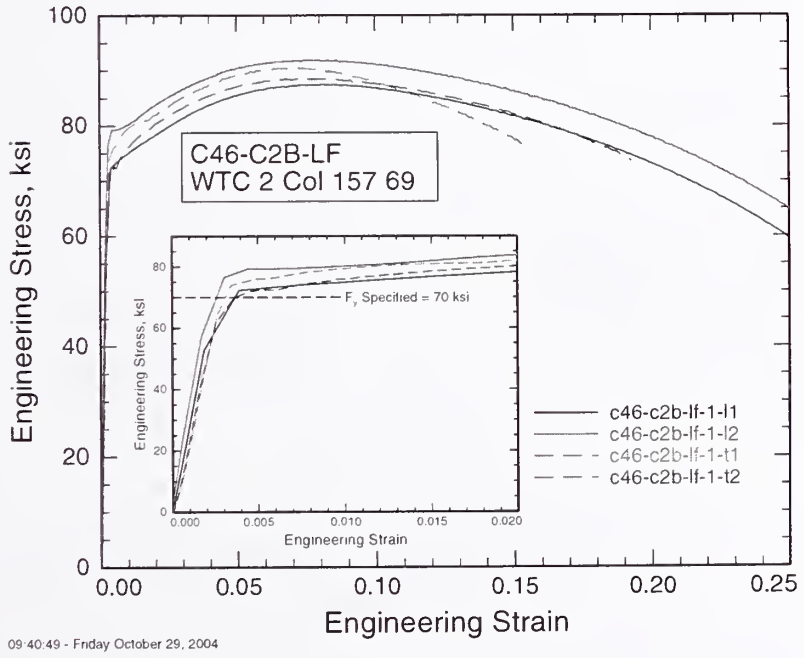

Figure A–11. Stress-strain curves for F_y = 70 ksi C-46.

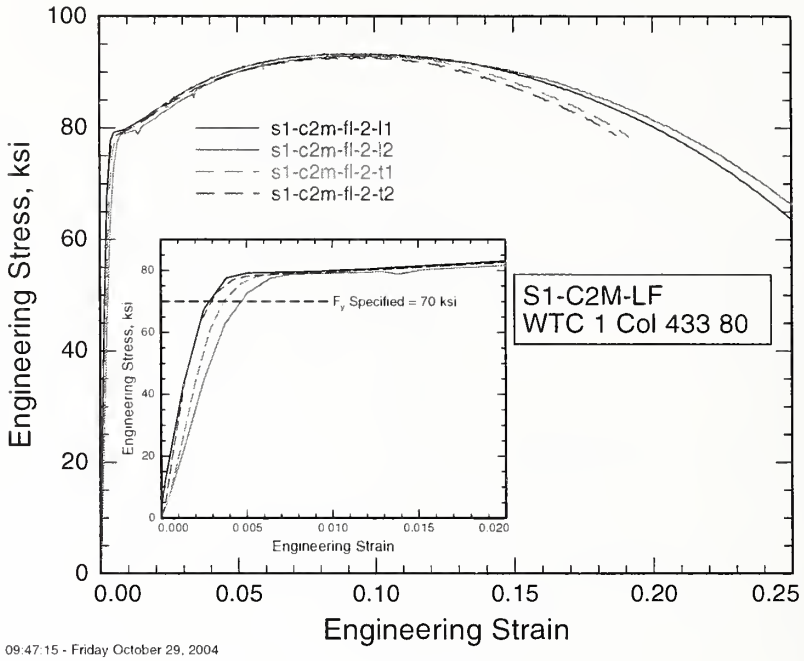

Figure A–12. Stress-strain curves for F_y = 70 ksi S-1.

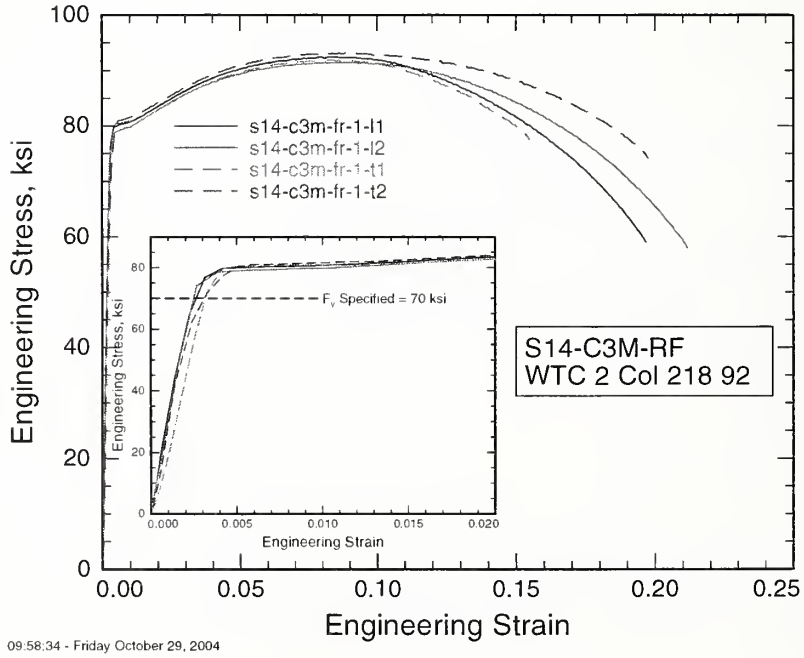

Figure A–13. Stress-strain curves for F_y = 70 ksi S-14.

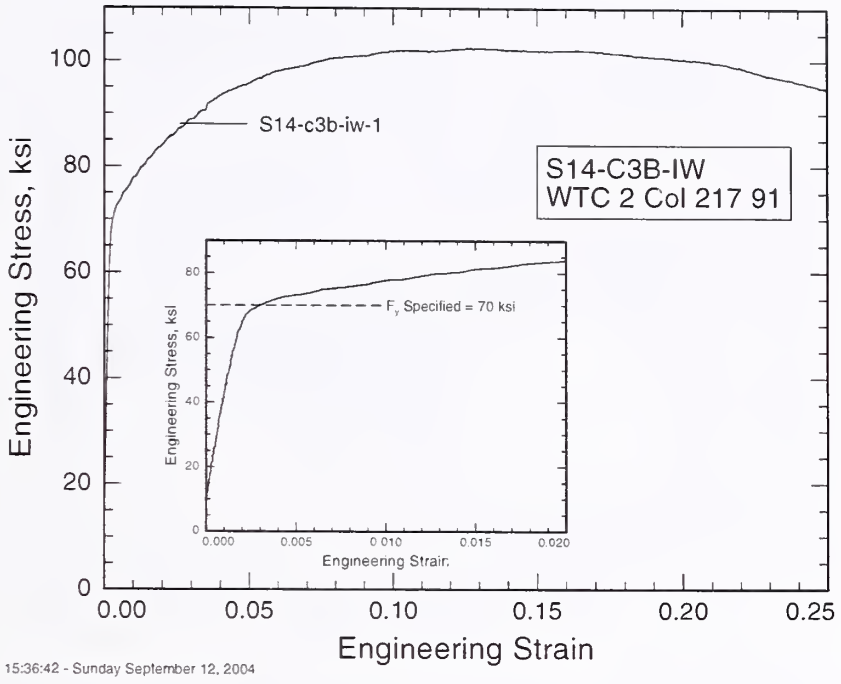

Figure A–14. Stress-strain curves for F_y = 70 ksi S-14 inner web.

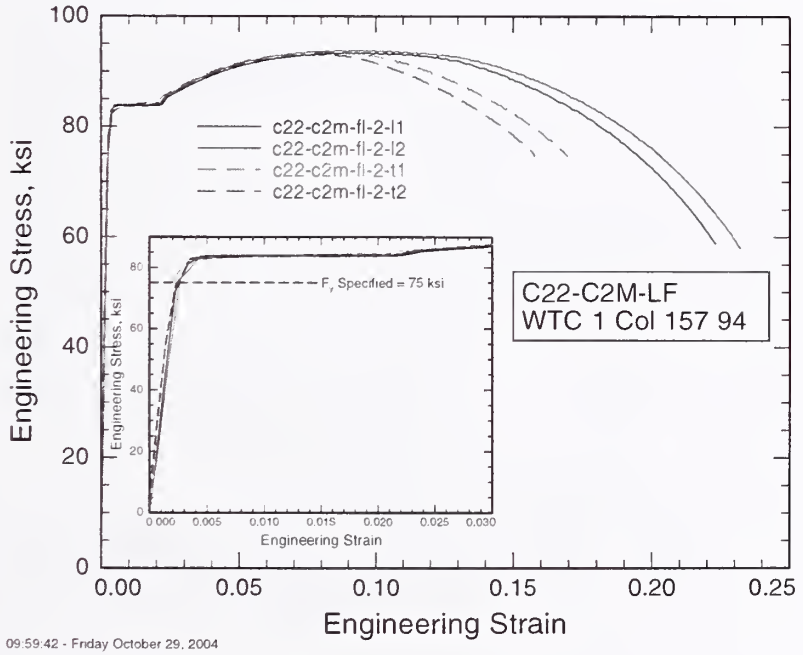

Figure A–15. Stress-strain curves for F_y = 75 ksi C-22.

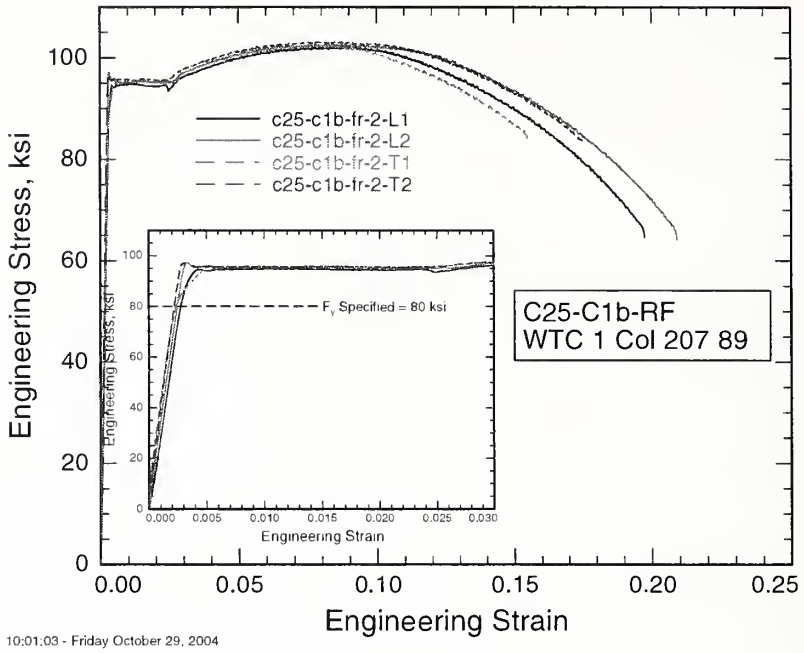

Figure A–16. Stress-strain curves for F_y = 80 ksi C-25.

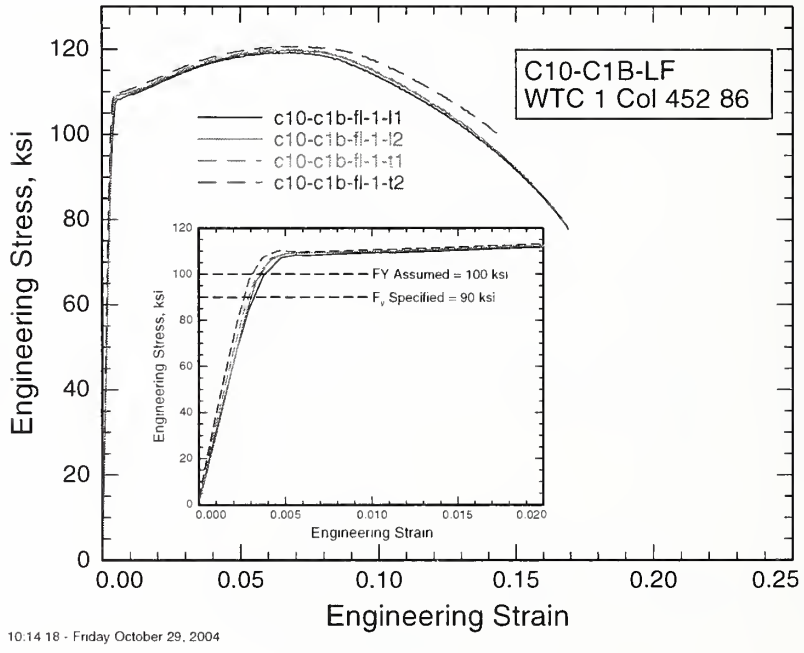

Figure A–17. Stress-strain curves for F_y = 100 ksi C-10.

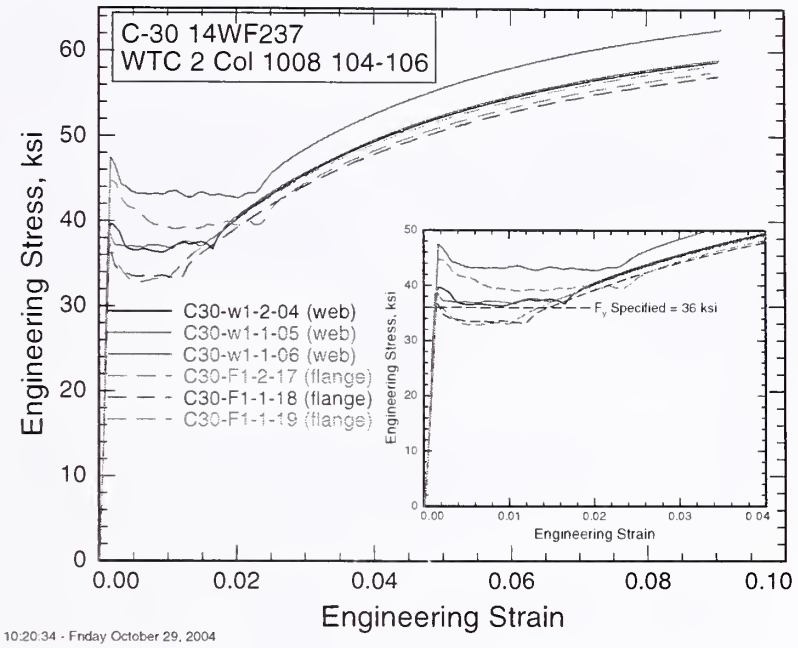

Figure A–18. Stress-strain curves for core wide-flange column C-30.

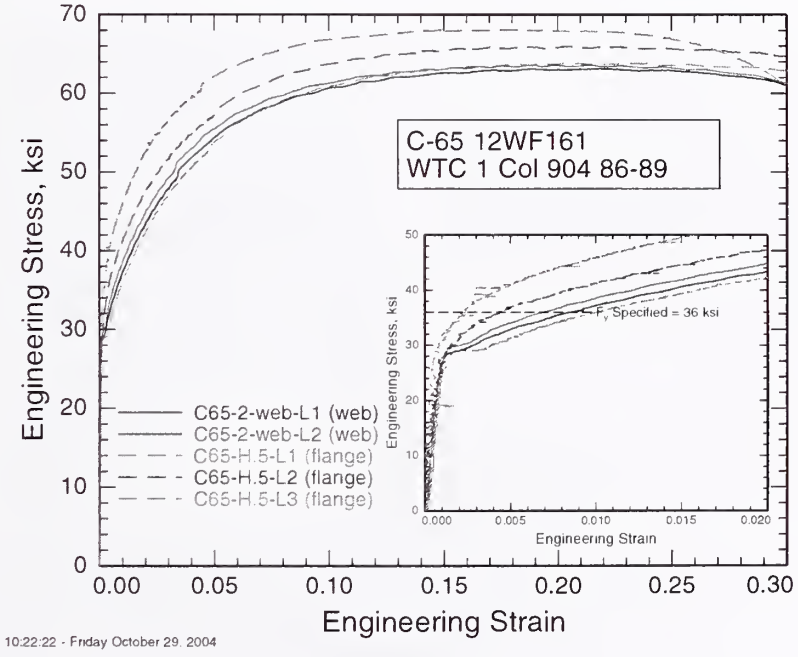

Figure A–19. Stress-strain curves for core wide-flange column C-65.

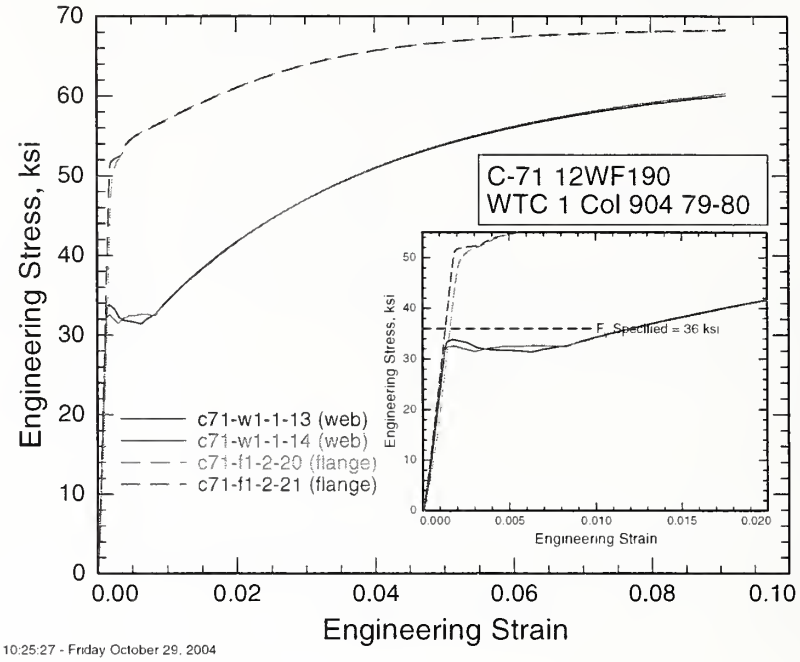

Figure A–20. Stress-strain curves for core wide-flange column C-71.

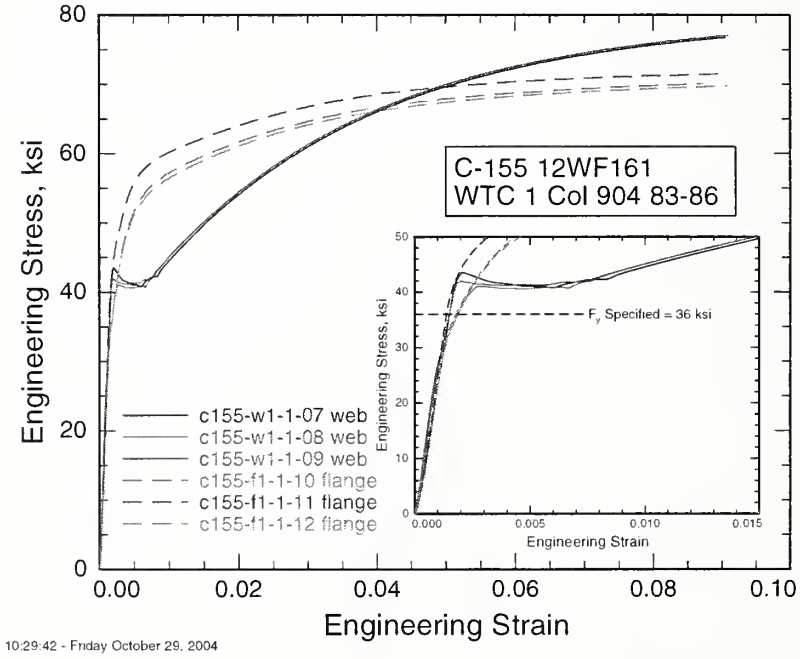

Figure A–21. Stress-strain curves for core wide-flange column C-155.

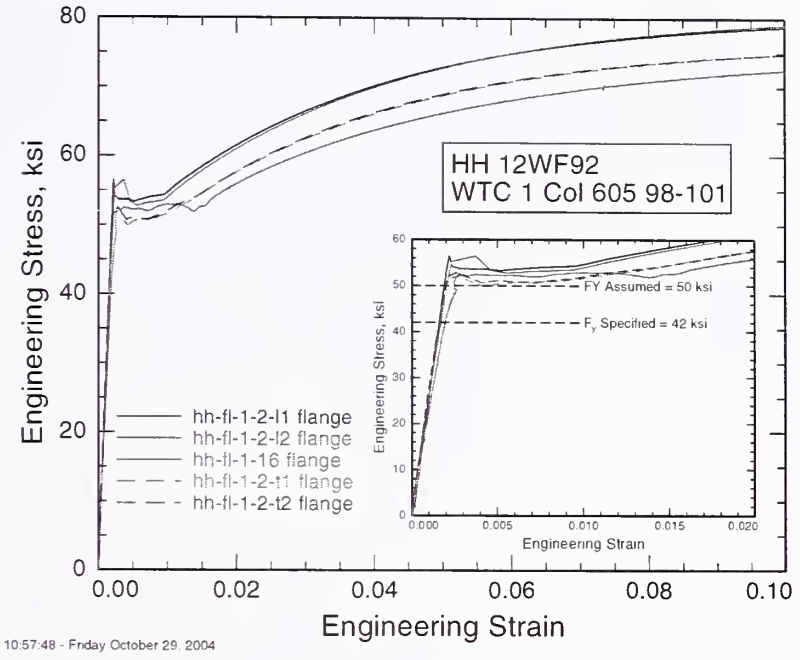

Figure A–22. Stress-strain curves for core wide-flange column HH.

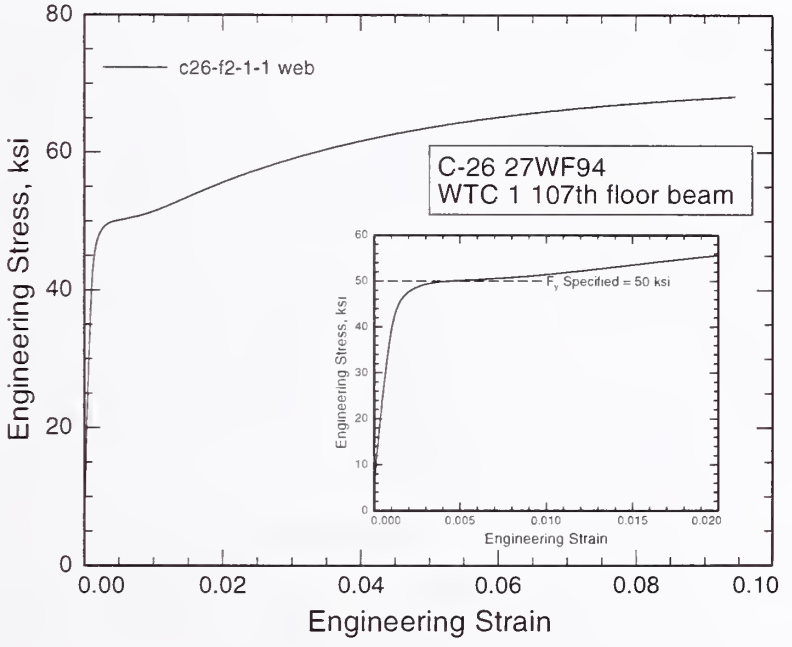

Figure A–23. Stress-strain curves for core wide-flange beam C-26.

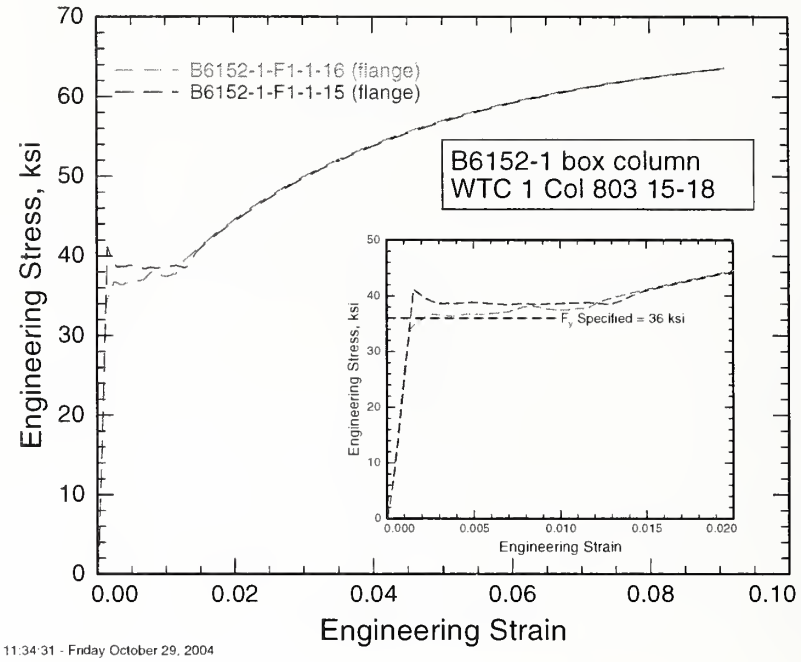

Figure A–24. Stress-strain curves for core box column B6152-1.

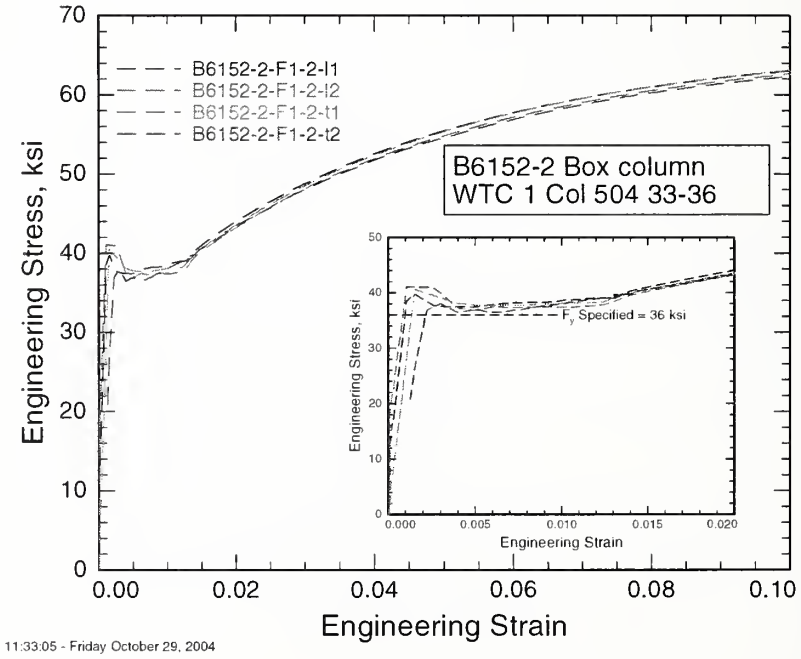

Figure A–25. Stress-strain curves for core box column B6152-2.

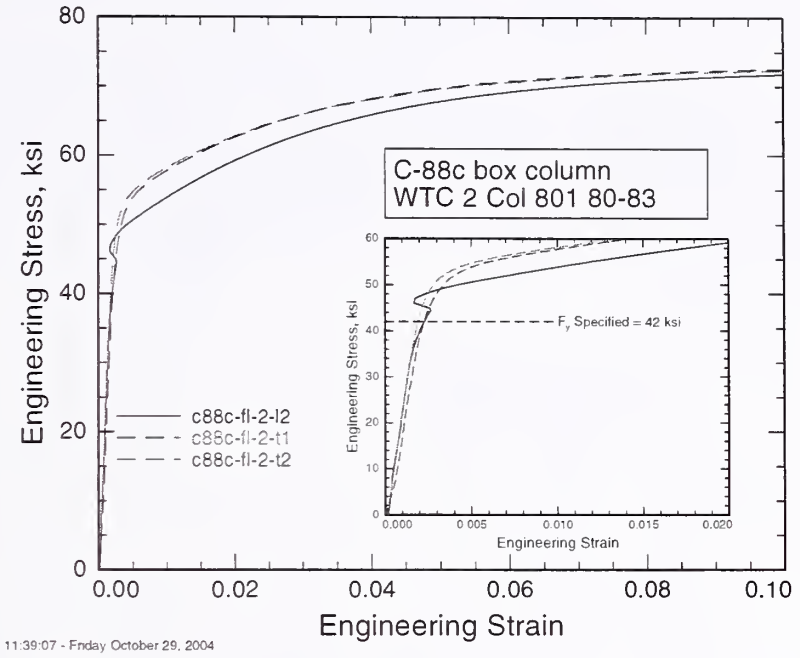

Figure A–26. Stress-strain curves for core box column C-88c.

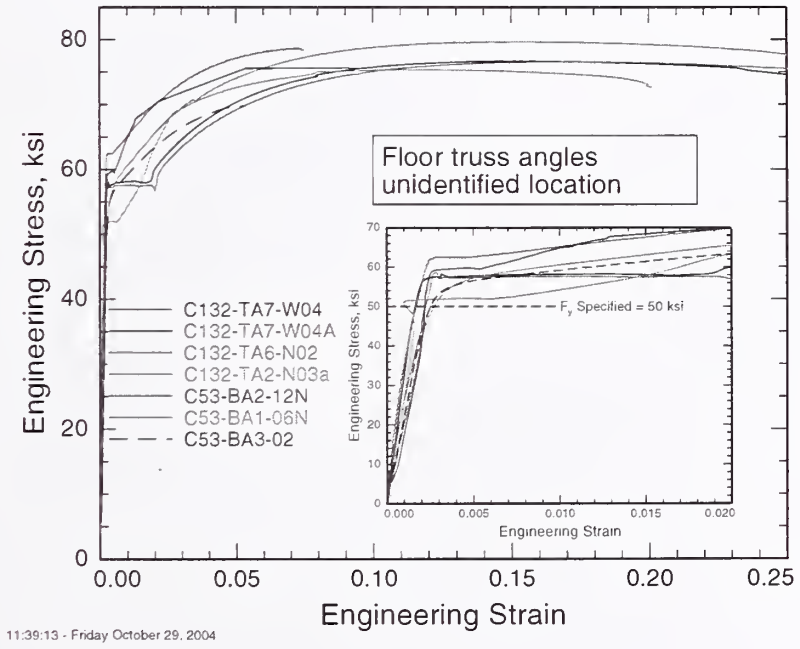

Figure A–27. Stress-strain curves for all truss angles.

A.5 SUPPLEMENTAL FIGURES FOR HIGH STRAIN-RATE PROPERTIES

Figures A–28 through A–37 summarize the stress-strain curves as a function of strain rate for perimeter column steels. Figures A–44 through A–52 summarize the curves for core-column steels. Figures A–53 through A–68 summarize the strain rate sensitivities for perimeter column steels. Figures A–69 through A–77 summarize the strain rate sensitivities for core column steels. Figure A–78 through A–80 summarize the dependence of total elongation, El_t, on strain rate. Figures A–81 through A–103 show the results of high strain-rate Kolsky tests.

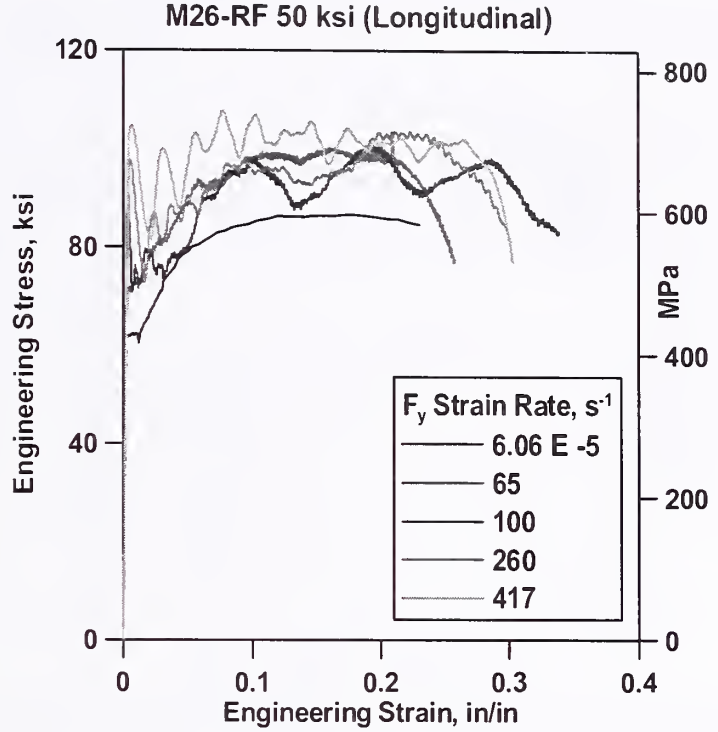

Figure A–28. Stress-strain curves for F_y = 50 ksi perimeter column M26-C1B1-RF longitudinal.

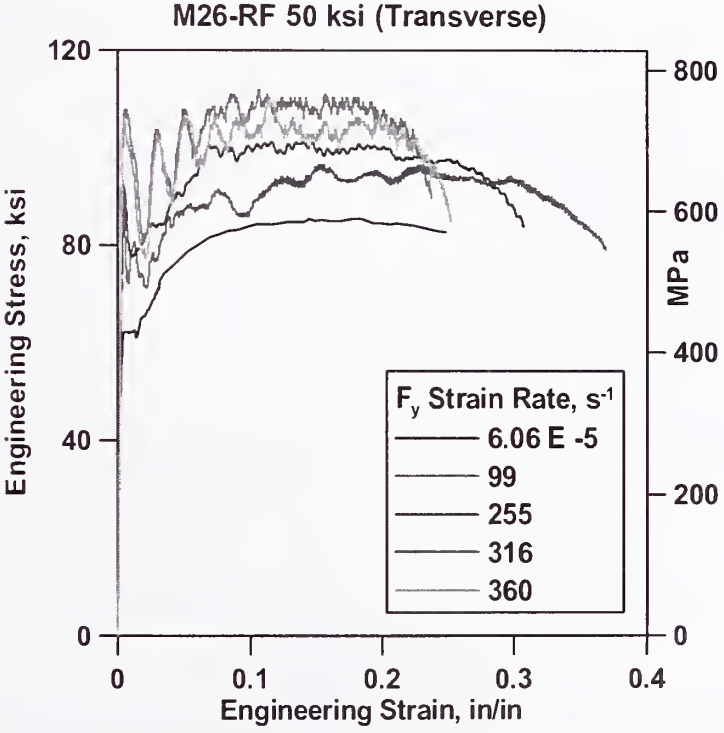

Figure A–29. Stress-strain curves for F_y = 50 ksi perimeter column M26-C1B1-RF transverse.

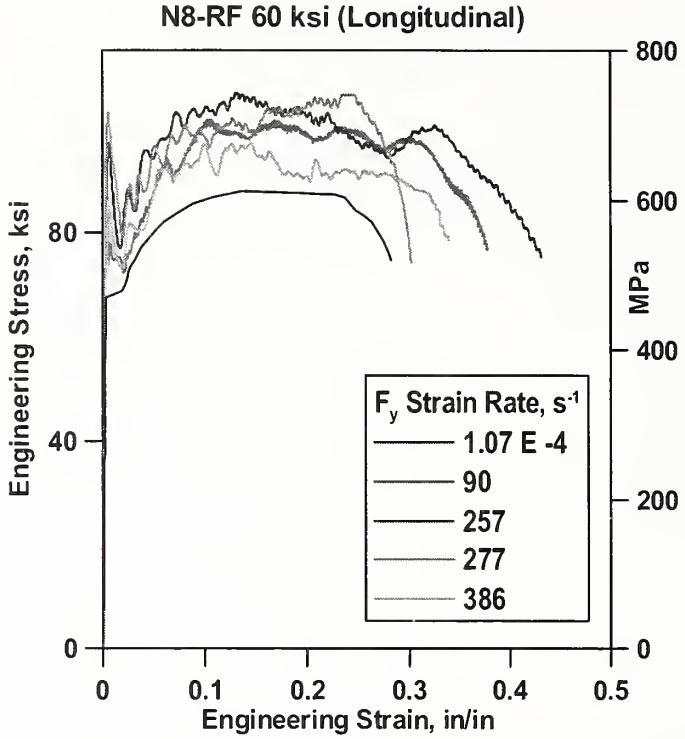

Figure A–30. Stress-strain curves for F_y = 60 ksi perimeter column N8-C1B1-RF longitudinal.

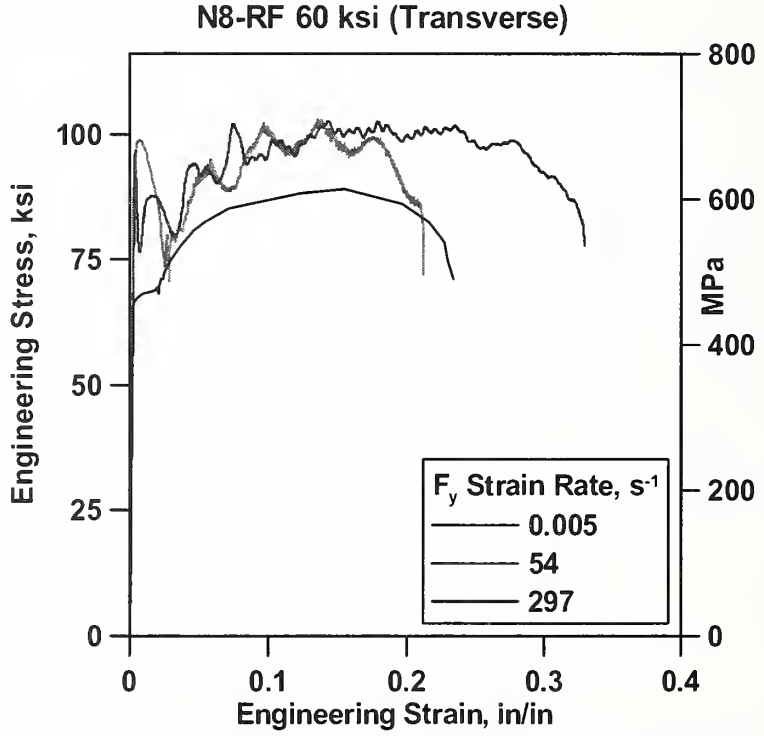

Figure A–31. Stress-strain curves for F_y = 60 ksi perimeter column N8-C1B1-C-RFtransverse.

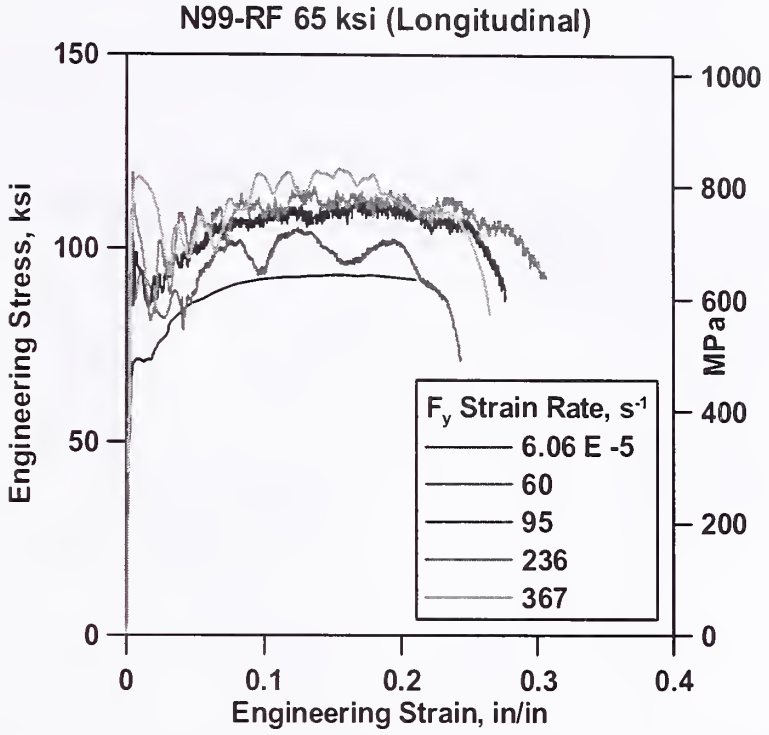

Figure A–32. Stress-strain curves for F_y = 65 ksi perimeter column N99-C3M1-RF longitudinal.

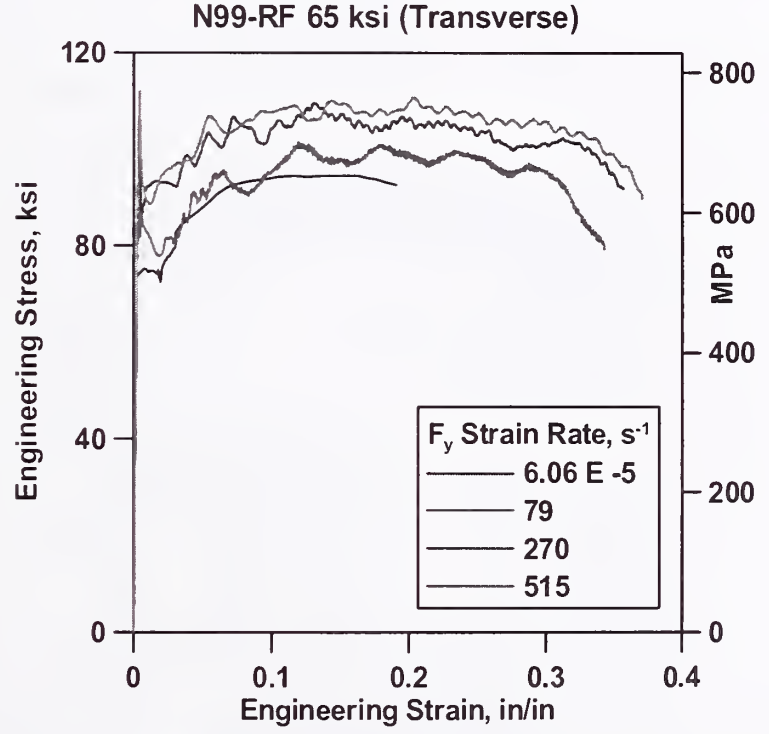

Figure A–33. Stress-strain curves for F_y = 65 ksi perimeter column N99-C3M1-RF transverse.

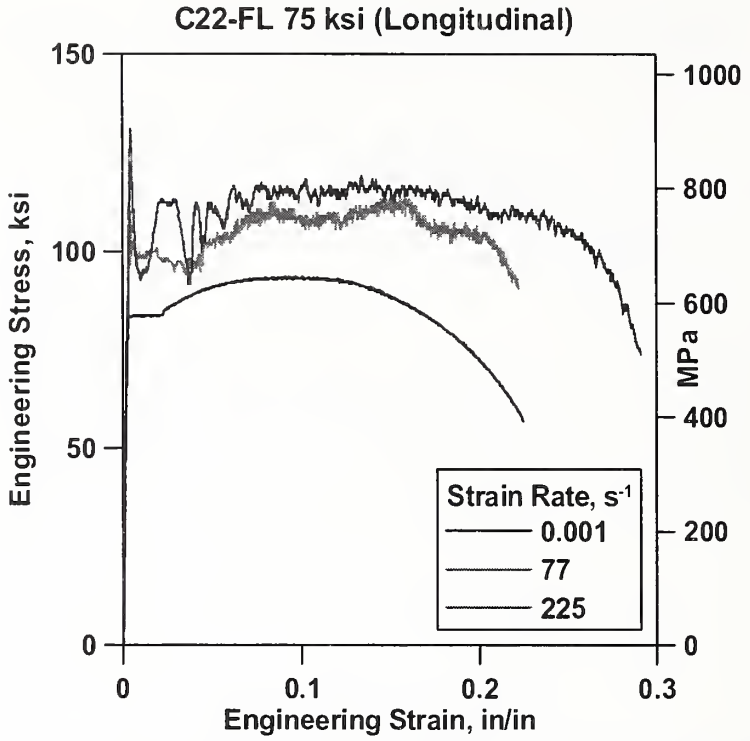

Figure A–34. Stress-strain curves for F_y = 75 ksi perimeter column C22-C2B-FL longitudinal.

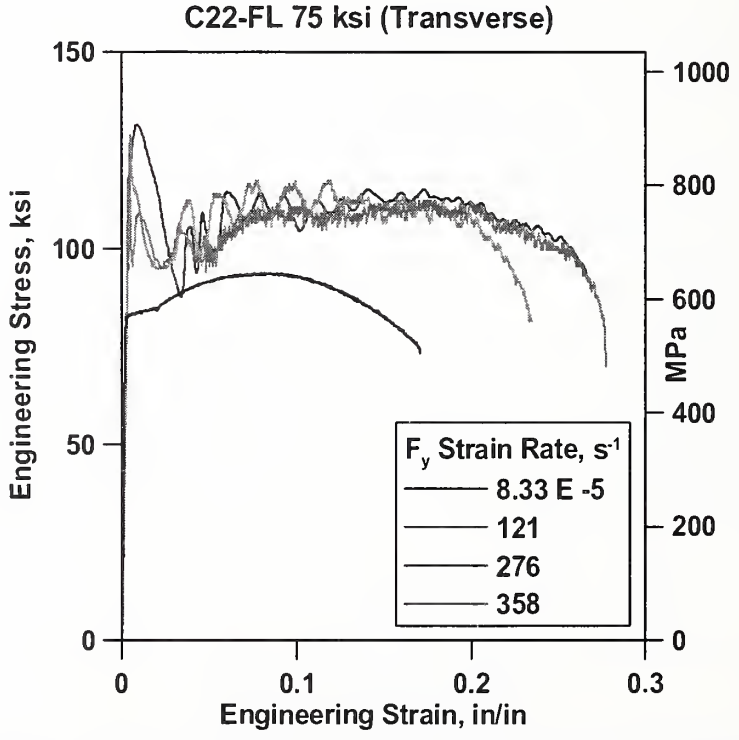

Figure A–35. Stress-strain curves for F_y = 75 ksi perimeter column C22-C2B-FL transverse.

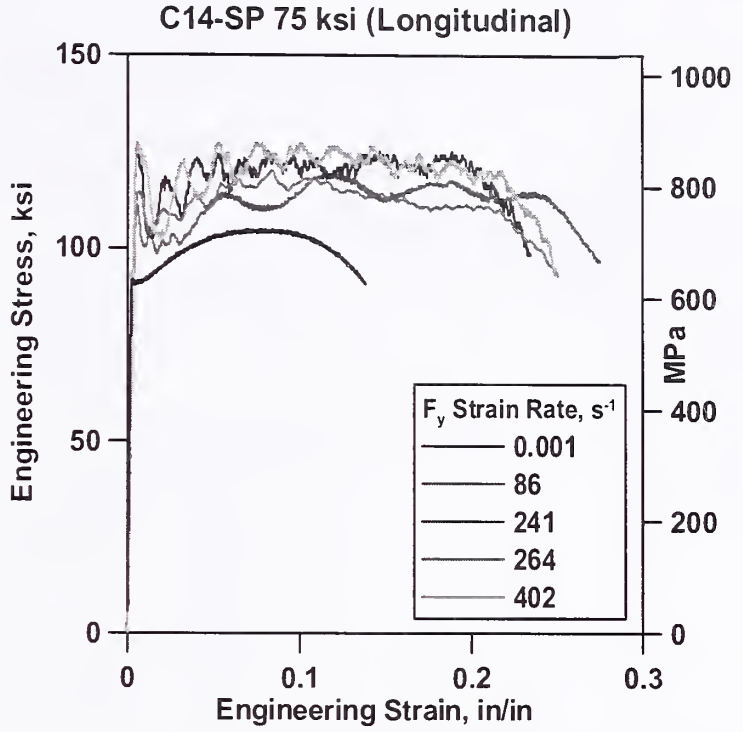

Figure A–36. Stress-strain curves for F_y = 75 ksi perimeter column spandrel C14-SP longitudinal.

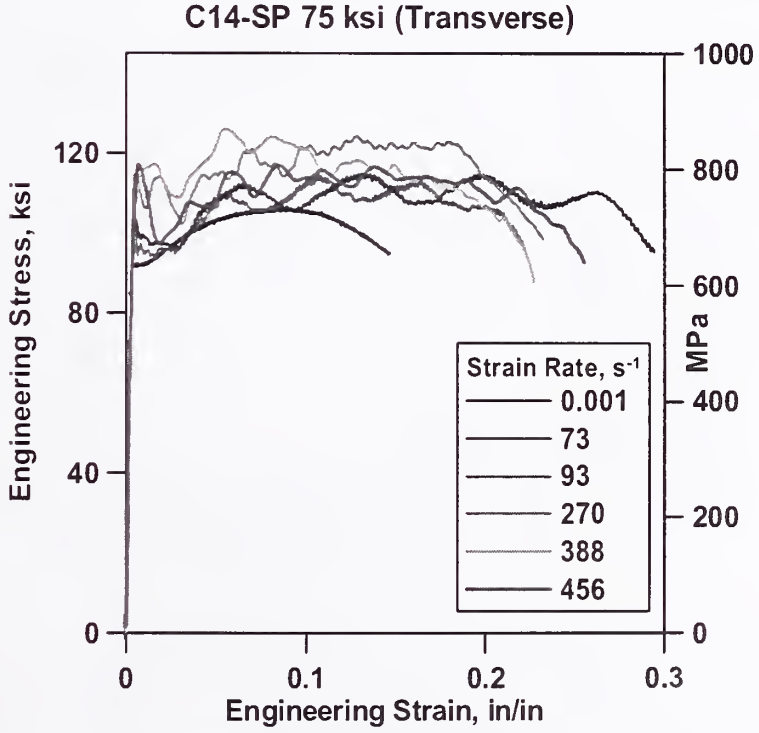

Figure A–37. Stress-strain curves for F_y = 75 ksi perimeter column spandrel C14-SP transverse.

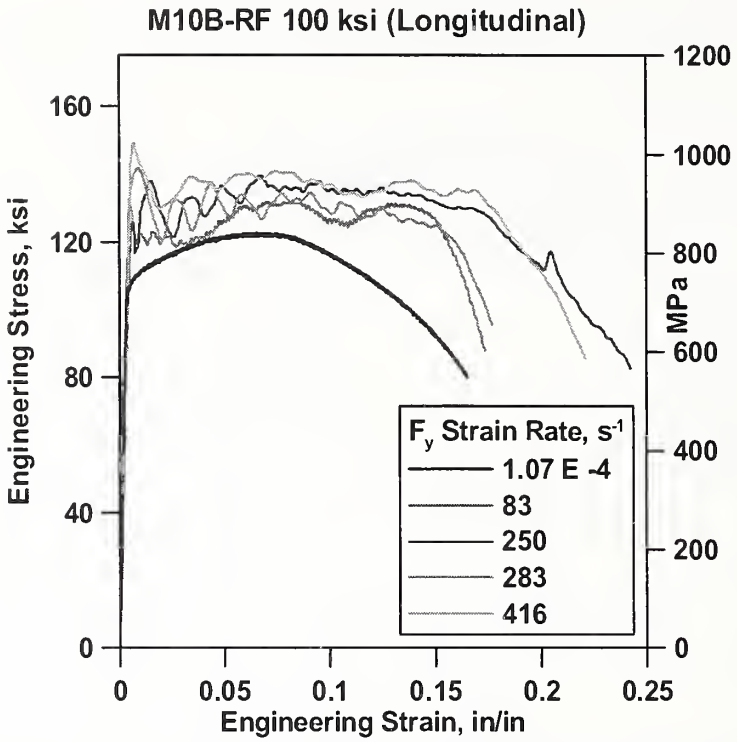

Figure A–38. Stress-strain curves for F_y = 100 ksi perimeter column M10B-C3B1-RF longitudinal.

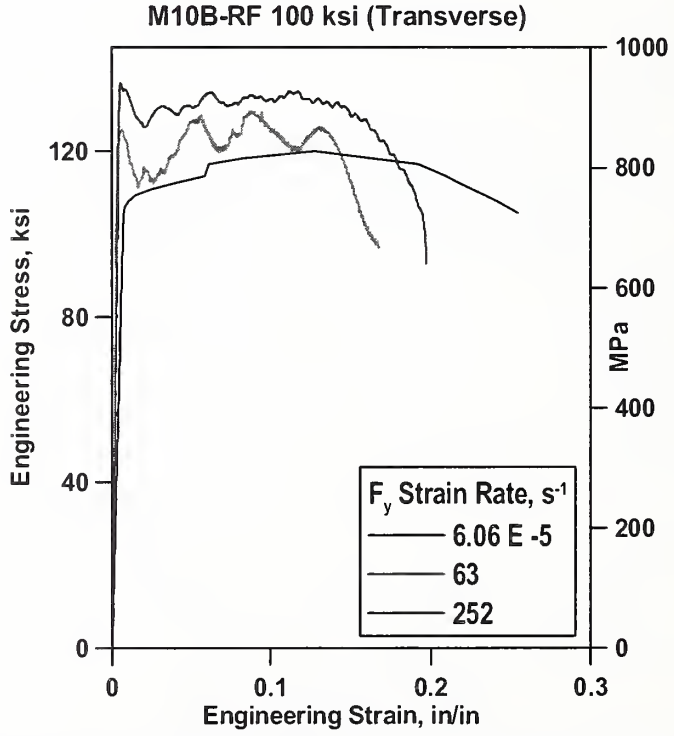

Figure A–39. Stress-strain curves for F_y = 100 ksi perimeter column M10B-C3B1-RF transverse.

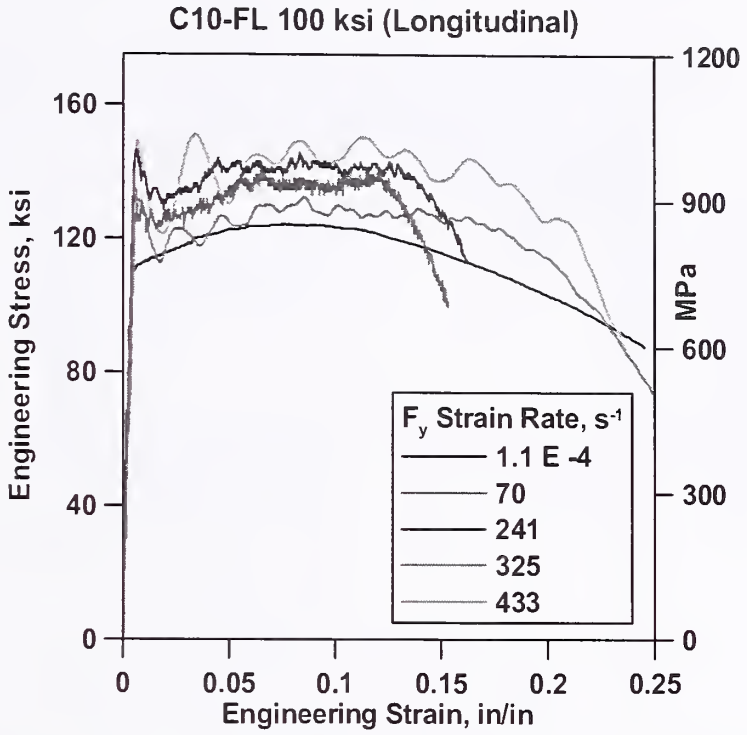

Figure A–40. Stress-strain curves for F_y = 100 ksi perimeter column C10-C1M1-FL longitudinal.

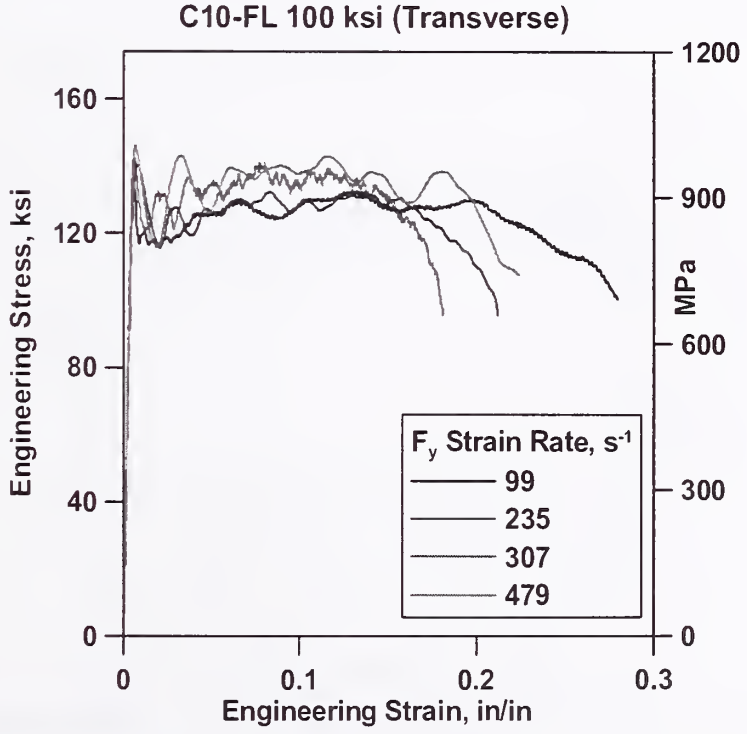

Figure A–41. Stress-strain curves for F_y = 100 ksi perimeter column C10-C1M1-FL transverse.

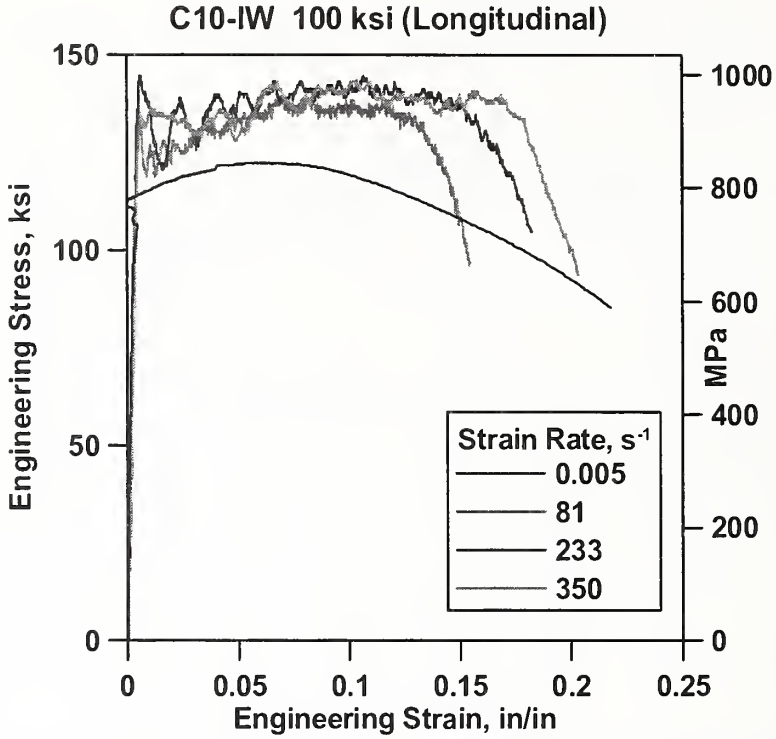

Figure A–42. Stress-strain curves for F_y = 100 ksi perimeter column C10-C1M1-IW longitudinal.

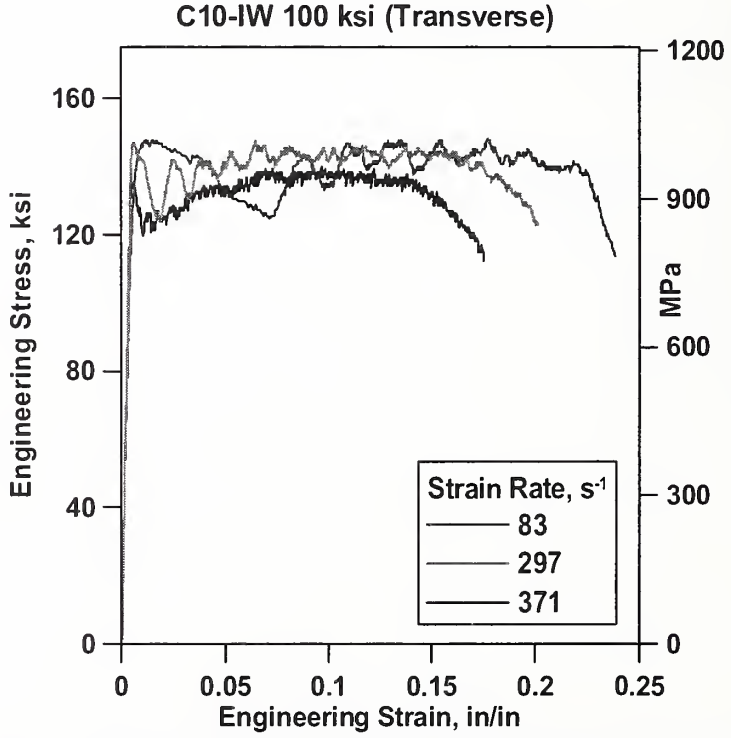

Figure A–43. Stress-strain curves for F_y = 100 ksi perimeter column C10-C1M1-IW transverse.

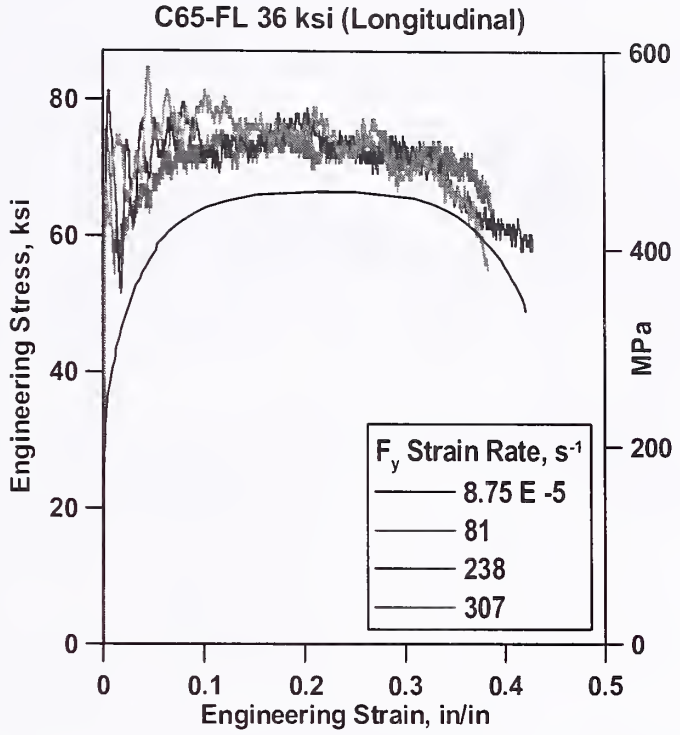

Figure A–44. Stress-strain curves for F_y = 36 ksi core wide-flange C65-FL longitudinal.

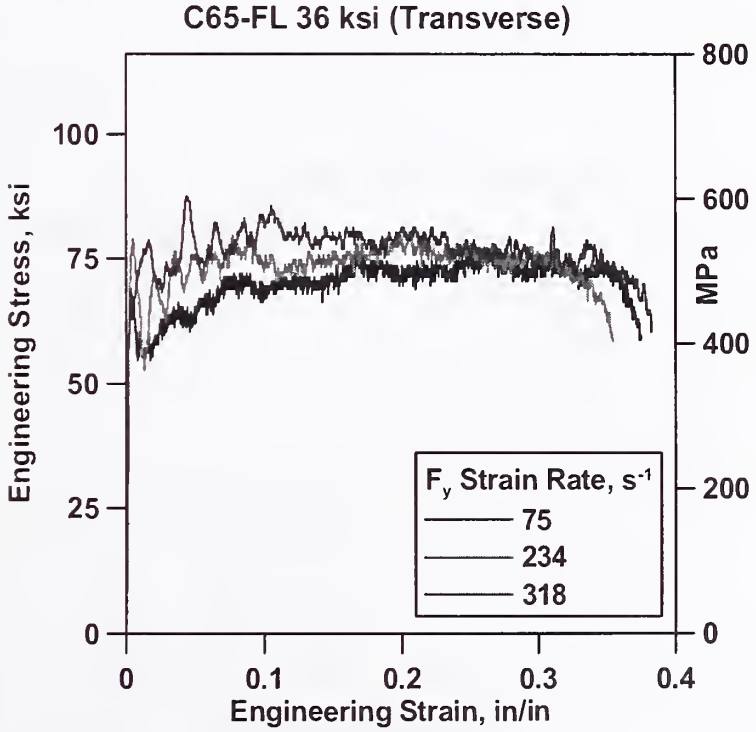

Figure A–45. Stress-strain curves for F_y = 36 ksi core wide-flange C65-FL transverse.

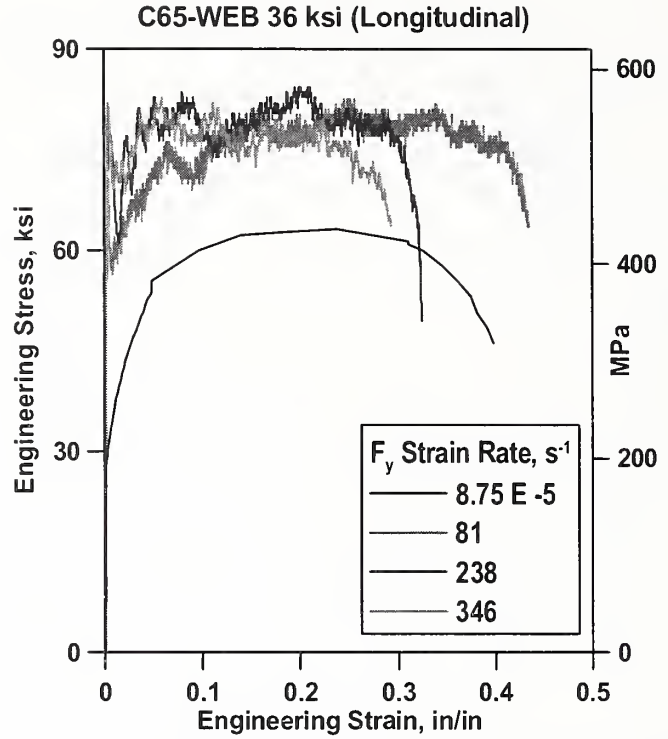

Figure A–46. Stress-strain curves for F_y = 36 ksi core wide-flange C65-WEB longitudinal.

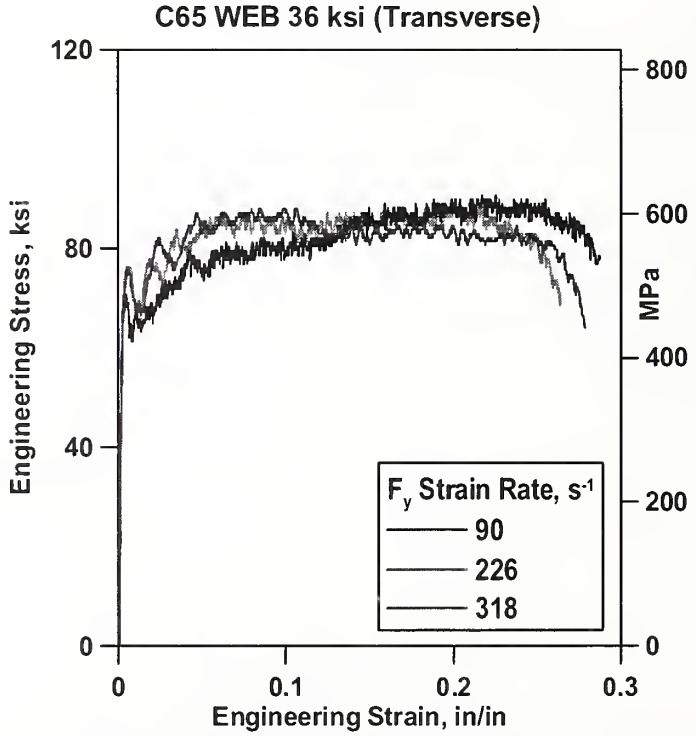

Figure A–47. Stress-strain curves for F_y = 36 ksi core wide-flange C65-WEB transverse.

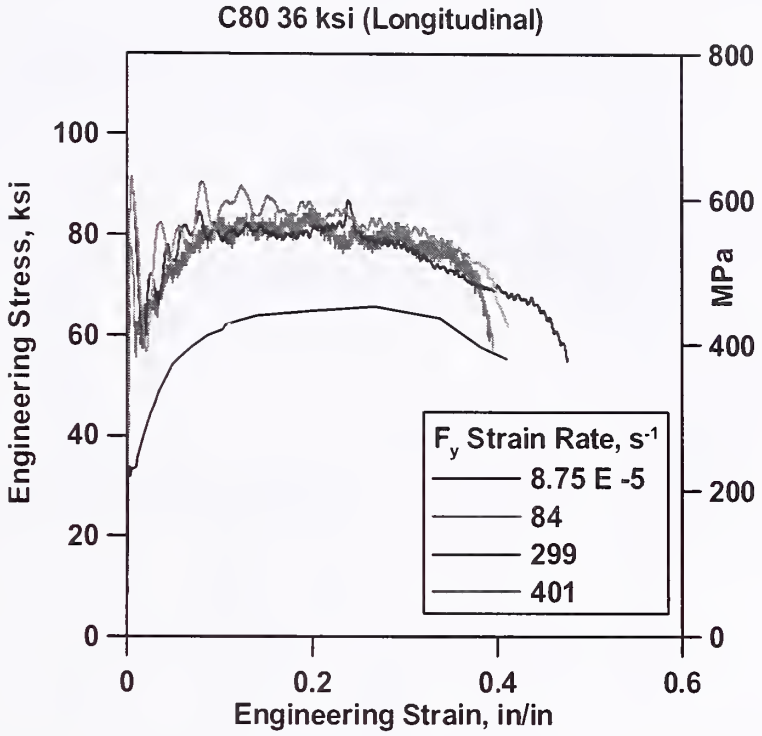

Figure A–48. Stress-strain curves for F_y = 36 ksi core wide-flange C80-A longitudinal.

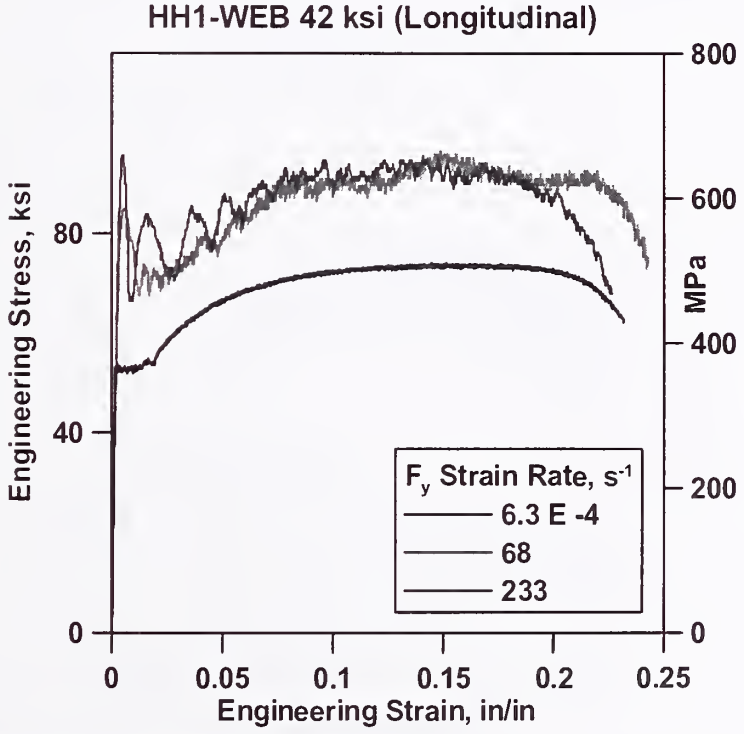

Figure A–49. Stress-strain curves for F_y = 42 ksi core wide-flange HH1-WEB longitudinal.

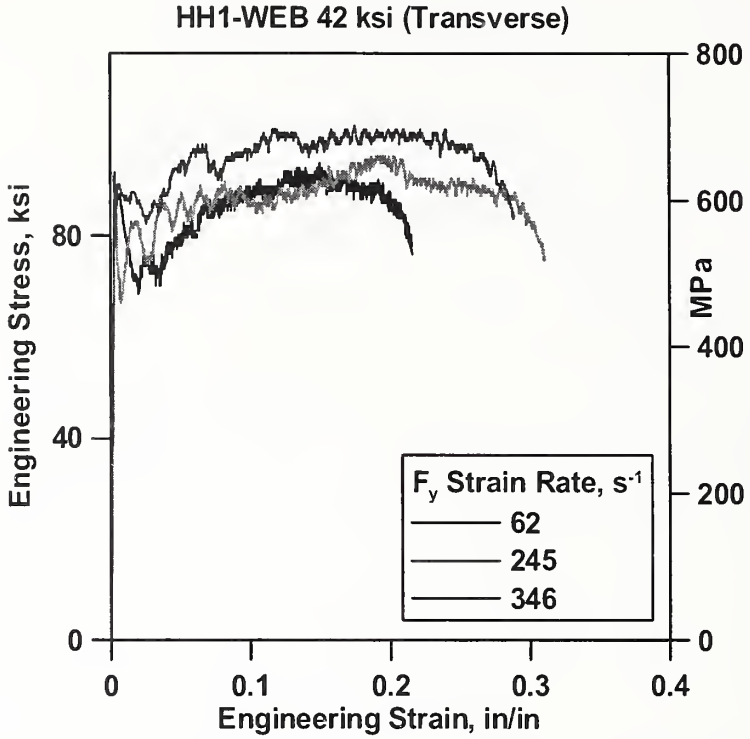

Figure A–50. Stress-strain curves for F_y = 42 ksi core wide-flange HH1-WEB transverse.

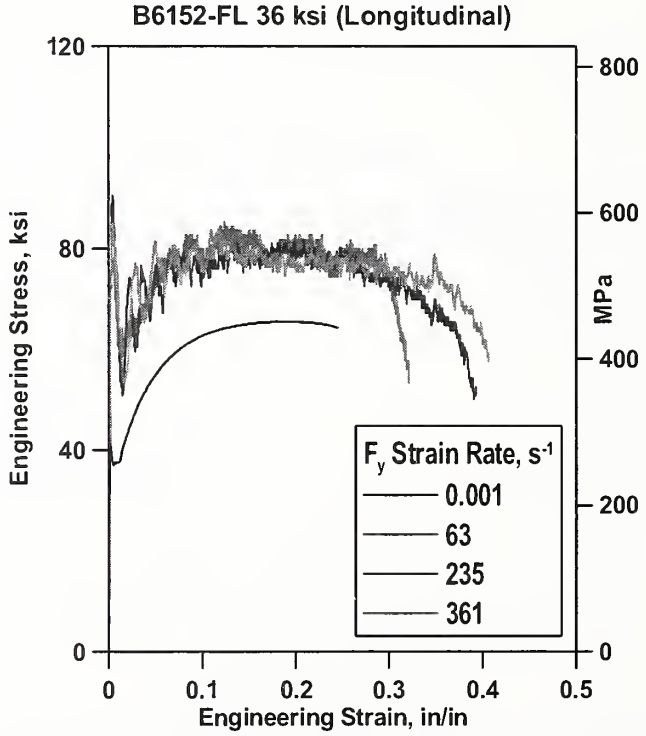

Figure A–51. Stress-strain curves for F_y = 36 ksi core box column B6152-FL longitudinal.

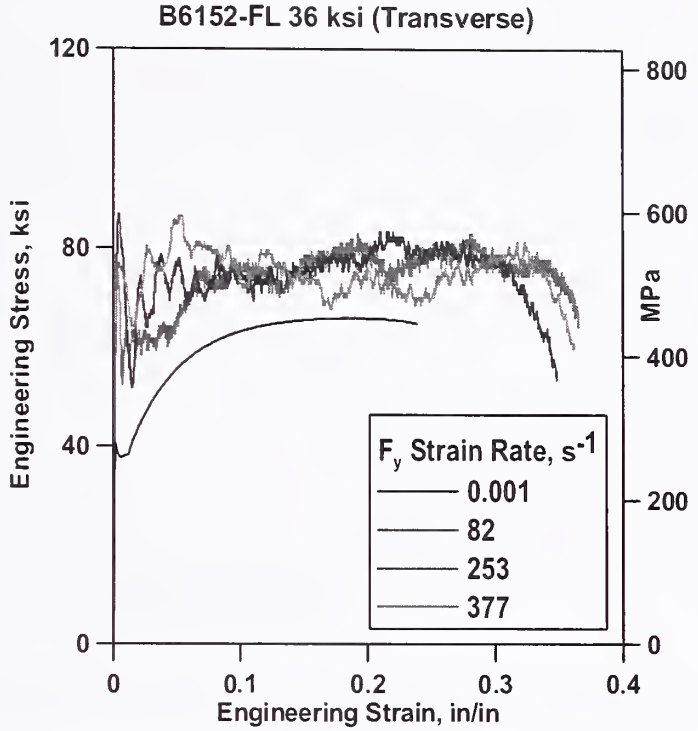

Figure A–52. Stress-strain curves for F_y = 36 ksi core box column B6152-FL transverse.

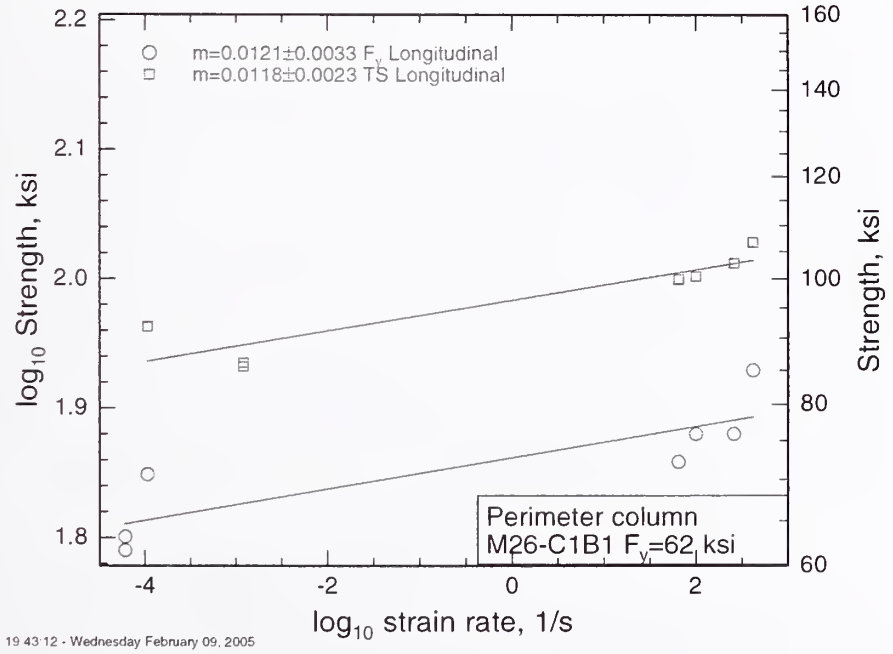

Figure A–53. Strain rate sensitivity for F_y = 50 ksi perimeter column M26-C1-RF longitudinal.

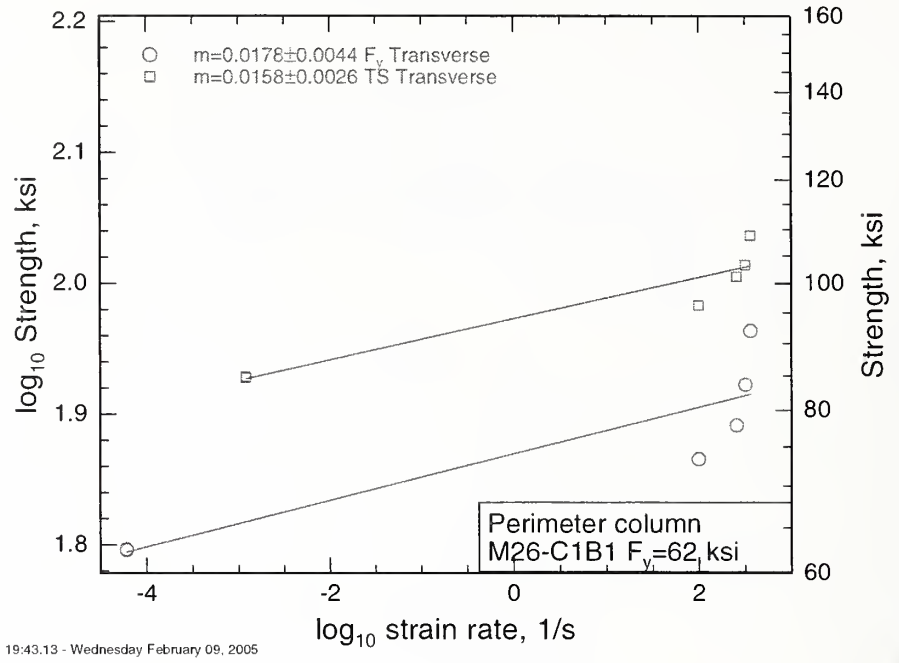

Figure A–54. Strain rate sensitivity for F_y = 50 ksi perimeter column M26-C1-RF transverse.

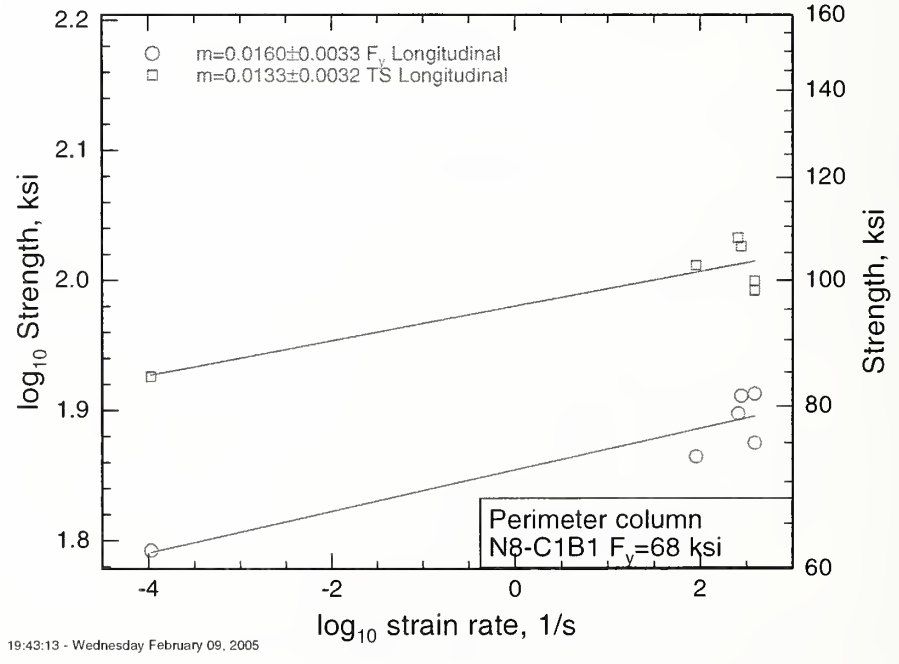

Figure A–55. Strain rate sensitivity for F_y = 60 ksi perimeter column N8-C1-RF longitudinal.

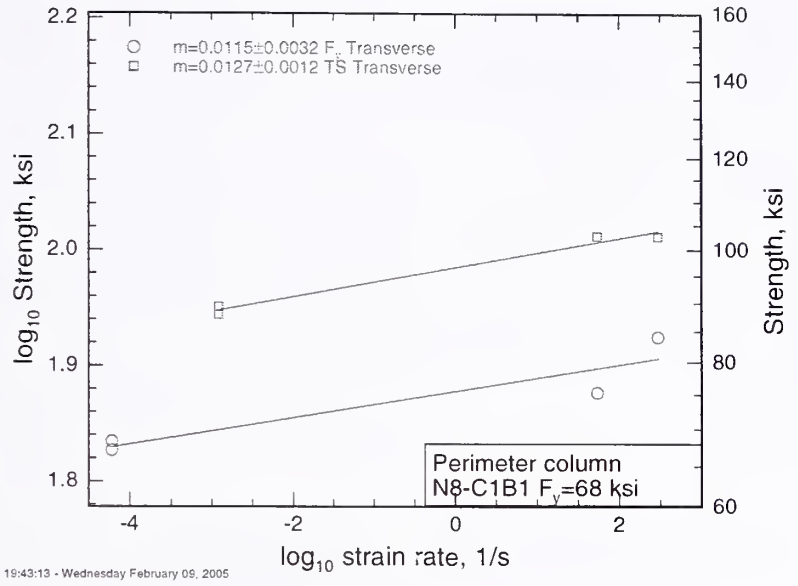

Figure A–56. Strain rate sensitivity for F_y = 60 ksi perimeter column N8-C1-RF transverse.

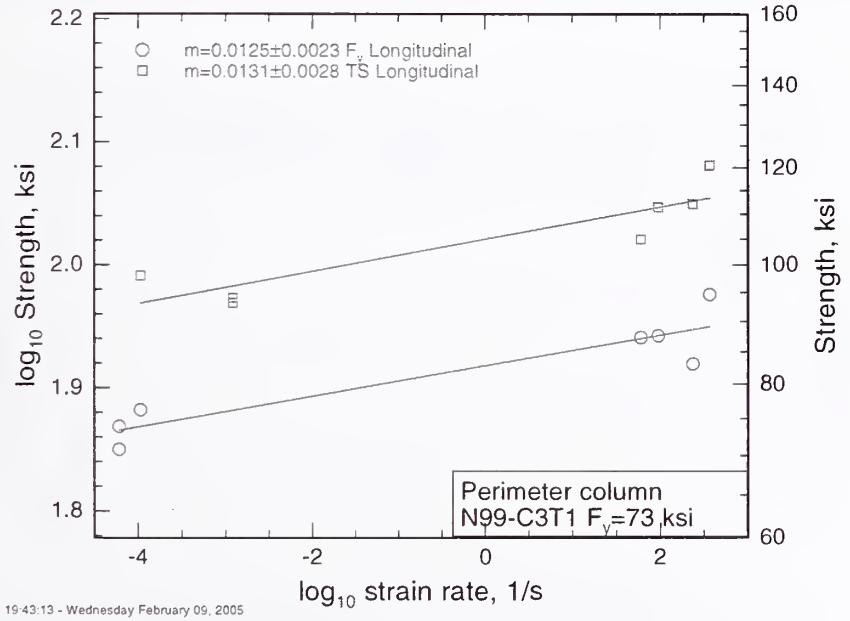

Figure A–57. Strain rate sensitivity for F_y = 65 ksi perimeter column N99-C3-RF longitudinal.

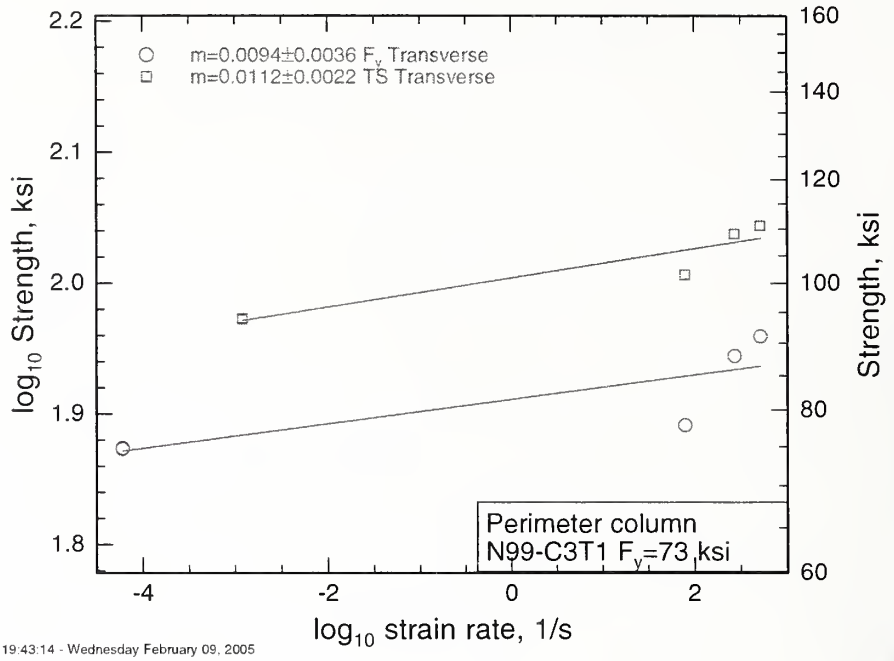

Figure A–58. Strain rate sensitivity for F_y = 65 ksi perimeter column N99-C3-RF transverse.

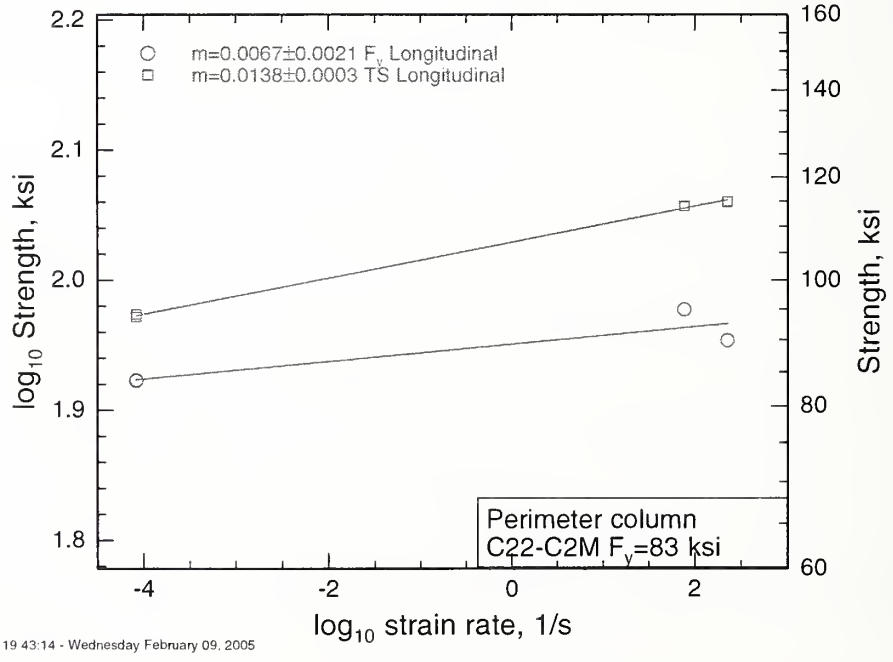

Figure A–59. Strain rate sensitivity for F_y = 75 ksi perimeter column C22-C2M-FL longitudinal

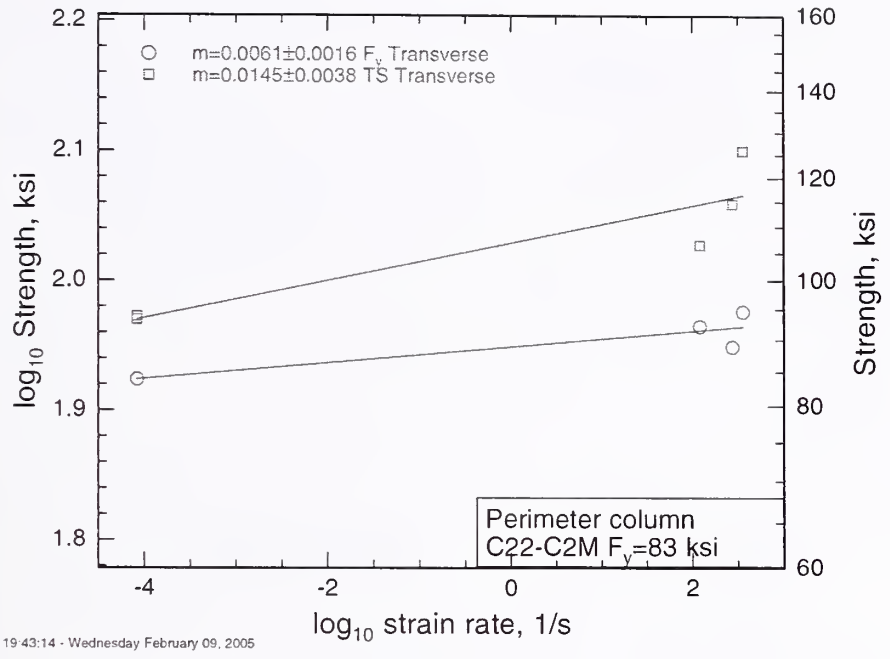

Figure A–60. Strain rate sensitivity for F_y = 75 ksi perimeter column C22-C2M-FL transverse.

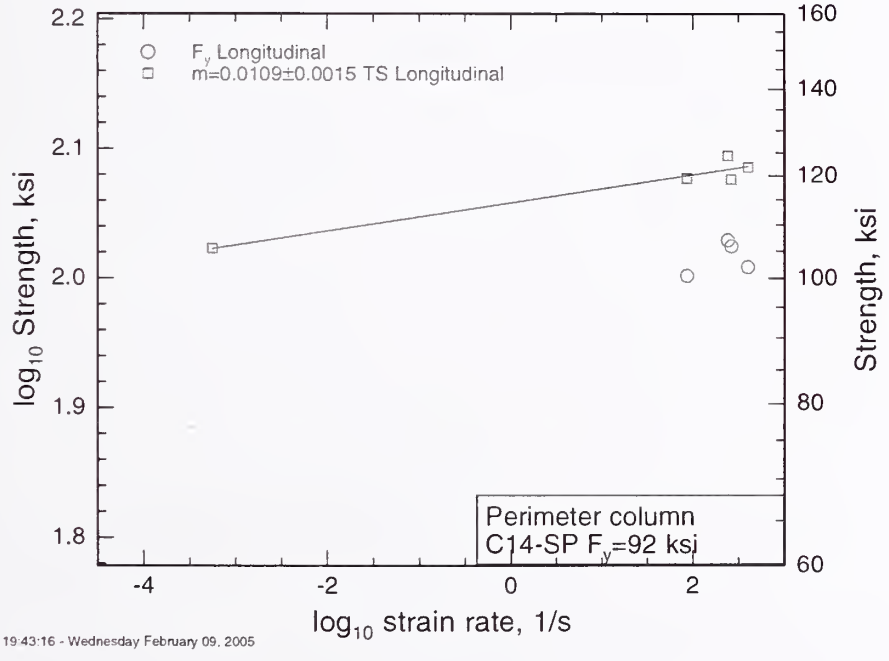

Figure A–61. Strain rate sensitivity for F_y = 75 ksi perimeter spandrel C14-SP-longitudinal.

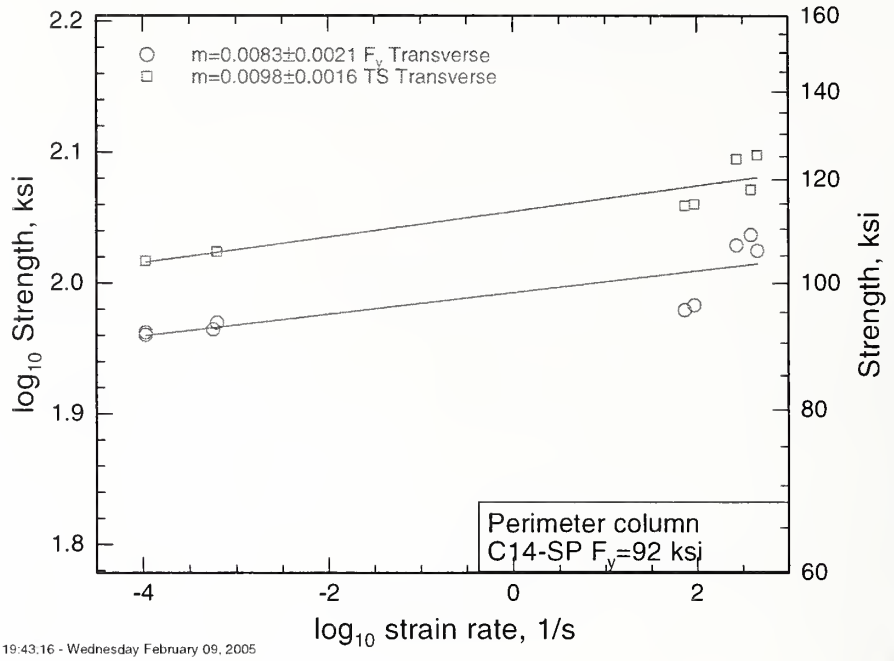

Figure A–62. Strain rate sensitivity for F_y = 75 ksi perimeter spandrel C14-SP transverse.

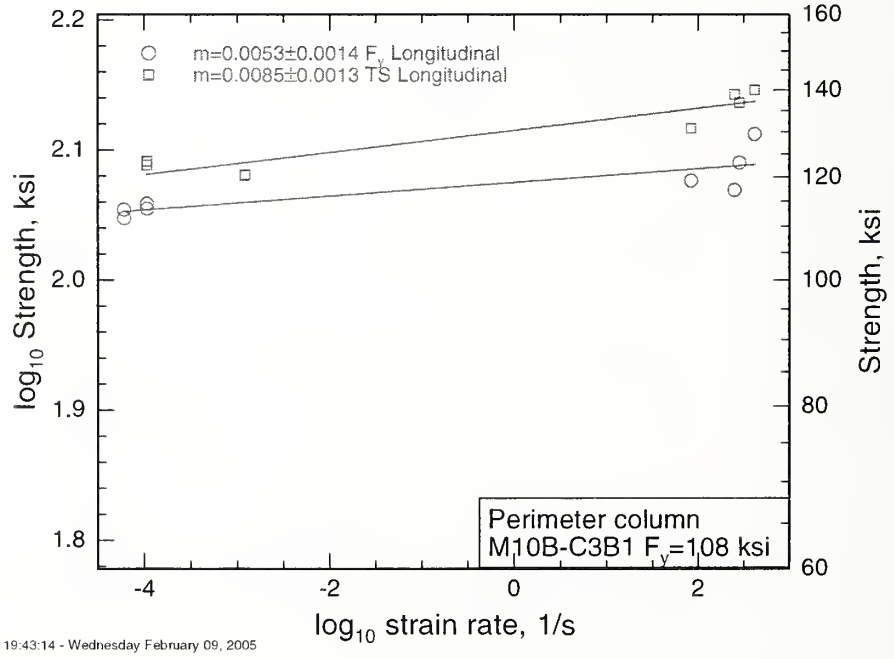

Figure A–63. Strain rate sensitivity for F_y = 100 ksi perimeter column M10B-C3B-RF longitudinal.

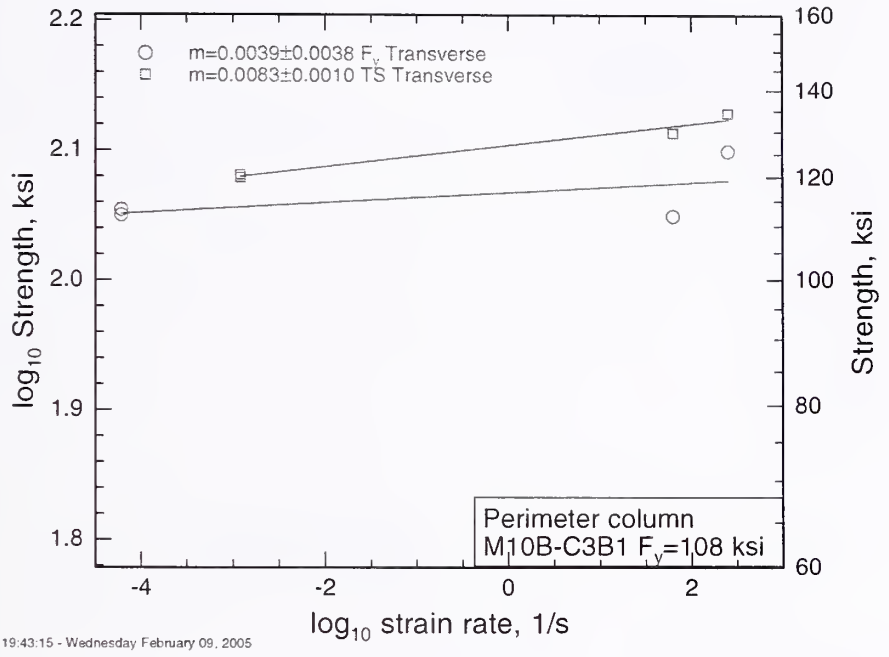

Figure A–64. Strain rate sensitivity for F_y = 100 ksi perimeter column M10B-C3B-RF-transverse.

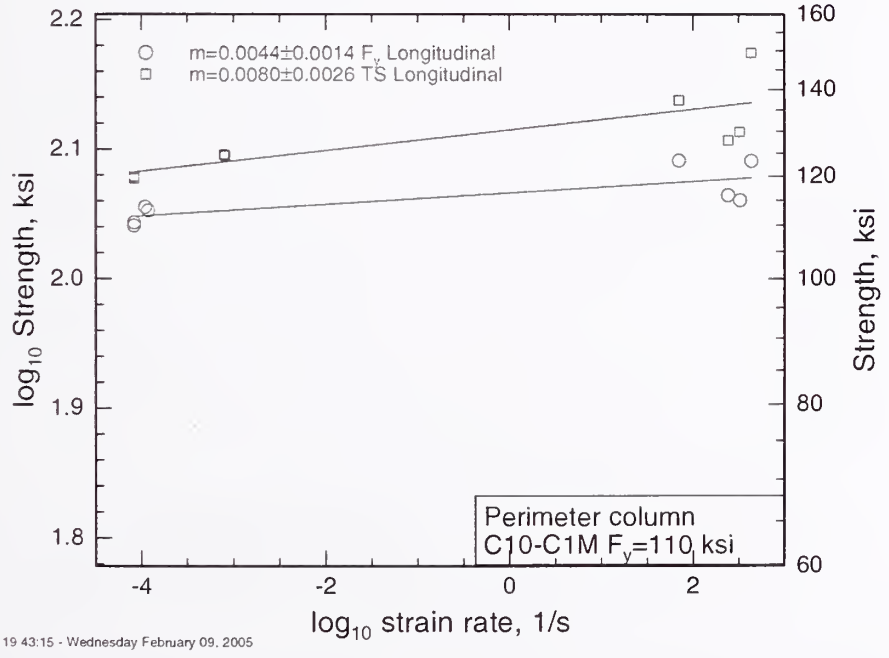

Figure A–65. Strain rate sensitivity for F_y = 100 ksi perimeter column C10-C1M1-FL longitudinal.

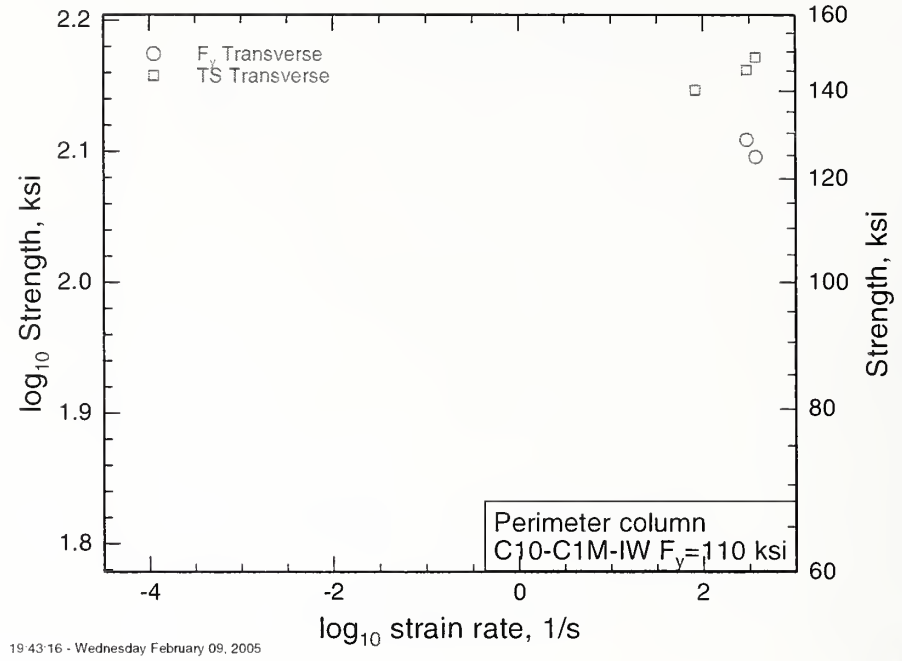

Figure A–66. Strain rate sensitivity for F_y = 100 ksi perimeter column C10-C1M1-FL transverse.

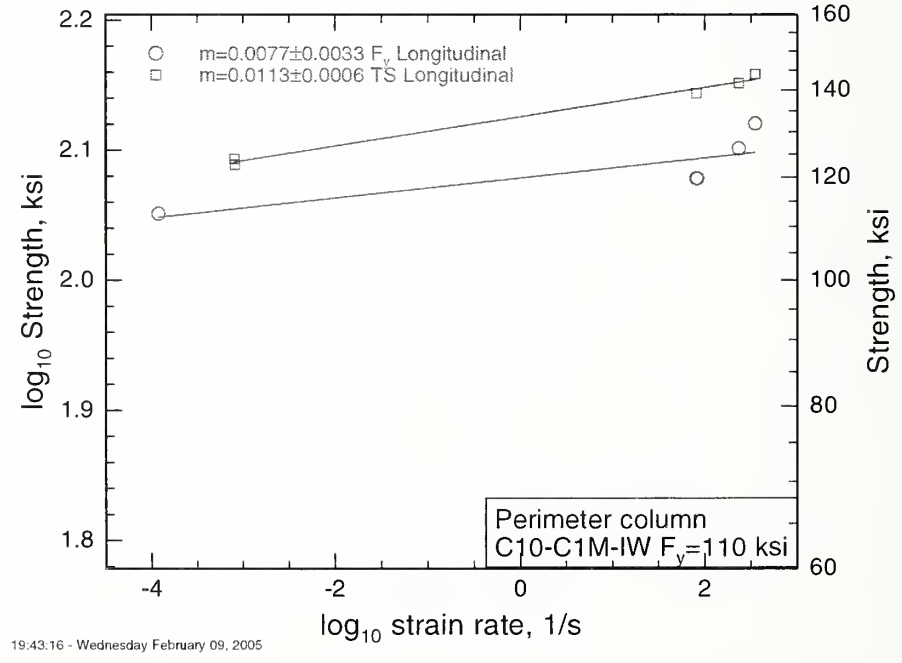

Figure A–67. Strain rate sensitivity for F_y = 100 ksi perimeter column C10-C1M1-IW-longitudinal.

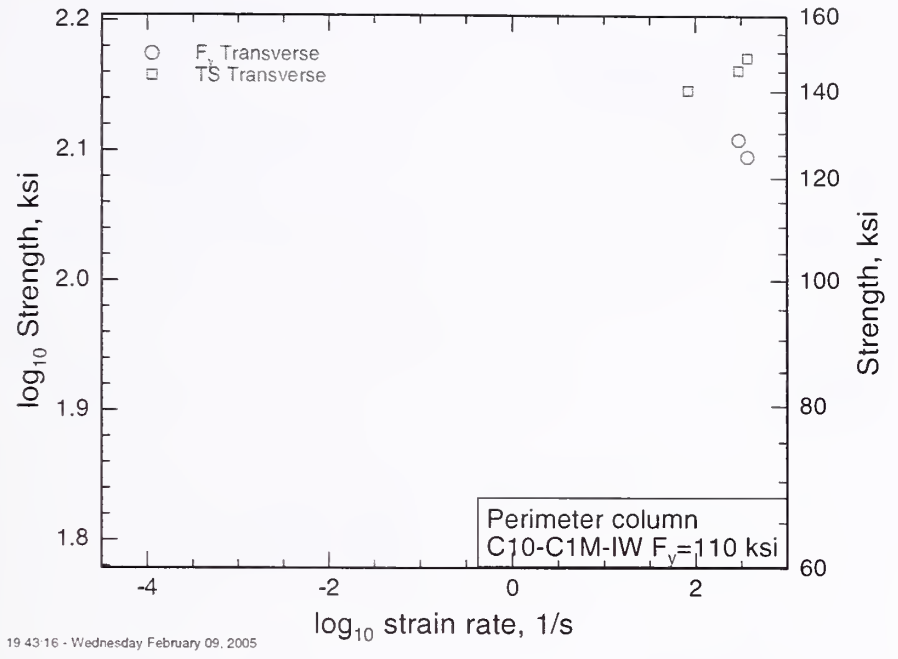

Figure A–68. Strain rate sensitivity for F_y = 100 ksi perimeter column C10-C1M1-IW transverse.

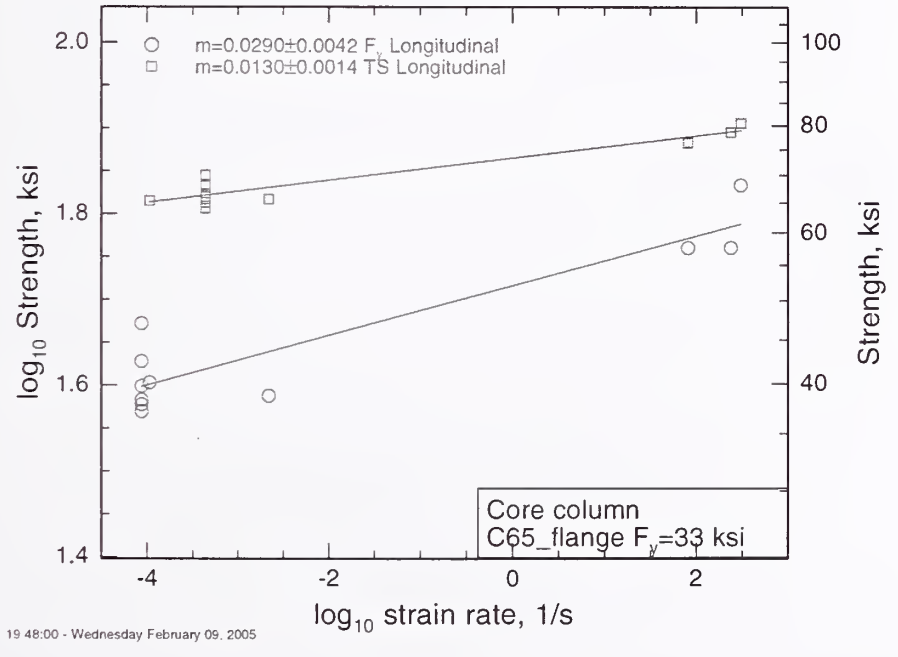

Figure A–69. Strain rate sensitivity for F_y = 36 ksi core wide-flange C65-FL longitudinal.

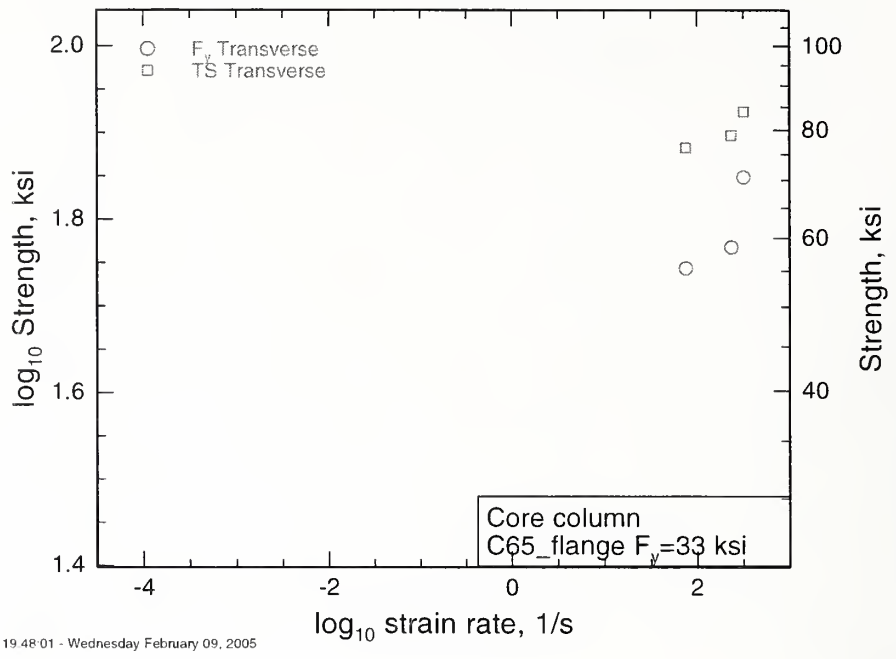

Figure A–70. Strain rate sensitivity for F_y = 36 ksi core wide-flange C65-FL transverse.

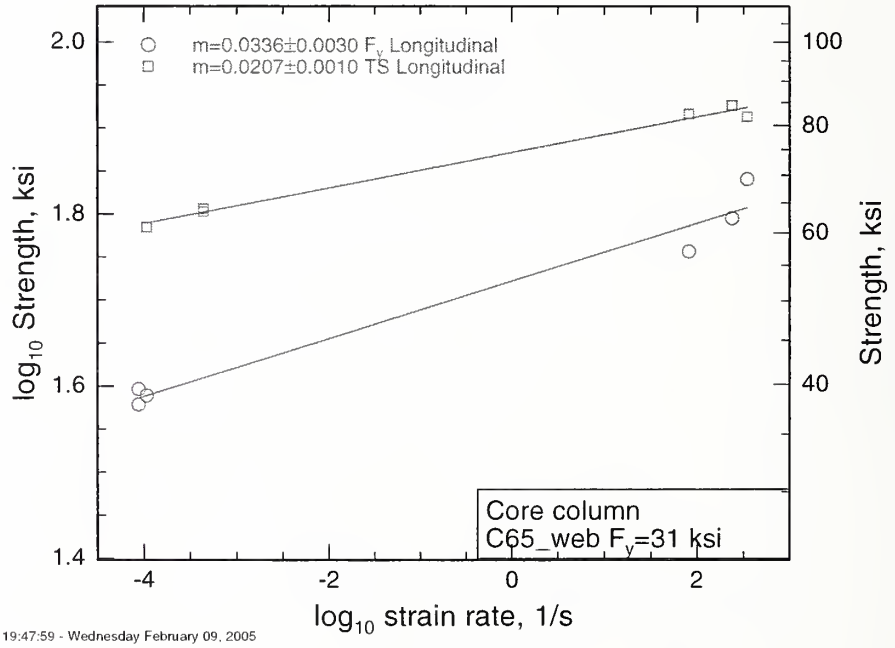

Figure A–71. Strain rate sensitivity for F_y = 36 ksi core wide-flange C65-WEB longitudinal

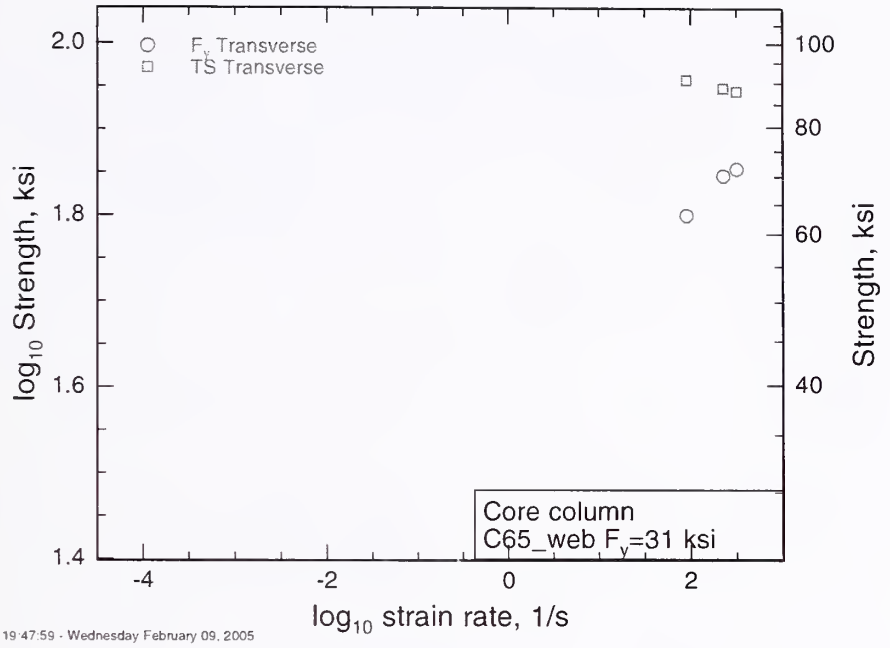

Figure A–72. Strain rate sensitivity for F_y = 36 ksi core wide-flange C65-WEB transverse.

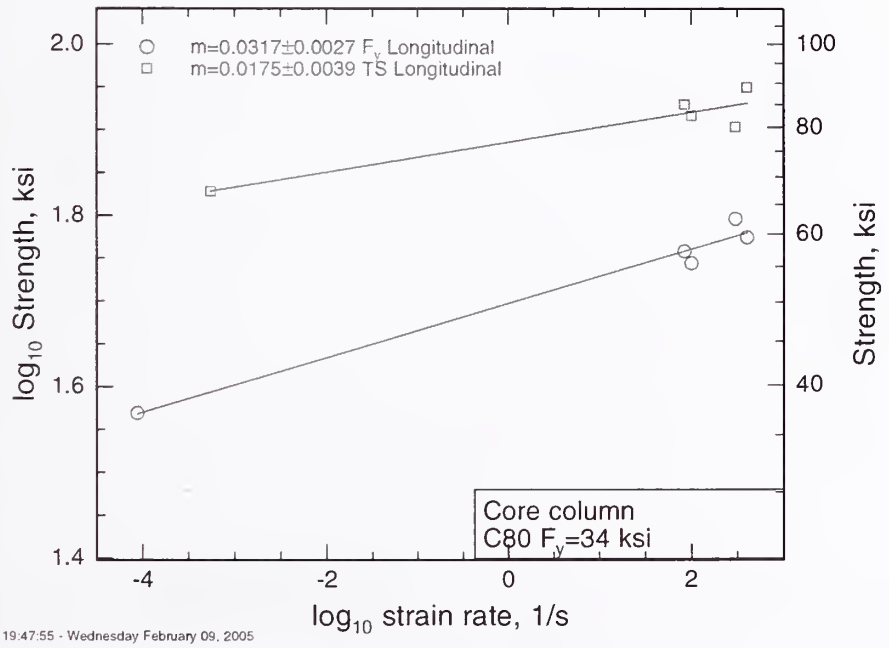

Figure A–73. Strain rate sensitivity for F_y = 36 ksi core wide-flange C80 longitudinal.

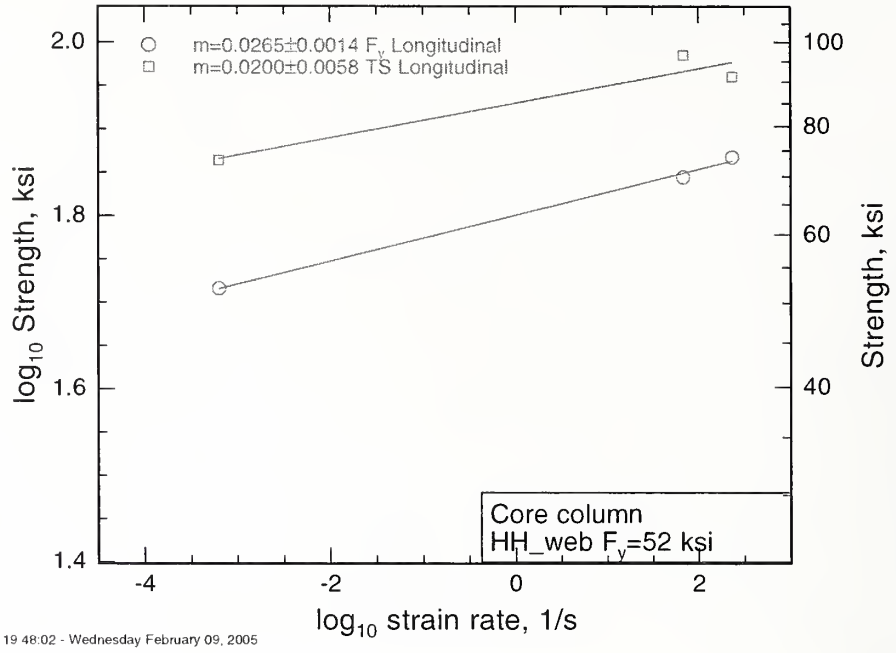

Figure A–74. Strain rate sensitivity for F_y = 42 ksi core wide-flange HH1-WEB longitudinal.

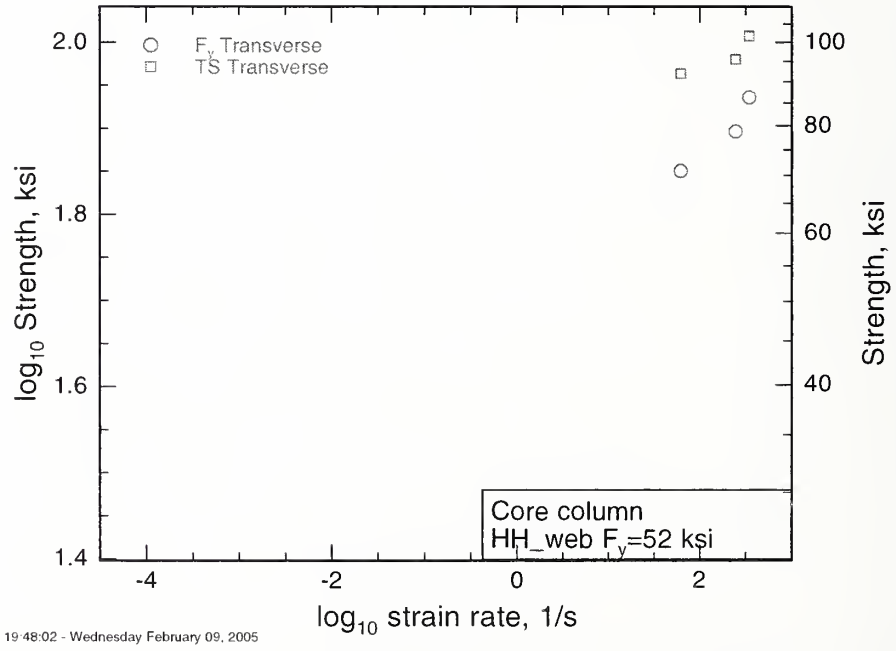

Figure A–75. Strain rate sensitivity for F_y = 42 ksi core wide-flange HH1-WEB transverse.

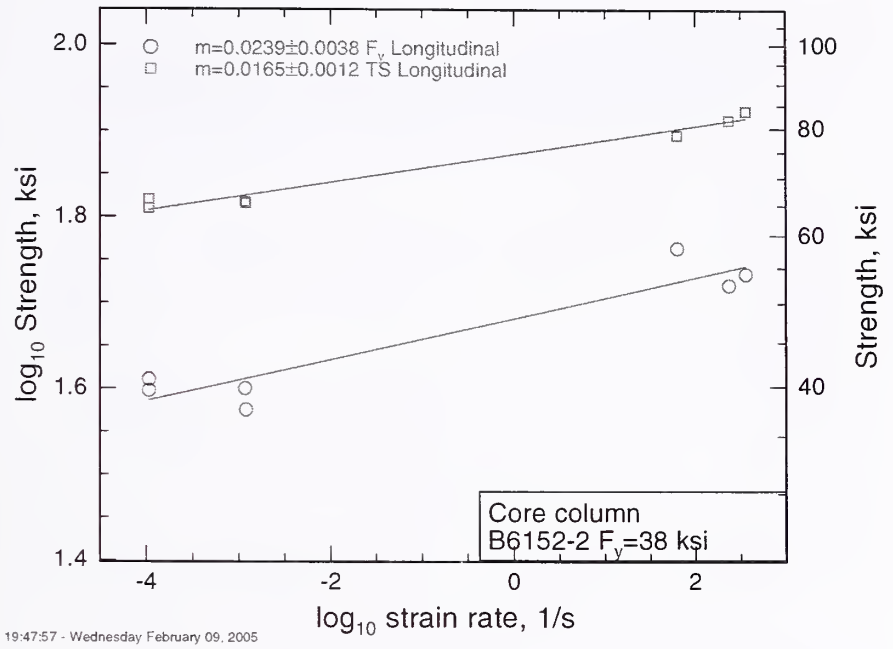

Figure A–76. Strain rate sensitivity for F_y = 36 ksi box column B6152-FL longitudinal.

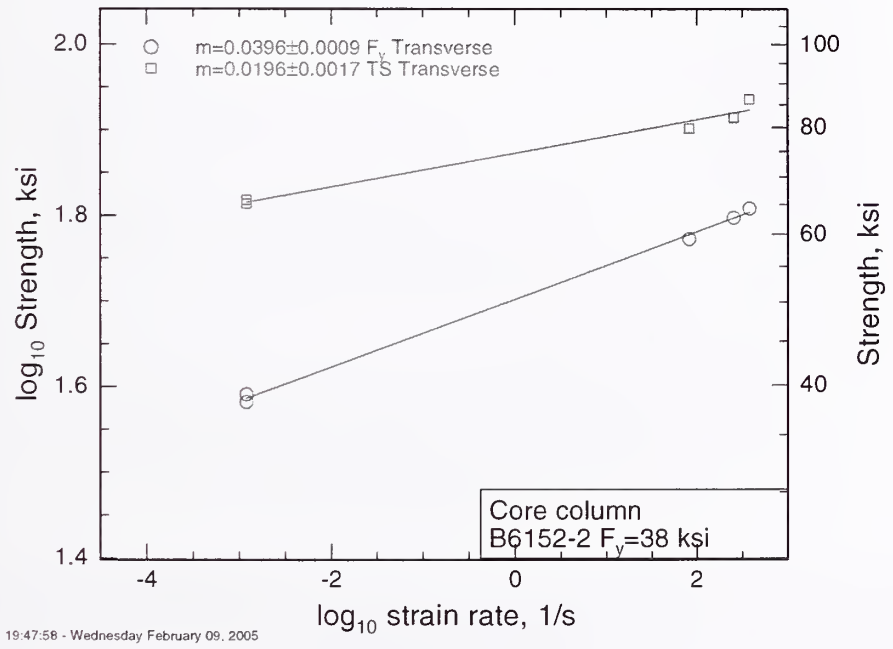

Figure A–77. Strain rate sensitivity for F_y = 36 ksi box column B6152-FL transverse.

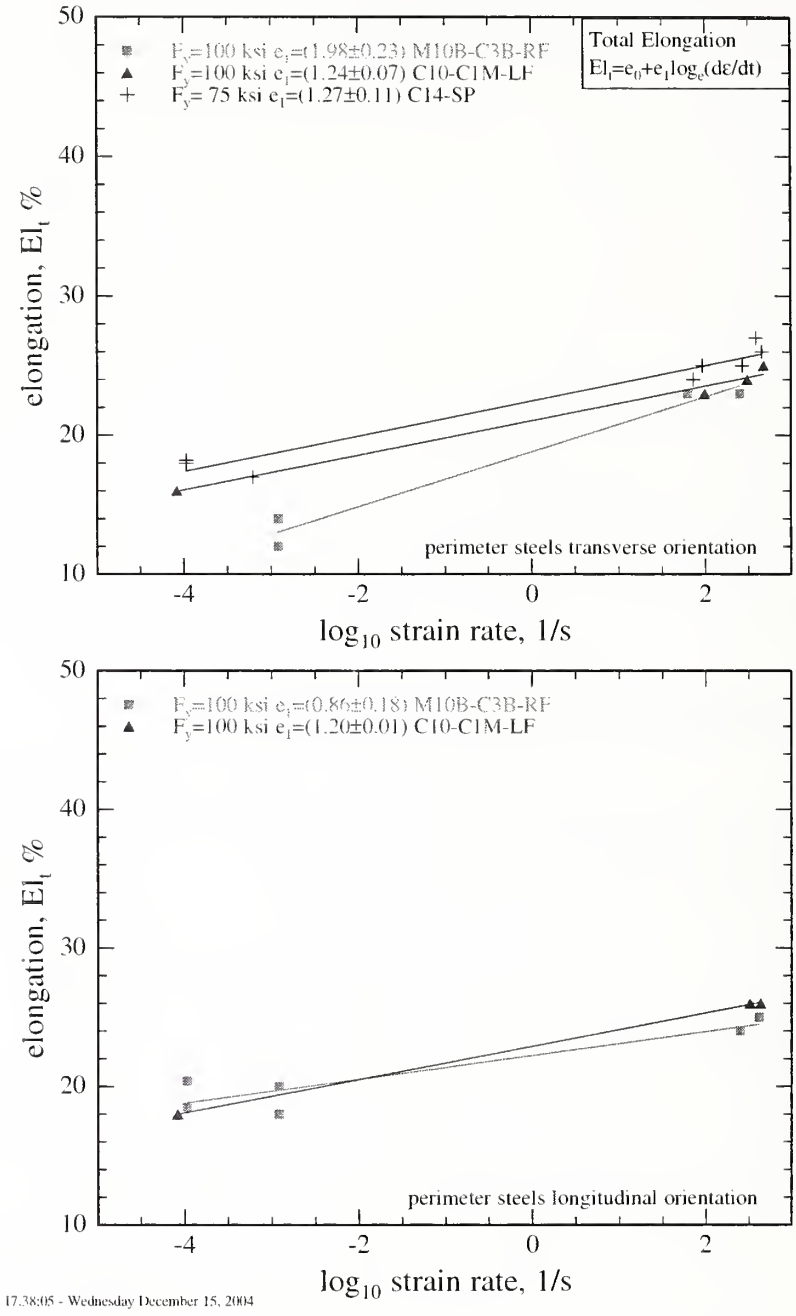

Figure A–78. Dependence of total elongation, El_t, on strain rate for high-strength perimeter columns.

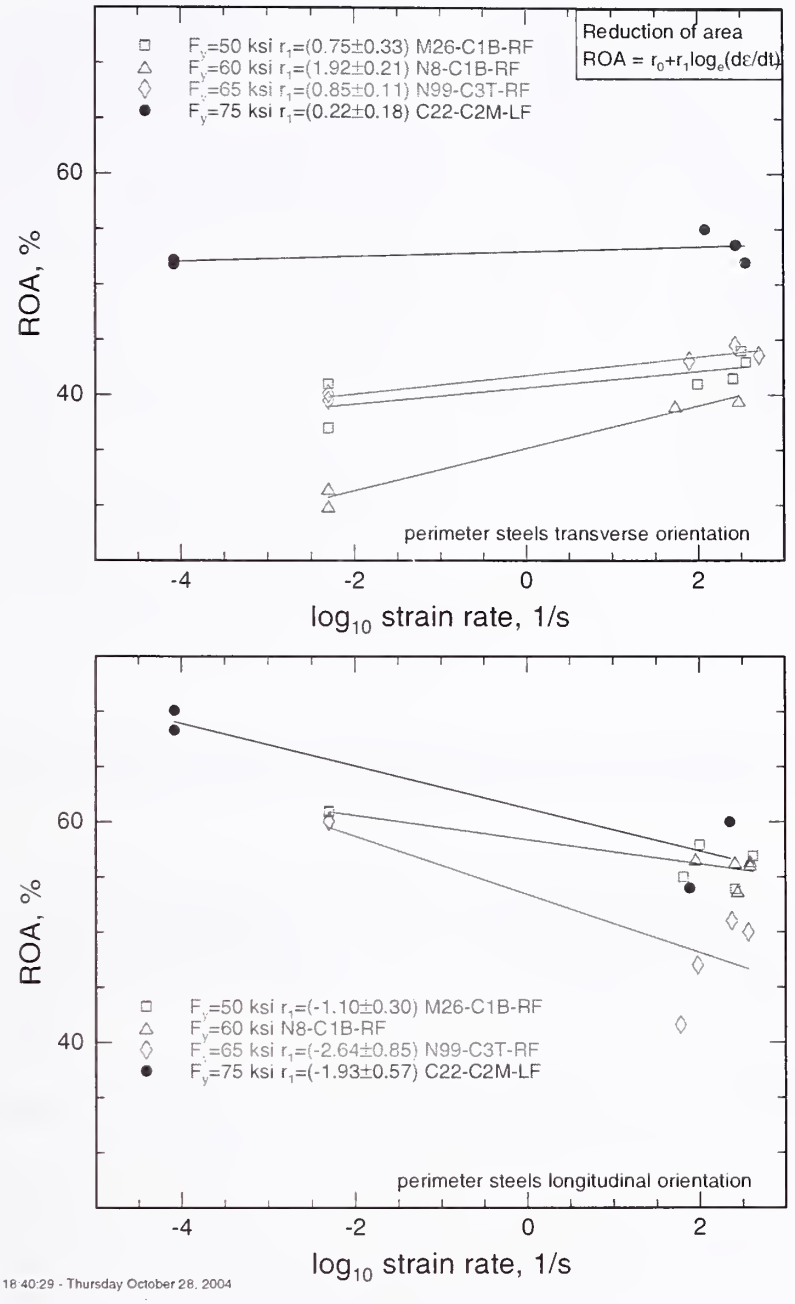

Figure A–79. Dependence of total elongation, El_t, on strain rate for low-strength perimeter columns.

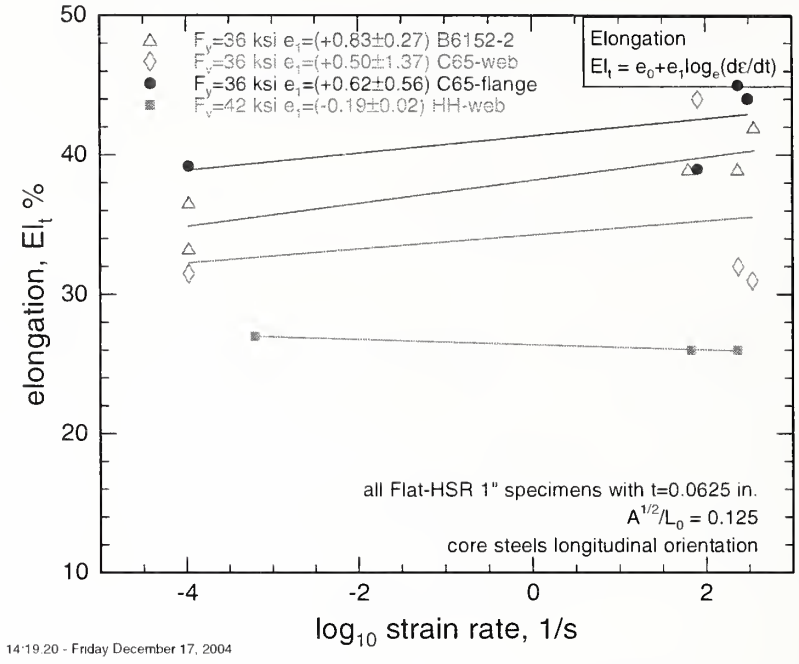

Figure A–80. Dependence of total elongation, El_t, on strain rate for core columns.

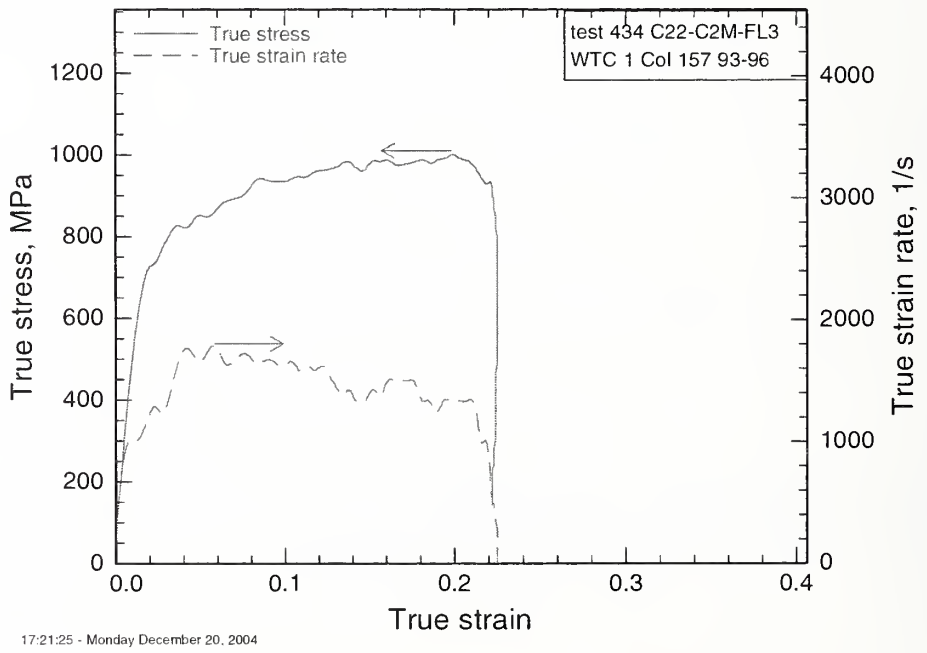

Figure A–81. Kolsky-test stress-strain behavior for F_y = 75 ksi perimeter column C22-C2M.

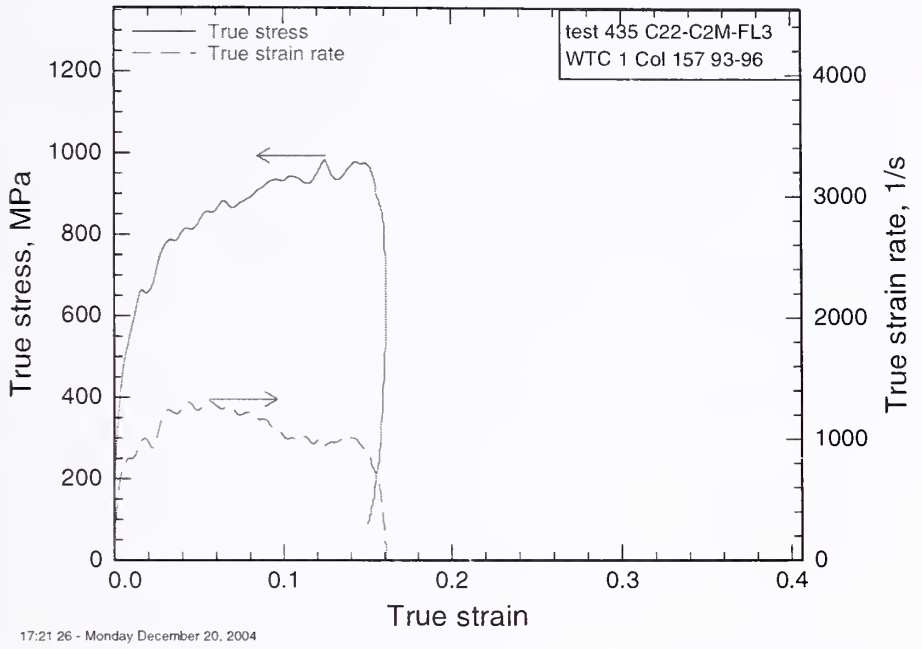

Figure A–82. Kolsky-test stress-strain behavior for F_y = 75 ksi perimeter column C22-C2M.

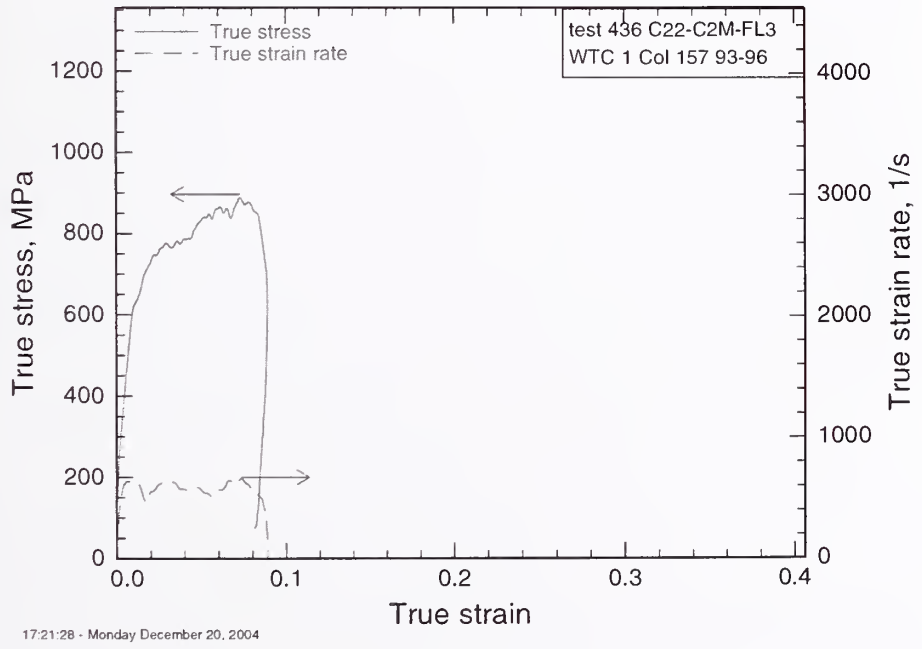

Figure A–83. Kolsky-test stress-strain behavior for F_y = 75 ksi perimeter column C22-C2M.

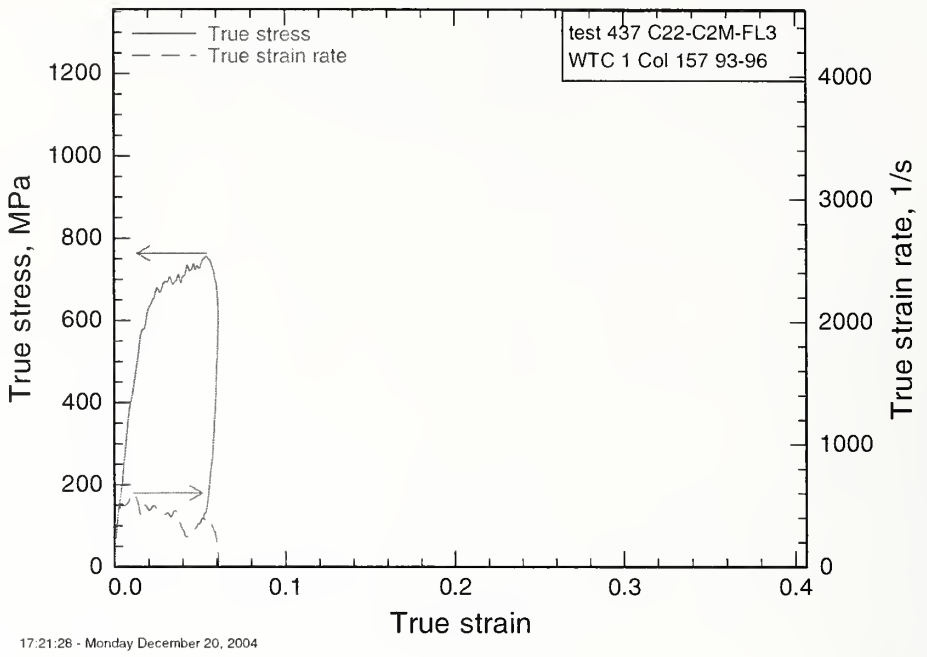

Figure A–84. Kolsky-test stress-strain behavior for F_y = 75 ksi perimeter column C22-C2M.

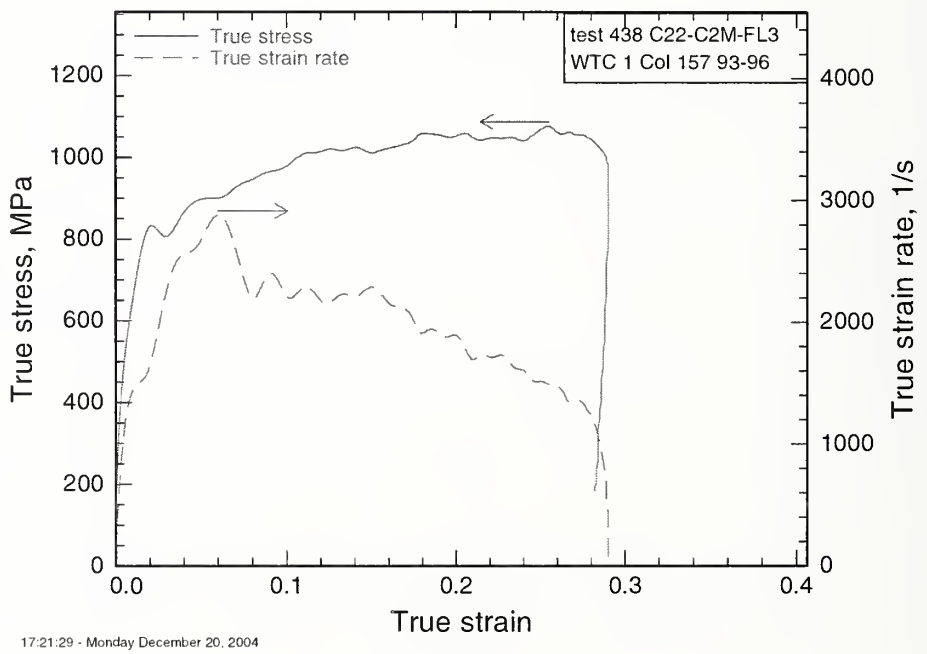

Figure A–85. Kolsky-test stress-strain behavior for F_y = 75 ksi perimeter column C22-C2M.

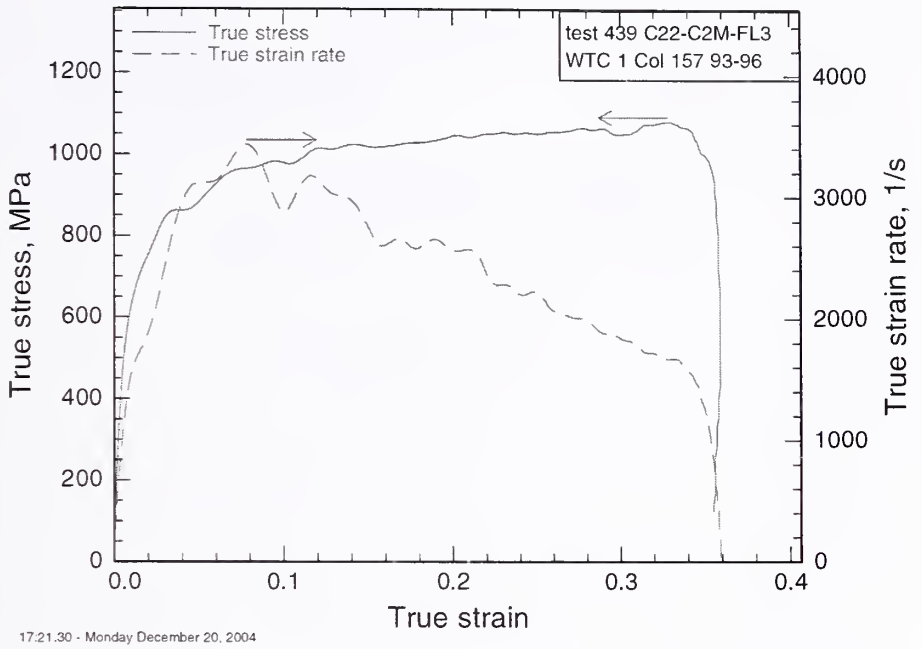

Figure A–86. Kolsky-test stress-strain behavior for F_y = 75 ksi perimeter column C22-C2M.

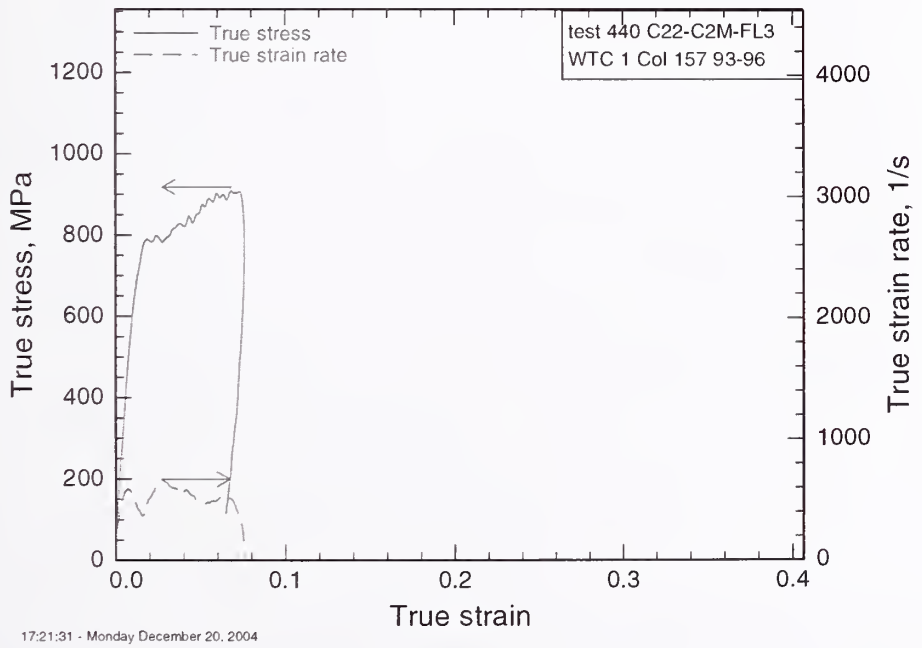

Figure A–87. Kolsky-test stress-strain behavior for F_y = 75 ksi perimeter column C22-C2M.

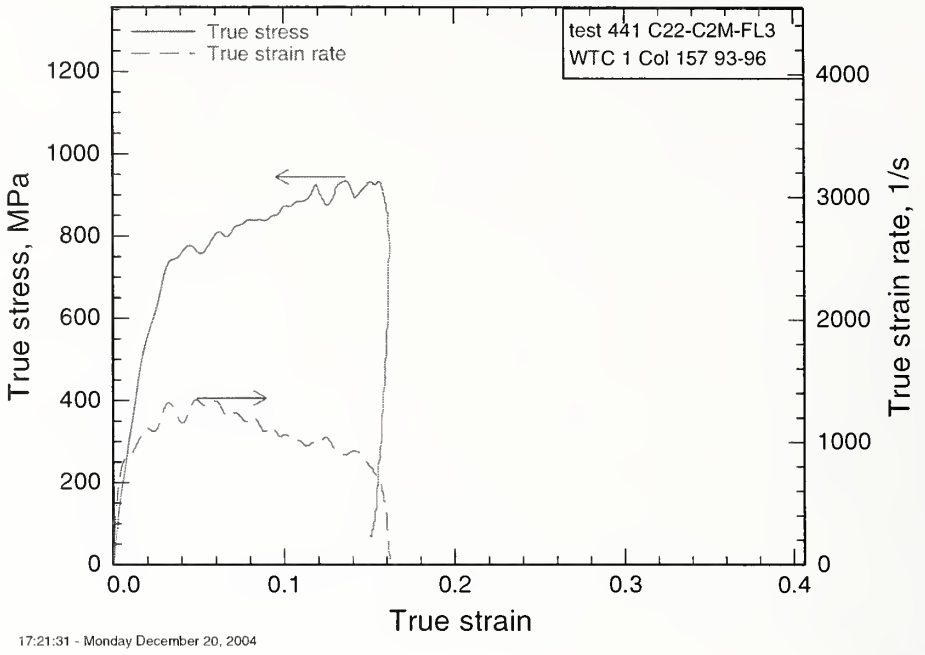

Figure A–88. Kolsky-test stress-strain behavior for F_y = 75 ksi perimeter column C22-C2M.

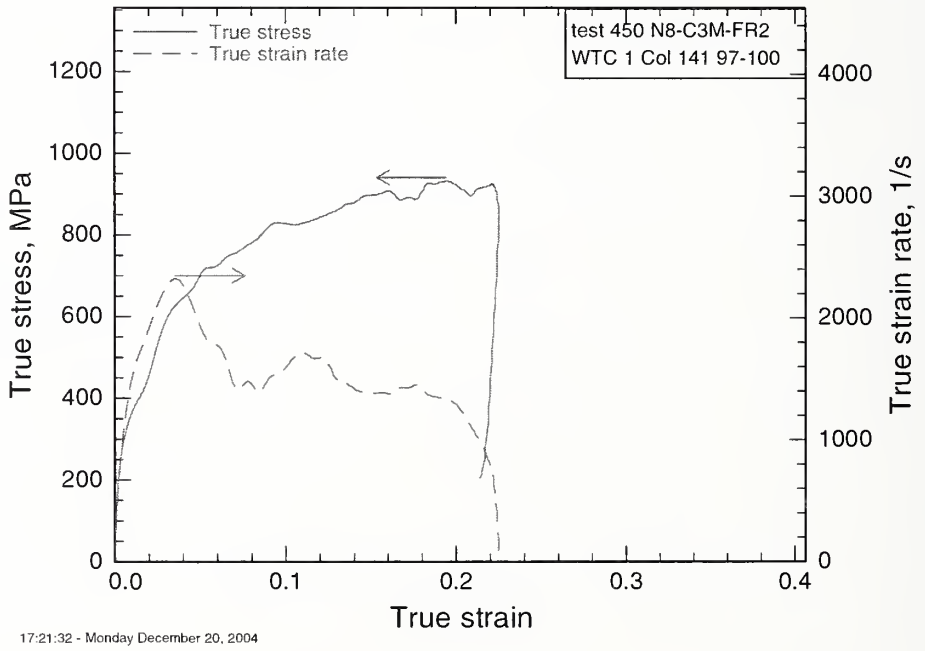

Figure A–89. Kolsky-test stress-strain behavior for F_y = 60 ksi perimeter column N8-C3M.

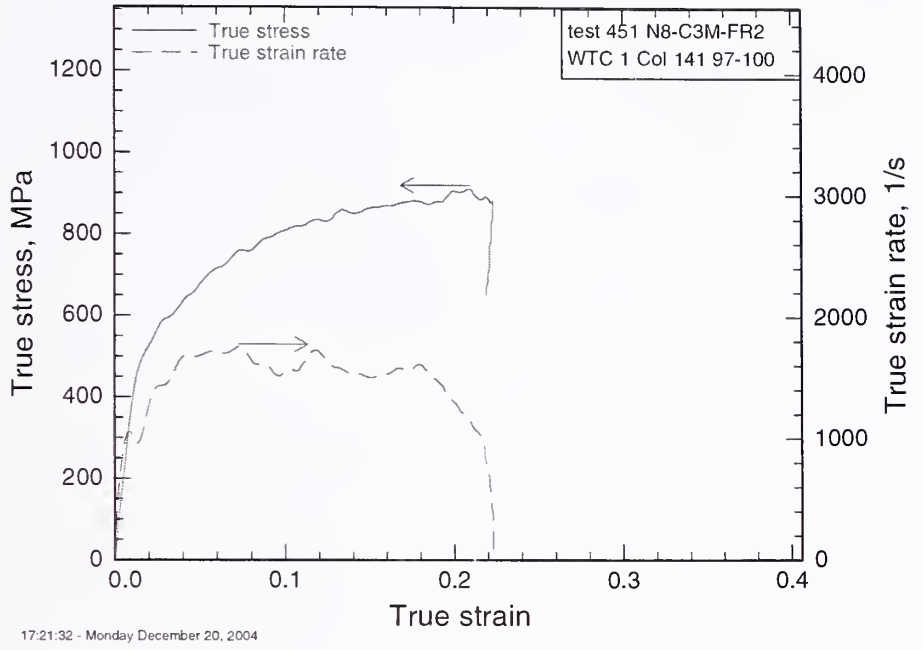

Figure A–90. Kolsky-test stress-strain behavior for F_y = 60 ksi perimeter column N8-C3M.

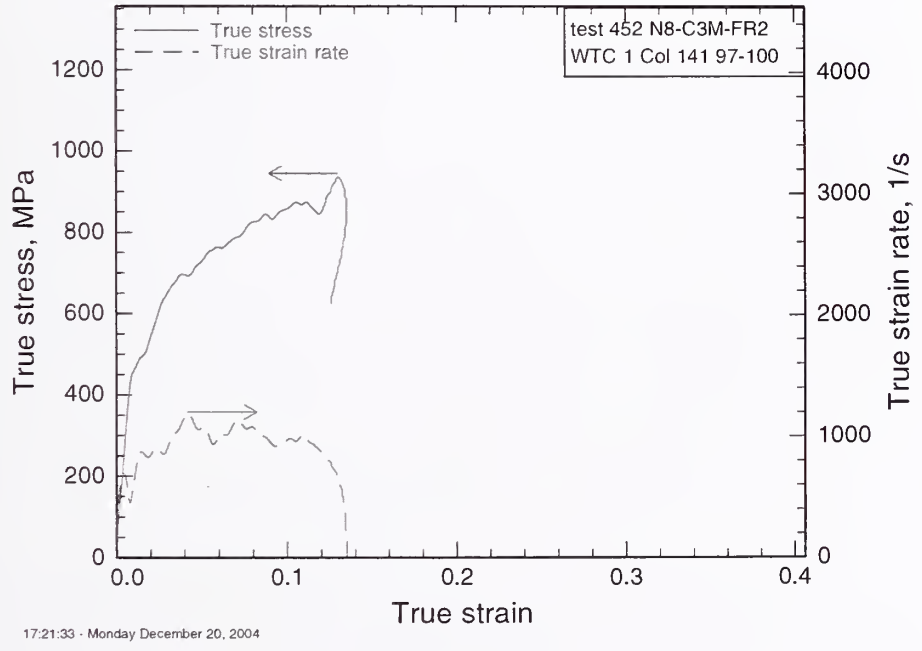

Figure A–91. Kolsky-test stress-strain behavior for F_y = 60 ksi perimeter column N8-C3M.

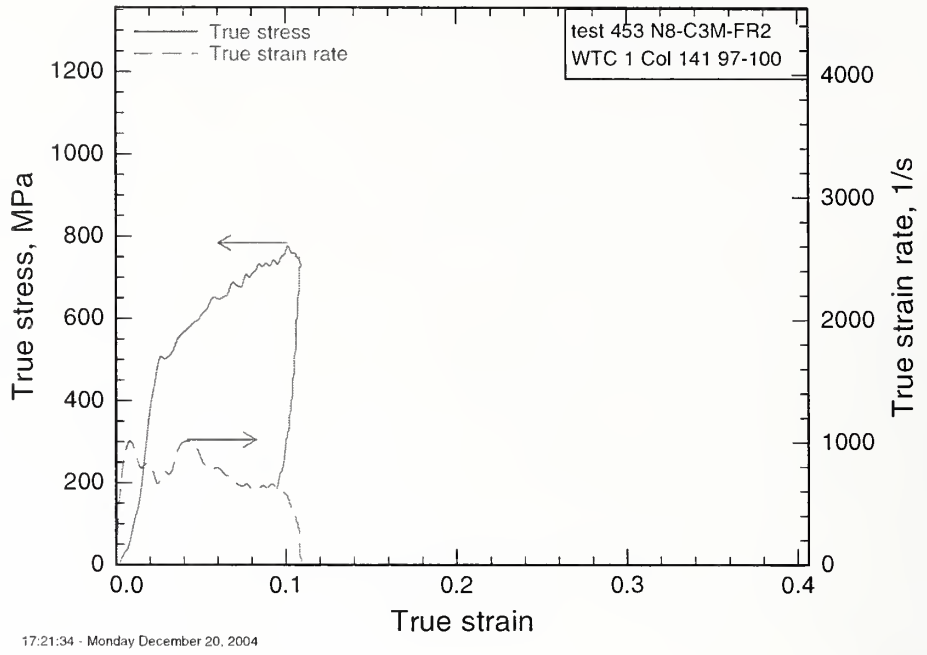

Figure A–92. Kolsky-test stress-strain behavior for F_y = 60 ksi perimeter column N8-C3M.

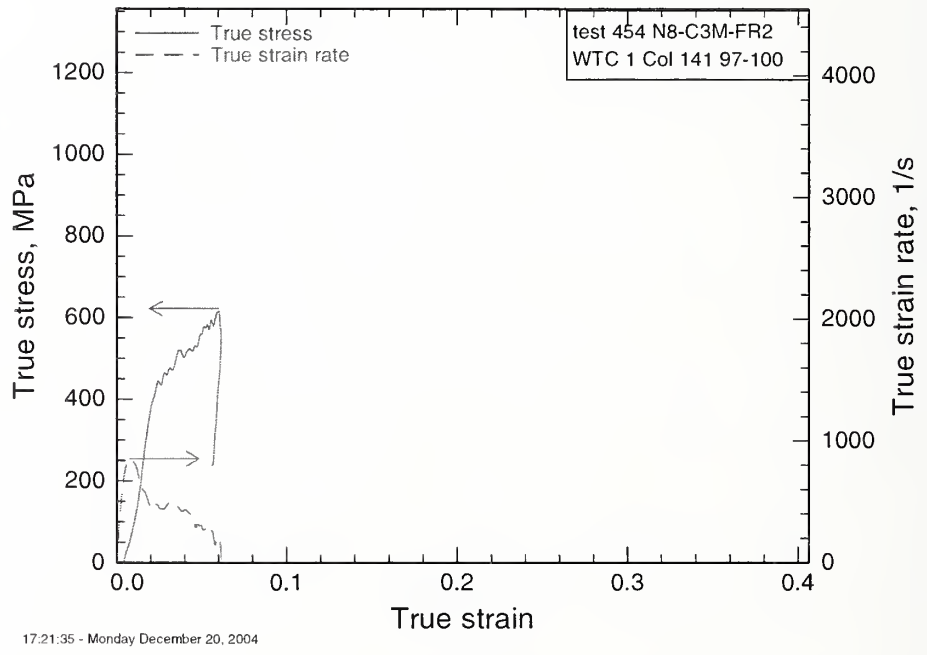

Figure A–93. Kolsky-test stress-strain behavior for F_y = 60 ksi perimeter column N8-C3M.

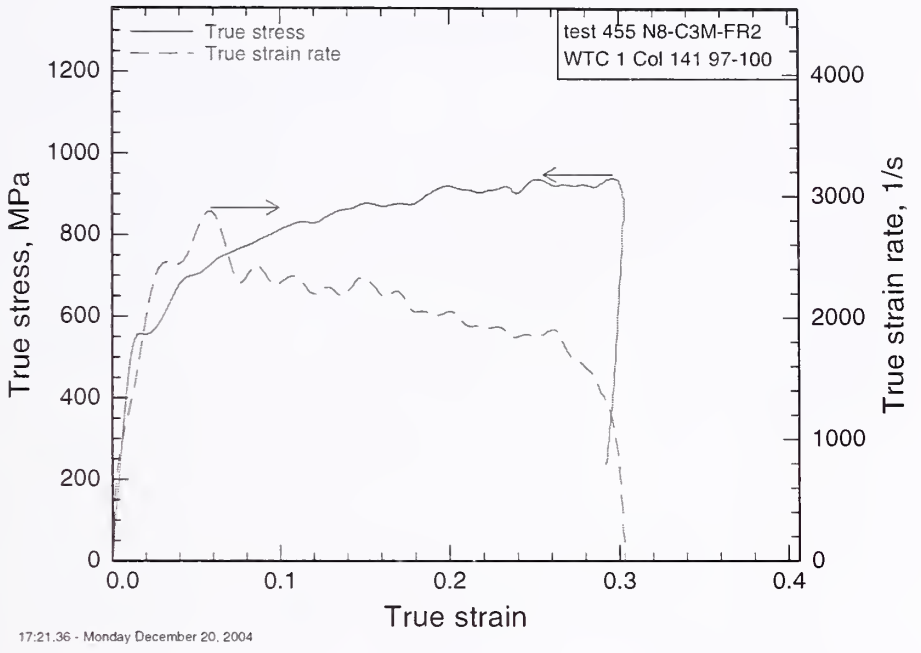

Figure A–94. Kolsky-test stress-strain behavior for F_y = 60 ksi perimeter column N8-C3M.

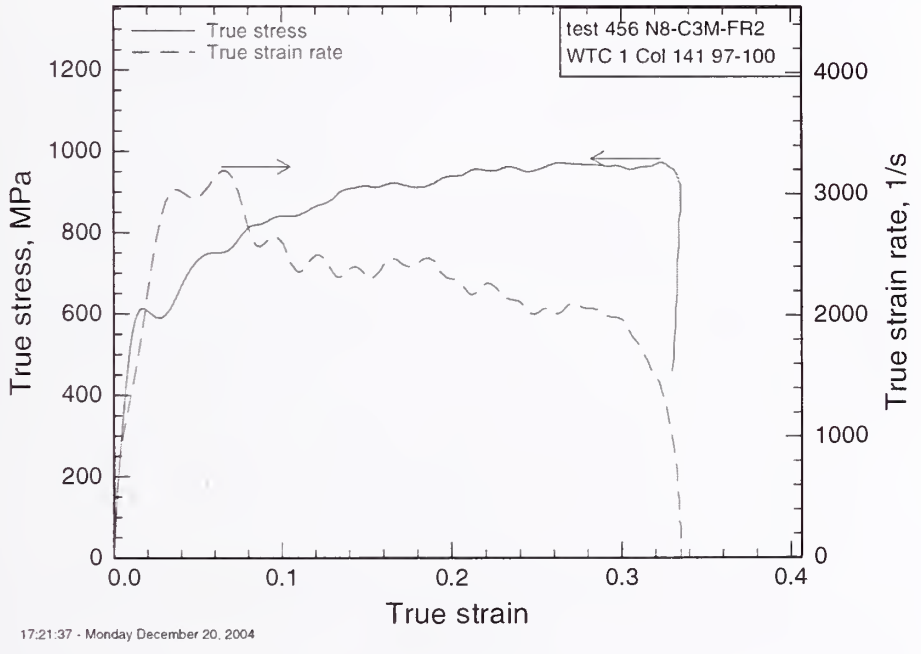

Figure A–95. Kolsky-test stress-strain behavior for F_y = 60 ksi perimeter column N8-C3M.

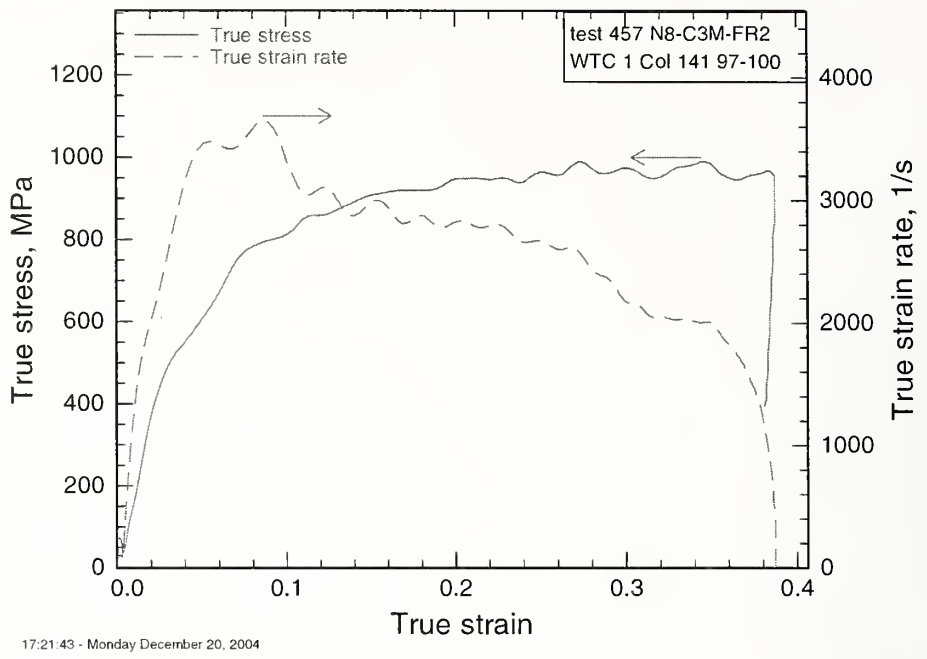

Figure A–96. Kolsky-test stress-strain behavior for F_y = 60 ksi perimeter column N8-C3M.

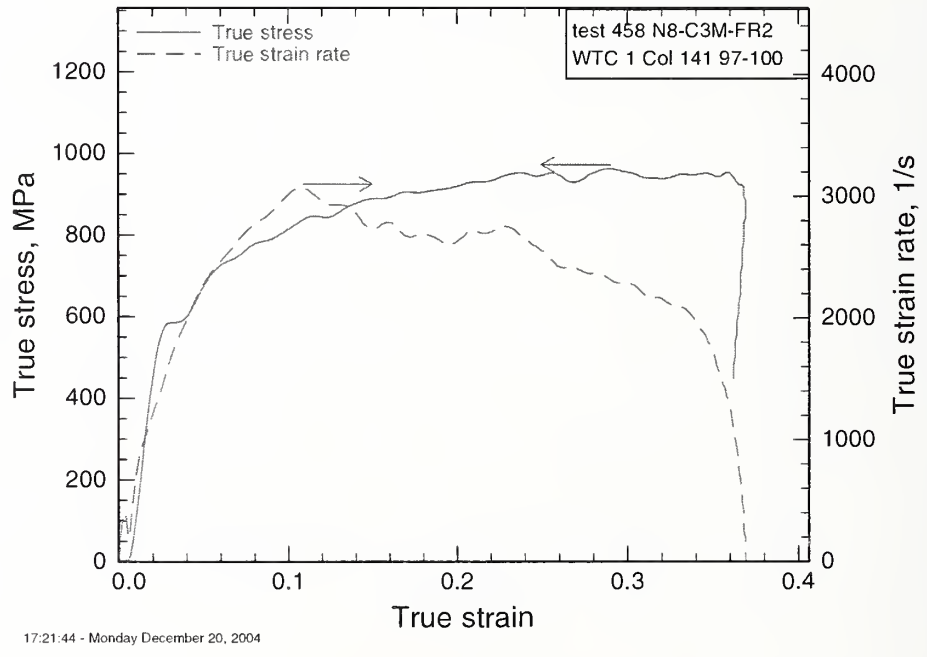

Figure A–97. Kolsky-test stress-strain behavior for F_y = 60 ksi perimeter column N8-C3M.

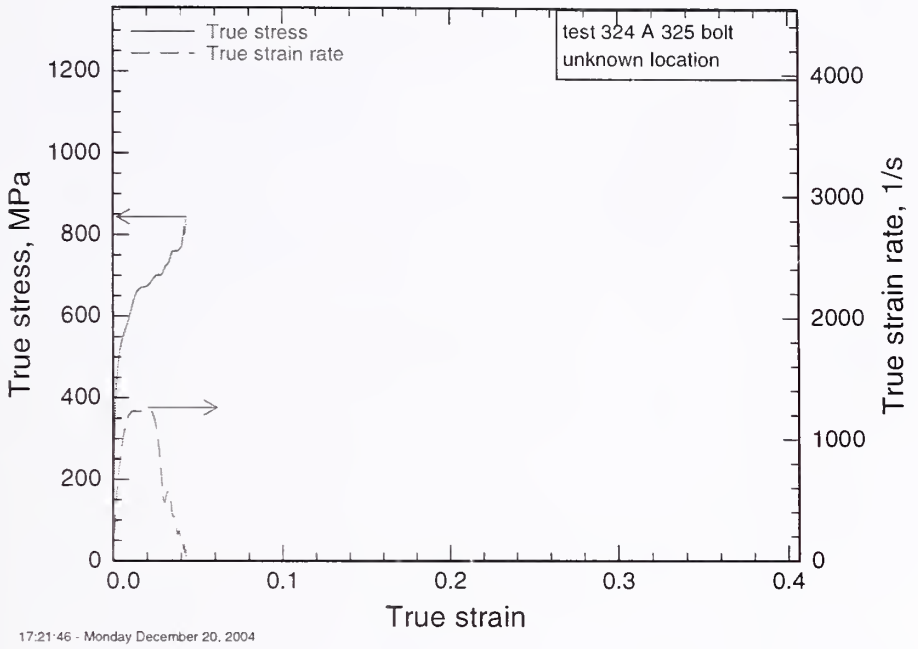

Figure A–98. Kolsky-test stress-strain behavior for A 325 bolt.

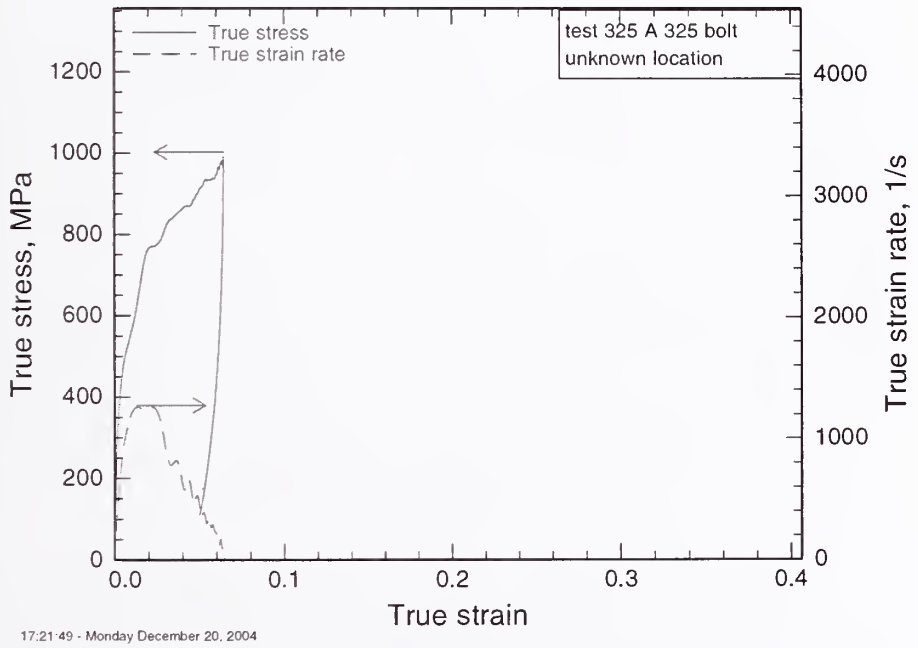

Figure A–99. Kolsky-test stress-strain behavior for A 325 bolt.

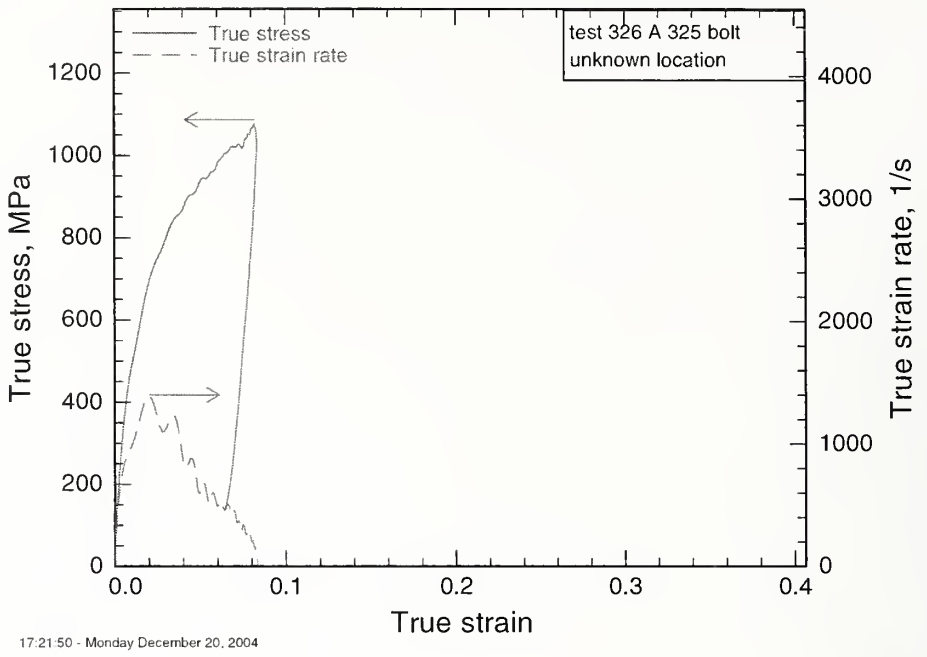

Figure A–100. Kolsky-test stress-strain behavior for A 325 bolt.

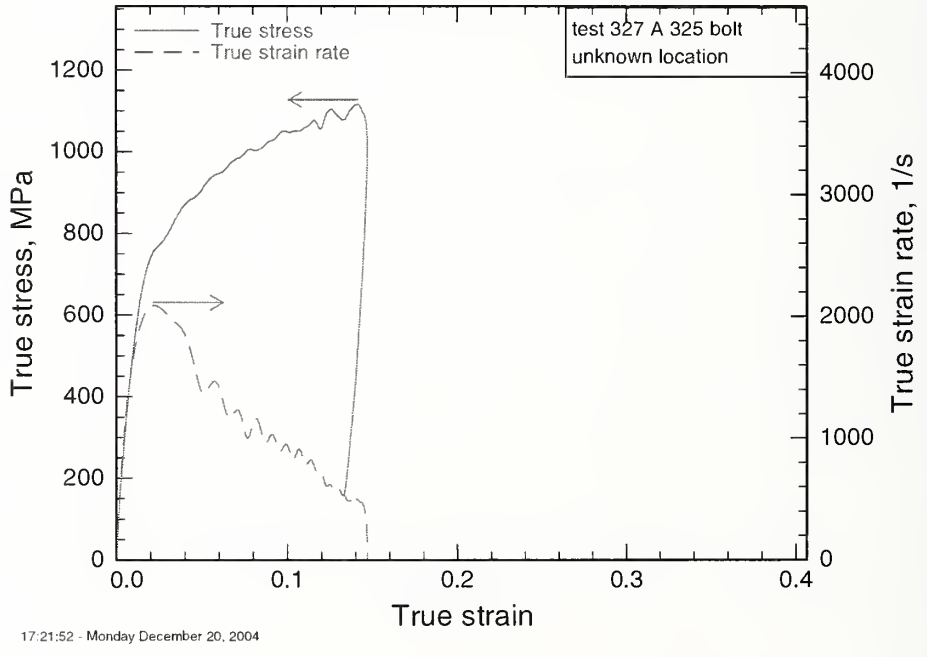

Figure A–101. Kolsky-test stress-strain behavior for A 325 bolt.

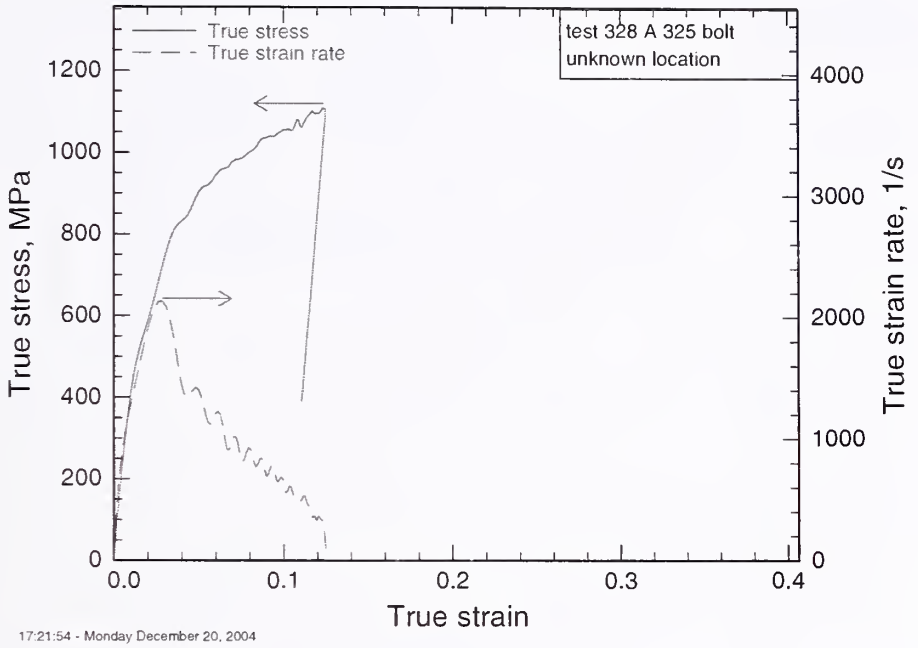

Figure A–102. Kolsky-test stress-strain behavior for A 325 bolt.

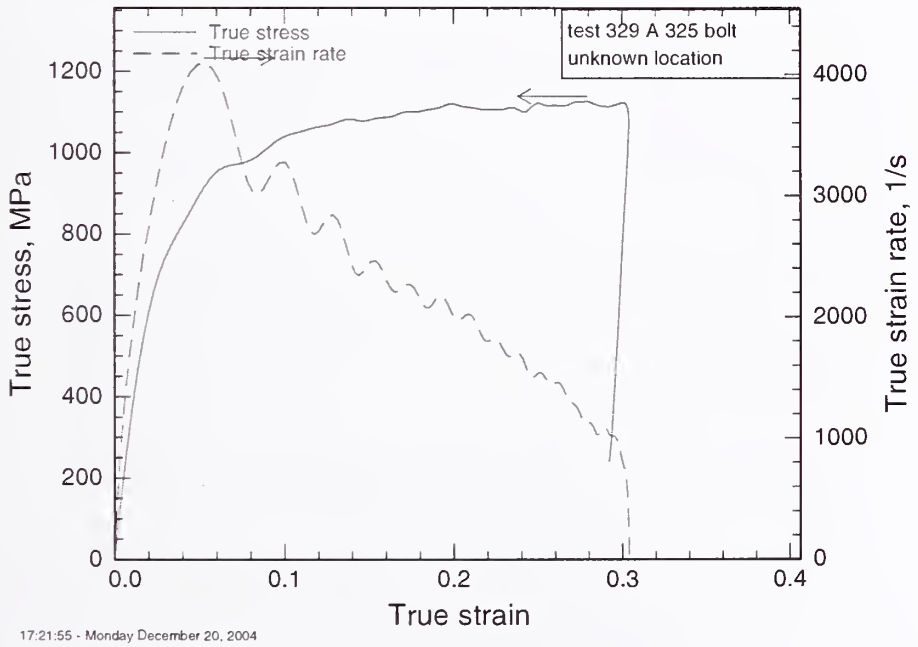

Figure A–103. Kolsky-test stress-strain behavior for A 325 bolt.

A.7 SUPPLEMENTAL FIGURES FOR ELEVATED-TEMPERATURE PROPERTIES

Figures A–104 through A–112 summarize the high-temperature stress-strain behavior of all steels tested.

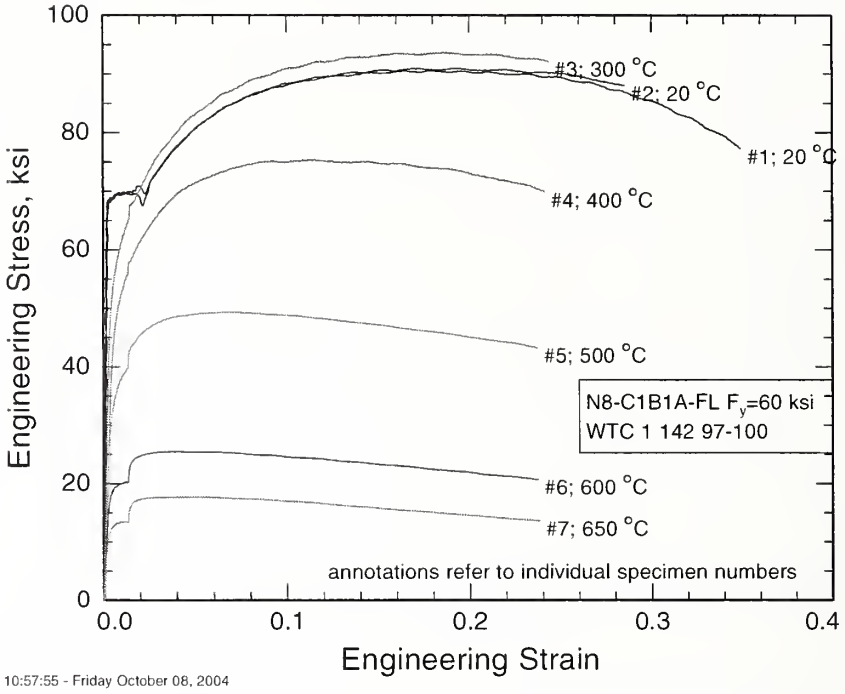

Figure A–104. Perimeter column F_y = 60 ksi N8-C1B-LF.

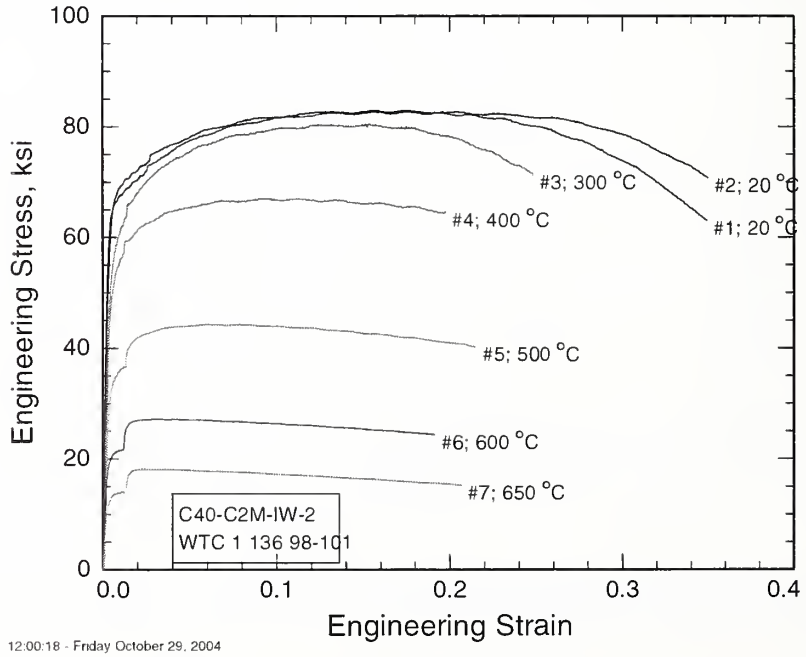

Figure A–105. Perimeter column F_y = 60 ksi C40-C2M-IW.

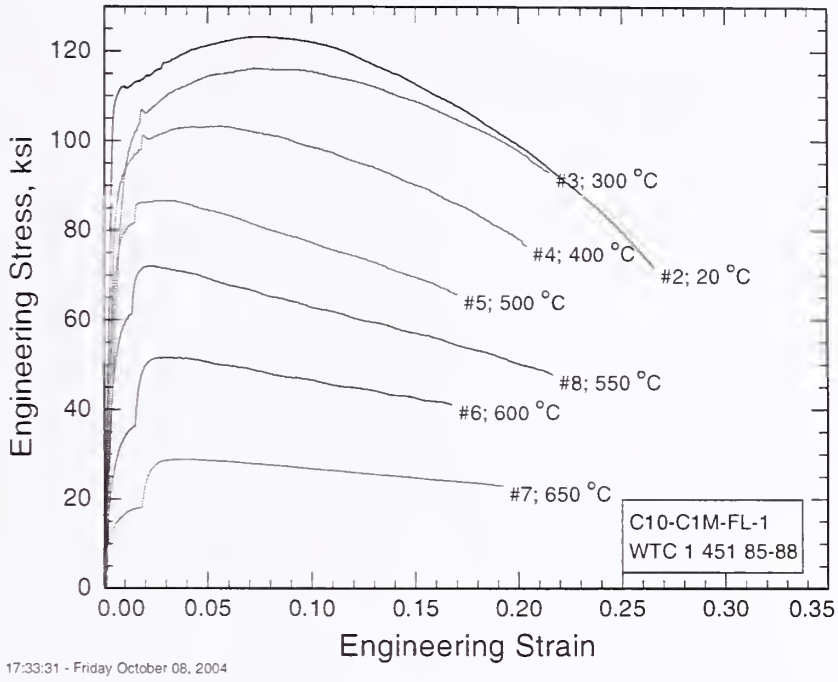

Figure A–106. Perimeter column F_y = 100 ksi C10-C1M-FL.

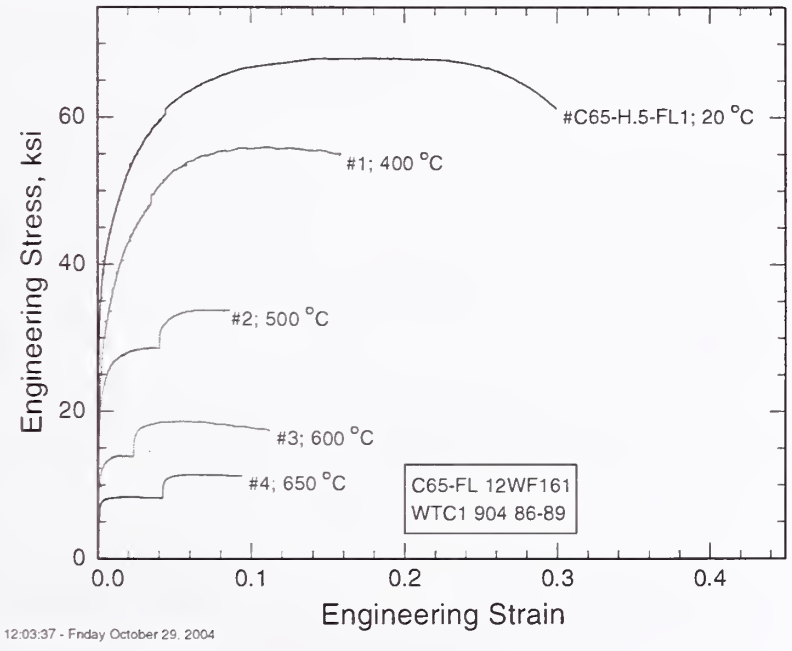

Figure A–107. Core wide-flange column F_y = 36 ksi C65-FL longitudinal.

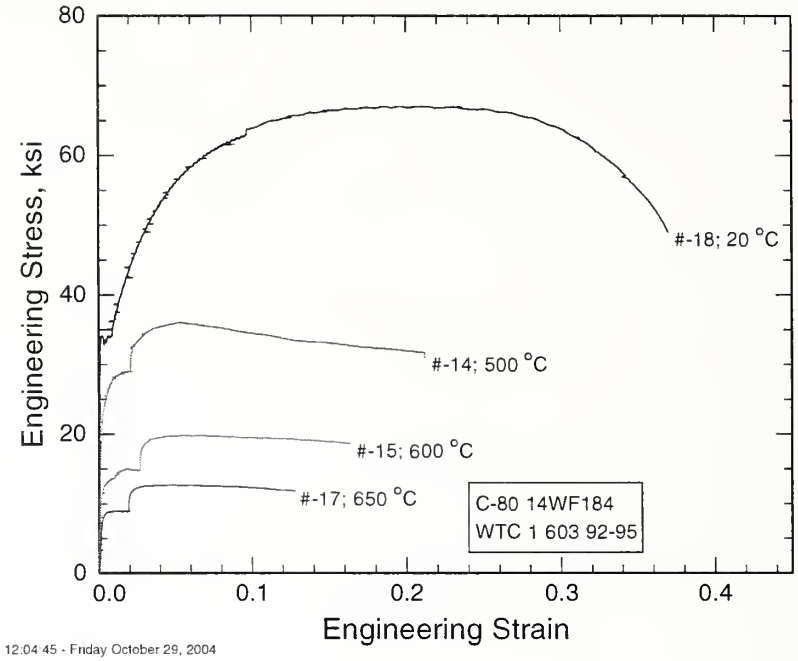

Figure A–108. Core wide-flange column F_y = 36 ksi C80.

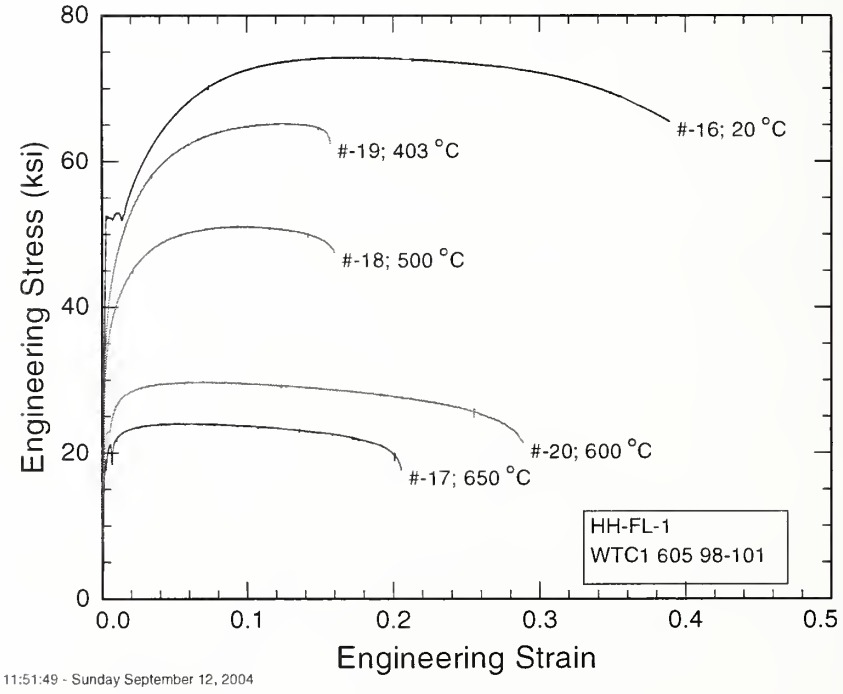

Figure A–109. Core wide-flange column F_y = 42 ksi HH.

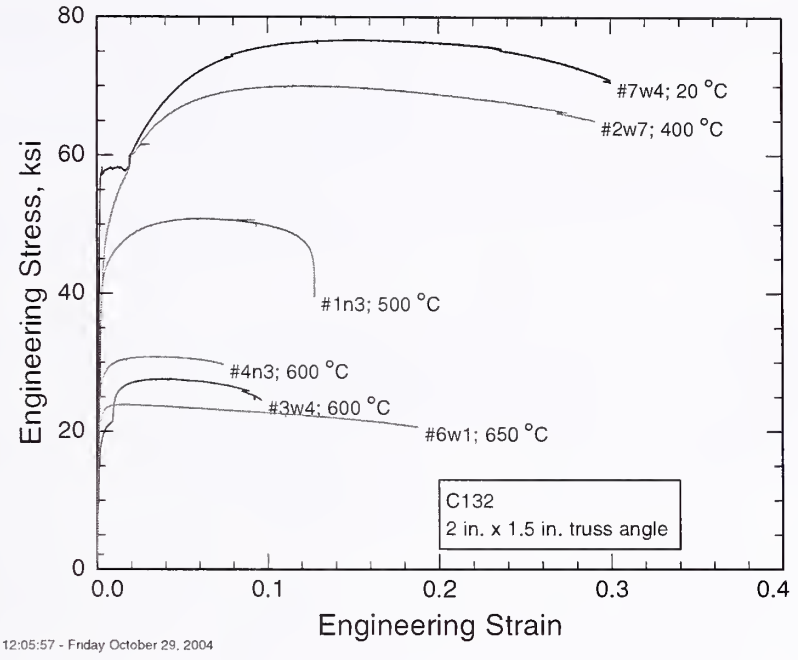

Figure A–110. Truss 2 in.x1.5 in.x0.25 in. angle F_y = 50 ksi C132.

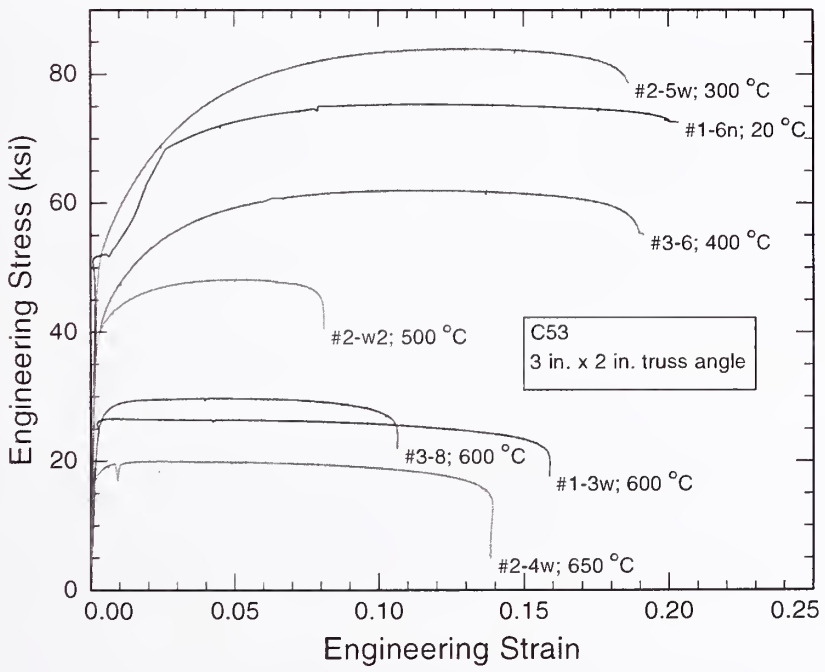

Figure A–111. Truss 3 in.x2 in.x0.37 in. angle F_y = 36 ksi.

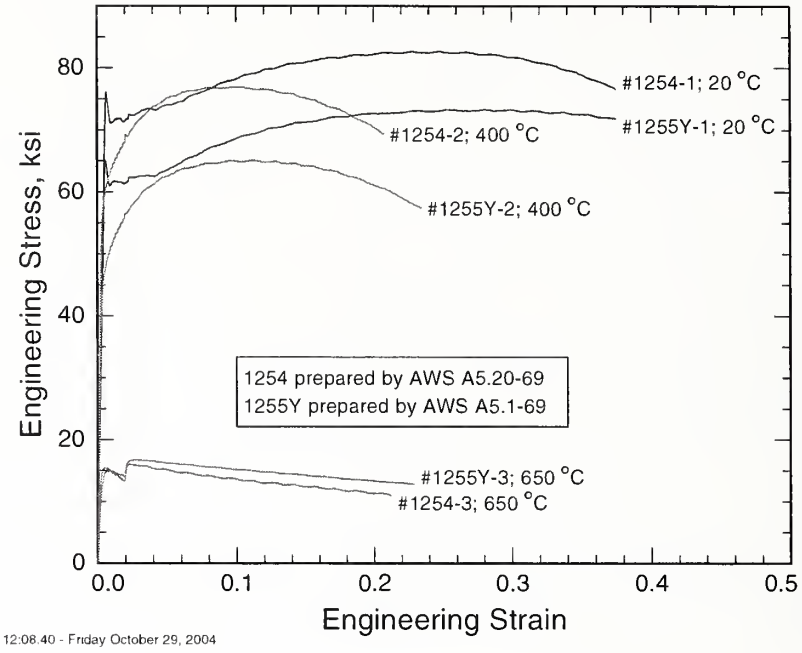

Figure A–112. Contemporary all weld metal specimens.

Appendix B
Effects of Deformation of Wide-Flange Core Columns on Measured Yield Strength

B.1 INTRODUCTION

Several of the stress-strain curves of specimens taken from wide-flange core columns differ significantly between the webs and the flanges. In particular, the stress-strain curves of specimens from the flanges of C-65, C-71, and C-155 and the webs of C-65 do not exhibit yield point or yield point elongation behavior. The yield strengths, *YS*, of specimens from the flanges of C-71 and C-155 are also much larger than those from the corresponding webs. Both effects are evidence of significant prior deformation.

Although National Institute of Standards and Technology (NIST) made every effort to sample the least-deformed material in core column, the condition of the core columns made it necessary to take material that was slightly deformed. Measurements of the shapes of the columns in their as-recovered state can be used to estimate the level of strain in tensile specimens harvested from those columns and characterized in the Investigation. This appendix summarizes this analysis.

B.2 ANALYSIS

Figure B–1 defines the variables that this analysis uses. In a typical wide-flange column, the moment of inertia about the *x*-*x* axis is about three times as large as the moment of inertia about the *y*-*y* axis. To a first approximation, a column will buckle about the axis with the lower moment of inertia; the major deformation will be about the *y*-*y* axis. The deformation of a wide-flange shape bent about the *x*-*x* axis is called camber, while the deformation about the *y*-*y* is called sweep, see Fig. B–2.

If the column bends around the *y*-*y* axis, the strain, ε_{yy} at any point in the flange is

$$\varepsilon_{yy} = \frac{l_s}{R} \qquad \text{B–8}$$

where l_s is the distance from the neutral axis *y*-*y* to the specimen position, and R is the radius of curvature the beam is bent to. Bending about the *y*-*y* axis produces much less strain in the web of the column because the neutral axis runs down the centerline of the web. Specimens from the web originate only a fraction of an inch from the neutral axis, in contrast to specimens from the flanges, which originate up to $l_s = 6$ in. from the neutral axis.

In practice, it is difficult to measure the radius of curvature, R. Instead, it is easier to measure the camber, h_x, and sweep, h_y, over a length l, of the column in the region where the tensile specimens originated. The radius of curvature, R, and the sweep, h_y, are related geometrically:

$$R = \frac{h_y^2 + \frac{l^2}{4}}{2h_y} \qquad \text{B–9}$$

Equation B–2 assumes that the radius of curvature, R, is much larger than the thickness of the piece. In practice, the sweep of a buckled column will usually be much larger than the camber, because the moment of inertia about the x-x axis is smaller.

B.3 RESULTS

Figures B–3 to B–6 are photo montages of the core columns C-30, C-65, C-71, and C-155 that describe the overall condition and specific origins of tensile test specimens. Table B–1 summarizes the important dimensions of these four columns. Table B–2 summarizes the measured sweeps, h_y, of the flanges and webs and their resulting strains. The sweep of column C-30 is indistinguishable from zero. The curvatures of columns C-71 and C-155 were verified by measuring the sweep of the flange on both sides of the web. As expected, it was positive on one side and negative and of approximately equal magnitude on the other. The large uncertainty in the sweep of the column, +/-0.02 in., arises from the rather irregular shape of the edge of the flanges, which were presumably damaged in the collapse and subsequent recovery.

Table B–3 summarizes the measured cambers of the four core columns. The cambers of the flanges of columns C-30, C-71, and C-155 are indistinguishable from zero. Although the sweep of column C-65 was indistinguishable from zero, its camber is measurable, Fig. B–4. Table B–3 also contains an entry for the deformation of the web of C-65. Its shape does not correspond to either camber or sweep. Instead, the shape of its web, Fig. B–4, is consistent with the entire web having buckled.

B.4 DISCUSSION

From the measured sweep, h_y, it is possible to estimate the strain, ε_{yy}, in the flange specimens using Equations B–1 and B–2. Table B–2 summarizes this information in the column labeled "ε_{yy} shape." The strain in the flange test specimens is about 1 percent in columns C-71 and C-155, where the sweeps could be measured. Based on the sign of the sweep on the side of the flange from which the test specimens originated, the strain is tensile in specimens from both columns. Table B–2 also summarizes the yield point behavior of the webs and flanges of all four columns. The strain estimated from the sweep of the flanges of C-71 and C-155 is certainly sufficient to remove the flange yield point behavior, and is the same magnitude as the typical yield point elongation. The flange tests of C-71 and C-155 do not exhibit any obvious yield point elongation behavior, consistent with the strain calculated from the sweep of the flange. Column C-30, which has no measurable sweep or camber, exhibits yield point behavior in both flange and web tests.

The sweeps reported in Table B–2 are roughly five times larger than the maximum sweep permissible in ASTM A 370, which is

$$h_y^{\max} = 0.125\,\text{in.}\left(\frac{l}{120\,\text{in.}}\right) \qquad \text{B–10}$$

The maximum allowable sweep and camber in A 370 is smaller than the smallest sweep measurable on the core columns, due to their short length and poor edge condition.

Both flange and web test specimens for column C-65 originated in deformed material. Because the deformation for these specimens is predominantly camber, rather than sweep, the magnitude of the pre-strain depends sensitively on the exact location of the specimen in the original billet. There were two types of flange specimens for column C-65. Some were 0.25 in. diameter rounds whose centerlines lay roughly at the 1/4-depth point of the flange. The others were 0.5 in. diameter rounds whose centerlines lay roughly on the mid-depth of the flange. Because of the camber of the flange, both types of specimens have non-uniform pre-strain across their widths. The deformation is probably sufficient to remove any yield point behavior, however.

It is also possible, neglecting any contribution of the Bauschinger effect, to roughly estimate the strain in the flange specimens of C-71 and C-155 by assuming that the web represents the undeformed behavior. This is a coarse assumption because the flanges typically lower yield strength. The flange strains predicted from the web stress-strain behavior are approximately 4 percent and 2 percent for C-71 and C-155 respectively.

B.5 SUMMARY

The magnitudes of the prior strains estimated from the tensile data are similar to those estimated from the measured sweep of core columns C-71 and C-155. It is likely, therefore, that the elevated yield strength and lack of yield point behavior in the flanges of these two columns arises from the prior deformation of the column. The deformation of column C-65 is sufficient to remove any yield point behavior from the tensile specimens cut from it.

Table B–1. Locations and dimension information for wide-flange core columns.

Specimen	Shape	Location	d (in.)	b_f (in.)	t_w (in.)	t_f (in.)	l_s (in.)
C-30	14WF237	WTC 2 Col. 1008 Fl. 104-106	16.12	15.91	1.09	1.75	5.0
C-65	12WF161	WTC 1 Col. 904 Fl. 86-89	13.88	12.52	0.91	1.49	2.3
C-71	12WF190	WTC 1 Col. 904 Fl. 79-80	14.38	12.67	1.06	1.74	4.0
C-155	12WF161	WTC 1 Col. 904 Fl. 83-86	13.88	12.52	0.91	1.49	4.0

Note: See Fig. B–1 for definitions of symbols.

Table B–2. Stress-strain behavior and sweep of core columns.

Specimen	Web F_y (ksi)	Flange F_y (ksi)	ε_{yy} Shape[a]	ε_{yy} Test[b]	Flange h_y[c] (in.)	Web h_y (in.)	l[d] (in.)	R (in.)
C-30	41.9 (YP)	39.6 (YP)	<0.004[e]	n/a	<0.02	<0.02	15	>1,400[e]
C-65	31.1 (NYP)	32.4 (NYP)	<0.0004[e]	n/a	<0.03	n/d	36	>5,400[e]
C-71	33.2 (YP)	53.4 (NYP)	+0.011	0.04	0.09	0.09	16	380
C-155	42.2 (YP)	50.9 (NYP)	+0.012	0.02	0.13	0.11	18	320

a. Estimated from sweep of flange, h_y, and location of specimens, l_s using Eqs. B–1 and B–2.
b. Estimated from stress-strain behavior of flange, relative to the web.
c. Uncertainties in h_y are approximately +/-0.02 in.
d. l is the length of the flange over which the sweep is measured, Fig. B–113.
e. Estimated from minimum measurable sweep, h_y.
Key: n/a, not applicable; n/d, not determined; NYP, no yield point behavior in stress-strain curve; YP, yield point behavior in stress-strain curve.

Table B–3. Stress-strain behavior and camber and deformation of core columns.

Specimen	Web F_y (ksi)	Flange F_y (ksi)	Measurement Type	Flange h_x[a] (in.)	l[b] (in.)
C-30	41.9 (YP)	39.6 (YP)	flange	<0.02	15
C-65	31.1 (NYP)	32.4 (NYP)	flange	0.17	36
C-65	31.1 (NYP)	32.4 (NYP)	web	0.38	9
C-71	33.2 (YP)	53.4 (NYP)	flange	<0.015	16
C-155	42.2 (YP)	50.9 (NYP)	flange	<0.015	18

a. Uncertainties in h_x are approximately +/-0.02 in.
b. l is the length of the flange over which the camber is measured.
Key: NYP, no yield point behavior in stress-strain curve; YP, yield point behavior in stress-strain curve.

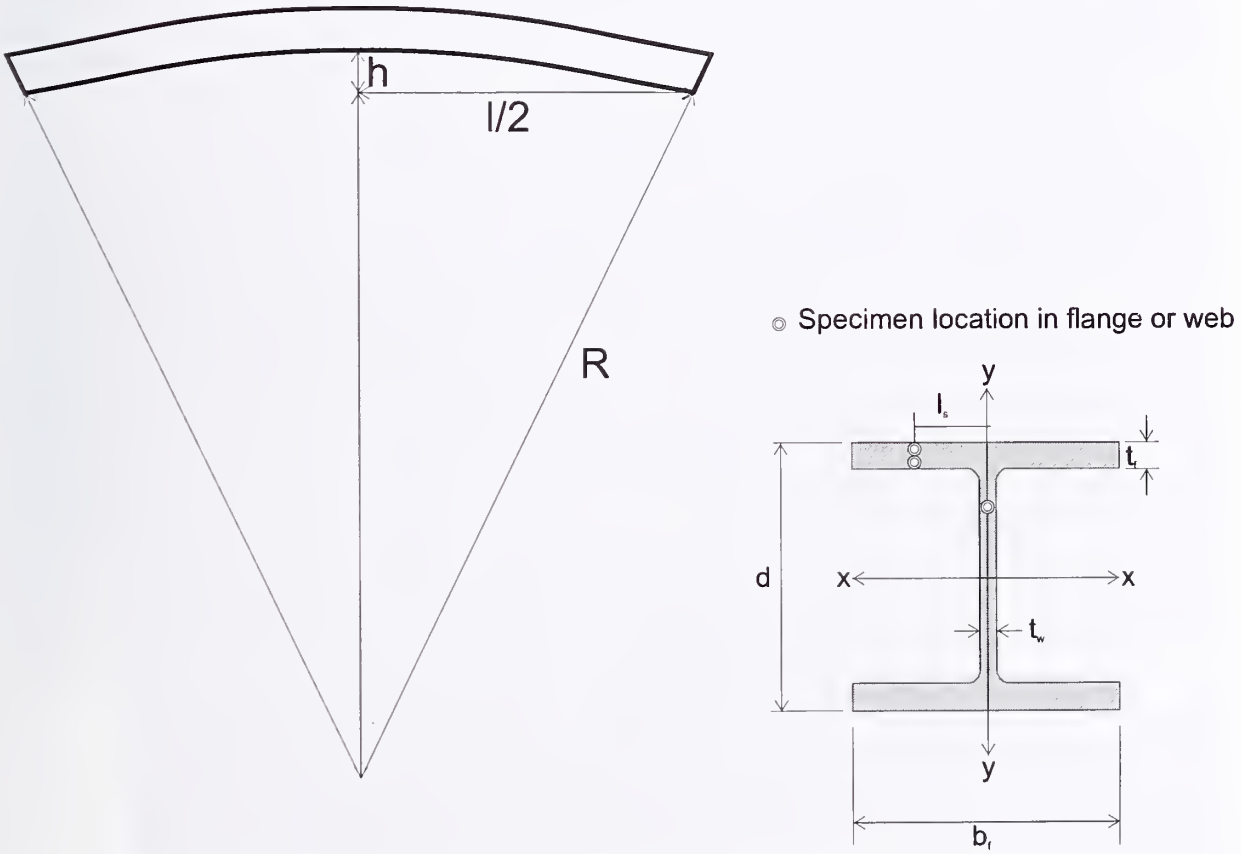

Figure B–1. Schematic diagram that defines the variables used in the analysis of the wide-flange bending.

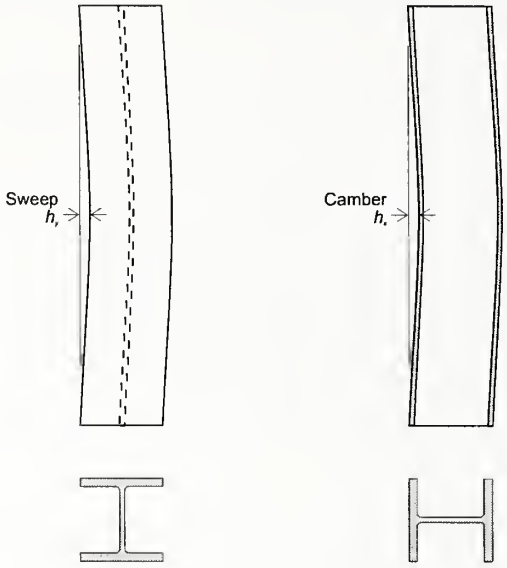

Figure B–2. Definitions of camber and sweep in wide-flange shapes.

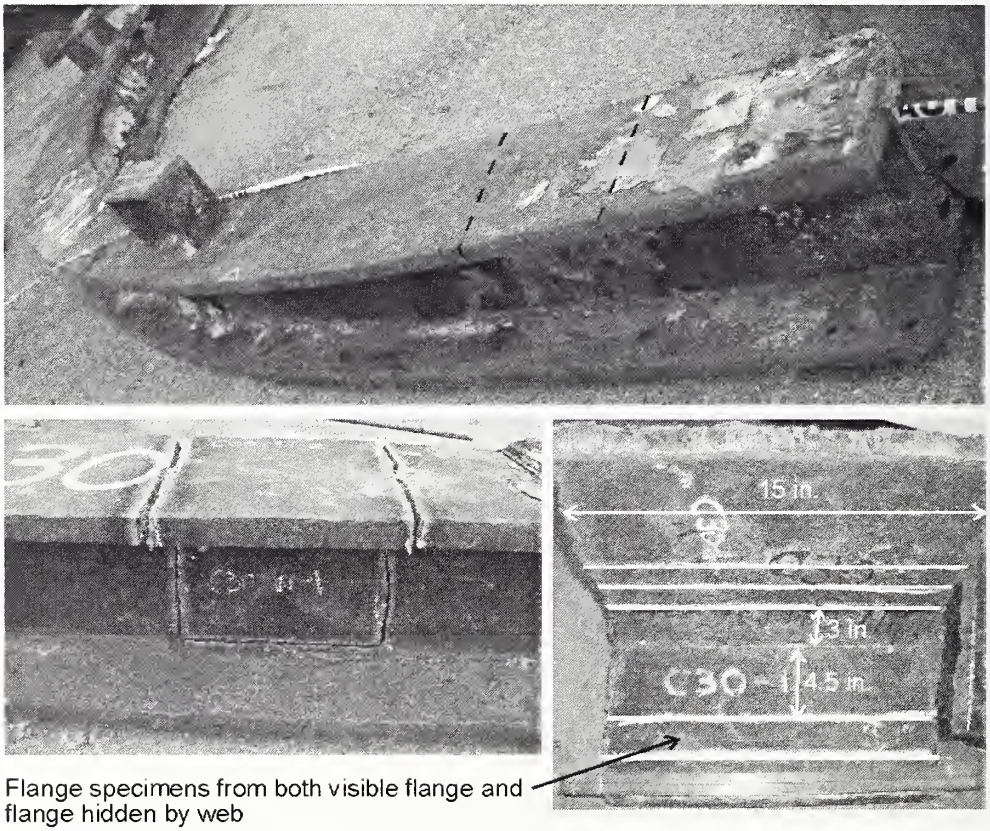

Flange specimens from both visible flange and flange hidden by web

Source: NIST.

Figure B–3. Montage of specimen C-30 that shows the overall state of the column and the region that provided the test specimens.

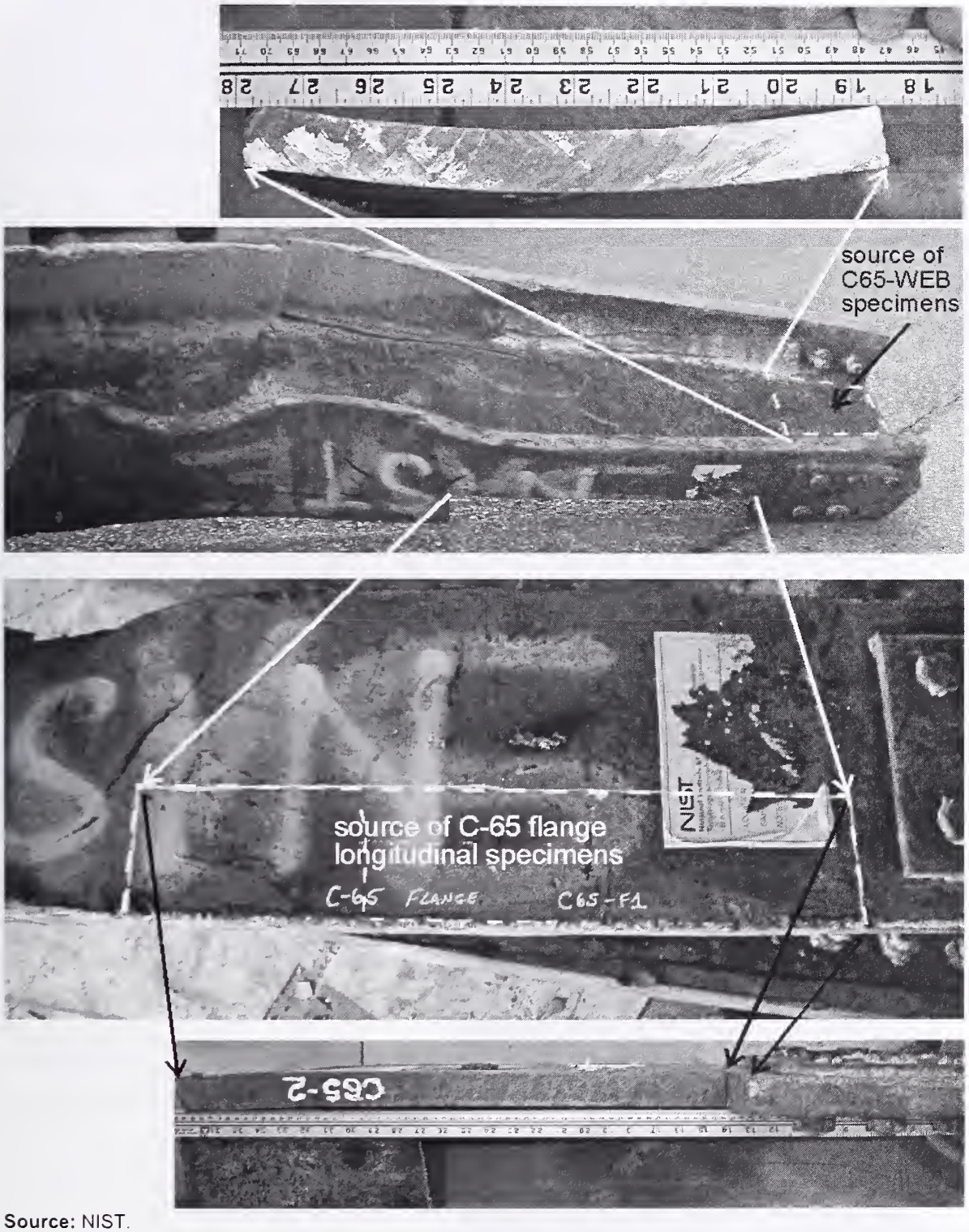

Source: NIST.

Figure B–4. Montage of specimen C-65 that shows the overall state of the column and the region that provided the test specimens.

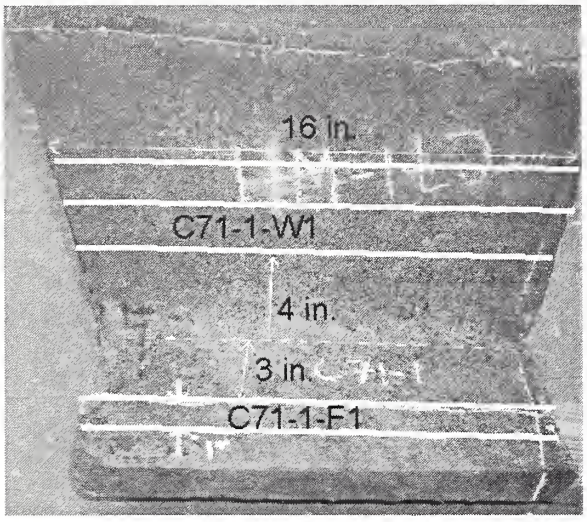

All tension specimens originated specimen C71-1-F2, which came from flange (hidden by web above) with tensile strain. Note that the curvature of the specimen area is opposite to the general curvature of column.

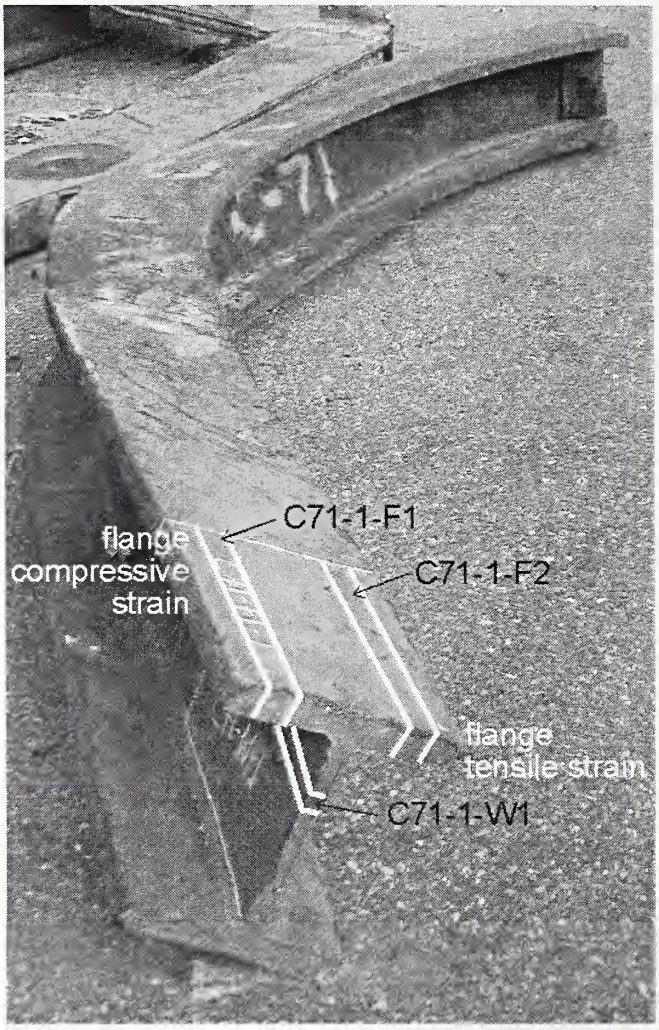

Source: NIST.

Figure B–5. Montage of specimen C-71 that shows the overall state of the column and the region that provided the test specimens.

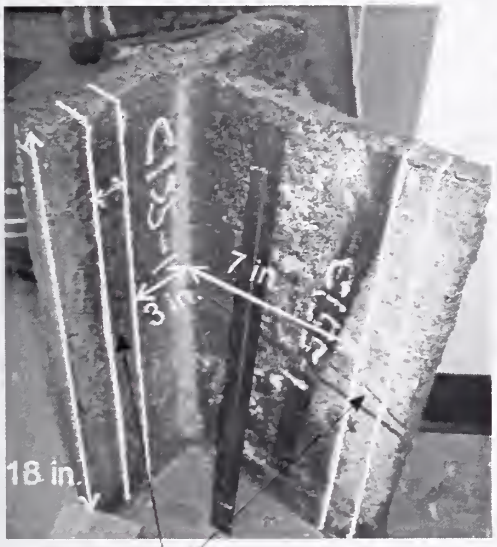

C155-1-W1
C155-1-F1

All flange specimens from C155-1-F1 (tension side). All web specimens from C155-1-W1

Source: NIST.

Figure B–6. Montage of specimen C-155 that shows the overall state of the column and the region that provided the test specimens.

This page intentionally left blank.

Appendix C
PROVISIONAL ANALYSIS OF HIGH-RATE DATA

Early in the Investigation, before testing was complete, it was necessary to provide high-strain-rate data to other Investigation Team members modeling the aircraft impact on the building. The accelerated schedule required that the model for the data be developed on a provisional set of the steels. This provisional data set includes the six steels listed in Table C–1. The reported values in Appendix A differ slightly from the provisional values used in the provisional analysis because the provisional analysis did not use the ESIS procedure for data reduction.

For use in the finite element model, the data had to be expressed in terms of the Cowper-Symonds equation:

$$\frac{\sigma}{\sigma_0} = 1 + \left(\frac{\dot{\varepsilon}}{C}\right)^{1/p} \qquad \text{C–1}$$

The Cowper-Symonds equation describes the increase in flow stress with strain rate using two parameters, C and p. In the Cowper-Symonds equation $\dot{\varepsilon}$ is the strain rate, σ is the stress (yield, tensile, or other stress) and σ_0 is the reference stress. Usually, σ_0 is the stress measured in a low-rate tensile test. The present analysis uses the yield strength.

Equation C–1 can be rewritten as

$$\frac{\sigma - \sigma_0}{\sigma_0} = \overline{S} = \left(\frac{\dot{\varepsilon}}{C}\right)^{1/p} \qquad \text{C–2}$$

Taking the natural logarithm of each side produces an equation linear in the Cowper-Symonds parameters:

$$\log_e \overline{S} = \frac{1}{p}\log_e \dot{\varepsilon} - \frac{1}{p}\log_e C \qquad \text{C–3}$$

The value of the stress at the lowest strain rate, σ_0, fixes the overall strain rate behavior, but this value cannot be included in a fit of Equation C–3, because at $\sigma = \sigma_0$, $\overline{S} = 0$.

To avoid this problem, NIST fit a line to the $\sigma - \log_e \dot{\varepsilon}$ data, as is commonly done in analysis of high-rate test data. Plotting this semi-log fit on log-log axes results in a curve. A linear fit of Equation C–3 to this curve yields the Cowper-Symonds parameters p and C.

In these fits for the provisional data, the Cowper-Symonds exponent, p, was constant among the steels, but the pre-factor C increased with the yield strength. The increase in C with increasing yield strength, F_y, can be represented with a second order polynomial of the natural logarithm of C:

$$\log_e C = C_0 + C_1 F_y + C_2 F_y^2 \qquad \text{C–4}$$

where F_y is the yield strength measured in the low-rate tensile test in units of ksi. The provisional Cowper-Symonds model, after incorporating the yield strength dependence of the parameter C is

$$\frac{\sigma}{\sigma_0} = 1 + \left(\frac{\dot{\varepsilon}}{C(F_y)} \right)^{1/p} \qquad \text{C–5}$$

Table C–2 summarizes the values of the parameters in the provisional model, Eq. C–5.

The predictions of Eq. C–5 to the individual provisional data sets for the six steels were reasonable in that the yield stress increases with increasing strain rate. Furthermore, predicting the behavior of low-strength steels, outside the strength range of the original data set, using Eq. C–5 does not produce anomalous behavior.

By analyzing the full data set collected as part of the Investigation in the same manner as the provisional data set, it is possible to assess the quality of the predictions of the provisional model. As in the analysis of the provisional data, the exponent p for the full data set does not vary between the steels: $p = 4.4053$. The normalizing constant C also increases with increasing yield strength; a second-order polynomial is sufficient to represent the behavior. Table C–2 summarizes the parameters in the Cowper-Symonds model for the full data set of 13 steels.

The model based on the full data set predicts the behavior of the six steels in the provisional data set about as well as the provisional model does. Of these six steels, the full model fits more accurately in half the cases, where the goodness-of-fit is taken as the sum of squares of the residuals. As expected, the full model fits the data of the steels not in the provisional set better than does the provisional model. In the cases of the high-strength steels, the differences are not substantial, however. Figures C–1 through C–13 illustrate the data and the predictions of both models for high and intermediate strength steels.

The provisional model tends to overpredict the strain-rate sensitivity of the low-strength, core column steels. Figures C–10 through C–13 show the predictions of the model for the low-strength, core-column steels that were not included in the provisional data set. Because the aircraft struck the perimeter columns first, the reduced fidelity for the core columns should not be a significant problem.

Table C–1. Specimens and orientations used in the provisional analysis to determine Cowper-Symonds parameters

Fy (ksi)	Specimen	Orientation
50	M26-C1B	L&T
60	N8-C1B	L
65	N99-C3T	L&T
75	C22-C2M	L
100	M10B-C3B	L&T
100	C10-C1M	L&T

Key: L, longitudinal; T, transverse.

Table C–2. Comparison of provisional and final Cowper-Symonds parameters, Eq. C–5, for the high-strain rate data.

Data Set	# of Steels	p	*Parameters in Equation C–4*		
			C_0	C_1	C_2
Complete	13	4.4053	-4.7374	0.3614	-0.001707
Provisional (Table C–1)	6	6.7824	-17.391	0.74512	-0.0035253

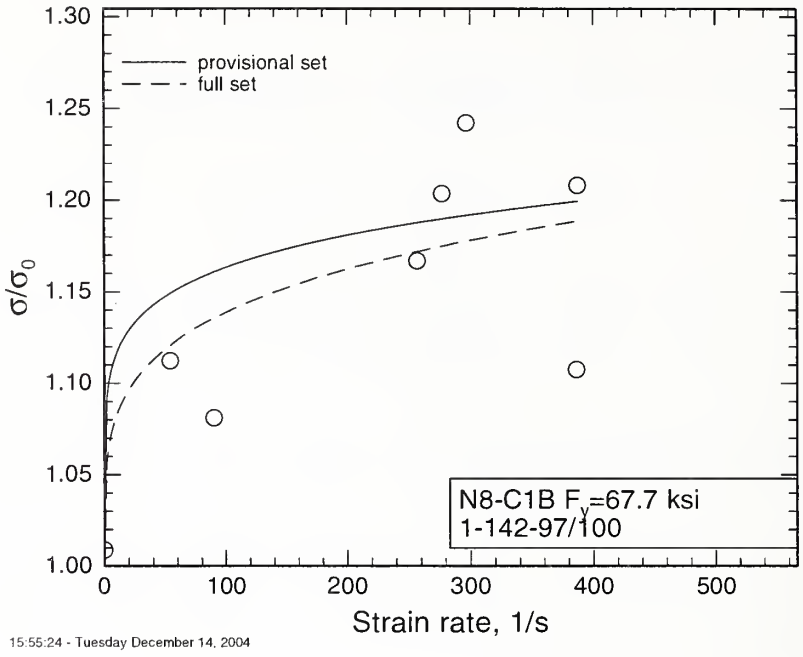

Figure C–1. Predictions of the provisional and full Cowper-Symonds model for perimeter column steel C10-C1M1-FL , which is in the provisional data set.

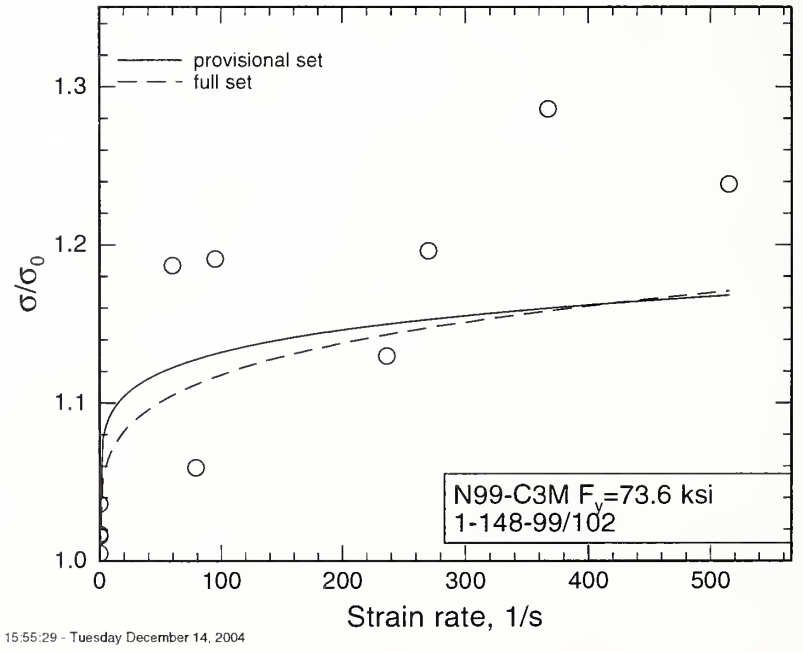

Figure C–2. Predictions of the provisional and full Cowper-Symonds model for perimeter column steel C10-C1M1-IW , which is not in the provisional data set.

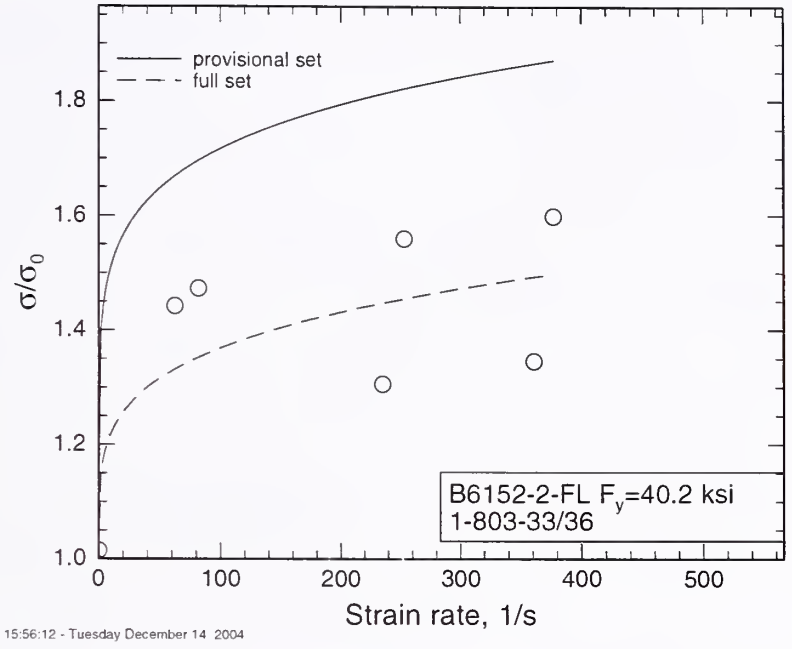

Figure C–3. Predictions of the provisional and full Cowper-Symonds model for perimeter column steel M10b-C3B1-RF, which is in the provisional data set.

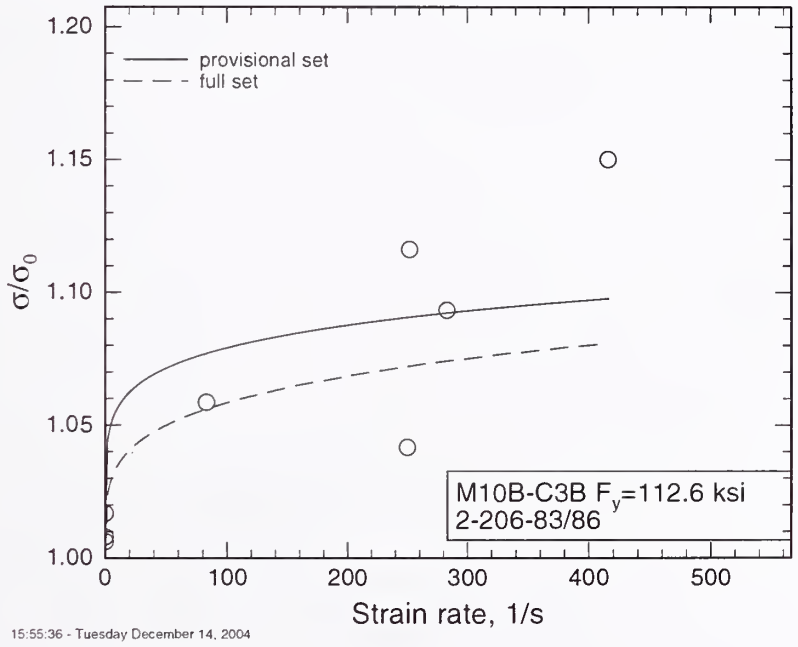

Figure C–4. Predictions of the provisional and full Cowper-Symonds model for perimeter column steel C22-C2M, which is in the provisional data set.

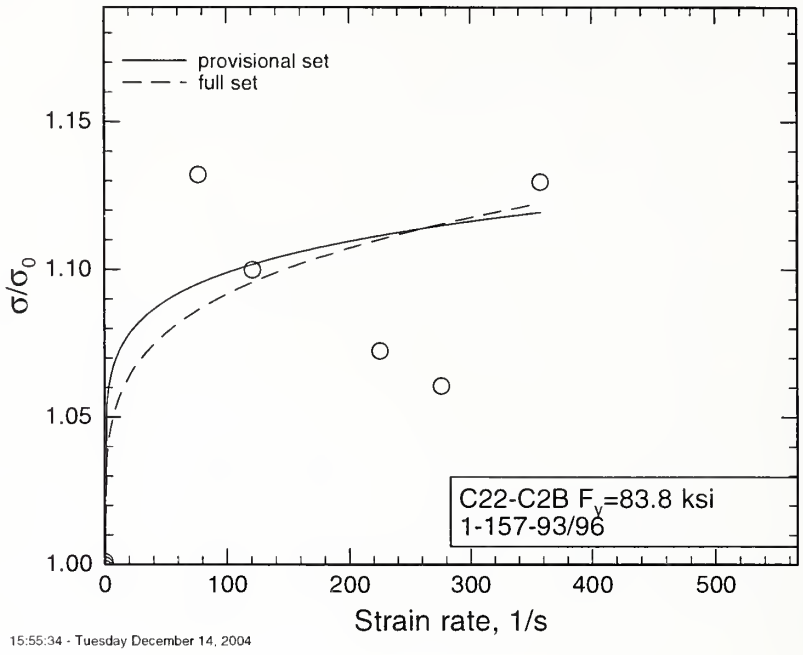

Figure C–5. Predictions of the provisional and full Cowper-Symonds model for perimeter column spandrel steel C14-S, which is not in the provisional data set.

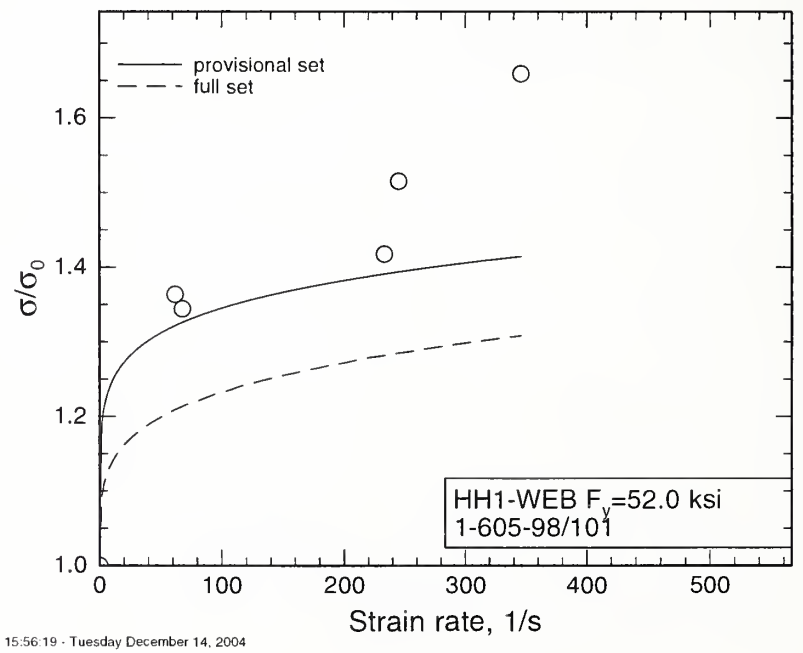

Figure C–6. Predictions of the provisional and full Cowper-Symonds model for perimeter column steel N99-C3T, which is in the provisional data set.

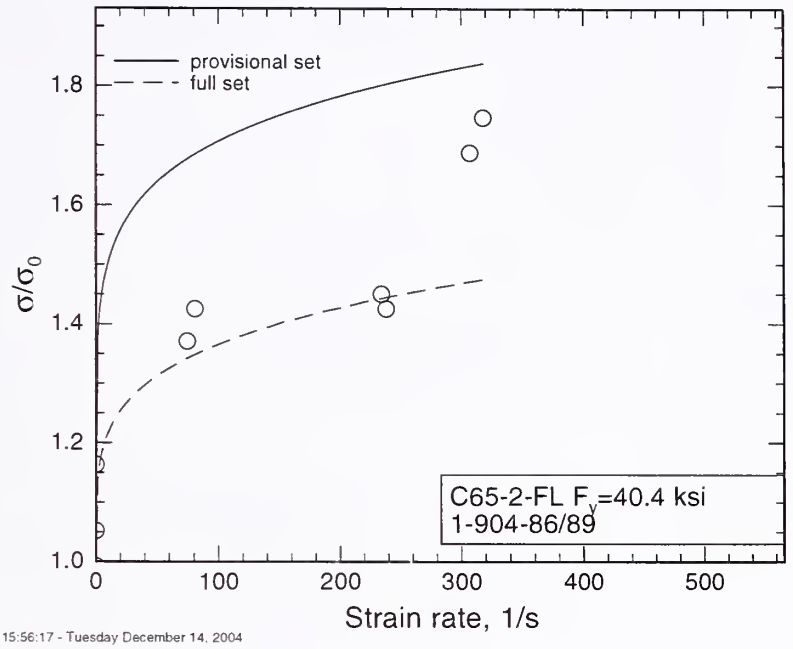

Figure C–7. Predictions of the provisional and full Cowper-Symonds model for perimeter column steel N8-C1B, which is in the provisional data set.

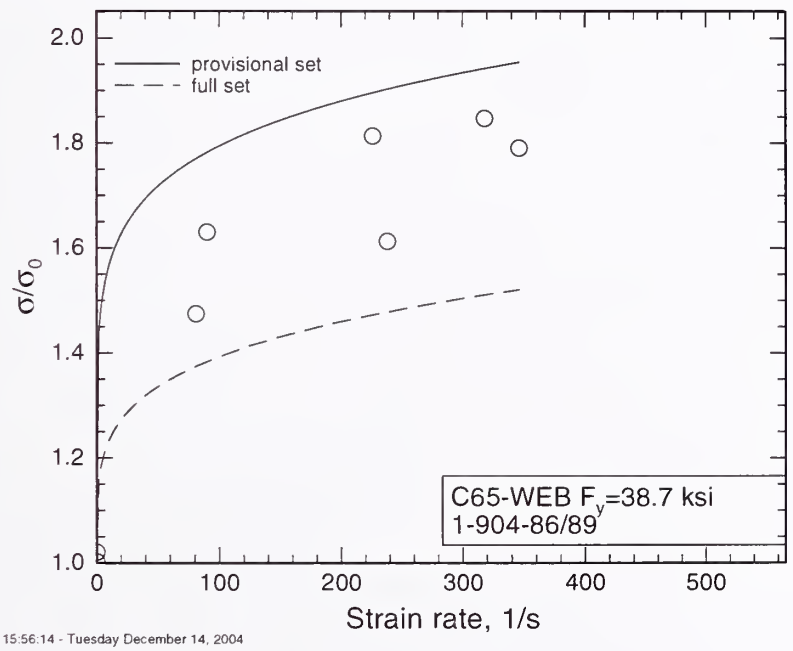

Figure C–8. Predictions of the provisional and full Cowper-Symonds model for perimeter column wide-flange steel M26-C1B, which is in the provisional data set.

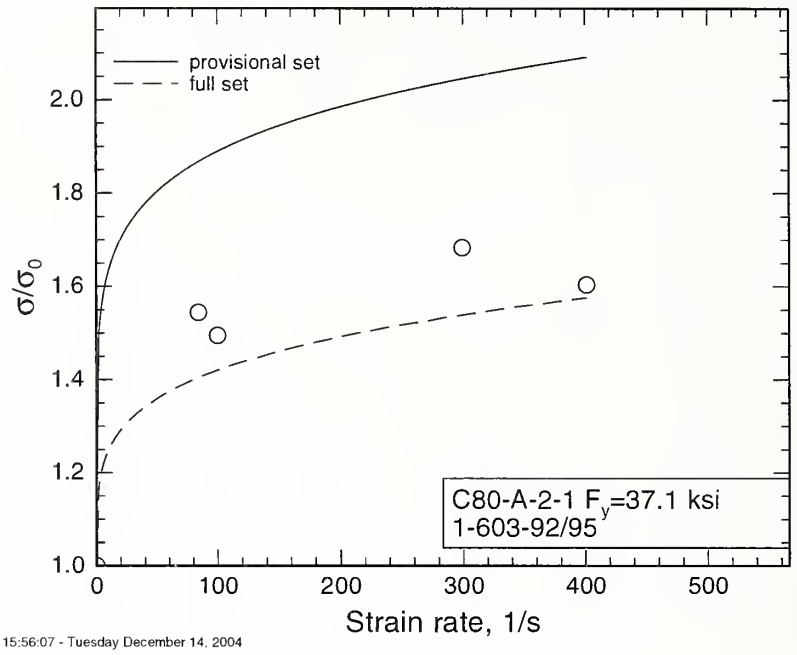

Figure C–9. Predictions of the provisional and full Cowper-Symonds model for core column wide-flange steel HH-WEB, which is not in the provisional data set.

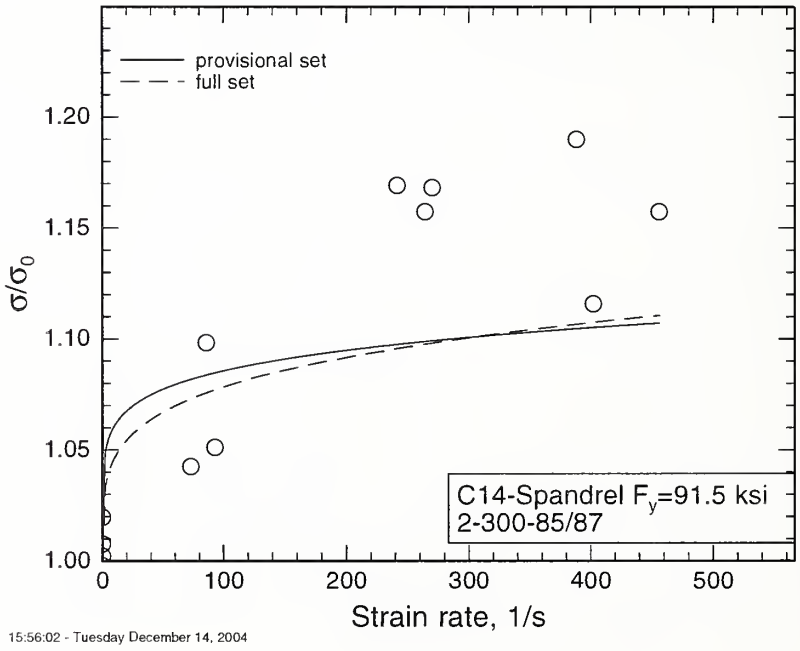

Figure C–10. Predictions of the provisional and full Cowper-Symonds model for core column wide-flange steel C80, which is not in the provisional data set.

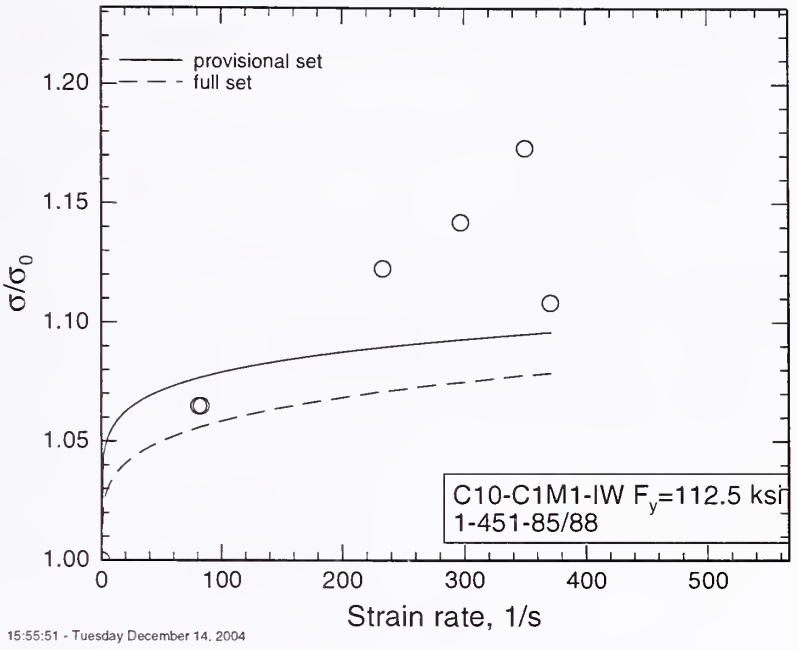

Figure C–11. Predictions of the provisional and full Cowper-Symonds model for core column steel C65-WEB, which is not in the provisional data set.

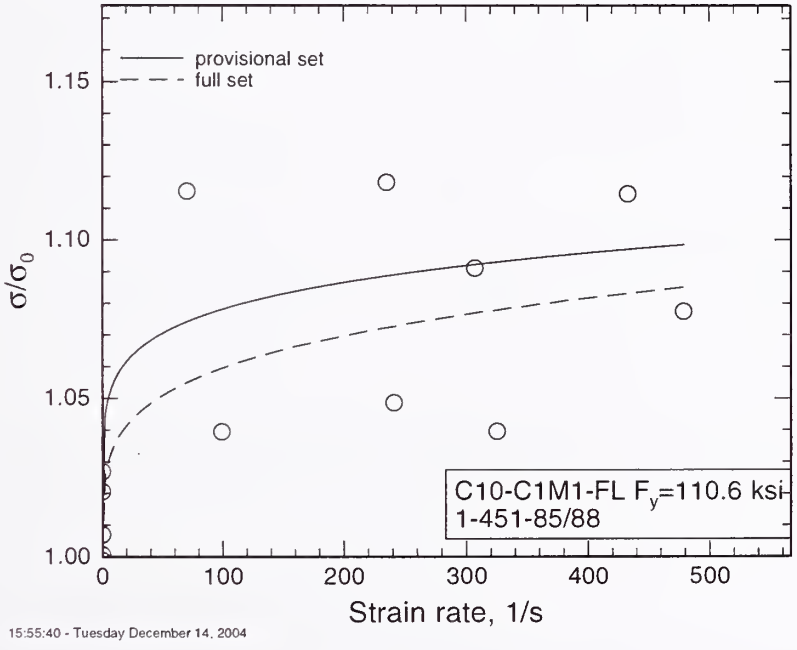

Figure C–12. Predictions of the provisional and full Cowper-Symonds model for core column wide-flange steel C65-FL2, which is not in the provisional data set.

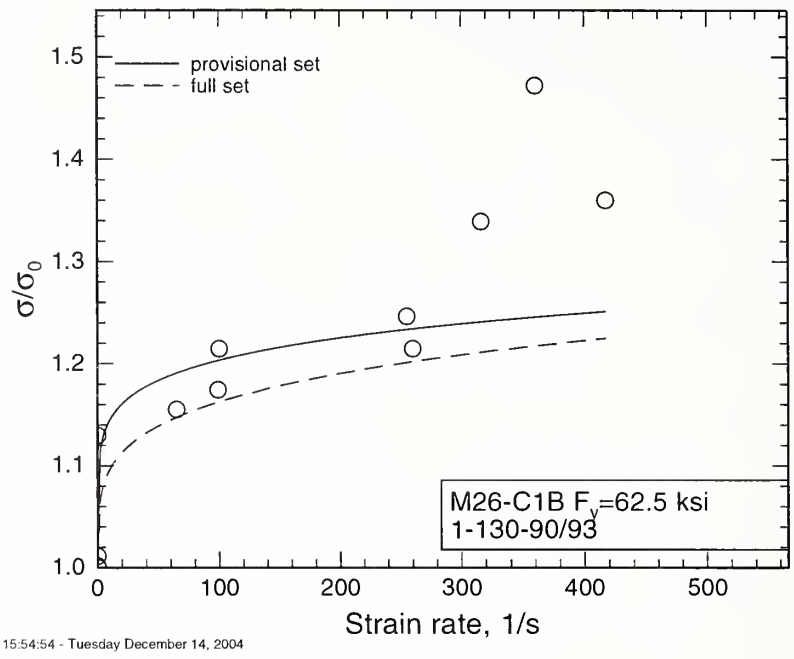

Figure C–13. Predictions of the provisional and full Cowper-Symonds model for core box column steel B6152-2, which is not in the provisional data set.

Appendix D
DEFORMATION OF STEELS USED IN WTC 7

D.1 INTRODUCTION

Unlike World Trade Center (WTC) 1 and WTC 2, no recovered steel in the National Institute of Standards and Technology (NIST) inventory can be unambiguously assigned to WTC 7. Therefore, properties must be estimated completely from the literature. Building plans called for rolled column shapes conforming to two ASTM International (ASTM) grades: A 36 and A 572 Grade 50. The heaviest rolled columns were built up with cover plates that were specified to several different ASTM specifications, by thickness: (in note 1 to drawing S-17)

$t < 2$ in.	A 36
2 in. $\leq t < 4$ in.	A 588 Grade 50
4 in. $\leq t < 6$ in.	A 572 Grade 42
$t > 6$ in.	A 588 Grade 42

About 26,000 tons of steel went into WTC 7 (Salvarinas 1986). Construction documents collected during the Investigation did not provide any information on steel suppliers, but a telephone interview with the former project manager for the construction of WTC 7 yielded some information (Salvarinas 2003). TradeARBED supplied the jumbo columns for the base of the building to ASTM specifications. British Steel (now Corus) and Bethlehem Steel supplied A 36 and Grade 50 steel. Algoma Steel supplied most of the beams used for the floors. These were rolled to a proprietary Algoma shape that was approximately 41 lb/ft (Salvarinas 2003). They were supplied to meet Canadian Standard CSA G40.21 ("General Requirements for Rolled or Welded Structural Quality Steel/Structural Quality Steel") Grade 44W. This was a $F_y = 44$ ksi steel, where the "W" designates "weldable."

The goal of this report is to estimate the relevant mechanical properties of the steels. The sections of this appendix follows outline of main report on mechanical properties.

D.2 ELASTIC PROPERTIES

Chapter 2 of this report summarizes the values for the elastic properties. NIST found no evidence that the Young's modulus or Poisson's ratio differs between structural steels, so the values in Chapter 2, Eqs. 2–2 and 2–3 can be used directly.

D.3 ROOM TEMPERATURE PROPERTIES

Because NIST recovered no steel from WTC 7, it is not possible to make any statements about its quality.

The values of the parameters that make up the expressions for the stress-strain behavior can be estimated using the same methodology that was used for the WTC 1 and WTC 2 steels. This section summarizes that methodology.

The static yield strength, σ_{ys} for rolled shapes was calculated using the expected historical value from literature data (Alpsten 1972):

$$\sigma_{ys} = k_s F_y + k_{\text{dynamic}} + k_{\text{flange}} \qquad \text{D–1 also 3-3}$$

where F_y is the specified minimum yield strength, The factor k_s = 1.2 corrects for the fact that, historically, the mill test report value of the yield strength of rolled shapes exceeds the specified value by about 20 percent. (Alpsten 1972). The factor k_{dynamic} = -3.6 ksi corrects the strength in the mill test report to the value the static value. The factor k_{flange} = –2.6 ksi corrects for the fact that, until recently, the specimen for the mill test report came from the higher-strength web, but the flange represents the majority of the load-carrying area. For core rolled plates the correction is slightly different:

$$\sigma_{\text{ys}} = k_p F_{\text{y}} + k_{\text{dynamic}} \qquad \text{D–2 also 3-4}$$

where k_p = 1.092 (Alpsten 1972).

The Voce hardening law can represent the increase in stress, σ, with plastic strain, ε_p, in the plastic regime. In this hardening rule the flow stress, σ, reaches a limiting stress, R_∞, with an exponential decay:

$$\sigma = R_0 \varepsilon_p + R_\infty \left(1 - \exp\left(- b\varepsilon_p\right)\right) \qquad \text{D–3 also 3-5}$$

This relation is available in most finite element packages.

Table D–1 summarizes the estimated static yield strengths and the parameters of the Voce hardening law for the steels from WTC 7.

Table D-1. Parameters for calculating room-temperature stress-strain curves.

Steel Description	F_y ksi	σ_{ys} ksi	TS ksi	ε_{max}	b	R_∞ ksi	R_0 ksi	Source of Plastic Portion
Fy = 36 ksi WF shapes	36	36.8	61.3	0.190	30.337	24.467	67.973	S9-C1T-S1 36 ksi perimeter steel
Fy = 50 ksi WF shapes	50	53.8	74.8	0.202	23.023	32.116	30.495	HH-FL-1 50 ksi core wide-flange
Fy = 36 ksi cover plates t < 2 in.	36	35.6	61.2	0.204	21.723	30.729	58.392	B6152-2-FL2 36 ksi box column steels
A 588 cover plates 2 in. ≤ t < 4 in.	50	50.8	72.5	0.202	23.023	32.116	30.495	HH-FL-1
A 572 cover plates 4 in. ≤ t < 6 in.	42	42.0	65.4	0.202	23.023	32.116	30.495	HH-FL-1
A 588 cover plates t ≥ 6.0 in.	42	42.0	65.4	0.202	23.023	32.116	30.495	HH-FL-1

Note: ε_{max} is the true strain at the tensile strength, *TS*. The static yield strength, σ_{ys}, is calculated from Eq. D–2. The column labeled "source of plastic portion" identifies the specific WTC specimen used to develop the voce hardening parameters

D.4 HIGH STRAIN RATE PROPERTIES

Because, prior to collapse, WTC 7 did not suffer any high strain rate events, NIST made no effort to estimate high-strain-rate properties of the steel.

D.5 IMPACT PROPERTIES

Because, prior to collapse, WTC 7 did not suffer any high strain rate events, and because there were no recovered steels to test, NIST made no effort to estimate impact properties of the steel.

D.6 ELEVATED-TEMPERATURE PROPERTIES

D.6.1 Stress-Strain Curves

The elevated-temperature stress-strain curves can be estimated using the methodology of Section 6.4.3.

The stress-strain curves for 0°C < T < 700°C for all WTC 7 steels is represented using a power-law work-hardening model:

$$\sigma = R_{TS} R_C K(T) \varepsilon^{n(T)} \qquad \text{D–4 also 6-4}$$

where σ has units of ksi, T has units of °C and K(T) and n(T) are defined in Eqs. 6-5 and 6-6. The parameter R_{TS} is the ratio of the room temperature tensile strength of the steel of interest, TS_i, to the room temperature tensile strength, TS_{ref}, of the steel used to develop the model expressed by Eq. D–4.

$$R_{TS} = \frac{TS_i}{TS_{\text{ref}}} \qquad \text{D–5 also 6-7}$$

The parameter R_C corrects for two additional phenomena. The temperature-dependent functions $K(T)$ and $n(T)$ (Eqs. 6-5 and 6-6) were originally developed using data that were not corrected to zero strain rate, whereas the stress-strain curves supplied to the Investigation teams for room temperature behavior are corrected to the zero strain rate. Secondly, because the temperature dependence of all the possible steels is represented using the behavior of only two different steels, it is possible that the stress-strain behavior predicted by Eq. D–4 at room temperature could differ from that predicted by the already generated room temperature stress-strain curve. The parameter R_C corrects the elevated-temperature stress-strain curve so that the value of stress predicted by Eq. D–4 for T = 25 °C at ε = 0.05 equals that of the room temperature model curve. In general, the correction is small: 0.9 < R_C < 1.04.

Table D–2 summarizes the values of the parameters necessary to calculate high-temperature stress-strain curves for the WTC 7 steels.

Table D-2. Parameters for estimating elevated-temperature stress-strain and creep curves.

Steel Description	F_y ksi	TS ksi	R_{TS}	R_C	R_σ
Parameter defined in Equation			6-7		6-19
F_y = 36 ksi WF shapes	36	61.3	1.03	0.90	1.15
F_y = 50 ksi WF shapes	50	74.8	1.01	0.97	0.94
F_y = 36 ksi cover plates $t < 2$ in.	36	63.4	1.07	0.86	1.11
A 588 cover plates 2 in $\leq t < 4$ in.	50	72.5	0.98	0.97	0.97
A 572 cover plates 4 in $\leq$ t $<$ 6 in.	42	65.4	0.88	0.94	1.08
A 588 cover plates t $\geq$ 6.0 in	42	65.4	0.88	0.94	1.08

Note: R_σ based on a reference tensile strength TS_{A149} = 70.65 ksi.

D.6.2 Creep Behavior

The creep behavior can be estimated using the methodology of Section 6.4.4. The creep strain as a function of time is represented by Eq. 6–10 using the parameters of Eqs. 6–11, 6–12, and 6–13.

$$\varepsilon_c = At^B\sigma^C \qquad \text{D–6 also 6-10}$$

The applied stress should be scaled by R_σ, ratio of the tensile strength of the steel in question to that of the reference AS A149 steel (TS_{A149} = 70.6 ksi) using Eq. 6–19.

$$\sigma_c = R_\sigma\sigma_a = \frac{TS_{A149}}{TS_{unt}}\sigma_a \qquad \text{D–7 also 6-19}$$

Table D–2 summarizes the values of the parameters necessary to calculate high-temperature creep curves for the WTC 7 steels.

D.7 REFERENCES

D.7.1 References Available from Publicly Available Sources

Salvarinas, John J. 1986. Seven World Trade Center, New York, Fabrication and Construction Aspects. *Canadian Structural Engineering Conference-1986 Proceedings*. Canadian Structural Steel Council, Willowdale, Ontario, Canada. ISBN 0-88811-062-6 pages 11-1 to 11-44.

D.7.2 References Available from Nonpublic Sources

Salvarinas, John J. 2003. Telephone interview with William Luecke. Salvarinas was the project manager for Frankel Steel during the erection of WTC 7. May 16.

This page intentionally left blank.

Appendix E
SPECIMEN GEOMETRY EFFECTS ON HIGH-RATE TENSILE PROPERTIES

E.1 INTRODUCTION

The test plan utilized several different specimen sizes and geometries to evaluate the strain rate sensitivity of the yield and tensile strength and the total elongation. Two types of high-rate specimens were used in an attempt to minimize the ringing in the load signal that complicated the data analysis. In addition, data from ordinary test specimens for assessing the quality of the steel and for characterizing room-temperature stress-strain behavior already existed. To evaluate the strain rate sensitivity, it was convenient to combine these data sets. This appendix describes the limitations of combining data developed from different specimen geometries and sizes and summarizes the calculations of the strain rate dependence of the total elongation to failure.

The analysis reaches two conclusions. Results from specimens with different geometry can be combined to evaluate the strain rate sensitivity of yield and tensile strength. To evaluate the strain rate sensitivity of the total elongation, the specimens may be different size, but they must be geometrically self-similar.

E.1.1 Estimating Specimen-Size Effects on Yield and Tensile Strength

To a first approximation, the details of the specimen shape should not affect the measured yield and tensile strength. If they did, the applicability of tension tests to determine material properties for use in constitutive models would be questionable.

E.1.2 Estimating Specimen-Geometry Effects on Ductility

The total elongation to failure of a specimen depends on the gauge length. In specimens with small gauge lengths, the neck occupies a greater fraction of the total elongation, which leads to greater measured total elongations. In general, geometrically similar specimens develop similar total elongations. This relation is called Barba's law (Metals Handbook, 1985), which relates the total elongation, El_f, to the specimen area A_0 and gauge length L_0:

$$El_f = \beta \frac{A_0^{1/2}}{L_0} + e_u \qquad \text{E–1}$$

The parameter β is a proportionality coefficient, and e_u is the engineering strain at the point of necking. Generally, specimens with different geometries will produce similar total elongations if the first term in Eq. E–1 is held constant. This relation underlies the choice of the geometries of the various round specimens in ASTM E 8, where the standard- and sub-size specimens have $A^{1/2}/L_0 = 0.177$.

E.2 PROCEDURE

In the course of the World Trade Center (WTC) Investigation, investigators employed a variety of different specimen geometries for tests at quasi-static rates to satisfy the constraints of the starting material and the test equipment available. The quasi-static strain rates, which were not identical between specimen geometries, were in the range 6×10^{-4} s^{-1} < dε/dt < 1.2×10^{-3} s^{-1}. Some of the quasi-static tests that used the ordinary tensile specimens followed E 8, which allows for an increased extension rate after the yield strength has been determined. For these specimens, the strain rate plotted is the rate appropriate for the tensile strength determination.

Table E–1 summarizes the different specimen geometries used for determining strain rate sensitivities. Note that the t = 0.25 in. Flat 2" specimen and the Flat-HSR-1"TK specimen not only have the same $A^{1/2}/L_0$ ratio, but their gauge lengths have the same width to thickness ratio. They are geometrically self-similar.

Table E–1. Specimen geometries used for establishing strain rate sensitivities.

Specimen Description	Specimen Designation	t in.	w in.	L_u in.	L_0 in.	A in.^{2}	$A^{0.5}/L_0$
High rate	Flat-HSR-1" TK	0.125	0.25	1.25	1	0.031	0.177
High rate	Flat-HSR-1" TN	0.0625	0.25	1.25	1	0.016	0.125
3 in. round for 1 in. elongation measurement	Rd 1"	D = 0.25 in	n/a	1.5	1	0.049	0.220
8 in. long flat[a]	Flat 2"	0.250	0.50	2.75	2	0.125	0.177
8 in. long flat[b]	Flat 2"	0.5625	0.50	2.75	2	0.281	0.260
4 in. long flat	Flat-C 1"	0.250	0.25	1.1	1	0.0625	0.250

a. Material thickness for Flat 2 in. specimens was generally 0.25 in.
b. Specimen M26-C1B1-RF came from a plate with t = 9/16 in.
Key: n/a, not applicable; A, area; L_u, length of uniform cross section; L_0, elongation gauge length; t, specimen thickness; w, specimen gauge section width.

E.3 RESULTS

Figures E–1 through E–7 show the quasi-static stress-strain curves for the different specimen geometries. In general, the agreement between the different specimen geometries is good for 1 percent offset yield strength and tensile strengths. Table E–2 summarizes the data from those figures. Total elongations should be taken from the table, because in some cases the operator removed the extensometer prior to failure. Although the yield and tensile strengths are not identical between the specimens, the differences are small enough so that the differences can be ignored and the data combined to evaluate the strain rate sensitivity.

The total elongation data generally follow Barba's law, Fig. E–9. The total elongation, El_t, in specimens with larger $A^{1/2}/L_0$ is correspondingly longer in five of the six cases. Specimen M10B provides a direct comparison between the large, Flat-2" specimen and the 1/4-size Flat-HSR 1"TK specimen. The $A^{1/2}/L_0$ ratio is identical for both test specimens. The total elongations for each specimen are statistically indistinguishable, which is consistent with the expected Barba's law behavior.

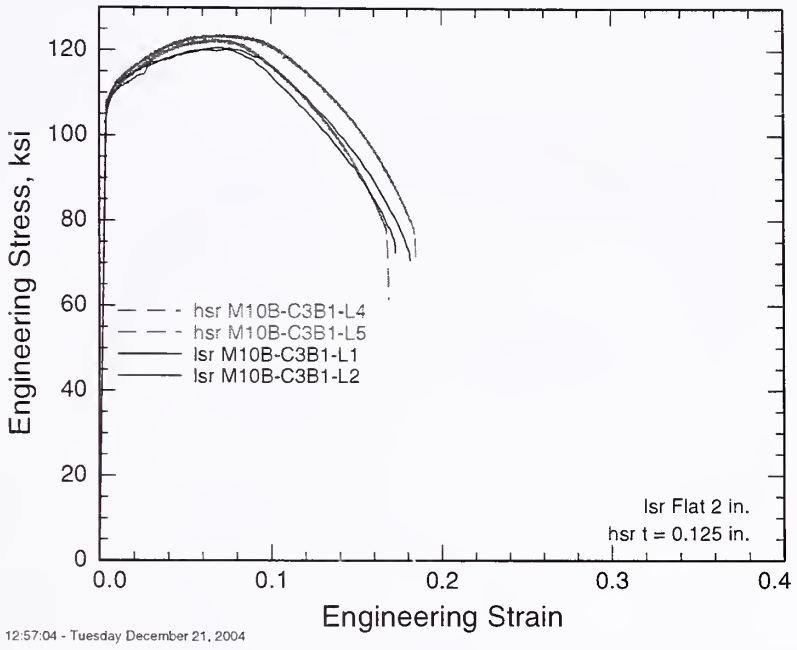

Figure E–1. Comparison of quasi-static stress strain curves obtained with high-rate style (HSR) and ordinary specimens for specimen M10B-C3B1-RF, F_y = 100 ksi.

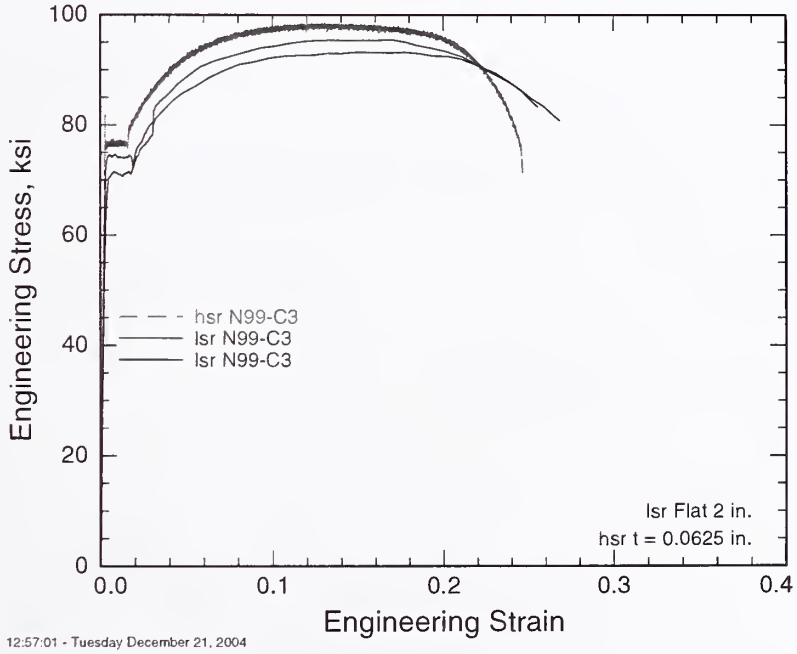

Figure E–2. Comparison of quasi-static stress strain curves obtained with high-rate style (HSR) and ordinary specimens for specimen N99-C3M1-RF, F_y = 65 ksi.

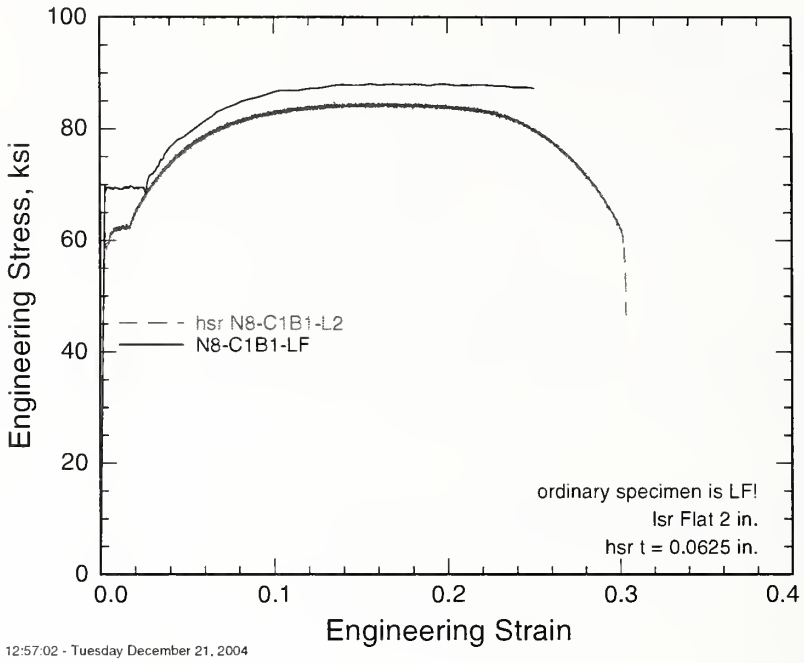

Figure E–3. Comparison of quasi-static stress strain curves obtained with high-rate style (HSR) and ordinary specimens for specimen N8-C1B1-RF, F_y = 60 ksi.

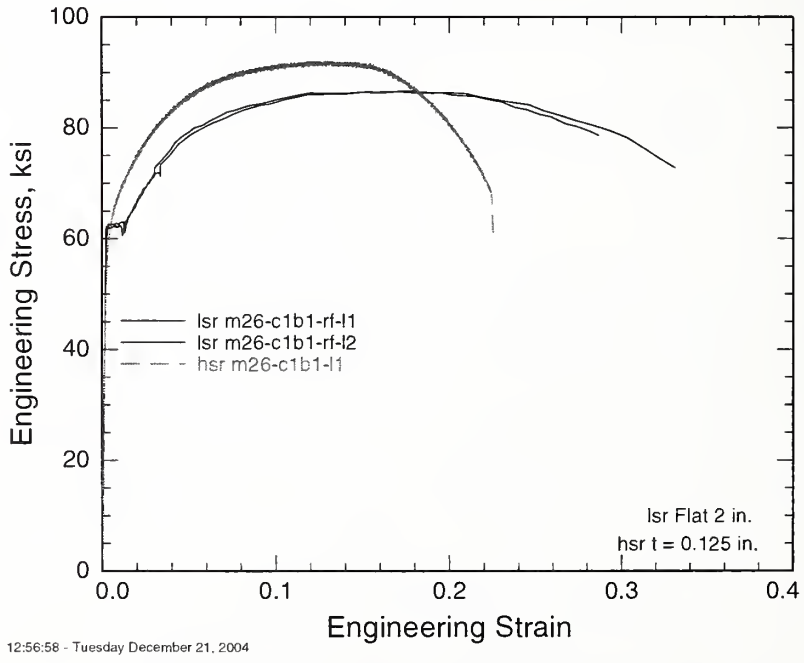

Figure E–4. Comparison of quasi-static stress strain curves obtained with high-rate style (HSR) and ordinary specimens for specimen M26-C1B1, F_y = 50 ksi.

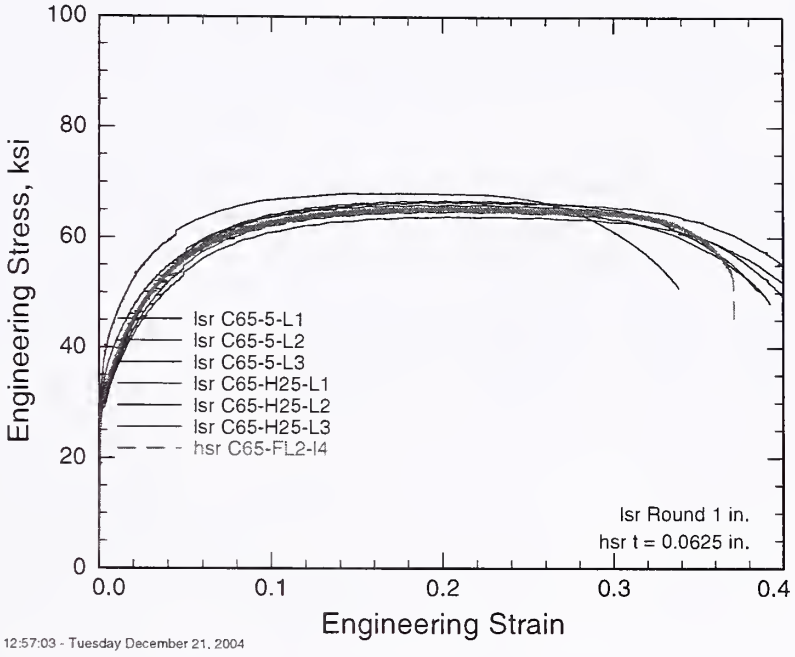

Figure E–5. Comparison of quasi-static stress strain curves obtained with high-rate style (HSR) and ordinary specimens for specimens from the flange of WF core shape C65-FL2, F_y = 36 ksi.

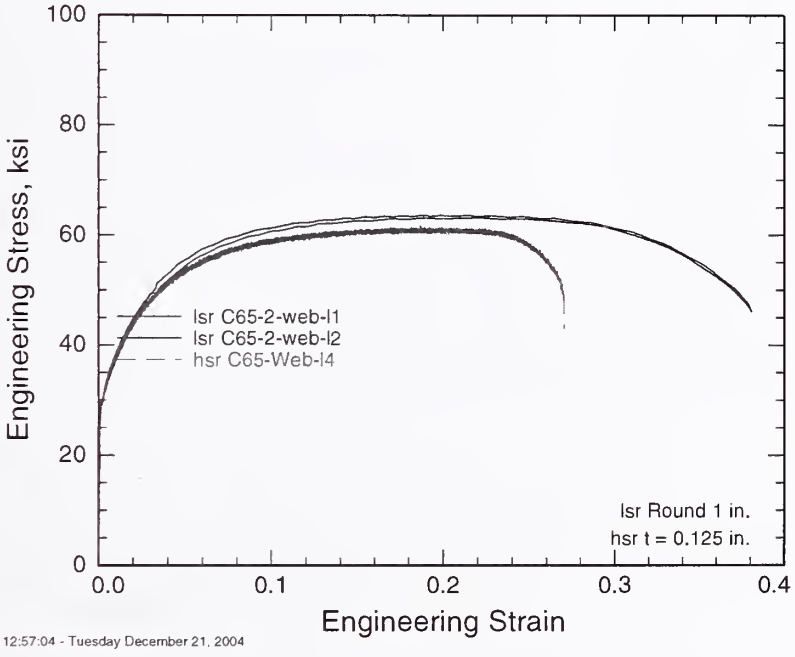

Figure E–6. Comparison of quasi-static stress strain curves obtained with high-rate style (HSR) and ordinary specimens for specimens from the web of WF core shape C65-WEB, F_y = 36 ksi.

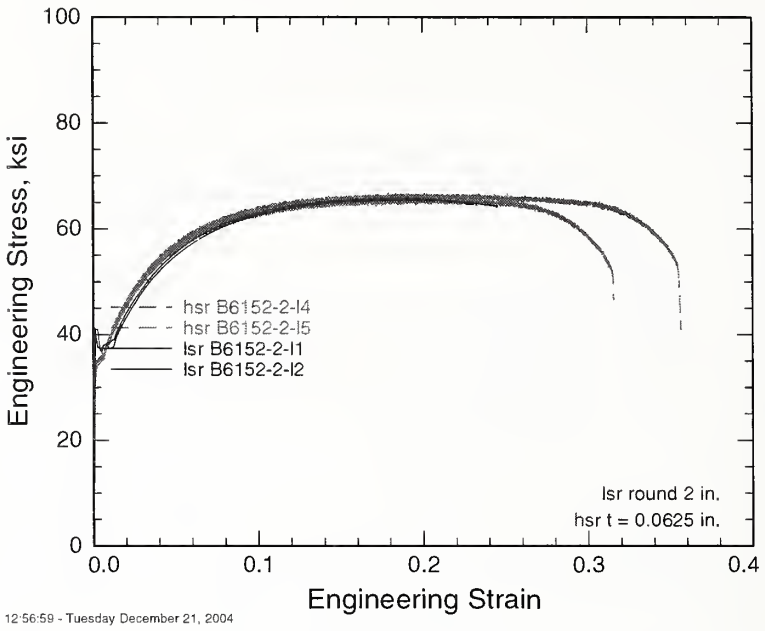

Figure E–7. Comparison of quasi-static stress strain curves obtained with high-rate style (HSR) and ordinary specimens for specimens from core box column B6152-2 F_y = 36 ksi.

Table E–2. Summary data for tests using different specimen geometries at quasi-static rates.

Strain Rate for F_y 1/s	F_y 1% offset ksi	Strain Rate for TS 1/s	TS ksi	El_t %	L_g in.	ROA %	t in.	$A^{0.5}/L_g$	F_y ksi	Specimen type	Sample #	Location
6.06E-5	63.2	1.21E-3	85.5	36.0	2	61	0.5625	0.265	50	Flat 2"	M26-C1B1-RF-L1	1-130-90/93
6.06E-5	61.7	1.21E-3	86.1	35.0	2	61	0.5625	0.265	50	Flat 2"	M26-C1B1-RF-L2	1-130-90/93
1.07E-4	70.6	1.07E-4	91.8	22.6	1	58	0.125	0.177	50	Flat HSR 1" TK	M26-C1B1-L1	1-130-90/93
1.07E-4	76.2	1.07E-4	98.0	24.1	1	51	0.0625	0.125	65	Flat HSR 1" TN	N99-C3M1-RF-L6	1-148-99/102
6.06E-5	70.8	1.21E-3	93.1	29.0	2	60	0.25	0.177	65	Flat 2"	N99-C3T1-RF-L1	1-148-99/102
6.06E-5	73.9	1.21E-3	94.0	30.0	2	60	0.25	0.177	65	Flat 2"	N99-C3T1-RF-L2	1-148-99/102
1.07E-4	113.5	1.07E-4	122.6	18.5	1	54	0.125	0.177	85	Flat HSR 1" TK	M10B-C3B1-RF-L4	2-206-83/86
1.07E-4	114.5	1.07E-4	123.4	20.4	1	54	0.125	0.177	85	Flat HSR 1" TK	M10B-C3B1-RF-L5	2-206-83/86
6.06E-5	111.6	1.21E-3	120.4	20.0	2	55	0.25	0.177	85	Flat 2"	M10B-C3B1-RF-L1	2-206-83/86
6.06E-5	113.3	1.21E-3	120.5	18.0	2	62	0.25	0.177	85	Flat 2"	M10B-C3B1-RF-L2	2-206-83/86
1.10E-4	113.6	7.88E-4	124.7	27.0	1	67	0.25	0.250	90	Flat-C 1"	C10-C1M-FL-1-1	1-451-85/88
1.19E-4	112.9	8.10E-4	124.4	23.0	1	66	0.25	0.250	90	Flat-C 1"	C10-C1M-FL-1-2	1-451-85/88
8.33E-5	109.9	8.33E-5	119.5	18.0	2	61	0.25	0.177	90	Flat 2"	C10-C1B-FL-1-L1	1-451-85/88
8.33E-5	110.5	8.33E-5	119.9	18.0	2	60	0.25	0.177	90	Flat 2"	C10-C1B-FL-1-L2	1-451-85/88
1.07E-4	39.6	1.07E-4	64.5	33.3	1	53	0.0625	0.125	36	Flat HSR 1" TN	B6152-2-FL-2-L4	1-504-33/36
1.07E-4	40.8	1.07E-4	66.1	36.6	1	51	0.0625	0.125	36	Flat HSR 1" TN	B6152-2-FL-2-L5	1-504-33/36
1.17E-3	39.8	1.17E-3	65.7	35.0	2	69	0.5	0.222	36	Rd 2"	B6152-2-FL-2-L1	1-504-33/36
1.20E-3	37.6	1.20E-3	65.4	36.0	2	67	0.5	0.222	36	Rd 2"	B6152-2-FL-2-L2	1-504-33/36
8.75E-5	37.9	4.37E-4	63.5	41.0	1	66	0.25	0.222	36	Rd 1"	C65-2-WEB-L1	1-904-86/89
8.75E-5	39.5	4.37E-4	64.0	42.0	1	63	0.25	0.222	36	Rd 1"	C65-2-WEB-L2	1-904-86/89
1.07E-4	38.8	1.07E-4	60.9	31.5	1	55	0.0625	0.125	36	Flat HSR 1" TN	C65-WEB-L4	1-904-86/89
8.75E-5	39.7	4.37E-4	66.6	43.0	1	63	0.25	0.222	36	Rd 1"	C65-H.25-L1	1-904-86/89
8.75E-5	37.8	4.37E-4	65.0	42.0	1	61	0.25	0.222	36	Rd 1"	C65-H.25-L2	1-904-86/89
8.75E-5	38.3	4.37E-4	70.0	43.0	1	62	0.25	0.222	36	Rd 1"	C65-H.25-L3	1-904-86/89
8.75E-5	47.0	4.37E-4	68.0	38.0	1	63	0.25	0.222	36	Rd 1"	C65-H.5-L1	1-904-86/89
8.75E-5	42.5	4.37E-4	66.0	42.0	1	62	0.25	0.222	36	Rd 1"	C65-H.5-L2	1-904-86/89
8.75E-5	37.1	4.37E-4	64.0	43.0	1	62	0.25	0.222	36	Rd 1"	C65-H.5-L3	1-904-86/89
2.19E-3	38.7	2.19E-3	65.6	42.0	1	62	0.25	0.222	36	Rd 1"	C65-H.5-L4	1-904-86/89
1.07E-4	40.1	1.07E-4	65.3	39.2	1	54	0.0625	0.125	36	Flat HSR 1" TN	C65-FL2-L4	1-904-86/89

E.4 DISCUSSION OF TOTAL ELONGATION BEHAVIOR

The excellent correspondence between the different-sized specimens of M10B indicates that, where possible, the different sized specimens with identical $A^{1/2}/L_0$ ratios can be combined to gain insight into the behavior of the total elongation with strain rate.

E.4.1 Limitations

Although the specimens are geometrically similar, the analysis does not account for the temperature rise in the specimen as the work of deformation is transformed into heat. High rate tests are generally assumed

to be adiabatic. Quasi-static tests have additional time for the specimen to cool during deformation, so the temperature rise will be less. For adiabatic conditions the temperature rise, ΔT, is

$$\Delta T = \frac{1}{\rho C_p} \int_e^{e_f} s(e)de \qquad \text{E–2}$$

for a material with density, ρ, heat capacity C_p, which deforms at engineering stress $s(e)$ to a final strain of e_f. For steel, assume that the failure strain is $e_f = 0.3$, the flow stress constant s = 830 MPa (120 ksi), C_p = 415 J/kg/K, and ρ = 7860 kg/m^3. Then

$$\Delta T = \frac{se_f}{\rho C_p} = 76.5 \text{ K} \qquad \text{E–3}$$

which represents an upper limit. The temperature rise of lower-strength specimens will be correspondingly smaller. Because the temperature rise of the quasi-static specimen is not zero, however, the effect of the temperature rise on the ductility of the high-rate specimens is probably not significant.

E.5 CONCLUSIONS

It is possible to combine ordinary and high-rate style specimens for determining the yield and tensile behavior as a function of strain rate. For determining the total elongation behavior as a function of strain rate, because of the Barba's law behavior, specimens can be mixed only if their width-to-thickness ratios are identical and their $A^{1/2}/L_0$ ratios are identical.

E.6 REFERENCES

Metals Handbook. 1985. Metals Handbook Ninth Edition. Volume 8 Mechanical Testing. American Society for Metals. Metals Park, OH. USA. p. 26.

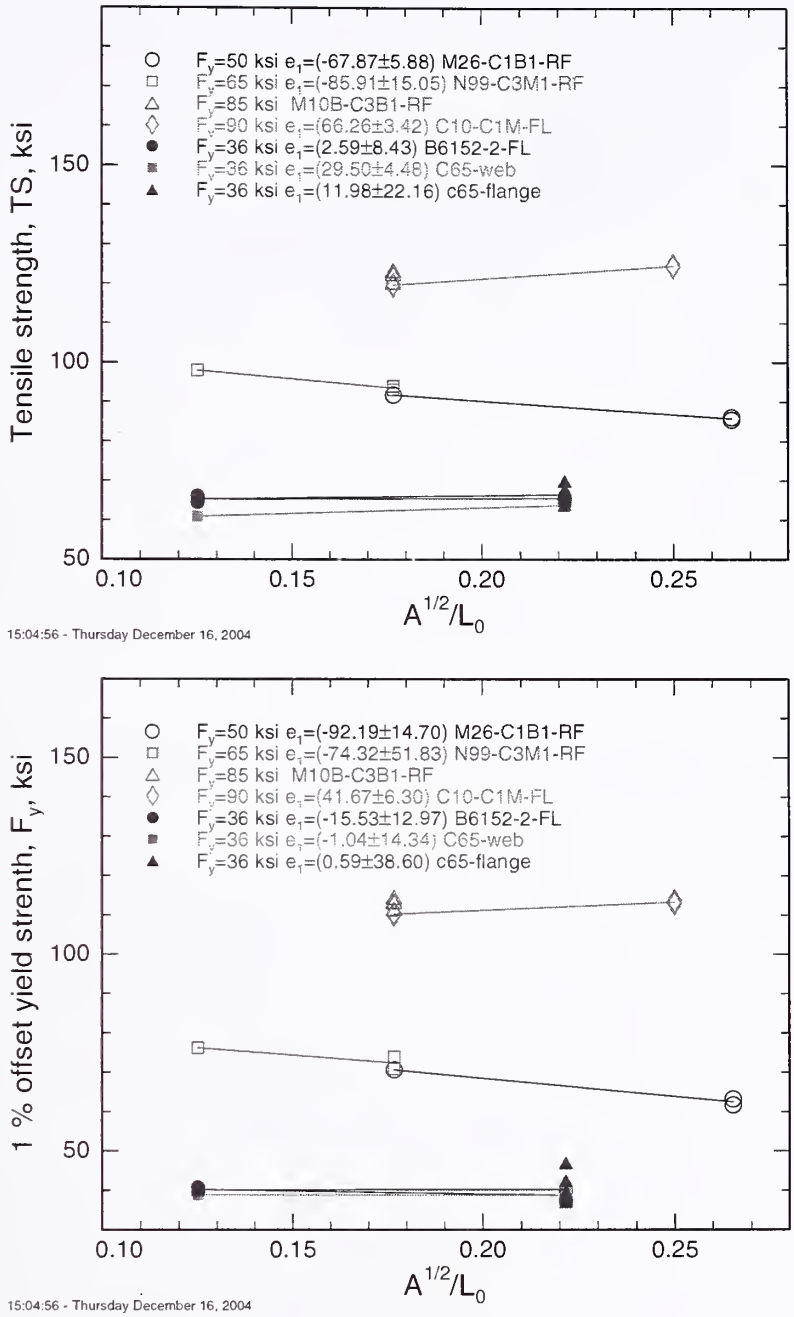

Figure E–8. Yield (1 percent offset) and tensile strength as a function of specimen geometry for specimens tested at quasistatic rates.

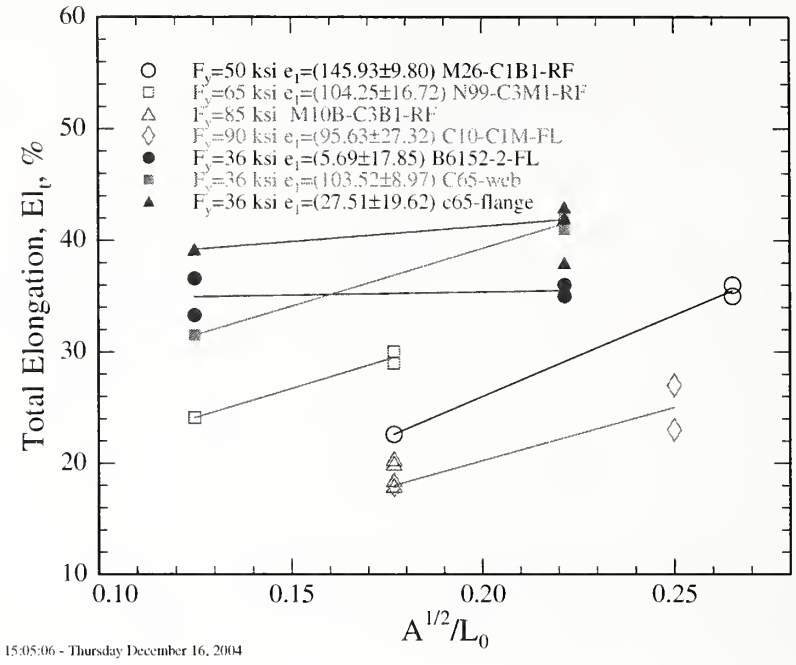

Figure E–9. Total elongation, El_t, as a function of specimen geometry for specimens tested at quasistatic rates.